



ADVANCES IN SULFATION PATHWAYS RESEARCH

EDITED BY: Jon Wolf Mueller, Tarsis G. Ferreira and Abby C. Collier
PUBLISHED IN: Frontiers in Molecular Biosciences



frontiers

Frontiers eBook Copyright Statement

The copyright in the text of individual articles in this eBook is the property of their respective authors or their respective institutions or funders. The copyright in graphics and images within each article may be subject to copyright of other parties. In both cases this is subject to a license granted to Frontiers.

The compilation of articles constituting this eBook is the property of Frontiers.

Each article within this eBook, and the eBook itself, are published under the most recent version of the Creative Commons CC-BY licence.

The version current at the date of publication of this eBook is CC-BY 4.0. If the CC-BY licence is updated, the licence granted by Frontiers is automatically updated to the new version.

When exercising any right under the CC-BY licence, Frontiers must be attributed as the original publisher of the article or eBook, as applicable.

Authors have the responsibility of ensuring that any graphics or other materials which are the property of others may be included in the CC-BY licence, but this should be checked before relying on the CC-BY licence to reproduce those materials. Any copyright notices relating to those materials must be complied with.

Copyright and source acknowledgement notices may not be removed and must be displayed in any copy, derivative work or partial copy which includes the elements in question.

All copyright, and all rights therein, are protected by national and international copyright laws. The above represents a summary only. For further information please read Frontiers' Conditions for Website Use and Copyright Statement, and the applicable CC-BY licence.

ISSN 1664-8714

ISBN 978-2-88976-535-5

DOI 10.3389/978-2-88976-535-5

About Frontiers

Frontiers is more than just an open-access publisher of scholarly articles: it is a pioneering approach to the world of academia, radically improving the way scholarly research is managed. The grand vision of Frontiers is a world where all people have an equal opportunity to seek, share and generate knowledge. Frontiers provides immediate and permanent online open access to all its publications, but this alone is not enough to realize our grand goals.

Frontiers Journal Series

The Frontiers Journal Series is a multi-tier and interdisciplinary set of open-access, online journals, promising a paradigm shift from the current review, selection and dissemination processes in academic publishing. All Frontiers journals are driven by researchers for researchers; therefore, they constitute a service to the scholarly community. At the same time, the Frontiers Journal Series operates on a revolutionary invention, the tiered publishing system, initially addressing specific communities of scholars, and gradually climbing up to broader public understanding, thus serving the interests of the lay society, too.

Dedication to Quality

Each Frontiers article is a landmark of the highest quality, thanks to genuinely collaborative interactions between authors and review editors, who include some of the world's best academicians. Research must be certified by peers before entering a stream of knowledge that may eventually reach the public - and shape society; therefore, Frontiers only applies the most rigorous and unbiased reviews.

Frontiers revolutionizes research publishing by freely delivering the most outstanding research, evaluated with no bias from both the academic and social point of view. By applying the most advanced information technologies, Frontiers is catapulting scholarly publishing into a new generation.

What are Frontiers Research Topics?

Frontiers Research Topics are very popular trademarks of the Frontiers Journals Series: they are collections of at least ten articles, all centered on a particular subject. With their unique mix of varied contributions from Original Research to Review Articles, Frontiers Research Topics unify the most influential researchers, the latest key findings and historical advances in a hot research area! Find out more on how to host your own Frontiers Research Topic or contribute to one as an author by contacting the Frontiers Editorial Office: frontiersin.org/about/contact

ADVANCES IN SULFATION PATHWAYS RESEARCH

Topic Editors:

Jon Wolf Mueller, University of Birmingham, United Kingdom

Tarsis G. Ferreira, Optimvia, United States

Abby C. Collier, University of British Columbia, Canada



Cover image: John Gage

Citation: Mueller, J. W., Ferreira, T. G., Collier, A. C., eds. (2022).
Advances in Sulfation Pathways Research. Lausanne: Frontiers Media SA.
doi: 10.3389/978-2-88976-535-5

Table of Contents

- 04 Editorial: Sulfation Pathways—There and Back Again**
Jon Wolf Mueller, Abby C. Collier and Tarsis F. Gesteira
- 07 In the Model Cell Lines of Moderately and Poorly Differentiated Endometrial Carcinoma, Estrogens Can Be Formed via the Sulfatase Pathway**
Renata Pavlič, Marija Gjorgoska, Eva Hafner, Maša Sinreih, Kristina Gajser, Stefan Poschner, Walter Jäger and Tea Lanišnik Rižner
- 24 Cellular ATP Levels Determine the Stability of a Nucleotide Kinase**
Oliver Brylski, Puja Shrestha, Patricia Gnutt, David Gnutt, Jonathan Wolf Mueller and Simon Ebbinghaus
- 36 A Sulfuryl Group Transfer Strategy to Selectively Prepare Sulfated Steroids and Isotopically Labelled Derivatives**
Jaber A. Alshehri, Daniel M. Gill and Alan M. Jones
- 42 Dissecting the Role of SAL1 in Metabolizing the Stress Signaling Molecule 3'-Phosphoadenosine 5'-Phosphate in Different Cell Compartments**
Natallia Ashykhmina, Kai Xun Chan, Henning Frerigmann, Frank Van Breusegem, Stanislav Kopriva, Ulf-Ingo Flügge and Tamara Gigolashvili
- 58 The Role of Sulfation in Nematode Development and Phenotypic Plasticity**
Catia Igreja and Ralf J. Sommer
- 71 Steroid Sulfation in Neurodegenerative Diseases**
Jana Vitku, Martin Hill, Lucie Kolatorova, Eva Kubala Havrdova and Radmila Kancheva
- 87 Profiling Urinary Sulfate Metabolites With Mass Spectrometry**
Christopher C. J. Fitzgerald, Rikard Hedman, Dimanthi R. Uduwela, Bettina Paszerbovics, Adam J. Carroll, Teresa Neeman, Adam Cawley, Lance Brooker and Malcolm D. McLeod
- 101 Human Sulfotransferase Assays With PAPS Production in situ**
Yanan Sun, Lukas Corbinian Harps, Matthias Bureik and Maria Kristina Parr
- 111 Disease-Related Protein Variants of the Highly Conserved Enzyme PAPSS2 Show Marginal Stability and Aggregation in Cells**
Oliver Brylski, Puja Shrestha, Philip J. House, Patricia Gnutt, Jonathan Wolf Mueller and Simon Ebbinghaus
- 119 Sulfation Pathways During Neurodevelopment**
Taylor Clarke, Francesca E. Fernandez and Paul A. Dawson
- 129 Role of the Steroid Sulfate Uptake Transporter Soat (Slc10a6) in Adipose Tissue and 3T3-L1 Adipocytes**
Emre Karakus, Andreas Schmid, Silke Leiting, Bärbel Fühler, Andreas Schäffler, Thilo Jakob and Joachim Geyer
- 143 Site-Specific Regulation of Sulfatase and Aromatase Pathways for Estrogen Production in Endometriosis**
Katiane de Almeida Da Costa, Helena Malvezzi, Cristine Dobo, Rosa Maria Neme, Renée Zon Filippi, Thiago Pinheiro Arrais Aloia, Elisa Rampazo Prado, Juliana Meola and Carla de Azevedo Piccinato



Editorial: Sulfation Pathways—There and Back Again

Jon Wolf Mueller^{1*}, Abby C. Collier^{2*} and Tarsis F. Gesteira^{3*}

¹Institute of Metabolism and Systems Research, University of Birmingham, Birmingham, United Kingdom, ²Faculty of Pharmaceutical Sciences, University of British Columbia, Vancouver, BC, Canada, ³College of Optometry, University of Houston, Houston, TX, United States

Keywords: PAPS synthase, sulfation pathways, protein folding/stability/aggregation, conjugate analytics/mass spectrometry, sulfo-metabolite synthesis/analytics

Editorial on the Research Topic

Advances in Sulfation Pathways Research

Sulfation Pathways are understood as the oxidative branch of sulfur metabolism (Günel et al., 2019). Core to sulfation pathways is sulfate activation, the transfer of sulfate to biological acceptor molecules and its dynamic cleavage in a spatially and temporally specific manner. The biochemical problem of sulfate activation is evident even in geological specimens—gypsum may be observed in orthopedic casts, an example of the highly inert sulfate ion (Figure 1). A significant amount of energy is needed to turn biological sulfate into PAPS (3'-phospho-adenosine-5'-phospho-sulfate), the active sulfate form.

The many and diverse sulfation acceptor molecules in biology dictate the molecular functions of ubiquitous sulfation pathways. Recent publications have highlighted doubly sulfated steroids (Lightning et al., 2021) as well as sulfo-conjugated vitamin D species (Jenkinson et al., 2022). This Research Topic focused on *Advances in Sulfation Pathways Research* features nine research articles and three reviews, authored by 63 individual scientists, significantly advancing the field of Sulfation Pathways, highlighted within the following paragraphs:

Research into sulfation pathways always relied on state-of-the-art analytical methods. Hence, we are pleased to present novel mass-spectrometry-based ways of profiling sulfated metabolites in urine by Fitzgerald et al. Developing mass spectrometry methods is impossible however without having the respective pure compounds readily at hand. In this regard, Alshehri et al. report a novel sulfation strategy to prepare steroid sulfates and isotopically labeled variations thereof, certainly an innovation with great importance for the field. Whenever coming from a genomic viewpoint, it may be necessary to characterize a sulfation enzyme with regards to its activity. With this in mind, Sun et al. have prepared a manuscript on optimized sulfotransferase assays.

Sulfation impacts greatly on steroidogenesis—sulfated steroids may represent transport forms and/or modulate downstream processing (Foster and Mueller, 2018). Two studies by Pavlič et al. and De Almeida Da Costa et al. independently provide experimental evidence that endometrial tissues can generate estrogens from circulating steroid sulfates. Sulfation of steroids predominantly occurs within the cytosol and sulfated steroids then need dedicated transporters to enter circulation and for the uptake into target tissues. Karakus et al. provide an in-depth study about the steroid sulfate uptake transporter SOAT (SLC10A6) in adipose tissue that illustrates this well.

When studying sulfated steroids, not only are circulating steroids important, but also sulfated neuro-steroids. This Research Topic features two review articles about steroid sulfation in neurodegenerative diseases by Vitku et al. and during neurodevelopment by Clarke et al. Fascinating topics that will enable exciting discoveries in future, with great potential for the development of novel therapeutics.

OPEN ACCESS

Edited and reviewed by:

Cecilia Giulivi,
University of California, Davis,
United States

*Correspondence:

Jon Wolf Mueller
j.w.mueller@bham.ac.uk
Abby C. Collier
abby.collier@ubc.ca
Tarsis F. Gesteira
tgferrei@central.uh.edu

Specialty section:

This article was submitted to
Cellular Biochemistry,
a section of the journal
Frontiers in Molecular Biosciences

Received: 04 April 2022

Accepted: 29 April 2022

Published: 16 May 2022

Citation:

Mueller JW, Collier AC and Gesteira TF
(2022) Editorial: Sulfation
Pathways—There and Back Again.
Front. Mol. Biosci. 9:912700.
doi: 10.3389/fmolb.2022.912700



FIGURE 1 | Sulfur and a rock of sulfate. A lump of elementary sulfur featuring many shades of sulfuric yellows (front) and a rock of gypsum (rear), also known as $\text{CaSO}_4 \cdot 2 \text{H}_2\text{O}$. Both specimens were kindly provided by the Lapworth Museum of Geology, University of Birmingham, for an outreach event (to JWM).

Aspects of sulfation pathways are highly conserved in multicellular organisms. Hence, the review article by Igreja and Sommer about sulfation pathways in nematode development will be of great interest to the community—much is known about the genetics of these pathways, however a lot remains to be uncovered from the metabolism side.

One part of sulfation pathways that differs greatly between species is degradation of the remnants of PAPS-dependent sulfation. 3'-Phospho-adenosine-5'-phosphate seems to be a waste product in humans—it however represents important signaling properties in plants. Ashykhmina et al. studied the divergent functions of this nucleotide in stress signaling, when encountered in different cellular compartments. It remains to be seen, if any of these signaling propensities would also be discovered in human sulfation pathways.

REFERENCES

- Brylski, O., Ebbinghaus, S., and Mueller, J. W. (2019). Melting Down Protein Stability: PAPS Synthase 2 in Patients and in a Cellular Environment. *Front. Mol. Biosci.* 6, 31. doi:10.3389/fmolb.2019.00031

From a synthetic biology perspective, some sulfation proteins have been characterized in their folding and protein stability, reviewed here (Brylski et al., 2019), following on from which Brylski et al. constructed a folding sensor that reports protein integrity *via* Förster resonance energy transfer. This elegant advance allowed measurement of protein unfolding within intact cells. With this approach, Brylski et al. established that cellular ATP levels determine the stability of a nucleotide kinase. The same team of researchers also studied the stability and aggregation behavior of disease-related protein variants of the highly conserved enzyme PAPSS2 (Brylski et al.).

We look towards a bright future in Sulfation Pathways research. New developments may bring insights in novel or overlooked sulfated metabolites. Linking sulfation pathways with other metabolic pathways may also be highly interesting—such as the study of two Golgi-residing heparan sulfate sulfotransferases that cooperatively act on their substrate (Gesteira et al., 2021). By investigation of patients with rare genetic mutations or by using omics and big data approaches, we also may be able to link sulfation pathways to other biological themes; and linking steroid sulfation to adrenal tumors (Mueller et al., 2021) is a first step towards this goal.

There were dedicated meetings on sulfation pathways back in the 1990s. Due to renewed interest and significant advances in the field, such meetings started again. SUPA meetings took place in Greifswald, Germany, in 2015; then continued in Birmingham, United Kingdom, in 2017, and Castle Rauischholzhausen, Germany, in 2019. Accompanying Research Topics on sulfation pathways were published in 2016 (Mueller and Muller, 2016) and 2018 (Mueller and Foster, 2018). We are delighted to present the current Research Topic, looking towards the SUPA 2023 meeting that is being organized already.

AUTHOR CONTRIBUTIONS

JWM drafted the manuscript. All authors approved the final version of this editorial.

ACKNOWLEDGMENTS

We cordially thank Annalisa Pastore for introducing us to the publisher Frontiers. We also thank all the listed reviewers as well as several anonymous reviewers for their invaluable input as expert referees.

- Foster, P. A., and Mueller, J. W. (2018). Sulfation Pathways: Insights into Steroid Sulfation and Desulfation Pathways. *J. Mol. Endocrinol.* 61 (2), T271–T283. doi:10.1530/JME-18-0086
- Gesteira, T. F., Marforio, T. D., Mueller, J. W., Calvaresi, M., and Coulson-Thomas, V. J. (2021). Structural Determinants of Substrate Recognition and Catalysis by Heparan Sulfate Sulfotransferases. *ACS Catal.* 11 (17), 10974–10987. doi:10.1021/acscatal.1c03088

- Günal, S., Hardman, R., Kopriva, S., and Mueller, J. W. (2019). Sulfation Pathways from Red to Green. *J. Biol. Chem.* 294 (33), 12293–12312. doi:10.1074/jbc.REV119.007422
- Jenkinson, C., Desai, R., McLeod, M. D., Mueller, J. W., Hewison, M., and Handelsman, D. J. (2022). Circulating Conjugated and Unconjugated Vitamin D Metabolite Measurements by Liquid Chromatography Mass Spectrometry. *J. Clin. Endocrinol. Metab.* 107 (2), 435–449. doi:10.1210/clinem/dgab708
- Lightning, T. A., Gesteira, T. F., and Mueller, J. W. (2021). Steroid Disulfates - Sulfation Double Trouble. *Mol. Cell. Endocrinol.* 524, 111161. doi:10.1016/j.mce.2021.111161
- Mueller, J. W., and Foster, P. A. (2018). Steroid Sulfation Research Has Come a Long Way. *J. Mol. Endocrinol.* 61 (2), E5–E6. doi:10.1530/JME-18-0109
- Mueller, J. W., Vogg, N., Lightning, T. A., Weigand, I., Ronchi, C. L., Foster, P. A., et al. (2021). Steroid Sulfation in Adrenal Tumors. *J. Clin. Endocrinol. Metab.* 106 (12), 3385–3397. doi:10.1210/clinem/dgab182
- Mueller, J. W., and Muller, S. (2016). Welcome to a SUPA Issue. *Chemico-Biological Interact.* 259 (Pt A), 1. doi:10.1016/j.cbi.2016.11.006

Conflict of Interest: The authors declare that the research was conducted in the absence of any commercial or financial relationships that could be construed as a potential conflict of interest.

Publisher's Note: All claims expressed in this article are solely those of the authors and do not necessarily represent those of their affiliated organizations, or those of the publisher, the editors and the reviewers. Any product that may be evaluated in this article, or claim that may be made by its manufacturer, is not guaranteed or endorsed by the publisher.

Copyright © 2022 Mueller, Collier and Gesteira. This is an open-access article distributed under the terms of the Creative Commons Attribution License (CC BY). The use, distribution or reproduction in other forums is permitted, provided the original author(s) and the copyright owner(s) are credited and that the original publication in this journal is cited, in accordance with accepted academic practice. No use, distribution or reproduction is permitted which does not comply with these terms.



In the Model Cell Lines of Moderately and Poorly Differentiated Endometrial Carcinoma, Estrogens Can Be Formed *via* the Sulfatase Pathway

Renata Pavlič¹, Marija Gjorgoska¹, Eva Hafner¹, Maša Sinreih¹, Kristina Gajser¹, Stefan Poschner², Walter Jäger² and Tea Lanišnik Rižner^{1*}

¹Laboratory for Molecular Basis of Hormone-Dependent Diseases and Biomarkers, Institute of Biochemistry and Molecular Genetics, Faculty of Medicine, University of Ljubljana, Ljubljana, Slovenia, ²Department of Pharmaceutical Sciences, University of Vienna, Vienna, Austria

OPEN ACCESS

Edited by:

Jon Wolf Mueller,
University of Birmingham,
United Kingdom

Reviewed by:

Paul Alexander Foster,
University of Birmingham,
United Kingdom
Carla Piccinato,
Independent Researcher, São Paulo,
Brazil

*Correspondence:

Tea Lanišnik Rižner
Tea.Lanisnik-Rizner@mf.uni-lj.si

Specialty section:

This article was submitted to
Cellular Biochemistry,
a section of the journal
Frontiers in Molecular Biosciences

Received: 18 July 2021

Accepted: 15 October 2021

Published: 05 November 2021

Citation:

Pavlič R, Gjorgoska M, Hafner E, Sinreih M, Gajser K, Poschner S, Jäger W and Rižner TL (2021) In the Model Cell Lines of Moderately and Poorly Differentiated Endometrial Carcinoma, Estrogens Can Be Formed *via* the Sulfatase Pathway. *Front. Mol. Biosci.* 8:743403. doi: 10.3389/fmolb.2021.743403

Endometrial cancer (EC) is the most common gynecological malignancy in resource-abundant countries. The majority of EC cases are estrogen dependent but the mechanisms of estrogen biosynthesis and oxidative metabolism and estrogen action are not completely understood. Here, we evaluated formation of estrogens in models of moderately and poorly differentiated EC: RL95-2 and KLE cells, respectively. Results revealed high expression of estrone-sulfate (E1-S) transporters (*SLCO1A2*, *SLCO1B3*, *SLCO1C1*, *SLCO3A1*, *SLC10A6*, *SLC22A9*), and increased E1-S uptake in KLE vs RL95-2 cells. In RL95-2 cells, higher levels of sulfatase and better metabolism of E1-S to E1 were confirmed compared to KLE cells. In KLE cells, disturbed balance in expression of *HSD17B* genes led to enhanced activation of E1 to E2, compared to RL95-2 cells. Additionally, increased *CYP1B1* expression and down-regulation of genes encoding phase II metabolic enzymes: *COMT*, *NQO1*, *NQO2*, and *GSTP1* suggested decreased detoxification of carcinogenic metabolites in KLE cells. Results indicate that in model cell lines of moderately and poorly differentiated EC, estrogens can be formed *via* the sulfatase pathway.

Keywords: sulfatase pathway, steroid sulfatase, endometrial cancer, estrone sulfate, estrone sulfate transporters, 17 β -hydroxysteroid dehydrogenase, oxidative metabolism of estrogens, estrogen biosynthesis

INTRODUCTION

Endometrial cancer (EC) is the most frequent gynecological cancer in the developed world (Bray et al., 2018), with a continuing trend for increased incidence over recent decades due to pandemic obesity and increased life expectancy (Lindemann et al., 2010). According to the Bokhman classification, EC histopathology defines two groups. Type I is characterized by well and moderately differentiated endometrioid histology (grades 1, 2), which comprises 70–80% of all cases. In contrast type II, includes clear-cell, serous, or squamous histology, or endometrioid tumors with poorly differentiated histology (grade 3) (Amant et al., 2005; Chiang and Soslow, 2014; Murali et al., 2014; Morice et al., 2016), which comprises 20% of all cases. Tumors that show combined morphological and molecular characteristics of types I and II are also common (Yeramian et al., 2013). In addition to these sporadic cases, about 10% of ECs are hereditary and are associated with Lynch syndrome (Amant et al., 2005). Based on integrated genomic, transcriptomic, and proteomic data, EC is now classified into four molecular subtypes (Kandoth et al., 2013).

EC type I is estrogen-dependent disease, which develops and progresses due to unopposed actions of endogenous and exogenous estrogens on endometrial cells (Inoue, 2001). EC type II is usually considered estrogen independent. However, this has been questioned by studies that have shown no differences in tissue and plasma estrogen concentrations between patients with EC types I and II. This indicates that estrogens also have roles in EC type II (Berstein et al., 2003; Brinton et al., 2016; Wan et al., 2016). EC develops mainly in postmenopausal women, and thus relies on local formation of active estrogens. Locally, estrogens can be formed from the adrenal precursors dehydroepiandrosterone sulfate (DHEA-S) and DHEA, and from circulating estrone sulfate (E1-S) (Rižner et al., 2017). To enter the cells, these sulfated precursors use transporters from the solute carrier gene (SLC) superfamily. These genes encode organic anion transporters and organic anion transporting polypeptides (Roth et al., 2012). The efflux of sulfated steroids is *via* ATP-binding cassette (ABC) transporters. Within cells, active estrogens can be synthesized *via* the so-called aromatase and sulfatase pathways by the actions of a series of enzymes that include sulfatase (STS) and aromatase (CYP19A1). The most potent estrogen is estradiol (E2), and it can be formed from DHEA-S or DHEA *via* androstenedione, through the actions of STS, 3 β -hydroxysteroid dehydrogenase (HSD3B), aromatase, and reductive 17 β -hydroxysteroid dehydrogenases (HSD17B1, HSD17B7, HSD17B12), and also from E1-S through the actions of STS and HSD17B1, HSD17B7, and HSD17B12 (Rižner, 2013). The oxidative enzymes HSD17B2, HSD17B4, HSD17B8, and HSD17B14 catalyze the inactivation of E2 to the less potent estrone (E1). Sulfotransferases SULT2A1 and SULT2B1 maintain the levels of DHEA-S, and SULT1E1 maintains the levels of E1 and estradiol sulfate (E2-S). Estrogens can activate nuclear receptors ER α and ER β and G protein coupled receptor (GPER), through which they either stimulate cell proliferation (ER α , GPER), induce apoptosis (ER β) or enhance migration of cancerous cells (GPER) (Paterni et al., 2014; Xu et al., 2019). Additionally, phase I metabolism of estrogens by the CYP enzymes (CYP1A1, CYP1A2, CYP1B1, CYP3A5, CYP3A7) leads to formation of 16 α -hydroxyestrogens and 2- and 4-hydroxyestrogens. These catechols can then be further oxidized to quinones, which can bind to DNA and form adducts (Hevir et al., 2011). The formation of estrogen quinones is opposed by phase II metabolism, which includes methylation (catechol-O-methyl transferase; COMT), sulfation (sulfotransferases; SULT1A1, SULT1E1, SULT2B1) and glucuronidation (UDP-glucuronyl transferase). The formation of DNA adducts is prevented by conjugation with glutathione (glutathione S-transferase; GSTP1) and reduction back to catechols by (NAD(P)H quinone dehydrogenases; NQO1, NQO2). Estrogens can stimulate cell proliferation, and can also have genotoxic effects; they can thus act as promoters and initiators of carcinogenesis (Cavalieri and Rogan, 2011; Rižner, 2013; Cavalieri and Rogan, 2016).

The altered uptake of sulfated steroid precursors, the mechanisms of estrogen biosynthesis and oxidative metabolism, and estrogen actions in EC are not completely understood. In the present study we hypothesized that local

formation of estrogens *via* the sulfatase pathway has roles in different histological types of endometrial cancer and also in metastatic cancer. We investigated estrogen biosynthesis and metabolism in the RL95-2 and KLE cell lines, as models of moderately and poorly differentiated EC, respectively. The aims were; (i) to examine expression of 20 genes that encode E1-S uptake and efflux transporters, and 31 genes that encode estrogen biosynthetic, phase I and II metabolic enzymes and receptors; (ii) to investigate the metabolism of DHEA-S and E1-S, and to quantify the metabolites they form; and (iii) to measure cell uptake of E1-S in the RL95-2 and KLE cell lines, as representative of moderately and poorly differentiated, metastatic EC.

MATERIALS AND METHODS

Reagents and Chemicals

The standards of E1 (1,3,5 (10)-estratrien-3-ol-17-one) and E2 (1,3,5-estratriene-3,17 β -diol) were from Steraloids (Newport, RI, United States), the standards of E1-S (1,3,5 (10)-estratrien-17-one 3-sulfate), E2-S (1,3,5 (10)-estratriene-3,17 β -diol sulfate), E2-d₂ (1,3,5 (10)-estratriene-2,4-d₂-3,17 β -diol) were from Sigma Aldrich (St. Louis, MO, United States). Methanol and ammonium fluoride (NH₄F) were from Honeywell International Inc. (Charlotte, NC, United States), and ethanol was from Merck (Darmstadt, Germany). Ultrapure water with a resistivity of 18.2 M Ω \times cm was obtained from a Milli-Q water purification system (Merck Millipore, Darmstadt, Germany). The STS inhibitor STX64 was a kind gift from Dr. Barry Potter (Oxford University, Oxford, United Kingdom).

Model Cell Lines

The RL95-2 cell line (RRID: CVCL_0505) was originally established from a grade 2 moderately differentiated adenocarcinoma of the endometrium from a 65-year-old patient (Way et al., 1983), and it was purchased from American Type Culture Collection (ATCC; CRL-1671; lot 62130010) on October 18, 2017, as passage 125. The RL95-2 cells were cultured in Dulbecco's modified Eagles's medium/F12 (D6421), with 10% fetal bovine serum (FBS; F9665), 2.5 mM L-glutamine (G7153), and 5 μ g/ml insulin (I9278) (all from Sigma-Aldrich GmbH). The RL95-2 cells were used as passages +8 to +14. Authentication by short tandem repeat (STR) profiling was performed by ATCC.

The KLE cell line (RRID: CVCL_1329) was originally established from a poorly differentiated endometrial carcinoma from a 68-year-old patient (Richardson et al., 1984), and it was purchased from ATCC (CRL-162; lot 70001143) on October 18, 2017, as passage +12. The KLE cells were cultured in Dulbecco's modified Eagles's medium/F12 (D6421) supplemented with 10% FBS (F9665) and 2.5 mM L-glutamine (G7153) (all from Sigma-Aldrich GmbH). The KLE cells were used as passages +21 to +27. Authentication by STR profiling was performed by ATCC.

The HIEEC cell line was obtained from Michael A. Fortier (Laval University, Quebec, Canada) on April 4, 2014, as passage

TABLE 1 | Details for the TaqMan “Assays on Demand” used for the genes investigated in this study.

Gene symbol	Assay ID	Gene name
COMT	Hs00241349_m1	Catechol-O-methyltransferase
CYP19A1	Hs00240671_m1	Cytochrome P450, family 19, subfamily A
CYP1A1	Hs00153120_m1	Cytochrome P450, family 1, subfamily A, polypeptide 1
CYP1A2	Hs00167927_m1	Cytochrome P450, family 1, subfamily A, polypeptide 2
CYP1B1	Hs00164383_m1	Cytochrome P450, family 1, subfamily B, polypeptide 1
CYP3A5	Hs00241417_m1	Cytochrome P450, family 3, subfamily A, polypeptide 5
CYP3A7	Hs00426361_m1	Cytochrome P450, family 3, subfamily A, polypeptide 7
ESR1	Hs00174860_m1	Estrogen receptor 1 (α)
ESR2	Hs00230957_m1	Estrogen receptor 2 (β)
GP1R v2	Hs00173506_m1	G-protein-coupled estrogen receptor 1 (gene variant 2)
GP1R v3, v4	Hs01116133_m1	G-protein-coupled estrogen receptor 1 (gene variants 3 and 4)
GSTP1	Hs00168310_m1	Glutathione S-transferase pi 1
HPRT1 ^a	Hs99999909_m1	Hypoxanthine phosphoribosyltransferase 1
HSD17B1	Hs00166219_g1	Hydroxysteroid (17 β) dehydrogenase 1
HSD17B10	Hs00189576_m1	Hydroxysteroid (17 β) dehydrogenase 10
HSD17B12	Hs00275054_m1	Hydroxysteroid (17 β) dehydrogenase 12
HSD17B14	Hs00212233_m1	Hydroxysteroid (17 β) dehydrogenase 14
HSD17B2	Hs00157993_m1	Hydroxysteroid (17 β) dehydrogenase 2
HSD17B4	Hs00264973_m1	Hydroxysteroid (17 β) dehydrogenase 4
HSD17B7	Hs00367686_m1	Hydroxysteroid (17 β) dehydrogenase 7
HSD17B8	Hs00367151_m1	Hydroxysteroid (17 β) dehydrogenase 8
HSD3B1	Hs00426435_m1	Hydroxy-delta-5-steroid dehydrogenase, 3 β , and steroid delta-isomerase 1
HSD3B2	Hs00605123_m1	Hydroxy-delta-5-steroid dehydrogenase, 3 β , and steroid delta-isomerase 2
NQO1	Hs00168547_m1	NAD(P)H dehydrogenase, quinone 1
NQO2	Hs00168552_m1	NAD(P)H dehydrogenase, quinone 2
POLR2A ^a	Hs00172187_m1	Polymerase (RNA) II (DNA directed) polypeptide A
RPLP0 ^a	Hs99999902_m1	Ribosomal protein lateral stalk subunit P0
STS	Hs00165853_m1	Steroid sulfatase (microsomal), isozyme S
SULT1A1	Hs00738644_m1	Sulfotransferase family 1A, member 1
SULT1E1	Hs00193690_m1	Sulfotransferase family 1 E, estrogen-preferring, member 1
SULT2A1	Hs00234219_m1	Sulfotransferase family, cytosolic, 2A, dehydroepiandrosterone-preferring, member 1
SULT2B1	Hs00190268_m1	Sulfotransferase family, cytosolic, 2B, member 1
UGT2B7	Hs00426592_m1	UDP glucuronosyltransferase 2 family, polypeptide B7

^aReference genes.

14. The HIEEC cells were grown in RPMI-1640 Medium supplemented with 2 mM L-glutamine and 10% fetal bovine serum (FBS) (all from Sigma-Aldrich, St. Louis, MI, United States). The HIEEC cells were used as passage +7. Cells in passage +8 were authenticated by STR profiling performed by ATCC on March 8, 2018.

These cell lines were all negative for *mycoplasma* infection, according to MycoAlert *mycoplasma* detection kits (Lonza, Basel, Switzerland).

RNA Isolation

The RL95-2 and KLE cells were cultured four different times independently ($n = 4$) as two replicates. The total RNA from RL95-2 and KLE cells was isolated and purified using RNA isolation kits (Nucleospin; Macherey-Nagel GmbH & Co. KG, Düren, Germany), according to the manufacturer instructions. The RNA quality was determined using a bioanalyzer (2100; Agilent) and RNA nanokits (RNA 600; Agilent Technologies Inc, Santa Clara, CA, United States). The mean RNA integrity number was 9.00 ± 0.53 , which demonstrated that the RNA was of good quality. Samples of the total RNA (4 μ g) were reverse transcribed into cDNA (in 40 μ g) using cDNA synthesis kits (SuperScript VILO; Invitrogen, Thermo Fisher Scientific, Carlsbad, CA,

United States), according to manufacturer instructions. The cDNA samples were stored at -20°C .

Quantitative PCR

The expression of the genes that encode the enzymes involved in estradiol biosynthesis and oxidative metabolism was examined using quantitative PCR (qPCR) with exon-spanning hydrolysis probes (dye labeled, FAM), as commercially available as ‘Assay on Demand’ (Applied Biosystems, Foster City, CA, United States) (Table 1), or with primers and probes for AKR1C3 that were designed by our group previously (Rižner et al., 2006) (Table 2), using TaqMan Fast Advanced Master Mix and the universal thermocycling parameters recommended by Applied Biosystems (1 cycle of 20 s at 50°C ; 1 cycle of 20 s at 95°C ; 40 cycles of 1 s at 95°C ; 20 s at 60°C). The expression of the genes that encode transporters was examined using SYBR green I master (Roche, Basel, Switzerland) and primers that were designed in our laboratory (Table 3), using the following program: 1 cycle of 5 min at 95°C ; 40 cycles of 10 s at 95°C ; 10 s at 60°C ; and 21 s at 72°C . Quantification was accomplished using a real-time PCR system (ViiA 7; Applied Biosystems, Thermo Fisher Scientific, Waltham, MA, United States). All of the cDNA samples were run on the PCR machine in triplicates, using 0.25 μ l cDNA, and the

TABLE 2 | Sequences of the primers and probe for specific amplification of *AKR1C3*.

Gene symbol	Gene name	Primers/probe	Sequence
<i>AKR1C3</i>	Aldo-keto reductase family 1, member C3 (17 β -hydroxysteroid dehydrogenase type 5)	Forward primers (5' to 3') Reverse primers (5' to 3') Fluorescent MGB-NFQ probe (5' to 3')	GTTGCCTATAGTGCTCTGGGATCT GGACTGGGTC CTCCAAGAGG CACCCATCGTTTGCTC FAM

TABLE 3 | Sequences of the primers for SYBR green evaluation of gene expression.

Gene symbol	Gene name	Forward primers (5' to 3')	Reverse primers (5' to 3')
<i>ABCC1</i>	Multidrug-resistance-associated protein 1	GGACTCAGGAGCACACGAAA	ACGGCGATCCCTTGTGAAAT
<i>ABCC11</i>	ATP-binding cassette sub-family C member 11	TCTCCATATATCCTGTAAAT	TATAGTTCTCCAGTCTCTTG
<i>ABCC4</i>	Multidrug-resistance-associated protein 4	AACTGCAACTTTTCACGGATG	AATGACTTTTCCAGGCGTA
<i>ABCG2</i>	Broad substrate specificity ATP-binding cassette transporter ABCG2	GGGTTTGGAACTGTGGGTAG	AGATGATTCTGACGCACACC
<i>HPRT1^a</i>	Hypoxanthine-guanine phosphoribosyltransferase	CCTGGCGTCGTGATTAGTC	TGAGGAATAAACACCCCTTTCCA
<i>POLR2A^a</i>	DNA-directed RNA polymerase II subunit RPB1	CAAGTTCAACCAAGCCATTG	GTGGCAGGTTCTCCAAGG
<i>RPLP0^a</i>	60S acidic ribosomal protein P0	AATGTGGGCTCCAAGCAGAT	TTCTTGCCCATCAGCACCAC
<i>SLC10A6</i>	Solute carrier family 10 member 6	TATGACAACCTGTTCCACCG	GAATGGTCAGGCACACAAGG
<i>SLC22A11</i>	Solute carrier family 22 member 11	CTACCTTCATCCTCCCTCG	CCATTGTCCAGCATGTGTGT
<i>SLC22A6</i>	Solute carrier family 22 member 6	CACAAGGAGGAGGAAGAGGA	ATGATGTGGTCTCTGGTGGGG
<i>SLC22A7</i>	Solute carrier family 22 member 7	CCTCCAGAGTCCAAGGGTCT	ATGCTGCTCACCACCAAT
<i>SLC22A8</i>	Solute carrier family 22 member 8	TACGCTGGTTGGTCTTGCT	CTCCCTCTCTCTTCTTGCCA
<i>SLC22A9</i>	Solute carrier family 22 member 9	CGGCTACCTATCTGACCCCA	TCTTGACGACTGTGCTTCCC
<i>SLC51A</i>	Organic solute transporter subunit alpha	GCCCTTTCCAATACGCCTTC	TCTGCTGGGTCATAGATGCC
<i>SLC51B</i>	Organic solute transporter subunit beta	GTGCTGTGAGTTTCTCTCCG	TCATGTGTCTGGCTTAGGATGG
<i>SLCO1A2</i>	Solute carrier organic anion transporter family member 1A2	GTTGGCATCATTCTGTGCAATGTT	AACGAGTGTGAGTGGGAGTTATGAT
<i>SLCO1B1</i>	Solute carrier organic anion transporter family member 1B1	CAAATTCTCATGTTTTACTG	GATTATTTCCATCATAGGTC
<i>SLCO1B3</i>	Solute carrier organic anion transporter family member 1B3	TCCAGTCATTGGCTTTGCAC	TCCAACCCAACGAGAGTCTCT
<i>SLCO1C1</i>	Solute carrier organic anion transporter family member 1C1	CACACAGACTACCAACACCC	TCACCATGCCGAACAGAGAA
<i>SLCO2B1</i>	Solute carrier organic anion transporter family member 2B1	AGAGCCCTGTGTTCCATTCT	CTCTTGCTCCAGAAATGGCC
<i>SLCO3A1</i>	Solute carrier organic anion transporter family member 3A1	CTACGACAATGTGGTCTAC	TTTTGATGTAGCGTTTATAG
<i>SLCO4A1</i>	Solute carrier organic anion transporter family member 4A1	ATGCACCAGTTGAAGGACAG	AACAAGGTGGCAGCTTCTGAG
<i>SLCO4C1</i>	Solute carrier organic anion transporter family member 4C1	CCAGGAGCCCCAGAAGTC	AACTCGGACAGCGACAGTG

^aReference genes.

reactions were performed in 384-well plates (MicroAmp Optical; Applied Biosystems, Thermo Fisher Scientific, Waltham, MA, United States), in a reaction volume of 5.0 μ l. The PCR amplification efficiency was determined from the slope of the log-linear portion of the calibration curve for each gene investigated, and this was allowed for in the further calculations.

For gene expression analysis in RL95-2 and KLE cells, the normalization factor for each sample was calculated based on the geometric mean of the three most stably expressed reference genes (*POLR2A*, *HPRT1*, *RPLP0*). The gene expression for each sample was calculated from the crossing-point value (C_q) as E^{-C_q} , divided by the normalization factor, and multiplied by 10^{13} . The Minimum Information for Publication of Quantitative Real-Time PCR Experiments (MIQE) guidelines were considered in the performance and interpretation of the qPCR reactions (Bustin et al., 2009).

For comparison of RL95-2 and KLE cell lines with HIEEC, expression of *HPRT1* was used as a normalization control. Inter-plate variability in comparison of these two cell lines with HIEEC cells was minimized by the use of relative quantification method

and by considering as important only the genes with 10-fold or higher significant differences in expression.

Western Blotting

Cell lysates were prepared using RIPA Lysis buffer (EMD Millipore Corporation, Temecula, CA, United States) according to the manufacturer instructions. Total protein concentrations were determined using Bradford reagent (Carl Roth GmbH + Co. KG, Karlsruhe, Germany), bovine serum albumin (BSA) as standard, and BioTek (Winooski, VT, United States) PowerWave XS Microplate reader.

Samples of 50 μ g protein were separated using SDS PAGE in 10% Tris-glycine gels, and then transferred to poly (vinylidene fluoride) membranes (Millipore, Billerica, MA, United States). For STS detection, the membranes were blocked in 5% non-fat milk overnight and 5% bovine serum albumin in TTBS buffer for 2 h. The membranes were incubated with primary anti-STS antibodies (1:5,000; in TTBS, 5% bovine serum albumin; 2 h at 4°C), which were kindly provided by Dr. Gerhard Schuler (Faculty of Veterinary Medicine, Justus-Liebig-University, Giessen, Germany). The membranes were then incubated for

2 h at 4°C with horseradish-peroxidase-conjugated secondary goat anti-rabbit antibodies (111-035-045, 1:5,000; in TTBS with 2.5% bovine serum albumin; Jackson ImmunoResearch Laboratories Inc, West Grove, PA, United States). For GAPDH detection, the membranes were blocked in 5% non-fat milk at room temperature, and incubated for 1 h in the primary anti-GAPDH antibody (G8795; lot number: 045M4799V; 1:5,000; in TTBS with 1% non-fat milk at room temperature; Sigma-Aldrich, St. Louis, MI, United States). The membranes were then incubated for 1 h at room temperature with the horseradish-peroxidase-conjugated secondary goat anti-mouse antibodies (115-035-062; 1:5,000; in TTBS with 1% nonfat milk; Jackson ImmunoResearch Laboratories Inc, West Grove, PA, United States). SuperSignal West Pico Chemiluminescent Substrate (Thermo Fischer Scientific, Waltham, MA, United States) was used for chemiluminescent detection, with a CCD camera (LAS-4000; Fujifilm, Tokyo, Japan). Differential expression of STS was determined after normalization to GAPDH, using the ImageJ program.

Steroid Metabolism and Quantification by LC-HRMS

The RL95-2 and KLE cell lines were seeded into six-well plates (92106; TPP, Sigma-Aldrich Chemie GmbH, Deisenhofen, Germany) at 3.5×10^6 cells/well and 3.0×10^5 cells/well, respectively. The next day, when they had reached 70% confluency, the cells were washed twice with Dulbecco's phosphate-buffered saline (DPBS) and treated with different concentrations of E1, E1-S, DHEA or DHEA-S (10, 100, 500, 1,000 nM), dissolved in dimethylsulfoxide (DMSO) and medium without phenol red and FBS. The final concentration of DMSO was 0.05%. The cells were treated for 48 h, and then the medium was removed and stored at -80°C in glass tubes (6 ml tubes; 986492; Wheaton, VWR, Pennsylvania, United States) until the liquid chromatography-high-resolution mass spectrometry (LC-HRMS) analysis. For normalization purposes, the cells in individual wells were counted using an automated cell counter (TC20; Bio-Rad, CA, United States). Two independent experiments were performed.

A selective and sensitive LC-HRMS assay was used for quantification of steroid precursors and estrogen metabolites (i.e., AD, DHEA, DHEA-S, E1, E1-S, E2, E2-S, E2-glucuronide, estriol, testosterone). This system was validated according to the Q2 (R1) International Conference on Harmonisation guidelines, as described previously (Poschner et al., 2017).

The HPLC system (UltiMate 3000 RSLC-series; Thermo Fisher Scientific, Inc, Waltham, MA, United States) was run with a C18 column (Phenomenex Luna 3 μ m C18 (2) 100 Å; 250 \times 4.6 mm ID; Phenomenex, Inc, Torrance, CA, United States), and with a C18 guard column (Hypersil BDS; 5 μ m, 10 \times 4.6 mm ID; Thermo Fisher Scientific, Inc). The column temperature was maintained at 43°C, with 100 μ l sample injected. The gradient elution used aqueous ammonium acetate buffer (10 mM, pH 5.0) as solvent A, and acetonitrile as solvent B. The gradient was as follows:

0.0–19.0 min, 25.0–56.3% B; 19.0–19.5 min, 56.3–90.0% B; 19.5–24.0 min, 90.0% B; 24.5–24.5 min, 90.0–25.0% B; 24.5–30.5 min, 25% B. The flow rate was 1.0 ml/min. The HPLC was coupled to a mass spectrometer (maXis HD ESI-Qq-TOF; Bruker Corporation, Bremen, Germany). Full-scan mass spectra were recorded from 150 m/z to 500 m/z.

Steroid Metabolism and Quantification by LC-MS/MS

The RL95-2 (passage, +10 to +15) and KLE (passage, +7 to +15) cells were plated into six-well plates at a cell density of 1.0×10^6 cells/well and 1.0×10^5 cells/well, respectively. After 24 h, the cells were washed with DPBS, and serum-free and phenol-red-free culture medium was added. The cells were then incubated with 2.3, 8.5, and 85 nM E1-S (in ethanol; final ethanol concentration, 0.25%). The effects of the STS inhibitor STX64 on E1-S metabolism was evaluated as follows: 30 min before addition of 2.3 nM E1-S, the cells were incubated with 10 nM STX64 (in anhydrous DMSO; final DMSO concentration, 0.25%). After 8, 24, 48, and 72 h of incubation, the cell culture medium was collected in microcentrifuge tubes (Eppendorf, Germany), and stored at -80°C until further processing. Three independent experiments were carried out, each performed in duplicate.

A deuterated internal standard of E2-d₂ was added to the cell culture medium samples following their thawing at room temperature. The lipophilic fraction containing the analytes of interest was extracted using solid-phase extraction (Strata-X polymer-based columns; Phenomenex, CA, United States). This method involved: column conditioning (1 ml methanol), column equilibration (1 ml water), sample loading, column drying (high vacuum, 10 min), and sample elution (1.5 ml methanol). The solvent was then evaporated off using a vacuum concentrator (Savant SPD 31 DDA-230; Thermo Fisher Scientific, Waltham, MA, United States), and reconstituted in a 100 μ l 70% methanol/0.2 mM NH₄F in water. The samples were stored at -20°C until LC-tandem mass spectrometry (MS/MS) analysis.

An LC-MS/MS system used for detection and quantification of E1, E1-S, E2, and E2-S comprised of a Shimadzu Nexera XR system (Shimadzu Corporation, Kyoto Japan) coupled to a triple quadrupole system (Triple Quad 3 500; AB Sciex Deutschland GmbH, Darmstadt, Germany), operating with the Analyst 1.6 software (AB Sciex Deutschland GmbH, Darmstadt, Germany). Chromatographic separation of the estrogens was performed using a C18 column (Kinetex 2.6 μ m XB; 100 \times 4.6 mm; Phenomenex, Aschaffenburg, Germany) equipped with a guard column and cartridges (Securityguard C18; 4 \times 3.0 mm; Phenomenex, Aschaffenburg, Germany). The mobile phases were 0.2 mM NH₄F, 5% methanol in water (A) and 0.2 mM NH₄F in methanol (B). Samples of 25 μ l were injected *via* an autosampler (SIL-20 AC XR; Shimadzu Corporation, Kyoto, Japan). The mobile phase flow rate was 0.5 ml/min, and the gradient elution was as follows: 0.0–3.0 min, 70% A; 3.0–8.0 min, 70–4% A; 8.0–8.01 min, 4–70% A; 8.01–15.0 min, 70% A. The column temperature was maintained at 38°C. The MS/MS

analysis was performed in negative ion mode with constant electrospray ionization conditions. The source-dependent parameters were as follows: curtain gas, 50; collision gas, 8; ion spray voltage, $-4,500$ V; source temperature, 600°C ; ion source gas 1, 40; ion source gas 2, 80. All transitions were recorded using the scheduled multiple reaction monitoring (MRM) algorithm. The target scan time was set to 1 s, with an MRM detection window of 120 s. The resolution for the first and third quadrupole (Q1, Q3) was set as UNIT, with the pause between the mass ranges set at 5 ms.

The concentration of each steroid was calculated using the internal standard approach. The standard calibration curves were constructed from 12 calibration concentrations prepared in 70% methanol/ 0.2 mM NH_4F , to cover the range from 0.01 to 100 ng/ml. An internal standard of E2- d_2 was added to each sample at a final concentration of 1 ng/ml. The retention times and monitoring transitions for the analytes are given in **Supplementary Table S1**. The limits of detection and quantification were calculated as $3\times$ and $10\times$ the signal/noise ratio. The limit of detection for E1, E1-S, E2, and E2-S was 1 pg/ml. The limit of quantification for E1 and E1-S was 5 pg/ml, and for E2 and E2-S, 10 pg/ml.

E1-S Uptake

For analysis of E1-S transport, RL95-2 and KLE cells were seeded into six-well plates at 1.0×10^6 cells/well and 1.2×10^5 cells/well, respectively, in triplicates. Here, RL95-2 cells were between passages +12 and +14, and KLE cells between passages +28 and +32. When the cells reached 60% confluency, full growth medium was replaced with medium without FBS, for 24 h. The cells were then washed twice with warm DPBS (S5652; Sigma-Aldrich, St. Louis, MO, United States) and incubated for 30 min at 37°C in 1.9 ml/well transport buffer (125 mM NaCl, 4.8 mM KCl, 1.2 mM CaCl_2 , 1.2 mM KH_2PO_4 , 12 mM MgSO_4 , 25 mM MES, 5.6 mM glucose, pH 5.5) with or without 10 μM inhibitor cyclosporine A (CsA, SML1018, Sigma-Aldrich, St. Louis, MI, United States) or 10 μM bromosulphophthalein (BSP, HY-D0217, MedChemExpress, Monmouth Junction, NJ, United States). After 30 min, steroid transport was initiated by addition of 100 μl transport buffer containing [^3H]E1-S (NET203250UC; Perkin Elmer Inc, MA, United States) to a final concentration of 16 nM, and the cells were incubated for 2, 5, 15, and 30 min at 37°C . The medium was collected and the uptake was stopped with 2 ml ice-cold DPBS. After five washes with DPBS, the cells were lysed by addition of 300 μl /well 1% Triton X-100, mixed for 30 min at 200 rpm at 4°C , and then frozen at -80°C . After thawing, the lysed cell samples were collected and centrifuged at $11,000 \times g$ for 15 min at 4°C . Finally, 250 μl of the cell lysates was mixed with 1.5 ml scintillation fluid (Quickszint Flow 302; Zinnsser Analytic, Frankfurt, Germany) and the radioactivity was determined in a scintillation counter (MicroBeta TriLux 1450; PerkinElmer, CT, United States). The [^3H]E1-S concentrations in the individual samples were then back-calculated from the disintegrations per minute (dpm) and the specific isotope activity (49.19 Ci/mmol) with the conversion of 1 Ci = 2.22×10^{12} dpm. The data were normalized to total protein concentrations, as determined using the protein assay kits (BCA protein assay;

Pierce, Thermo Scientific), according to manufacturer instructions. The E1-S transport was studied as two to three independent experiments.

Statistical Analysis

For evaluation of gene expression, RL95-2 and KLE cells were cultured independently on four different occasions; three times in duplicate, and once singly. The expression of the genes of interest and the reference genes was determined in each of these seven samples of three technical triplicates. The means for each independent experiment ($n = 4$) were considered in the statistical analysis. Western blotting was performed on protein samples from three biological replicates of each cell line. Cells for LC-HRMS and LC-MS/MS analyses were cultured in two and three independent experiments, respectively ($n = 2$ and 3), each in duplicate. E1-S uptake was performed independently two to three times, each time as triplicates.

Statistical evaluation was carried out using the GraphPad Prism software for Windows, version 8.0 (San Diego, CA, United States), with Mann-Whitney tests, Kruskal-Wallis tests followed by Dunn's multiple comparisons tests or ANOVA followed by Tukey's tests. Differences with $p < 0.05$ are considered as statistically significant. Unless stated otherwise, all of the data are shown as means \pm standard deviation (SD).

RESULTS

Here, we evaluated the expression of 51 genes that encode uptake and efflux transporters of sulfated steroid precursors, estrogen biosynthetic enzymes, estrogen receptors, and phase I and II estrogen metabolic enzymes, using model cell lines of moderately and poorly differentiated EC, as RL95-2 and KLE cells, respectively. The expression of these genes was compared on the basis of the changes from the moderately differentiated to poorly differentiated EC cells, as poorly differentiated EC cells KLE *vs* the moderately differentiated EC cells RL95-2. Furthermore, each of the RL95-2 and KLE cell lines were compared directly with HIEEC cells, which provided a model cell line of normal proliferative endometrium. For these comparison purposes, the raw gene expression data for HIEEC cells were obtained from our previously published studies (Hevir-Kene and Rižner, 2015; Pavlič et al., 2021). The data for all three cell lines were here normalized to the same house-keeping gene, *HPRT1*.

Differential Expression of E1-S Uptake Transporters in the RL95-2 and KLE Moderately and Poorly Differentiated Endometrial Cancer Cell Lines

After menopause, the ovaries cease to produce estrogens, and local E2 formation relies on the actions of transporters for the uptake of the inactive steroid precursors DHEA-S and E1-S into cells. We evaluated here the expression of 20 genes that encode

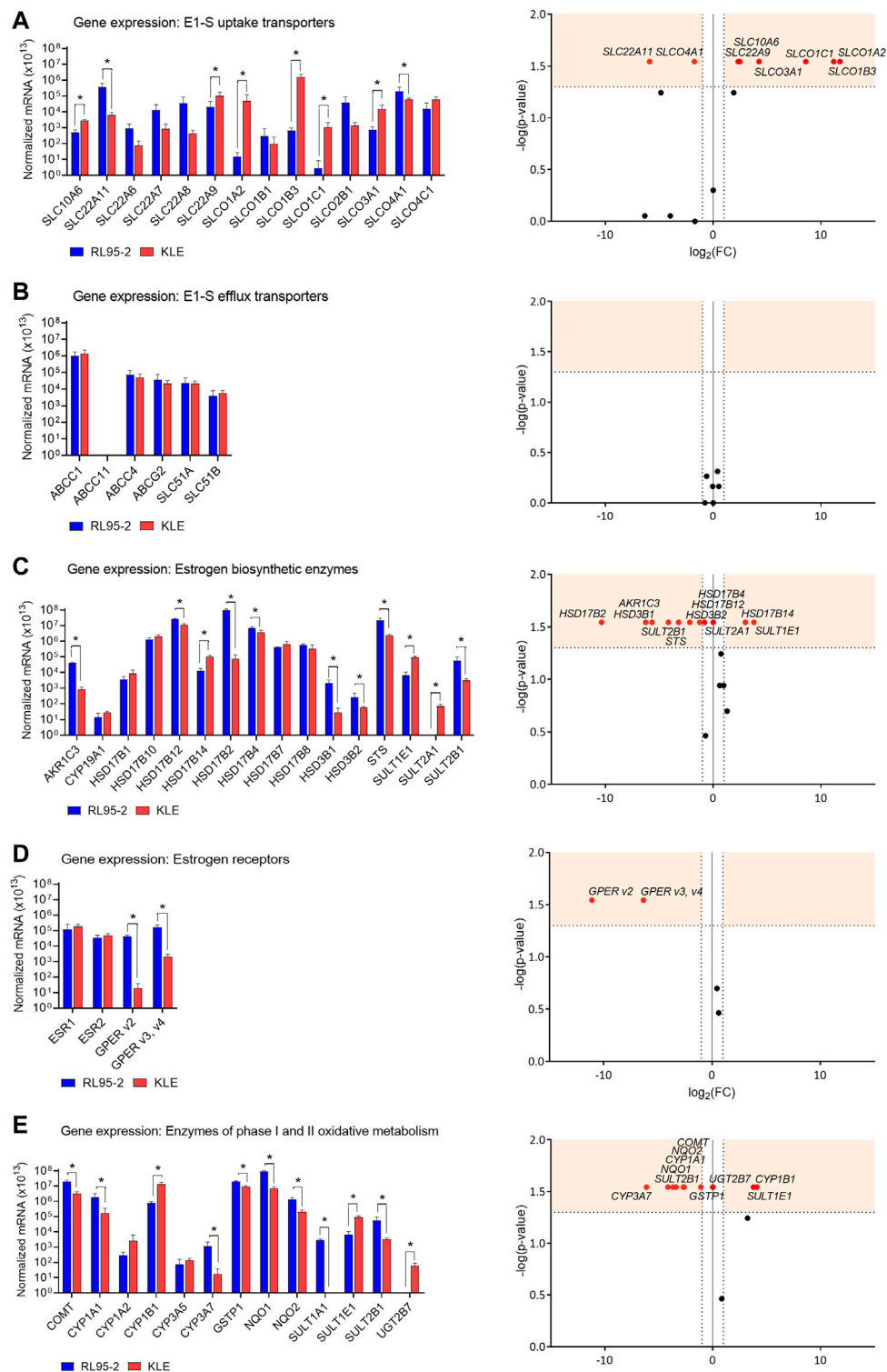
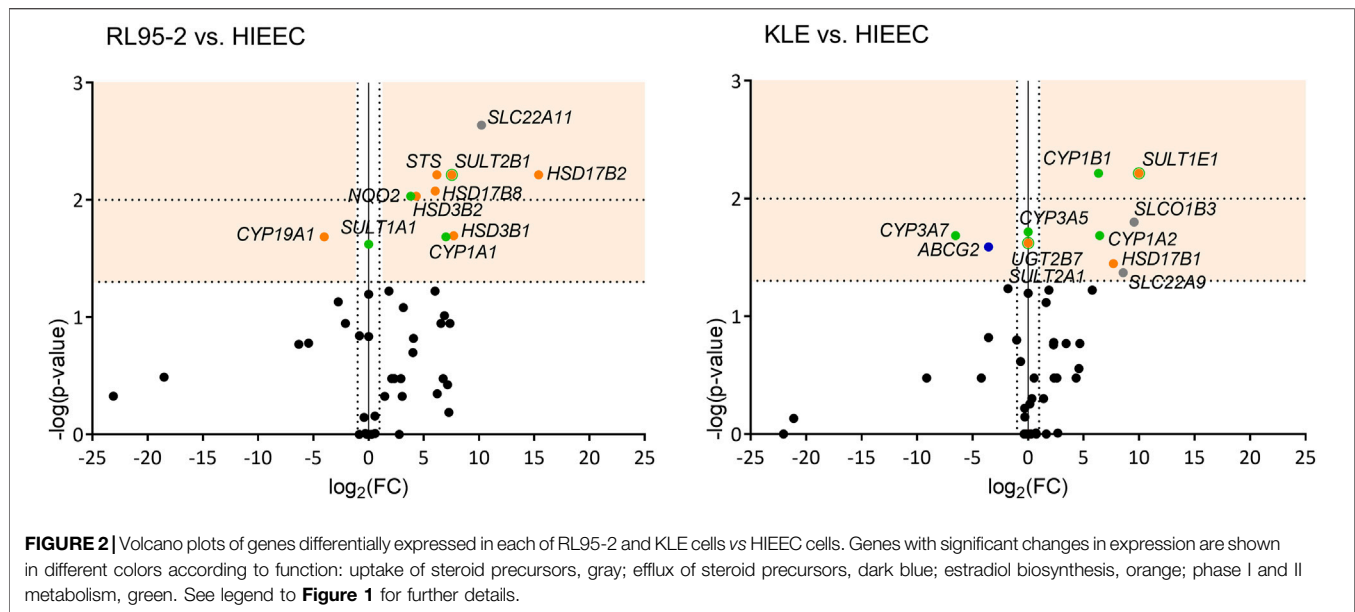


FIGURE 1 | Expression of genes that encode E1-S uptake (A) and efflux (B) transporters, estrogen biosynthetic enzymes (C), estrogen receptors (D) and enzymes of phase I and II oxidative metabolism (E). Left: Expression levels in RL95-2 and KLE cells, as normalized to the three reference genes, *POLR2A*, *HPRT1*, and *RPLP0* ($n = 4$). *, $p < 0.05$ (Mann-Whitney tests). Right: Volcano plots for relative expression of the genes (KLE vs RL95-2 cells). FC, fold change; horizontal dashed line, cut-off for experimental significance (shaded; $-\log(1.3)$; $p < 0.05$); vertical dashed lines, cut-off for genes similarly expressed in both cell lines (FC, ± 2.0); vertical line ($x = 0$), genes not expressed in either cell line; red symbols, differentially expressed genes; black symbols, non-differentially expressed genes.



15 E1-S uptake and four E1-S efflux transporters (**Figure 1**, **Supplementary Table S2**). The great majority of the genes that encoded these E1-S uptake and efflux transporters were expressed in both the RL95-2 and KLE cells.

For the relative expression of the poorly differentiated (KLE) EC cells compared to the moderately differentiated (RL95-2) EC cells (i.e., KLE vs RL95-2 relative expression), differences were seen for several of the E1-S uptake transporters (**Figure 1A**). These showed higher expression for six E1-S uptake transporters (KLE vs RL95-2): *SLCO1A2* (3433.6-fold), *SLCO1B3* (2301.5-fold), *SLCO1C1* (381.2-fold), *SLCO3A1* (19.0-fold), *SLC10A6* (5.5-fold), and *SLC22A9* (5.0-fold). Two E1-S uptake transporters showed lower expression instead (KLE vs RL95-2): *SLC22A11* (59.3-fold) and *SLC4A1* (3.4-fold) (**Supplementary Table S2**). No differences were seen for the E1-S efflux transporters (**Figure 1B**).

Comparisons of these RL95-2 and KLE cells with the model of normal endometrium, HIEEC cells, showed several differences in the expression of the E1-S uptake transporters (**Figure 2**, **Supplementary Table S3**). For RL95-2 vs HIEEC cells, the relative expression was higher for *SLC22A11* (1199.8-fold). Then for KLE vs HIEEC, this was higher for *SLCO1B3* (754.9-fold) and *SLC22A9* (380.3-fold). For the efflux transporters, for KLE vs HIEEC cells, the relative expression was lower for *ABCG2* efflux transporter (11.9-fold).

This gene expression analysis thus initially indicated that both of these EC cell lines can carry out E1-S uptake. The increased relative expression of six of these E1-S uptake transporters in the poorly differentiated KLE EC cells vs the moderately differentiated RL95-2 EC cells, and the higher expression of two of these genes for KLE cells vs HIEEC cells (over RL95-2 cells vs HIEEC cells) imply that more sulfated steroid precursors can enter KLE cells.

Higher Expression of STS and Negligible Expression of *CYP19A1* in RL95-2 and KLE Endometrial Cancer Cell Lines Support the Importance of the Sulfatase Pathway for E2 Formation

After the steroid precursors enter the cells, these can be further transformed through multiple steps into the most potent estrogen, E2. This can occur *via* the sulfatase and aromatase pathways, where E2 can be formed from E1-S and from DHEA-S (*via* androstenedione), respectively. The expression of 16 genes of these pathways was examined here for the RL95-2 and KLE model cell lines.

Both RL95-2 and KLE cells showed 10⁵-fold–10⁶-fold higher expression of *STS* compared to *CYP19A1* (**Figure 1C**). This suggests that these cell lines form estrogens only through the sulfatase pathway. Additionally, these data indicated that RL95-2 and KLE cells differ in their E2 formation. KLE vs RL95-2 relative expression was lower for the sulfatase pathway *STS* (9.3-fold), as also for the aromatase pathway *HSD3B1* (76.2-fold), *HSD3B2* (4.5-fold), and *AKR1C3* (50.7-fold). For *AKR1C3* lower protein levels were seen in KLE cells as compared to RL95-2 (**Supplementary Figures S1A, S2**).

The genes that encode the HSD17B enzymes were also differentially expressed. The greatest difference for KLE vs RL95-2 cells was lower relative expression for *HSD17B2* (1303.7-fold), the enzyme product of which has the highest catalytic efficiency for inactivation of E2 to E1. Similarly, this was lower for another oxidative HSD17B, *HSD17B4* (1.8-fold). On the other hand, this was higher for *HSD17B14* (7.9-fold), which also catalyzes oxidation of E2 to E1, but with lower catalytic efficiency. Additionally, KLE vs RL95-2 relative expression was lower for *HSD17B12* (2.4-fold), which encodes an enzyme for reduction of E1 to E2. The gene that encodes the major reductive

HSD17B1 enzyme was not differentially expressed. For KLE cells, these alterations in gene expression of the reductive and oxidative HSD17B enzymes would shift the balance between E1 and E2 towards E2 formation.

Differences in KLE vs RL95-2 relative expression of genes for the sulfotransferase enzymes were also seen. The relative expression here was lower for the gene that encodes DHEA sulfotransferases, *SULT2B1* (17.7-fold), while expression of *SULT2A1* was only detected in KLE cells. Higher relative expression was instead seen for the gene encoding E1 and E2 sulfotransferase, *SULT1E1* (13.6-fold). This differential expression of these genes suggests that KLE cells followed more sulfation of DHEA (higher relative expression of *SULT2A1*), E1 and E2 (higher relative expression of *SULT1E1*) compared to RL95-2 cells.

Comparing RL95-2 cells to HIEEC cells, relative expression was lower for *CYP19A1* (16.1-fold), and higher for *STS* (73.1-fold) (**Figure 2, Supplementary Table S3**). This suggests that for RL95-2 cells, E1 and E2 can be formed *via* the sulfatase pathway. Several other genes involved in the aromatase and the sulfatase pathways also showed higher relative expression here: *HSD17B2* (43,060.2-fold), *HSD3B1* (209.0-fold), and *SULT2B1* (185.8-fold). Other genes with higher relative expression in RL95-2 cells vs HIEEC cells were *HSD17B8* (65.4-fold) and *HSD3B2* (19.9-fold). This higher expression of *HSD3B1* and *HSD3B2* suggests that in RL95-2 cells, DHEA can be metabolized to androstenedione, although DHEA can also be sulfated due to higher expression of *SULT2B1*. Higher expression of several genes for oxidative HSD17B enzymes suggest that for RL95-2 cells compared to HIEEC cells, the balance between E1 and E2 will be shifted towards E1.

For KLE vs HIEEC cells, relative expression was higher for *HSD17B1* (204.6-fold), which encodes reductive HSD17B, *SULT1E1* (1020.7-fold), and *SULT2A1*, which was expressed in KLE cells but not in HIEEC cells. These data indicate that for KLE cells, more E2 can be formed, but conjugation to E2-S would prevail.

RL95-2 and KLE Cell Line Models of Moderately and Poorly Differentiated Endometrial Cancer Express *ESR1* and *ESR2*, but Differ in *GPER* Expression

The actions of estrogens are mediated through their binding to and activation of nuclear estrogen receptors and membrane-bound receptors. Here, expression was evaluated for *ESR1* and *ESR2*, which encode nuclear receptors ER α and ER β , respectively, and the three *GPER* transcript variants, as $v2$ and $v3$ plus $v4$ (Hevir-Kene and Rižner, 2015) (**Figure 1D**).

Both *ESR1* and *ESR2* were expressed in RL95-2 and KLE cells, with no difference between these. For KLE vs RL95-2 relative expression, this was lower for *GPER v2* (2189.7-fold) and *GPER v3* plus $v4$ (80.9-fold). When RL95-2 and KLE cells were compared to the control cell line, HIEEC cells, there were no significant differences in gene expression of estrogen receptors *ESR1*, *ESR2* and *GPER* (**Figure 2, Supplementary Table S3**). The expression of *ESR1* surmounted expression of

ESR2 in all three cell lines RL95-2, KLE and HIEEC for 3-fold, 3-fold and 67-fold, respectively (**Supplementary Table S4**).

These data suggest that in moderately differentiated EC (RL95-2 cells), estrogens might act *via* nuclear and membrane bound receptors, while in poorly differentiated EC (KLE cells), estrogens might preferentially activate the nuclear receptors.

Decreased Expression of Genes Encoding Phase II Enzymes in the KLE Cell Line, as a Model of Poorly Differentiated Endometrial Cancer

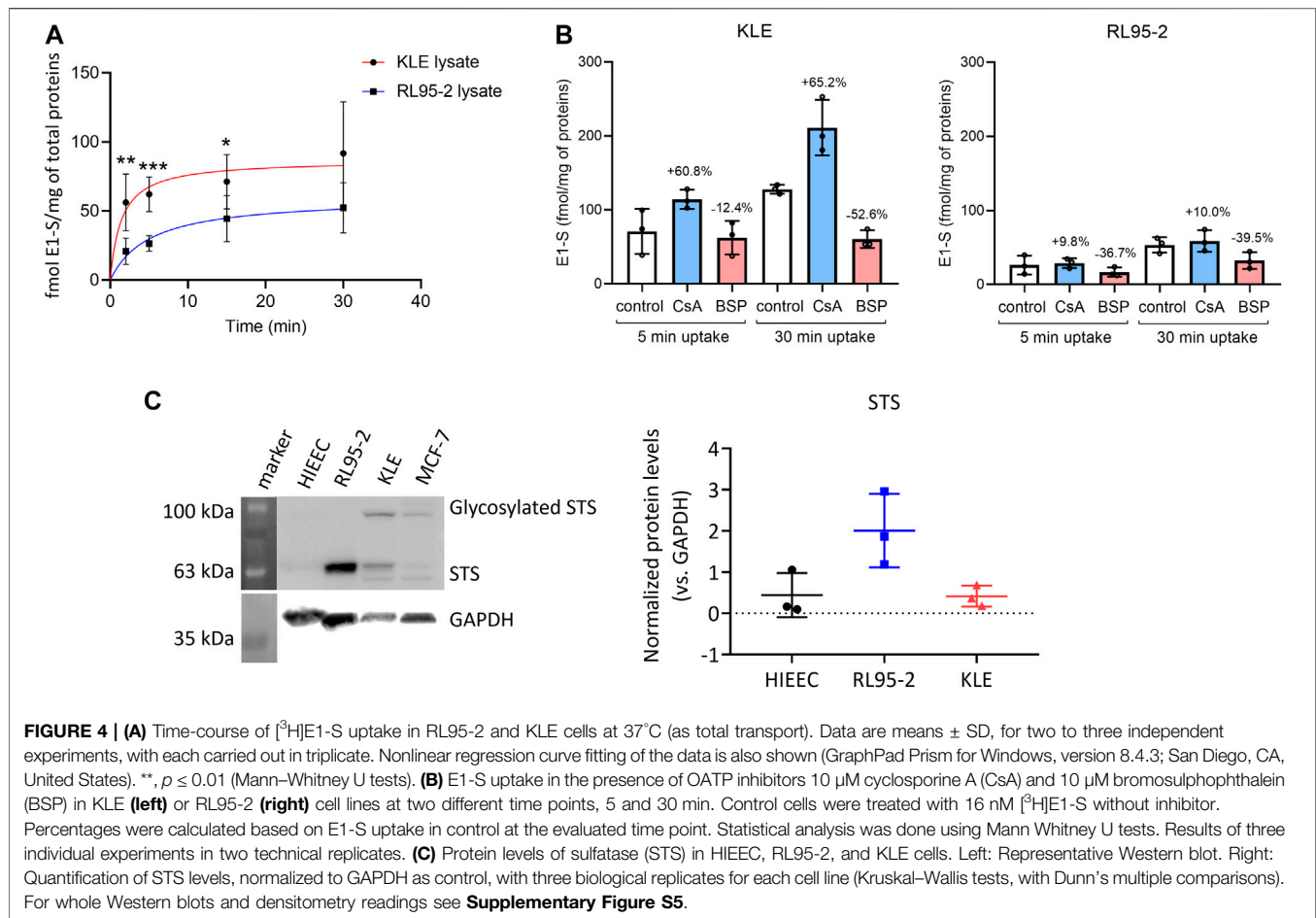
For phase I metabolism inside cells estrogens can be metabolized to 2-, 4- or 16 α -hydroxy-estrogens by the actions of different CYP enzymes. Catechol estrogens (2- or 4-OH-E1/E2) can be oxidized to semiquinones or quinones, which are associated with DNA damage. To avoid cell damage, these catechols and quinones are further conjugated and detoxified in phase II metabolism, by the COMT, SULT, UGT, GSTP1, NQO1, and NQO2 enzymes (Rižner, 2013; Hevir-Kene and Rižner, 2015). The expression of 13 genes that encode phase I and II metabolic enzymes was evaluated in these model cell lines (**Figure 1E**).

The relative expression of genes involved in phase I metabolism for KLE vs RL95-2 cells was higher for *CYP1B1* (17.1-fold), which encodes a 4-hydroxylase, but lower for *CYP1A1* (10.6-fold) and *CYP3A7* (70.1-fold), which encode a 2-hydroxylase and a 16 α -hydroxylase, respectively.

For expression of the eight genes of phase II metabolism that were evaluated, KLE vs RL95-2 relative expression was higher for *SULT1E1* (13.6-fold), while expression of *UGT2B7* was only detected in KLE cells. All of the other genes that encode detoxification-associated enzymes showed lower relative expression for KLE vs RL95-2 cells, as *SULT2B1* (17.7-fold), *NQO1* (12.7-fold), *NQO2* (6.6-fold), *COMT* (6.3-fold), and *GSTP1* (2.2-fold), with *SULT1A1* not expressed in KLE cells. This was confirmed at the protein level for soluble COMT in KLE as compared to RL95-2 cells (**Supplementary Figures S1B, S3**). These changes imply that more 4-hydroxy-estrogens can be formed in KLE cells, along with more genotoxic 3,4-quinones, as a result of lower expression of genes that encode phase II metabolic enzymes.

Comparisons of RL95-2 and KLE cells with HIEEC cells for expression of genes encoding phase I metabolic enzymes revealed some significant differences (**Figure 2, Supplementary Table S3**). RL95-2 vs HIEEC relative expression was higher for *CYP1A1* (127.6-fold), while for KLE vs HIEEC cells, this was higher for *CYP1A2* (87.2-fold), *CYP1B1* (81.1-fold) and *CYP3A5* which was expressed in KLE but not in HIEEC cells. On the other hand, KLE cells showed lower relative expression for *CYP3A7* (93.2-fold). These data suggest that more 2-hydroxyestrogens can be formed in RL95-2 vs HIEEC cells, and more 4-hydroxyestrogens in KLE vs HIEEC cells.

Genes of phase II metabolism were also differentially expressed between each of these EC cell lines and HIEEC cells (**Figure 2,**



inhibition of E1-S uptake by bromosulphophthalein, a known inhibitor of OATP1B1, OATP1B3, OATP1A2, OATP2B1 (König et al., 2006). Increased E1-S uptake in KLE cells in the presence of cyclosporine A, which also inhibits E1-S efflux transporters (Dantzie et al., 2018), imply that these efflux ABC transporters importantly regulate E1-S uptake in KLE cells. Furthermore, for KLE cells, the active estrogens formed from E1-S *via* the sulfatase pathway would be expected to act *via* nuclear receptors ER α and ER β (i.e., lower relative expression of GPER, compared with RL95-2 cells).

Additionally, again for KLE vs RL95-2 cells expression data suggest that the KLE cells may show lower levels of 2-hydroxyestrogens and 16 α -hydroxyestrogens (i.e., lower relative expression of *CYP1A1*, *CYP3A7*), but more 4-hydroxycatechols (i.e., higher relative expression of *CYP1B1*), which can be oxidized to carcinogenic 3,4-quinones. In KLE cells, lower detoxification levels of catechols (i.e., lower relative expression of *COMT* and lower S-COMT protein levels, **Supplementary Figure S1**) and quinones (i.e., lower relative expression of *NQO1*, *NQO2*, *GSTP1*) would also indicate higher levels of DNA adducts, compared to RL95-2 cells.

A similar summarized comparison between RL95-2 and HIEEC cells (**Figure 2**, **Supplementary Figure S6**) suggests

enhanced hydrolysis of E1-S to E1 (i.e., increased levels of STS), hindered reduction of E1-S to E2 (i.e., higher expression of *HSD17B2*) and hydroxylation of E1 at the C2 position to form 2-hydroxyestrogens (i.e., higher expression of *CYP1A1*).

For the comparison between KLE and HIEEC cells (**Figure 2**, **Supplementary Figure S7**), this would support increased E1-S uptake (i.e., high relative expression of *SLCO1B3*, *SLC22A9*), but also enhanced activation of E1 to E2 and conjugation to E2-S, or formation of 2-hydroxy or 4-hydroxy-estrogens (i.e., higher relative expression of *HSD17B1*, *SULT1E1*, *CYP1A2*, *CYP1B1*).

In RL95-2 and KLE Cells as Model Cell Lines of Moderately and Poorly Differentiated Endometrial Cancer, Estrogens Are Not Formed From DHEA-S and DHEA

To evaluate the formation of active estrogens in the RL95-2 and KLE cells, the metabolism of 10 nM, 100 nM, 500 nM, and 1000 nM DHEA-S, DHEA, E1-S, and E1 was studied following their addition to the cells, with their products separated and quantified by LC-HRMS (**Figure 5**).

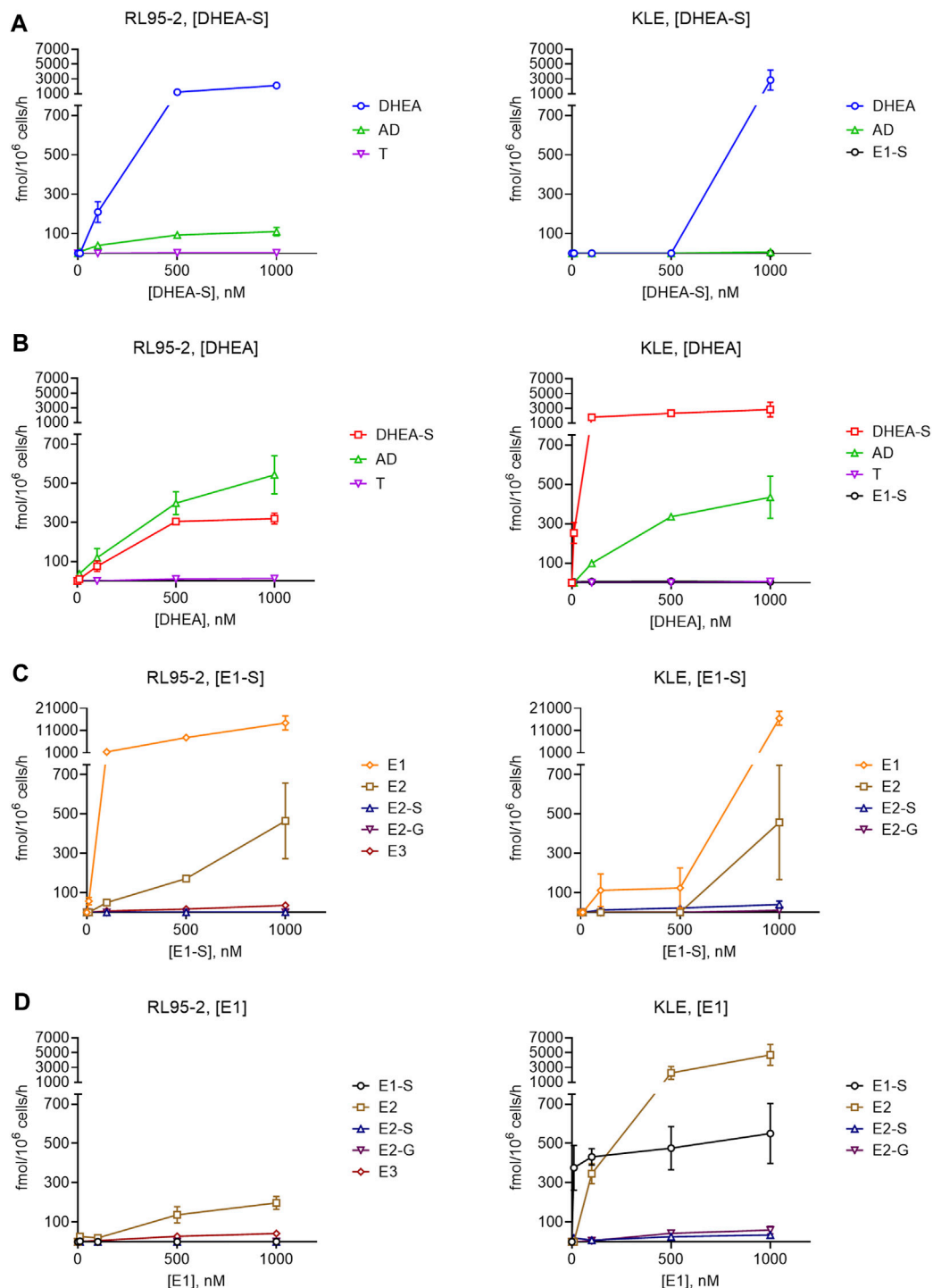


FIGURE 5 | Metabolism of DHEA-S (A), DHEA (B), E1-S (C) and E1 (D) in RL95-2 (left) and KLE (right) cells. Metabolites were separated and quantified by LC-HRMS. AD, androstenedione; E2-G, E2-glucuronide; E3, estriol; T, testosterone; for other abbreviations see main text.

These data showed more efficient DHEA-S metabolism in RL95-2 cells compared to KLE cells. In RL95-2 cells, DHEA-S was metabolized to DHEA and lower levels of androstenedione. In KLE cells, DHEA-S was only metabolized to DHEA at the highest, non-physiological,

DHEA-S concentration (i.e., 1,000 nM), which is in line with the lower levels of STS seen previously for KLE cells (Figure 4).

In contrast, metabolism of DHEA was more efficient in KLE cells, where DHEA was the major product, followed by

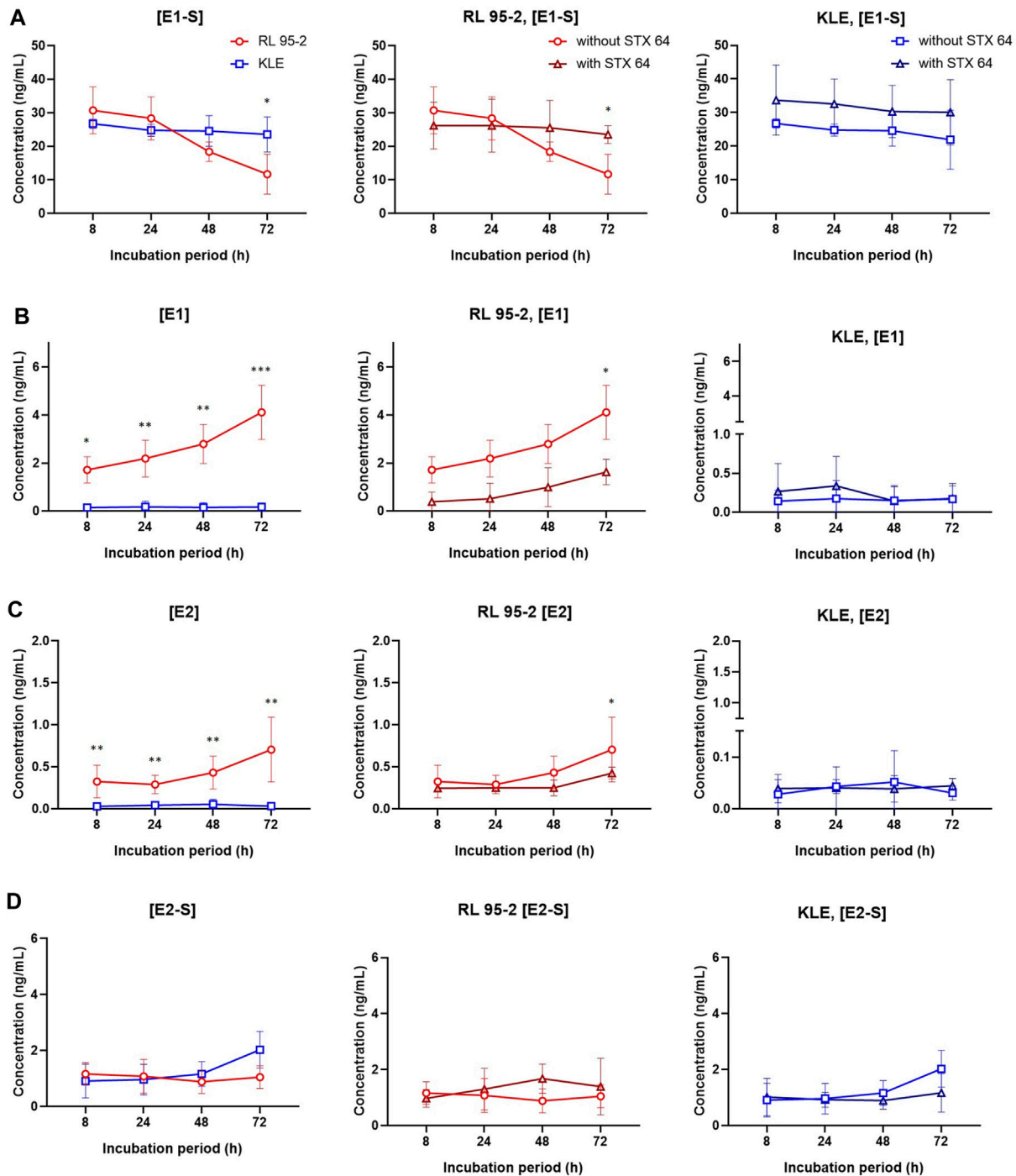


FIGURE 6 | E1-S metabolism in RL95-2 and KLE cells. Time courses for the estrogen metabolites following addition of 2.3 nM E1-S to the cells, for E1-S (**A**), E1 (**B**), E2 (**C**), and E2-S (**D**), in the presence and absence of 10 nM STX64 (sulfatase inhibitor). Data are means \pm SD. *, $p < 0.05$; **, $p < 0.01$; ***, $p < 0.001$ (ANOVA plus Tukey's tests).

androstenedione. Here, DHEA-S production can be explained by expression of *SULT2A1*. In RL95-2 cells, DHEA was instead mainly metabolized to androstenedione, with very low levels of testosterone. Here, in RL95-2 cells, the lower DHEA-S production is supported by

the higher relative expression of *HSD3B1*, *HSD3B2*, and *AKR1C3*. These data confirm that DHEA-S and DHEA cannot serve as precursors for estrogen biosynthesis in these cells, as no estrogens were formed here from these steroid precursors.

In RL95-2 and KLE Cells as Model Cell Lines of Moderately and Poorly Differentiated Endometrial Cancer, E1-S Is Metabolized to Active Estrogens

Incubations with E1-S revealed that both EC cell lines can take up and metabolize the E1-S steroid precursor, to form active E2. For KLE vs RL95-2 cells, lower levels of E1 and E2 were seen, with E2 formed only at the supraphysiological 1000 nM E1-S. This can be explained by higher relative expression of STS in RL95-2 cells. In contrast, incubation of EC cell lines with E1 showed that in KLE cells, there is greater metabolism of E1 to E2 and E1-S, which would be due to lower expression of *HSD17B2* and higher expression of *SULT1E1*, compared to RL95-2 cells. In RL95-2 cells, formation of very low levels of estriol was seen after addition of E1-S and E1, which is in line with higher relative expression of *CYP3A7*, and for KLE cells, E2-glucuronides were detected as a result of *UGT2B7* activity (Figure 1).

To better simulate the physiological conditions, the metabolism of E1-S in these EC cell lines was also studied at lower E1-S concentrations: 2.3, 8.5, and 85 nM (Figure 6, Supplementary Figure S8). After 72 h for KLE vs RL95-2 cells, metabolism of 2.3 nM E1-S resulted in lower levels of E1, E2 and E2-S; for KLE cells here, E1 and E2 were formed, but E2-S was the major product. The profiles of the metabolites remained the same at the higher, 8.5 and 85 nM E1-S concentrations (Supplementary Figure S8).

When comparing the EC cell lines to HIEEC cells, more E1 and E2 were formed from E1-S for RL95-2 cells, which is in line with higher levels of STS, and more E2-S was formed for KLE cells, which can be explained by higher relative expression of *HSD17B1* and *SULT1E1* (Figure 2, Supplementary Figures S6, S7). The importance of the sulfatase pathway for formation of E2 from E1-S was additionally confirmed using a specific and potent STS inhibitor, STX64; this shows an IC_{50} of 8 nM at 20 μ M E1-S (Malini et al., 2000), and was used at 10 nM STX64. In RL95-2 cells, this addition of STX64 in combination with 2.3 nM E1-S resulted in an almost complete block of the sulfatase pathway, with significantly lower levels of E1 and E2 formed (Figure 6). In KLE cells, where less E1 was formed from E1-S, addition of STX64 affected the levels of E1 and E2, although a significant difference was only seen for E1-S (Figure 6).

DISCUSSION

The current understanding of estrogen formation and actions in moderately and poorly differentiated EC is very limited (Berstein et al., 2003). We aimed to contribute to the clarification of estrogen formation from steroid precursors DHEA-S, DHEA, E1, and E1-S in the RL95-2 and KLE cell lines, as models of moderately differentiated and poorly differentiated metastatic (Van Nyen et al., 2018) EC, respectively. We focused on two well-characterized cell lines that are commonly used, uncontaminated, with known STR profile and histopathological characteristics. Although with these two model cell lines we did not cover inter-individual variability

among patients, the results of our study may help to determine whether blockade of estrogen actions at the pre-receptor or receptor levels can be considered as new options for treatments of individual patients with these histological types of EC.

Transport of steroid sulfates *via* organic anion transporters (*SLC*), organic anion transporter polypeptides (*SLCO*), ABC transporters, and OSTa β (dimer *SLC15A*, *SLC51B*) is an important process after menopause, which is when production of lipid-soluble estrogens diminishes, and the water-soluble sulfated precursors, DHEA-S and E1-S, are still present at relatively high levels in the plasma (Rižner et al., 2017). In the present study, we evaluated the expression of 19 transporters encoded by 20 genes.

Comparisons between these EC cell lines suggested increased uptake of E1-S and DHEA-S in the poorly differentiated KLE EC cells, as six uptake transporters (i.e., *SLCO1A2*, *SLCO1B3*, *SLCO1C1*, *SLCO3A1*, *SLC10A6*, *SLC22A9*) showed higher relative expression in KLE cells vs the moderately differentiated RL95-2 EC cell line, and as the expression of the efflux transporters was not different. These expression data were also supported by E1-S uptake inhibition by bromosulphophthalein and by the E1-S uptake studies that show increased influx in KLE cells compared to RL95-2 cells. Comparisons of gene expression in these EC cell lines with that of the control HIEEC cell line indicated their increased uptake of steroid precursors. This was due to higher expression of *SLC22A11* in RL95-2 cells and *SLCO1B3* and *SLC22A9* in KLE cells, vs HIEEC cells. This would be combined with decreased efflux of the steroid precursors in the EC cells, as the gene for efflux transporter *ABCG2* showed lower expression in KLE cells, and the gene for *ABCC11* was not expressed in RL95-2 and KLE cells. All in all, these gene expression and functional studies confirm E1-S uptake in these moderately and poorly differentiated EC cells, with higher uptake seen in the poorly differentiated KLE EC cells.

These differences in expression of the transporters might also be associated with menopausal status of the patients who donated tissues for the original establishment of these HIEEC, RL95-2, and KLE cell lines. The HIEEC cell line was derived from the proliferative endometrium of a 37-year-old woman (Chapdelaine et al., 2006), and the RL95-2 and KLE cell lines were established from tissues of postmenopausal patients. However, to the best of our knowledge, there are no suitable control endometrial cell lines that would originate from postmenopausal women. We recently investigated the HEC-1A cell line, a model of postmenopausal well-differentiated EC cells. Compared with HIEEC cells, HEC-1A cells showed higher expression of *SLCO1B3*, followed by *SLCO1B1* and *SLCO2B1*, where silencing of *SLCO1B3* decreased E1-S uptake. Comparison of Ishikawa cells, which are a model for premenopausal EC, vs HIEEC cells as the control again, showed higher expression for *SLCO1C1* and *SLCO1A2*, but lower expression of *SLCO3A1*. *ABCG2*, which encodes an efflux transporter, showed lower expression in both HEC-1A and Ishikawa cells, compared to HIEEC cells (Pavlič et al., 2021). These data support the role of these *SLCO* and *ABC* transporters in EC.

We and others have previously reported on the importance of the sulfatase pathway for E2 formation in EC tissue samples and model cell lines (Hevir-Kene and Rižner, 2015; Sinreih et al., 2017; Cornel et al., 2018). The crucial role of sulfatase was also confirmed in mouse endometrial cancer xenograft model where STS inhibitor STX64 significantly inhibited tumour growth (Foster et al., 2008). STS inhibitor STX64, also known as irosustat, has also been investigated in a phase II clinical study (NCT00910091) in patients with advanced/metastatic or recurrent endometrial cancer. In this study irosustat showed lower clinical benefit compared to progestin megestrol acetate. However, expression of STS has not been determined in these patients, which can explain the observed weak response to irosustat. Similarly as shown here for KLE, patients with metastatic cancer probably had low levels of STS in cancer tissue, and varied STS levels in other tissues.

Here we confirmed the crucial role of the sulfatase pathway once again, with 10^5 -fold– 10^6 -fold higher expression of *STS* compared to *CYP19A1* in both RL95-2 and KLE cells. Gene expression analysis indicated that E2 can be formed from E1-S in both of these EC cell lines. In KLE vs RL95-2 cells, lower levels of E1 would be expected due to lower relative expression of *STS*, but higher activation to E2 would be expected due to lower relative expression of the major oxidative *HSD17B2* and *HSD17B4* genes (Rižner, 2013). Additionally, when compared to HIEEC cells, KLE cells showed higher expression of the major reductive *HSD17B1* gene, which supports higher E2 formation, and higher expression of *SULT1E1*, which leads to E2-S as the major product of E1 metabolism and questions the action of estrogens in this cell line. The E1-S metabolism supported these data, with production of E1, E2, and very low levels of estriol in RL95-2 cells, and production of E1, E2 and E2-S in KLE cells. The metabolism of E1 was more efficient in KLE cells, with the formation of E2, E1-S, E2-S, and E2-glucuronide, while in RL95-2 cells, E2, estriol, and E1-S were formed. At 2.3 nM E1-S, E1 and E2 were the main products for RL95-2 cells, and E2-S for KLE cells. For RL95-2 cells vs HIEEC cells, there was >85-fold higher expression of *STS*, with increased STS protein levels also seen. This indicates enhanced hydrolysis of E1-S to E1 in RL95-2 cells, and supports the importance of the sulfatase pathway. This was also confirmed by the E1-S metabolism in the presence of the STS inhibitor STX64. For KLE vs HIEEC cells, there were no significant differences in expression of *STS*, while there was higher expression of *HSD17B1* and *SULT1E1*, thus allowing hydrolysis of E1-S to E1, and promoting formation of E2 and E2-S. These data confirm that these cell lines of moderately and poorly differentiated EC have a capacity for E1-S metabolism and E2 formation.

Also, higher expression of DHEA sulfotransferases supported the biosynthesis of E2 from E1-S via the sulfatase pathway. *SULT2B1* was expressed in both RL95-2 and KLE EC cell lines, with higher relative expression in RL95-2 cells vs KLE and HIEEC cells, while the more efficient *SULT2A1* (Lu et al., 2008) was expressed only in KLE cells. These data suggest that in KLE cells, DHEA sulfation would prevail over hydrolysis of DHEA-S. In RL95-2 vs HIEEC cells, higher expression of *HSD3B1* and *HSD3B2* with concurrent higher expression of *HSD17B2* and *HSD17B8*

imply that DHEA metabolism proceeds to androstenedione, while lower relative expression of *AKR1C3* in KLE vs RL95-2 cells suggests that more testosterone will be formed in the moderately differentiated RL95-2 cells. This supports the protective role of androgens in EC (Gibson et al., 2014; Simitsidellis et al., 2017). The results of the DHEA-S and DHEA metabolism studies are also in line with the gene expression data. In RL95-2 cells, the balance between hydrolysis of DHEA-S and sulfation of DHEA was shifted towards hydrolysis to DHEA, with further metabolism to androstenedione and testosterone; instead, in KLE cells, sulfation prevails.

Binding of estrogens to their receptors is crucial for estrogen actions. In our previous study, *ESR1* and *ESR2* showed higher expression in Ishikawa vs HIEEC cells, while *ESR1* was not expressed in HEC-1A cells (Hevir-Kene and Rižner, 2015). Here, both the RL95-2 and KLE moderately and poorly differentiated EC cell lines expressed the genes that encode ER α and ER β and the expression of *ESR1* prevailed. For these RL95-2 and KLE EC cell lines compared to the model HIEEC cell line, there was no difference in expression of *ESR1*. This is surprising, as differences in ER α have previously been associated with histology, response to therapy, and metastatic potential of EC (Swasti, 2018). Previously, we showed lower *GPER* expression in HEC-1A vs HIEEC cells (v2), and vs Ishikawa cells (v3, v4) (Hevir-Kene and Rižner, 2015). For Ishikawa and HEC-1A cells, other studies have reported that E2 and 4-hydroxytamoxifen stimulate cell proliferation via *GPER* and via the MAPK and PI3K pathways (Vivacqua et al., 2006). In the present study, there were important difference in *GPER* expression, with lower relative expression for KLE vs RL95-2 cells, which suggests that estrogen action via *GPER* might be hampered in poorly differentiated EC. These data thus suggest that in moderately differentiated EC, estrogens might act via ER α and ER β or *GPER*, while in poorly differentiated EC, estrogens might act preferentially via ER α and ER β , and less via *GPER*. However, further studies are needed to clarify estrogen action in these cell lines.

Also phase I and phase II metabolism may differ between these EC cell lines. Compared to the KLE cells, RL95-2 cells differentially expressed genes of phase I and II metabolism in favor of 2-MeOE1/E2 formation (higher relative expression of *CYP1A1*, *COMT*) and 4-MeOE1/E2 formation (higher relative expression of *NQO2*, *COMT*). Formation of these metabolites has a protective role since harmful hydroxyl-E1/E2 are deactivated and also 2-MeOE2 is known to have antiproliferative, antiangiogenic, and proapoptotic effects (Lépine et al., 2010; Hevir et al., 2011). Expression patterns of these phase I and II metabolism genes might to some extent be associated with EC; however, on the other hand, correlations have also been reported between age of patients and formation of 2-MeO and 4-MeO E1/E2 (Brinton et al., 2016), with more 2-MeO and 4-MeO E1/E2 formed in older patients.

For KLE vs RL95-2 cells, lower relative expression of *CYP1A1* and *CYP3A7* and higher relative expression of *CYP1B1* are in favor of the formation of 4-hydroxyestrogens in KLE cells and 2-OH or 16 α OH estrogens in RL95-2 cells. Also, KLE cells will probably form more catechol glucuronides and less 2- or 4-MeO

E1/E2 and glutathione conjugates, compared to RL95-2 cells. This will be due to higher relative expression of *UGT2B7* (i.e., for catechol glucuronides) and lower relative expression of *COMT* and *GSTP1* (i.e., for 2- and 4-MeO E1/E2 and glutathione conjugates). Additionally, for KLE vs RL95-2 cells, lower relative expression of *GSTP1*, *NQO1*, and *NQO2* favors higher DNA adduct formation in poorly differentiated EC.

For KLE cells vs control HIEEC cells, higher expression of *CYP1A2* and *CYP1B1*, and lower expression of *CYP3A7* indicate that in KLE cells, E1 or E2 are primarily transformed into 2-OH E1/E2 or 4-OH E1/E2, and less so into 16 α -OH E1/E2. Higher expression of *SULT1E1* for KLE vs HIEEC cells indicates increased formation of catechol sulfates, which have potential protective roles. Higher expression of *CYP1A2* and *CYP1B1* might lead to increased formation of E1/E2-2,3- or E1/E2-3,4-quinones, and thus to higher probability of the formation of depurinating estrogen–DNA adducts, which are associated with carcinogenesis (Cavalieri and Rogan, 2016). In model EC cell lines of lower grade EC, as RL95-2 (G2), HEC-1-A (G2), and Ishikawa (G1) cells (Hevir-Kene and Rižner, 2015), increased *CYP1A2* and *CYP1B2* expression has not been reported previously, compared to HIEEC cells. To clarify the formation and action of the oxidative metabolites of estrogens and their conjugates further studies are needed.

CONCLUSION

Here, we carried out gene expression analysis supported by E1-S uptake, metabolism studies for DHEA-S, DHEA, E1-S, and E1, and quantification of metabolites by LC-HRMS and LC-MS/MS. These analyses have revealed that the RL95-2 and KLE model cell lines of moderately and poorly differentiated EC, respectively, differ significantly. In both of these cell lines, DHEA-S and DHEA cannot serve as precursors for estrogen formation. RL95-2 cells show metabolism of DHEA-S to DHEA and androstenedione, while KLE cells show little DHEA-S metabolism to DHEA, and DHEA-S production from DHEA, along with androstenedione. In contrast E1-S is metabolized to active estrogens in both of the RL95-2 and KLE cell lines. For RL95-2 cells, as a model of moderately differentiated EC, E1 and E2 are formed, as also for KLE cells, as a model of poorly differentiated EC; however, in KLE cells, E2-S is the major product at physiological E1-S concentrations. Lack of understanding of estrogen action in

these model cell lines of moderately and poorly differentiated EC calls for further studies that may reveal new avenues for treatment.

DATA AVAILABILITY STATEMENT

The original contributions presented in the study are included in the article/**Supplementary Material**, further inquiries can be directed to the corresponding author.

AUTHOR CONTRIBUTIONS

Methodology, validation, RP, MG, EH, KG, MS, SP; formal analysis, RP, MG, MS, SP; investigation, RP, MG, SP, WJ; data curation, RP, MG, MS, SP; writing—original draft preparation, RP and TLR; visualization, RP, EH, MS, MG; funding acquisition, conceptualization, supervision, writing—review and editing, TLR. All authors have read and agreed to the published version of the manuscript.

FUNDING

This study was funded by the Slovenian Research Agency, grants J3-8212 and J3-2535 to TLR, and a Young Researcher grant to RP, and by the Austrian Science Fund (FWF), grant I 3417-B31 to WJ.

ACKNOWLEDGMENTS

The authors would like to acknowledge Mrs. Špela Kos from the Institute of Biochemistry and Molecular Genetics, Faculty of Medicine, University of Ljubljana, for help in performance of experiments, and Dr. Chris Berrie for critical reading of the manuscript.

SUPPLEMENTARY MATERIAL

The Supplementary Material for this article can be found online at: <https://www.frontiersin.org/articles/10.3389/fmolb.2021.743403/full#supplementary-material>

REFERENCES

- Amant, F., Moerman, P., Neven, P., Timmerman, D., Van Limbergen, E., and Vergote, I. (2005). Endometrial Cancer. *Lancet* 366 (9484), 491–505. doi:10.1016/s0140-6736(05)67063-8
- Berstein, L. M., Tchernobrovkina, A. E., Gamajunova, V. B., Kovalevskij, A. J., Vasilyev, D. A., Chepik, O. F., et al. (2003). Tumor Estrogen Content and Clinico-Morphological and Endocrine Features of Endometrial Cancer. *J. Cancer Res. Clin. Oncol.* 129 (4), 245–249. doi:10.1007/s00432-003-0427-9
- Bray, F., Ferlay, J., Soerjomataram, I., Siegel, R. L., Torre, L. A., and Jemal, A. (2018). Global Cancer Statistics 2018: GLOBOCAN Estimates of Incidence and Mortality Worldwide for 36 Cancers in 185 Countries. *CA: A Cancer J. Clin.* 68 (6), 394–424. doi:10.3322/caac.21492
- Brinton, L. A., Trabert, B., Anderson, G. L., Falk, R. T., Felix, A. S., Fuhrman, B. J., et al. (2016). Serum Estrogens and Estrogen Metabolites and Endometrial Cancer Risk Among Postmenopausal Women. *Cancer Epidemiol. Biomarkers Prev.* 25 (7), 1081–1089. doi:10.1158/1055-9965.epi-16-0225
- Bustin, S. A., Benes, V., Garson, J. A., Hellemans, J., Huggett, J., Kubista, M., et al. (2009). The MIQE Guidelines: Minimum Information for Publication of Quantitative Real-Time PCR Experiments. *Clin. Chem.* 55 (4), 611–622. doi:10.1373/clinchem.2008.112797
- Cavalieri, E. L., and Rogan, E. G. (2011). Unbalanced Metabolism of Endogenous Estrogens in the Etiology and Prevention of Human Cancer. *J. Steroid Biochem. Mol. Biol.* 125 (3–5), 169–180. doi:10.1016/j.jsbmb.2011.03.008

- Cavalieri, E. L., and Rogan, E. G. (2016). Depurinating estrogen-DNA Adducts, Generators of Cancer Initiation: Their Minimization Leads to Cancer Prevention. *Clin. Transl. Med.* 5, 12. doi:10.1186/s40169-016-0088-3
- Chapdelaine, P., Kang, J., Boucher-Kovalik, S., Caron, N., Tremblay, J. P., and Fortier, M. A. (2006). Decidualization and Maintenance of a Functional Prostaglandin System in Human Endometrial Cell Lines Following Transformation with SV40 Large T Antigen. *Mol. Hum. Reprod.* 12 (5), 309–319. doi:10.1093/molehr/gal034
- Chiang, S., and Soslow, R. A. (2014). Updates in Diagnostic Immunohistochemistry in Endometrial Carcinoma. *Semin. Diagn. Pathol.* 31 (3), 205–215. doi:10.1053/j.semdp.2014.03.002
- Cornel, K. M. C., Delvoux, B., Saya, T., Xanthouleas, S., Konings, G. F. J., Kruitwagen, R. P. F. M., et al. (2018). The Sulfatase Pathway as Estrogen Supply in Endometrial Cancer. *Steroids* 139, 45–52. doi:10.1016/j.steroids.2018.09.002
- Dantzie, D., Noel, P., Merien, F., Liu, D.-X., Lu, J., Han, H., et al. (2018). The Effects of Synthetically Modified Natural Compounds on ABC Transporters. *Pharmaceutics* 10 (3), 127. doi:10.3390/pharmaceutics10030127
- Foster, P. A., Woo, L. W., Potter, B. V. L., Reed, M. J., and Purohit, A. (2008). The Use of Steroid Sulfatase Inhibitors as a Novel Therapeutic Strategy against Hormone-dependent Endometrial Cancer. *Endocrinology* 149 (8), 4035–4042. doi:10.1210/en.2008-0223
- Gibson, D. A., Simitsidelis, I., Collins, F., and Saunders, P. T. K. (2014). Evidence of Androgen Action in Endometrial and Ovarian Cancers. *Endocr. Relat. Cancer* 21 (4), T203–T218. doi:10.1530/ERC-13-0551
- Hevir, N., Šinkovec, J., and Rižner, T. L. (2011). Disturbed Expression of Phase I and Phase II Estrogen-Metabolizing Enzymes in Endometrial Cancer: Lower Levels of CYP1B1 and Increased Expression of S-COMT. *Mol. Cell Endocrinol.* 331 (1), 158–167. doi:10.1016/j.mce.2010.09.011
- Hevir-Kene, N., and Rižner, T. L. (2015). The Endometrial Cancer Cell Lines Ishikawa and HEC-1A, and the Control Cell Line HIEEC, Differ in Expression of Estrogen Biosynthetic and Metabolic Genes, and in Androstenedione and Estrone-Sulfate Metabolism. *Chem. Biol. Interact.* 234, 309–319. doi:10.1016/j.cbi.2014.11.015
- Inoue, M. (2001). Current Molecular Aspects of the Carcinogenesis of the Uterine Endometrium. *Int. J. Gynecol. Cancer* 11 (5), 339–348. doi:10.1046/j.1525-1438.2001.01046.x
- Kandoth, C., Kandoth, C., Schultz, N., Cherniack, A. D., Akbani, R., Liu, Y., et al. (2013). Integrated Genomic Characterization of Endometrial Carcinoma. *Nature* 497 (7447), 67–73. doi:10.1038/nature12113
- König, J., Seithel, A., Gradhand, U., and Fromm, M. F. (2006). Pharmacogenomics of Human OATP Transporters. *Naunyn Schmied Arch. Pharmacol.* 372 (6), 432–443. doi:10.1007/s00210-006-0040-y
- Le'pine, J., Audet-Walsh, E., Grégoire, J., Têtu, B., Plante, M., Me'nard, V., et al. (2010). Circulating Estrogens in Endometrial Cancer Cases and Their Relationship with Tissue Expression of Key Estrogen Biosynthesis and Metabolic Pathways. *J. Clin. Endocrinol. Metab.* 95 (6), 2689–2698. doi:10.1210/jc.2010-2648
- Lindemann, K., Eskild, A., Vatten, L. J., and Bray, F. (2010). Endometrial Cancer Incidence Trends in Norway during 1953–2007 and Predictions for 2008–2027. *Int. J. Cancer* 127 (11), 2661–2668. doi:10.1002/ijc.25267
- Lu, L.-Y., Hsieh, Y.-C., Liu, M.-Y., Lin, Y.-H., Chen, C.-J., and Yang, Y.-S. (2008). Identification and Characterization of Two Amino Acids Critical for the Substrate Inhibition of Human Dehydroepiandrosterone Sulfotransferase (SULT2A1). *Mol. Pharmacol.* 73 (3), 660–668. doi:10.1124/mol.107.041038
- Malini, B., Purohit, A., Ganeshapillai, D., Woo, L. W., Potter, B. V., and Reed, M. J. (2000). Inhibition of Steroid Sulphatase Activity by Tricyclic Coumarin Sulphamates. *J. Steroid Biochem. Mol. Biol.* 75 (4–5), 253–258. doi:10.1016/s0960-0760(00)00178-3
- Morice, P., Leary, A., Creutzberg, C., Abu-Rustum, N., and Darai, E. (2016). Endometrial Cancer. *Lancet* 387 (10023), 1094–1108. doi:10.1016/S0140-6736(15)00130-0
- Murali, R., Soslow, R. A., and Weigelt, B. (2014). Classification of Endometrial Carcinoma: More Than Two Types. *Lancet Oncol.* 15 (7), e268–e278. doi:10.1016/s1470-2045(13)70591-6
- Paterni, I., Granchi, C., Katzenellenbogen, J. A., and Minutolo, F. (2014). Estrogen Receptors Alpha (ERα) and Beta (ERβ): Subtype-Selective Ligands and Clinical Potential. *Steroids* 90, 13–29. doi:10.1016/j.steroids.2014.06.012
- Pavlič, R., Vidic, S., Anko, M., Knific, T., Büdefeld, T., Marton, K., et al. (2021). Altered Profile of E1-S Transporters in Endometrial Cancer: Lower Protein Levels of ABCG2 and OSTβ and Up-Regulation of SLC01B3 Expression. *Ijms* 22 (8), 3819. doi:10.3390/ijms22083819
- Poschner, S., Zehl, M., Maier-Salamon, A., and Jäger, W. (2017). Simultaneous Quantification of Estrogens, Their Precursors and Conjugated Metabolites in Human Breast Cancer Cells by LC-HRMS without Derivatization. *J. Pharm. Biomed. Anal.* 138, 344–350. doi:10.1016/j.jpba.2017.02.033
- Richardson, G. S., Dickersin, G. R., Atkins, L., MacLaughlin, D. T., Raam, S., Merk, L. P., et al. (1984). KLE: a Cell Line with Defective Estrogen Receptor Derived from Undifferentiated Endometrial Cancer. *Gynecol. Oncol.* 17 (2), 213–230. doi:10.1016/0090-8258(84)90080-5
- Rižner, T. L., Šmuc, T., Ruprecht, R., Šinkovec, J., and Penning, T. M. (2006). AKR1C1 and AKR1C3 May Determine Progesterone and Estrogen Ratios in Endometrial Cancer. *Mol. Cell. Endocrinol.* 248 (1–2), 126–135. doi:10.1016/j.mce.2005.10.009
- Rižner, T. L., Thalhammer, T., and Özyeğy-Laczka, C. (2017). The Importance of Steroid Uptake and Intracrine Action in Endometrial and Ovarian Cancers. *Front. Pharmacol.* 8, 346. doi:10.3389/fphar.2017.00346
- Rižner, T. L. (2013). Estrogen Biosynthesis, Phase I and Phase II Metabolism, and Action in Endometrial Cancer. *Mol. Cell Endocrinol.* 381 (1–2), 124–139. doi:10.1016/j.mce.2013.07.026
- Roth, M., Obaidat, A., and Hagenbuch, B. (2012). OATPs, OATs and OCTs: the Organic Anion and Cation Transporters of the SLC0 and SLC22A Gene Superfamilies. *Br. J. Pharmacol.* 165 (5), 1260–1287. doi:10.1111/j.1476-5381.2011.01724.x
- Simitsidelis, I., Saunders, P. T. K., and Gibson, D. A. (2018). Androgens and Endometrium: New Insights and New Targets. *Mol. Cell Endocrinol.* 465, 48–60. doi:10.1016/j.mce.2017.09.022
- Sinreih, M., Knific, T., Anko, M., Hevir, N., Vouk, K., Jerin, A., et al. (2017). The Significance of the Sulfatase Pathway for Local Estrogen Formation in Endometrial Cancer. *Front. Pharmacol.* 8, 368. doi:10.3389/fphar.2017.00368
- Swasti (2018). Estrogen and Progesterone Receptors in Endometrial Cancer: Where Are We Today? *Gynecol. Obstet.* 8 (2), e127. doi:10.4172/2161-0932.1000e127
- Van Nyen, T., Moiola, C. P., Colas, E., Annibali, D., and Amant, F. (2018). Modeling Endometrial Cancer: Past, Present, and Future. *Ijms* 19 (8), 2348. doi:10.3390/ijms19082348
- Vivacqua, A., Bonfiglio, D., Recchia, A. G., Musti, A. M., Picard, D., Andò, S., et al. (2006). The G Protein-Coupled Receptor GPR30 Mediates the Proliferative Effects Induced by 17β-Estradiol and Hydroxytamoxifen in Endometrial Cancer Cells. *Mol. Endocrinol.* 20 (3), 631–646. doi:10.1210/me.2005-0280
- Wan, J., Gao, Y., Zeng, K., Yin, Y., Zhao, M., Wei, J., et al. (2016). The Levels of the Sex Hormones Are Not Different between Type 1 and Type 2 Endometrial Cancer. *Sci. Rep.* 6, 39744. doi:10.1038/srep39744
- Way, D. L., Grosso, D. S., Davis, J. R., Surwit, E. A., and Christian, C. D. (1983). Characterization of a New Human Endometrial Carcinoma (RL95-2) Established in Tissue Culture. *In Vitro* 19 (3 Pt 1), 147–158. doi:10.1007/BF02618053
- Xu, S., Yu, S., Dong, D., and Lee, L. T. O. (2019). G Protein-Coupled Estrogen Receptor: A Potential Therapeutic Target in Cancer. *Front. Endocrinol.* 10, 725. doi:10.3389/fendo.2019.00725
- Yeremian, A., Moreno-Bueno, G., Dolcet, X., Catusas, L., Abal, M., Colas, E., et al. (2013). Endometrial Carcinoma: Molecular Alterations Involved in Tumor Development and Progression. *Oncogene* 32 (4), 403–413. doi:10.1038/onc.2012.76

Conflict of Interest: The authors declare that the research was conducted in the absence of any commercial or financial relationships that could be construed as a potential conflict of interest.

Publisher's Note: All claims expressed in this article are solely those of the authors and do not necessarily represent those of their affiliated organizations, or those of the publisher, the editors and the reviewers. Any product that may be evaluated in this article, or claim that may be made by its manufacturer, is not guaranteed or endorsed by the publisher.

Copyright © 2021 Pavlič, Gjorgoska, Hafner, Sinreih, Gajser, Poschner, Jäger and Rižner. This is an open-access article distributed under the terms of the Creative Commons Attribution License (CC BY). The use, distribution or reproduction in other forums is permitted, provided the original author(s) and the copyright owner(s) are credited and that the original publication in this journal is cited, in accordance with accepted academic practice. No use, distribution or reproduction is permitted which does not comply with these terms.



Cellular ATP Levels Determine the Stability of a Nucleotide Kinase

Oliver Brylski^{1,2,3}, Puja Shrestha^{1,2}, Patricia Gnutz³, David Gnutz^{1,2,3},
Jonathan Wolf Mueller^{4,5*} and Simon Ebbinghaus^{1,2,3*}

¹Institute of Physical and Theoretical Chemistry, TU Braunschweig, Braunschweig, Germany, ²Braunschweig Integrated Centre of Systems Biology (BRICS), Braunschweig, Germany, ³Institute of Physical Chemistry II, Ruhr University, Bochum, Germany, ⁴Institute of Metabolism and Systems Research (IMSR), University of Birmingham, Birmingham, United Kingdom, ⁵Centre for Endocrinology, Diabetes and Metabolism (CEDAM), Birmingham Health Partners, Birmingham, United Kingdom

OPEN ACCESS

Edited by:

Cesare Indiveri,
University of Calabria, Italy

Reviewed by:

Kai Tittmann,
University of Göttingen, Germany
Arnold J. Boersma,
DWI—Leibniz-Institut für Interaktive
Materialien, Germany

*Correspondence:

Jonathan Wolf Mueller
j.w.mueller@bham.ac.uk
Simon Ebbinghaus
s.ebbinghaus@tu-braunschweig.de

Specialty section:

This article was submitted to
Cellular Biochemistry,
a section of the journal
Frontiers in Molecular Biosciences

Received: 06 October 2021

Accepted: 26 November 2021

Published: 13 December 2021

Citation:

Brylski O, Shrestha P, Gnutz P,
Gnutz D, Mueller JW and Ebbinghaus S
(2021) Cellular ATP Levels Determine
the Stability of a Nucleotide Kinase.
Front. Mol. Biosci. 8:790304.
doi: 10.3389/fmolb.2021.790304

The energy currency of the cell ATP, is used by kinases to drive key cellular processes. However, the connection of cellular ATP abundance and protein stability is still under investigation. Using Fast Relaxation Imaging paired with alanine scanning and ATP depletion experiments, we study the nucleotide kinase (APSK) domain of 3'-phosphoadenosine-5'-phosphosulfate (PAPS) synthase, a marginally stable protein. Here, we show that the in-cell stability of the APSK is determined by ligand binding and directly connected to cellular ATP levels. The observed protein stability change for different ligand-bound states or under ATP-depleted conditions ranges from $\Delta G_f^0 = -10.7$ to $+13.8$ kJ/mol, which is remarkable since it exceeds changes measured previously, for example upon osmotic pressure, cellular stress or differentiation. The results have implications for protein stability during the catalytic cycle of APS kinase and suggest that the cellular ATP level functions as a global regulator of kinase activity.

Keywords: PAPS synthase, ATP depletion, in-cell spectroscopy, protein folding stability, alanine scanning, ligand binding, sulfation pathways, cellular stress

INTRODUCTION

In eukaryotic cells, there is abundant ATP at millimolar concentrations (Traut, 1994). Under conditions of stress, such as starvation (Maddocks et al., 2013; Petrovska et al., 2014) or DNA damage (Bonora et al., 2012), the ATP concentration is fluctuating inside cells. Recently, ATP was attributed an additional role as a 'biological hydrotrope'; it controls the solubility and stability of proteins and protein complexes and governs liquid-liquid phase separation (Patel et al., 2017; Hayes et al., 2018; Gnutz et al., 2019b).

A class of proteins traditionally linked to ATP are P-loop kinases; they are ATP-dependent phosphate-transferring enzymes (Leipe et al., 2003). Nucleotide kinases are a kinase sub-family—they have ATP and some other nucleotide as their substrates. A special class of nucleotide kinases are those that phosphorylate the atypical nucleotide adenosine-5'-phosphosulfate (APS). Because APS is created in an upstream reaction that strongly relies on ATP as a substrate (Mueller and Shafqat, 2013), all substrates and all products of the reaction catalyzed by APS kinase (APSK) directly or indirectly depend on ATP availability (Brylski et al., 2019).

APSK enzymes sit at the center of sulfation pathways, as they are essential to produce active sulfate in the form of 3'-phosphoadenosine-5'-phosphosulfate (PAPS) (Gunal et al., 2019). With more than 50 PAPS-utilizing sulfotransferases encoded in the human genome, for example generating heparan sulfate (Gesteira et al., 2021), defects in the supply of the active sulfate PAPS should result in multi systems-defects. Clinical mutations in the human APS kinase-

containing enzyme PAPS synthase 1 (PAPSS1) have not been described so far. However, disease-relevant point mutations in PAPSS2 have been linked specifically to bone and cartilage mal-formation (Iida et al., 2013) as well as dysregulation of steroid hormone action (Noordam et al., 2009; Oostdijk et al., 2015; Mueller et al., 2018). Noteworthy, a previous report classified PAPSS2 as a marginally stable protein, when being studied as recombinant protein (van den Boom et al., 2012). It remains unclear whether this marginal stability and possibly misfolding and subsequent aggregation of disease-related mutant proteins is a cause of the diseases mentioned above (Brylski et al., 2019).

Alternatively, the marginal stability of the PAPSS2 enzyme could actually serve a biological role in regulating enzymatic activity in sulfation pathway (Brylski et al., 2019). PAPS synthase isoforms are only marginally stable when studied as recombinant proteins, but they are stabilized by binding of their natural nucleotide ligands (van den Boom et al., 2012; Brylski et al., 2019). Most proteins should be stabilized by ligand binding (Luque et al., 2002), which may also serve as a protective measure from degradation (Staniec et al., 2015). However, a high affinity of two binding partners and high binding energies do not necessarily result in a stabilization of the full protein structure, as observed very recently for the protein complex of human proteins histone H1 and prothymosin- α (Borgia et al., 2018). This demonstrates the necessity to study individual protein-ligand interactions and their effect on protein stability on a case-by-case basis. For PAPS synthases, the main stabilizing ligands are PAPS, ADP as well as APS (Mueller and Shafqat, 2013); they all preferentially bind to the APSK (van den Boom et al., 2012). The protein-ligand interactions and stability of the respective ligand-bound states were traditionally studied using recombinant proteins and in aqueous buffers. Hence, it remains unclear if the stabilization of APSK by ligand binding (van den Boom et al., 2012) is preserved inside crowded cells and how protein stability of the APSK kinase domain is affected by fluctuating cellular ATP levels.

Here, we measure the in-cell stability of the APS kinase domain (APSK) of PAPSS2 under different conditions, using *Fast Relaxation Imaging* in combination with the engineered FRET-based fluorescent folding sensor APSK37. By alanine-scanning mutagenesis, we probe the stability changes of the APS kinase domain in different ensembles of substrate bound states. The observed stability changes correlate with the type of interaction deleted and its impact on the catalytic cycle. This implicates a changing protein stability for different states of the catalytic cycle. Further, we monitor the stability of this kinase domain at different intracellular ATP levels to determine the impact of ATP on the regulatory mechanism of sulfation pathways. Here, the overall protein stability of this kinase is directly coupled to cellular ATP levels, with marginal stability at low cellular ATP levels. In summary, we demonstrate that the APS kinase domain undergoes a protein-stability cycle that is coupled to the different ligand-bound states during its catalytic cycle and cellular ATP levels.

MATERIALS AND METHODS

Plasmid Preparation

Full-length human PAPS synthase 2b (NM_001015880) in a EGFP-C1 vector was described previously (Schroder et al., 2012). The APS kinase domain of PAPSS2 was subcloned into a modified pDream2.1 vector with an N-terminal AcGFP1 and a C-terminal mCherry by PCR (In-Fusion, Clontech). The AcGFP1 is additionally tagged with an 6-His-Tag for protein purification. Point-mutations were introduced using site-directed mutagenesis (QuikChange Lightning, Agilent Technologies). Plasmid DNA was amplified in NEB5 α (New England Biolabs), Stellar (Clontech) or XL10 Gold (Agilent Technologies) competent *E. coli* cells and purified using Zymoprep Miniprep plasmid preparation kits (Zymo Research). DNA was quantified by UV/Vis spectroscopy (NanoDrop 2000; Thermo Fisher) and sequenced at an intramural facility (RUB Bochum).

Protein Purification

NiCo21(DE3) competent *E. coli* (New England Biolabs) were transformed with plasmid DNA. A single colony was grown at 37°C and moderate shaking at 220 rpm to OD₆₀₀ 0.6 in LB broth medium and then induced by addition of 100 μ M IPTG. Protein expression was allowed overnight (~16 h) at 18°C. Cells were harvested via centrifugation and lysed using xTractor buffer (Clontech). Protein suspension was transferred onto gravity flow His60 Ni Gravity Flow columns (Clontech) and purified according to the manufacturers protocol. Buffer was exchanged using Amicon Ultra (MWCO 30 kDa) to PBS (137 mM NaCl, 2.7 mM KCl, 10 mM Na₂HPO₄, 1.8 mM KH₂PO₄) at pH 7.4. Proteins were aliquoted and shock-frozen for long-term storage. Purity was evaluated via SDS-PAGE.

Cell Culture and Plasmid Transfection

HeLa cells were grown in DMEM supplemented with 10% FBS, 100 U/ml penicillin and 0.1 mg/ml streptomycin as an adherent culture (Sarstedt) in a humidified atmosphere (37°C, 5% CO₂). Cells were passaged in a 1:4 or 1:6 ratio after 2 to 3 days upon reaching 80–90% confluence using trypsin digestion. For experimental preparation, cells were seeded on six-well plates (Sarstedt) and transfected at 80–90% confluence using Lipofectamine 3,000 (Thermo Fisher) according to the manufacturers protocol. Briefly, 125 μ l Opti-MEM (Thermo Fisher) was supplemented with 2 μ g of according plasmid DNA and 4 μ l P3000 reagent. Mixture was transferred and mixed with 125 μ l Opti-MEM supplemented with 4 μ l Lipofectamine3000 reagent after 5 min of incubation. Transfection mixture was added to the cellular growth medium and cell culture incubated for 6 hours. After incubation, cells were passaged using trypsin digestion and seeded on 35 mm glass bottom dishes (Fluorodish, World Precision Instruments) and grown for 2 days at regular cell culture conditions.

Sample Preparation

In-cell measurements using Fast Relaxation Imaging were performed with transfected cells grown on 35 mm glass bottom dishes (Fluorodish, World Precision Instruments). Growth medium was aseptically removed and cells washed with DPBS (Sigma-Aldrich). Glass bottom dishes with cells were placed on a glass cover slip (Menzel #1.0) with a 120 μm thick imaging spacer (Sigma-Aldrich) and covered with 30 μl Leibovitz's L15 medium supplemented with 30% FBS. For measurements at ATP depleted conditions, Leibovitz's L15 medium was supplemented with 1 mM KCN (Sigma-Aldrich) and 10 mM 2-deoxyglucose (Sigma-Aldrich) and cells incubated for the respective time prior to the FReI measurement.

Measurements in buffered solutions were performed at 10 μM protein concentration in PBS supplemented with 10 μM MgCl_2 . Nucleotides were dissolved in PBS and added at desired concentration. 20 μl of sample were sealed between a glass cover slip with a 120 μm thick imaging spacer and a 35 mm glass bottom dish.

HeLa cells transfected with the ATeam1.03-nD/nA protein sensor were not sealed as the ATP depleting agents had to be supplemented during the measurement.

Fast Relaxation Imaging Measurements

Fast Relaxation Imaging combines millisecond temperature jumps with wide field fluorescence microscopy (Ebbinghaus et al., 2010). The microscope setup as well as the fluorophore pair used in this study have been described and characterized earlier (Dhar et al., 2011; Gao et al., 2016; Buning et al., 2017). Briefly, the specimen is rapidly heated by an IR diode laser (m2k-Laser, 2,200 nm) in the millisecond range while recording change of fluorescent signal using CCD cameras. The temperature jumps were calibrated using the temperature sensitive dye Rhodamine B (Vopel et al., 2015; Gao et al., 2016; Buning et al., 2017). The heating profile used throughout this study consisted of individual 2.2°C temperature jumps at intervals of 50 s (Supplementary Figure 1), covering a temperature range from 23.0°C to 58.2°C in 16 steps. Images were recorded at a frame rate of 1 fps and image acquisition times were between 50–200 ms with LED exposure only during acquisition times. At least three technical replicates ($N \geq 3$), including separate cell culturing and measuring, were performed for in-cell measurements. For *in vitro* measurements at least three technical replicates were performed ($N \geq 3$).

Images were processed and evaluated using ImageJ (National Institute of Health, United States). Retrieved intensity data were further evaluated using self-written MatLab (Mathworks) codes and GraphPad Prism 6 (GraphPad). The cytoplasmic region of the cell was defined by excluding the visible nuclear area and fluorescence intensity averaged throughout this region of interest for each channel individually. *In vitro* samples were averaged throughout a defined region covering about 90% of the image.

After subtraction of the background signal for the individual donor (D) and acceptor (A) channels, the ratio D/A was calculated for an initial evaluation of data and $D-\alpha A$ for kinetic analysis (Dhar et al., 2011). Single temperature jumps and their unfolding kinetics were fitted to single exponentials, reflecting a two-state folding behavior, and the kinetic amplitudes

($D-\alpha A(T)$) plotted against temperature. These amplitudes were then fitted to the thermodynamic model introduced as *Better thermodynamics from kinetics* (Girdhar et al., 2011):

$$D - \alpha A(T) = \frac{-\delta g_1 T \Delta \cdot T_M}{R(T - \Delta T/2)^2} \cdot (A_0 + m_A(T - T_M)) \cdot \frac{\exp(-\delta g_1(T - (\Delta T/2) - T_M) \cdot (R(T - \Delta T/2))^{-1})}{(1 + \exp(-\delta g_1(T - (\Delta T/2) - T_M) \cdot (R(T - \Delta T/2))^{-1}))^2}$$

The determined fitting parameters are δg_1 and T_M . δg_1 is the pre-factor of the linear Taylor approximation of the two-state population and T_M the melting point of the protein unfolding transition analyzed. ΔT is the amplitude of the temperature (set to 2.2°C) and A_0 and m_A the fitting parameters of the underlying baseline (with m_A set to 0). The melting point T_M was compared for individual point-mutants measured. Fits were performed using GraphPad Prism 6.

The pre-factor of the linear Taylor approximation δg_1 as well as T_M are used to calculate the standard free energy of folding (Dhar et al., 2011; Girdhar et al., 2011):

$$\Delta G_f^0 = -\delta g_1(T_M - T)$$

with T being the reference temperature of 37°C or 310.15 K respectively.

The results of the different solvated alanine mutants need to be compared to the wildtype APSK37 sensor as an internal standard and depict a lower limit of the actual thermodynamic contribution.

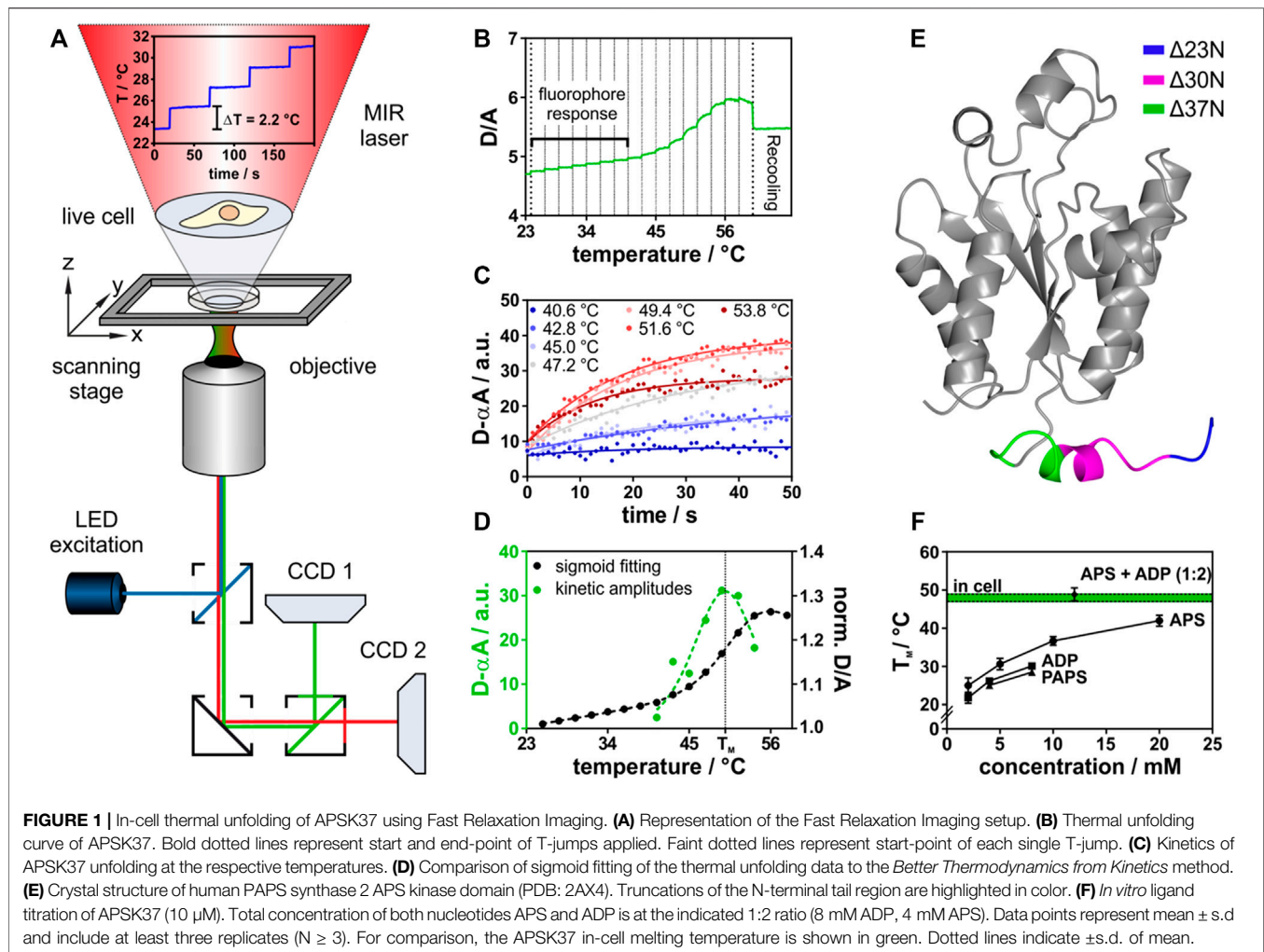
ATP Depletion Experiments

The ATeam1.03-nD/nA protein sensor used for depletion experiments is based on the ϵ -subunit of the bacterial F_0F_1 -ATP synthase (Kotera et al., 2010). Recordings of ATP depletion were performed using an Olympus FV3000 CLSM confocal microscope. Transfected HeLa cells were supplemented with 1 mM KCN and 10 mM 2-deoxyglucose during the measurement and the solution carefully mixed using a pipette. The sensor was excited using a 445 nm laser and the signal recorded via an UPLXAPO $\times 20$ objective (NA 0.8, Olympus). Donor and acceptor signals were detected on separate detectors for 50 min in 5 s intervals. Two technical replicates ($N = 2$), including new passaging of cells and transfection, were performed to determine relative ATP concentration changes during treatment.

RESULTS

Determining the in-Cell Stability of APS Kinases *in vitro* and in the Cell

In order to study protein-ligand interactions and their effects on protein stability in the complex environment of the cell, we use *Fast Relaxation Imaging*. It is a unique tool to study protein folding kinetics and thermal stability in single living cells with high spatial and temporal resolution (Ebbinghaus et al., 2010; Dhar et al., 2011; Wirth et al., 2013). *Fast Relaxation Imaging* combines wide-field fluorescence microscopy with consecutive



temperature jumps utilizing a mid-infrared laser and Förster Resonance Energy Transfer (FRET) (Figure 1A). Analysis of kinetic amplitudes of protein unfolding at the respective temperatures allows to determine the thermal stability of the protein in the cell (Dhar et al., 2011; Girdhar et al., 2011).

In this study, a temperature profile with 16 consecutive temperature jumps was used. This resulted in individual temperature jumps of 2.2°C covering a temperature range from 23.0°C to 58.2°C (Supplementary Figure 1). The consecutive temperature jumps allowed to measure the thermal melting curve of a FRET-labeled APS kinase (Figure 1B) within 16 min. The respective unfolding kinetics at each temperature jump were fitted (Figure 1C) using the *Better Thermodynamics from Kinetics* method (Girdhar et al., 2011) (see Material and Methods for details). The amplitudes of the unfolding kinetics were analyzed, showing a maximum at the melting temperature (T_M) due to the highest population shift between folded and unfolded states. In common fitting of thermal melting curves folded and unfolded baselines need to be resolved, which does not need to be accounted for in this model (Figure 1D), making the fitting procedure more robust (Girdhar et al., 2011). The standard free energy of folding at

37°C (ΔG_f^0) was then determined by a linear Taylor approximation as described earlier (Dhar et al., 2011; Girdhar et al., 2011).

This method was applied both in aqueous buffered solution *in vitro* and in the cell under the same experimental conditions. For FRET detection, we constructed a fusion protein of the APS kinase domain of human PAPS synthase 2 (Figure 1E). The APS kinase domain catalyzes the rate-limiting step in PAPS synthesis (Grum et al., 2010) and harbors four of the six known disease-mutations (Kurima et al., 1998; Noordam et al., 2009; Iida et al., 2013). To construct the fusion protein, we truncated the two-domain bifunctional PAPSS2 protein between two isoleucine residues (I220 and I221) within the flexible linker region connecting the kinase and sulfurylase domain (Harjes et al., 2005). In bacteria, fungi and plants, APS kinase and ATP sulfurylase are not observed as fusion proteins (Patron et al., 2008) and crystal structures (Sekulic et al., 2007a) as well as enzymology studies (Harjes et al., 2005; Sekulic et al., 2007a) indicate that the isolated APS kinase remains fully functional, rationalizing the choice of truncation for the experiment. Next, we step-wise truncated the flexible and disordered N-terminal region. An APS kinase variant, shortened by 37 amino acids

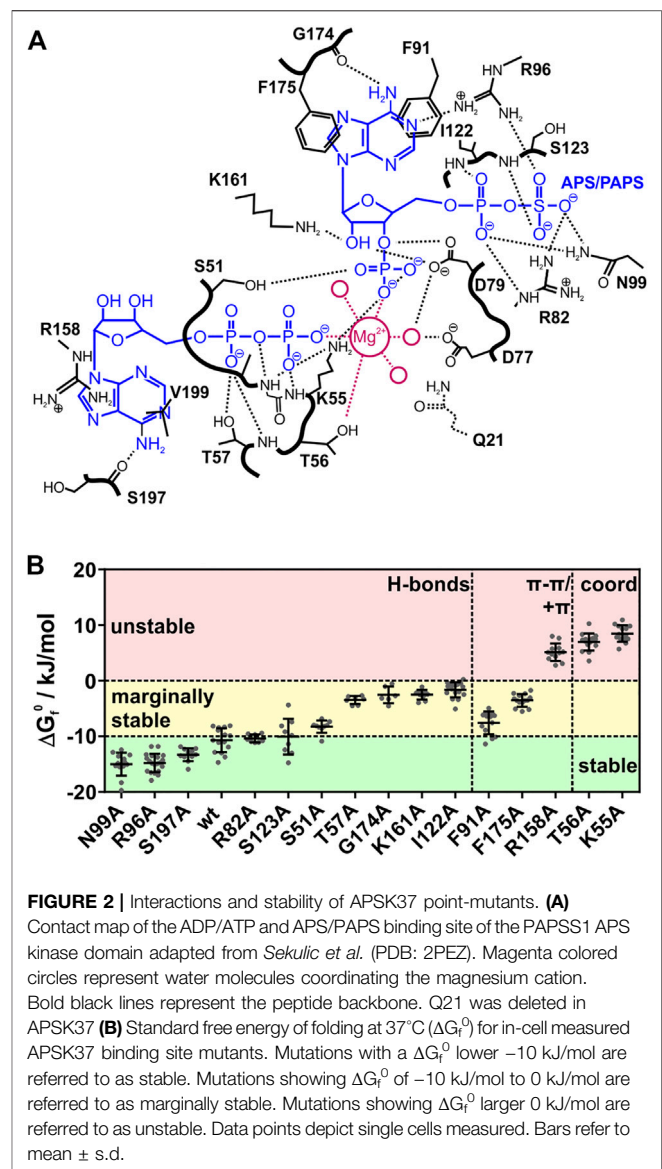
($\Delta 37N$), resembles a truncation variant of the PAPSS1 homolog that retained catalytic activity (Sekulic et al., 2007a). Only this variant allowed us to study the conformational dynamics of the monomer by intramolecular FRET using AcGFP1 (N-terminus) and mCherry (C-terminus) as fusion proteins (Supplementary Figure 2). We refer to this newly engineered folding reporter as APSK37 from now on.

APSK37 showed an intrinsic donor (D) to acceptor (A) fluorescence intensity increase upon IR-laser heating (Figure 1B, fluorophore response), resulting from the different temperature dependency of quantum efficiencies of the FRET pair AcGFP1 and mCherry (Dhar et al., 2011). Thermal unfolding was then observed at $T_M = 48.0 \pm 1.7^\circ\text{C}$ giving rise to an unfolding curve with a single transition. The unfolding process is reversible for a fraction of the protein ensemble as indicated by recovery towards the initial D/A ratio upon temperature relapse (Feng et al., 2019) (Supplementary Figure 3). Unfolding kinetics at the respective temperatures show single exponential behavior, suggesting two-state unfolding (Figure 1D).

For *in vitro* experiments, we purified the recombinant APSK37 fusion protein from *E. coli* to investigate its substrate binding capacity (see Material and Methods). Reversible unfolding and refolding of the protein *in vitro* requires the addition of nucleotides (Supplementary Figure 4), illustrating their role in determining folding stability. Titrations of the recombinant APSK37 protein with different nucleotides showed a pronounced stabilization by APS followed by a less pronounced stabilization by ADP and PAPS (Figure 1F) which is in good agreement with previous *in vitro* studies of full-length PAPS synthase 2 (van den Boom et al., 2012). Combination of the nucleotides ADP and APS at a ratio of 2:1, as found in nucleotide-soaked crystals of the PAPSS1 APS kinase domain (PDB: 2PEY), stabilized the protein to a much larger extent than addition of only one nucleotide alone. In fact, joint binding of ADP and APS nucleotides to APSK37 resulted in similar T_M values to the ones determined inside live cells (Figure 1F) ($48.0 \pm 1.7^\circ\text{C}$ compared to $48.9 \pm 1.7^\circ\text{C}$). Experiments in buffered solutions neglect excluded-volume (Zimmerman and Trach, 1991) and non-specific binding (McConkey, 1982) present inside crowded cells, however these results show that both nucleotide binding sites of this kinase need to be occupied to compensate for being naturally fragile (van den Boom et al., 2012).

APSK37 in-Cell Thermal Stability is Determined by Ligand Binding

Next, we used APSK37 to elucidate the influence of substrate, product and co-factor binding on protein stability inside cells, by systematically alanine-scanning its ligand binding sites. We know that ADP, APS and PAPS stabilize the PAPS synthases proteins (van den Boom et al., 2012). Analogous in-cell nucleotide titrations are not feasible as nucleotide concentrations cannot be controlled inside cells in a quantitative manner. To introduce changes in binding affinity of the protein to its nucleotide ligands and the metal co-factor, we probed the protein environment of the ATP/ADP and the APS/PAPS nucleotide binding sites as well as the P-loop coordinating the Mg^{2+} cation by alanine scanning



mutagenesis (Figure 2A, see Table 1). Binding sites of the APS kinase domain of human PAPS synthases have been characterized structurally before (Harjes et al., 2005; Rabeh et al., 2005; Sekulic et al., 2007a). This allowed us to selectively delete different types of chemical contacts, such as hydrogen bonds, π - π or cation- π -stacking interactions or cation coordination (see Table 1). Deletion of the stronger interactions, such as cation coordination or stacking interactions, is expected to reduce affinity more than deleting a single H-bond. This approach enabled us to evaluate the in-cell stability change of APSK37 in an indirect way that is comparable to classic titration experiments with recombinant proteins and different ratios of bound and unbound substrate ensembles.

We determined the in-cell melting temperature T_M as well as the standard free energy of folding at 37°C (ΔG_f°) of the respective alanine mutations. Mutants showing a ΔG_f° energy of less than -10 kJ/mol are referred to as stable mutants. Mutants with ΔG_f°

TABLE 1 | Summary of APSK37 in-cell binding-site analysis. Mutations are split into stable, marginally stable and unstable variants and sorted according to their ΔG_f^0 . ΔG_f^0 corresponds to the standard free energy of folding at 37°C. Asterisks depict mutations originally interacting with the nucleotide *via* their peptide backbone. Values are depicted as mean \pm s.d.

Mutation	Interaction	Nucleotide	Partner	$T_M/^\circ\text{C}$	$\Delta G_f^0/\text{kJ/mol}$	n
Stable						
N99A	H-bond	APS/PAPS	α -phosphate/ β -sulfate	47.8 ± 0.6	-15.1 ± 2.1	13
R96A	H-bond	APS/PAPS	β -sulfate/adenine base	50.5 ± 0.6	-14.8 ± 1.6	20
*S197A	H-bond	ATP/ADP	adenine base	49.8 ± 0.6	-13.3 ± 1.2	11
Wt	---	---	---	48.0 ± 1.7	-10.7 ± 2.2	15
R82A	H-bond	APS/PAPS	α -phosphate/ β -sulfate	47.7 ± 1.9	-10.4 ± 0.7	8
*S123A	H-bond	APS/PAPS	α -phosphate/ β -sulfate	48.6 ± 3.3	-10.1 ± 3.2	9
Marginally stable						
S51A	H-bond	APS/PAPS	3'-phosphate	46.4 ± 1.3	-8.3 ± 1.1	9
F91A	π - π	APS/PAPS	adenine base	47.1 ± 2.7	-7.6 ± 2.0	13
F175A	π - π	APS/PAPS	adenine base	40.9 ± 2.3	-3.5 ± 1.1	14
T57A	H-bond	ATP/ADP	α -phosphate	40.9 ± 1.1	-3.4 ± 0.7	7
*G174A	H-bond	APS/PAPS	adenine base	38.4 ± 0.7	-2.5 ± 1.5	6
K161A	H-bond	APS/PAPS	4'-hydroxide	39.5 ± 1.4	-2.5 ± 0.9	9
*I122A	H-bond	APS/PAPS	α -phosphate	38.9 ± 1.9	-1.6 ± 1.4	17
Unstable						
R158A	$+\pi$	ATP/ADP	adenine base	33.2 ± 1.3	5.1 ± 1.6	12
T56A	$+\text{coord}$	---	Mg^{2+} cation	29.2 ± 0.9	7.0 ± 1.5	15
K55A	$+\text{coord via H-bond}$	ATP/ADP APS/PAPS	β -phosphate/3'-phosphate	28.1 ± 0.8	8.5 ± 1.5	14

energies between -10 kJ/mol and 0 kJ/mol are referred to as marginally stable mutants, in accordance with a recent definition (Pastore et al., 2019), and mutants with a ΔG_f^0 energy of more than 0 kJ/mol are referred to as unstable (Figure 2B, see Table 1).

Alanine-scanning of hydrogen bonding, which we expected to have a small impact on affinity changes upon deletion, showed largely varying protein stabilities. The stable mutants R96A, N99A and S197A show ΔG_f^0 values in a range of -15 to -13 kJ/mol, being more stable than the wild type. Mutants R82A and S123A do not change in their ΔG_f^0 values from the wild type. Here, the hydrogen bonds are formed via the peptide backbone or the side-chain with either the β -sulfate of APS/PAPS or the adenine bases of the nucleotides. The deletion of their interactions does seemingly not alter the affinity of the protein to its ligands and co-factor.

However, alanine variants with deleted hydrogen bonds are also found in the marginally stable energy range. Mutation S51A showed a minor destabilization with a difference of 2.4 kJ/mol to the APSK37 wild type. Mutations T57A, I122A, K161A and G174A represent a more destabilized, but still marginally stable group at physiological conditions indicated by the negative ΔG_f^0 , ranging from -3.4 to -1.6 kJ/mol. S51 interacts with the 3'-phosphate of PAPS, T57 interacts with the α -phosphate of ATP/ADP and I122 with the one of APS/PAPS via its peptide backbone, K161 with the ribose 4'-hydroxide of APS/PAPS and G174 *via* its peptide backbone with the adenine base of APS/PAPS. Surprisingly, the peptide backbone interactions with the α -phosphate and APS/PAPS adenine base via I122 and G174 result in a pronounced destabilization, which we did not expect to occur from exchanges in the side-chains. The effects must therefore be

connected to the gain (I122A) or loss (G174A) of flexibility and the consequences for the structural integrity of the APS/PAPS binding-site. Here, the interactions of marginally stable H-bonds residing close to the center of catalysis, the transfer of the γ -phosphate of ATP onto the 3' hydroxide of APS, are highly stabilizing. Hence, the effect of hydrogen bonds appears to depend on the localization within the protein.

Deleted stacking interactions, occurring either as π - π stacking with the adenine base of APS/PAPS (F91, F175) or cation- π stacking with the ATP/ADP adenine base (R158), range from marginally stable to unstable. Deletion of π - π interactions differently impacts on the destabilization comparing the ΔG_f^0 values of -7.6 kJ/mol (F91A) and -3.5 kJ/mol (F175A). However, the loss of π - π interactions is overall destabilizing, making the protein marginally stable. Deletion of cation- π stacking in the ATP/ADP binding site resulted in a severe destabilization, shifting the APSK37 protein from a stable protein to an unstable one by deletion of a single protein-ligand interaction.

The cation coordination of the p-loop mutants T56 and K55 is of similar importance as the stacking interaction of R158, indicated by ΔG_f^0 values ranging from 7.0 to 8.5 kJ/mol. According to the pronounced destabilization compared to wild-type APSK37, the cation coordination within the p-loop in a direct (T56) or indirect manner via orientation of the nucleotides phosphates (K55) (Figure 2A) is crucial for protein stability. These data suggest that cation coordination within APSK37 is essential for the protein to fold.

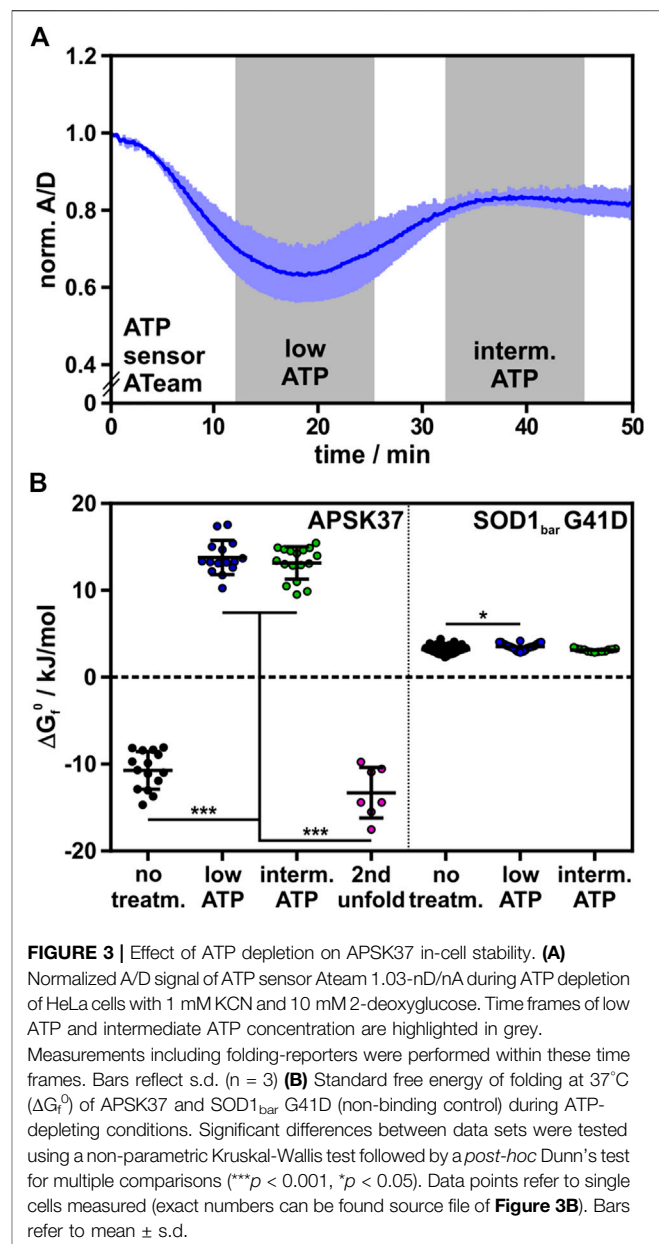
Next, we analyzed initial and final D/A values in our experiments that are representative of the initial and final conformational states of the different mutants (Supplementary Figure 5). Folded mutants (stable and marginally stable) show largely identical initial D/A values, indicative of a similar folded

fraction of protein at the beginning of the experiment (Supplementary Figure 5). The exceptions within the folded mutants are N99A and G174A. N99A shows low initial D/A values prior to the temperature jumps and similar final D/A values after temperature relaxation compared to other mutants. G174A shows low initial as well as final D/A values. This exception may be attributed to protein oligomerization prior to the experiment. Still, unfolding transitions could clearly be observed for this mutant.

In contrast to the folded mutants, we found that the unstable mutants K55A, T56A and R158A showed decreased initial (3.5 compared to 4.5 for wild-type) and final D/A values (3.5 compared to 5.2 for wild-type) (Supplementary Figure 5). Further, the determined in-cell ΔG_f^0 is smaller than 0 kJ/mol (5.1–8.7 kJ/mol), reflecting proteins which are unfolded at physiological conditions. The final D/A decreased below the initial ratio and the negative D/A response at elevated temperatures for these three mutants due to intermolecular FRET (Ebbinghaus et al., 2010; Buning et al., 2017) (Supplementary Figure 5, 6; see negative kinetic amplitudes at T larger 36°C) indicates aggregation of the respective mutants prior and during the experiment at high temperatures. Again, unfolding transitions were still observable clearly for these mutants.

We could correlate the observed changes in standard folding free energy ΔG_f^0 due to the type and localization of the deleted protein-ligand interaction with the ligand titrations of the recombinant APSK37 protein (Figure 1F). Thus, we could estimate qualitatively how the population of the enzyme devoid of substrates and possibly co-factor, single-bound and fully occupied APSK37 shifted within the cell. For the stable mutants (see Table 1), the population at the beginning of the in-cell experiment should be predominantly on the side of occupied APSK37, as stability is not affected for the stable mutants. The deletion of their interactions seemingly does not alter the affinity of the protein to its ligands and co-factor. For the marginally stable mutants (see Table 1), the ensemble of APSK37 binding states should shift towards less stable states due to a major loss in affinity. Except for T57A, all mutations are located within the APS/PAPS binding site. Therefore, the single-bound state with only the ATP/ADP binding site occupied and the Mg^{2+} cation coordinated should most likely reflect the marginally stable mutants. For the unstable mutants (see Table 1), the population of APSK37 binding-states should shift to predominantly being the state devoid of substrates. Considering the type and localization of the interactions, the loss of coordination sites for the Mg^{2+} cation does largely affect ligand binding, resulting in low affinity of all binding sites, to their respective binding partner including the cation itself.

Here we have shown by alanine-scanning that nucleotide ligands and the metal co-factor binding determine APSK37 stability in living cells at physiological substrate and co-factor concentrations. Most deleted H-bonds do not shift populations of different ligand-binding states notably towards unstable states free of bound ligands. Deletion of stronger interactions, such as π - π or cation- π interactions however shift the APSK37 complex towards the substrate-free state, as noted by the pronounced



destabilization. The largest effects were observed for deleted interactions necessary for cation-coordination, being the most crucial contacts to stabilize APSK37 upon ligand binding. Strikingly, the deletion of a single interaction is connected to the expected loss in affinity and results in pronounced protein destabilization, due to less protein population in ligand bound states.

ATP Depletion Strongly Destabilizes the APSK37 Kinase Domain

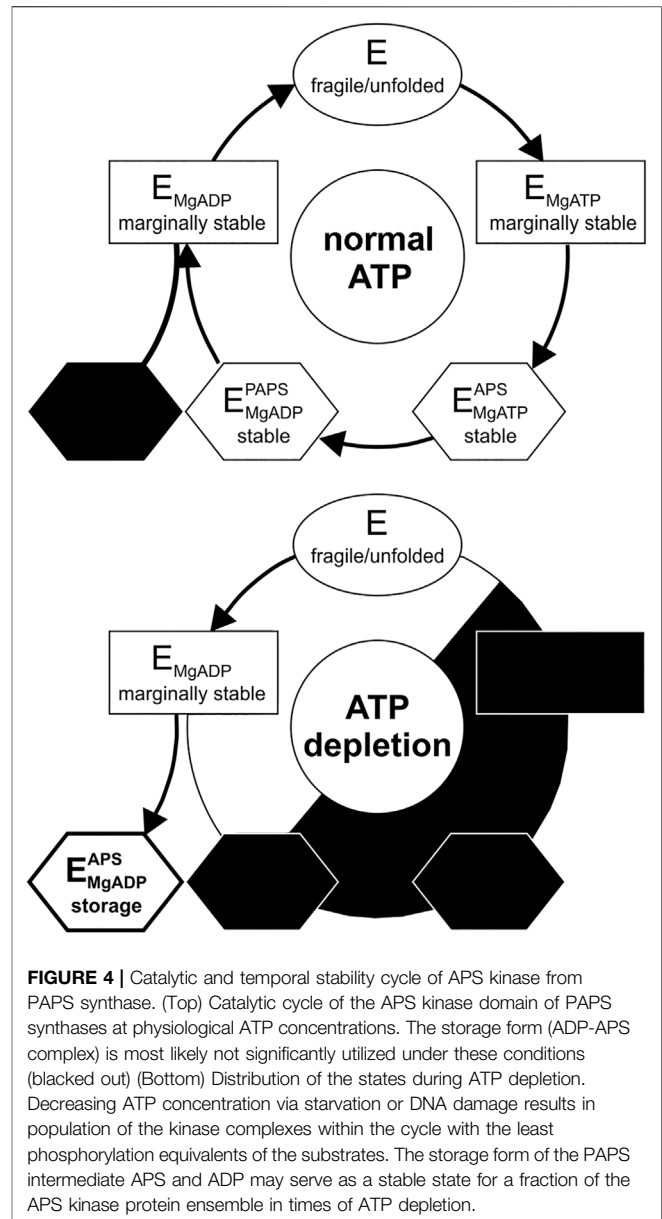
We have shown how changing the binding affinity of all ligands mutating their binding sites impacts on APSK37 stability. The catalytic cycle of PAPS synthases shows that the key determinant

for the availability of the stabilizing ligands, APS, PAPS and ADP, is ATP availability. The cellular ATP concentration, however, is prone to changes during stresses such as DNA damage (Dmitrieva et al., 2011) or cellular starvation (Maddocks et al., 2013; Petrovska et al., 2014). Depending on the nutrition or even the organelle investigated the ATP concentration may range from 8–10 mM to a low micromolar level (Imamura et al., 2009). Especially in active neurons, the ATP:ADP ratio can change on a minute timescale upon excitation from 40 to 1 (Tantama et al., 2013). For comparison, the half-life of PAPS synthases in different cell types can be up to 100 h (Mathieson et al., 2018) and therefore the APS kinase domain is necessarily affected by changing ATP concentrations due to cellular events. Therefore, we investigated how cellular ATP levels influence APSK37 stability.

We depleted HeLa cells of ATP, using potassium cyanide (KCN) and 2-deoxyglucose (2DG), to poison the oxidative phosphorylation machinery and to clear the ATP pool available for APSK37 ligand binding and nucleotide ligand synthesis (Imamura et al., 2009). The change in cellular ATP during the treatment was detected using the FRET-based ATP protein-sensor ATeam (Kotera et al., 2010). The relative ATP concentration is reported as the acceptor to donor ratio (A/D) with decreasing ratios showing reduced FRET-efficiency and release of ATP from the sensor due to decreasing cellular concentrations. Incubation with KCN and 2DG led to a rapid decrease of ATP levels inside cells followed by a regeneration phase reaching an intermediate ATP level (**Figure 3A**) as described by Imamura et al. (Imamura et al., 2009). In-cell protein stability of APSK37 was measured before and after depletion of ATP, representing high, low and intermediate ATP levels (**Figure 3A**).

Stability of wild-type APSK37 at low and intermediate cellular ATP levels did not differ significantly. Compared to untreated cells, APSK37 is destabilized by 24.5 ± 2.9 kJ/mol at low cellular ATP levels and 23.9 ± 2.9 kJ/mol for intermediate ones. The observed range of destabilization exceeded the effect of the most severe alanine mutants, which showed a destabilization up to 19.2 ± 2.7 kJ/mol for APSK37 variant K55A (**Figures 2B, 3B**). The pronounced destabilization at lowered ATP levels may be attributed to a depletion of APS and PAPS as both nucleotides are generated from ATP. At low and intermediate ATP, the accessible pool of nucleotide binding partners appears to be mostly depleted, resulting in highly destabilized APSK37 within cells.

In addition to the low-temperature unfolding event described above, we observed a second high-temperature unfolding event within ATP-depleted cells, which shows similar ΔG_r^0 energies to the wild-type at regular ATP levels (**Figure 3B**); suggestive of two distinct protein populations in the observed protein ensemble. Unfolding at low temperatures resembles the unfolding of substrate-free APSK37 protein, best approximated by the K55A mutant. As the protein stability of the wild-type APSK37, which predominantly occurs in fully occupied binding states, is comparable to the high-temperature unfolding event, this state may be attributed to a fully occupied binding state as well. Lately, the inhibitory ADP-APS complex of APSK was proposed to may serve as a storage form in



times of ATP depletion (Brylski et al., 2019). This suggests that the high-temperature event of unfolding, visible in ATP-depleted cells, may be connected to the highly stable ADP-APS-complex (**Figure 4**), which may protect the APSK from misfolding and aggregation.

We finally compared our measurements to the stability of an in-cell folding reporter that does not feature kinase activity or co-factor binding sites, the G41D mutation of the SOD1_{bar} protein (Gnutt et al., 2019b), as a control. We measured the stability of this folding reporter under the same experimental conditions and indeed found that this protein's stability is insensitive to intracellular ATP concentration. We found only a minor destabilization at low ATP levels and no significant destabilization at intermediate ones (**Figure 3B**). This shows that not the treatment with KCN and 2DG itself, but the

resulting depletion of ATP and consequently APS and PAPS is responsible for the severe destabilization of APSK37 in these measurements.

Taken together, ATP depletion caused a pronounced destabilization of the APSK37 wild-type kinase. Complementing the alanine-scanning that focused on site-directed reduction of affinity to the ligands, these data show that the stability of APSK37 is directly connected to the cellular ATP concentration and consequently the available nucleotide ligand pool.

DISCUSSION

Cells maintain abundant pools of ATP at millimolar concentrations (Traut, 1994). The necessity of such high ATP levels and their costly maintenance are not fully understood. For an enzyme like PAPS synthase where all stabilizing substrates need to be generated from ATP, stability of the enzyme is necessarily connected to the availability of ATP inside the cell. The nucleotide kinase domain of human PAPSS2, a naturally fragile protein, was the starting point for developing the FRET-based folding reporter APSK37. Using alanine-mutagenesis and ATP depletion experiments of APSK37 in living cells, we investigated the effect of ligand binding on APSK37 stability and how it is connected to cellular ATP levels.

By alanine-mutagenesis of amino acids interacting with the nucleotide ligands and the metal co-factor, the number of intermolecular interactions and ultimately affinity of APSK37 to either APS/PAPS or ATP/ADP is reduced. This allows to study the effect of ligand binding to APSK37 stability inside cells and to shift the ratios of the possible protein-ligand complexes formed towards single-bound or substrate-free form. Each alanine mutation was classified according to its ΔG_f^0 value (Figure 2B) into stable mutants, marginally stable (Pastore et al., 2019) and unstable proteins. The loss of hydrogen bonds to the nucleotide substrates results in stable and marginally stable protein. Noteworthy, half of the hydrogen bonds deleted (R82A, R96A, N99A, S123A and S197A) do not alter protein stability and most likely do not impair affinity, compared to an expected loss of binding energy of 4 kJ/mol (Davis and Teague, 1999). Alanine mutation of the other half resides close to the catalytic center (S51A, T57A, I122A, K161A and G174A) and showed surprisingly large effects. Differences in stabilization between the two sets of hydrogen bonds can be explained by the apparent gain of unwanted flexibility by reducing steric hindrance, for example affecting contacts in the cation-binding p-loop. Other mutations may lead to unwanted rigidity in the protein, leading to less stable contact formation in adjacent parts of the proteins (e.g., stacking interactions affected by G174A).

A loss of stacking interactions with the nucleotide ligands, proposed to be in the range of 16 kJ/mol (Gallivan and Dougherty, 1999; Huber et al., 2014), severely destabilizes APSK37. For the cation- π stacking interaction, the loss of binding energy translates directly into a similar loss in protein stability. Loss of π - π stacking resulted in marginally stable protein variants; however, the destabilization was less pronounced as

expected for stacking interactions. The destabilization ranged from 3.1 kJ/mol for F91A to 7.2 kJ/mol for F175A. Targeting interactions of the p-loop residues K55 and T56 with the Mg^{2+} cation translated to the largest destabilization of the protein of up to 19.2 kJ/mol (K55A).

In summary, our data showed that substrate and co-factor binding determine the APSK37 in-cell protein stability. The spread in protein stability ΔG_f^0 from -10.7 to +8.5 kJ/mol is remarkable. Considering that the effect of the solvent water on the thermodynamic stability range is unknown, these values may be a lower limit of the actual effect on the protein. They may even be more precisely determined in a homogeneous *in vitro* environment using calorimetric measurement approaches such as isothermal titration calorimetry. Still, in the heterogeneous cellular environment the effects by far exceed the changes that had been reported previously for conditions such as osmotic pressure, cellular stress or differentiation (Stadmler et al., 2017; Gnutt et al., 2019a): Hyperosmotic stress of *E. coli*, by adding 300 mM NaCl to regular buffer conditions, destabilized the expressed SH3 protein by ~4.2 kJ/mol (Stadmler et al., 2017). Cellular stress, induced by inhibition of the 26S proteasome using MG132, showed a destabilization of a SOD1-based folding reporter of ~1 kJ/mol (Gnutt et al., 2019a). The SOD1-based folding reporter was also tested with regard to protein stability in differentiated and undifferentiated PC12 cells; it did not show significant changes in the standard folding free energies, but minor changes to thermal stability and folding properties (Gnutt et al., 2019a).

When comparing *in vitro* and in-cell results for different biomolecules, cellular crowding genuinely affects in-cell stability in a range of up to 7 kJ/mol as observed for cell surface antigen VlsE (Guzman et al., 2014) or SOD1 (Danielsson et al., 2015; Gnutt et al., 2019b), which are destabilized, an RNA hairpin (Gao et al., 2016) marginally affected and PGK (Dhar et al., 2011) which is stabilized in cells. Quinary interactions, that lead to (intracellular) fifth order structure of proteins change the conformational stability by up to ~4.7 kJ/mol (Cohen and Pielak, 2016). Compared to the aforementioned cases of in-cell protein stability and their modulation by up to 7 kJ/mol, our study shows that ligand binding is a crucial factor to determine the in-cell stability of a protein, as indicated by the pronounced stability effects of 19.2 kJ/mol. It adds a novel descriptor to the recently discussed effects of quinary interactions and crowding, largely exceeding these effects in the systems studied so far. For this specific protein an interaction with its binding partners becomes stability-wise just as crucial as the induced folding of intrinsically disordered proteins by ligand binding (Fuxreiter and Peter, 2012). Ligand binding induced stability shifts will also be crucial to consider for marginally stable proteins that participate in liquid-liquid phase separation (Samanta et al., 2021).

What are the implications of the stability changes of the enzyme for the catalytic cycle? The APS kinase domain of PAPS synthase undergoes a series of ligand binding and releasing events during its catalytic cycle (Sekulic et al., 2007a; Ravilious and Jez, 2012; Brylski et al., 2019) (Figure 4A). Our in-cell results at ATP-depleted conditions show that the APS kinase

free of bound substrates is highly unstable - as we have assigned the unfolding event at $\sim 17.5^\circ\text{C}$ to this form due to its pronounced instability. Proceeding in the cycle, the kinase then preferentially binds either ATP or ADP (Ravilious and Jez, 2012) leading to a re-structuring within the otherwise flexible lid region (P151-S180) (Harjes et al., 2005; Sekulic et al., 2007b). This conformational change opens the APS/PAPS binding site for binding (Sekulic et al., 2007b). The severe destabilization of the R158A as well as the T56A and K55A mutations (**Figure 2B**) show, that the occupation of the ATP/ADP binding site and the resulting conformational change are essential for an initial stabilization to a marginal stability level. The K55 and T56 side-chains are responsible for the Mg^{2+} cation coordination. The R158 side chain interacts via cation- π -stacking with the adenine base of ATP/ADP and has been attributed to the structuring of the lid region of APSK (Sekulic et al., 2007b). The pronounced stabilization induced by the second ligand-binding event of APS/PAPS is best explained by the additive effect of ADP and APS we have observed *in vitro* (**Figure 1F**). In summary, during the catalytic cycle the actual stability of the APSK is subjected to temporal changes ranging from intrinsically unstable in its apo-form as well as without any substrate bound to marginal and great stabilization upon substrate binding in its two nucleotide binding sites.

As ATP fuels the PAPS cycle, physiological ATP concentrations will keep the PAPS synthase fraction in stable binding conformations, while ATP depletion should shift these fractions to less stable ones (**Figure 4**). Further, the intrinsic instability of the protein devoid of substrates and single-bound ligand complexes also sheds new light on the inhibitory PAPS synthase complex with ADP and APS bound (Brylski et al., 2019). The complex might not have only evolved as an inhibitory complex regulating activity but in addition may serve as a stable storage form of the APS kinase during ATP depletion (Brylski et al., 2019). The proposed storage complex is also a less ATP-dependent conformation in which effectively ADP and APS show only three phosphorylation equivalents, compared to ATP-APS and ADP-PAPS complexes having one more phosphorylation equivalent. The second unfolding event that we observed at high temperatures during ATP depletion of cells indicates that the ADP-APS binding conformation may be maintained for a fraction of the protein in cells at times of low ATP levels.

Temporal stability changes and control over pathways by ligand concentration changes are factors to consider when it comes to the properties of marginally stable proteins, such as PAPS synthases, inside cells. As the APS kinase plays a crucial role in the generation of the unique activated sulfate PAPS and catalyzes the rate-limiting step in PAPS biosynthesis (Grum et al., 2010), the temporal stability changes during the catalytic cycle and changing cellular ATP concentration observed suggest that sulfation pathways may be regulated by intracellular ATP levels. Decreasing ATP concentration under starvation or stress may destabilize key ATP-dependent enzymes to slow down metabolic activity. Thereby, the abundance of ATP in cells may be utilized to maintain ATP levels beyond what is needed for energy supply and to use it to additionally control metabolic activity. The excess pool may be used to stabilize proteins such as PAPS synthases and provide a 'regulatory buffer' in which ATP changes may be tolerated by cells.

In summary, we show APS kinase (APSK) stability and therefore its activity is highly determined by several factors including ligand binding capability and intracellular ATP levels. We engineered the FRET-based folding sensor APSK37 and used it for alanine-scanning mutagenesis of the ligand binding site. This revealed that the potential protein-ligand complexes have different impact on the overall protein stability. Further, pharmacological in-cell depletion of ATP levels inside cells confirmed, that APSK stability is directly connected to the accessible ATP as all ligands binding to APSK are generated from it. This connection has major implications for the catalytic cycle of the APSK kinase enzyme, which experiences significant changes in its stability during catalysis. The second unfolding event observed, suggests that in times of ATP depletion, the inhibitory ADP-APS complex may still be populated as a storage form to protect a fraction of APSK from aggregation and degradation. Our results show that the stability of catalytically active proteins inside cells may be primarily determined by ligand and co-factor binding, in addition to crowding effects and quinary interactions that determine the in-cell stability of proteins. This suggests a novel regulatory layer of catalytic activity by co-factor and ligand dependent stability regulation of the involved enzymes. This idea may be particularly applicable to enzymes that show marginal stability in the cell and are highly stabilized by ligand binding. The proposed mechanism will initiate further studies on different kinases and their associated regulatory complexes.

DATA AVAILABILITY STATEMENT

The original contributions presented in the study are included in the article/**Supplementary Material**, further inquiries can be directed to the corresponding authors.

AUTHOR CONTRIBUTIONS

OB designed and performed experiments, analyzed data and wrote the paper; PG, PS, and DG performed experiments; JM and SE designed experiments, analyzed data and wrote the paper.

FUNDING

We acknowledge funding from the Cluster of Excellence RESOLV (EXC 1069). OB was supported by the Graduate School of Solvation Science (Ruhr University Bochum). JM was supported by the European Commission Marie Curie Fellowship SUPA-HD (625451) and the Biochemical Society UK (Eric Reid Fund).

SUPPLEMENTARY MATERIAL

The Supplementary Material for this article can be found online at: <https://www.frontiersin.org/articles/10.3389/fmolb.2021.790304/full#supplementary-material>

REFERENCES

- Bonora, M., Patergnani, S., Rimessi, A., De Marchi, E., Suski, J. M., Bononi, A., et al. (2012). ATP Synthesis and Storage. *Purinergic Signal.* 8, 343–357. doi:10.1007/s11302-012-9305-8
- Borgia, A., Borgia, M. B., Bugge, K., Kissling, V. M., Heidarsson, P. O., Fernandes, C. B., et al. (2018). Extreme Disorder in an Ultrahigh-Affinity Protein Complex. *Nature* 555, 61–66. doi:10.1038/nature25762
- Bryliski, O., Ebbinghaus, S., and Mueller, J. W. (2019). Melting Down Protein Stability: PAPS Synthase 2 in Patients and in a Cellular Environment. *Front. Mol. Biosci.* 6, 31. doi:10.3389/fmolb.2019.00031
- Büning, S., Sharma, A., Vachharajani, S., Newcombe, E., Ormsby, A., Gao, M., et al. (2017). Conformational Dynamics and Self-Association of Intrinsically Disordered Huntingtin Exon 1 in Cells. *Phys. Chem. Chem. Phys.* 19, 10738–10747. doi:10.1039/c6cp08167c
- Cohen, R. D., and Pielak, G. J. (2016). Electrostatic Contributions to Protein Quinary Structure. *J. Am. Chem. Soc.* 138, 13139–13142. doi:10.1021/jacs.6b07323
- Danielsson, J., Mu, X., Lang, L., Wang, H., Binolfi, A., Theillet, F.-X., et al. (2015). Thermodynamics of Protein Destabilization in Live Cells. *Proc. Natl. Acad. Sci. USA* 112, 12402–12407. doi:10.1073/pnas.1511308112
- Davis, A. M., and Teague, S. J. (1999). Hydrogen Bonding, Hydrophobic Interactions, and Failure of the Rigid Receptor Hypothesis. *Angew. Chem. Int. Ed.* 38, 736–749. doi:10.1002/(sici)1521-3773(19990315)38:6<736:aid-anie736>3.0.co;2-r
- Dhar, A., Girdhar, K., Singh, D., Gelman, H., Ebbinghaus, S., and Gruebele, M. (2011). Protein Stability and Folding Kinetics in the Nucleus and Endoplasmic Reticulum of Eucaryotic Cells. *Biophysical J.* 101, 421–430. doi:10.1016/j.bpj.2011.05.071
- Dmitrieva, N. I., Cui, K., Kitchaev, D. A., Zhao, K., and Burg, M. B. (2011). DNA Double-Strand Breaks Induced by High NaCl Occur Predominantly in Gene Deserts. *Proc. Natl. Acad. Sci.* 108, 20796–20801. doi:10.1073/pnas.1114677108
- Ebbinghaus, S., Dhar, A., McDonald, J. D., and Gruebele, M. (2010). Protein Folding Stability and Dynamics Imaged in a Living Cell. *Nat. Methods* 7, 319–323. doi:10.1038/nmeth.1435
- Feng, R., Gruebele, M., and Davis, C. M. (2019). Quantifying Protein Dynamics and Stability in a Living Organism. *Nat. Commun.* 10, 1179. doi:10.1038/s41467-019-09088-y
- Fuxreiter, M., and Tompa, P. (2012). Fuzzy Complexes: a More Stochastic View of Protein Function. *Fuzziness* 725, 1–14. doi:10.1007/978-1-4614-0659-4_1
- Gallivan, J. P., and Dougherty, D. A. (1999). Cation- π Interactions in Structural Biology. *Proc. Natl. Acad. Sci.* 96, 9459–9464. doi:10.1073/pnas.96.17.9459
- Gao, M., Gnut, D., Orban, A., Appel, B., Righetti, F., Winter, R., et al. (2016). RNA Hairpin Folding in the Crowded Cell. *Angew. Chem. Int. Ed.* 55, 3224–3228. doi:10.1002/anie.201510847
- Gesteira, T. F., Marforio, T. D., Mueller, J. W., Calvaresi, M., and Coulson-Thomas, V. J. (2021). Structural Determinants of Substrate Recognition and Catalysis by Heparan Sulfate Sulfotransferases. *ACS Catal.* 11, 10974–10987. doi:10.1021/acscatal.1c03088
- Girdhar, K., Scott, G., Chemla, Y. R., and Gruebele, M. (2011). Better Biomolecule Thermodynamics from Kinetics. *J. Chem. Phys.* 135, 015102. doi:10.1063/1.3607605
- Gnut, D., Sistemich, L., and Ebbinghaus, S. (2019a). Protein Folding Modulation in Cells Subject to Differentiation and Stress. *Front. Mol. Biosci.* 6, 38. doi:10.3389/fmolb.2019.00038
- Gnut, D., Timr, S., Ahlers, J., König, B., Manderfeld, E., Heyden, M., et al. (2019b). Stability Effect of Quinary Interactions Reversed by Single Point Mutations. *J. Am. Chem. Soc.* 141, 4660–4669. doi:10.1021/jacs.8b13025
- Grum, D., Van Den Boom, J., Neumann, D., Matena, A., Link, N. M., and Mueller, J. W. (2010). A Heterodimer of Human 3'-Phospho-Adenosine-5'-Phosphosulphate (PAPS) Synthases Is a New Sulphate Activating Complex. *Biochem. Biophysical Res. Commun.* 395, 420–425. doi:10.1016/j.bbrc.2010.04.039
- Günal, S., Hardman, R., Kopriva, S., and Mueller, J. W. (2019). Sulfation Pathways from Red to green. *J. Biol. Chem.* 294, 12293–12312. doi:10.1074/jbc.rev119.007422
- Guzman, I., Gelman, H., Tai, J., and Gruebele, M. (2014). The Extracellular Protein VlsE Is Destabilized inside Cells. *J. Mol. Biol.* 426, 11–20. doi:10.1016/j.jmb.2013.08.024
- Harjes, S., Bayer, P., and Scheidig, A. J. (2005). The crystal Structure of Human PAPS Synthetase 1 Reveals Asymmetry in Substrate Binding. *J. Mol. Biol.* 347, 623–635. doi:10.1016/j.jmb.2005.01.005
- Hayes, M. H., Peuchen, E. H., Dovichi, N. J., and Weeks, D. L. (2018). Dual Roles for ATP in the Regulation of Phase Separated Protein Aggregates in Xenopus Oocyte Nucleoli. *Elife* 7, e35224. doi:10.7554/eLife.35224
- Huber, R. G., Margreiter, M. A., Fuchs, J. E., Von Grafenstein, S., Tautermann, C. S., Liedl, K. R., et al. (2014). Heteroaromatic π -Stacking Energy Landscapes. *J. Chem. Inf. Model.* 54, 1371–1379. doi:10.1021/ci500183u
- Iida, A., Simsek-Kiper, P. Ö., Mizumoto, S., Hoshino, T., Elcioglu, N., Horemuzova, E., et al. (2013). Clinical and Radiographic Features of the Autosomal Recessive Form of Brachyolmia Caused by PAPSS2 Mutations. *Hum. Mutat.* 34, 1381–1386. doi:10.1002/humu.22377
- Imamura, H., Huynh Nhat, K. P., Togawa, H., Saito, K., Iino, R., Kato-Yamada, Y., et al. (2009). Visualization of ATP Levels inside Single Living Cells with Fluorescence Resonance Energy Transfer-Based Genetically Encoded Indicators. *Pnas* 106, 15651–15656. doi:10.1073/pnas.0904764106
- Kotera, I., Iwasaki, T., Imamura, H., Noji, H., and Nagai, T. (2010). Reversible Dimerization of Aequorea victoria Fluorescent Proteins Increases the Dynamic Range of FRET-Based Indicators. *ACS Chem. Biol.* 5, 215–222. doi:10.1021/cb900263z
- Kurima, K., Warman, M. L., Krishnan, S., Domowicz, M., Krueger, R. C., Jr., Deyrup, A., et al. (1998). A Member of a Family of Sulfate-Activating Enzymes Causes Murine Brachymorphism. *Proc. Natl. Acad. Sci.* 95, 8681–8685. doi:10.1073/pnas.95.15.8681
- Leipe, D. D., Koonin, E. V., and Aravind, L. (2003). Evolution and Classification of P-Loop Kinases and Related Proteins. *J. Mol. Biol.* 333, 781–815. doi:10.1016/j.jmb.2003.08.040
- Luque, I., Levitt, S. A., and Freire, E. (2002). The Linkage between Protein Folding and Functional Cooperativity: Two Sides of the Same coin. *Annu. Rev. Biophys. Biomol. Struct.* 31, 235–256. doi:10.1146/annurev.biophys.31.082901.134215
- Maddocks, O. D. K., Berkers, C. R., Mason, S. M., Zheng, L., Blyth, K., Gottlieb, E., et al. (2013). Serine Starvation Induces Stress and P53-dependent Metabolic Remodelling in Cancer Cells. *Nature* 493, 542–546. doi:10.1038/nature11743
- Mathieson, T., Franken, H., Kosinski, J., Kurzawa, N., Zinn, N., Sweetman, G., et al. (2018). Systematic Analysis of Protein Turnover in Primary Cells. *Nat. Commun.* 9 (1), 689. doi:10.1038/s41467-018-03106-1
- McConkey, E. H. (1982). Molecular Evolution, Intracellular Organization, and the Quinary Structure of Proteins. *Proc. Natl. Acad. Sci.* 79, 3236–3240. doi:10.1073/pnas.79.10.3236
- Mueller, J. W., Idkowiak, J., Gesteira, T. F., Vallet, C., Hardman, R., Van Den Boom, J., et al. (2018). Human DHEA Sulfation Requires Direct Interaction between PAPS Synthase 2 and DHEA Sulfotransferase SULT2A1. *J. Biol. Chem.* 293, 9724–9735. doi:10.1074/jbc.ra118.002248
- Mueller, J. W., and Shafqat, N. (2013). Adenosine-5'-phosphosulfate - a Multifaceted Modulator of Bifunctional 3'-Phospho-Adenosine-5'-Phosphosulfate Synthases and Related Enzymes. *FEBS J.* 280, 3050–3057. doi:10.1111/febs.12252
- Noordam, C., Dhir, V., Mcnelis, J. C., Schlereth, F., Hanley, N. A., Krone, N., et al. (2009). Inactivating PAPSS2 Mutations in a Patient with Premature Pubarche. *N. Engl. J. Med.* 360, 2310–2318. doi:10.1056/nejmoa0810489
- Oostdijk, W., Idkowiak, J., Mueller, J. W., House, P. J., Taylor, A. E., O'reilly, M. W., et al. (2015). PAPSS2 Deficiency Causes Androgen Excess via Impaired DHEA Sulfation-In Vitro and In Vivo Studies in a Family Harboring Two Novel PAPSS2 Mutations. *J. Clin. Endocrinol. Metab.* 100, E672–E680. doi:10.1210/jc.2014-3556
- Pastore, A., Martin, S. R., and Temussi, P. A. (2019). Generalized View of Protein Folding: In Medio Stat Virtus. *J. Am. Chem. Soc.* 141, 2194–2200. doi:10.1021/jacs.8b10779
- Patel, A., Malinowska, L., Saha, S., Wang, J., Alberti, S., Krishnan, Y., et al. (2017). ATP as a Biological Hydrotrope. *Science* 356, 753–756. doi:10.1126/science.aaf6846
- Patron, N. J., Durnford, D. G., and Kopriva, S. (2008). Sulfate Assimilation in Eukaryotes: Fusions, Relocations and Lateral Transfers. *BMC Evol. Biol.* 8, 39. doi:10.1186/1471-2148-8-39

- Petrovska, I., Nuske, E., Munder, M. C., Kulasegaran, G., Malinowska, L., Kroschwald, S., et al. (2014). Filament Formation by Metabolic Enzymes Is a Specific Adaptation to an Advanced State of Cellular Starvation. *Elife* 3, e02409. doi:10.7554/eLife.02409
- Rabeh, W. M., Nedyalkova, L., Ismail, S., Park, H., Arrowsmith, C., Edwards, A., et al. (2005). *Crystal Structure of the Kinase Domain of PAPSS2*.
- Ravilious, G. E., and Jez, J. M. (2012). Nucleotide Binding Site Communication in *Arabidopsis thaliana* Adenosine 5'-Phosphosulfate Kinase. *J. Biol. Chem.* 287, 30385–30394. doi:10.1074/jbc.m112.387001
- Samanta, N., Ribeiro, S. S., Becker, M., Laborie, E., Pollak, R., Timr, S., et al. (2021). Sequestration of Proteins in Stress Granules Relies on the In-Cell but Not the *In Vitro* Folding Stability. *J. Am. Chem. Soc.* 143, 19909–19918. doi:10.1021/jacs.1c09589
- Schröder, E., Gebel, L., Ereemeev, A. A., Morgner, J., Grum, D., Knauer, S. K., et al. (2012). Human PAPS Synthase Isoforms Are Dynamically Regulated Enzymes with Access to Nucleus and Cytoplasm. *PLoS One* 7, e29559. doi:10.1371/journal.pone.0029559
- Sekulic, N., Dietrich, K., Paarmann, I., Ort, S., Konrad, M., and Lavie, A. (2007a). Elucidation of the Active Conformation of the APS-Kinase Domain of Human PAPS Synthetase 1. *J. Mol. Biol.* 367, 488–500. doi:10.1016/j.jmb.2007.01.025
- Sekulic, N., Konrad, M., and Lavie, A. (2007b). Structural Mechanism for Substrate Inhibition of the Adenosine 5'-Phosphosulfate Kinase Domain of Human 3'-Phosphoadenosine 5'-Phosphosulfate Synthetase 1 and its Ramifications for Enzyme Regulation. *J. Biol. Chem.* 282, 22112–22121. doi:10.1074/jbc.m701713200
- Stadtmiller, S. S., Gorensek-Benitez, A. H., Guseman, A. J., and Pielak, G. J. (2017). Osmotic Shock Induced Protein Destabilization in Living Cells and its Reversal by Glycine Betaine. *J. Mol. Biol.* 429, 1155–1161. doi:10.1016/j.jmb.2017.03.001
- Staniec, D., Ksiazek, M., Thøgersen, I. B., Enghild, J. J., Sroka, A., Bryzek, D., et al. (2015). Calcium Regulates the Activity and Structural Stability of Tpr, a Bacterial Calpain-like Peptidase. *J. Biol. Chem.* 290, 27248–27260. doi:10.1074/jbc.m115.648782
- Tantama, M., Martínez-François, J. R., Mongeon, R., and Yellen, G. (2013). Imaging Energy Status in Live Cells with a Fluorescent Biosensor of the Intracellular ATP-To-ADP Ratio. *Nat. Commun.* 4, 2550. doi:10.1038/ncomms3550
- Traut, T. W. (1994). Physiological Concentrations of Purines and Pyrimidines. *Mol. Cell Biochem* 140, 1–22. doi:10.1007/bf00928361
- van den Boom, J., Heider, D., Martin, S. R., Pastore, A., and Mueller, J. W. (2012). 3'-Phosphoadenosine 5'-Phosphosulfate (PAPS) Synthases, Naturally Fragile Enzymes Specifically Stabilized by Nucleotide Binding. *J. Biol. Chem.* 287, 17645–17655. doi:10.1074/jbc.m111.325498
- Vöpel, T., Scholz, R., Davico, L., Gross, M., Büning, S., Kareth, S., et al. (2015). Infrared Laser Triggered Release of Bioactive Compounds from Single Hard Shell Microcapsules. *Chem. Commun.* 51, 6913–6916. doi:10.1039/c4cc09745a
- Wirth, A. J., Platkov, M., and Gruebele, M. (2013). Temporal Variation of a Protein Folding Energy Landscape in the Cell. *J. Am. Chem. Soc.* 135, 19215–19221. doi:10.1021/ja4087165
- Zimmerman, S. B., and Trach, S. O. (1991). Estimation of Macromolecule Concentrations and Excluded Volume Effects for the Cytoplasm of *Escherichia coli*. *J. Mol. Biol.* 222, 599–620. doi:10.1016/0022-2836(91)90499-v

Conflict of Interest: The authors declare that the research was conducted in the absence of any commercial or financial relationships that could be construed as a potential conflict of interest.

Publisher's Note: All claims expressed in this article are solely those of the authors and do not necessarily represent those of their affiliated organizations, or those of the publisher, the editors and the reviewers. Any product that may be evaluated in this article, or claim that may be made by its manufacturer, is not guaranteed or endorsed by the publisher.

Copyright © 2021 Brylski, Shrestha, Gnut, Gnut, Mueller and Ebbinghaus. This is an open-access article distributed under the terms of the Creative Commons Attribution License (CC BY). The use, distribution or reproduction in other forums is permitted, provided the original author(s) and the copyright owner(s) are credited and that the original publication in this journal is cited, in accordance with accepted academic practice. No use, distribution or reproduction is permitted which does not comply with these terms.



A Sulfuryl Group Transfer Strategy to Selectively Prepare Sulfated Steroids and Isotopically Labelled Derivatives

Jaber A. Alshehri, Daniel M. Gill and Alan M. Jones *

Molecular Synthesis Laboratory, School of Pharmacy, Institute of Clinical Sciences, University of Birmingham, Edgbaston, United Kingdom

OPEN ACCESS

Edited by:

Tarsis G Ferreira,
University of Houston, United States

Reviewed by:

Jozef Stec,
Marshall B. Ketchum University,
United States
Malcolm McLeod,
Australian National University,
Australia
Fernando Ogata,
Federal University of São Paulo, Brazil

*Correspondence:

Alan M. Jones
a.m.jones.2@bham.ac.uk

Specialty section:

This article was submitted to
Cellular Biochemistry,
a section of the journal
Frontiers in Molecular Biosciences

Received: 14 September 2021

Accepted: 15 November 2021

Published: 24 December 2021

Citation:

Alshehri JA, Gill DM and Jones AM
(2021) A Sulfuryl Group Transfer
Strategy to Selectively Prepare
Sulfated Steroids and Isotopically
Labelled Derivatives.
Front. Mol. Biosci. 8:776900.
doi: 10.3389/fmolb.2021.776900

The treatment of common steroids: estrone, estradiol, cortisol, and pregnenolone with tributylsulfoammonium betaine (TBSAB) provides a convenient chemoselective conversion of the steroids alcohol/phenol moiety to the corresponding steroidal organosulfate. An important feature of the disclosed methodology is the millimolar scale of the reaction, and the isolation of the corresponding steroid sulfates as their biologically relevant sodium salts without the need for ion-exchange chromatography. The scope of the method was further explored in the estradiol and pregnanediol steroid systems with the bis-sulfated derivatives. Ultimately, a method to install an isotopic label, deuterium (^2H) combined with estrone sulfation is a valuable tool for its mass-spectrometric quantification in biological studies.

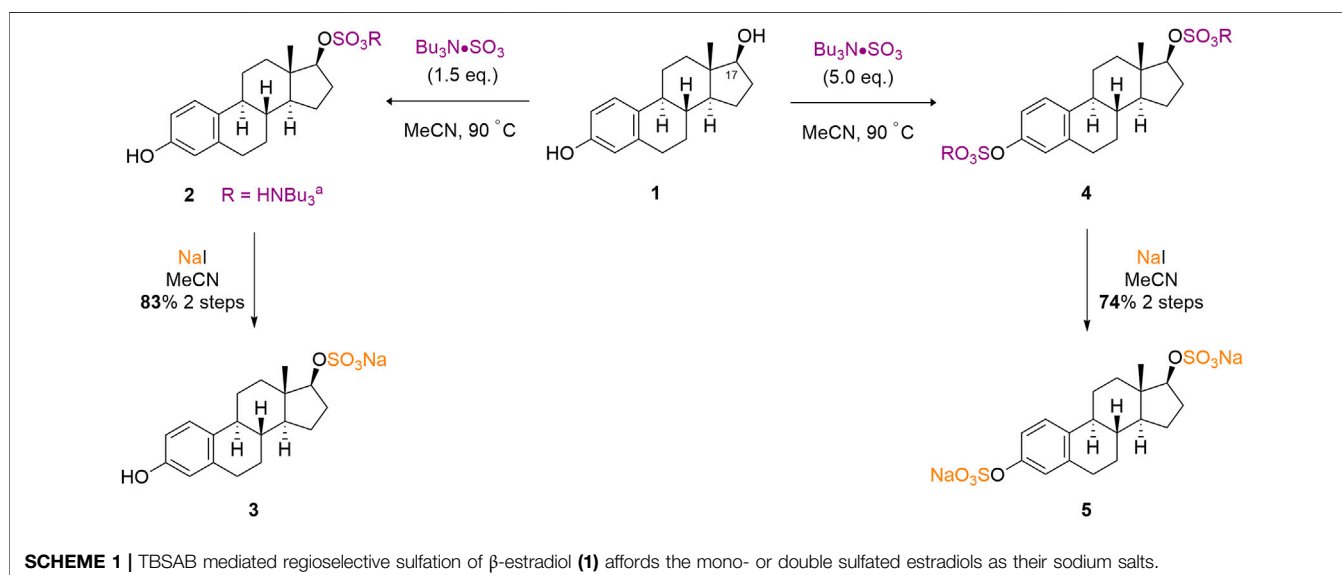
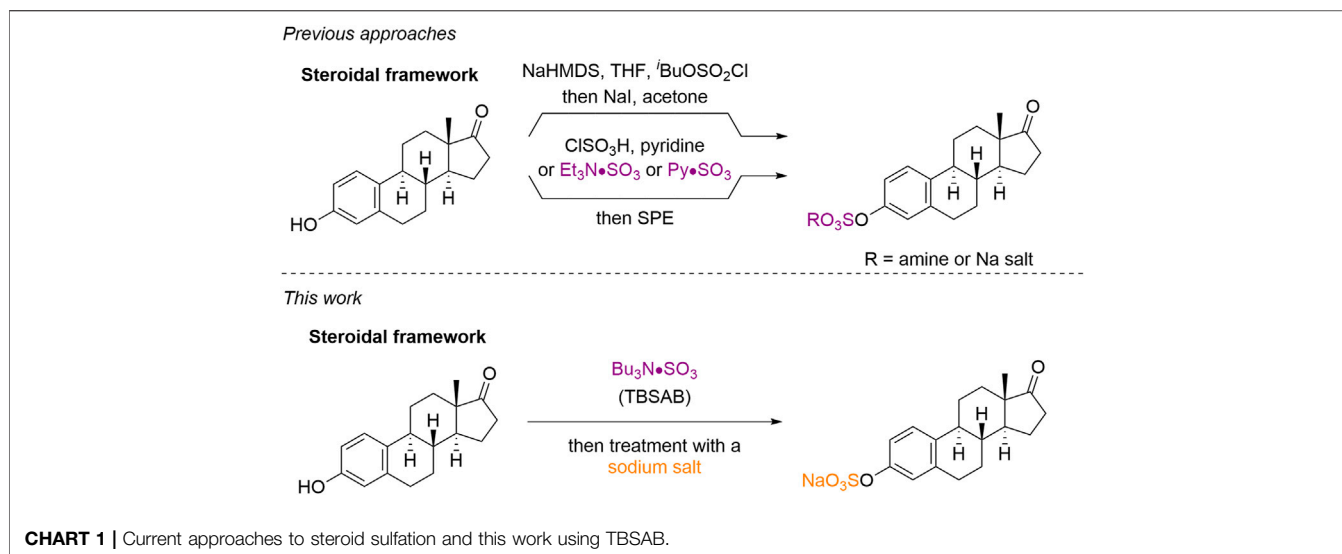
Keywords: sulfation, selectivity, isotopic labelling, sulfuryl transfer, TBSAB

INTRODUCTION

The preparation of authentic reference samples of sulfated steroids with either regioselective mono or disulfation patterns, (Lightning et al., 2021) combined with methods to isotopically label the resulting sulfated steroids is an ongoing challenge to their biological study. The resulting authentic sulfated steroids are key reference standards of paramount importance to the understanding of sulfatases (Mueller et al., 2015), (Günel et al., 2019), (Foster and Mueller, 2018), the role of steroid sulfation in diseases (Mueller et al., 2021) and the fields of detection of steroids, whether in abuse (Waller and McLeod, 2014) or in the environment, (Petrie et al., 2013) using spectroscopic techniques (Hill et al., 2019). Furthermore, the development of improved sulfation methods can be applied to both sulfated steroid containing natural products synthesis and structural elucidation studies (Hoye et al., 2007).

Current methods to sulfate steroids fall into two main categories (**Chart 1**). The use of a protected sulfate group (e.g., isobutyl protected sulfate esters) with subsequent deprotection (Simpson and Widlanski, 2006), or the use of a sulfur trioxide equivalent (e.g., chlorosulfonic acid or pyridine-sulfur trioxide complex) (Waller and McLeod, 2014), (Hungerford et al., 2006). Although these methods are effective, they suffer from the additional steps of deprotection and/or purification cascades. Issues with toxicity regarding pyridine contamination from the use of pyridine-sulfur trioxide complex in related carbohydrate scaffolds (Gabriel et al., 2020), (Vo et al., 2021) requires either an exceptionally vigilant isolation and analysis; or an improved overall method for steroid sulfation.

Our own current interest in the sulfation field derives from the development of tributylsulfoammonium betaine (TBSAB) (Gill et al., 2019a), (Jones, 2021) as a convenient one-pot method for the sulfation of heteroatom containing bioactive molecules. (Benedetti et al., 2020), (Alshehri et al., 2020) This was initiated due to challenges encountered with the purification of sulfated small molecule heparin sulfate glycomimetics (Gill et al., 2021), (Gill et al., 2019b),



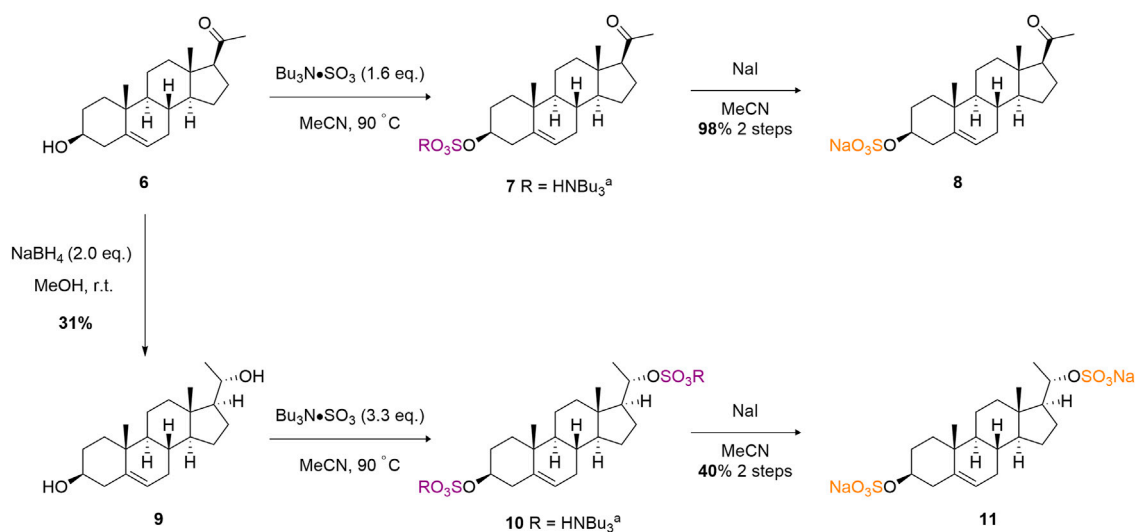
(Mahmoud et al., 2019), (Langford-Smith et al., 2019), (Mahmoud et al., 2017) with conventional, pre-existing sulfation methods. A key advantage of TBSAB over similar amine containing-sulfur trioxide complexes (e.g., triethylamine-sulfur trioxide) is the lipophilic nature of the counterion avoiding the need for ion-exchange chromatography. Herein we report our findings on the use of TBSAB as a general, scalable and regioselective sulfating reagent for steroids, and the application of TBSAB in conjugation with isotopic labelling for steroidal-organosulfate reference standards.

RESULTS AND DISCUSSION

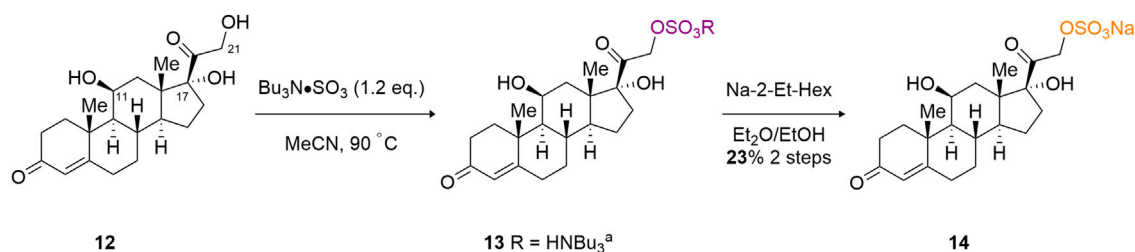
Our initial exploration of the method builds upon early screening results of TBSAB, including a single example on β-estradiol (**1**) (Gill

et al., 2019a). We firstly sought to demonstrate the reproducibility of this method on a 1.0 mmol scale, thus taking commercially available β-estradiol (**1**) and treating it with TBSAB resulted in exclusive C (17), secondary alcohol, sulfation (**2**). Furthermore the same conditions using an excess of TBSAB resulted in both C (17) sulfation and C (3), phenol, sulfation of (**4**) presumably occurs via initial C (17) alcohol sulfation in a stepwise installation. In both cases, a work-up using sodium iodide isolated the mono (**3**) and double (**5**) sulfated steroids as their sodium salts, in good yields without the risk of pyridinium ion contamination (**Scheme 1**).

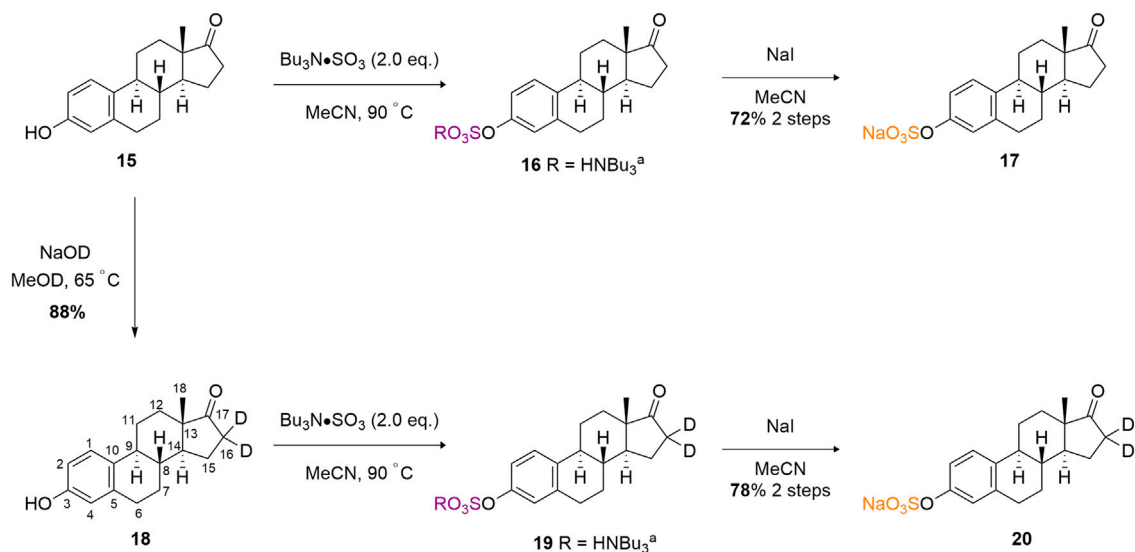
Next, we considered sulfation of a more challenging biologically active substrate, pregnenolone (**6**). (Harteneck, 2013). Under analogous conditions to the β-estradiol examples, and on a 0.3 mmol scale, steroidal sulfate **8** was afforded after sodium exchange in an excellent 98% isolated yield (**Scheme 2**). Diastereoselective reduction of the ketone



SCHEME 2 | Sulfation of the pregnenolone (**6**) and pregnandiol (**9**) steroids.



SCHEME 3 | Regioselective C (21) sulfate ester formation on cortisol (**12**).



SCHEME 4 | Estrone and estrone- d_2 sulfation using TBSAB.

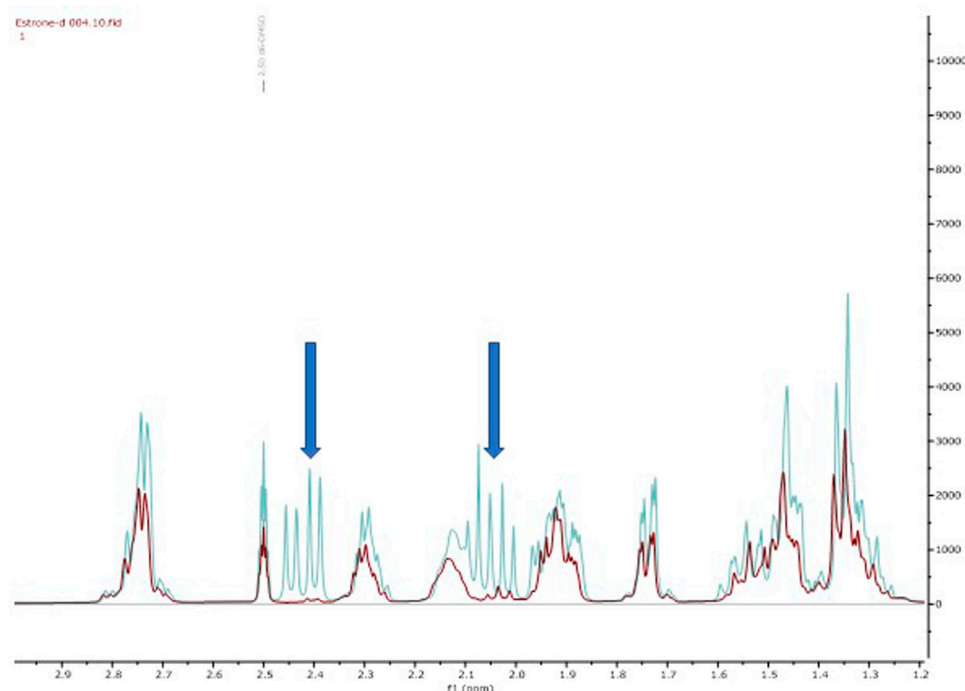


FIGURE 1 | Overlay of ^1H NMR spectra of estrone (blue, **15**) and estrone- d_2 (red, **18**) shows the diagnostic reduction of the diastereotopic C (16) protons.

moiety of pregnenolone using sodium borohydride afforded pregnanediol in 31% yield (**9**). Crystallographic data of the bulk material from d_6 -DMSO crystallisation supports the assignment of the major diastereomer as *R* at the newly set stereocentre (**Supplementary Figure S3**) (2120263 contain, 2120). As **9** contains two secondary alcohol motifs, treatment with TBSAB afforded the double sulfated pregnanediol (**11**) in a modest 40% isolated yield on a 0.6 mmol scale.

The ultimate test of the TBSAB method, in relation to regioselective sulfation, is the complex triol, cortisol (**12**) (**Scheme 3**). Cortisol contains three potentially reactive hydroxyl motifs at the C (11), C (17) and C (21) positions. It was anticipated that a regioselective sulfation of the primary C (21) alcohol would result over the C (11), secondary, or C (17), tertiary, alcohol moieties, despite the presence of the α -ketone affecting the reactivity of the C (21)-OH. To our delight, a microscale (8 mg) treatment of cortisol with TBSAB afforded the C (21) organosulfate in a modest 17% overall yield (23% based on recovered starting material) as the sodium salt (**14**). Furthermore, no unwanted C (11) or indeed C (17) sulfate ester formation was observed.

Finally, we sought to develop a proof-of-concept isotopic labelling-chemoselective sulfation method for the estrone scaffold (**15**) (**Scheme 4**). Prior to developing a deuterium labelling method at the C (16) methylene position, a model non-deuterated estrone was sulfated at the C (3) phenolic position in good 72% isolated yield as the sodium salt (**17**). A higher equivalence of TBSAB (2.0 eq) was used to ensure complete sulfation at the sole reactive C (3) phenolic centre. This provided confidence that sulfation should occur readily at

the C (3) position using TBSAB on the deuterium labeled substrate.

Firstly, we adapted the method of Rudqvist for C (19) deuteration (Rudqvist, 1983). Treatment of the estrone with NaOD in MeOD resulted in estrone- d_2 formation (**18**). The C (16)- H_2 protons were selectively deuterated by enolate formation with sodium deuteroxide and resultant deuterium incorporation by quenching the enolate with methanol- D (CH_3OD). This was confirmed via comparative 2D-NMR spectroscopic studies (see Supporting Information) but the key disappearance of the C (16) protons can be clearly observed in the ^1H -NMR spectral overlay (**Figure 1**). It should be noted that deuteration next to a carbonyl group is not usually recommended for applied quantification studies as the deuterium label could readily back exchange through a keto-enol tautomerisation leading to a loss of the label (Wudy, 1990). In our system we observed, a decline of deuterium label in solution based mass-spectrometry studies (**Supplementary Figures S1, S2**).

Finally, the treatment of estrone- d_2 with TBSAB afforded the sulfated and isotopically labelled estrone- d_2 sulfate in 78% isolated yield and 67% incorporation of the deuterium label (**20**).

CONCLUSION

In summary, we have demonstrated a general method for the synthesis of mono- or di-sulfated steroidal skeletons of importance to the fields of biology and spectroscopic detection. We have

showcased chemo-selective sulfation within a variety of complex structures, such as cortisol, and developed a simplified deuterium labeling-sulfation strategy for estrone. Overall, these approaches provide tractable routes on preparative scales to multiple sulfated steroid classes as reference compounds for detection of substances of abuse through to cancer diagnosis applications.

DATA AVAILABILITY STATEMENT

The original contributions presented in the study are included in the article/**Supplementary Materials**, further inquiries can be directed to the corresponding author. The data files can be found at the following doi: <https://doi.org/10.25500/edata.bham.00000720>.

AUTHOR CONTRIBUTIONS

Conducted experiments, spectral analysis, and revised manuscript (JA and DG); provided materials and supervision,

REFERENCES

- Alshehri, J. A., Benedetti, A. M., and Jones, A. M. (2020). A Novel Exchange Method to Access Sulfated Molecules. *Sci. Rep.* 10, 16559. doi:10.1038/s41598-020-72500-x
- Benedetti, A. M., Gill, D. M., Tsang, C. W., and Jones, A. M. (2020). Chemical Methods for N- and O-Sulfation of Small Molecules, Amino Acids and Peptides. *ChemBioChem* 21, 938–942. doi:10.1002/cbic.201900673
- CCDC 2120263 Contains the Supplementary Crystallographic Data for This Paper. These Data Can Be Obtained Free of Charge from the Cambridge Crystallographic Data Centre. Available at: www.ccdc.cam.ac.uk/data_request/cif.
- Foster, P. A., and Mueller, J. W. (2018). SULFATION PATHWAYS: Insights into Steroid Sulfation and Desulfation Pathways. *J. Mol. Endocrinol.* 61, T271–T283. doi:10.1530/JME-18-0086
- Gabriel, L., Günther, W., Pielenz, F., and Heinze, T. (2020). Determination of the Binding Situation of Pyridine in Xylan Sulfates by Means of Detailed NMR Studies. *Macromol. Chem. Phys.* 221, 1900327. doi:10.1002/macp.201900327
- Gill, D. M., Male, L., and Jones, A. M. (2019). A Structure-Reactivity Relationship of the Tandem Asymmetric Dihydroxylation on a Biologically Relevant Diene: Influence of Remote Stereocenters on Diastereofacial Selectivity. *Eur. J. Org. Chem.* 2019, 7568–7577. doi:10.1002/ejoc.201901474
- Gill, D. M., Male, L., and Jones, A. M. (2019). Sulfation Made Simple: a Strategy for Synthesising Sulfated Molecules. *Chem. Commun.* 55, 4319–4322. doi:10.1039/C9CC01057B
- Gill, D. M., R. Pavinelli, A. P., Zazeri, G., Shamir, S. A., Mahmoud, A. M., Wilkinson, F. L., et al. (2021). The Modulatory Role of Sulfated and Non-sulfated Small Molecule Heparan Sulfate-Glycomimetics in Endothelial Dysfunction: Absolute Structural Clarification, Molecular Docking and Simulated Dynamics, SAR Analyses and ADMET Studies. *RSC Med. Chem.* 12, 779–790. doi:10.1039/D0MD00366B
- Günal, S., Hardman, R., Kopriva, S., and Mueller, J. W. (2019). Sulfation Pathways from Red to green. *J. Biol. Chem.* 294, 12293–12312. doi:10.1074/jbc.REV119.007422
- Harteneck, C. (2013). Pregnenolone Sulfate: From Steroid Metabolite to TRP Channel Ligand. *Molecules* 18, 12012–12028. doi:10.3390/molecules181012012
- Hill, M., Hána, V., Velíková, M., Pařízek, A., Kolátorová, L., Vítků, J., et al. (2019). A Method for Determination of One Hundred Endogenous Steroids in Human Serum by Gas Chromatography-Tandem Mass Spectrometry. *Physiol. Res.* 68, 179–207. doi:10.33549/physiolres.934124
- Hoye, T. R., Dvornikovs, V., Fine, J. M., Anderson, K. R., Jeffrey, C. S., Muddiman, D. C., et al. (2007). Details of the Structure Determination of the Sulfated

analysed results, drafted and revised manuscript (AJ). All authors agree to be accountable for the content of the work.

ACKNOWLEDGMENTS

The authors thank the above funding bodies for supporting our research programme. The authors thank Louise Male for X-ray crystallography, Allen Bowden for HPLC analysis, Chris Williams for mass-spectroscopic studies, and Cecile Le Duff for NMR assistance. Requests for milligram samples will be considered by the authors until samples are exhausted.

SUPPLEMENTARY MATERIAL

The Supplementary Material for this article can be found online at: <https://www.frontiersin.org/articles/10.3389/fmolb.2021.776900/full#supplementary-material>

- Steroids PSDS and PADS: New Components of the Sea Lamprey (*Petromyzon marinus*) Migratory Pheromone. *J. Org. Chem.* 72, 7544–7550. doi:10.1021/jo0709571
- Hungerford, N. L., McKinney, A. R., Stenhouse, A. M., and McLeod, M. D. (2006). Selective Manipulation of Steroid Hydroxyl Groups with Boronate Esters: Efficient Access to Antigenic C-3 Linked Steroid-Protein Conjugates and Steroid Sulfate Standards for Drug Detection. *Org. Biomol. Chem.* 4, 3951–3959. doi:10.1039/b610499a
- Jones, A. M. (2021). Tributylsulfoammonium Betaine. *Encyclopaedia Reagents Org. Synth.*, 1–3. doi:10.1002/047084289X.rn02393
- Langford-Smith, A. W. W., Hasan, A., Weston, R., Edwards, N., Jones, A. M., Boulton, A. J. M., et al. (2019). Diabetic Endothelial colony Forming Cells Have the Potential for Restoration with Glycomimetics. *Sci. Rep.* 9, 2309. doi:10.1038/s41598-019-38921-z
- Lightning, T. A., Gesteira, T. F., and Mueller, J. W. (2021). Steroid Disulfates - Sulfation Double Trouble. *Mol. Cell Endocrinol.* 524, 111161. doi:10.1016/j.mce.2021.111161
- Mahmoud, A. M., Jones, A. M., Sidgwick, G., Arafat, A. M., Wilkinson, F. L., and Alexander, M. Y. (2019). Small Molecule Glycomimetics Inhibit Vascular Calcification via C-Met/Notch3/HES1 Signalling. *Cell Physiol Biochem* 53, 323–336. doi:10.33594/000000141
- Mahmoud, A. M., Wilkinson, F. L., Jones, A. M., Wilkinson, J. A., Romero, M., Duarte, J., et al. (2017). A Novel Role for Small Molecule Glycomimetics in the protection against Lipid-Induced Endothelial Dysfunction: Involvement of Akt/eNOS and Nrf2/ARE Signaling. *Biochim. Biophys. Acta (Bba) - Gen. Subjects* 1861, 3311–3322. doi:10.1016/j.bbagen.2016.08.013
- Mueller, J. W., Gilligan, L. C., Idkowiak, J., Arlt, W., and Foster, P. A. (2015). The Regulation of Steroid Action by Sulfation and Desulfation. *Endocr. Rev.* 36, 526–563. doi:10.1210/er.2015-1036
- Mueller, J. W., Vogg, N., Lightning, T. A., Weigand, I., Ronchi, C. L., Foster, P. A., et al. (2021). Steroid Sulfation in Adrenal Tumors. *J. Clin. Endocrinol. Metab.*, 106: Dgab182. doi:10.1210/clinem/dgab182
- Petrie, B., McAdam, E. J., Richards, K. H., Lester, J. N., and Cartmell, E. (2013). Application of Ultra-performance Liquid Chromatography-Tandem Mass Spectrometry for the Determination of Steroid Oestrogens in Wastewaters. *Int. J. Environ. Anal. Chem.* 93 (13), 1343–1355. doi:10.1080/03067319.2012.717272
- Rudqvist, U. (1983). Synthesis of C19 Steroid Monosulphates Labelled with Deuterium at Specific Positions. *J. Label Compd. Radiopharm.* 20, 1159–1170. doi:10.1002/jlcr.2580201005
- Simpson, L. S., and Widlanski, T. S. (2006). A Comprehensive Approach to the Synthesis of Sulfate Esters. *J. Am. Chem. Soc.* 128, 1605–1610. doi:10.1021/ja056086j
- Vo, Y., Schwartz, B. D., Onagi, H., Ward, J. S., Gardiner, M. G., Banwell, M. G., et al. (2021). A Rapid and Mild Sulfation Strategy Reveals Conformational

- Preferences in Therapeutically Relevant Sulfated Xylooligosaccharides. *Chem. Eur. J.* 27, 9830–9838. doi:10.1002/chem.202100527
- Waller, C. C., and McLeod, M. D. (2014). A Simple Method for the Small Scale Synthesis and Solid-phase Extraction Purification of Steroid Sulfates. *Steroids* 92, 74–80. doi:10.1016/j.steroids.2014.09.006
- Wudy, S. A. (1990). Synthetic Procedures for the Preparation of Deuterium-Labeled Analogs of Naturally Occurring Steroids. *Steroids* 55, 463–471. doi:10.1016/0039-128X(90)90015-4

Conflict of Interest: The authors declare that the research was conducted in the absence of any commercial or financial relationships that could be construed as a potential conflict of interest.

Publisher's Note: All claims expressed in this article are solely those of the authors and do not necessarily represent those of their affiliated organizations, or those of the publisher, the editors, and the reviewers. Any product that may be evaluated in this article, or claim that may be made by its manufacturer, is not guaranteed or endorsed by the publisher.

Copyright © 2021 Alshehri, Gill and Jones. This is an open-access article distributed under the terms of the Creative Commons Attribution License (CC BY). The use, distribution or reproduction in other forums is permitted, provided the original author(s) and the copyright owner(s) are credited and that the original publication in this journal is cited, in accordance with accepted academic practice. No use, distribution or reproduction is permitted which does not comply with these terms.



Dissecting the Role of SAL1 in Metabolizing the Stress Signaling Molecule 3'-Phosphoadenosine 5'-Phosphate in Different Cell Compartments

Natallia Ashykhmina^{1†}, Kai Xun Chan^{2,3†}, Henning Frerigmann⁴, Frank Van Breusegem^{2,3}, Stanislav Kopriva¹, Ulf-Ingo Flügge¹ and Tamara Gigolashvili^{1*}

¹Institute for Plant Sciences, Cologne Biocenter, University of Cologne, Cologne, Germany, ²Department of Plant Biotechnology and Bioinformatics, Ghent University, Ghent, Belgium, ³VIB Center for Plant Systems Biology, Ghent, Belgium, ⁴Max Planck Institute for Plant Breeding Research, Cologne, Germany

OPEN ACCESS

Edited by:

Robert David Hall,
Wageningen University and Research,
Netherlands

Reviewed by:

Charlotte Gommers,
Wageningen University and Research,
Netherlands
Eva Knoch,
Ludwig Maximilian University of
Munich, Germany

*Correspondence:

Tamara Gigolashvili
t.gigolashvili@uni-koeln.de

[†]These authors have contributed
equally to this work

Specialty section:

This article was submitted to
Metabolomics,
a section of the journal
Frontiers in Molecular Biosciences

Received: 10 September 2021

Accepted: 24 November 2021

Published: 21 January 2022

Citation:

Ashykhmina N, Chan KX,
Frerigmann H, Van Breusegem F,
Kopriva S, Flügge U-I and Gigolashvili T
(2022) Dissecting the Role of SAL1 in
Metabolizing the Stress Signaling
Molecule 3'-Phosphoadenosine 5'-
Phosphate in Different
Cell Compartments.
Front. Mol. Biosci. 8:763795.
doi: 10.3389/fmolb.2021.763795

Plants possess the most highly compartmentalized eukaryotic cells. To coordinate their intracellular functions, plastids and the mitochondria are dependent on the flow of information to and from the nuclei, known as retrograde and anterograde signals. One mobile retrograde signaling molecule is the monophosphate 3'-phosphoadenosine 5'-phosphate (PAP), which is mainly produced from 3'-phosphoadenosine 5'-phosphosulfate (PAPS) in the cytosol and regulates the expression of a set of nuclear genes that modulate plant growth in response to biotic and abiotic stresses. The adenosine bisphosphate phosphatase enzyme SAL1 dephosphorylates PAP to AMP in plastids and the mitochondria, but can also rescue *sal1 Arabidopsis* phenotypes (PAP accumulation, leaf morphology, growth, etc.) when expressed in the cytosol and the nucleus. To understand better the roles of the SAL1 protein in chloroplasts, the mitochondria, nuclei, and the cytosol, we have attempted to complement the *sal1* mutant by specifically cargoing the transgenic SAL1 protein to these four cell compartments. Overexpression of SAL1 protein targeted to the nucleus or the mitochondria alone, or co-targeted to chloroplasts and the mitochondria, complemented most aspects of the *sal1* phenotypes. Notably, targeting SAL1 to chloroplasts or the cytosol did not effectively rescue the *sal1* phenotypes as these transgenic lines accumulated very low levels of SAL1 protein despite overexpressing SAL1 mRNA, suggesting a possibly lower stability of the SAL1 protein in these compartments. The diverse transgenic SAL1 lines exhibited a range of PAP levels. The latter needs to reach certain thresholds in the cell for its impacts on different processes such as leaf growth, regulation of rosette morphology, sulfate homeostasis, and glucosinolate biosynthesis. Collectively, these findings provide an initial platform for further dissection of the role of the SAL1–PAP pathway in different cellular processes under stress conditions.

Keywords: 3'-phosphoadenosine 5'-phosphate (PAP), chloroplasts, mitochondria, nuclei, cytosol, metabolite signaling, SAL1, nucleotidase/phosphatase

1 INTRODUCTION

Eukaryotic cells are highly organized into different compartments, such as the mitochondria, the endoplasmic reticulum, peroxisomes, and the Golgi apparatus. Additionally, plant cells possess plastids, large vacuoles, and the apoplast, each with a unique set of enzymes and functions. Chloroplasts not only perform photosynthesis but also participate in the assimilation of mineral nutrients (e.g., S, N, and P) and synthesize numerous compounds, including secondary metabolites [phenylpropanoids and glucosinolates (GSLs)], fatty acids, and amino acids (Bhardwaj et al., 2015). Mitochondria are essential for cellular respiration and contribute to the generation of reactive oxygen species (ROS) (Wang et al., 2018). The major protein complexes of chloroplasts and the mitochondria are combinations of nuclear- and organelle-encoded subunits; therefore, appropriate gene expression involves a tight coordination between the nucleus and organelles. Plastids and the mitochondria produce retrograde signals that modulate nuclear gene expression and organellar biogenesis or optimize their performance (Chi et al., 2015). Many signals in organellar retrograde pathways have been identified, including chlorophyll intermediates, ROS, and other metabolites (Chan et al., 2016; Ishiga et al., 2017; Pesaresi and Kim, 2019). For example, the SAL1–PAP retrograde signaling pathway is implicated in responses to drought and high-light stresses (Estavillo et al., 2011). The retrograde signaling molecule PAP (3'-phosphoadenosine 5'-phosphate) is generated by the sulfate assimilation pathway and degraded by SAL1 into AMP and inorganic phosphate. During stress conditions, PAP accumulates, as it can no longer be degraded by the nucleotidase/phosphatase SAL1, which becomes inactivated by oxidation (Chan et al., 2016). Transcriptome analysis has also shown that SAL1 regulates an overlapping set of genes with 3' exoribonucleases (XRNs), suggesting that they function in a common signaling pathway (Estavillo et al., 2011).

The nuclear-encoded SAL1 belongs to a small family of six nucleotidase/phosphatase proteins in *Arabidopsis thaliana*, and out of these six proteins, only SAL1 contains a dual-targeting signal, which directs the protein to both the mitochondria and chloroplasts. Previous research has partly elucidated the role of SAL1 in sulfur metabolism and retrograde signaling (Lee et al., 2012; Chan et al., 2013). Several *sal1* mutant alleles have been identified by genetic screens: *fiery1* through an elevated abscisic acid (ABA) response (Xiong et al., 2001), *alx8* was identified in a screen for the elevated expression of *ASCORBATE PEROXIDASE2* at high- and low-light conditions, *fou8* possesses elevated jasmonic acid (JA) levels (Rodríguez et al., 2010), and *ron1* was isolated from a screen for mutants with aberrant vascular patterning (Robles et al., 2010) and has rounder leaves and altered auxin signaling. The *alx8* and *fry1* alleles can rescue stomatal closure in ABA-insensitive mutants, while *fou8* has a high jasmonate level (Rodríguez et al., 2010), suggesting that SAL1 regulates development and stress responses via at least three of the main phytohormone signaling pathways. Consistently, Ishiga et al. (2017) have recently shown that the SAL1–PAP pathway is

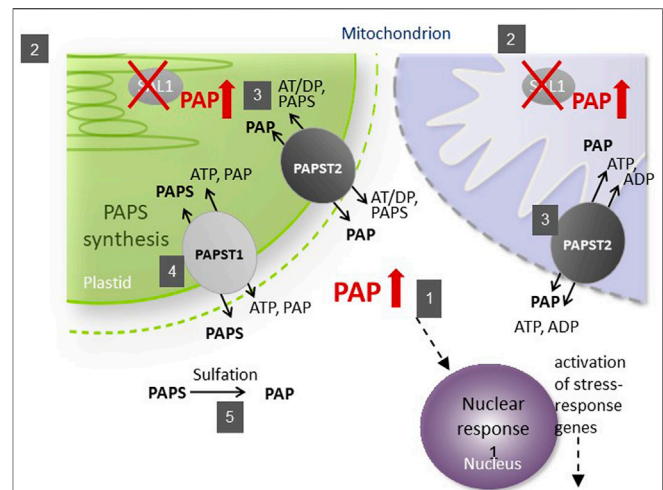


FIGURE 1 | Schematic illustration of phosphoadenosine 5'-phosphate (PAP) catabolism in the *sal1* mutant. The SAL1 (2) protein is localized to plastids and the mitochondria, where it regulates the intercellular PAP concentration (1). PAPST2 (3) and PAPST1 (4) import cytosolic PAP into the mitochondria and plastids. PAPST1 (4) delivers newly synthesized PAPS from the plastid to the cytosol in exchange for PAP. In the cytosol and the Golgi apparatus, PAPS consumption via sulfotransferases results in PAP release (5). A defect in SAL1 activity leads to PAP accumulation in these organelles, which decelerates PAP uptake. The resulting increase in cytosolic PAP induces nuclear responses and phenotypes recorded previously for *sal1* mutants.

important for the regulation of retrograde signaling in plant immunity and that the salicylic acid (SA) and JA pathways are compromised in *sal1*, thereby confirming a role for the SAL1–PAP pathway in the antagonistic interaction between SA and ABA, JA and ABA, and SA and JA.

The subcellular localization of its components is important for the function of the SAL1–PAP pathway in retrograde signaling (Figure 1). As the precursor of PAP, 3'-phosphoadenosine 5'-phosphosulfate (PAPS) is mainly synthesized in chloroplasts and transported into the cytosol by PAPST1 (Gigolashvili et al., 2012) and, to a lesser extent, by PAPST2 (Tee, 2018; Ashykhmina et al., 2019), where it is used as a sulfate donor by sulfotransferases (SOTs) for various sulfation reactions. These reactions generate PAP in the cytosol, which is then transported into chloroplasts and the mitochondria for degradation by SAL1 (Estavillo et al., 2011). Unless it is transported back into organelles, PAP regulates nuclear gene expression (Dichtl et al., 1997) and inhibits SOTs in the cytosol (Rens-Domiano and Roth, 1987), thus modulating sulfur assimilation in plant cells (Lee et al., 2012; Chan et al., 2013). To modulate the concentration of PAP in the cytosol, its transport into chloroplasts and the mitochondria is mainly mediated by PAPST2 (Ashykhmina et al., 2019) and, to a lesser extent, by PAPST1 (Gigolashvili et al., 2012).

The dual localization of SAL1 in plastids and the mitochondria and the presence of two different PAP transporters in these compartments are indicative of distinct SAL1 functions in these two compartments. For example, studies that targeted

yeast SAL1 (Sc-SAL1) to the chloroplast only (Rodríguez et al., 2010; Estavillo et al., 2011), as well as the nuclear- and cytosolic-specific expression of a truncated (missing chloroplastidic localization sequence) SAL1 construct (Kim and von Arnim 2009), complemented *sal1* mutant phenotypes to different extents. Furthermore, although the *papst1* mutant showed inhibited plant growth associated with lowered levels of PAPS and invariant levels of cellular PAP (Gigolashvili et al., 2012), the *papst2* transfer DNA (T-DNA) and artificial microRNA (amiRNA) mutant lines displayed a larger rosette than did the wild type and moderately increased PAP levels (Ashykhmina et al., 2019). Remarkably, morphological phenotypes in the high-PAP-accumulating *sal1* were partially restored to wild type in the *sal1 papst1* double mutant, coincident with a lower cytosolic PAP content and a higher chloroplastic PAP level than in *sal1*. This is due to a decrease in PAPS transport *via* PAPST1 and, consequently, a reduced PAP formation in the cytosol. In contrast, *sal1 papst2* showed an enhancement compared to the *sal1* phenotype, with higher cytosolic and chloroplastic PAP contents than *sal1*.

Collectively, the above observations suggest that PAP has complex effects on plant growth, not only depending on its dosage but also on the subcellular location. This intriguing hypothesis prompted us to deconvolute the role of SAL1 in different cell compartments by systematically expressing it in chloroplasts, the mitochondria, nuclei, and the cytosol and assessing its ability to complement the morphological, physiological, and chemical phenotypes of the *sal1* mutant (Ashykhmina et al., 2019).

2 RESULTS

2.1 Generation of Chimeric Constructs to Direct SAL1 Protein Into Different Cell Compartments

To achieve the compartment-specific accumulation of SAL1 and expression of *SAL1*, we generated six chimeric constructs (Supplementary Figure S1). Constructs *SAL1_I* to *SAL1_IV* consisted of a truncated *SAL1* (*SAL1tr*) backbone fused to various organellar targeting sequences. This *SAL1tr* backbone was previously reported to be localized to the cytosol and the nucleus and to complement the *sal1* phenotype, in the absence of organellar targets (Kim and von Arnim, 2009). *SAL1_I* was designed to express the protein exclusively in the nucleus and contained *SAL1tr* fused to a nuclear localization sequence (NLS) at the C-terminus. Construct *SAL1_II* was created to express *SAL1tr* exclusively in the cytosol and was a fusion of the *SAL1tr* backbone to the nucleus exclusion sequence (NES) from At1g07140. This NES was necessary to avoid *SAL1* localization to the nuclei, as described by Kim and von Arnim (2009). To constructs II–V, we added NES at the C-terminus of *SAL1* by incorporating it into primers by PCR. Construct *SAL1_III* was designed to express *SAL1* exclusively in plastids and consisted of *SAL1tr* fused to the chloroplast pre-sequence (cPS) of the Rubisco small subunit (SSU) at the

N-terminus and to the NES at the C-terminus. Construct *SAL1_IV* aimed to express *SAL1* exclusively in the mitochondria and contained *SAL1tr* fused to the mitochondrial pre-sequence (mPS) or transit peptide of heat shock protein 90 (Hsp90) (Krishna and Gloor, 2001) at the N-terminus and NES at the C-terminus. Construct *SAL1_V* encoded the native *SAL1* pre-sequence and full-length *SAL1* fused to the NES at the C-terminus and should target *SAL1* to plastids and the mitochondria. *SAL1tr*, as described by Kim and von Arnim (2009), was designated *SAL_VI*.

To confirm the subcellular localization of *SAL1* fusion proteins experimentally, we used *Arabidopsis* root cell suspension cultures and mesophyll protoplasts (Figure 2 and Supplementary Figure S2). Suspension cells from *Arabidopsis* roots were transformed with *Agrobacterium* carrying constructs encoding *SAL1_I*–*VI* fused to green fluorescent protein (GFP) at the C-terminus (Berger et al., 2007), and protoplasts were isolated from the mesophyll of leaves and transfected using purified plasmid DNA (Yoo et al., 2007). Fluorescence confocal microscopic analysis, shown in Figure 2 and Supplementary Figure S2, confirmed the expected localization of the transiently expressed *SAL1*_(I–VI):GFP fusion proteins in the designated compartments. DAPI staining of *Arabidopsis* root cells expressing *SAL1_I*-GFP and *SAL1_VI*-GFP (Figures 2A,F) confirmed the nuclear localization of both constructs (nuclei of cells containing both DAPI and *SAL1*-GFP are indicated by white arrows). The cytosolic localization of *SAL1_II*-GFP and *SAL1_VI*-GFP was observed in cells showing equal distribution of GFP in the cytosol (Figures 2B,F). Cells transfected with the *SAL1_VI* construct and showing *SAL1*-GFP in the cytosol are marked by red arrows (Figure 2F). The chloroplastidic localization of *SAL1_III*-GFP can be also confirmed (Figure 2C) as chlorophyll autofluorescence coincides with the GFP signal. Similarly, the mitochondrial localization of *SAL1_IV* (Figure 2D) was revealed by confirming the presence of the MitoTracker signal in the same structures as *SAL1_IV*-GFP. The GFP signal of *SAL1_V* was difficult to interpret as the expression level of this construct was weak (adjustments of levels were applied in Photoshop CS3). Nevertheless, the presence of *SAL1_V* protein in chloroplasts and in some mitochondria-like structures in the cytosol can be assumed (Figure 2E). The co-localization of *SAL1_V* with the MitoTracker was not successful as the GFP signal was too weak for this assay. Interestingly, the expression of *SAL1_V* in *Arabidopsis* suspension cells from roots, which lack chloroplasts (Supplementary Figure S2), showed intensive GFP staining in tiny mitochondria-like structures in the cytosol. In line with this observation Chen et al. (2011) and Estavillo et al. (2011) have previously demonstrated that when the full-length protein of *SAL1* is fused to GFP (similar to the *SAL1_V* construct used in this work), *SAL1* will be found in both chloroplasts and mitochondria. The only difference in the *SAL1_V* construct used in this work from that used by Chen et al. (2011) and Estavillo et al. (2011) is that our construct contained NES. However, as NES did not lead to mislocalization of constructs *SAL1_II*, *SAL1_III*, and *SAL1_IV*, the potential mislocalization of *SAL1_V*-GFP is less probable.

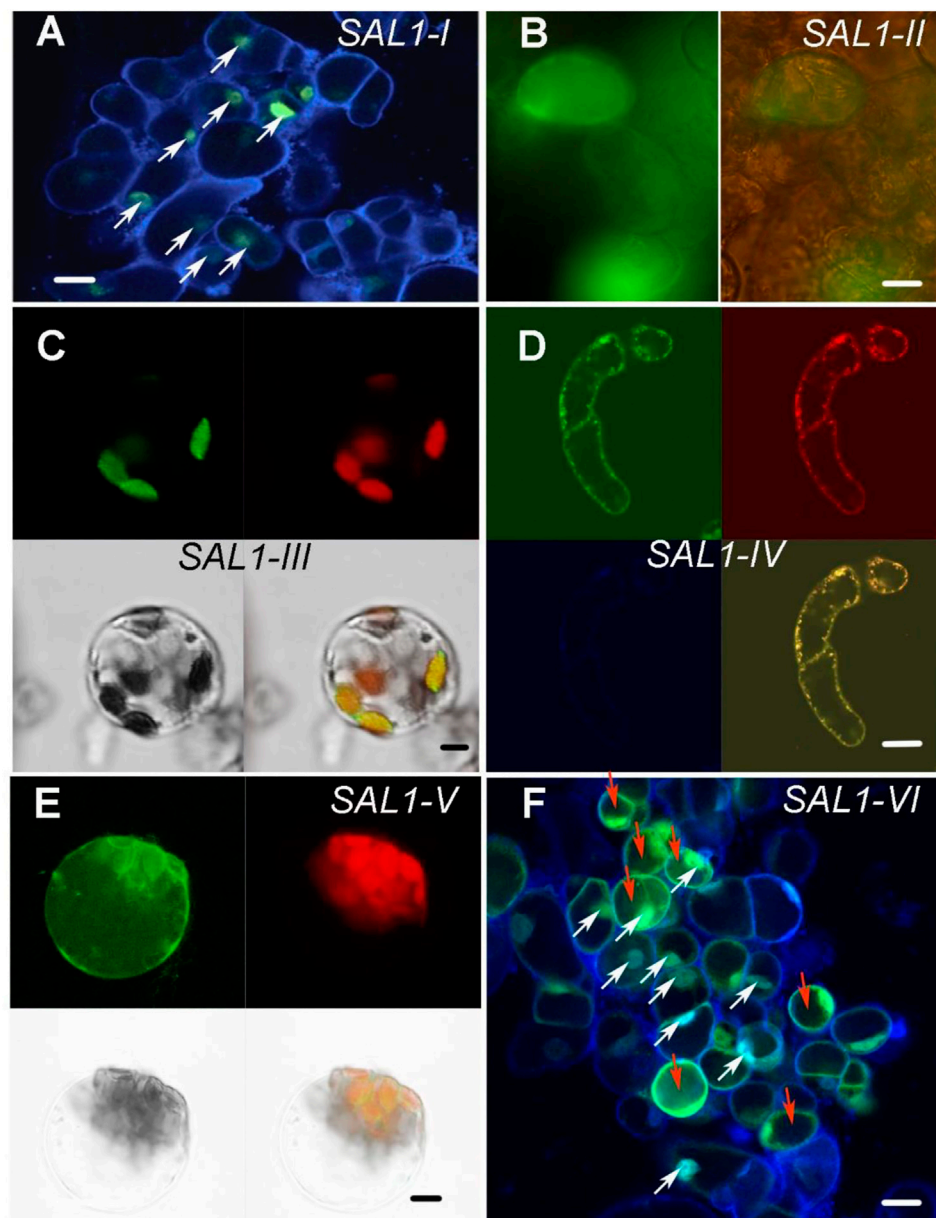
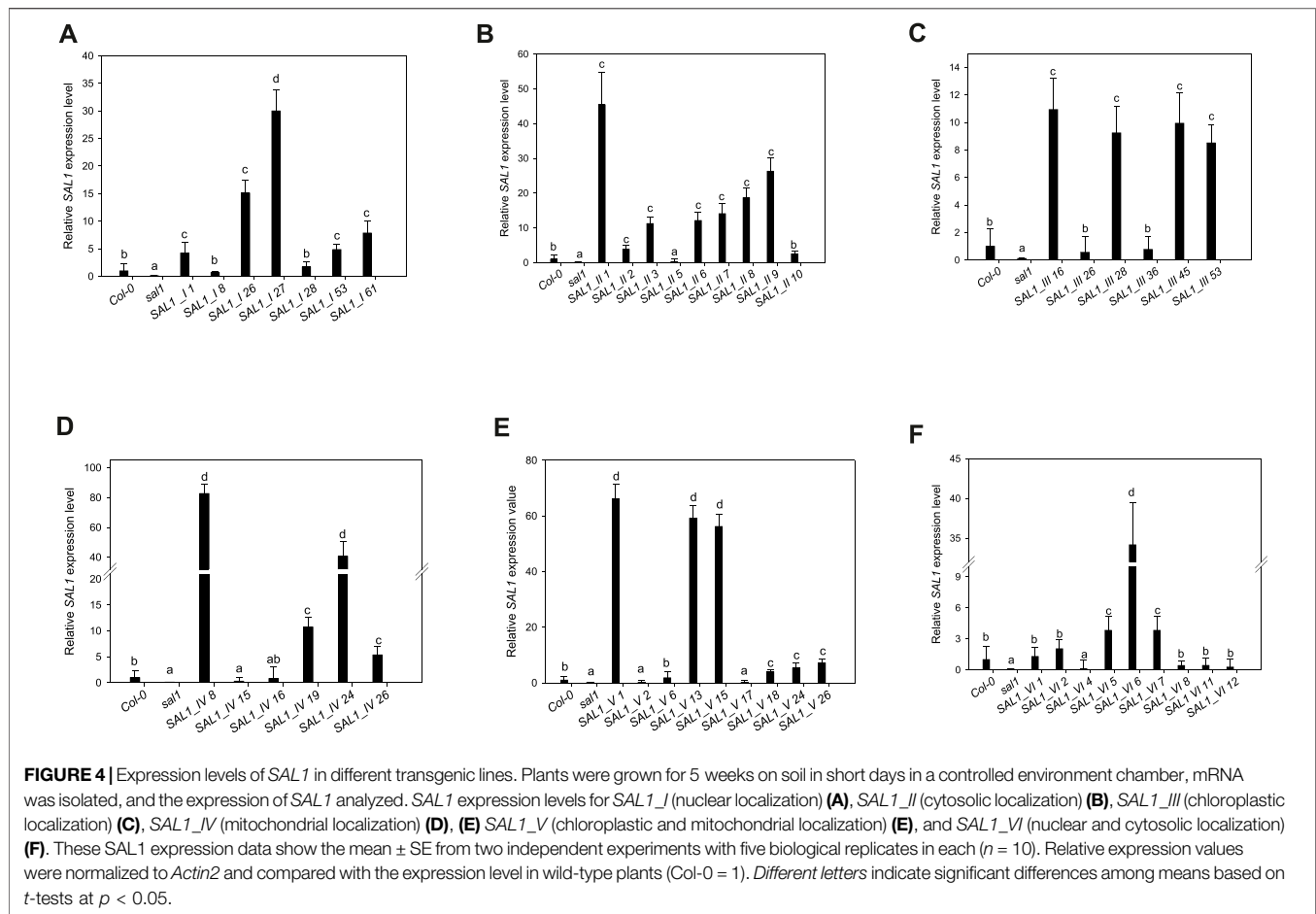


FIGURE 2 | Subcellular localization of SAL1_I–SAL1_VI proteins in *Arabidopsis* root cell suspension cultures, protoplasts from the mesophyll, and in *Nicotiana benthamiana*. Transient expression of SAL1 protein chimeras fused to green fluorescent protein (GFP) under control of the 35S *CaMV* promoter in various subcellular compartments of cells from *Arabidopsis* root cell suspension culture, as revealed by confocal fluorescence microscopy. **(A)** DAPI-stained *Arabidopsis* suspension cells form roots showing the nuclear localization of SAL1_I:GFP. White arrows show cells in which both GFP and DAPI are visible in the nuclei. Bar = 20 μ m. **(B)** Cytosolic localization of SAL1_II:GFP shown with GFP filter and bright field and GFP. Bar = 40 μ m. **(C)** Chloroplastic localization of SAL1_III:GFP in *Arabidopsis* protoplasts from the mesophyll four fields with GFP, chlorophyll autofluorescence, bright field, and overlay of GFP and chlorophyll signals. Bar = 10 μ m. **(D)** Mitochondrial localization of SAL1_IV:GFP in *Arabidopsis* suspension cells form roots four fields with GFP, MitoTracker in red, DAPI staining, and overlay of both MitoTracker with GFP. Bar = 20 μ m. **(E)** SAL1_V:GFP localization in *Arabidopsis* protoplasts from the mesophyll. It shows the presence of SAL1 in chloroplasts and in some tiny dot-like structures in the cytosol, which can be the mitochondria. Four fields show GFP, chlorophyll autofluorescence, bright field, and overlay of GFP and chlorophyll signals. Bar = 10 μ m. **(F)** DAPI-stained *Arabidopsis* suspension cells form roots, showing both the cytosolic and nuclear localization of GFP. White arrows show cells in which both GFP and DAPI are visible in the nuclei. Red arrows show cells in which GFP is visible in the cytosol. Bars = 20 μ m.



FIGURE 3 | Morphological phenotypes of plants expressing SAL1 chimeric constructs in different cell compartments. Plants were grown for 5 weeks on soil in short days in a controlled environment chamber. Bar = 2 cm. SAL1_I, nuclear localization; SAL1_II, cytosolic localization; SAL1_III, chloroplastic localization; SAL1_IV, mitochondrial localization; SAL1_V, chloroplastic and mitochondrial localization; and SAL1_VI, nuclear and cytosolic localization, which served as a positive control for the complementation (Kim and von Arnim, 2009).



2.2 Selection of Partly and Fully Complemented Transgenic Mutant Lines With Varying *SAL1* Expression Levels

To study the function of *SAL1* in different cell compartments *in planta*, *sal1* mutant plants were transformed with the respective *SAL1* chimeric constructs. We selected independent transgenic lines that showed varying *SAL1* transcript levels and that were either marginally, moderately, or fully complemented in terms of the overall rosette morphology (Figure 3). We isolated 77 independent transgenic lines for each of *SAL1_I*, *SAL1_III*, and *SAL1_IV*, 40 lines for *SAL1_V*, and 12 lines for each of *SAL1_II* and *SAL1_VI*. Although we repeated the transformation process several times, we were not able to significantly increase the number of transgenic lines for constructs *SAL1_II* and *SAL1_VI*, indicating that *SAL1* localization in the cytosol was probably not indiscriminate for the survival of transgenic plants. We then selected six to nine lines for each construct, which showed different levels of complementation. These lines were first compared to wild type and *sal1* in their visual appearance of rosette morphology, *SAL1* mRNA levels, shoot fresh weight (biomass) of fully developed 5-week-old adult plants, and PAP levels (Figures 3–5).

2.3 Complementation of PAP Levels and Biomass Following *SAL1* Expression in Different Compartments

2.3.1 Nucleus

Seven independent lines with varying *SAL1* expression levels were analyzed in detail and are presented here. The extent to which the different *sal1* phenotypes were complemented correlated well with the degree of nuclear-targeted *SAL1* transcript levels. *SAL1_I* lines 26 and 27 showed the highest *SAL1* mRNA levels at 15- to 30-fold that of the wild type (Figure 4A). Adult plants of these lines were fully complemented in terms of rosette morphology, showed higher biomass than did the wild type, and had PAP levels that were either similar to those of the wild type or significantly decreased compared to those of *sal1* (Figures 4A, 5A,G). The *SAL1_I* lines 1, 53, and 61 with moderate *SAL1* overexpression (five to eight fold higher than that of the wild type) only showed partial complementation in rosette morphology, biomass, and PAP levels, whereas lines 8 and 28 with wild-type levels of *SAL1* expression only partially complemented leaf shape, but not biomass or PAP (Figures 4A, 5A,G).

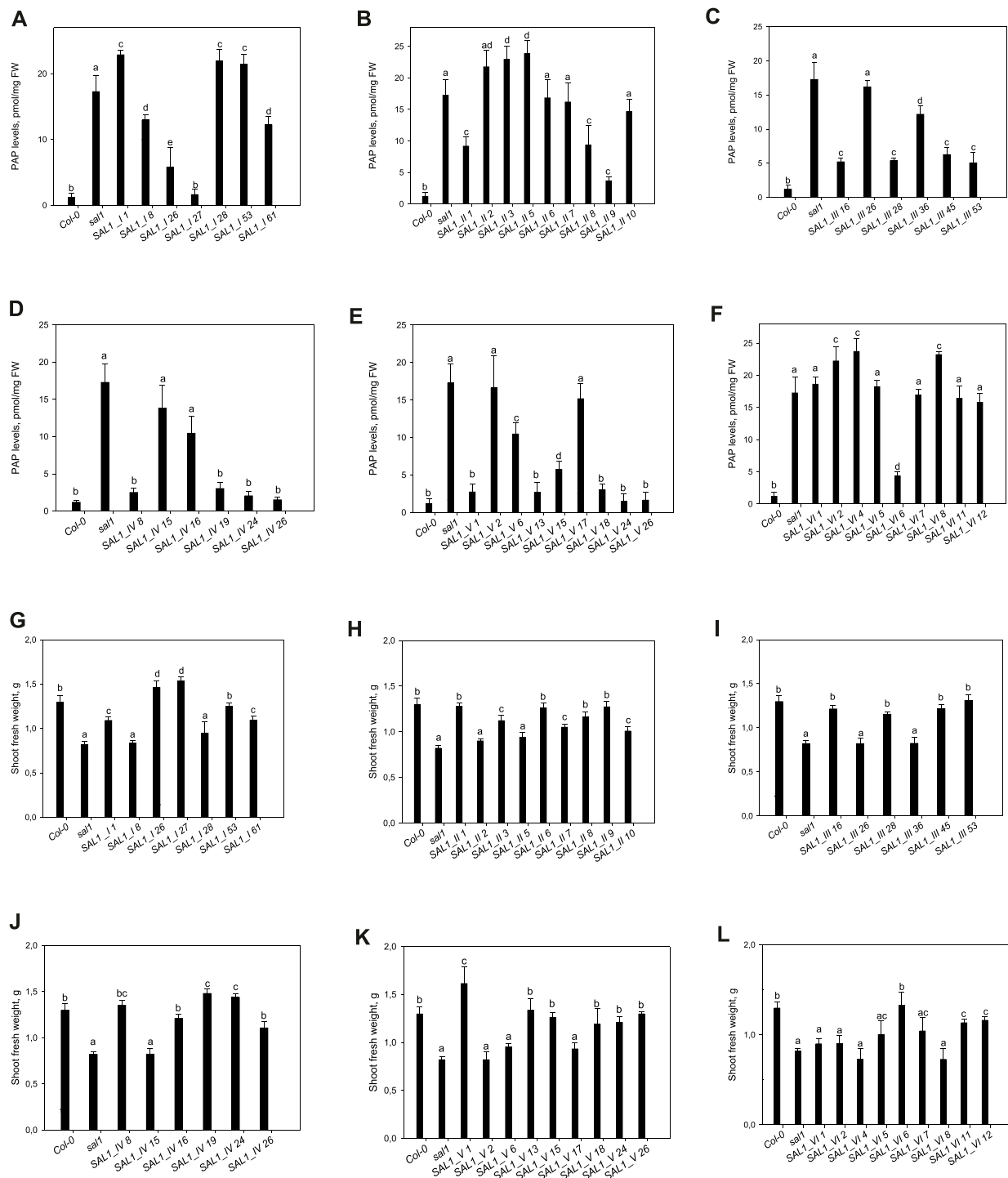


FIGURE 5 | Phosphoadenosine 5'-phosphate (PAP) levels and shoot fresh weight in *sal1* mutants with the directed expression of *SAL1* to various cell compartments. **(A–F)** PAP levels in rosette leaves of 5-week-old *SAL1* and stably transformed *sal1* transgenic plants overexpressing *SAL1* chimeric proteins. **(A)** *SAL1_I* (nuclear localization). **(B)** *SAL1_II* (cytosolic localization). **(C)** *SAL1_III* (chloroplastic localization). **(D)** *SAL1_IV* (mitochondrial localization). **(E)** *SAL1_V* (chloroplastic and mitochondrial localization). **(F)** *SAL1_VI* (nuclear and cytosolic localization). Plants were grown on soil in short days in a controlled environment chamber. Data show the mean \pm SD ($n = 3$). FW, fresh weight. Different letters indicate significant differences among means based on t -tests at $p < 0.05$. **(G–L)** Shoot fresh weight of *sal1* mutants complemented with *SAL1* expressed in different cell compartments. Shoot fresh weight of wild-type, *sal1*, and stably transformed *sal1* transgenic plants overexpressing *SAL1* chimeric proteins. **(G)** *SAL1_I* (nuclear localization). **(H)** *SAL1_II* (cytosolic localization). **(I)** *SAL1_III* (chloroplastic localization). **(J)** *SAL1_IV* (mitochondrial localization). **(K)** *SAL1_V* (chloroplastic and mitochondrial localization). **(L)** *SAL1_VI* (nuclear and cytosolic localization). Plants were grown for 4 weeks on MS agar plated under short-day conditions in an environment-controlled chamber. Data show the mean \pm SD ($n = 9$). Different letters indicate significant differences among means based on t -tests at $p < 0.05$.

2.3.2 Cytosol

Following the localization of *SAL1* to the cytosol by construct *SAL1_II*, we obtained 12 independent transgenic lines with a stable phenotype. We analyzed nine lines that showed varying levels of *SAL1* expression in detail. All lines showed only partial complementation and a disconnect between their growth/development phenotypes and PAP levels, despite high the *SAL1* expression level in several transgenic lines (*SAL1_II* 1, 3, 6, 7, 8, and 9) (Figures 4B, 5B,H). For instance, biomass was complemented to Col-0 levels in three out of nine lines (*SAL1_II* 1, 8, and 9) (Figure 5H), but both the PAP levels and morphological phenotype of these lines were intermediate between that of Col-0 and *sal1* (Figures 4B, 5B). Similarly, *SAL1_II* lines 3 and 7 showed partially complemented biomass (Figure 5H) despite accumulating similar or higher levels of PAP compared to *sal1* (Figure 5B). *SAL1_II* lines 2, 3, and 5 accumulated higher levels of PAP than did *sal1* and largely failed to restore biomass and rosette morphology (Figures 4B, 5H). This observation was similar to that for the *SAL1-I* construct (*SAL1-I* lines 1, 28, and 53). Finally, the cytosolic expression of *SAL1* at levels similar to those of the wild type (in lines 2 and 10) (Figure 4B) was not sufficient to complement the biomass phenotype (Figure 5H) or the high PAP levels (Figure 5B) of *sal1*.

2.3.3 Chloroplast

Surprisingly, the transformation of *sal1* by construct *SAL1_III* (targeting of *SAL1* to the chloroplast) only led to partial complementation across lines with different *SAL1* expression levels (Figure 4C). Multiple lines such as *SAL1_III* 16, 28, 45, and 53 showed full complementation of biomass, but not other parameters (Figures 3, 5C,I). Despite having comparable shoot fresh weight to that of wild-type plants (Figure 5I), the PAP levels in these lines were only partially decreased (Figure 5C) (from 17 to 5 pmol/mg) compared to those in *sal1*, and their rosette morphology was intermediate between that of Col-0 and *sal1*. As expected, two lines (*SAL1_III* line 26 and *SAL1_III* line 36) with only moderately decreased PAP contents showed no complementation of biomass and rosette morphology (Figures 3, 5C,I).

2.3.4 Mitochondria

Complementation of *sal1* by construct *SAL1_IV* (targeted expression of *SAL1* to the mitochondria) was extremely effective. Sixty-five out of 77 independent transgenic lines (85%) were fully complemented (data not shown). Here, we show six representative lines (Figures 4D, 5D,J) to illustrate the range of complementation observed. Lines *SAL1_IV* 8, 19, 24, and 26 had fully complemented PAP levels, whereas line *SAL1_IV* 16 showed partial complementation and *SAL1_IV* line 15, which had lower *SAL1* transcript levels than the wild type, was not complemented. The extent to which the PAP levels and rosette morphology were complemented correlated well with the PAP levels of these lines (Figures 3, 5D).

2.3.5 Chloroplasts and Mitochondria

Complementation of *sal1* by construct *SAL1_V* (*SAL1* targeted to the mitochondria and chloroplasts) was functionally effective, as

expected. Here, we present the data for nine representative independent transgenic lines with a range of phenotypes (Figures 4E, 5E,K). Six of these lines (*SAL1_V* 1, 13, 15, 18, 24, and 26) showed wild-type phenotypes, including leaf blade shape (Figure 3), PAP levels (Figure 5E), and biomass (Figure 5K). Nevertheless, line *SAL1-V* 6, which had a comparable *SAL1* expression level to that of the wild type, was phenotypically similar to *sal1* in terms of biomass and rosette morphology, although the PAP level was moderately but significantly decreased. Only lines *SAL1_V* 2 and *SAL1_V* 17 were not complemented, presumably due to their very low *SAL1* expression (Figure 4E).

2.3.6 Cytosol and Nucleus

Following transformation with *SAL1_VI*, which served as a positive control for complementation (Kim and von Arnim, 2009), we obtained 12 independent transgenic lines with a stable phenotype and analyzed nine representative lines in detail (Figures 3, 4F, 5F,L). Only one line (*SAL1_VI* 6) was complemented in terms of leaf morphology and growth (Figure 4) and shoot fresh weight (Figure 5L), with its PAP level almost restored to that of the wild type (Figure 5F). The remaining eight lines all had similar or significantly higher PAP levels compared to *sal1* and showed limited complementation in terms of rosette morphology and biomass (Figures 3, 4L). We did not expect to find only 1 out of 12 lines to be complemented or to show a wild-type phenotype because this construct was previously reported to be able to complement *sal1* (Kim and von Arnim, 2009). Thus, complementation of *sal1* by co-targeting *SAL1* to the nucleus and the cytosol is possible in principle, but is not a guaranteed outcome (see Section 3).

2.4 The Sulfur Assimilation Pathway and Accumulation of Secondary Sulfated Compounds in Selected *SAL1* Complemented Lines

Loss of *SAL1* function results in low total sulfate levels, a decreased accumulation of GSLs, an increased level of desulfoprecursors, and a decreased level of thiols (Lee et al., 2012). Furthermore, sulfur assimilation in *sal1* mutants was not only affected at the metabolic level, but the transcript profile of genes was similar to that of sulfate-starved plants (Lee et al., 2012). Therefore, in addition to the general processes related to growth and stress response, the nutritional status was also impaired in *sal1* plants. To address the role of the compartmentalization of *SAL1* in sulfur assimilation, we selected the best-complemented transgenic lines, *SAL1_I* 26, *SAL1_II* 1, *SAL1_III* 53, *SAL1_IV* 8, *SAL1_V* 13, and *SAL1_VI* 6 (Figures 4, 5), and analyzed their sulfur metabolite profiles (Figure 6). The accumulation of sulfur metabolites in phenotypically weakly complemented lines is shown in Supplementary Figure S3.

The sulfate content in the selected lines revealed that *SAL1* can rescue the low-sulfate phenotype of *sal1* in all compartments, even when it is expressed in the cytosol or the nucleus alone (Figure 6A). However, in weakly expressing lines, complementation of low sulfate levels only occurred when

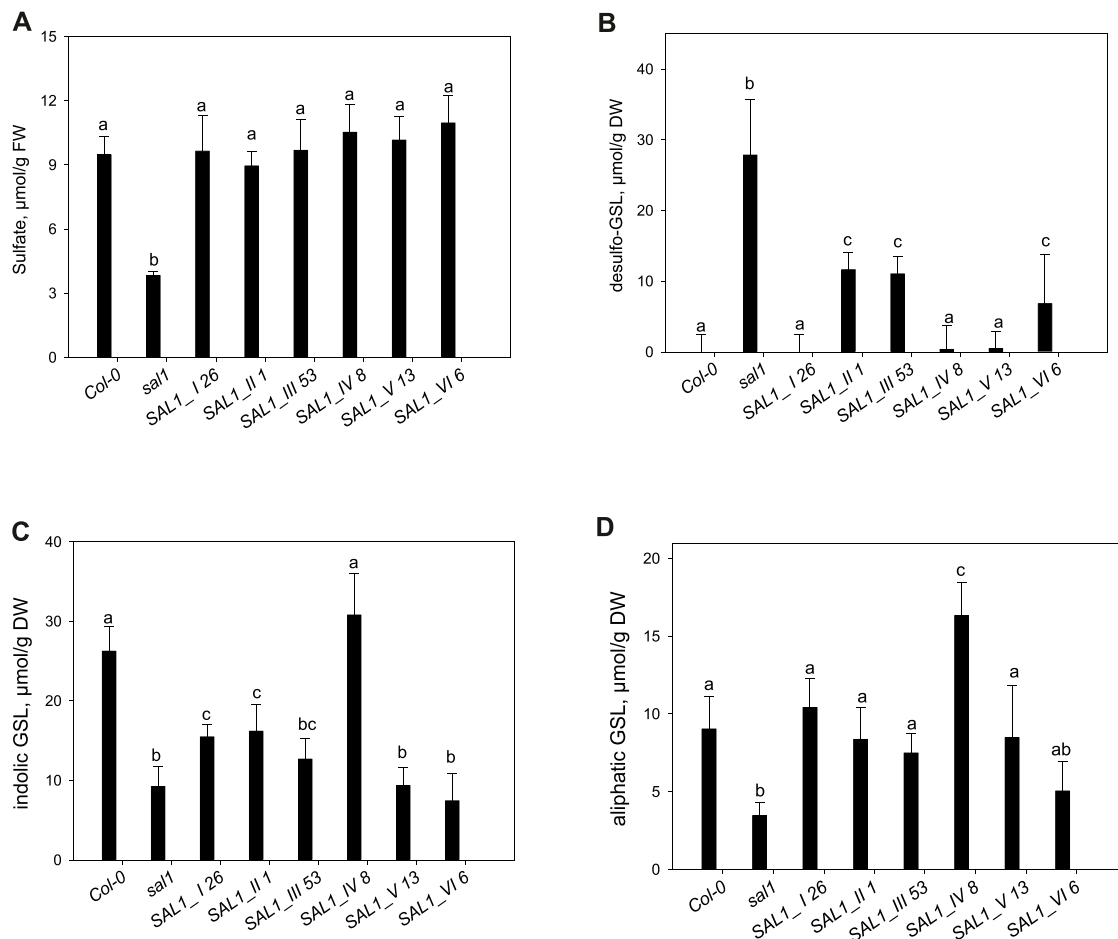


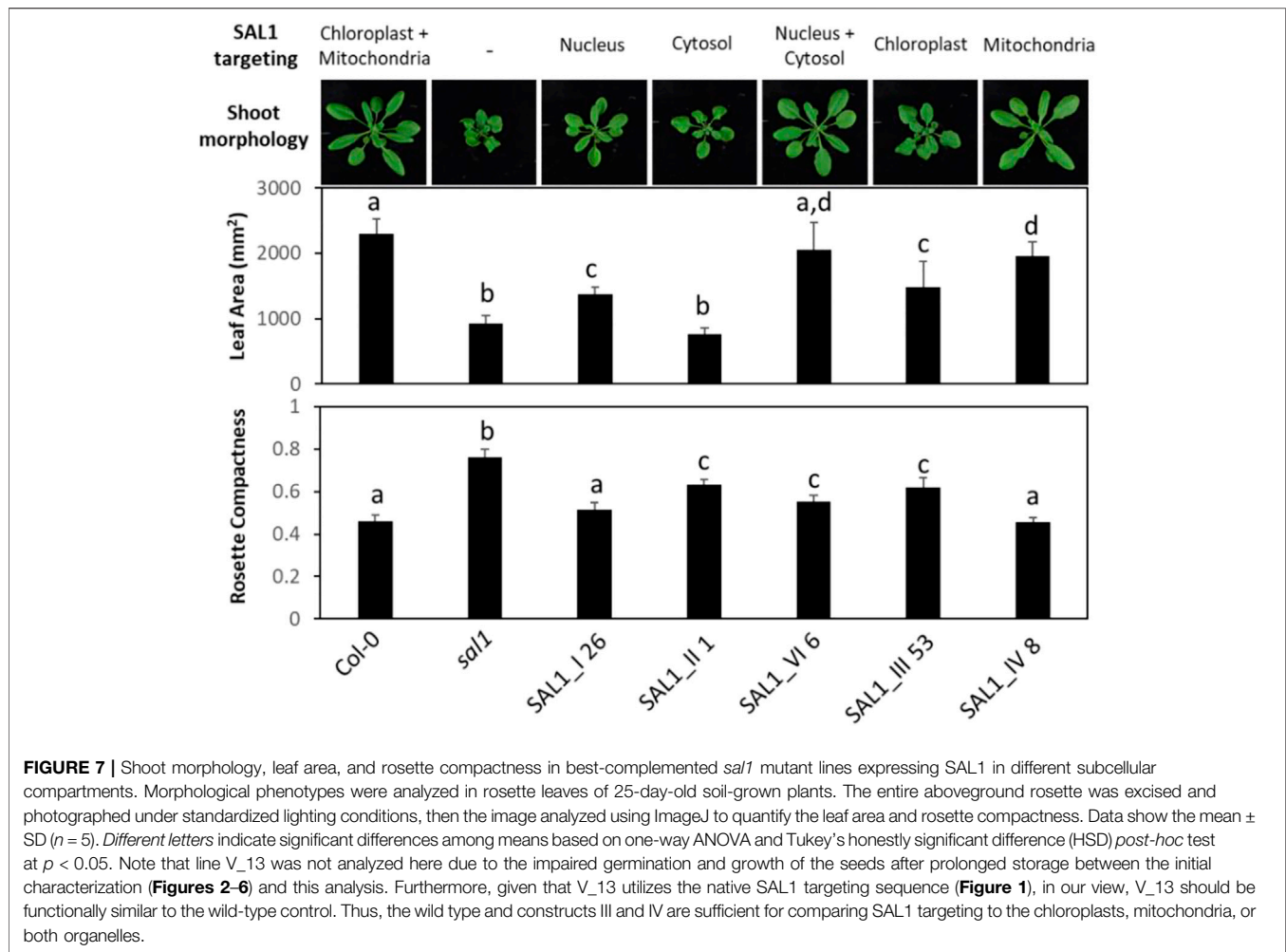
FIGURE 6 | Analysis of sulfate, desulfo-glucosinolate (GSL), and aliphatic and indolic GSL levels in complemented *sal1* mutant lines. The levels of sulfate (**A**), desulfo-GSL (**B**), indolic GSL (**C**), and aliphatic GSL (**D**) were analyzed in rosette leaves of 5-week-old *sal1* and complemented lines *SAL1_I_26*, *SAL1_II_1*, *SAL1_III_53*, *SAL1_IV_8*, *SAL1_V_13*, and *SAL1_VI_6*. Sulfur metabolites of partially complemented lines are shown in **Supplementary Figure S3**. Plants were grown on soil in short days in an environment-controlled chamber. Data show the mean \pm SD ($n = 4$). FW, fresh weight. Different letters indicate significant differences among means based on *t*-tests at $p < 0.05$.

SAL1 was expressed in the nucleus, mitochondria, or chloroplasts, but not when *SAL1* was present in the cytosol (constructs II and VI) (**Supplementary Figure S3**).

As sulfate is required for the sulfation of GSLs, we additionally measured the accumulation of indolic (IG) and aliphatic (AG) GSLs and their desulfo-precursors. The desulfo-GSLs (ds-GSLs), which accumulate to high levels in *sal1*, were fully complemented by *SAL1* expression in the nucleus, mitochondria, and by the native *SAL1* construct. However, the cytosolic and chloroplastic expression of *SAL1* only led to a 50% decrease in the accumulation of ds-GSL, which could not restore the wild-type level of ds-GSL (**Figure 6B**). In contrast to ds-GSLs, we observed less phenotypic variation among the *SAL1*-expressing lines for AGs and IGs. The production of AGs was fully complemented in all lines, with the exception of line VI in which the low AG level only slightly increased (**Figure 6D**). Conversely, the production of IGs was fully complemented only when *SAL1* was targeted to the mitochondria (**Figure 6C**).

2.5 Phenotypic Comparison of Complementation Efficiency by *SAL1* in Different Subcellular Compartments

We further characterized the best-complemented lines in **Figure 6** by quantifying their leaf phenotypes in more detail. We did comparative analysis of the following transgenic lines: 1) plants expressing *SAL1* in the compartments in which PAP is proposed to act (nucleus, cytosol, or both) compared to the wild type and 2) plants expressing *SAL1* in a single organelle (chloroplast or the mitochondria) compared to both organelles where *SAL1* is normally found (wild type). Targeting *SAL1* to both the cytosol and the nucleus (*SAL1_VI_6*) showed an additive effect compared to either the nucleus (*SAL1_I_26*) or the cytosol (*SAL1_II_1*) alone in restoring leaf area to wild-type levels (**Figures 6, 7**). In contrast, *SAL1* in either the cytosol or the nucleus alone was similarly effective as *SAL1* in both the cytosol and the nucleus in rescuing rosette compactness (**Figure 7**). In the second set of comparisons, targeting *SAL1* to chloroplasts alone



(*SAL1_III 53*) only partially rescued leaf area and rosette compactness. Similarly, targeting SAL1 to the mitochondria (*SAL1_IV*) did not completely restore leaf area, although it rescued rosette compactness to wild-type levels (Figure 7). Taken together, these results suggest that PAP most likely exerts its effects in both the cytosol and the nucleus, albeit unequally, and that the presence of SAL1 in both chloroplasts and the mitochondria is required for PAP homeostasis.

2.6 Re-Evaluating Complementation Efficiency by SAL1 in the Context of SAL1 mRNA and Protein Levels *In Vivo*

The unequal complementation obtained with the different constructs (Figures 3–7) was striking and unexpected, given that *SAL1* was driven by a strong promoter that, in theory, should drive overexpression in all constructs. Therefore, we first examined for any possible relationship between the different phenotypes and *SAL1* mRNA levels in lines of the different constructs. *SAL1* overexpression at 5- to 10-fold of the wild-type levels was sufficient to completely restore the PAP levels in *SAL1_IV 26*, but not in lines of the other

constructs such as *SAL1_I 53*, *SAL1_II 2*, *SAL1_III 53*, and *SAL1_VI 5* (Figures 4, 5). Similarly, *SAL1* expression at levels comparable to those of wild-type Col-0 restored plant biomass and significantly decreased the PAP levels only in construct IV, but not in lines of the other constructs (Figures 4, 5).

To address the possibility that the mRNA levels of transgenic *SAL1* are uncoupled from the protein levels of SAL1 in the different constructs, we first compared selected lines with similar *SAL1* mRNA expression levels (~10-fold higher than that of Col-0) irrespective of their targeting. The different constructs showed significantly different degrees of leaf complementation despite their similar levels of *SAL1* mRNA (Figure 8). Interestingly, the variance in leaf phenotype complementation appeared linked to substantial variation in the protein levels of SAL1, with the Western blot of lines *SAL1_III 16* and *28* in particular showing much weaker SAL1 protein bands compared to *SAL1_II 3* and *SAL1_VI 6* (Figure 9B). This was further confirmed by comparing the protein and mRNA levels of SAL1 in the best-complemented lines of each construct regardless of their *SAL1* mRNA levels (Figure 9A). Although the *SAL1_I 26*, *III 53*, and *VI 6* lines all expressed *SAL1* mRNA at 10- to 15-fold that of the wild type,

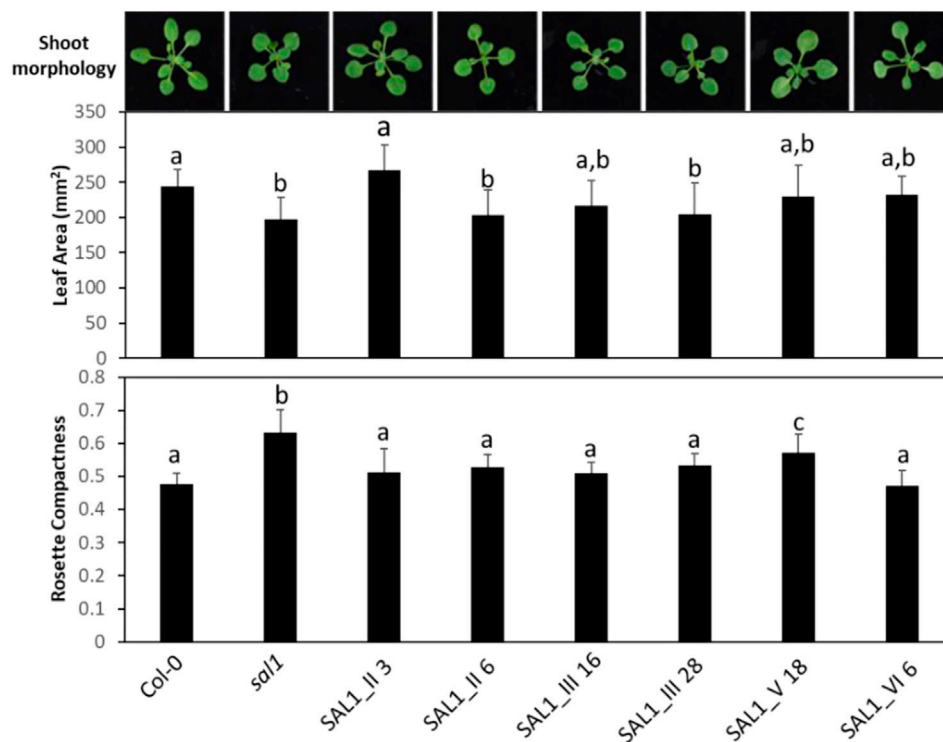


FIGURE 8 | Shoot morphology, leaf area, and rosette compactness in complemented *sal1* mutant lines expressing *SAL1* mRNA at similar levels. Morphological phenotypes were analyzed in rosette leaves of 25-day-old soil-grown plants. The entire aboveground rosette was excised and photographed under standardized lighting conditions, then the image analyzed using ImageJ to quantify the leaf area and rosette compactness. All lines shown here have *SAL1* mRNA overexpressed at ~10-fold the levels of Col-0. Data show the mean \pm SD ($n = 5$). Different letters indicate significant differences among means based on one-way ANOVA and Tukey's honestly significant difference (HSD) *post-hoc* test at $p < 0.05$. Note that, similar to **Figure 7**, there was either complete or serious loss in germination rate and/or seedling growth in lines of interest, which were not seen in earlier experiments (e.g., lines I_61, IV_19, IV_26, and V_13). We decided to omit representatives from certain lines (e.g., construct IV) because no other representative within that construct had similar *SAL1* mRNA expression to the rest of the constructs. However, we attempted to compensate for this deficiency by studying two representatives of certain constructs (II and III), in cases where they have similar *SAL1* mRNA expression to the rest of the constructs.

their *SAL1* protein levels varied substantially, with *III 53* showing very low *SAL1* protein abundance. *SAL1_II 1* had similar *SAL1* protein abundance to *III 53* despite overexpressing *SAL1* mRNA to a greater extent (40- vs. 10-fold, respectively). Similarly, *SAL1_V 13* accumulated substantially more *SAL1* protein than *SAL1_IV 8* despite overexpressing *SAL1* mRNA to a lesser degree (60 vs. 80-fold). Therefore, instead of *SAL1* mRNA being the primary determinant of complementation, targeting *SAL1* to different subcellular compartments may lead to different levels of the *SAL1* protein *in vivo* through unknown mechanism(s), thus causing unequal complementation.

3 DISCUSSION

The accumulation of PAP differs in different subcellular compartments due to the activities of *SAL1*. Based on current knowledge concerning the *SAL1*–PAP pathway and taking all phenotypes reported for *sal1* mutants into consideration, we hypothesized that PAP can act in different compartments, where PAP signaling can potentially execute different functions (Phua et al., 2018). These intriguing scenarios

prompted us to design experiments addressing the role of *SAL1* in different cell compartments by expressing it in chloroplasts, the mitochondria, the nucleus, and the cytosol. This set of experiments aimed to compare the ability of *SAL1* expressed in different compartments to complement the morphological, physiological, and chemical phenotypes of *sal1*, thereby revealing initial hints on how PAP might differentially affect multiple growth- and sulfur metabolism-related phenotypes.

Our results indicated that *SAL1* expression in the nucleus (construct I) was sufficient to complement the *sal1* phenotypes (**Figures 4–7**). This finding, which is consistent with previous observations by Kim and von Arnim (2009), pointed that: 1) PAP is present in the nucleus due to diffusion from the cytosol and that 2) modulating nuclear the PAP levels can revert the phenotype of *sal1* to that of the wild type. This finding is also consistent with the localization of two known PAP targets, *XRN2* and *XRN3*, in the nucleus. PAP inhibits the 5'–3' exoribonuclease activity of the *XRN* proteins, most likely by binding to the active site of *XRN*s (Nagarajan et al., 2013), as suggested by *in vitro* assays and the protein crystallography of PAP-inhibited exoribonucleases (Yun et al., 2018). In contrast, the high mRNA level of

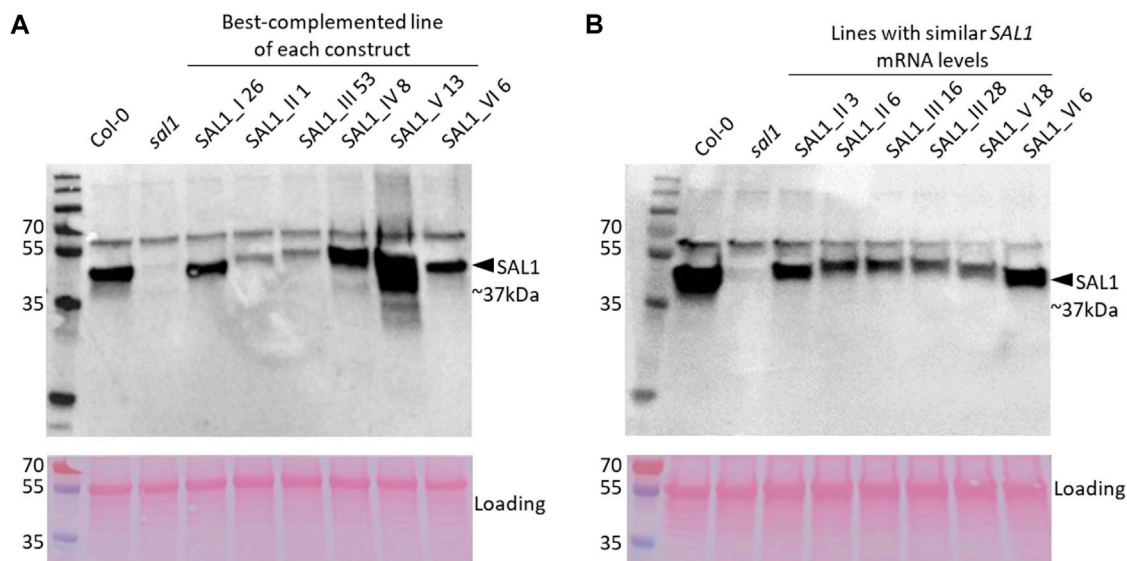


FIGURE 9 | SAL1 protein levels in best-complemented *sal1* lines expressing SAL1 in different subcellular compartments and in complemented *sal1* lines expressing similar SAL1 mRNA levels. SAL1 protein levels were analyzed in total protein extracts of 25-day-old rosette leaves from the best-complemented line of *sal1* expressing the different constructs I–VI (**A**) and diverse complemented *sal1* lines with similar SAL1 mRNA levels (~10-fold overexpression compared to Col-0) (**B**). Immunoblotting was performed with an anti-SAL1 antibody and a horseradish peroxidase (HRP)-conjugated secondary antibody against 20 µg total protein per sample. The SAL1 protein was detected at approximately 37 kDa, with no SAL1 protein in the *sal1* mutant sample, as expected. A higher band at 55 kDa is most likely the result of nonspecific antibody binding to Rubisco (upper panels). The blots were subsequently stained with Ponceau S and re-imaged to evaluate equal loading between samples (lower panels). In both (**A**) and (**B**), the upper and lower panels were generated from the same blot that was independently imaged twice after incubation with HRP chemiluminescence substrate and Ponceau S, respectively.

cytosol-targeted SAL1 did not fully complement *sal1* with respect to leaf shape, PAP level, plant biomass, and GLs (*SAL1_II* lines; **Figures 4–6**). This is counterintuitive because PAP is generated in the cytosol and, therefore, the cytosolic expression of SAL1 was predicted to directly detoxify PAP without the requirement for PAP transport into organelles or its diffusion into the nucleus. Similarly, targeting SAL1 to the chloroplast, which is one of the organelles in which SAL1 is normally located in wild-type plants, should have enabled efficient complementation of *sal1* phenotypes. These discrepancies can be explained by the low levels of transgenic SAL1 protein when expressed exclusively in the cytosol or in the chloroplast (**Figure 9**). It is also possible that the introduction of a NES or the Rubisco SSU targeting peptide to the SAL1 sequences in *SAL1_II* and *SAL1_III* lines, respectively, could have negatively impacted its protein folding or structure since even relatively few (one to four) codon changes to the SAL1 sequence are sufficient to decrease its protein abundance in *Arabidopsis* (Wilson et al., 2009) and *Escherichia coli* (Chan et al., 2016). Interestingly, in an experiment aiming at the subcellular localization of native SAL1_V_GFP, we also observed low levels of the GFP protein, which can be caused by both GFP and NES. Although the NES was also present in SAL1 sequences of the well-complemented *SAL1_IV* 8 and *SAL1_V* 13 lines, these two lines had among the highest levels of SAL1 mRNA overexpression across all the lines tested, which could have partially compensated for the decreased protein stability.

As demonstrated by line *SAL1_IV* 8, all secondary sulfate metabolism metabolites, including sulfate, ds-GSL, and aliphatic

and indolic GSLs, were also fully restored to wild-type levels (**Figure 6**). Notably, sulfur assimilation (**Supplementary Figure S3**) was highly stimulated by the mitochondrial expression of SAL1. Aliphatic and indolic GSLs reached levels significantly higher than those in the wild type (**Figures 6C, D**). Taken together, these observations confirmed the transport of PAP into the mitochondria for degradation by SAL1, which was previously only inferred based on the localization data for SAL1 and the PAPS/PAP transporter PAPST2 (Estavillo et al., 2011; Ashykhmina et al., 2019). Nevertheless, PAP degradation by SAL1 in both chloroplasts and the mitochondria may still be required for complete regulation of PAP-mediated signaling since the leaf area was still significantly, albeit only slightly, lower in *SAL1_IV* 8 compared to the wild type (**Figure 9**).

When comparing the PAP levels, leaf area, and rosette compactness between the different lines (**Figures 5, 7**), it appears that the same level of PAP may exert different impacts on individual growth phenotypes. A moderately elevated PAP level compared to that of the wild-type was sufficient to suppress the altered leaf area, but not rosette compactness (e.g., *SAL1_V* 13 and *SAL1_VI* 6), whereas higher PAP levels that were intermediate between the wild type and *sal1* also had an impact on rosette morphology (*SAL1_II* 1 and *SAL1_III* 53). Similarly, the lines *SAL1_II* 6, *SAL1_III* 16, and *SAL1_III* 28, all of which have similar PAP contents, have suppressed leaf area like *sal1*, but have wild type-like rosette compactness. Notably, rosette compactness is highly influenced by petiole length (Vanhaeren et al., 2015), which is

regulated by light signaling components such as PhyB that are also influenced by PAP accumulation (Kim and von Arnim, 2009). Leaf area is a function of cell size and number, which in turn are regulated by several complex factors such as cell expansion, cell wall composition, and the cell cycle (Gonzalez et al., 2012). How PAP signaling influences these processes is still not clear. Given that a small increase in cytosolic PAP levels, as observed here for the *SAL1_IV* lines or in the *papst2* mutant (Ashykhmina et al., 2019), actually enhances plant growth while further PAP elevations suppress growth, it may be that at least one of the parameters governing cell growth and replication is highly tuned to fluctuations in the intracellular PAP levels.

Similarly, the production of indolic GSLs seemed more sensitive to PAP accumulation than that of aliphatic GSLs. Both *SAL1_II 1* and *SAL1_III 53* had only partially complemented ds-GSLs and indolic GSLs, yet exhibited complete complementation of aliphatic GSLs. Given that SOT16 highly prefers indolic ds-GSLs whereas SOT18 prefers aliphatic ds-GSLs *in vitro* (Klein and Papenbrock, 2009), it is possible that PAP exerted a stronger inhibitory effect on SOT16 than on SOT18 *in vivo*. The inhibition kinetics of PAP have only been determined for SOT18 so far (Hirschmann et al., 2017). Alternatively, it may be that the effect of PAP on indolic GSLs was more pronounced due to their greater abundance *in vivo* compared to aliphatic GSLs (Figure 6).

All of the best-complemented lines from each construct showed complete recovery of the sulfate levels. This suggests that the regulation of total sulfate is relatively insensitive to PAP accumulation until a very high threshold is reached, as shown by *SAL1_II 1*, which had wild-type sulfate content despite accumulating 50% of the PAP levels in *sal1* (Figures 5, 6). Recently, it has been shown that GSLs serve as a sulfate reservoir and can be catabolized to release free sulfate (Sugiyama et al., 2021), so it is tempting to speculate that a high PAP may affect the sulfate levels at least partly *via* GSLs. It is also possible that PAP affects sulfate by modulating sulfate transport since the expressions of some sulfate transporters were affected in *fry1-6* (Estavillo et al., 2011).

Collectively, our results indicate that the role of the SAL1–PAP pathway in different cell compartments, environmental conditions, and signaling pathways is likely to be more complex than previously assumed. Understanding how PAP exerts differential effects on diverse processes, such as leaf morphology, growth, and sulfur metabolism, as we have shown here, could be the key to unraveling its role in the integration of retrograde, light, and hormonal signaling (Rodríguez et al., 2010; Estavillo et al., 2011; Ishiga et al., 2017; Phua et al., 2018), as well as in nutrient (Hirsch et al., 2011; Lee et al., 2012) and pathogen signaling (Ishiga et al., 2017).

4 MATERIALS AND METHODS

4.1 Plant Material and Growth Conditions

Seeds of *A. thaliana* ecotype Col-0, the T-DNA insertion mutant, and complemented transgenic plants were sown on soil or culture plates containing 1/2 Murashige and Skoog medium. The seeds

were stratified for 2–3 days in the dark, and the plants were cultivated under short-day (8-h light and 16-h dark) conditions with an average photon flux density of 100–150 $\mu\text{mol m}^{-2} \text{s}^{-1}$. White light was provided by Fluora L58W/77 fluorescent tubes. The temperature was kept at 22°C during the light period and 18°C during the dark period. The relative humidity was ~40%.

4.2 Isolation of *sal1* Mutant

The homozygous mutant *sal1* line (At5g63980, SALK_020882, and SALK_005741) was identified and the insertion position of the T-DNA in the target gene was confirmed by sequencing previously (Ashykhmina et al., 2019). In this manuscript, we present data on the analysis and complementation of SALK_020882 line, named here also as *sal1*.

4.3 Cloning of Chimeric *SAL1* Constructs

To achieve the compartment-specific accumulation of *SAL1*, we generated six chimeric constructs, as shown in **Supplementary Figure S1**. The *SAL1tr* backbone was amplified from *Arabidopsis* cDNA and fused with different DNA pieces using fusion PCR, as described in Section 2.

In our cloning procedure, all six constructs were inserted into the entry pDONOR207 vector. pDONOR207 vectors containing six different *SAL1*s were recombined with either the binary vector pGWB5 (for GFP localization studies) or pGWB2 (for the complementation of *sal1*) under the control of the 35S cauliflower mosaic virus promoter. All constructs of interest were transformed into *Arabidopsis* mesophyll protoplasts or root suspension cells.

4.4 GFP-Based Subcellular Localization of *SAL1* Proteins in *Arabidopsis* Protoplasts and in *Arabidopsis* Suspension Cell Culture From Roots

To confirm the subcellular localization of *SAL1* fusion proteins experimentally, *Arabidopsis* mesophyll protoplasts and root cell suspension cultures were transformed with *Agrobacterium* carrying constructs encoding *SAL1_I–VI* fused to the GFP at the C-terminus. Transfection of *Arabidopsis* mesophyll protoplasts was performed as described by Yoo et al. (2007) using 20–40 μg of plasmid DNA. Transformation of *Arabidopsis* root suspension cells was performed as described previously (Berger et al., 2007).

For staining with 4',6-diamidino-2-phenylindol (DAPI), *Arabidopsis* cells were incubated in 2 $\mu\text{g ml}^{-1}$ (*w/v*) solution of DAPI for 5 min in the dark, followed by one to two times rinsing with cell culture media (Berger et al., 2007). For MitoTracker staining, the cells were removed from the medium and exposed in 500 nmol concentrated MitoTracker dye for 45–60 min. Cells were rinsed several times with cell culture media prior to imaging.

The GFP expression patterns in dark-grown cultured *Arabidopsis* or protoplasts from mesophyll tissue were recorded by confocal laser scanning microscopy (Zeiss, Jena, Germany). Images were acquired as *z*-series with a 1- to 3- μm interval with 25 frames using a Zeiss LSM510 confocal laser scanning microscope. Green fluorescent protein was visualized with a 488-nm laser and a band-pass (BP) 500–530 filter and the

MitoTracker stain with a 543-nm laser and a BP 565–615 filter. For the visualization of DAPI, we used ultraviolet light and a BP 385–470 filter.

Co-localization of the GFP signal with chlorophyll autofluorescence indicated chloroplastidic localization. A co-labeling of GFP with the DNA fluorescent stain DAPI was interpreted as a nuclear localization, whereas a co-labeling of GFP with the MitoTracker indicated a mitochondrial localization.

Results were documented with Discus and Zeiss software. Images were processed using Photoshop CS3 (Adobe Systems, San Jose, CA, USA). Adjustment of levels was applied to the SAL1-V construct to make weak GFP signals better visible in protoplasts.

4.5 Complementation of *sal1* Mutant Using SAL1 I to VI Constructs

To complement *sal1*, we utilized constructs SAL1 I to VI without GFP and generated stable *Arabidopsis* transgenic lines. All six SAL1 constructs were recombined from pDONR207 into the Gateway destination pGWB2 vector (35S cauliflower mosaic virus promoter), and correctness of constructs was verified by sequencing. SAL1 I to VI were delivered to *sal1* *Arabidopsis* plants by *Agrobacterium*-mediated transformation, and positive transformants were selected using kanamycin. The homozygous SAL1ox lines I to VI were isolated following segregation analysis of populations.

4.6 Analysis of Shoot Fresh Weight of Complemented Plants

Individual *Arabidopsis* plants were grown on MS agar media for 4 weeks as described above. To measure the shoot fresh weight of complemented *sal1* mutants, the aboveground rosettes were excised at the hypocotyl and individual weight was recorded. At least nine seedlings per construct were analyzed.

4.7 RNA Extraction and RT-qPCR

To measure the transcript levels in the wild type and the different complemented mutant plants, total RNA was isolated from leaves, cDNA was reversely transcribed, and reverse transcription quantitative PCR (RT-qPCR) was performed as described previously (Gigolashvili et al., 2009). The relative quantification of the expression levels was performed using the comparative delta C_t method, and the calculated relative expression values were normalized to *Actin2* and compared with the expression level in wild-type plants ($Col-0 = 1$).

4.8 Extraction and Measurement of Sulfated Compounds and of Sulfate

GSs and their desulfo-precursors were extracted from the lyophilized plant material as reported previously (Ashykhmina et al., 2019). Sulfate was detected as previously reported in Mugford et al. (2009).

4.9 Quantification of PAP in Plant Extracts

Plant material was collected and frozen in liquid nitrogen. The extraction and chromatographic detection of PAP

were performed as reported previously (Ashykhmina et al., 2019).

4.10 Quantification of Rosette Parameters

Individual *Arabidopsis* plants were grown on separate soil-filled pots for 25 days under long-day conditions (18-h light and 6-h darkness at $\sim 100 \mu\text{mol photons m}^{-2} \text{ s}^{-1}$, 22°C/20°C day/night cycle). For imaging, the aboveground rosettes were excised at the hypocotyl with sharp scissors and immediately photographed using an in-house imaging platform comprising a Canon DSLR camera and controlled fluorescent lighting. The images were analyzed in ImageJ to quantify the leaf area (area of green pixels) and the rosette compactness (ratio of leaf area relative to the convex hull) (Vanhaeren et al., 2015).

4.11 Protein Extraction and Western Blot

Approximately 100 mg leaf tissue harvested from 25-day-old soil-grown *Arabidopsis* plants was snap-frozen in liquid nitrogen, ground to fine powder using a ball mill at 20 Hz for 1 min (Retsch, Haan, Germany), and then resuspended in 300 μl RIPA extraction buffer (1% NP-40, 0.5% sodium deoxycholate, 0.1% sodium dodecyl sulfate, and 10% glycerol) supplemented with 1 mM phenylmethylsulfonyl fluoride (PMSF). Cellular debris was removed by centrifugation ($14,000 \times g$ for 10 min at 4°C) and the supernatant moved to a fresh tube. Total protein was quantified using the Bradford assay. For SDS-PAGE and Western blotting, 20 μg total protein was loaded per sample onto 12% Mini-PROTEAN® TGX™ Precast Gels (Bio-Rad, Hercules, CA, United States) and resolved at 200 V for 30 min. The proteins were then transferred onto PVDF membranes using the Trans-Blot Turbo Transfer System (Bio-Rad). The membranes were incubated in blocking solution (5% milk, 1 \times PBS, and 0.05% Tween) for 1 h at room temperature. This was followed by an anti-SAL1 antibody (Agrisera AS07 256; 1:1,000 dilution in 1% milk, 1 \times PBS, and 0.05% Tween) overnight at 4°C and a secondary antibody (ECL™ Donkey anti-rabbit IgG, horseradish peroxidase linked; GE Healthcare, Chicago, IL, United States) for 1 h at room temperature, with three 15-min washes (1 \times PBS and 0.05% Tween) after every incubation step. The blots were developed using ECL imaging solution (Clarity Western Peroxide Reagent and Clarity Western Luminol/Enhancer Reagent; Bio-Rad). Chemiluminescence was visualized using the ChemiDoc system (Bio-Rad). To visualize all proteins present on the blot, the membrane was incubated for 5 min in Ponceau S solution (Sigma-Aldrich, St. Louis, MO, USA) and washed with distilled water to remove background staining.

4.12 Statistical Analysis

Comparison of means was performed to determine statistical significance using a two-sample Student's *t*-test or an ANOVA (Tukey's test). Constant variance and normal distribution of data were verified prior to statistical analysis.

In the first phase of the project, comparison to wild type with repeated *t*-tests seemed to be the most accessible method of choice, as we were most interested in whether an individual line was not significantly different from the wild type (indicating complete complementation) rather than possible

differences between certain lines (partial complementation). Prior to the *t*-test, a two-sample *F*-test for variances was implemented to check for scedasticity, shown in **Figures 4–6**. If the variances differed, a heteroscedastic two-tailed *t*-test was performed, while equal variances led to the choice of a homoscedastic *t*-test. For **Figures 7, 8**, homogeneity of the variances was verified using the Levene's test for equality of variances in SPSS Statistics version 27 (IBM, Armonk, NY, USA). All datasets passed the test for equal variances, returning significance values between 0.3 and 0.6 (significance values higher than 0.05 indicate equal variance). The datasets were subsequently analysed by ANOVA.

DATA AVAILABILITY STATEMENT

The original contributions presented in the study are included in the article/**Supplementary Material**. Further inquiries can be directed to the corresponding author.

AUTHOR CONTRIBUTIONS

NA and KXC performed most of the experiments and analyzed the data. HF did analysis of the glucosinolates and contributed to data analysis. TG and U-IF made the original experimental design. KXC, SK, and FVB contributed to the experimental design and editing. TG and KXC wrote the manuscript.

REFERENCES

- Ashykhmina, N., Lorenz, M., Frerigmann, H., Koprivova, A., Hofsetz, E., Stührwoldt, N., et al. (2019). PAPST2 Plays Critical Roles in Removing the Stress Signaling Molecule 3'-Phosphoadenosine 5'-Phosphate from the Cytosol and its Subsequent Degradation in Plastids and Mitochondria. *Plant Cell* 31, 231–249. doi:10.1105/tpc.18.00512
- Berger, B., Stracke, R., Yatusovich, R., Weisshaar, B., Flügge, U.-I., and Gigolashvili, T. (2007). A Simplified Method for the Analysis of Transcription Factor-Promoter Interactions that Allows High-Throughput Data Generation. *Plant J.* 50, 911–916. doi:10.1111/j.1365-3113x.2007.03088.x
- Chan, K. X., Mabbitt, P. D., Phua, S. Y., Mueller, J. W., Nisar, N., Gigolashvili, T., et al. (2016). Sensing and Signaling of Oxidative Stress in Chloroplasts by Inactivation of the SAL1 Phosphoadenosine Phosphatase. *Proc. Natl. Acad. Sci.* 113, 201604936. doi:10.1073/pnas.1604936113
- Chan, K. X., Wirtz, M., Phua, S. Y., Estavillo, G. M., and Pogson, B. J. (2013). Balancing Metabolites in Drought: the Sulfur Assimilation Conundrum. *Trends Plant Sci.* 18, 18–29. doi:10.1016/j.tplants.2012.07.005
- Chen, H., Zhang, B., Hicks, L. M., and Xiong, L. (2011). A Nucleotide Metabolite Controls Stress-Responsive Gene Expression and Plant Development. *Plos One* 6, e26661. doi:10.1371/journal.pone.0026661
- Chi, W., Feng, P., Ma, J., and Zhang, L. (2015). Metabolites and Chloroplast Retrograde Signaling. *Curr. Opin. Plant Biol.* 25, 32–38. doi:10.1016/j.pbi.2015.04.006
- Dichtl, B., Stevens, A., and Tollervey, D. (1997). Lithium Toxicity in Yeast Is Due to the Inhibition of RNA Processing Enzymes. *Embo J.* 16, 7184–7195. doi:10.1093/emboj/16.23.7184
- Estavillo, G. M., Crisp, P. A., Pornsiriwong, W., Wirtz, M., Collinge, D., Carrie, C., et al. (2011). Evidence for a SAL1-PAP Chloroplast Retrograde Pathway that

FUNDING

This work was supported by Deutsche Forschungsgemeinschaft grant (GI-824/2-1) and the Deutsche Forschungsgemeinschaft Heisenberg Fellowship (GI-824/4-1). Research in SK's lab is supported by Deutsche Forschungsgemeinschaft under Germany's Excellence Strategy (EXC 2048/1)—project 390686111. KXC is funded by a Postdoctoral Fellowship from the Research Foundation—Flanders (FWO; grant no. 12N4818N). FVB is funded by Fonds Wetenschappelijk Onderzoek and Fonds De La Recherche Scientifique—FNRS (EOS project no. 30829584).

ACKNOWLEDGMENTS

We thank Bastian Walter and Claudia Nothelle (University of Cologne) for technical assistance with anion and thiol analysis and greatly acknowledge undergraduate students Eduard Hofsetz, Yvonne Peters, and Olga Spit for their assistance in the lab. We very much appreciate the financial support from the Deutsche Forschungsgemeinschaft grant (FL-126/24-1).

SUPPLEMENTARY MATERIAL

The Supplementary Material for this article can be found online at: <https://www.frontiersin.org/articles/10.3389/fmolb.2021.763795/full#supplementary-material>

- Functions in Drought and High Light Signaling in Arabidopsis. *The Plant Cell Online* 23, 3992–4012. doi:10.1105/tpc.111.091033
- Gigolashvili, T., Geier, M., Ashykhmina, N., Frerigmann, H., Wulfert, S., Krueger, S., et al. (2012). The Arabidopsis Thylakoid ADP/ATP Carrier TAAC Has an Additional Role in Supplying Plastidic Phosphoadenosine 5'-Phosphosulfate to the Cytosol. *Plant Cell* 24, 4187–4204. doi:10.1105/tpc.112.101964
- Gigolashvili, T., Yatusovich, R., Rollwitz, I., Humphry, M., Gershenzon, J., and Flügge, U.-I. (2009). The Plastidic Bile Acid Transporter 5 Is Required for the Biosynthesis of Methionine-Derived Glucosinolates in Arabidopsis Thaliana. *Plant Cell* 21, 1813–1829. doi:10.1105/tpc.109.066399
- Gonzalez, N., Vanhaeren, H., and Inzé, D. (2012). Leaf Size Control: Complex Coordination of Cell Division and Expansion. *Trends Plant Science* 17, 332–340. doi:10.1016/j.tplants.2012.02.003
- Hirsch, J., Misson, J., Crisp, P. A., David, P., Bayle, V., Estavillo, G. M., et al. (2011). A Novel Fry1 Allele Reveals the Existence of a Mutant Phenotype Unrelated to 5'->3' Exoribonuclease (XRN) Activities in Arabidopsis thaliana Roots. *Plos One* 6, e16724. doi:10.1371/journal.pone.0016724
- Hirschmann, F., Krause, F., Baruch, P., Chizhov, I., Mueller, J. W., Manstein, D. J., et al. (2017). Structural and Biochemical Studies of Sulphotransferase 18 from Arabidopsis thaliana Explain its Substrate Specificity and Reaction Mechanism. *Sci. Rep.* 7, 4160. doi:10.1038/s41598-017-04539-2
- Ishiga, Y., Watanabe, M., Ishiga, T., Tohge, T., Matsuura, T., Ikeda, Y., et al. (2017). The SAL-PAP Chloroplast Retrograde Pathway Contributes to Plant Immunity by Regulating Glucosinolate Pathway and Phytohormone Signaling. *Mpmi* 30, 829–841. doi:10.1094/mpmi-03-17-0055-r
- Kim, B.-H., and von Arnim, A. G. (2009). FIERY1 regulates Light-Mediated Repression of Cell Elongation and Flowering Time via its 3'(2'),5'-bisphosphate Nucleotidase Activity. *Plant J.* 58, 208–219. doi:10.1111/j.1365-3113x.2008.03770.x

- Klein, M., and Papenbrock, J. (2009). Kinetics and Substrate Specificities of Desulfo-Glucosinolate Sulfotransferases in *Arabidopsis thaliana*. *Physiologia Plantarum* 135, 140–149. doi:10.1111/j.1399-3054.2008.01182.x
- Krishna, P., and Gloor, G. (2001). The Hsp90 Family of Proteins in *Arabidopsis thaliana*. *Cell Stress Chapter* 6, 238–246. doi:10.1379/1466-1268(2001)006<0238:thfopi>2.0.co;2
- Lee, B.-R., Huseby, S., Koprivova, A., Chételat, A., Wirtz, M., Mugford, S. T., et al. (2012). Effects of Fou8/fry1 Mutation on Sulfur Metabolism: Is Decreased Internal Sulfate the Trigger of Sulfate Starvation Response? *PLoS One* 7, e39425. doi:10.1371/journal.pone.0039425
- Mugford, S. G., Yoshimoto, N., Reichelt, M., Wirtz, M., Hill, L., Mugford, S. T., et al. (2009). Disruption of Adenosine-5'-Phosphosulfate Kinase in *Arabidopsis* Reduces Levels of Sulfated Secondary Metabolites. *Plant Cell* 21, 910–927. doi:10.1105/tpc.109.065581
- Nagarajan, V. K., Jones, C. I., Newbury, S. F., and Green, P. J. (2013). XRN 5'→3' Exoribonucleases: Structure, Mechanisms and Functions. *Biochim. Biophys. Acta (Bba) - Gene Regul. Mech.* 1829, 590–603. doi:10.1016/j.bbagr.2013.03.005
- Pesaresi, P., and Kim, C. (2019). Current Understanding of GUN1: a Key Mediator Involved in Biogenic Retrograde Signaling. *Plant Cell Rep.* 38, 819–823. doi:10.1007/s00299-019-02383-4
- Phua, S. Y., Yan, D., Chan, K. X., Estavillo, G. M., Nambara, E., and Pogson, B. J. (2018). The *Arabidopsis* SAL1-PAP Pathway: A Case Study for Integrating Chloroplast Retrograde, Light and Hormonal Signaling in Modulating Plant Growth and Development? *Front. Plant Sci.* 9, 1171. doi:10.3389/fpls.2018.01171
- Poonam, R., Bhardwaj, R., Kaur, R., Bali, S., Kaur, P., Sirhindi, G., et al. (2015). Role of Various Hormones in Photosynthetic Responses of green Plants under Environmental Stresses. *Curr. Protein Pept. Sci.* 16, 435–449. doi:10.2174/1389203716666150330125215
- Rens-Domiano, S. S., and Roth, J. A. (1987). Inhibition of M and P Phenol Sulfotransferase by Analogues of 3'-Phosphoadenosine-5'-Phosphosulfate. *J. Neurochem.* 48, 1411–1415. doi:10.1111/j.1471-4159.1987.tb05679.x
- Robles, P., Fleury, D., Candela, H., Cnops, G., Alonso-Peral, M. M., Anami, S., et al. (2010). The RON1/FRY1/SAL1 Gene Is Required for Leaf Morphogenesis and Venation Patterning in *Arabidopsis*. *Plant Physiol.* 152, 1357–1372. doi:10.1104/pp.109.149369
- Rodríguez, V. M., Chételat, A., Majcherczyk, P., and Farmer, E. E. (2010). Chloroplastic Phosphoadenosine Phosphosulfate Metabolism Regulates Basal Levels of the Prohormone Jasmonic Acid in *Arabidopsis* Leaves. *Plant Physiol.* 152, 1335–1345. doi:10.1104/pp.109.150474
- Sugiyama, R., Li, R., Kuwahara, A., Nakabayashi, R., Sotta, N., Mori, T., et al. (2021). Retrograde Sulfur Flow from Glucosinolates to Cysteine in *Arabidopsis thaliana*. *Proc. Natl. Acad. Sci.* 118, e2017890118. doi:10.1073/pnas.2017890118
- Tee, E. E. (2018). Too Much, Take it Back: PAP Moves from the Cytosol to Plastids and Mitochondria for Degradation via PAPST2. *The Plant Cell* 31 (1), 15–16. doi:10.1105/tpc.18.00944
- Vanhaeren, H., Gonzalez, N., and Inzé, D. (2015). A Journey through a Leaf: Phenomics Analysis of Leaf Growth in *Arabidopsis thaliana*. *The Arabidopsis Book* 13, e0181. doi:10.1199/tab.0181
- Wang, Y., Berkowitz, O., Selinski, J., Xu, Y., Hartmann, A., and Whelan, J. (2018). Stress Responsive Mitochondrial Proteins in *Arabidopsis thaliana*. *Free Radic. Biol. Med.* 122, 28–39. doi:10.1016/j.freeradbiomed.2018.03.031
- Wilson, P. B., Estavillo, G. M., Field, K. J., Pornsiriwong, W., Carroll, A. J., Howell, K. A., et al. (2009). The Nucleotidase/phosphatase SAL1 Is a Negative Regulator of Drought Tolerance in *Arabidopsis*. *Plant J.* 58, 299–317. doi:10.1111/j.1365-3113.2008.03780.x
- Xiong, L., Lee, B., Ishitani, M., Lee, H., Zhang, C., and Zhu, J. K. (2001). FIERY1 Encoding an Inositol Polyphosphate 1-Phosphatase is a Negative Regulator of Absciscic Acid and Stress Signaling in *Arabidopsis*. *Genes Dev.* 15 (15), 1971–1984. doi:10.1101/gad.891901
- Yoo, S.-D., Cho, Y.-H., and Sheen, J. (2007). *Arabidopsis* Mesophyll Protoplasts: a Versatile Cell System for Transient Gene Expression Analysis. *Nat. Protoc.* 2, 1565–1572. doi:10.1038/nprot.2007.199
- Yun, J.-S., Yoon, J.-H., Choi, Y. J., Son, Y. J., Kim, S., Tong, L., et al. (2018). Molecular Mechanism for the Inhibition of DXO by Adenosine 3',5'-bisphosphate. *Biochem. biophysical Res. Commun.* 504, 89–95. doi:10.1016/j.bbrc.2018.08.135

Conflict of Interest: The authors declare that the research was conducted in the absence of any commercial or financial relationships that could be construed as a potential conflict of interest.

Publisher's Note: All claims expressed in this article are solely those of the authors and do not necessarily represent those of their affiliated organizations, or those of the publisher, the editors, and the reviewers. Any product that may be evaluated in this article, or claim that may be made by its manufacturer, is not guaranteed or endorsed by the publisher.

Copyright © 2022 Ashykhmina, Chan, Frerigmann, Van Breusegem, Kopriva, Flüge and Gigolashvili. This is an open-access article distributed under the terms of the Creative Commons Attribution License (CC BY). The use, distribution or reproduction in other forums is permitted, provided the original author(s) and the copyright owner(s) are credited and that the original publication in this journal is cited, in accordance with accepted academic practice. No use, distribution or reproduction is permitted which does not comply with these terms.



The Role of Sulfation in Nematode Development and Phenotypic Plasticity

Catia Igreja^{*†} and Ralf J. Sommer^{*†}

Max Planck Institute for Biology, Tübingen, Germany

OPEN ACCESS

Edited by:

Jon Wolf Mueller,
University of Birmingham,
United Kingdom

Reviewed by:

Paul Alexander Foster,
University of Birmingham,
United Kingdom
Michael Duffel,
The University of Iowa, United States

*Correspondence:

Catia Igreja
catia.igreja@tuebingen.mpg.de
Ralf J. Sommer
ralf.sommer@tuebingen.mpg.de

†ORCID:

Catia Igreja
orcid.org/0000-0003-3563-1788
Ralf J. Sommer
orcid.org/0000-0003-1503-7749

Specialty section:

This article was submitted to
Cellular Biochemistry,
a section of the journal
Frontiers in Molecular Biosciences

Received: 20 December 2021

Accepted: 24 January 2022

Published: 10 February 2022

Citation:

Igreja C and Sommer RJ (2022) The
Role of Sulfation in Nematode
Development and
Phenotypic Plasticity.
Front. Mol. Biosci. 9:838148.
doi: 10.3389/fmolb.2022.838148

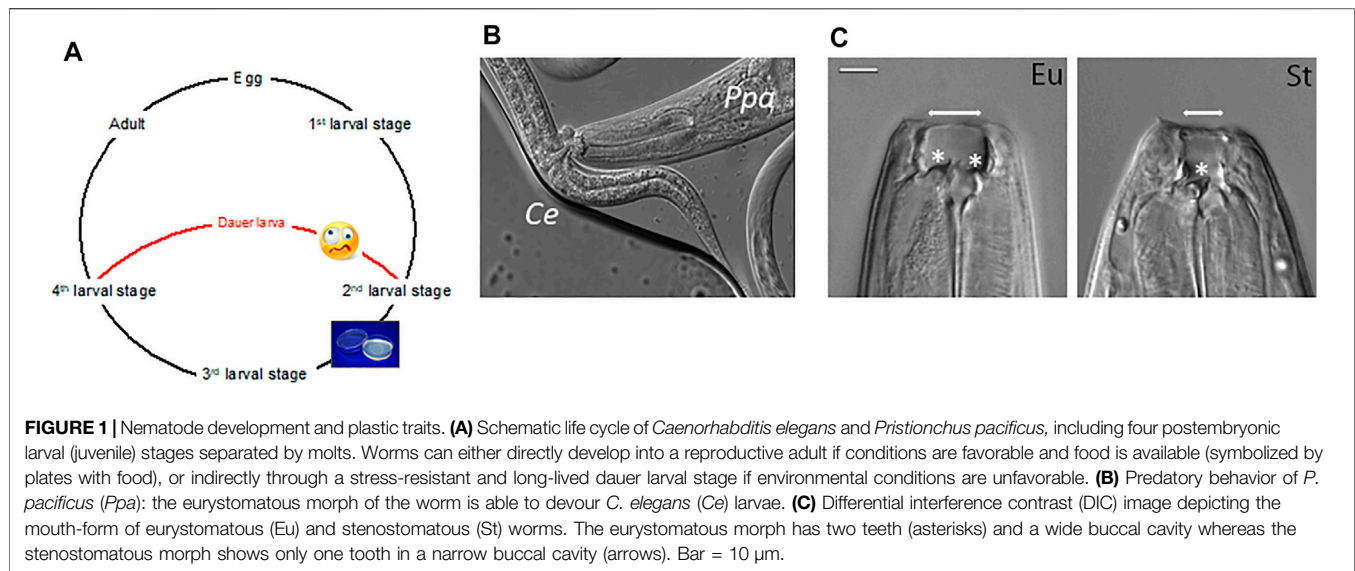
Sulfation is poorly understood in most invertebrates and a potential role of sulfation in the regulation of developmental and physiological processes of these organisms remains unclear. Also, animal model system approaches did not identify many sulfation-associated mechanisms, whereas phosphorylation and ubiquitination are regularly found in unbiased genetic and pharmacological studies. However, recent work in the two nematodes *Caenorhabditis elegans* and *Pristionchus pacificus* found a role of sulfatases and sulfotransferases in the regulation of development and phenotypic plasticity. Here, we summarize the current knowledge about the role of sulfation in nematodes and highlight future research opportunities made possible by the advanced experimental toolkit available in these organisms.

Keywords: nematodes, sulfatases, *Caenorhabditis elegans*, *Pristionchus pacificus*, sulfotransferases, *eud-1*, developmental switch, developmental plasticity

INTRODUCTION

Sulfation, sulfonation or sulfoconjugation, is an essential and ubiquitous biochemical reaction that modifies a wide range of xenobiotic and endogenous molecules. From bacteria to plants and animals, perturbation of the molecular processes that regulate the biologic ratio of sulfated and unconjugated substrates is likely to alter cellular and organismal physiology (Leung et al., 2016; Langford et al., 2017; Gunal et al., 2019). The sulfation pathways are catalyzed by two types of enzymes, the sulfotransferases (sulfuryltransferases) and the sulfatases. The sulfotransferases transfer a sulfonyl group (SO₃) from the universal donor PAPS (3'-phosphoadenosine 5'-phosphosulfate) to the hydroxyl or amino group of numerous compounds (Strott, 2002; Coughtrie, 2016). The presence of the charged sulfate group changes the physiochemical properties (water solubility and conformation) of the acceptor molecules and has therefore a major role in the detoxification and elimination of various xenobiotics (Strott, 2002; Leung et al., 2016). Multiple endogenous compounds including carbohydrates, lipids, proteins and hormone precursors (steroids) are also modified by sulfotransferases. In their case, sulfation has significant influence on the biological activity of the modified molecules and consequently in multiple biological processes (for details see (Strott, 2002; Mueller et al., 2015; Leung et al., 2016)).

The sulfatases, on the other hand, hydrolyze the sulfate ester bonds to the unconjugated form of the substrate (Hanson et al., 2004). These hydrolytic enzymes are part of the alkaline phosphatase superfamily and share a post-translational modification that greatly enhances enzymatic activity: a cysteine or serine in the catalytic center is converted to a formylglycine (Schmidt et al., 1995; Dierks et al., 1997; Dierks et al., 1998a; Dierks et al., 1998b). This review elaborates on the players, molecular mechanisms and roles of the sulfation pathways in *Caenorhabditis elegans* and *Pristionchus pacificus*. We especially highlight the use of these nematode model organisms to investigate the poorly



understood relevance of the sulfation pathways in organismal development. Finally, the emerging topics and questions on sulfation in nematodes are discussed.

The Nematode Model Organisms: *C. elegans* and *P. pacificus*

Nematodes, or roundworms, are one of the largest animal phyla and are found in all ecosystems: marine, fresh-water and soil (van den Hoogen et al., 2019). In addition, many nematode species are parasites of plants, animals, life stock or humans, resulting in their economic importance for agriculture, breeding and health (Lee et al., 2002). Most of these parasites are hard to culture in the laboratory, whereas some free-living species are among the most rapidly reproducing and most easily culturable species of all metazoans. One example is *Caenorhabditis elegans*, which was introduced as a potential model organism by Sydney Brenner in the 1960ies (Brenner, 1974). Building on a unique set of life history traits and a growing functional toolkit, the ‘*C. elegans* research community’ has grown rapidly to make fundamental discoveries in all areas of the life sciences. *C. elegans* can be grown on small agar plates in the laboratory, feeds on *Escherichia coli* and completes its life cycle in 3 days at 20 °C (Figure 1A). This species reproduces primarily by selfing of hermaphrodites, which produce around 200–300 sperm during larval development before switching to a female fate with oocyte production as adults. Consequently, the progenies of hermaphrodites are genetically identical and the resulting isogenic propagation represents a unique advantage among all animal model organisms. Original unbiased forward genetic screens have identified many mutants essential for animal survival, egg-laying, neurogenesis or life span (Wood and Researchers, 1988). With *RNA interference* and CRISPR/Cas9-based genome engineering being implemented, large scale reverse genetic screens have been performed aiming at the analysis of the knock-down or knock-out of all genes in the genome (Fire

et al., 1998; Dickinson and Goldstein, 2016). Indeed, when the *C. elegans* genome was fully sequenced, the 100 Mb genome was shown to encode around 20,000 genes with several thousands of them being functionally characterized (Consortium, 1998). Together, these features made *C. elegans* one of the most important study systems in modern biology.

The related nematode *Pristionchus pacificus* shares many of these features with *C. elegans* and similarly builds on a short generation time (4 days, 20°C), self-fertilizing hermaphroditism, forward and reverse genetic tools and a fully sequenced genome (Sommer and Sternberg, 1996; Dieterich et al., 2008; Han et al., 2020). *P. pacificus* and *C. elegans*, like many nematodes, can undergo direct and indirect development (Figure 1A). Under favorable environmental conditions and the availability of food, they undergo direct development, rapidly proceeding through four juvenile (larval) stages to become adults. In contrast, in the absence of food and other unfavorable circumstances, they arrest in a long-lived and stress-resistant “dauer” stage, which is adapted to survive harsh environmental conditions (Figure 1A) (for review see (Sommer and Mayer, 2015)). Besides these conserved features, *P. pacificus* differs from *C. elegans* with regard to several morphological and organismal features that turned out to be under the control of sulfation-mediated processes. Specifically, while *P. pacificus* can be cultured on *E. coli* as single food source indefinitely, it is a potential predator of other nematodes (Figure 1B). It forms teeth-like denticles in its mouth that are unknown in *C. elegans* or most other free-living nematodes (Figure 1C) (Bento et al., 2010). These teeth come in two alternative mouth-forms, representing an example of developmental (phenotypic) plasticity (Sommer, 2020). Worms can either form a “eury stomatous” (Eu) morph with two teeth and a wide buccal cavity, or, alternatively, a “stenostomatous” (St) morph with a single tooth and a narrow opening (Figure 1C) (Ragsdale et al., 2013). While both morphs can feed on bacteria, only the Eu form is a potential predator with associated self-recognition systems preventing the killing of kin

TABLE 1 | Cytosolic and membrane-bound sulfotransferases in nematodes and corresponding human orthologues.

	<i>H. sapiens</i>	<i>C. elegans</i>	<i>P. pacificus</i>	<i>S. ratti</i>	
Cytosolic SULTs	SULT1B1 SULT2A1 SULT2B1	SSU-1	SULT-1 (PPA12547)	SRP02937 SRP02634 SRP05555 SRP07442	1-hydroxypyrene sulfotransferase activity and arylsulfotransferase activity; cytosolic
			SULT-2 (PPA36905)	SRP08825 SRP08910 SRP09379	
			SULT-3 (PPA06620)	SRP09540	
			SULT-4 (PPA22156)		
			SULT-5 (PPA41942)		
	SULTs		PPA20882 PPA16538 PPA00693 PPA22912		
Protein-tyrosine sulfotransferase	TPST1 TPST2 TPST1 TPST2	TPST-1 TPST-2	TPST-1 (PPA25491) —	SRP01681 SRP00103 SRP09791	Golgi; Tyrosylprotein sulfotransferase 1 Protein-tyrosine sulfotransferase; Golgi
Heparan sulfate proteoglycan biosynthetic process	NDST1 NDST2 NDST4 HS2ST1	HST-1	HST-1 (PPA38610)	SRP03281	Heparan sulfate-glucosamine N-sulfotransferase and deacetylase activity
	HS3ST5	HST-2	HST-2 (PPA21724)	SRP00819	Heparan sulfate-glucosamine 2-O-sulfotransferase activity
	HS3ST6	HST-3.1 (transmembrane protein)	HST-3.1 (PPA39158)	SRP08308	Heparan sulfate-glucosamine 3-sulfotransferase 1 activity
	HS6ST1 HS6ST3	HST-3.2 (secreted protein)	HST-3.2 (PPA32231)	SRP04407	Heparan sulfate-glucosamine 3-sulfotransferase 1 activity
		HST-6	HST-6 (PPA28737)	SRP12180	Heparan sulfate- 6-O-sulfotransferase activity
Chondroitin sulfate biosynthetic process	CHSTs	B0273.115	PPA19622	SRP00399 SRP00911 SRP01497 SRP01663 SRP02672 SRP02896 SRP03731 SRP03749 SRP04122 SRP04305 SRP04354 SRP04890 SRP05289 SRP05718 SRP06402 SRP06805 SRP06991 SRP07055 SRP07472 SRP08449 SRP08386 SRP08576 SRP09039 SRP09641 SRP09844 SRP10988 SRP11197 SRP11358	Chondroitin 4-sulfotransferase activity
		C31B8.9			
		C54F6.3			
		F01D5.10			
		F17B5.4			
		F25E5.2			
		F36D1.8			
		F40C5.1			

(Continued on following page)

TABLE 1 | (Continued) Cytosolic and membrane-bound sulfotransferases in nematodes and corresponding human orthologues.

<i>H. sapiens</i>	<i>C. elegans</i>	<i>P. pacificus</i>	<i>S. ratti</i>
	F49D11.3		SRP11499
	F49D11.6		
	F55B12.2		SRP11527
	F56H6.4		
	F56H6.13		
	F59D12.3		
	K06H6.5		
	K07H8.8		
	T15D6.1		
	T24A6.16		
	T27C5.12		
	ZK1025.2		
	ZK1025.8		
	CHST-1	PPA16534	SRP10755
	C18B2.1		
	C18B2.2		
	F20C5.7		SRP09150
	T09E11.3		
	Y87G2A.16		
	Y48G1BL.7	PPA09342	

Protein searches were performed on the *C. elegans* genome at Wormbase (version WS282), the *P. pacificus* transcriptome (El_Paco_V3 annotation), and the *S. ratti* genome (PRJEB125 version WBPS16). Human orthologous proteins were assigned according to Wormbase curation and/or literature. Note that nematode nomenclature of sulfotransferases follows the standard nomenclature rules of *C. elegans*, for example *ssu-1*, follows the 3-letter code of genetic mutants and was isolated as a Suppressor of Stomatin mutant Uncoordination. All other genes, were described based on sequence homology and often related to the corresponding enzymes in humans.

(Lightfoot et al., 2019). The role of sulfation enzymes, the sulfatase *eud-1* and the sulfotransferase *seud-1/sult-1*, in the regulation of mouth-form plasticity were discovered through unbiased forward genetic screens and will be described below (Ragsdale et al., 2013; Bui et al., 2018; Namdeo et al., 2018).

Sulfotransferases in Nematodes

Eukaryotes express cytosolic and membrane-bound sulfotransferases. Cytosolic sulfotransferases (termed SULTs) sulfate xenobiotics and small molecules like neurotransmitters and hormones. The membrane-bound sulfotransferases reside in the Golgi and mediate the post-translational sulfation of endogenous macromolecules (proteins, lipids and glycosaminoglycans) in the secretory pathway (Bojarova and Williams, 2008; Leung et al., 2016). Despite low sequence conservation, sulfotransferases possess a conserved protein structure and catalytic properties, which include the binding to the PAPS cofactor. However, sulfotransferases show broad substrate specificity and may sulfate an unlimited number of substrates (Mueller et al., 2015; Langford et al., 2017). The human genome contains 13 cytoplasmic and 39 membrane-bound sulfotransferases (Langford et al., 2017; Gunal et al., 2019). Based on published literature and Wormbase (version WS282), **Table 1** lists the cytosolic and membrane-bound sulfotransferases currently identified in *C. elegans* (36), *P. pacificus* (18) and *Strongyloides ratti* (48), a common gastrointestinal parasitic worm of the rat (Streit, 2008).

Nematode Cytosolic Sulfotransferases

ssu-1 (suppressor of stomatin mutant uncoordination) is the only member of the cytosolic sulfotransferase gene family present in the genome of *C. elegans* (Carroll et al., 2006; Hattori et al., 2006; Mizuguchi et al., 2009). Orthologous proteins include the human SULT1B1, SULT2A1 and SULT2B1 enzymes (Wormbase curation). This sulfotransferase is expressed throughout development, particularly in embryos and adult stages, but shows increased levels in dauer larvae. Recombinant protein is able to sulfate simple phenol substrates, such as bisphenol A (Hattori et al., 2006). Expression of SSU-1 has also been detected in the amphid sensory neurons located in the head of the worm where it is hypothesized to modify endocrine signals (Carroll et al., 2006). A recent study observed that mutant *ssu-1* animals failed to arrest development in response to osmotic stress. The authors suggest that in the sensory neurons SSU-1 sulfates a ligand of the nuclear hormone receptor NHR-1 to activate a transcriptional response to osmotic stress and induce developmental arrest (Burton et al., 2018).

Five paralogs of *C. elegans* SSU-1 are found in *P. pacificus*, termed SULT-1 to SULT-5 (**Table 1**) (Namdeo et al., 2018). CRISPR/Cas9-mediated knockout of these cytosolic sulfotransferases and a genetic screen for suppressors of an all-stenostomatous mutant of *P. pacificus* has identified a role for SULT-1 (PPA12547) in the regulation of mouth-form plasticity (see details below) (Bui et al., 2018; Namdeo et al., 2018). Additional SULTs can also be found in *P. pacificus* (4) and *S. ratti* (8). Their biological role remains unknown.

Nematode Membrane-Bound Sulfotransferases

Tyrosylprotein Sulfotransferases

The genomes of nematodes also contain genes encoding TPSTs (**Table 1**) (Namdeo et al., 2018), integral membrane glycoproteins of the *trans*-Golgi network that post translationally sulfate tyrosine residues of soluble and membrane proteins of the secretory pathway. Sulfation is the most common modification of tyrosine residues and regulates biological activity and correct cellular processing (Monigatti et al., 2006; Stone et al., 2009; Yang et al., 2015). Two types of tyrosylprotein sulfotransferases (TPST1 and TPST2) with distinct substrate preference are present in animals; *P. pacificus* lacks the second TPST gene and *S. ratti* encodes three TPST enzymes (**Table 1**) (Beisswanger et al., 1998; Ouyang and Moore, 1998; Mizuguchi et al., 2009; Namdeo et al., 2018). In *C. elegans*, TPST-1 activity is required for cuticle organization as it controls collagen secretion (Kim et al., 2005; Kim et al., 2010).

Carbohydrate Sulfotransferases

Sulfotransferases also extensively modify carbohydrates/sugars along the secretory pathway. Carbohydrate sulfoforms function on the cell surface and in the extracellular matrix where they provide structural support and mediate communication between cells and the surrounding environment (Bowman and Bertozzi, 1999). Sulfation of carbohydrates creates structural variety, enables electrostatic interactions and generates ligands for specific receptors. The biological significance of the sulfation of carbohydrates is therefore broad as it regulates multiple processes, such as organ development, extracellular signaling, and inflammation, among others (Bowman and Bertozzi, 1999; Strott, 2002). Carbohydrate sulfotransferases are integral membrane enzymes of the Golgi apparatus that sulfate glycans attached to lipids and proteins (Bowman and Bertozzi, 1999; Strott, 2002). Recognizable carbohydrate sulfotransferases in nematodes modify the scaffold of proteoglycans (glycosaminoglycan chains constituted by repeating disaccharide units attached to core proteins) to produce variable sulfoforms. Two groups of carbohydrate sulfotransferases are present in *C. elegans*, *P. pacificus* and *S. ratti*: heparan sulfate (HS) and chondroitin sulfate (CS) sulfotransferases (**Table 1**). Sequence homology searches revealed 28 CS-6-O-sulfotransferases-like genes (CHST) in *C. elegans* (Mizuguchi et al., 2009), with three orthologs in *P. pacificus* (Namdeo et al., 2018) and 32 in *S. ratti* (**Table 1**). Five HS-sulfotransferases (HSTs) are also encoded in the genomes of the three nematodes (Mizuguchi et al., 2009; Namdeo et al., 2018) (**Table 1**).

a) Biological roles of CS-sulfotransferases in *C. elegans*

Chondroitin sulfate chains are composed of disaccharide units of glucuronic acid (GlcUA) and iduronic acid-*N*-acetylgalactosamine (GalNAc) heterogeneously sulfated (Sugahara et al., 2003). Sulfation of CS occurs on the 4- and 6-hydroxyl groups of GalNAc and on the 2-hydroxyl group of

GlcUA. CS is the main structural component of the extracellular matrix in the brain and cartilage. In addition, CS sulfoforms regulate cell signaling through specific receptor-ligand binding influencing processes such as neuronal and skeletal development, and infection by pathogens (Bowman and Bertozzi, 1999; Sugahara et al., 2003).

Nematodes produce vast amounts of non-sulfated chondroitin (Yamada et al., 1999; Toyoda et al., 2000; Olson et al., 2006; Lawrence et al., 2008), which in *C. elegans* is crucial for cell division during embryogenesis and vulva morphogenesis (Herman et al., 1999; Hwang et al., 2003; Mizuguchi et al., 2003). Mutations or RNAi depletion of the nematode chondroitin synthase gene are proposed to decrease chondroitin hydration activity controlling tissue osmotic pressure (structural role) and/or disrupt cell signaling (Hwang et al., 2003; Mizuguchi et al., 2003). Although the presence of CS in *C. elegans* has been controversial, several studies detected different sulfoforms in the worms (Schimpf et al., 1999; Beeber and Kieras, 2002; Dierker et al., 2016). Recently, the first CS sulfotransferase enzyme has also been characterized in *C. elegans*, CHST-1 (**Table 1**) (Dierker et al., 2016), suggesting that sulfate CS has a biological role also in nematodes. Recombinant CHST-1 utilizes PAPS to sulfate a chondroitin substrate, and the levels of 4-*O*-sulfation in chondroitin are dramatically reduced in the *chst-1* mutant strain (Dierker et al., 2016). Whether the 26 other putative CS-sulfotransferases present in *C. elegans* genome encode for functional sulfotransferases with effects on CS sulfation and worm biology remains unclear, similar to the function of CS sulfotransferases in other nematodes.

b) Biological roles of HS-sulfotransferases in *C. elegans*

HS molecules are linear glycosaminoglycan polysaccharides composed of glucuronic acid (GlcUA) and iduronic acid-*N*-acetylglucosamine (GlcNAc) repeat units covalently bound to a protein core. As components of extracellular matrices and cell surfaces, HS function in a wide range of cellular processes, are essential in development and homeostasis, and have several implications in disease (Bowman and Bertozzi, 1999; Strott, 2002; Lindahl and Li, 2009). Three different types of HS are present in cells: syndecans (transmembrane proteins), glycosylphosphatidylinositol (GPI)-anchored proteins (e.g., glypicans) and secreted molecules (e.g., perlecan, agrin, and collagen XVIII) (Lindahl and Li, 2009). The genome of *C. elegans* contains single orthologues of these major proteoglycans (syndecan/F57C7.3, glypican/F59D12.4, perlecan (*unc-52*) and agrin/F41G3.8) (Rogalski et al., 1993; Hutter et al., 2000; Ackley et al., 2001; Bulow and Hobert, 2004; Minniti et al., 2004; Gumienny et al., 2007). After synthesis in the Golgi complex, heparan sulfate polymers are highly modified by deacetylation, sulfation and epimerization catalyzed by specific HS modifying enzymes at selective positions. The bifunctional enzyme *N*-deacetylase/*N*-sulfotransferases (Ndst) removes the acetyl group from GlcNAc and substitutes it with a sulfuryl group (Wei et al., 1993). The reactions catalyzed by Ndst allow the subsequent epimerization of glucuronic acid to iduronic acid and sulfation of HS, as the other enzymes

recognize the N-sulfate groups on the molecule (Habuchi, 2000). The HS C-5 glucuronyl-epimerase is responsible for epimerization, while the HS 2-O, HS 6-O, HS 3-O sulfotransferases add SO₃ at the C2 hydroxyl group of hexuronic acids and the C6 or C3 of glucosamine units, respectively (Habuchi, 2000; Turnbull et al., 2001; Lindahl and Li, 2009). Orthologues of all of these enzymes are present in nematodes (Table 1). These modifications increase the structural diversity of HS and influence cellular processes such as cell migration, axon guidance and pathogen infection as they are binding sites for multiple ligands, receptors, growth factors, enzymes, extracellular matrix proteins and adhesion proteins found in pathogens. These interactions are specific and perform regulatory roles (Turnbull et al., 2001; Lindahl and Li, 2009).

Work in *C. elegans* has increased the understanding of the relationships among HS modifications and specific proteoglycans in defined biological processes. The HS-modifying enzymes have differential effects in the development of the nervous system. For example, the modifications catalyzed by C-5 glucuronyl-epimerase (*hse-5*), HS 2-O (*hst-2*) and HS 6-O (*hst-6*)-sulfotransferases have been described to differentially regulate specific signaling pathways controlling axonal development (Bulow and Hobert, 2004). Efficient Robo, Ephrin and possibly Integrin-associated signaling pathways are dependent on distinct HS modifications to properly guide axon patterning in specific cellular contexts. These signaling pathways act in concert with precise modifications on components of the extracellular matrix to organize the complexity of the nervous system (Bulow and Hobert, 2004). In addition, the activity of HST-6 has been shown to modulate the function of anosmin (Kallman protein, *kal-1*), a secreted neural cell adhesion molecule with roles in axonal growth (Bulow et al., 2002). Parallel HS modifications also participate in the migration of *C. elegans* hermaphrodite specific neurons (HSNs), the pair of neurons that coordinates contraction of the vulval muscles to initiate egg laying (Desai et al., 1988; Kinnunen et al., 2005; Kinnunen, 2014). The migration of these neurons that are born in the posterior towards the mid body region is supported by HST-6-dependent sulfation of syndecan and HST-2-mediated sulfation of glypican. Genetic elimination of *hst-2* (expressed in the muscle and hypodermis) and *hst-6* (predominantly expressed in neurons) causes severe defects in the migration of the HSNs (Kinnunen, 2014). RNAi of the *hst-2* gene in *C. elegans* also causes aberrant morphology of the gonad and defects in egg laying, suggesting that sulfated HS chains are required for normal development and function of the reproductive tissues (Turnbull et al., 2003; Kinnunen et al., 2005).

The function of HST-3 enzymes has likewise been investigated in *C. elegans*. In *loss-of-function* mutants of *hst-3.1* and *hst-3.2*, worm viability and overall neuronal development are not affected. Yet, HS-3-O-sulfation has a specialized role in HSNs. Together with KAL-1, both enzymes are important for the branching of neurites in these neurons (Tecle et al., 2013). Forward genetic screens, have also identified *hst-6* and *hst-3.2* as modifiers of *kal-1*-dependent neurite branching of AIY neurons, a left/right pair of interneurons with axons that

innervate the nerve ring in the head of the worm (Diaz-Balzac et al., 2014). Thus, different HS modifications regulate *kal-1*-dependent branching in distinct tissues. As KAL-1/anosmin is the underlying gene causing hereditary Kallman syndrome in humans (Franco et al., 1991; Legouis et al., 1991), these studies highlight the importance of using nematode model systems to understand the role of HS in development and disease-associated processes.

Mating behavior between hermaphrodites and males is also controlled by sulfation of HS molecules. During mating, the male will press its tail against the body of the hermaphrodite and move backwards in search for the vulva (Liu and Sternberg, 1995). Abnormal response to mate contact has been observed in *hst-2*, *hst-3.1* and *hse-5* mutant worms, suggesting that HS modifications are required for the response to hermaphrodite contact by the male worm (Lazaro-Pena et al., 2018). Specifically, 3-O-sulfation of glypicans regulates synaptogenesis in neurons controlling male mating behavior, the B-type ray sensory neurons (Liu and Sternberg, 1995; Koo et al., 2011; Lazaro-Pena et al., 2018).

Finally, HS modifications have also been shown to regulate cilia structure in *C. elegans* (Acker et al., 2021). The cilia protrusions are organized in highly compartmentalized microtubule-based domains and disruption of their composition and structure results in ciliopathies (Reiter and Leroux, 2017). Null alleles of *hst-3.1* show defects in the localization of complement factor H (CFH) to the cilia of mechanosensory neurons. A potential interaction of CFH with modified HS appears to control cilia structural organization. HST-3.1 is proposed to modify the HS chain of proteoglycans that recruit CFH in the mechanosensory neurons. In the absence of this modification, CFH is not properly localized in the cilia and the animals show defects in mechanosensory neuron function (Acker et al., 2021). The role of HS modifications in cilia structure is another example of how studies in nematodes increase our knowledge on disease associated processes, since CFH is a major risk factor for age-related macular degeneration and blindness in humans (Edwards et al., 2005; Hageman et al., 2005; Haines et al., 2005; Klein et al., 2005; Zarepari et al., 2005).

In summary, the differential modification of molecules of HS provide a “code” that mediates the selective interaction with a set of signaling factors and molecules that define the migration, patterning and function of different neurons (Bulow and Hobert, 2004; Lindahl and Li, 2009; Kinnunen, 2014).

Sulfatases in Nematodes

From prokaryotes to eukaryotes sulfatases are highly conserved in sequence, structure and mechanism of action (Hanson et al., 2004; Ghosh, 2007). They share a highly conserved N-terminal region containing two consensus sulfatase motifs. The first motif is characterized by the conserved sequence C/SxPxRxxxxTG (x is any amino acid) and is crucial to generate the post-translationally modified active-site aldehyde residue, the α-formylglycine (FGly; 2-amino-3-oxopropanoic acid) (Knaust et al., 1998; Dierks et al., 1999). The second sulfatase signature motif is a 12-mer sequence GY/VxS/T-xxxGKxxH. The Lys and His residues are part of the active-site and required for catalysis (Waldow et al., 1999). The

TABLE 2 | Sulfatases in nematodes and corresponding human orthologues.

	<i>H. sapiens</i>	<i>C. elegans</i>	<i>P. pacificus</i>	<i>S. ratti</i>	
Heparan sulfate proteoglycan biosynthetic process	SULF1	SUL-1	SUL-1 (PPA46687)	SRP07877	Extracellular sulfatases; Removal of 6-O-sulfate from heparan sulfate
	SULF2				
	ARSL/E	SUL-2	SUL-2.1 (PPA21290) SUL-2.2.1 (PPA06135)EUD-1 (PPA43535)	SRP01584	Golgi; ER (steroid sulfates)
	STS				Lysosome (chondroitin sulfate, keratan sulfate)
	GALNS				Lysosome
	ARSB	SUL-3	SUL-3 (PPA23475)	SRP06160	
	ARSI				
	ARSJ				ER, secreted

Protein searches were performed on the *C. elegans* genome at Wormbase (version WS282), the *P. pacificus* transcriptome (EI_Paco_V3 annotation), and the *S. ratti* genome (PRJEB125 version WBPS16). Human orthologous proteins were assigned according to Wormbase curation and/or literature.

C-terminal region of sulfatases is the most diverse; however, it is proposed that this region provides substrate specificity (Hanson et al., 2004). Although a large number of eukaryotic sulfatases are active on small aromatic sulfates (aryl substrates) *in vitro* and thus classified as arylsulfatases, many sulfatases show strong substrate specificity, specific subcellular location and optimal activity under defined conditions (Hanson et al., 2004). Sulfatase genes encode proteins with a wide range of substrate specificity but little functional redundancy, and deficiency in a single sulfatase can lead to unique disorders and developmental defects in animals (Langford et al., 2017).

Eukaryotic sulfatases are targeted to the secretory pathway. In the endoplasmic reticulum (ER), the sulfatases are modified by glycosylation and FGly is generated (Dierks et al., 1997; Dierks et al., 1998a; Hanson et al., 2004). They can then remain in the ER, be secreted, or transported to other subcellular compartments, such as the Golgi complex and the lysosome (Table 2) (Hanson et al., 2004). The steroid sulfatase (STS, human arylsulfatase C) is integrated into the membrane of the ER or Golgi apparatus (Willemsen et al., 1988; Hernandez-Guzman et al., 2003) where it plays an important role in the regulation of endocrine responses and xenobiotic metabolism. STS is the main enzyme involved in steroid desulfation and regulates hormone levels by removing sulfate from precursors, such as estrone sulfate and dehydroepiandrosterone (DHEAS), and originating active steroid hormones (for review see (Mueller et al., 2015)). Lysosome-located sulfatases (human arylsulfatases A and B) participate in the catabolism of defective and unwanted sulfated glycolipids (sulfatides) and proteoglycans that are imported into this organelle by endocytosis. Lysosome storage disorders are therefore a consequence of lysosome-sulfatase deficiency (Langford et al., 2017). The secreted sulfatases, known as Sulfs, remove the 6-O-sulfate groups of the glucosamine units of HS regulating multiple developmental processes (Hanson et al., 2004; Bojarova and Williams, 2008; Langford et al., 2017).

Nematodes also contain multiple sulfatase genes: three in *C. elegans* and *S. ratti*, and five in *P. pacificus* (Table 2). Sequence-wise Wormbase indicates that SUL-1 proteins are orthologues of the secreted SULF-1 and SULF-2 sulfatases that act on HS. In contrast, SUL-2 proteins show similarity with the human arylsulfatases A, B that participate in the degradation of

cerebroside-3-sulfate and keratan/dermatan sulfate or CS, respectively, the steroid sulfatase (STS) and N-acetylglucosamine-6-sulfatase (GALNS) (Ragsdale et al., 2013; Perez-Jimenez et al., 2021), another lysosome-resident protein involved in the catabolism of HS (Schlotawa et al., 2020). SUL-3 proteins are most similar to the lysosome sulfatase human arylsulfatase B that participates in the degradation of keratan/dermatan sulfate and CS, or the potentially secreted arylsulfatases I and J with currently uncharacterized substrates. The biological function, localization and substrates of the nematode sulfatases are largely unexplored. To date, efforts to understand desulfation in worms have been restricted to *C. elegans* SUL-2 and *P. pacificus* EUD-1 (SUL-2 paralog). The role of EUD-1 in the regulation of mouth-form and predation is discussed below.

C. elegans SUL-2, the worm steroid sulfatase (Perez-Jimenez et al., 2021), is expressed in sensory neurons of the head of the worm where it is proposed to regulate the levels of steroid hormones. Worms with *loss-of-function* mutation of *sul-2* or treated with the steroid sulfatase (STS) inhibitor STX64 have higher levels of sulfate steroid hormones and increased longevity. The authors of the study hypothesize that sulfated steroid hormones produced in the gonads of the worm may act in response to environmental cues, such as nutrient availability, to alter neurotransmission and promote longevity. Furthermore, higher levels of sulfated hormones as a result of reduced SUL-2 activity, or treatment of worms with sulfated steroid hormones, reduced protein aggregation and proteotoxic stress in models of Parkinson and Huntington neurodegenerative disorders. These data indicate that inhibitors of STS activity and sulfated steroid hormones have great potential in the treatment of aging-related diseases (Perez-Jimenez et al., 2021). In the same study, genetic ablation of *sul-1* and *sul-3* had no effects on lifespan.

The post-translational modification that enhances sulfatase activity is catalyzed by an endoplasmic reticulum (ER)-resident protein, the FGE-generating enzyme (FGE, sulfatase modifying factor 1, *SUMF1*) (Dierks et al., 1998a; Cosma et al., 2003; Dierks et al., 2003; Appel and Bertozzi, 2015). The FGly modification is essential for sulfatase activity (Dierks et al., 1998b; Recksiek et al., 1998) and is able to greatly stimulate catalytic proficiency, which can reach a rate enhancement (k_{cat}/k_{uncat}) of 10^{26} for alkylsulfates

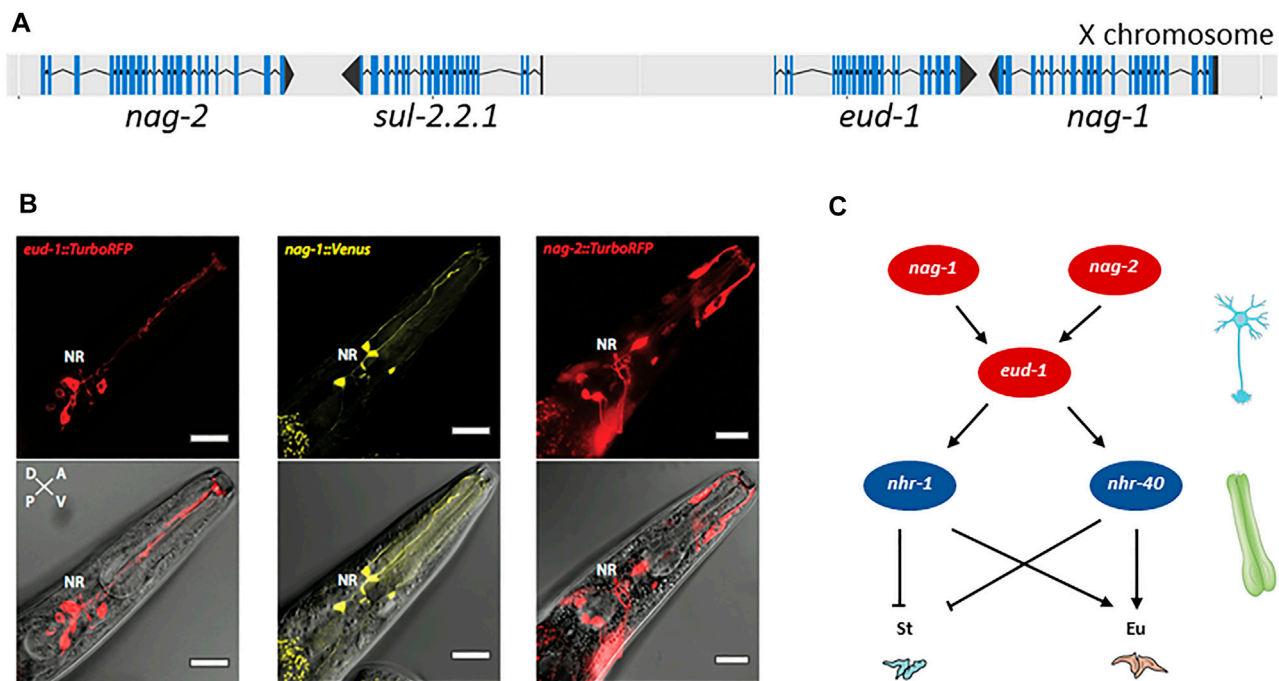


FIGURE 2 | Genes involved in mouth-form dimorphism. **(A)** The switch gene *eud-1* is located on the X chromosome of *P. pacificus* in an inverted tandem configuration (head-to-head orientation) with its paralog *sul-2.2.1*. In the same gene cluster, the two sulfatase genes are surrounded by a pair of inverted and duplicated genes encoding the α -N-acetylglucosaminidases NAG-1 and NAG-2. Blue lines indicate the coding sequence (CDS); black lines represent the untranslated regions (UTRs) of the gene. Figure adapted from (Sieriebriennikov et al., 2018). **(B)** *eud-1*, *nag-1* and *nag-2* are expressed in distinct sensory neurons. Depicted are head sections of worms overexpressing fluorescent *eud-1*, *nag-1* or *nag-2* transcriptional reporters. Bottom: overlay of a DIC image with the TurboRFP (red fluorescent protein) or Venus fluorescence. Top: the same without the DIC image. Bar = 20 μ m. **(C)** Partial genetic network involved in mouth-form plasticity indicating some of the key players, the α -N-acetylglucosaminidases *nag-1* and *nag-2*, the sulfatase-encoding gene *eud-1* and the nuclear hormone receptors *nhr-40* and *nhr-1*. *nag-1*, *nag-2* and *eud-1* are expressed in sensory neurons whereas *nhr-40* and *nhr-1* expression is mainly detected in the pharyngeal muscle cells, which are thought to secrete the structural components of the teeth. St: stenostomatous; Eu: eurystomatous.

(most efficient enzymes known to date) (Edwards et al., 2012). In humans, lack of FGly modification in sulfatases due to mutations in FGE that alter its activity causes multiple sulfatase deficiency (Schmidt et al., 1995; Schlotawa et al., 2020). FGE orthologues are found in prokaryotes and eukaryotes. Yet, homology searches indicate that FGE homologs are not present in plants (which also lack sulfatases), nematodes and fungi, although these last two groups of organisms contain cysteine-type sulfatase genes (Landgrebe et al., 2003; Appel and Bertozzi, 2015). This observation is suggestive of a different FGly-generating system in nematodes and fungi with a yet elusive enzyme. Alternatively, as FGly modification has not been studied so far in these groups of organisms, it remains unknown if their sulfatases require this post-translational modification to be active.

Sulfatases in *P. pacificus*

The sulfatase-encoding gene *eud-1* was the first gene identified to regulate mouth-form plasticity in *P. pacificus* (Ragsdale et al., 2013). In the *P. pacificus* wild type strain PS312, the majority of animals express the predatory Eu mouth-form. Therefore, genetic screens aimed at identifying eurystomatous form defective (*eud*) mutants that would only generate St animals. From a screen of less than 4,000 haploid genomes, 17 mutants with a *Eud* phenotype were isolated. Of these, four were dominant with

heterozygous animals having a mutant all-St phenotype and all of them turned to be alleles of the same gene, *eud-1*. The cloning of *eud-1* not only revealed this gene to encode a sulfatase but also that all four mutations reduce or eliminate gene function (Ragsdale et al., 2013). These *reduction-of-function* mutations and the associated dominant phenotype indicate this gene to be haploinsufficient and to act as a developmental switch. Indeed, *eud-1* mutants can be rescued by the overexpression of a wild type copy of *eud-1*, whereas overexpression of the mutant version of *eud-1* will not cause a Eu phenotype in wild type animals (Ragsdale et al., 2013). It should be noted that such dominant *reduction-of-function* mutants are extremely rare with only one example known in *C. elegans* after more than 50 years of forward genetic screening, whereas *gain-of-function* mutants with a dominant phenotype are quite common (Hodgkin, 2005).

Further characterization revealed that EUD-1 might act as a sulfatase. *Ppa-EUD-1*, like *Cel-SUL-2*, is most similar to the human arylsulfatases A, GALNS and STS (Table 2). Application of sulfate and phosphate ions in the worm diet, which are known inhibitors of arylsulfatases, mimicked the *eud-1* phenotype (Ragsdale et al., 2013). As indicated above, the *P. pacificus* genome contains more sulfatase genes than the *C. elegans* genome and *eud-1* is indeed one of the genes resulting from lineage-specific gene duplications. While the arylsulfatase

Cel-sul-2 is a single copy gene on chromosome IV, there are three *sul-2*-related genes in *P. pacificus* (Table 2). The ancestral gene is also located on chromosome IV and is termed *Ppa-sul-2.1*. The two additional copies, *eud-1* and *Ppa-sul-2.2.1*, are located on the X chromosome with an interesting head to head organization and a separation by 7 kb of potential regulatory sequence (Figure 2A). *Ppa-sul-2.2.1* and *Ppa-sul-2.1* were soon shown to play no role in mouth-form specification (Ragsdale and Ivers, 2016). However, the full complexity of the *eud-1* locus was only revealed through several additional experiments. First, the conserved histone-acetyltransferase *Ppa-lsy-12* is required for *eud-1* expression suggesting that *eud-1* expression and mouth-form regulation are subject to epigenetic control (Seroby et al., 2016). Second, an antisense-*eud-1* message exists at the locus that acts as a positive regulator of *eud-1* (Seroby et al., 2016). Finally, two more enzyme encoding genes are part of the *eud-1* locus. These genes encode for N-acetylglucosaminidases (*nag*) and *nag-1* and *nag-2* are located adjacent to *sul-2.2.1* and *eud-1*, respectively (Figure 2A). Inactivation of both genes results in the opposite phenotype of *eud-1* mutants: all animals have the Eu mouth-form even in liquid culture conditions that induce the St morph in wild type animals (Sieriebriennikov et al., 2018). Interestingly, *nag-1*, *nag-2* and *eud-1* are expressed in a small set of different sensory neurons suggesting that they play a key role in environmental perception (Figure 2B). Importantly, *eud-1* is epistatic over *nag-1* and *nag-2* as a quadruple knockout of the complete multigene locus has an all-St phenotype similar to *eud-1* single mutants (Sieriebriennikov et al., 2018). Thus, the sulfatase EUD-1 plays a crucial role in mouth-form regulation as the central developmental switch. First, it is involved in the sensing of the environment and second, it integrates different environmental inputs to guide final decision making of mouth-form. It is important to note that while these genetic experiments clearly show a key role of a sulfatase in regulating a plastic developmental decision, the exact biochemical function and the potential substrates remain currently unknown. It has been speculated based on the physical proximity of sulfatases and N-acetylglucosaminidases that they might act on the extracellular matrix of neurons. However, no experimental support of this hypothesis is currently available and future studies have to shed light on the actual substrates of EUD-1.

Sulfotransferases in *P. pacificus*

Further genetic studies have identified a complex gene regulatory network (GRN) to control mouth-form plasticity with *eud-1* representing the key developmental switch (Figure 2C) (Sieriebriennikov et al., 2020). The identification of this GRN was in large parts based on the strong all-St phenotype of the *eud-1* mutant itself, which allowed unbiased genetic screens for suppressors resulting in all-Eu animals.

First, three suppressor alleles with an all-Eu phenotype were shown to result from mutations in the nuclear hormone receptor *Ppa-nhr-40* (Kieninger et al., 2016) and were later on shown to result from *gain-of-function* mutations (Sieriebriennikov et al., 2020). In contrast, the *loss-of-function* phenotype of *Ppa-nhr-40* is all-St and thus, similar to the *eud-1* mutant phenotype

(Sieriebriennikov et al., 2020). Also, *loss-of-function* mutations in another nuclear hormone receptor, *Ppa-nhr-1*, have an all-St phenotype, but with additional morphological defects in teeth formation unknown from other mutants (Sieriebriennikov et al., 2020). These studies would be compatible with the EUD-1 protein regulating the sulfation state of potential ligands of nuclear hormone receptors. Note that while nematodes have undergone a substantial expansion of nuclear hormone receptors with more than 250 genes in *P. pacificus* and *C. elegans*, only one ligand has been identified: the steroid hormone dafachronic acid that regulates the nuclear hormone receptor DAF-12 in multiple nematode species (Motola et al., 2006; Ogawa et al., 2009). Thus, the ligands of nematode nuclear hormone receptors remain little understood and similarly, nothing is known about a potential role of sulfation in the regulation of such ligands.

Second, the same genetic screen for *eud-1* suppressors resulted in the identification of a sulfotransferase, mutations in which also produced an all-Eu phenotype and thus were named *seud-1* (suppressor of *eud-1*) (Bui et al., 2018). Transgenic overexpression of *seud-1* revealed the sulfotransferase to be dosage-dependent, similar to *eud-1* (Bui et al., 2018). When mutants of *eud-1* and *seud-1* were used to produce all types of homozygous and heterozygous combinations, a graduation of phenotypes was observed. For example, animals with one copy of the sulfotransferase *seud-1* and two copies of the sulfatase *eud-1* were Eu (Bui et al., 2018). Besides the work of Bui and co-workers, an independent study resulted in the identification of the same sulfotransferase. A pharmacological screen found bisphenol A to induce the St mouth phenotype in wild type animals (Namdeo et al., 2018). As already indicated above, in *C. elegans* the sulfotransferase *ssu-1* sulfates bisphenol A (Hattori et al., 2006). Indeed, a systematic screen of the five sulfotransferases of *P. pacificus* that are most similar in sequence to *Cel-ssu-1*, identified a single gene, named *sult-1*, to control mouth-form plasticity (Namdeo et al., 2018). Note that these independent studies have named the same sulfotransferase gene as *seud-1* and *sult-1*. Importantly, the expression of SEUD-1/SULT-1 (pharyngeal muscle cells) is distinct from EUD-1 (sensory neurons) and therefore, it is possible that two independent sulfation processes regulate mouth-form plasticity (Bui et al., 2018; Namdeo et al., 2018).

Sulfolipids of *P. pacificus* Induce Escape Behavior in *C. elegans*

Completely independent insight pointing towards the role of sulfated molecules in the biology of *P. pacificus* nematodes came from studies in analytical chemistry. The predatory behavior of *P. pacificus* is thought to be of importance in the context of the ecology of this nematode. While *P. pacificus* is a soil nematode, it is most reliably found in association with adult scarab beetles, i.e. cock chafers, stag beetles and dung beetles. On the living beetle, nematodes are found in the dauer stage, the arrested and stress-resistant, alternative larval stage that can survive long periods of harmful conditions. It is important to note that several, unrelated nematode species can be found on beetles and also other insects,

and many of them wait for their vector to die. Indeed, after the beetles' death back in the soil, bacteria and fungi will grow on the carcass. These food signals will cause the exit of the nematodes from the dauer stage and they rapidly mature to feed and reproduce on this time-limited food source. Indeed, recent studies in *P. pacificus* have indicated the dynamics and succession of nematodes on beetle carcasses in the context of the microbiome of the insect cadaver (Meyer et al., 2017; Renahan et al., 2021; Renahan and Sommer, 2021). The predatory behavior of Eu animals of *P. pacificus* is thought to serve a dual role: on the one hand, it allows supplementation of its bacterial diet by preying on nematodes; on the other hand, it will result in the elimination of competitors for the limited bacterial food available. This phenomenon is known as intraguild predation and represents an important concept in ecology (Polis and Holt, 1992; Quach and Chalasani, 2020).

While there is no obvious evidence that *P. pacificus* and *C. elegans* share the same ecosystem, a study by Liu and co-workers indicated a defensive response of *C. elegans* when it is exposed to *P. pacificus* predators (Liu et al., 2018). Subsequent studies revealed the behavioral details of this predator-prey competition (Quach and Chalasani, 2020). Strikingly, the original defensive response of *C. elegans* larvae towards *P. pacificus* is caused by predator-secreted sulfolipids. Specifically, fractionation of the *P. pacificus* secretome and analytical chemistry identified several (w-1)-branched-chain sulfolipids to induce the escape behavior in *C. elegans* prey (Liu et al., 2018). These findings are consistent with previous studies that showed an avoidance behavior of *C. elegans* against sodium dodecyl sulfate (SDS) (Hilliard et al., 2004). Importantly, the production and secretion of branched chain fatty acids is specific to *P. pacificus* and likely its relatives (Liu et al., 2018). The presence of multiple secreted sulfolipids in *P. pacificus* might open the door to several independent functions in the organism. For example, it might well be that branched chain fatty acids can serve as ligands for nuclear hormone receptors although no functional studies are yet available to support this hypothesis. In conclusion, genetic and chemical studies provide strong support for the role of sulfation in the development and the behavior of this nematode.

Open Questions and Future Perspectives

The literature described in this review highlights the significance of sulfation and desulfation pathways during development of different nematodes. From neuronal organization, to the regulation of phenotypic traits and behavior, sulfatases and sulfotransferases appear to modify a wide range of substrates also in nematodes. Despite the work done so far, we still possess a

limited understanding on the localization, substrates and regulation of the panoply of sulfation-associated enzymes present in worms. Many of the sulfotransferases and sulfatases remain uncharacterized; their substrates are unknown, we have no understanding of their biological significance or subcellular localization, and we lack defined knowledge on their pattern of expression. Moreover, specific sulfated molecules, such as sulfolipids, act as signaling molecules between animals (Quach and Chalasani, 2020). However, we still do not understand the molecular mechanisms that generate, interpret, and execute, or the universality of this communication pathway.

An exciting research area in sulfation relates to the regulation of the enzymatic activity by post-translational modifications, such as FGly and glycosylation. As mentioned above, nematodes lack a recognizable FGE. Future studies that aim at detecting this unique modification in the proteome of nematodes, the corresponding modifying enzyme and its mechanism of action have great potential to elucidate alternative systems that introduce the FGly modification in eukaryotic sulfatases.

The significance of sulfation pathways in parasitic nematodes, like *S. ratti*, has never been addressed. With the development of specific sulfatase inhibitors, it is therefore of great importance to study their impact on the infection and ability of the parasite to invade the host. A deeper understanding on the sulfation players and their functions in these pathogenic worms may lead to improved therapeutic strategies that aim at eliminating the pathogen from their natural host. We are therefore looking forward to use nematodes in the quest to obtain a comprehensive understanding of the mechanisms and roles that sulfation plays in organismal development.

AUTHOR CONTRIBUTIONS

All authors listed have made a substantial, direct, and intellectual contribution to the work and approved it for publication.

ACKNOWLEDGMENTS

We thank the members of the Sommer laboratory, in particular Radhika Sharma and Alejandra Schäfer, for inspiring discussions, and Wen-Sui Lo and Alejandra Schäfer for help with bioinformatic analysis of nematode sulfatase and sulfotransferase genes. We are grateful to Bogdan Seriebriennikov for the fluorescence images depicted in **Figure 2B**.

REFERENCES

- Acker, N., Smith, H., Devine, C., Oltjen, S. L., Tsiropoulou, S., Smit-Mcbride, Z., et al. (2021). A Complement Factor H Homolog, Heparan Sulfation, and Syndecan Maintain Inversin Compartment Boundaries in *C. elegans* Cilia. *Proc. Natl. Acad. Sci. U S A.* 118. doi:10.1073/pnas.2016698118
- Ackley, B. D., Crew, J. R., Elamaa, H., Pihlajaniemi, T., Kuo, C. J., and Kramer, J. M. (2001). The NC1/endostatin Domain of *Caenorhabditis elegans* Type XVIII Collagen Affects Cell Migration and Axon Guidance. *J. Cel Biol* 152, 1219–1232. doi:10.1083/jcb.152.6.1219
- Appel, M. J., and Bertozzi, C. R. (2015). Formylglycine, a post-translationally Generated Residue with Unique Catalytic Capabilities and Biotechnology Applications. *ACS Chem. Biol.* 10, 72–84. doi:10.1021/cb500897w
- Beeber, C., and Kieras, F. J. (2002). Characterization of the Chondroitin Sulfates in Wild Type *Caenorhabditis elegans*. *Biochem. Biophysical Res. Commun.* 293, 1374–1376. doi:10.1016/s0006-291x(02)00399-6

- Beisswanger, R., Corbeil, D., Vannier, C., Thiele, C., Dohrmann, U., Kellner, R., et al. (1998). Existence of Distinct Tyrosylprotein Sulfotransferase Genes: Molecular Characterization of Tyrosylprotein Sulfotransferase-2. *Proc. Natl. Acad. Sci.* 95, 11134–11139. doi:10.1073/pnas.95.19.11134
- Bento, G., Ogawa, A., and Sommer, R. J. (2010). Co-option of the Hormone-Signalling Module Dafachronic Acid-DAF-12 in Nematode Evolution. *Nature* 466, 494–497. doi:10.1038/nature09164
- Bojarová, P., and Williams, S. J. (2008). Sulfotransferases, Sulfatases and Formylglycine-Generating Enzymes: a Sulfation Fascination. *Curr. Opin. Chem. Biol.* 12, 573–581. doi:10.1016/j.cbpa.2008.06.018
- Bowman, K. G., and Bertozzi, C. R. (1999). Carbohydrate Sulfotransferases: Mediators of Extracellular Communication. *Chem. Biol.* 6, R9–R22. doi:10.1016/s1074-5521(99)80014-3
- Brenner, S. (1974). The Genetics of *Caenorhabditis elegans*. *Genetics* 77, 71–94. doi:10.1093/genetics/77.1.71
- Bui, L. T., Ivers, N. A., and Ragsdale, E. J. (2018). A Sulfotransferase Dosage-Dependently Regulates Mouthpart Polyphenism in the Nematode *Pristionchus pacificus*. *Nat. Commun.* 9, 4119. doi:10.1038/s41467-018-05612-8
- Bulow, H. E., Berry, K. L., Topper, L. H., Peles, E., and Hobert, O. (2002). Heparan Sulfate Proteoglycan-dependent Induction of Axon Branching and Axon Misrouting by the Kallmann Syndrome Gene Kal-1. *Proc. Natl. Acad. Sci.* 99, 6346–6351. doi:10.1073/pnas.092128099
- Bulow, H. E., and Hobert, O. (2004). Differential Sulfations and Epimerization Define Heparan Sulfate Specificity in Nervous System Development. *Neuron* 41, 723–736. doi:10.1016/s0896-6273(04)00084-4
- Burton, N. O., Dwivedi, V. K., Burkhart, K. B., Kaplan, R. E. W., Baugh, L. R., and Horvitz, H. R. (2018). Neurohormonal Signaling via a Sulfotransferase Antagonizes Insulin-like Signaling to Regulate a *Caenorhabditis elegans* Stress Response. *Nat. Commun.* 9, 5152. doi:10.1038/s41467-018-07640-w
- Carroll, B. T., Dubyak, G. R., Sedensky, M. M., and Morgan, P. G. (2006). Sulfated Signal from ASJ Sensory Neurons Modulates Stomatin-dependent Coordination in *Caenorhabditis elegans*. *J. Biol. Chem.* 281, 35989–35996. doi:10.1074/jbc.m606086200
- Consortium, C. E. S. (1998). Genome Sequence of the Nematode *C. elegans*: a Platform for Investigating Biology. *Science* 282, 2012–2018. doi:10.1126/science.282.5396.2012
- Cosma, M. P., Pepe, S., Annunziata, I., Newbold, R. F., Grompe, M., Parenti, G., et al. (2003). The Multiple Sulfatase Deficiency Gene Encodes an Essential and Limiting Factor for the Activity of Sulfatases. *Cell* 113, 445–456. doi:10.1016/s0092-8674(03)00348-9
- Coughtrie, M. W. H. (2016). Function and Organization of the Human Cytosolic Sulfotransferase (SULT) Family. *Chemico-Biological Interactions* 259, 2–7. doi:10.1016/j.cbi.2016.05.005
- Desai, C., Garriga, G., McIntire, S. L., and Horvitz, H. R. (1988). A Genetic Pathway for the Development of the *Caenorhabditis elegans* HSN Motor Neurons. *Nature* 336, 638–646. doi:10.1038/336638a0
- Díaz-Balzac, C. A., Lázaro-Peña, M. I., Teclé, E., Gomez, N., and Bülow, H. E. (2014). Complex Cooperative Functions of Heparan Sulfate Proteoglycans Shape Nervous System Development in *Caenorhabditis elegans*. *G3 (Bethesda)* 4, 1859–1870. doi:10.1534/g3.114.012591
- Dickinson, D. J., and Goldstein, B. (2016). CRISPR-based Methods for *Caenorhabditis elegans* Genome Engineering. *Genetics* 202, 885–901. doi:10.1534/genetics.115.182162
- Dierker, T., Shao, C., Haitina, T., Zaia, J., Hinas, A., and Kjellén, L. (2016). Nematodes Join the Family of Chondroitin Sulfate-Synthesizing Organisms: Identification of an Active Chondroitin Sulfotransferase in *Caenorhabditis elegans*. *Sci. Rep.* 6, 34662. doi:10.1038/srep34662
- Dierks, T., Lecca, M. R., Schlotterhose, P., Schmidt, B., and Von Figura, K. (1999). Sequence Determinants Directing Conversion of Cysteine to Formylglycine in Eukaryotic Sulfatases. *EMBO J.* 18, 2084–2091. doi:10.1093/emboj/18.8.2084
- Dierks, T., Lecca, M. R., Schmidt, B., and Von Figura, K. (1998a). Conversion of Cysteine to Formylglycine in Eukaryotic Sulfatases Occurs by a Common Mechanism in the Endoplasmic Reticulum. *FEBS Lett.* 423, 61–65. doi:10.1016/s0014-5793(98)00065-9
- Dierks, T., Miech, C., Hummerjohann, J., Schmidt, B., Kertesz, M. A., and Von Figura, K. (1998b). Posttranslational Formation of Formylglycine in Prokaryotic Sulfatases by Modification of Either Cysteine or Serine. *J. Biol. Chem.* 273, 25560–25564. doi:10.1074/jbc.273.40.25560
- Dierks, T., Schmidt, B., Borissenko, L. V., Peng, J., Preusser, A., Mariappan, M., et al. (2003). Multiple Sulfatase Deficiency Is Caused by Mutations in the Gene Encoding the Human Ca-Formylglycine Generating Enzyme. *Cell* 113, 435–444. doi:10.1016/s0092-8674(03)00347-7
- Dierks, T., Schmidt, B., and Von Figura, K. (1997). Conversion of Cysteine to Formylglycine: a Protein Modification in the Endoplasmic Reticulum. *Proc. Natl. Acad. Sci.* 94, 11963–11968. doi:10.1073/pnas.94.22.11963
- Dieterich, C., Clifton, S. W., Schuster, L. N., Chinwalla, A., Delehaunty, K., Dinkelacker, I., et al. (2008). The *Pristionchus pacificus* Genome Provides a Unique Perspective on Nematode Lifestyle and Parasitism. *Nat. Genet.* 40, 1193–1198. doi:10.1038/ng.227
- Edwards, A. O., Ritter, R., 3rd, Abel, K. J., Manning, A., Panhuysen, C., and Farrer, L. A. (2005). Complement Factor H Polymorphism and Age-Related Macular Degeneration. *Science* 308, 421–424. doi:10.1126/science.1110189
- Edwards, D. R., Lohman, D. C., and Wolfenden, R. (2012). Catalytic Proficiency: the Extreme Case of S-O Cleaving Sulfatases. *J. Am. Chem. Soc.* 134, 525–531. doi:10.1021/ja208827q
- Fire, A., Xu, S., Montgomery, M. K., Kostas, S. A., Driver, S. E., and Mello, C. C. (1998). Potent and Specific Genetic Interference by Double-Stranded RNA in *Caenorhabditis elegans*. *Nature* 391, 806–811. doi:10.1038/35888
- Franco, B., Guioli, S., Pragliola, A., Incerti, B., Bardoni, B., Tonlorenzi, R., et al. (1991). A Gene Deleted in Kallmann's Syndrome Shares Homology with Neural Cell Adhesion and Axonal Path-Finding Molecules. *Nature* 353, 529–536. doi:10.1038/353529a0
- Ghosh, D. (2007). Human Sulfatases: a Structural Perspective to Catalysis. *Cell. Mol. Life Sci.* 64, 2013–2022. doi:10.1007/s00018-007-7175-y
- Gumienny, T. L., Macneil, L. T., Wang, H., De Bono, M., Wrana, J. L., and Padgett, R. W. (2007). Glypican LON-2 Is a Conserved Negative Regulator of BMP-like Signaling in *Caenorhabditis elegans*. *Curr. Biol.* 17, 159–164. doi:10.1016/j.cub.2006.11.065
- Günal, S., Hardman, R., Kopriva, S., and Mueller, J. W. (2019). Sulfation Pathways from Red to green. *J. Biol. Chem.* 294, 12293–12312. doi:10.1074/jbc.rev119.007422
- Habuchi, O. (2000). Diversity and Functions of Glycosaminoglycan Sulfotransferases. *Biochim. Biophys. Acta (Bba) - Gen. Subjects* 1474, 115–127. doi:10.1016/s0304-4165(00)00016-7
- Hageman, G. S., Anderson, D. H., Johnson, L. V., Hancox, L. S., Taiber, A. J., Hardisty, L. I., et al. (2005). From the Cover: A Common Haplotype in the Complement Regulatory Gene Factor H (HF1/CFH) Predisposes Individuals to Age-Related Macular Degeneration. *Proc. Natl. Acad. Sci.* 102, 7227–7232. doi:10.1073/pnas.0501536102
- Haines, J. L., Hauser, M. A., Schmidt, S., Scott, W. K., Olson, L. M., Gallins, P., et al. (2005). Complement Factor H Variant Increases the Risk of Age-Related Macular Degeneration. *Science* 308, 419–421. doi:10.1126/science.1110359
- Han, Z., Lo, W.-S., Lightfoot, J. W., Witte, H., Sun, S., and Sommer, R. J. (2020). Improving Transgenesis Efficiency and CRISPR-Associated Tools through Codon Optimization and Native Intron Addition in *Pristionchus* Nematodes. *Genetics* 216, 947–956. doi:10.1534/genetics.120.303785
- Hanson, S. R., Best, M. D., and Wong, C.-H. (2004). Sulfatases: Structure, Mechanism, Biological Activity, Inhibition, and Synthetic Utility. *Angew. Chem. Int. Ed.* 43, 5736–5763. doi:10.1002/anie.200300632
- Hattori, K., Inoue, M., Inoue, T., Arai, H., and Tamura, H.-o. (2006). A Novel Sulfotransferase Abundantly Expressed in the Dauer Larvae of *Caenorhabditis elegans*. *J. Biochem.* 139, 355–362. doi:10.1093/jb/mvj041
- Herman, T., Hartwig, E., and Horvitz, H. R. (1999). Sqv Mutants of *Caenorhabditis elegans* Are Defective in Vulval Epithelial Invagination. *Proc. Natl. Acad. Sci.* 96, 968–973. doi:10.1073/pnas.96.3.968
- Hernandez-Guzman, F. G., Higashiyama, T., Pangborn, W., Osawa, Y., and Ghosh, D. (2003). Structure of Human Estrone Sulfatase Suggests Functional Roles of Membrane Association. *J. Biol. Chem.* 278, 22989–22997. doi:10.1074/jbc.m211497200
- Hilliard, M. A., Bergamasco, C., Arbucci, S., Plasterk, R. H., and Bazzicalupo, P. (2004). Worms Taste Bitter: ASH Neurons, QUI-1, GPA-3 and ODR-3 Mediate Quinine Avoidance in *Caenorhabditis elegans*. *EMBO J.* 23, 1101–1111. doi:10.1038/sj.emboj.7600107
- Hodgkin, J. (2005). *Karyotype, Ploidy, and Gene Dosage*. WormBook, 1–9. doi:10.1895/wormbook.1.3.1

- Hutter, H., Vogel, B. E., Plenefisch, J. D., Norris, C. R., Proenca, R. B., Spieth, J., et al. (2000). Conservation and novelty in the Evolution of Cell Adhesion and Extracellular Matrix Genes. *Science* 287, 989–994. doi:10.1126/science.287.5455.989
- Hwang, H.-Y., Olson, S. K., Esko, J. D., and Robert Horvitz, H. (2003). *Caenorhabditis elegans* Early Embryogenesis and Vulval Morphogenesis Require Chondroitin Biosynthesis. *Nature* 423, 439–443. doi:10.1038/nature01634
- Kieninger, M. R., Ivers, N. A., Rödelberger, C., Markov, G. V., Sommer, R. J., and Ragsdale, E. J. (2016). The Nuclear Hormone Receptor NHR-40 Acts Downstream of the Sulfatase EUD-1 as Part of a Developmental Plasticity Switch in *Pristionchus*. *Curr. Biol.* 26, 2174–2179. doi:10.1016/j.cub.2016.06.018
- Kim, T. H., Hwang, S. B., Jeong, P.-Y., Lee, J., and Cho, J. W. (2005). Requirement of Tyrosylprotein Sulfotransferase-A for Proper Cuticle Formation in the nematode *C. elegans*. *FEBS Lett.* 579, 53–58. doi:10.1016/j.febslet.2004.11.044
- Kim, T. H., Kim, D. H., Nam, H. W., Park, S. Y., Shim, J., and Cho, J. W. (2010). Tyrosylprotein Sulfotransferase Regulates Collagen Secretion in *Caenorhabditis elegans*. *Mol. Cell* 29, 413–418. doi:10.1007/s10059-010-0049-4
- Kinnunen, T., Huang, Z., Townsend, J., Gatdula, M. M., Brown, J. R., Esko, J. D., et al. (2005). Heparan 2-O-Sulfotransferase, Hst-2, Is Essential for normal Cell Migration in *Caenorhabditis elegans*. *Proc. Natl. Acad. Sci.* 102, 1507–1512. doi:10.1073/pnas.0401591102
- Kinnunen, T. K. (2014). Combinatorial Roles of Heparan Sulfate Proteoglycans and Heparan Sulfates in *Caenorhabditis elegans* Neural Development. *PLoS One* 9, e102919. doi:10.1371/journal.pone.0102919
- Klein, R. J., Zeiss, C., Chew, E. Y., Tsai, J.-Y., Sackler, R. S., Haynes, C., et al. (2005). Complement Factor H Polymorphism in Age-Related Macular Degeneration. *Science* 308, 385–389. doi:10.1126/science.1109557
- Knaust, A., Schmidt, B., Dierks, T., von Bülow, R., and Von Figura, K. (1998). Residues Critical for Formylglycine Formation And/or Catalytic Activity of Arylsulfatase A. *Biochemistry* 37, 13941–13946. doi:10.1021/bi9810205
- Koo, P. K., Bian, X., Sherlekar, A. L., Bunkers, M. R., and Lints, R. (2011). The Robustness of *Caenorhabditis elegans* Male Mating Behavior Depends on the Distributed Properties of ray Sensory Neurons and Their Output through Core and Male-specific Targets. *J. Neurosci.* 31, 7497–7510. doi:10.1523/jneurosci.6153-10.2011
- Landgrebe, J., Dierks, T., Schmidt, B., and Von Figura, K. (2003). The Human SUMF1 Gene, Required for Posttranslational Sulfatase Modification, Defines a New Gene Family Which Is Conserved from Pro- to Eukaryotes. *Gene* 316, 47–56. doi:10.1016/s0378-1119(03)00746-7
- Langford, R., Hurrion, E., and Dawson, P. A. (2017). Genetics and Pathophysiology of Mammalian Sulfate Biology. *J. Genet. Genomics* 44, 7–20. doi:10.1016/j.jgg.2016.08.001
- Lawrence, R., Olson, S. K., Steele, R. E., Wang, L., Warrior, R., Cummings, R. D., et al. (2008). Evolutionary Differences in Glycosaminoglycan fine Structure Detected by Quantitative Glycan Reductive Isotope Labeling. *J. Biol. Chem.* 283, 33674–33684. doi:10.1074/jbc.m804288200
- Lázaro-Peña, M. I., Díaz-Balzac, C. A., Bülow, H. E., and Emmons, S. W. (2018). Synaptogenesis Is Modulated by Heparan Sulfate in *Caenorhabditis elegans*. *Genetics* 209, 195–208. doi:10.1534/genetics.118.300837
- Lee, D. W., Choo, H. Y., Kaya, H. K., Lee, S. M., Smitley, D. R., Shin, H. K., et al. (2002). Laboratory and Field Evaluation of Korean Entomopathogenic Nematode Isolates against the oriental Beetle *Exomala orientalis* (Coleoptera: Scarabaeidae). *J. Econ. Entomol.* 95, 918–926. doi:10.1093/jee/95.5.918
- Legouis, R., Hardelin, J.-P., Levilliers, J., Claverie, J.-M., Compain, S., Wunderle, V., et al. (1991). The Candidate Gene for the X-Linked Kallmann Syndrome Encodes a Protein Related to Adhesion Molecules. *Cell* 67, 423–435. doi:10.1016/0092-8674(91)90193-3
- Leung, A. W. Y., Backstrom, I., and Bally, M. B. (2016). Sulfonation, an Underexploited Area: from Skeletal Development to Infectious Diseases and Cancer. *Oncotarget* 7, 55811–55827. doi:10.18632/oncotarget.10046
- Lightfoot, J. W., Wilecki, M., Rödelberger, C., Moreno, E., Susoy, V., Witte, H., et al. (2019). Small Peptide-Mediated Self-Recognition Prevents Cannibalism in Predatory Nematodes. *Science* 364, 86–89. doi:10.1126/science.aav9856
- Lindahl, U., and Li, J. p. (2009). Chapter 3 Interactions between Heparan Sulfate and Proteins-Design and Functional Implications. *Int. Rev. Cel Mol Biol* 276, 105–159. doi:10.1016/s1937-6448(09)76003-4
- Liu, K. S., and Sternberg, P. W. (1995). Sensory Regulation of Male Mating Behavior in *Caenorhabditis elegans*. *Neuron* 14, 79–89. doi:10.1016/0896-6273(95)90242-2
- Liu, Z., Kariya, M. J., Chute, C. D., Pribadi, A. K., Leinwand, S. G., Tong, A., et al. (2018). Predator-secreted Sulfolipids Induce Defensive Responses in *C. elegans*. *Nat. Commun.* 9, 1128. doi:10.1038/s41467-018-03333-6
- Meyer, J. M., Baskaran, P., Quast, C., Susoy, V., Rödelberger, C., Glöckner, F. O., et al. (2017). Succession and Dynamics of *Pristionchus* Nematodes and Their Microbiome during Decomposition of *Oryctes* Borbonicus on La Réunion Island. *Environ. Microbiol.* 19, 1476–1489. doi:10.1111/1462-2920.13697
- Minniti, A. N., Labarca, M., Hurtado, C., and Brandan, E. (2004). *Caenorhabditis elegans* Syndecan (SDN-1) Is Required for normal Egg Laying and Associates with the Nervous System and the Vulva. *J. Cel Sci* 117, 5179–5190. doi:10.1242/jcs.01394
- Mizuguchi, S., Dejima, K., and Nomura, K. (2009). Sulfation and Related Genes in *Caenorhabditis elegans*. *Tigg* 21, 179–191. doi:10.4052/tigg.21.179
- Mizuguchi, S., Uyama, T., Kitagawa, H., Nomura, K. H., Dejima, K., Gengyo-Ando, K., et al. (2003). Chondroitin Proteoglycans Are Involved in Cell Division of *Caenorhabditis elegans*. *Nature* 423, 443–448. doi:10.1038/nature01635
- Monigatti, F., Hekking, B., and Steen, H. (2006). Protein Sulfation Analysis-A Primer. *Biochim. Biophys. Acta (Bba) - Proteins Proteomics* 1764, 1904–1913. doi:10.1016/j.bbapap.2006.07.002
- Motola, D. L., Cummins, C. L., Rottiers, V., Sharma, K. K., Li, T., Li, Y., et al. (2006). Identification of Ligands for DAF-12 that Govern Dauer Formation and Reproduction in *C. elegans*. *Cell* 124, 1209–1223. doi:10.1016/j.cell.2006.01.037
- Mueller, J. W., Gilligan, L. C., Idkowiak, J., Arlt, W., and Foster, P. A. (2015). The Regulation of Steroid Action by Sulfation and Desulfation. *Endocr. Rev.* 36, 526–563. doi:10.1210/er.2015-1036
- Namdeo, S., Moreno, E., Rödelberger, C., Baskaran, P., Witte, H., and Sommer, R. J. (2018). Two Independent Sulfation Processes Regulate Mouth-form Plasticity in the Nematode *Pristionchus Pacificus*. *Development* 145, 166272
- Ogawa, A., Streit, A., Antebi, A., and Sommer, R. J. (2009). A Conserved Endocrine Mechanism Controls the Formation of Dauer and Infective Larvae in Nematodes. *Curr. Biol.* 19, 67–71. doi:10.1016/j.cub.2008.11.063
- Olson, S. K., Bishop, J. R., Yates, J. R., Oegema, K., and Esko, J. D. (2006). Identification of Novel Chondroitin Proteoglycans in *Caenorhabditis elegans*: Embryonic Cell Division Depends on CPG-1 and CPG-2. *J. Cel Biol* 173, 985–994. doi:10.1083/jcb.200603003
- Ouyang, Y.-B., and Moore, K. L. (1998). Molecular Cloning and Expression of Human and Mouse Tyrosylprotein Sulfotransferase-2 and a Tyrosylprotein Sulfotransferase Homologue in *Caenorhabditis elegans*. *J. Biol. Chem.* 273, 24770–24774. doi:10.1074/jbc.273.38.24770
- Pérez-Jiménez, M. M., Monje-Moreno, J. M., Brokate-Llanos, A. M., Venegas-Calerón, M., Sánchez-García, A., Sansigre, P., et al. (2021). Steroid Hormones Sulfatase Inactivation Extends Lifespan and Ameliorates Age-Related Diseases. *Nat. Commun.* 12, 49. doi:10.1038/s41467-020-20269-y
- Polis, G. A., and Holt, R. D. (1992). Intraguild Predation: The Dynamics of Complex Trophic Interactions. *Trends Ecol. Evol.* 7, 151–154. doi:10.1016/0169-5347(92)90208-s
- Quach, K. T., and Chalasani, S. H. (2020). Intraguild Predation between *Pristionchus Pacificus* and *Caenorhabditis elegans*: a Complex Interaction with the Potential for Aggressive Behaviour. *J. Neurogenet.* 34, 404–419. doi:10.1080/01677063.2020.1833004
- Ragsdale, E. J., and Ivers, N. A. (2016). Specialization of a Polyphenism Switch Gene Following Serial Duplications in *Pristionchus* Nematodes. *Evolution* 70, 2155–2166. doi:10.1111/evo.13011
- Ragsdale, E. J., Müller, M. R., Rödelberger, C., and Sommer, R. J. (2013). A Developmental Switch Coupled to the Evolution of Plasticity Acts through a Sulfatase. *Cell* 155, 922–933. doi:10.1016/j.cell.2013.09.054
- Recksiek, M., Selmer, T., Dierks, T., Schmidt, B., and Von Figura, K. (1998). Sulfatases, Trapping of the Sulfated Enzyme Intermediate by Substituting the Active Site Formylglycine. *J. Biol. Chem.* 273, 6096–6103. doi:10.1074/jbc.273.11.6096

- Reiter, J. F., and Leroux, M. R. (2017). Genes and Molecular Pathways Underpinning Ciliopathies. *Nat. Rev. Mol. Cel Biol* 18, 533–547. doi:10.1038/nrm.2017.60
- Renahan, T., Lo, W. S., Werner, M. S., Roach, J., Herrmann, M., and Sommer, R. J. (2021). Nematode Biphasic 'boom and Bust' Dynamics Are Dependent on Host Bacterial Load while Linking Dauer and Mouth-form Polyphenisms. *Environ. Microbiol.* 23, 5102–5113. doi:10.1111/1462-2920.15438
- Renahan, T., and Sommer, R. J. (2021). Nematode Interactions on Beetle Hosts Indicate a Role of Mouth-form Plasticity in Resource Competition. *Front. Ecol. Evol.* doi:10.3389/fevo.2021.752695
- Rogalski, T. M., Williams, B. D., Mullen, G. P., and Moerman, D. G. (1993). Products of the Unc-52 Gene in *Caenorhabditis elegans* Are Homologous to the Core Protein of the Mammalian Basement Membrane Heparan Sulfate Proteoglycan. *Genes Dev.* 7, 1471–1484. doi:10.1101/gad.7.8.1471
- Schimpf, J., Sames, K., and Zwilling, R. (1999). Proteoglycan Distribution Pattern during Aging in the Nematode *Caenorhabditis elegans*: an Ultrastructural Histochemical Study. *Histochem. J.* 31, 285–292. doi:10.1023/a:1003761817109
- Schlotawa, L., Adang, L. A., Radhakrishnan, K., and Ahrens-Nicklas, R. C. (2020). Multiple Sulfatase Deficiency: A Disease Comprising Mucopolysaccharidosis, Sphingolipidosis, and More Caused by a Defect in Posttranslational Modification. *Int. J. Mol. Sci.* 21. doi:10.3390/ijms21103448
- Schmidt, B., Selmer, T., Ingendoh, A., and Figurat, K. v. (1995). A Novel Amino Acid Modification in Sulfatases that Is Defective in Multiple Sulfatase Deficiency. *Cell* 82, 271–278. doi:10.1016/0092-8674(95)90314-3
- Seroby, V., Xiao, H., Namdeo, S., Rödelberger, C., Sieriebriennikov, B., Witte, H., et al. (2016). Chromatin Remodelling and Antisense-Mediated Up-Regulation of the Developmental Switch Gene Eud-1 Control Predatory Feeding Plasticity. *Nat. Commun.* 7, 12337. doi:10.1038/ncomms12337
- Sieriebriennikov, B., Prabh, N., Dardiry, M., Witte, H., Röseler, W., Kieninger, M. R., et al. (2018). A Developmental Switch Generating Phenotypic Plasticity Is Part of a Conserved Multi-Gene Locus. *Cel Rep.* 23, 2835–2843. doi:10.1016/j.celrep.2018.05.008
- Sieriebriennikov, B., Sun, S., Lightfoot, J. W., Witte, H., Moreno, E., Rödelberger, C., et al. (2020). Conserved Nuclear Hormone Receptors Controlling a Novel Plastic Trait Target Fast-Evolving Genes Expressed in a Single Cell. *Plos Genet.* 16, e1008687. doi:10.1371/journal.pgen.1008687
- Sommer, R. J., and Mayer, M. G. (2015). Toward a Synthesis of Developmental Biology with Evolutionary Theory and Ecology. *Annu. Rev. Cel Dev. Biol.* 31, 453–471. doi:10.1146/annurev-cellbio-102314-112451
- Sommer, R. J. (2020). Phenotypic Plasticity: From Theory and Genetics to Current and Future Challenges. *Genetics* 215, 1–13. doi:10.1534/genetics.120.303163
- Sommer, R. J., and Sternberg, P. W. (1996). Apoptosis and Change of Competence Limit the Size of the Vulva Equivalence Group in *Pristionchus Pacificus*: a Genetic Analysis. *Curr. Biol.* 6, 52–59. doi:10.1016/s0960-9822(02)00421-9
- Stone, M. J., Chuang, S., Hou, X., Shoham, M., and Zhu, J. Z. (2009). Tyrosine Sulfation: an Increasingly Recognised post-translational Modification of Secreted Proteins. *New Biotechnol.* 25, 299–317. doi:10.1016/j.nbt.2009.03.011
- Streit, A. (2008). Reproduction in Strongyloidea (Nematoda): a Life between Sex and Parthenogenesis. *Parasitology* 135, 285–294. doi:10.1017/s003118200700399x
- Strott, C. A. (2002). Sulfonation and Molecular Action. *Endocr. Rev.* 23, 703–732. doi:10.1210/er.2001-0040
- Sugahara, K., Mikami, T., Uyama, T., Mizuguchi, S., Nomura, K., and Kitagawa, H. (2003). Recent Advances in the Structural Biology of Chondroitin Sulfate and Dermatan Sulfate. *Curr. Opin. Struct. Biol.* 13, 612–620. doi:10.1016/j.sbi.2003.09.011
- Tecle, E., Diaz-Balzac, C. A., and Bülow, H. E. (2013). Distinct 3-O-Sulfated Heparan Sulfate Modification Patterns Are Required for kal-1-Dependent Neurite Branching in a Context-dependent Manner in *Caenorhabditis elegans*. *G3 (Bethesda)* 3, 541–552. doi:10.1534/g3.112.005199
- Toyoda, H., Kinoshita-Toyoda, A., and Selleck, S. B. (2000). Structural Analysis of Glycosaminoglycans in *Drosophila* and *Caenorhabditis elegans* and Demonstration that Tout-Vel, a *Drosophila* Gene Related to EXT Tumor Suppressors, Affects Heparan Sulfate *In Vivo*. *J. Biol. Chem.* 275, 2269–2275. doi:10.1074/jbc.275.4.2269
- Turnbull, J., Drummond, K., Huang, Z., Kinnunen, T., Ford-Perriss, M., Murphy, M., et al. (2003). Heparan Sulfate Sulphotransferase Expression in Mice and *Caenorhabditis elegans*. *Biochem. Soc. Trans.* 31, 343–348. doi:10.1042/bst0310343
- Turnbull, J., Powell, A., and Guimond, S. (2001). Heparan Sulfate: Decoding a Dynamic Multifunctional Cell Regulator. *Trends Cel Biol.* 11, 75–82. doi:10.1016/s0962-8924(00)01897-3
- Van Den Hoogen, J., Geisen, S., Routh, D., Ferris, H., Traunspurger, W., Wardle, D. A., et al. (2019). Soil Nematode Abundance and Functional Group Composition at a Global Scale. *Nature* 572, 194–198. doi:10.1038/s41586-019-1418-6
- Waldow, A., Schmidt, B., Dierks, T., von Bülow, R., and Von Figura, K. (1999). Amino Acid Residues Forming the Active Site of Arylsulfatase A. *J. Biol. Chem.* 274, 12284–12288. doi:10.1074/jbc.274.18.12284
- Wei, Z., Swiedler, S. J., Ishihara, M., Orellana, A., and Hirschberg, C. B. (1993). A Single Protein Catalyzes Both N-Deacetylation and N-Sulfation during the Biosynthesis of Heparan Sulfate. *Proc. Natl. Acad. Sci.* 90, 3885–3888. doi:10.1073/pnas.90.9.3885
- Willemssen, R., Kroos, M., Hoogveen, A. T., Van Dongen, J. M., Parenti, G., Van Der Loos, C. M., et al. (1988). Ultrastructural Localization of Steroid Sulphatase in Cultured Human Fibroblasts by Immunocytochemistry: a Comparative Study with Lysosomal Enzymes and the Mannose 6-phosphate Receptor. *Histochem. J.* 20, 41–51. doi:10.1007/bf01745968
- Wood, W. B., and Researchers, C. O. C. E. (1988). *The Nematode Caenorhabditis Elegans*. Cold Spring Harbor, NY: Cold Spring Harbor Laboratory Press.
- Yamada, S., Van Die, I., Van Den Eijnden, D. H., Yokota, A., Kitagawa, H., and Sugahara, K. (1999). Demonstration of Glycosaminoglycans in *Caenorhabditis Elegans*. *FEBS Lett.* 459, 327–331. doi:10.1016/s0014-5793(99)01286-7
- Yang, Y.-S., Wang, C.-C., Chen, B.-H., Hou, Y.-H., Hung, K.-S., and Mao, Y.-C. (2015). Tyrosine Sulfation as a Protein post-translational Modification. *Molecules* 20, 2138–2164. doi:10.3390/molecules20022138
- Zarepari, S., Branham, K. E. H., Li, M., Shah, S., Klein, R. J., Ott, J., et al. (2005). Strong Association of the Y402H Variant in Complement Factor H at 1q32 with Susceptibility to Age-Related Macular Degeneration. *Am. J. Hum. Genet.* 77, 149–153. doi:10.1086/431426

Conflict of Interest: The authors declare that the research was conducted in the absence of any commercial or financial relationships that could be construed as a potential conflict of interest.

Publisher's Note: All claims expressed in this article are solely those of the authors and do not necessarily represent those of their affiliated organizations, or those of the publisher, the editors, and the reviewers. Any product that may be evaluated in this article, or claim that may be made by its manufacturer, is not guaranteed or endorsed by the publisher.

Copyright © 2022 Igreja and Sommer. This is an open-access article distributed under the terms of the Creative Commons Attribution License (CC BY). The use, distribution or reproduction in other forums is permitted, provided the original author(s) and the copyright owner(s) are credited and that the original publication in this journal is cited, in accordance with accepted academic practice. No use, distribution or reproduction is permitted which does not comply with these terms.



Steroid Sulfation in Neurodegenerative Diseases

Jana Vitku^{1*}, Martin Hill¹, Lucie Kolatorova¹, Eva Kubala Havrdova² and Radmila Kancheva¹

¹Department of Steroids and Proteofactors, Institute of Endocrinology, Prague, Czechia, ²Department of Neurology and Center of Clinical Neuroscience, First Faculty of Medicine, Charles University and General University Hospital in Prague, Prague, Czechia

Steroid sulfation and desulfation participates in the regulation of steroid bioactivity, metabolism and transport. The authors focused on sulfation and desulfation balance in three neurodegenerative diseases: Alzheimer's disease (AD), Parkinson's disease (PD), and multiple sclerosis (MS). Circulating steroid conjugates dominate their unconjugated counterparts, but unconjugated steroids outweigh their conjugated counterparts in the brain. Apart from the neurosteroid synthesis in the central nervous system (CNS), most brain steroids cross the blood-brain barrier (BBB) from the periphery and then may be further metabolized. Therefore, steroid levels in the periphery partly reflect the situation in the brain. The CNS steroids subsequently influence the neuronal excitability and have neuroprotective, neuroexcitatory, antidepressant and memory enhancing effects. They also exert anti-inflammatory and immunoprotective actions. Like the unconjugated steroids, the sulfated ones modulate various ligand-gated ion channels. Conjugation by sulfotransferases increases steroid water solubility and facilitates steroid transport. Steroid sulfates, having greater half-lives than their unconjugated counterparts, also serve as a steroid stock pool. Sulfotransferases are ubiquitous enzymes providing massive steroid sulfation in adrenal *zona reticularis* and *zona fasciculata*. Steroid sulfatase hydrolyzing the steroid conjugates is exceedingly expressed in placenta but is ubiquitous in low amounts including brain capillaries of BBB which can rapidly hydrolyze the steroid sulfates coming across the BBB from the periphery. Lower dehydroepiandrosterone sulfate (DHEAS) plasma levels and reduced sulfotransferase activity are considered as risk factors in AD patients. The shifted balance towards unconjugated steroids can participate in the pathophysiology of PD and anti-inflammatory effects of DHEAS may counteract the MS.

OPEN ACCESS

Edited by:

Jon Wolf Mueller,
University of Birmingham,
United Kingdom

Reviewed by:

William Davies,
Cardiff University, United Kingdom
Giovanna Di Nardo,
University of Turin, Italy

*Correspondence:

Jana Vitku
jvitku@endo.cz

Specialty section:

This article was submitted to
Cellular Biochemistry,
a section of the journal
Frontiers in Molecular Biosciences

Received: 20 December 2021

Accepted: 20 January 2022

Published: 23 February 2022

Citation:

Vitku J, Hill M, Kolatorova L,
Kubala Havrdova E and Kancheva R
(2022) Steroid Sulfation in
Neurodegenerative Diseases.
Front. Mol. Biosci. 9:839887.
doi: 10.3389/fmolb.2022.839887

Keywords: steroid sulfotransferases, steroid sulfatase, neuroactive steroids, neurosteroids, brain, Alzheimer's disease, Parkinson's disease, multiple sclerosis

INTRODUCTION

Steroids are important components of endogenous signaling in the organism. Steroidogenesis takes place prominently in peripheral glands such as adrenals, gonads, placenta. However, some other tissues and organs, including the brain are also able to metabolize cholesterol to steroid molecules and exert effects in autocrine and paracrine manner (Labrie, 1991; Pluchino et al., 2019; Giatti et al., 2020a). The group of steroids that can influence actions in nervous system are called neuroactive steroids (NAS), with the subgroup of steroids—neurosteroids—that act in the nervous system and are also synthesized there (Corpéchet et al., 1981).

Under physiological conditions, NAS influence a broad spectrum of functions, such as brain development, sexual behavior, stress response, emotions, memory, and cognition (Vallée et al., 1997; Serra et al., 2000; Frye, 2001; Darnaudéry et al., 2002; Johansson et al., 2002; Hampl et al., 2015). In various pathophysiological states of the central nervous system (CNS), such as epilepsy, depression, anxiety and neurodegenerative diseases neuroactive steroid levels are altered (Hillen et al., 2000; Kancheva et al., 2010; Hill et al., 2011; MacKenzie and Maguire, 2013; Kanceva et al., 2015).

The most discussed NAS in humans include metabolites of progesterone, i.e., pregnanolone isomers, 5 α / β -reduced metabolites of cortisol, sulfates of pregnanolone isomers, dehydroepiandrosterone sulfate (DHEAS) and pregnenolone sulfate (PregS). Furthermore, classical steroid hormones such as 17 β -estradiol (E2) (Xu et al., 2008; Jiang et al., 2009) testosterone (Park-Chung et al., 1999), and progesterone (Wu et al., 1990) can act as NAS in the brain (reviewed in (Giatti et al., 2019)).

Biosynthesis of NAS, especially pregnane steroids, shows marked differences depending on the gender, age, menstrual cycle and pregnancy status (Kancheva et al., 2007). In premenopausal women, the largest proportion of pregnanolone isomers arise from progesterone synthesized in corpus luteum with the dominant metabolite allopregnanolone (3 α -hydroxy-5 α -pregnan-20-one) (Hill et al., 2005; Ottander et al., 2005; Hill and Očenášková, 2007). Gonadal pregnane may easily surpass the blood-brain barrier (BBB) as the brain concentrations reflect the ovarian production (Bixo et al., 1997).

Outside of pregnancy and the luteal phase of the menstrual cycle, the adrenal cortex produces most NAS and their precursors. Human *zona fasciculata* produces PregS (Hill and Očenášková, 2007) in relatively high concentrations. In addition, *zona fasciculata* synthesizes mainly cortisol whose 5 α / β -reduced metabolites can act as NAS (Strömberg et al., 2005); *zona reticularis* primarily produces massive amounts of DHEAS (Mueller et al., 2015).

Additionally, the CNS can synthesize neurosteroids directly in the CNS or from peripheral precursors (Corpéchet et al., 1981; Corpéchet et al., 1983; Luchetti et al., 2011). Maintaining a pool of the bioavailable steroids in the site of action is a dynamic process where different steroidogenic enzymes are involved. One of the systems regulating the activity of steroids are sulfotransferases (SULTs) and steroid sulfatase (STS), which add or detach sulfate moiety, respectively. This balance could be of importance in neurodegenerative processes as well as for the transport of soluble steroid conjugates to the respective active sites.

The role of unconjugated NAS in various neurodegenerative diseases were intensively reviewed recently (Melcangi et al., 2016; Yilmaz et al., 2019; Giatti et al., 2020b; Kudova, 2021) as well as in the past (Luchetti et al., 2011; Melcangi et al., 2008; Wang et al., 2001; Melcangi and Panzica, 2009; Melcangi et al., 2011; di Michele et al., 2003). In this review, we focused mainly on sulfated steroids and sulfation and desulfation pathways in three neurodegenerative diseases: Alzheimer's disease (AD), Parkinson's disease (PD), multiple sclerosis (MS), while the dysregulation of sulfation processes can change the

bioavailability and activity of NAS and may influence the pathogenesis and progression of some diseases.

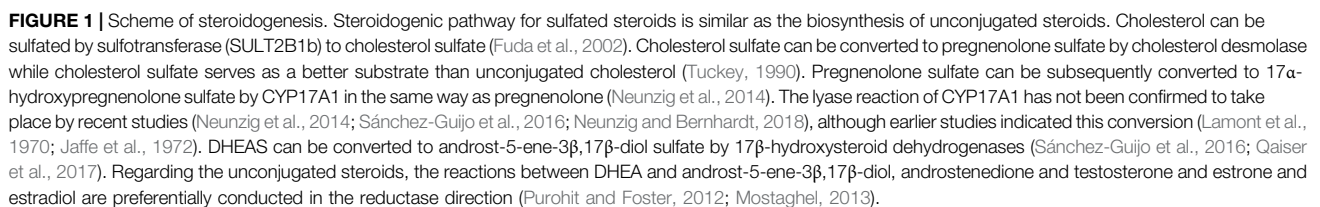
UNCONJUGATED STEROIDS

Unconjugated (free) steroids are predominantly lipophilic compounds, which can enter the cells and pass the BBB by simple nonsaturable diffusion. A major fraction of numerous steroids in circulation is bound to albumin. However, steroids can easily dissociate from the albumin complex and pass the BBB as well (Pardridge and Mietus, 1979; Pardridge and Mietus, 1980). Steroids that are bound to selective transport proteins (CBD-transcortin, SHBG-sex hormone binding globulin), are not transported through the BBB (Compagnone and Mellon, 2000). Part of steroids can be also synthesized *de novo* in CNS (Corpéchet et al., 1983). However, a substantial part of steroids can be synthesized from steroid precursors from periphery or can be transported from the periphery thus partly reflecting the circulating levels (Bixo et al., 1995; Kancheva et al., 2010; Kancheva et al., 2011). Therefore, the contribution of peripheral steroids to the steroid pool in CNS is important and changes in the steroid milieu in the CNS can subsequently have an impact on neuronal activity in brain (Vaňková et al., 2016). The steroid levels in cerebrospinal fluid (CSF) are generally lower than in circulation, while some CNS steroids (especially DHEA and some of its metabolites; allopregnanolone and cortisol) correlate with their peripheral levels (Kancheva et al., 2010).

Main unconjugated NAS include metabolites of progesterone (allopregnanolone, isopregnanolone, pregnanolone, epipregnanolone and pregnanediols), DHEA, E2, testosterone and their metabolites (androsterone, epiandrosterone, etiocholanolone, 3 α -hydroxy-5 α / β ,17 β -diols), 5 α / β -reduced metabolites of glucocorticoids (3 α -hydroxy, 5 α / β -tetrahydro-cortisols, 3 α -hydroxy-5 α / β -tetrahydro-cortisones). Basic scheme of steroidogenesis is shown in **Figure 1**.

DHEA is mainly of adrenal origin, but it can also be synthesized in gonads (10–20%) (Nieschlag et al., 1973) and most probably also in the CNS (Stárka et al., 2015). DHEA is a substrate for testosterone production and subsequently for estrogen synthesis. These processes occur also in the human brain (Steckelbroeck et al., 2002) and may subsequently influence the nervous system by genomic as well as by non-genomic pathways. Furthermore, DHEA itself serves as neuroactive steroid (Stárka et al., 2015). DHEA has neuroprotective, anti-glucocorticoid, anti-apoptotic, anti-inflammatory and anti-oxidative properties, increases neurite growth and has impact on neurogenesis and catecholamine synthesis and secretion. However, it can also be neurotoxic (reviewed in (Maninger et al., 2009; Stárka et al., 2015)).

Pregnanolone isomers are progesterone metabolites originated through the action of ubiquitous 5 α -reductase (SRD5As) and liver 5 β -reductase (AKR1D1) forming 5 α - and 5 β -dihydroprogesterone, respectively (Havlíková et al., 2006). The subsequent metabolism to individual pregnanolone isomers is provided by a system of subfamily 1C aldoketoreductases (AKR1Cs) and 17 β -hydroxysteroid



Sex hormones are also active in the CNS. Particularly E2 exert pleiotropic effects there, facilitating learning and memory (Frick, 2015; Sun et al., 2019; Luine and Frankfurt, 2012; Tozzi et al., 2020; Dieni et al., 2020), as well as influencing emotional (Altemus, 2019) and sexual behavior (Diotel et al., 2018). They

TABLE 1 | Positive and negative modulators of selected membrane receptors.

Modulation of GABA_A receptor			
Positive		Negative	
3 α -OH-pregnanolone isomers (allopregnanolone, pregnanolone)	Majewska et al. (1986); Park-Chung et al. (1999); Strömberg et al. (2005)	3 β -OH-pregnanolone isomers (isopregnanolone, epipregnanolone)	Wang et al. (2000), Wang et al. (2002); Lundgren et al. (2003)
3 α -androstane steroids (androstene, etiocholanolone, 5 α -androstane-3 α , 17 β , diol)	Turner et al. (1989); Park-Chung et al. (1999); Kaminski et al. (2005)	PregS	Park-Chung et al. (1999); Majewska and Schwartz, (1987)
3 α ,5 α /5 β - THDOC	Majewska et al. (1986); Turner et al. (1989); Strömberg et al. (2005)	DHEAS	Park-Chung et al. (1999); Majewska et al. (1990)
weak: progesterone	Wu et al. (1990); Park-Chung et al. (1999)	Sulfates of pregnanolone isomers (pregnanoloneS, epipregnanoloneS, isopregnanoloneS)	Park-Chung et al. (1999)
weak: androstenedione	Park-Chung et al. (1999)	3 β 5 β -THDOC	Wang et al. (2002)
weak: testosterone	Park-Chung et al. (1999)	sulfates of 5 α -androstane isomers (androsteneS and epiandrosteroneS)	Park-Chung et al. (1999)
weak: 11-keto-PregS	Park-Chung et al. (1999)	11 β -hydroxy-PregS	Park-Chung et al. (1999)
—	—	weak: E2 sulfate	Park-Chung et al. (1999)
—	—	weak: DHEA	Park-Chung et al. (1999)
→ neuroinhibition		→ neuroactivation	
Modulation of glycine receptor			
Positive		Negative	
Allopregnanolone (nM-1 μ M concentrations)	Weir et al. (2004); Jiang et al. (2006)	progesterone	Wu et al. (1990)
—	—	deoxycorticosterone	Wu et al. (1990)
—	—	17 α -OH-progesterone	Wu et al. (1990)
—	—	corticosterone	Wu et al. (1997); Maksay et al. (2001)
—	—	pregS	Wu et al. (1997); Maksay et al. (2001)
—	—	DHEAS	Maksay et al. (2001)
—	—	pregnanolone	Jiang et al. (2006)
—	—	E2	Jiang et al. (2009)
—	—	testosterone	Bukanova et al. (2020)
—	—	epitestosterone	Bukanova et al. (2020)
—	—	5 α DHT	Bukanova et al. (2020)
—	—	epiandrosterone	Bukanova et al. (2020)
—	—	dihydroandrostendione	Bukanova et al. (2020)
—	—	androstenedione	Bukanova et al. (2020)
—	—	androstendiol	Bukanova et al. (2020)
—	—	DHEA	Bukanova et al. (2020)
—	—	etiocholanedione	Bukanova et al. (2020)
—	—	Allopregnanolone (40 μ M concentration)	Fodor et al. (2006)
→ neuroinhibition		→ neuroactivation	
Modulation of sigma (σ) 1 receptor			
Positive		Negative	
DHEAS	Monnet et al. (1995)	PregS	Monnet et al. (1995)
—	—	progesterone	Monnet et al. (1995)
→ neuroactivation		→ neuroinhibition	
Modulation of NMDA receptor			
Positive		Negative	
Sulfates of 5 α -pregnanolone isomers	Weaver et al. (2000)	Sulfates of 5 β -pregnanolone steroids (pregnanoloneS)	Yaghoubi et al. (1998); Park-Chung et al. (1994); Weaver et al. (2000)
PregS	Wu et al. (1991); Irwin et al. (1992)	E2 (μ M concentrations)	Weaver et al. (1997)

(Continued on following page)

TABLE 1 | (Continued) Positive and negative modulators of selected membrane receptors.

Modulation of NMDA receptor			
DHEAS	Park-Chung et al. (1994)	—	—
E2 (pM-nM concentrations)	Foy et al. (1999)	—	—
→ neuroactivation		→ neuroinhibition	
Modulation of kainate receptor			
Positive		Negative	
progesterone	Wu and Chen, (1997)	PregS	Wu et al. (1991)
—	—	PregnanolonS	Park-Chung et al. (1994)
→ neuroactivation		→ neuroinhibition	
Modulation of AMPA receptor			
Positive		Negative	
—	—	pregS	Wu et al. (1991); Shirakawa et al. (2005)
—	—	pregnanolonS	Park-Chung et al. (1994)
—	—	→ neuroinhibition	
Modulation of voltage-gated ion channels (L-type)			
Positive		Negative	
E2 (pM concentrations)	Wu et al. (2005); Sarkar et al. (2008)	E2 (nM concentration)	Brewer et al. (2009); Sribnick et al. (2009); Sánchez et al. (2014)
—	—	allopregnanolone	Hu et al. (2007); Earl and Tietz, (2011)
—	—	progesterone	Luoma et al. (2012)
→ neuroactivation		→ neuroinhibition	
Modulation of serotonin (5-HT3) receptor			
Positive		Negative	
—	—	E2	Wetzel et al. (1998)
—	—	progesterone	Wetzel et al. (1998); Wu et al. (2000)
—	—	testosterone	Wetzel et al. (1998)
—	—	allopregnanolone	Wetzel et al. (1998)
—	—	→ neuroinhibition	
Modulation of transient receptor potential (TRP) ion channels			
Positive		Negative	
PregS (TRPM3)	Wagner et al. (2008)	E2 (TRPV1)	Xu et al. (2008)
—	—	DHEA (TRPV1)	Chen et al. (2004)
—	—	progesterone (TRPM3)	Majeed et al. (2012)
→ neuroactivation		→ neuroinhibition	

Abbreviations: DHEA, dehydroepiandrosterone; DHEAS, dehydroepiandrosterone sulfate; E2, 17 β -estradiol; PregS, pregnenolone sulfate; THDOC, tetrahydrodeoxycorticosterone.

generally act as neuroprotective substances (Fargo et al., 2009; Spence and Voskuhl, 2012; Duong et al., 2020; Yang et al., 2020) and promote neurogenesis and neuro-regeneration (Pillerová et al., 2021; Azcoitia et al., 2019). These processes in the brain take place through classical nuclear steroid receptors (estrogen receptor α and β -ER α and ER β , androgen receptor-AR, progesterone receptor-PR), non-classical membrane-associated steroid receptors (AR, ER α , ER β) and transmembrane receptors (zinc transporter protein 9, G protein coupled estrogen receptor 1) (Pillerová et al., 2021).

Finally, E2 can exert its action through neurotransmitter receptors such as serotonin receptor (Wetzel et al., 1998), L-type voltage gated channel (Sribnick et al., 2009; Vega-Vela et al., 2017; Sánchez et al., 2014) or N-methyl-D-aspartate (NMDA) receptor (Weaver et al., 1997; Foy et al., 1999). The action of E2 on L-type voltage channel as well as NMDA receptor appears to be concentration dependent (Table 1). Progesterone has also therapeutic benefits such as reduction of inflammation and edema, preventing myelin degradation and reducing excitotoxic neuronal death (Luoma et al., 2012).

CONJUGATED STEROIDS

Conjugated steroids predominantly include steroid sulfates and glucuronides. Namely the sulfates have an important role in the regulation of steroid metabolism and transport. Steroid sulfates are hydrophilic compounds. Therefore, their passive diffusion through BBB is limited when compared with their unconjugated counterparts. Organic anion transporters (OATs) belonging to the solute carrier (SLC) transporters superfamily are the primary transporters for cellular influx of steroid sulfates. On the other hand, multidrug resistance proteins (MRP) from the ATP-binding cassette (ABC) transporter superfamily provides efflux of steroid sulfates (Sodani et al., 2012; Mueller et al., 2015). Steroid sulfates are transported from the cell mainly through MRP1 and MRP4. The same types of transporters (ABC and SLC transporters) are present on the BBB (Grube et al., 2018). It is assumed that there is a predominant influx of steroid sulfates from the circulation across the BBB to the brain due to huge concentration gradient (Wang et al., 1997; Qaiser et al., 2017; Grube et al., 2018).

The most important conjugated NAS include DHEAS, PregS and conjugated 5 α / β reduced pregnane and androstane isomers. The steroid conjugates in the blood dominate over their free counterparts from one to four orders of magnitude. On the other hand, the levels of unconjugated DHEA, Preg, and reduced 5 α -pregnane steroids were found in substantially higher amounts in all brain regions compared to their conjugated counterparts (Weill-Engerer et al., 2002). Looking more closely to individual brain regions, the highest levels of DHEAS were found in striatum, hypothalamus and cerebellum and those of PregS in striatum and hypothalamus (Weill-Engerer et al., 2002).

DHEAS exert neuroprotective, neuroexcitatory, antidepressant and memory enhancing effects. Together with DHEA, DHEAS has anti-inflammatory and immunomodulating effects, positive effects on neurite growth, neurogenesis and neuronal survival as described earlier (reviewed in (Maninger et al., 2009; Stárka et al., 2015)).

PregS, similarly as DHEAS, is an excitatory NAS. It has enhancing effects on the adult hippocampal neurogenesis, neurite growth and the survival of newborn neurons (Xu et al., 2012). It plays a role in the modulation of memory and learning (Smith et al., 2014; Wong et al., 2015).

MECHANISM OF ACTION OF NEUROACTIVE STEROIDS

Genomic Action

Steroids can surpass the BBB from periphery to the brain either by passive diffusion (unconjugated steroids) or in cooperation with transporter proteins mentioned above (steroid conjugates). Unconjugated or deconjugated steroids can bind to intracellular receptors in the brain and act as transcriptional factors regulating gene expression (Rupprecht et al., 1996). This action may be preceded by intracellular metabolism of the steroids (Rupprecht,

2003). This genomic effect is generally delayed in the onset, because it is limited by the rate of protein synthesis, but it has longer lasting effects.

Non-Genomic Action

In addition to this classical genomic effect, NAS (unconjugated as well as conjugated) are able to bind to various membrane receptors where they can act as their allosteric modulators and induce fast nongenomic effects in values from milliseconds to seconds (McEwen, 1991; Joëls, 1997). Both fast and delayed actions can potentially/subsequently alter membrane excitability (Joëls, 1997).

The mechanism of action of NAS lies mainly in affecting the excitability of the nervous cells. They are able to modulate permeability of ion channels. In the CNS, the best-known receptors modulated by NAS are type A γ -aminobutyric acid (GABA_A) receptors and glutamate receptors including NMDA receptors, α -amino-3-hydroxy-5-methyl-4-isoxazolepropionic acid (AMPA) receptors and kainate receptors (Joëls, 1997; Wu and Chen, 1997; Wu et al., 1998; Yaghoubi et al., 1998; Beyenburg et al., 2001; Rupprecht, 2003; Shirakawa et al., 2005). Furthermore, interactions of NAS with glycine, transient receptor potential (TRP), nicotinic acetylcholine, muscarinic acetylcholine, sigma (σ)-receptors and several types of voltage-gated calcium channel were reported (Klangkalya and Chan, 1988; Valera et al., 1992; Monnet et al., 1995; Hu et al., 2007; Xu et al., 2008; Majeed et al., 2012; Bukanova et al., 2020).

Stereoselectivity is an important property when binding to GABA_A and NMDA receptors. The presence of a 3 α -hydroxy group on the A ring is necessary for the positive modulation of GABA_A receptor. The GABA_A receptor positive modulators include 3 α -pregnane steroids (Majewska et al., 1986), including the tetrahydrodeoxycorticosterone (THDOC) isomers, as well as 3 α -androstane metabolites (Turner et al., 1989; Kaminski et al., 2005). These substances act via increasing the frequency and opening time of the GABA_A receptor (for chloride ions). The influx of chlorides into nerve cells reduce the neuronal excitability. Thus, these substances are neuroinhibitory and exhibit sedative, hypnotic, anesthetic, anxiolytic and anticonvulsant properties. The 3 β -pregnane steroids (Wang et al., 2000), and particularly their conjugates (Park-Chung et al., 1999) as well as the Δ^5 steroid sulfates (PregS, DHEAS) act as negative GABA_A receptor modulators and activate the neuronal activity in this way. Nanomolar concentrations of steroids are necessary for the positive modulation of GABA_AR, while the antagonists act only in micromolar amounts (Park-Chung et al., 1999). Steroid modulators of selected membrane receptors are shown in Table 1.

Positive and negative steroid modulators are also known for the NMDA receptor. Positive modulators, upon binding to the receptor, increase the influx of calcium ions into the cell and thus cause activation of the neuron. These include Δ^5 steroid sulfates (Wu et al., 1991; Irwin et al., 1992) and polar conjugates of 5 α -pregnane steroids (predominantly sulfates) (Weaver et al., 2000). Polar conjugates of 5 β -pregnane steroids have the opposite effect (Park-Chung et al., 1994; Yaghoubi et al., 1998; Weaver et al.,

2000). These substances are summarized in **Table 1** together with positive and negative modulators of further receptors.

CONJUGATION AND DECONJUGATION

Steroids can be conjugated either by sulfotransferases (SULTs) to form sulfates or by uridine 5'-diphospho (UDP)-glucuronosyltransferases to form glucuronides (**Figure 2**). These processes increase their polarity and water solubility and facilitate the excretion in urine and bile (Schiffer et al., 2019). Furthermore, sulfates having greater half-lives than their unconjugated counterparts, also function as a steroid pool in the circulation (mainly DHEAS and estrone sulfate). Finally, sulfated steroids (e.g., PregS and DHEAS) may modulate some ligand-gated ion channels in the CNS as was described above.

The form of conjugation (sulfation/glucuronidation) depends on the structure of the steroid. Sulfation occurs mainly in Δ^5 steroids such as DHEA, pregnenolone and estrogens (estrone). Alternatively, glucuronidation takes place mainly in the phase 2 metabolism of Δ^4 steroids (Mueller et al., 2015; Schiffer et al., 2019).

Sulfotransferases

Sulfation takes place by two-step enzymatic reactions; 1) activation of the sulfate group in the form of 3'-phosphoadenosine-5'-phosphosulfate (PAPS) by PAPS synthase and 2) transfer of activated sulfate on hydroxyl group of the steroid by SULT (Schiffer et al., 2019). Five cytoplasmic SULTs are known to be involved in steroid metabolism—SULT1A1, SULT1E1, SULT2A1 and 2 isoforms of SULT2B1 (SULT2B1a and SULT2B1b) (Hempel et al., 2000; Fuda et al., 2002; Chang et al., 2004; Gamage et al., 2005). They possess broad substrate specificity; instead of steroid sulfation they can also metabolize phenolic drugs and catecholamines (SULT1A), thyroid hormones (SULT1B) and sterols (SULT2B) (Strott, 2002). Regarding steroids, they can have preferred substrate e.g. SULT1E1 preferentially sulfates estrogens and SULT2A1 most androgens and pregnenolone (reviewed in (Mueller et al., 2015)) and SULT2B1 isoforms stereo-specifically sulfate β -hydroxysteroids (e.g., pregnenolone, cholesterol) (Meloche and Falany, 2001; Fuda et al., 2002). SULTs are ubiquitous enzymes with the highest concentrations found in the liver and intestine compared to the kidney and lung (Riches et al., 2009). SULT2A1 is strongly expressed in adrenal *zona reticularis*, *zona fasciculata* and the liver. SULT2A1 probably has a dual function: in adrenals it is responsible for massive sulfation of DHEA and pregnenolone and it detoxifies xenobiotics in the liver (Falany and Rohn-Glowacki, 2013).

Regarding the detailed expression of SULTs in brain, SULT1A1 expression was detected in several brain regions (Salman et al., 2009). SULT2A1 was detected exclusively in the thalamus and hypothalamus (Shimizu and Tamura, 2002), it was not detected in other brain regions. These findings are in agreement with the those of Salman et al. who analyzed specimens of prefrontal cortex, hippocampus, and cerebellum (Salman et al., 2011). The results on SULT2B1b

expression are ambiguous. No mRNA expression of SULT2B1b in the brain was reported by some authors (Her et al., 1998; Meloche and Falany, 2001), conversely, SULT2B1b mRNA expression was reported in a large number of sections of the human brain by other research groups (Shimizu and Tamura, 2002; Salman et al., 2011). Although SULT2B1a mRNA was detected by Salman et al. (but not by (Shimizu and Tamura, 2002)), no SULT2B1a immunoreactive protein was observed. SULT1E1 expression was not found in human brain in one study (Salman et al., 2011). Taken together, some types of SULTs are apparently available in the brain and therefore may play a crucial role in neurosteroid sulfation and control.

Steroid Sulfatase

Sulfation is reversible; steroid sulfate can be desulfated by steroid sulfatase (EC 3.1.6.2, STS, aryl sulfatase C) to unconjugated steroids in the target tissue. STS belongs to the sulfatase family containing 17 members, while only STS uses steroids as substrates (Diez-Roux and Ballabio, 2005). It is expressed as a membrane associated enzyme. Immunohistochemical techniques showed localization mainly in the rough endoplasmic reticulum. Furthermore, it is localized in Golgi cisternal, trans-Golgi reticulum, plasma membranes, endosomes and lysosomes (Willemssen et al., 1988; Stein et al., 1989). The main substrates for STS are estrone sulfate, DHEAS, PregS and cholesterol sulfate (Mueller et al., 2015). It is most abundantly expressed in placenta, however, it is believed to be ubiquitous in low amounts (Reed et al., 2005) in other tissues including the brain (Iwamori et al., 1976; Steckelbroeck et al., 2004). Within the brain the high activity of STS was observed in the thalamus, hypothalamus, hippocampus and temporal lobe (Perumal and Robins, 1973; Steckelbroeck et al., 2004). Furthermore, reports from rat studies indicate that STS is present in brain capillaries of BBB and can rapidly desulfate DHEAS that comes across the BBB from the circulation (Nicolas and Fry, 2007; Kaiser et al., 2017).

Mutations in the gene for STS result in X-linked ichthyosis, which is a rare skin disorder. Several extracutaneous manifestations have been associated with this disease including corneal opacities, cryptorchidism and chondrodysplasia punctata (Fernandes et al., 2010). While STS is expressed in various brain structures, it can be hypothesized that alterations in brain function might be present. Neurological (mental retardation, epilepsy), neurodevelopmental (attention deficit hyperactivity disorder, autism) and mood disorders are more frequent in individuals with X-linked ichthyosis compared to the general population (Fernandes et al., 2010; Chatterjee et al., 2016). From neuroanatomical point of view, structural changes in basal ganglia (reduced right putamen and pallidum volume, and left accumbens volume) in female carriers were reported (Brcic et al., 2020). The described structural changes seem to be also involved in the degeneration in PD. The recent results of Hickman et al. (2022) showed that neurodevelopmental and neurodegenerative diseases may overlap. The genetic alterations which can lead to AD and PD were also described in detail by the authors (Hickman et al., 2022).

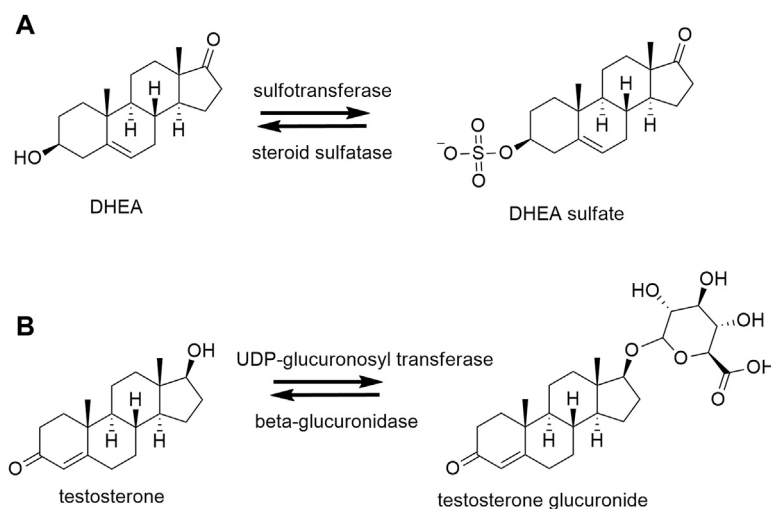


FIGURE 2 | Conjugation and deconjugation reactions. **(A)** Example of sulfation and desulfation reactions of dehydroepiandrosterone (DHEA) by sulfotransferase and steroid sulfatase, respectively. **(B)** Example of glucuronidation and deglucuronidation of testosterone by uridine 5'-diphospho (UDP)-glucuronosyltransferase and β -glucuronidase, respectively.

Uridine 5'-Diphospho-Glucuronosyl Transferases and β -glucuronidase

For completeness, except for sulfation, steroids may be conjugated to steroid glucuronides by UDP-glucuronosyl transferases (UGT), with the UGT1 a 2. However, this process is irreversible in the humans except for the activity of certain gut bacteria that possess β -glucuronidase activity (Schiffer et al., 2019). The process of glucuronidation is used for excretion through bile and urine and steroid glucuronides are not neuroactive.

Balances Between Conjugated and Unconjugated Neuroactive Steroids

Balances between conjugated and unconjugated NAS, except for adrenal sulfated Δ^5 steroids, are ensured mainly by hepatic STS, SULTs, and possibly UDP-glucuronosyltransferases. Sulfation pathways prevail in healthy brain, colon, adrenal, and kidney while desulfation dominates in breast, ovary, prostate, testis, placenta and uterus (Mueller et al., 2015). These balances may be of great importance as unconjugated and sulfated steroids act in many cases in opposite ways on the same receptors.

For example, $5\alpha/\beta$ -reduced metabolites with a hydroxy group in the 3α -position are positive modulators of GABA_A receptors. However their sulfation reverses their action from the positive to negative modulation (Park-Chung et al., 1999). Additionally, the sulfation in the 3α -position enables steroid modulation at NMDA receptor. These data suggest that sulfation and desulfation might be the critical point in steroid regulation of GABAergic and glutamatergic neurotransmission (Park-Chung et al., 1994; Park-Chung et al., 1999). Sulfation also increases the polarity of substances and contributes to their better solubility in the circulation, while rather inhibiting their passage through the BBB.

SULFATION IN NEURODEGENERATIVE DISEASES

Neurodegenerative diseases including multiple sclerosis (MS), Alzheimer's disease (AD) and Parkinson's disease (PD) are generally characterized by progressive alterations in the brain and the spinal cord (Bianchi et al., 2020). These diseases are usually accompanied by neuroinflammation, which may contribute to neurodegeneration (Yilmaz et al., 2019). In addition, neurosteroid synthesis can be affected by neuroinflammation and *vice versa*, neuroactive steroids can influence neuroinflammation. Alterations in neurosteroids (mainly unconjugated) in the aforementioned neurodegenerative diseases were thoroughly reviewed in 2011 by Luchetti et al. (2011). The current review presents the results of some of the later published studies.

Alzheimer's Disease

The pathophysiology of Alzheimer's disease (AD) is characterized by a formation of extracellular amyloid plaques in the cortex and limbic system, aggregation of hyperphosphorylated τ -protein causing intracellular neurofibrillary tangles and is often accompanied by reactive microgliosis and loss of synapses, cholinergic, serotonergic, and noradrenergic function together with glutamatergic dysfunction (López and DeKosky, 2008; Reitz and Mayeux, 2014; Vaňková et al., 2016). The clinical picture is formed by memory loss and cognitive impairment that are often accompanied by various neurological and psychiatric symptoms (López and DeKosky, 2008).

The study of Vaňková et al. (2016) examined 16 AD female patients and 22 sex- and age-matched healthy controls. The measurement of 30 unconjugated steroids and 17 conjugates in the circulation of the AD patients showed altered various

steps of the steroidogenesis. The authors found a shift from conjugated to free (unconjugated) steroids in the AD patients probably due to the reduced SULT2A1 activity in the liver and the adrenal *zona reticularis*. Despite this finding, the relative overproduction of C21 steroids was sufficient to maintain higher levels of sulfates such as PregS, allopregnanolone sulfate, conjugated pregnanolone and conjugated 5 β -pregnane-3 α ,20 α -diol in AD patients (Vaňková et al., 2016). The same findings of attenuated sulfotransferase activity measured as the ratio between conjugated and corresponding unconjugated steroids were confirmed in the cohort of 18 male and 16 female AD patients compared to corresponding age- and gender-controls (Vaňková et al., 2015).

Generally, lower plasma levels of DHEAS in AD patients are reported when compared with control subjects (Näsman et al., 1991; Genedani et al., 2004; Aldred and Mecocci, 2010; Pan et al., 2019). Besides the lower plasma levels of DHEAS, Yanase et al. also found lower values of DHEAS/DHEA ratio in patients with AD and cerebrovascular dementia. This indicates decreased peripheral sulfotransferase activity in dementias in general (Yanase et al., 1996). A recent meta-analysis showed lower DHEAS plasma levels in AD patients (Pan et al., 2019), in accordance with reduced sulfotransferase activity in AD patients. Furthermore, AD patients with higher DHEAS plasma levels were more successful in some memory tasks than patients with lower DHEAS levels (Carlson et al., 1999). Moreover, the results from a prospective study supported the role of lower DHEAS as a risk factor for AD (Hillen et al., 2000) and indicates attenuated sulfotransferase activity even before the development of the disease.

The conclusions drawn from the examinations of the circulating steroids are in line with the observations in CSF, where the steroid levels may also reflect the steroid production and metabolism in the brain. Higher DHEA but lower DHEAS levels in CSF were reported in patients with AD and vascular dementia (Kim et al., 2003). This indicates the attenuated sulfation in the brain of patients with dementia and suggests that DHEA itself does not protect from neurodegeneration. However, it may be a compensatory mechanism against the neurodegenerative process. Lower DHEAS and PregS levels were found in certain brain regions of AD patients examined *postmortem* together with negative correlation of these sulfates with key proteins involved in plaque formation (Weill-Engerer et al., 2002). These results allow to speculate about the neuroprotective role of sulfated steroids and/or the sulfation in AD.

Data from genome wide association study (GWAS) showed downregulation of *STS* gene in patients with AD (Wu et al., 2019). Further GWAS revealed eight independent single nucleotide polymorphisms (SNPs) associated with serum DHEAS concentration. The results elucidated a certain role for *SULT2A1* gene which provides information about key mechanisms of degeneration and aging (Zhai et al., 2011).

STS inhibitors influence the ratio between sulfated and non-sulfated steroids which subsequently modulate brain function. Administration of the STS inhibitor DU-14 to rats increased

plasma DHEAS, decreased plasma DHEA and enhanced hippocampal acetylcholine release and memory (Rhodes et al., 1997). Additionally, significantly higher levels of serotonin in the striatum and hippocampus were reported in mice lacking *STS* gene (Trent et al., 2012). Therefore, steroid sulfation may influence processes in the hippocampus (one of the earliest sites affected in AD (Braak et al., 1993; Mu and Gage, 2011)) by multiple mechanisms, including an alteration of the cholinergic and serotonergic signaling (Trent et al., 2012).

A recent study of Pérez-Jiménez et al. showed that the treatment with STS inhibitor STX64 (Irosustat) resulted in higher pool of sulfated steroids and subsequently increased longevity, improved cognitive symptoms and plaque formation in a chronic AD murine model (Pérez-Jiménez et al., 2021). Furthermore, the use of another STS inhibitor DU-14 in chronic AD murine model decreased the cognitive deficits in spatial learning and memory and protected hippocampal synaptic plasticity (Yue et al., 2016). These data may be of importance for treatment of age-related diseases such as AD in humans. Interestingly, the concept of inhibition of STS has been longer studied in the context of hormone dependent cancers (reviewed in (Foster, 2021)). The use of STS inhibitor STX64 in phase II clinical trial was efficient for the treatment of breast cancer with an acceptable safety profile (Palmieri et al., 2017).

Parkinson's Disease

Parkinson's disease (PD) is a neurodegenerative disorder that predominantly presents in later life with bradykinesia and at least one other symptom of resting tremor or rigidity. People with PD can develop cognitive impairment, including memory loss and dementia. Parkinson's dementia is the second most common dementia after AD and is characterized by neurodegeneration in areas related to motor control, coordination and cognitive function (Mendell and MacLusky, 2018). These features are caused by a massive loss of dopaminergic neurons in the *substantia nigra pars compacta* and consequent striatal dopamine deficiency (di Michele et al., 2013). The pathological hallmark is α -synuclein aggregation into intraneuronal inclusions named Lewy bodies (Mahul-Mellier et al., 2020). Prevalence of PD is twice higher in men than in women, however, women have higher mortality rate and faster progression of the disease (Cerri et al., 2019).

The mechanism how steroid sulfation may be involved in the pathophysiology of PD might lie in the modulation of dopaminergic neurons in substantia nigra that are also under control of the excitatory glutamatergic and inhibitory GABAergic systems (Cobb and Abercrombie, 2002).

The few studies which examined alterations in neurosteroid levels in PD were mostly focusing on unconjugated NAS such as allopregnanolone (di Michele et al., 2003). While DHEAS was found to be lower in AD and vascular dementia (Yanase et al., 1996), no changes were observed in DHEAS levels in PD patients when compared with healthy controls in circulation (Genedani et al., 2004). However, the expression of *SULT2B1* was

downregulated in *substantia nigra* of PD patients with no changes in sulfatase expression (Luchetti et al., 2010). These results indicate that there can be brain region-specific changes in the bioavailability of neuroactive sulfate steroids, which may consequently affect the balance between GABAergic and glutamatergic systems and finally worsen the degeneration of dopaminergic cells (di Michele et al., 2013). The question is whether the decreased levels of neuroprotective NAS contribute to the neurodegeneration or they may be the primary cause of it (Luchetti et al., 2011).

STS inhibitors as well as mutations in STS gene were tested in *Caenorhabditis elegans* PD model. Mutation in STS gene or administration of STX64 improved mobility and decreased the number of α -synuclein aggregates (Pérez-Jiménez et al., 2021) indicating that the use of STS inhibitors in PD could be also a promising treatment option.

Multiple Sclerosis

Multiple sclerosis (MS) is an autoimmune inflammatory and demyelinating disease of the central nervous system with symptoms occurring most often between age of 20–40. Clinical representation is variable with either cognitive and/or motor impairment depending on the localization of the lesion(s). Compared to PD, the prevalence of MS is, on the contrary, at least twice higher in women than in men (Luchetti et al., 2014).

Several studies examined changes in unconjugated NAS in the brain of MS patients. DHEA and allopregnanolone levels in the white matter of MS patients were reported to be decreased (Noorbakhsh et al., 2011; Boghözian et al., 2017). Gender-dependent changes in progesterone and estradiol synthesis and signaling in MS lesions have been described where estrogen pathways were predominantly activated in MS lesions of male patients whereas progesterone pathways were predominantly activated in MS lesions of female patients (Luchetti et al., 2014). In CSF of MS patients, increased levels of pregnenolone and DHEA compared to control groups were reported (Orefice et al., 2016). Additionally, an increase in pregnenolone and isopregnanolone levels together with a decrease in dihydropregesterone and allopregnanolone levels in CSF of male MS patients were observed in the study of Caruso *et al.* (Caruso et al., 2014). Dysregulation in biosynthesis of allopregnanolone of MS patients and its potentially therapeutic role was recently reviewed (Melcangi and Panzica, 2014; Noorbakhsh et al., 2014; Balan et al., 2019). To the best of the authors' knowledge, no information about sulfated steroids and sulfation pathways in MS patients in brain tissue or CSF is available.

At the peripheral level, low plasma testosterone was found in men as well as in women with MS (Foster et al., 2003; Tomassini et al., 2005; Foroughipour et al., 2012). A recent study of Cheng *et al.* found changes in isopregnanolone and allopregnanolone plasma levels when comparing patients with relapsing-remitting MS and patients with a clinically isolated syndrome (Cheng et al., 2021).

In a study of Kancheva *et al.*, 51 steroids and steroid polar conjugates were analyzed in 12 women with MS and 6 sex- and

age-matched controls in follicular phase of menstrual cycle. Intriguingly, the results showed higher levels of C21 steroids including pregnenolone and 3 α / β pregnane isomers and also higher levels of conjugated steroids such as PregS, 20 α -dihydropregnenolone sulfate, conjugates of 3 α / β pregnane isomers and certain bioactive C19 steroids (androsterone, 5-androsten-3 β ,7 α ,17 β -triol) in MS patients (Kanceva et al., 2015) similarly as in AD patients (Vaňková et al., 2016). The altered levels of these steroids may influence neural activity by interacting with various neurotransmitter receptors on a neuronal membrane and affect the balance between neuroprotection and excitotoxicity.

The results regarding DHEAS levels in MS are ambiguous. Levels of DHEAS did not differ between MS and control patients in the above mentioned study of Kanceva et al. (2015). On the other hand, two studies found lower levels of DHEAS in MS in comparison with healthy subjects (Ramsaransing et al., 2005; Foroughipour et al., 2012) and one study found higher DHEAS in MS patients (Ysraelit et al., 2008). Further, lower serum levels of DHEAS and DHEA were found in patients with fatigue in comparison with those without fatigue within the progressive form of MS (Téllez et al., 2006).

The research also reveals the role of glutamate in the pathophysiology of MS. Higher glutamate concentrations were found in acute lesions and normal-appearing white matter (Srinivasan et al., 2005) and appear to contribute to the progression of the disease (Azevedo et al., 2014). GWAS which used *in vivo* glutamate concentration as a quantitative trait discovered that several SNPs are associated with glutamate concentrations. One of these SNPs is rs794185 ($p < 6.44 \times 10^{-7}$), which is within the *sulfatase modifying factor 1* (SUMF1) gene (Baranzini et al., 2010). SUMF1 is an essential factor for sulfatase activities, including the one of STS. The dysregulation of SUMF1 can lead to its diminished activity (Fraldi et al., 2007). Subsequently, an imbalance between conjugated and unconjugated steroids that can modulate glutamatergic receptors occurs.

The available data concerning the NAS and particularly sulfation pathways in association to MS in humans are limited. Therefore, the data from animal models may be helpful. In the mouse model of MS—experimental autoimmune encephalomyelitis (EAE)—a protective effect of unconjugated DHEA on the development and severity of the EAE was repeatedly reported (Du et al., 2001; Aggelakopoulou et al., 2016). Similarly, DHEAS administration to mice ameliorated EAE severity and improved neurological outcomes in EAE, possibly through anti-inflammatory effects (Boghözian et al., 2017).

CONCLUSION

The expression of SULTs and STS is brain region specific, the explanation of these differences across brain region remains to be elucidated. The balance between steroid sulfation and desulfation is critical to maintaining the balance between unconjugated and conjugated steroids, especially when their CNS action is reversed. In neurodegenerative diseases such as Parkinson's disease and Alzheimer's disease the reduced SULT expression and lower levels of steroid sulfates were reported in the brain. In

multiple sclerosis, no information about steroid sulfation and steroid sulfate levels is available yet. However, as with other neurodegenerative diseases, changes in steroid sulfation could be expected. Changes in sulfation in neurodegenerative diseases occur also at the peripheral level as mainly documented by changed ratios of conjugated steroids to their unconjugated counterparts. These alterations may subsequently affect the neuronal activity in the CNS, as the circulating unconjugated steroids and to a lesser extent also the steroid conjugates from periphery surpass the BBB and enter the brain. Therefore, further research of the steroid sulfation in periphery and in brain deserves attention.

Future studies aiming to decipher the relative contributions of the effects of steroid sulfation on neurodegeneration by neurochemical/inflammatory/developmental/general health process may choose different approaches to answer these scientific questions. Animal experiments may be one of the options. However, the limitations of the animal studies are due to the different steroidogenesis in humans and commonly used laboratory animals. In fact, compared to primates, laboratory rodents have negligible steroid sulfate production and generally very different adrenal steroidogenesis (Schuler, 2021). Another route may be GWAS or transcriptomic studies, which are promising approaches suitable for studying the genome or transcriptome and the pathophysiology of human diseases. However, their disadvantage might be the need for a larger

sample size (Hong and Park, 2012). Finally, steroidomic studies may also be designed to explore the mutual association between the metabolites studied.

STS inhibitors are gaining increased attention in the context of aging and age-related diseases. Use of STS inhibitors in animal studies shows promising results in increasing longevity and reducing protein aggregation in protein aggregation diseases such as AD and PD (Pérez-Jiménez et al., 2021). Based on the promising animal results clinical studies in humans are justifiable and warranted.

AUTHOR CONTRIBUTIONS

The authors confirm contribution to the paper as follows: draft manuscript preparation–JV; study conception and supervision–RK; visualization and critical review of the manuscript–MH; literature review and critical review of the manuscript–LK; EKH–critical review and the revision of the manuscript.

FUNDING

The work was supported by a grant NU20-04-00450 of the Ministry of Health of the Czech Republic.

REFERENCES

- Aggelakopoulou, M., Kourepini, E., Paschalidis, N., Simoes, D. C. M., Kalavrizioti, D., Dimisianios, N., et al. (2016). $\text{Er}\beta$ -Dependent Direct Suppression of Human and Murine Th17 Cells and Treatment of Established Central Nervous System Autoimmunity by a Neurosteroid. *J. Immunol.* 197 (7), 2598–2609. doi:10.4049/jimmunol.1601038
- Aldred, S., and Mecocci, P. (2010). Decreased Dehydroepiandrosterone (DHEA) and Dehydroepiandrosterone Sulfate (DHEAS) Concentrations in Plasma of Alzheimer's Disease (AD) Patients. *Arch. Gerontol. Geriatr.* 51 (1), e16–e18. doi:10.1016/j.archger.2009.07.001
- Altemus, M. (2019). Neuroendocrine Networks and Functionality. *Med. Clin. North America* 103 (4), 601–612. doi:10.1016/j.mcna.2019.03.003
- Azcoitia, I., Barreto, G. E., and Garcia-Segura, L. M. (2019). Molecular Mechanisms and Cellular Events Involved in the Neuroprotective Actions of Estradiol. Analysis of Sex Differences. *Front. Neuroendocrinology* 55, 100787. doi:10.1016/j.yfrne.2019.100787
- Azevedo, C. J., Kornak, J., Chu, P., Sampat, M., Okuda, D. T., Cree, B. A., et al. (2014). *In Vivo* evidence of Glutamate Toxicity in Multiple Sclerosis. *Ann. Neurol.* 76 (2), 269–278. doi:10.1002/ana.24202
- Balan, I., Beattie, M. C., O'Buckley, T. K., Aurelian, L., and Morrow, A. L. (2019). Endogenous Neurosteroid (3 α ,5 α)3-Hydroxypregnan-20-One Inhibits Toll-Like-4 Receptor Activation and Pro-inflammatory Signaling in Macrophages and Brain. *Sci. Rep.* 9 (1), 1220. doi:10.1038/s41598-018-37409-6
- Baranzini, S. E., Srinivasan, R., Khankhanian, P., Okuda, D. T., Nelson, S. J., Matthews, P. M., et al. (2010). Genetic Variation Influences Glutamate Concentrations in Brains of Patients with Multiple Sclerosis. *Brain* 133 (9), 2603–2611. doi:10.1093/brain/awq192
- Beyenburg, S., Stoffel-Wagner, B., Bauer, J., Watzka, M., Blümcke, I., Bidlingmaier, F., et al. (2001). Neuroactive Steroids and Seizure Susceptibility. *Epilepsy Res.* 44 (2–3), 141–153. doi:10.1016/s0920-1211(01)00194-2
- Bianchi, V. E., Rizzi, L., Bresciani, E., Omeljaniuk, R. J., and Torsello, A. (2020). Androgen Therapy in Neurodegenerative Diseases. *J. Endocr. Soc.* 4 (11), bvaa120. doi:10.1210/endo/bvaa120
- Bixo, M., Andersson, A., Winblad, B., Purdy, R. H., and Bäckström, T. (1997). Progesterone, 5 α -Pregnane-3,20-Dione and 3 α -Hydroxy-5 α -Pregnane-20-One in Specific Regions of the Human Female Brain in Different Endocrine States. *Brain Res.* 764 (1–2), 173–178. doi:10.1016/s0006-8993(97)00455-1
- Bixo, M., Bäckström, T., Winblad, B., and Andersson, A. (1995). Estradiol and Testosterone in Specific Regions of the Human Female Brain in Different Endocrine States. *J. Steroid Biochem. Mol. Biol.* 55 (3–4), 297–303. doi:10.1016/0960-0760(95)00179-4
- Boghossian, R., McKenzie, B. A., Saito, L. B., Mehta, N., Branton, W. G., Lu, J., et al. (2017). Suppressed Oligodendrocyte Steroidogenesis in Multiple Sclerosis: Implications for Regulation of Neuroinflammation. *Glia* 65 (10), 1590–1606. doi:10.1002/glia.23179
- Braak, H., Braak, E., and Bohl, J. (1993). Staging of Alzheimer-Related Cortical Destruction. *Eur. Neurol.* 33 (6), 403–408. doi:10.1159/000116984
- Brcic, L., Underwood, J. F., Kendall, K. M., Caseras, X., Kirov, G., and Davies, W. (2020). Medical and Neurobehavioural Phenotypes in Carriers of X-Linked Ichthyosis-Associated Genetic Deletions in the UK Biobank. *J. Med. Genet.* 57 (10), 692–698. doi:10.1136/jmedgenet-2019-106676
- Brewer, L. D., Dowling, A. L. S., Curran-Rauhut, M. A., Landfield, P. W., Porter, N. M., and Blalock, E. M. (2009). Estradiol Reverses a Calcium-Related Biomarker of Brain Aging in Female Rats. *J. Neurosci.* 29 (19), 6058–6067. doi:10.1523/jneurosci.5253-08.2009
- Bukanova, J. V., Solntseva, E. I., and Kudova, E. (2020). Neurosteroids as Selective Inhibitors of Glycine Receptor Activity: Structure-Activity Relationship Study on Endogenous Androstanes and Androstenes. *Front. Mol. Neurosci.* 13, 44. doi:10.3389/fnmol.2020.00044
- Carlson, L. E., Sherwin, B. B., and Chertkow, H. M. (1999). Relationships between Dehydroepiandrosterone Sulfate (DHEAS) and Cortisol (CRT) Plasma Levels and Everyday Memory in Alzheimer's Disease Patients Compared to Healthy Controls. *Horm. Behav.* 35 (3), 254–263. doi:10.1006/hbeh.1999.1518
- Caruso, D., Melis, M., Fenu, G., Giatti, S., Romano, S., Grimoldi, M., et al. (2014). Neuroactive Steroid Levels in Plasma and Cerebrospinal Fluid of Male Multiple Sclerosis Patients. *J. Neurochem.* 130 (4), 591–597. doi:10.1111/jnc.12745

- Cerri, S., Mus, L., and Blandini, F. (2019). Parkinson's Disease in Women and Men: What's the Difference. *J. Parkinsons Dis.* 9 (3), 501–515. doi:10.3233/jpd-191683
- Chang, H.-J., Shi, R., Rehse, P., and Lin, S.-X. (2004). Identifying Androsterone (ADT) as a Cognate Substrate for Human Dehydroepiandrosterone Sulfotransferase (DHEA-ST) Important for Steroid Homeostasis. *J. Biol. Chem.* 279 (4), 2689–2696. doi:10.1074/jbc.M310446200
- Chatterjee, S., Humby, T., and Davies, W. (2016). Behavioural and Psychiatric Phenotypes in Men and Boys with X-Linked Ichthyosis: Evidence from a Worldwide Online Survey. *PLoS One* 11 (10), e0164417. doi:10.1371/journal.pone.0164417
- Chen, S.-C., Chang, T.-J., and Wu, F.-S. (2004). Competitive Inhibition of the Capsaicin Receptor-Mediated Current by Dehydroepiandrosterone in Rat Dorsal Root Ganglion Neurons. *J. Pharmacol. Exp. Ther.* 311 (2), 529–536. doi:10.1124/jpet.104.069096
- Cheng, C., Gomez, D., McCombe, J. A., Smyth, P., Giuliani, F., Blevins, G., et al. (2021). Disability Progression in Multiple Sclerosis Is Associated with Plasma Neuroactive Steroid Profile. *Neurol. Sci.* 42, 5241–5247. doi:10.1007/s10072-021-05203-4
- Cobb, W. S., and Abercrombie, E. D. (2002). Distinct Roles for Nigral GABA and Glutamate Receptors in the Regulation of Dendritic Dopamine Release under normal Conditions and in Response to Systemic Haloperidol. *J. Neurosci.* 22 (4), 1407–1413. doi:10.1523/jneurosci.22-04-01407.2002
- Compagnone, N. A., and Mellon, S. H. (2000). Neurosteroids: Biosynthesis and Function of These Novel Neuromodulators. *Front. Neuroendocrinology* 21 (1), 1–56. doi:10.1006/frne.1999.0188
- Corpéchet, C., Robel, P., Axelsson, M., Sjövall, J., and Baulieu, E. E. (1981). Characterization and Measurement of Dehydroepiandrosterone Sulfate in Rat Brain. *Proc. Natl. Acad. Sci.* 78 (8), 4704–4707. doi:10.1073/pnas.78.8.4704
- Corpéchet, C., Synguelakis, M., Talha, S., Axelsson, M., Sjövall, J., Vihko, R., et al. (1983). Pregnenolone and its Sulfate Ester in the Rat Brain. *Brain Research* 270 (1), 119–125. doi:10.1016/0006-8993(83)90797-7
- Darnaudéry, M., Pallarès, M., Piazza, P.-V., Le Moal, M., and Mayo, W. (2002). The Neurosteroid Pregnenolone Sulfate Infused into the Medial Septum Nucleus Increases Hippocampal Acetylcholine and Spatial Memory in Rats. *Brain Res.* 951 (2), 237–242. doi:10.1016/s0006-8993(02)03166-9
- di Michele, F., Longone, P., Romeo, E., Lucchetti, S., Brusa, L., Pierantozzi, M., et al. (2003). Decreased Plasma and Cerebrospinal Fluid Content of Neuroactive Steroids in Parkinson's Disease. *Neurol. Sci.* 24 (3), 172–173. doi:10.1007/s10072-003-0115-1
- di Michele, F., Lucchetti, S., Bernardi, G., Romeo, E., and Longone, P. (2013). Neurosteroid and Neurotransmitter Alterations in Parkinson's Disease. *Front. Neuroendocrinology* 34 (2), 132–142. doi:10.1016/j.yfrne.2013.03.001
- Dieni, C. V., Contemori, S., Biscarini, A., and Panichi, R. (2020). De Novo Synthesized Estradiol: A Role in Modulating the Cerebellar Function. *Int. J. Mol. Sci.* 21 (9), 3316. doi:10.3390/ijms21093316
- Diez-Roux, G., and Ballabio, A. (2005). Sulfatases and Human Disease. *Annu. Rev. Genom. Hum. Genet.* 6, 355–379. doi:10.1146/annurev.genom.6.080604.162334
- Diotel, N., Charlier, T. D., Lefebvre d'Helencourt, C., Couret, D., Trudeau, V. L., Nicolau, J. C., et al. (2018). Steroid Transport, Local Synthesis, and Signaling within the Brain: Roles in Neurogenesis, Neuroprotection, and Sexual Behaviors. *Front. Neurosci.* 12, 84. doi:10.3389/fnins.2018.00084
- Du, C., Khalil, M. W., and Sriram, S. (2001). Administration of Dehydroepiandrosterone Suppresses Experimental Allergic Encephalomyelitis in SJL/J Mice. *J. Immunol.* 167 (12), 7094–7101. doi:10.4049/jimmunol.167.12.7094
- Duong, P., Tenkorang, M. A. A., Trieu, J., McCuiston, C., Rybalchenko, N., and Cunningham, R. L. (2020). Neuroprotective and Neurotoxic Outcomes of Androgens and Estrogens in an Oxidative Stress Environment. *Biol. Sex. Differ.* 11 (1), 12. doi:10.1186/s13293-020-0283-1
- Earl, D. E., and Tietz, E. I. (2011). Inhibition of Recombinant I-type Voltage-Gated Calcium Channels by Positive Allosteric Modulators of GABAA Receptors. *J. Pharmacol. Exp. Ther.* 337 (1), 301–311. doi:10.1124/jpet.110.178244
- Falany, C. N., and Rohn-Glowacki, K. J. (2013). SULT2B1: Unique Properties and Characteristics of a Hydroxysteroid Sulfotransferase Family. *Drug Metab. Rev.* 45 (4), 388–400. doi:10.3109/03602532.2013.835609
- Fargo, K. N., Foecking, E. M., Jones, K. J., and Sengelaub, D. R. (2009). Neuroprotective Actions of Androgens on Motoneurons. *Front. Neuroendocrinology* 30 (2), 130–141. doi:10.1016/j.yfrne.2009.04.005
- Fernandes, N. F., Janniger, C. K., and Schwartz, R. A. (2010). X-linked Ichthyosis: an Oculocutaneous Genodermatosis. *J. Am. Acad. Dermatol.* 62 (3), 480–485. doi:10.1016/j.jaad.2009.04.028
- Fodor, L., Boros, A., Dezso, P., and Maksay, G. (2006). Expression of Heteromeric glycine Receptor-Channels in Rat Spinal Cultures and Inhibition by Neuroactive Steroids. *Neurochem. Int.* 49 (6), 577–583. doi:10.1016/j.neuint.2006.04.013
- Foroughipour, A., Norbakhsh, V., Najafabadi, S. H., and Meamar, R. (2012). Evaluating Sex Hormone Levels in Reproductive Age Women with Multiple Sclerosis and Their Relationship with Disease Severity. *J. Res. Med. Sci.* 17 (9), 882–885. https://www.ncbi.nlm.nih.gov/pmc/articles/PMC3697216/pdf/JRMS-17-882.pdf
- Foster, P. A. (2021). Steroid Sulphatase and its Inhibitors: Past, Present and Future. *Molecules* 26 (10), 2852. doi:10.3390/molecules26102852
- Foster, S. C., Daniels, C., Bourdette, D. N., and Bebo, B. F., Jr. (2003). Dysregulation of the Hypothalamic-Pituitary-Gonadal axis in Experimental Autoimmune Encephalomyelitis and Multiple Sclerosis. *J. Neuroimmunol.* 140 (1–2), 78–87. doi:10.1016/s0165-5728(03)00177-2
- Foy, M. R., Xu, J., Xie, X., Brinton, R. D., Thompson, R. F., and Berger, T. W. (1999). 17 β -Estradiol Enhances NMDA Receptor-Mediated EPSPs and Long-Term Potentiation. *J. Neurophysiol.* 81 (2), 925–929. doi:10.1152/jn.1999.81.2.925
- Fraldi, A., Biffi, A., Lombardi, A., Visigalli, I., Pepe, S., Settembre, C., et al. (2007). SUMF1 Enhances Sulfatase Activities *In Vivo* in Five Sulfatase Deficiencies. *Biochem. J.* 403 (2), 305–312. doi:10.1042/bj20061783
- Frick, K. M. (2015). Molecular Mechanisms Underlying the Memory-Enhancing Effects of Estradiol. *Horm. Behav.* 74, 4–18. doi:10.1016/j.yhbeh.2015.05.001
- Frye, C. A. (1995). The Neurosteroid 3 Alpha, 5 Alpha-THP Has Antiseizure and Possible Neuroprotective Effects in an Animal Model of Epilepsy. *Brain Res.* 696 (1–2), 113–120. doi:10.1016/0006-8993(95)00793-p
- Frye, C. A. (2001). The Role of Neurosteroids and Non-genomic Effects of Progestins and Androgens in Mediating Sexual Receptivity of Rodents. *Brain Res. Rev.* 37 (1–3), 201–222. doi:10.1016/s0165-0173(01)00119-9
- Fuda, H., Lee, Y. C., Shimizu, C., Javitt, N. B., and Strott, C. A. (2002). Mutational Analysis of Human Hydroxysteroid Sulfotransferase SULT2B1 Isoforms Reveals that Exon 1B of the SULT2B1 Gene Produces Cholesterol Sulfotransferase, whereas Exon 1A Yields Pregnenolone Sulfotransferase. *J. Biol. Chem.* 277 (39), 36161–36166. doi:10.1074/jbc.M207165200
- Game, N. U., Tsvetanov, S., Duggleby, R. G., McManus, M. E., and Martin, J. L. (2005). The Structure of Human SULT1A1 Crystallized with Estradiol. *J. Biol. Chem.* 280 (50), 41482–41486. doi:10.1074/jbc.M508289200
- Genedani, S., Rasio, G., Cortelli, P., Antonelli, F., Guidolin, D., Galantucci, M., et al. (2004). Studies on Homocysteine and Dehydroepiandrosterone Sulphate Plasma Levels in Alzheimer's Disease Patients and in Parkinson's Disease Patients. *Neurotox Res.* 6 (4), 327–332. doi:10.1007/bf03033443
- Giatti, S., Divicaro, S., Falvo, E., Garcia-Segura, L. M., and Melcangi, R. C. (2020). Physiopathological Role of the Enzymatic Complex 5 α -Reductase and 3 α / β -Hydroxysteroid Oxidoreductase in the Generation of Progesterone and Testosterone Neuroactive Metabolites. *Front. Neuroendocrinology* 57, 100836. doi:10.1016/j.yfrne.2020.100836
- Giatti, S., Divicaro, S., Serafini, M. M., Caruso, D., Garcia-Segura, L. M., Viviani, B., et al. (2020). Sex Differences in Steroid Levels and Steroidogenesis in the Nervous System: Physiopathological Role. *Front. Neuroendocrinology* 56, 100804. doi:10.1016/j.yfrne.2019.100804
- Giatti, S., Garcia-Segura, L. M., Barreto, G. E., and Melcangi, R. C. (2019). Neuroactive Steroids, Neurosteroidogenesis and Sex. *Prog. Neurobiol.* 176, 1–17. doi:10.1016/j.pneurobio.2018.06.007
- Grube, M., Hagen, P., and Jedlitschky, G. (2018). Neurosteroid Transport in the Brain: Role of ABC and SLC Transporters. *Front. Pharmacol.* 9, 354. doi:10.3389/fphar.2018.00354
- Hampl, R., Bičíková, M., and Sosvorová, L. (2015). Hormones and the Blood-Brain Barrier. *Horm. Mol. Biol. Clin. Investig.* 21 (3), 159–164. doi:10.1515/hmbci-2014-0042
- Havliková, H., Hill, M., Kancheva, L., Vrbíková, J., Pouzar, V., Cerný, I., et al. (2006). Serum Profiles of Free and Conjugated Neuroactive Pregnenolone Isomers in Nonpregnant Women of fertile Age. *J. Clin. Endocrinol. Metab.* 91 (8), 3092–3099. doi:10.1210/jc.2005-2785

- He, X.-Y., Dobkin, C., and Yang, S.-Y. (2019). 17β -Hydroxysteroid Dehydrogenases and Neurosteroid Metabolism in the central Nervous System. *Mol. Cell Endocrinol.* 489, 92–97. doi:10.1016/j.mce.2018.10.002
- Hempel, N., Barnett, A. C., Bolton-Grob, R. M., Liyou, N. E., and McManus, M. E. (2000). Site-directed Mutagenesis of the Substrate-Binding Cleft of Human Estrogen Sulfotransferase. *Biochem. Biophysical Res. Commun.* 276 (1), 224–230. doi:10.1006/bbrc.2000.3473
- Her, C., Wood, T. C., Eichler, E. E., Mohrenweiser, H. W., Ramagli, L. S., Siciliano, M. J., et al. (1998). Human Hydroxysteroid Sulfotransferase SULT2B1: Two Enzymes Encoded by a Single Chromosome 19 Gene. *Genomics* 53 (3), 284–295. doi:10.1006/geno.1998.5518
- Hickman, R. A., O'Shea, S. A., Mehler, M. F., and Chung, W. K. (2022). Neurogenetic Disorders across the Lifespan: from Aberrant Development to Degeneration. *Nat. Rev. Neurol.* doi:10.1038/s41582-021-00595-5 <https://www.nature.com/articles/s41582-021-00595-5>
- Hill, M. (2007). "Neuroaktivní Pregnanové Deriváty - Fyziologie a Patofyziologie," in *Pokroky V Endokrinologii*. Editor J. Očenášková (Prague: Maxdorf).
- Hill, M., Popov, P., Havliková, H., Kancheva, L., Vrbíková, J., Kancheva, R., et al. (2005). Altered Profiles of Serum Neuroactive Steroids in Premenopausal Women Treated for Alcohol Addiction. *Steroids* 70 (8), 515–524. doi:10.1016/j.steroids.2005.02.013
- Hill, M., Vrbíková, J., Zárubová, J., Kancheva, R., Velíková, M., Kancheva, L., et al. (2011). The Steroid Metabolome in Lamotrigine-Treated Women with Epilepsy. *Steroids* 76 (12), 1351–1357. doi:10.1016/j.steroids.2011.07.002
- Hill, M., Zárubová, J., Marušić, P., Vrbíková, J., Velíková, M., Kancheva, R., et al. (2010). Effects of Valproate and Carbamazepine Monotherapy on Neuroactive Steroids, Their Precursors and Metabolites in Adult Men with Epilepsy. *J. Steroid Biochem. Mol. Biol.* 122 (4), 239–252. doi:10.1016/j.jsbmb.2010.06.003
- Hillen, T., Lun, A., Reischies, F. M., Borchelt, M., Steinhagen-Thiessen, E., and Schaub, R. T. (2000). DHEA-S Plasma Levels and Incidence of Alzheimer's Disease. *Biol. Psychiatry* 47 (2), 161–163. doi:10.1016/s0006-3223(99)00217-6
- Hong, E. P., and Park, J. W. (2012). Sample Size and Statistical Power Calculation in Genetic Association Studies. *Genomics Inform.* 10 (2), 117–122. doi:10.5808/gi.2012.10.2.117
- Hu, A.-Q., Wang, Z.-M., Lan, D.-M., Fu, Y.-M., Zhu, Y.-H., Dong, Y., et al. (2007). Inhibition of Evoked Glutamate Release by Neurosteroid Allopregnanolone via Inhibition of L-type Calcium Channels in Rat Medial Prefrontal Cortex. *Neuropsychopharmacol* 32 (7), 1477–1489. doi:10.1038/sj.npp.1301261
- Irwin, R. P., Maragakis, N. J., Rogawski, M. A., Purdy, R. H., Farb, D. H., and Paul, S. M. (1992). Pregnenolone Sulfate Augments NMDA Receptor Mediated Increases in Intracellular Ca^{2+} in Cultured Rat Hippocampal Neurons. *Neurosci. Lett.* 141 (1), 30–34. doi:10.1016/0304-3940(92)90327-4
- Iwamori, M., Moser, H. W., and Kishimoto, Y. (1976). Steroid Sulfatase in Brain: Comparison of Sulfohydrolase Activities for Various Steroid Sulfates in normal and Pathological Brains, Including the Various Forms of Metachromatic Leukodystrophy. *J. Neurochem.* 27 (6), 1389–1395. doi:10.1111/j.1471-4159.1976.tb02620.x
- Jaffe, R. B., Pérez-palacios, G., and Diczfalusy, E. (1972). Conversion of Pregnenolone and Pregnenolone Sulfate to Other Steroid Sulfates by the Human Fetus Perfused at Midgestation. *J. Clin. Endocrinol. Metab.* 35 (5), 646–654. doi:10.1210/jcem-35-5-646
- Jiang, P., Kong, Y., Zhang, X.-B., Wang, W., Liu, C.-F., and Xu, T.-L. (2009). Glycine Receptor in Rat Hippocampal and Spinal Cord Neurons as a Molecular Target for Rapid Actions of 17β -Estradiol. *Mol. Pain* 5, 1744–8069. doi:10.1186/1744-8069-5-2
- Jiang, P., Yang, C.-X., Wang, Y.-T., and Xu, T.-L. (2006). Mechanisms of Modulation of Pregnanolone on Glycinergic Response in Cultured Spinal Dorsal Horn Neurons of Rat. *Neuroscience* 141 (4), 2041–2050. doi:10.1016/j.neuroscience.2006.05.009
- Joëls, M. (1997). Steroid Hormones and Excitability in the Mammalian Brain. *Front. Neuroendocrinology* 18 (1), 2–48. doi:10.1006/frne.1996.0144
- Johansson, I.-M., Birzniece, V., Lindblad, C., Olsson, T., and Bäckström, T. (2002). Allopregnanolone Inhibits Learning in the Morris Water Maze. *Brain Res.* 934 (2), 125–131. doi:10.1016/s0006-8993(02)02414-9
- Kaminski, R. M., Marini, H., Kim, W.-J., and Rogawski, M. A. (2005). Anticonvulsant Activity of Androsterone and Etiocholanolone. *Epilepsia* 46 (6), 819–827. doi:10.1111/j.1528-1167.2005.00705.x
- Kancheva, R., Stárka, L., Kancheva, L., Hill, M., Velíková, M., and Havrdová, E. (2015). Increased Serum Levels of C21 Steroids in Female Patients with Multiple Sclerosis. *Physiol. Res.* 64 (Suppl. 2), S247–S254. doi:10.33549/physiolres.933145
- Kancheva, R., Hill, M., Cibula, D., Včoela 'kova', H., Kancheva, L., Vrbí 'kova', J., et al. (2007). Relationships of Circulating Pregnanolone Isomers and Their Polar Conjugates to the Status of Sex, Menstrual Cycle, and Pregnancy. *J. Endocrinol.* 195 (1), 67–78. doi:10.1677/joe-06-0192
- Kancheva, R., Hill, M., Novák, Z., Chrastina, J., Kancheva, L., and Stárka, L. (2011). Neuroactive Steroids in Periphery and Cerebrospinal Fluid. *Neuroscience* 191, 22–27. doi:10.1016/j.neuroscience.2011.05.054
- Kancheva, R., Hill, M., Novák, Z., Chrastina, J., Velíková, M., Kancheva, L., et al. (2010). Peripheral Neuroactive Steroids May Be as Good as the Steroids in the Cerebrospinal Fluid for the Diagnostics of CNS Disturbances. *J. Steroid Biochem. Mol. Biol.* 119 (1-2), 35–44. doi:10.1016/j.jsbmb.2009.12.006
- Kim, S.-B., Hill, M., Kwak, Y.-T., Hampl, R., Jo, D.-H., and Morfin, R. (2003). Neurosteroids: Cerebrospinal Fluid Levels for Alzheimer's Disease and Vascular Dementia Diagnostics. *J. Clin. Endocrinol. Metab.* 88 (11), 5199–5206. doi:10.1210/jc.2003-030646
- Klangkalya, B., and Chan, A. (1988). Structure-activity Relationships of Steroid Hormones on Muscarinic Receptor Binding. *J. Steroid Biochem.* 29 (1), 111–118. doi:10.1016/0022-4731(88)90384-6
- Klein, P., and Herzog, A. G. (1998). Hormonal Effects on Epilepsy in Women. *Epilepsia* 39 (Suppl. 8), S9–S16. doi:10.1111/j.1528-1157.1998.tb02602.x
- Kudova, E. (2021). Rapid Effects of Neurosteroids on Neuronal Plasticity and Their Physiological and Pathological Implications. *Neurosci. Lett.* 750, 135771. doi:10.1016/j.neulet.2021.135771
- Labrie, F. (1991). Intracrinology. *Mol. Cell Endocrinol.* 78 (3), C113–C118. doi:10.1016/0303-7207(91)90116-a
- Lamont, K. G., Pérez-Palacios, G., Pérez, A. E., and Jaffe, R. B. (1970). Pregnenolone and Pregnenolone Sulfate Metabolism by Human Fetal Testes. *In Vitro. Steroids* 16 (1), 127–140. doi:10.1016/s0039-128x(70)80101-5
- López, O. L., and DeKosky, S. T. (2008). "Clinical Symptoms in Alzheimer's Disease," in *Handbook of Clinical Neurology* (Amsterdam, Netherlands: Elsevier), 207–216. doi:10.1016/s0072-9752(07)01219-5
- Luchetti, S., Bossers, K., Frajese, G. V., and Swaab, D. F. (2010). Neurosteroid Biosynthetic Pathway Changes in Substantia Nigra and Caudate Nucleus in Parkinson's Disease. *Brain Pathol.* 20 (5), 945–951. doi:10.1111/j.1750-3639.2010.00396.x
- Luchetti, S., Huitinga, I., and Swaab, D. F. (2011). Neurosteroid and GABA-A Receptor Alterations in Alzheimer's Disease, Parkinson's Disease and Multiple Sclerosis. *Neuroscience* 191, 6–21. doi:10.1016/j.neuroscience.2011.04.010
- Luchetti, S., van Eden, C. G., Schuurman, K., van Strien, M. E., Swaab, D. F., and Huitinga, I. (2014). Gender Differences in Multiple Sclerosis. *J. Neuropathol. Exp. Neurol.* 73 (2), 123–135. doi:10.1097/nen.0000000000000037
- Luine, V. N., and Frankfurt, M. (2012). Estrogens Facilitate Memory Processing through Membrane Mediated Mechanisms and Alterations in Spine Density. *Front. Neuroendocrinology* 33 (4), 388–402. doi:10.1016/j.yfrne.2012.07.004
- Lundgren, P., Strömberg, J., Bäckström, T., and Wang, M. (2003). Allopregnanolone-stimulated GABA-Mediated Chloride Ion Flux Is Inhibited by 3β -Hydroxy-5 α -Pregnan-20-One (Isoallopregnanolone). *Brain Res.* 982 (1), 45–53. doi:10.1016/s0006-8993(03)02939-1
- Luoma, J. I., Stern, C. M., and Mermelstein, P. G. (2012). Progesterone Inhibition of Neuronal Calcium Signaling Underlies Aspects of Progesterone-Mediated Neuroprotection. *J. Steroid Biochem. Mol. Biol.* 131 (1-2), 30–36. doi:10.1016/j.jsbmb.2011.11.002
- MacKenzie, G., and Maguire, J. (2013). Neurosteroids and GABAergic Signaling in Health and Disease. *Biomol. Concepts* 4 (1), 29–42. doi:10.1515/bmc-2012-0033
- Mahul-Mellier, A.-L., Burtcher, J., Maharjan, N., Weerens, L., Croisier, M., Kuttler, F., et al. (2020). The Process of Lewy Body Formation, rather Than Simply α -synuclein Fibrillization, Is One of the Major Drivers of Neurodegeneration. *Proc. Natl. Acad. Sci. USA* 117 (9), 4971–4982. doi:10.1073/pnas.1913904117
- Majeed, Y., Tumova, S., Green, B. L., Seymour, V. A. L., Woods, D. M., Agarwal, A. K., et al. (2012). Pregnenolone Sulphate-independent Inhibition of TRPM3 Channels by Progesterone. *Cell Calcium* 51 (1), 1–11. doi:10.1016/j.ceca.2011.09.005

- Majewska, M. D., and Schwartz, R. D. (1987). Pregnenolone-sulfate: an Endogenous Antagonist of the Gamma-Aminobutyric Acid Receptor Complex in Brain. *Brain Res.* 404 (1-2), 355–360. doi:10.1016/0006-8993(87)91394-1
- Majewska, M. D., Demirgören, S., Spivak, C. E., and London, E. D. (1990). The Neurosteroid Dehydroepiandrosterone Sulfate Is an Allosteric Antagonist of the GABA Receptor. *Brain Res.* 526 (1), 143–146. doi:10.1016/0006-8993(90)90261-9
- Majewska, M. D., Harrison, N. L., Schwartz, R. D., Barker, J. L., and Paul, S. M. (1986). Steroid Hormone Metabolites Are Barbiturate-like Modulators of the GABA Receptor. *Science* 232 (4753), 1004–1007. doi:10.1126/science.2422758
- Maksay, G., Laube, B., and Betz, H. (2001). Subunit-specific Modulation of glycine Receptors by Neurosteroids. *Neuropharmacology* 41 (3), 369–376. doi:10.1016/s0028-3908(01)00071-5
- Maninger, N., Wolkowitz, O. M., Reus, V. I., Epel, E. S., and Mellon, S. H. (2009). Neurobiological and Neuropsychiatric Effects of Dehydroepiandrosterone (DHEA) and DHEA Sulfate (DHEAS). *Front. Neuroendocrinology* 30 (1), 65–91. doi:10.1016/j.yfrne.2008.11.002
- McEwen, B. S. (1991). Non-genomic and Genomic Effects of Steroids on Neural Activity. *Trends Pharmacol. Sci.* 12 (4), 141–147. doi:10.1016/0165-6147(91)90531-v
- Melcangi, R. C., Garcia-Segura, L. M., and Mensah-Nyagan, A. G. (2008). Neuroactive Steroids: State of the Art and New Perspectives. *Cell. Mol. Life Sci.* 65 (5), 777–797. doi:10.1007/s00018-007-7403-5
- Melcangi, R. C., Giatti, S., and Garcia-Segura, L. M. (2016). Levels and Actions of Neuroactive Steroids in the Nervous System under Physiological and Pathological Conditions: Sex-specific Features. *Neurosci. Biobehavioral Rev.* 67, 25–40. doi:10.1016/j.neubiorev.2015.09.023
- Melcangi, R. C., and Panzica, G. C. (2014). Allopregnanolone: State of the Art. *Prog. Neurobiol.* 113, 1–5. doi:10.1016/j.pneurobio.2013.09.005
- Melcangi, R. C., Panzica, G., and Garcia-Segura, L. M. (2011). Neuroactive Steroids: Focus on Human Brain. *Neuroscience* 191, 1–5. doi:10.1016/j.neuroscience.2011.06.024
- Melcangi, R. C., and Panzica, G. (2009). Neuroactive Steroids: an Update of Their Roles in central and Peripheral Nervous System. *Psychoneuroendocrinology* 34 (Suppl. 1), S1–S8. doi:10.1016/j.psyneuen.2009.11.001
- Meloche, C. A., and Falany, C. N. (2001). Expression and Characterization of the Human 3 Beta-Hydroxysteroid Sulfotransferases (SULT2B1a and SULT2B1b). *J. Steroid Biochem. Mol. Biol.* 77 (4-5), 261–269. doi:10.1016/s0960-0760(01)00064-4
- Mendell, A. L., and MacLusky, N. J. (2018). Neurosteroid Metabolites of Gonadal Steroid Hormones in Neuroprotection: Implications for Sex Differences in Neurodegenerative Disease. *Front. Mol. Neurosci.* 11, 359. doi:10.3389/fnmol.2018.00359
- Miller, W. L., and Auchus, R. J. (2011). The Molecular Biology, Biochemistry, and Physiology of Human Steroidogenesis and its Disorders. *Endocr. Rev.* 32 (1), 81–151. doi:10.1210/er.2010-0013
- Monnet, F. P., Mahé, V., Robel, P., and Baulieu, E. E. (1995). Neurosteroids, via Sigma Receptors, Modulate the [3H]norepinephrine Release Evoked by N-Methyl-D-Aspartate in the Rat hippocampus. *Proc. Natl. Acad. Sci.* 92 (9), 3774–3778. doi:10.1073/pnas.92.9.3774
- Mostaghel, E. A. (2013). Steroid Hormone Synthetic Pathways in Prostate Cancer. *Transl. Androl. Urol.* 2 (3), 212–227. doi:10.3978/j.issn.2223-4683.2013.09.16
- Mu, Y., and Gage, F. H. (2011). Adult Hippocampal Neurogenesis and its Role in Alzheimer's Disease. *Mol. Neurodegeneration* 6, 85. doi:10.1186/1750-1326-6-85
- Mueller, J. W., Gilligan, L. C., Idkowiak, J., Arlt, W., and Foster, P. A. (2015). The Regulation of Steroid Action by Sulfation and Desulfation. *Endocr. Rev.* 36 (5), 526–563. doi:10.1210/er.2015-1036
- Näsman, B., Olsson, T., Bäckström, T., Eriksson, S., Grankvist, K., Viitanen, M., et al. (1991). Serum Dehydroepiandrosterone Sulfate in Alzheimer's Disease and in Multi-Infarct Dementia. *Biol. Psychiatry* 30 (7), 684–690. doi:10.1016/0006-3223(91)90013-c
- Neunzig, J., and Bernhardt, R. (2018). Effect of Sulfonated Steroids on Steroidogenic Cytochrome P450-dependent Steroid Hydroxylases. *J. Steroid Biochem. Mol. Biol.* 179, 3–7. doi:10.1016/j.jsbmb.2017.07.004
- Neunzig, J., Sánchez-Guijo, A., Mosa, A., Hartmann, M. F., Geyer, J., Wudy, S. A., et al. (2014). A Steroidogenic Pathway for Sulfonated Steroids: the Metabolism of Pregnenolone Sulfate. *J. Steroid Biochem. Mol. Biol.* 144 B, 324–333. doi:10.1016/j.jsbmb.2014.07.005
- Nicolas, L. B., and Fry, J. P. (2007). The Steroid Sulfatase Inhibitor COUMATE Attenuates rather Than Enhances Access of Dehydroepiandrosterone Sulfate to the Brain in the Mouse. *Brain Res.* 1174, 92–96. doi:10.1016/j.brainres.2007.07.078
- Nieschlag, E., Loriaux, D. L., Ruder, H. J., Zucker, I. R., Kirschner, M. A., and Lipsett, M. B. (1973). The Secretion of Dehydroepiandrosterone and Dehydroepiandrosterone Sulphate in Man. *J. Endocrinol.* 57 (1), 123–134. doi:10.1677/joe.0.0570123
- Noorbakhsh, F., Baker, G. B., and Power, C. (2014). Allopregnanolone and Neuroinflammation: a Focus on Multiple Sclerosis. *Front. Cel. Neurosci.* 8, 134. doi:10.3389/fncel.2014.00134
- Noorbakhsh, F., Ellestad, K. K., Maingat, F., Warren, K. G., Han, M. H., Steinman, L., et al. (2011). Impaired Neurosteroid Synthesis in Multiple Sclerosis. *Brain* 134 (Pt 9), 2703–2721. doi:10.1093/brain/awr200
- Orefice, N., Carotenuto, A., Mangone, G., Bues, B., Rehm, R., Cerillo, I., et al. (2016). Assessment of Neuroactive Steroids in Cerebrospinal Fluid Comparing Acute Relapse and Stable Disease in Relapsing-Remitting Multiple Sclerosis. *J. Steroid Biochem. Mol. Biol.* 159, 1–7. doi:10.1016/j.jsbmb.2016.02.012
- Ottander, U., Poromaa, I. S., Bjurulf, E., Skytt, A., Bäckström, T., and Olofsson, J. I. (2005). Allopregnanolone and Pregnanolone Are Produced by the Human Corpus Luteum. *Mol. Cell Endocrinol.* 239 (1-2), 37–44. doi:10.1016/j.mce.2005.04.007
- Palmieri, C., Stein, R. C., Stein, R. C., Liu, X., Hudson, E., Nicholas, H., et al. (2017). IRIS Study: a Phase II Study of the Steroid Sulfatase Inhibitor Irosustat when Added to an Aromatase Inhibitor in ER-Positive Breast Cancer Patients. *Breast Cancer Res. Treat.* 165 (2), 343–353. doi:10.1007/s10549-017-4328-z
- Pan, X., Wu, X., Kaminga, A. C., Wen, S. W., and Liu, A. (2019). Dehydroepiandrosterone and Dehydroepiandrosterone Sulfate in Alzheimer's Disease: A Systematic Review and Meta-Analysis. *Front. Aging Neurosci.* 11, 61. doi:10.3389/fnagi.2019.00061
- Pardridge, W. M., and Mietus, L. J. (1979). Transport of Steroid Hormones through the Rat Blood-Brain Barrier. *J. Clin. Invest.* 64 (1), 145–154. doi:10.1172/jci109433
- Pardridge, W. M., and Mietus, L. J. (1980). Transport of Thyroid and Steroid Hormones through the Blood-Brain Barrier of the Newborn Rabbit: Primary Role of Protein-Bound Hormone*. *Endocrinology* 107 (6), 1705–1710. doi:10.1210/endo-107-6-1705
- Park-Chung, M., Wu, F. S., and Farb, D. H. (1994). 3 Alpha-Hydroxy-5 Beta-Pregnan-20-One Sulfate: a Negative Modulator of the NMDA-Induced Current in Cultured Neurons. *Mol. Pharmacol.* 46 (1), 146–150.
- Park-Chung, M., Malayev, A., Purdy, R. H., Gibbs, T. T., and Farb, D. H. (1999). Sulfated and Unsulfated Steroids Modulate γ -aminobutyric acidA Receptor Function through Distinct Sites. *Brain Res.* 830 (1), 72–87. doi:10.1016/s0006-8993(99)01381-5
- Pérez-Jiménez, M. M., Monje-Moreno, J. M., Brokate-Llanos, A. M., Venegas-Calerón, M., Sánchez-García, A., Sansigre, P., et al. (2021). Steroid Hormones Sulfatase Inactivation Extends Lifespan and Ameliorates Age-Related Diseases. *Nat. Commun.* 12 (1), 49. doi:10.1038/s41467-020-20269-y
- Perumal, A. S., and Robins, E. (1973). Regional and Subcellular Distribution of Aryl- and Steroid Sulfatases in Brain. *Brain Res.* 59, 349–358. doi:10.1016/0006-8993(73)90273-4
- Pillerová, M., Borbélyová, V., Hodosy, J., Riljak, V., Renczés, E., Frick, K. M., et al. (2021). On the Role of Sex Steroids in Biological Functions by Classical and Non-classical Pathways. An Update. *Front. Neuroendocrinology* 62, 100926. doi:10.1016/j.yfrne.2021.100926
- Pluchino, N., Ansaldi, Y., and Genazzani, A. R. (2019). Brain Intracrinology of Allopregnanolone during Pregnancy and Hormonal Contraception. *Horm. Mol. Biol. Clin. Investig.* 37 (1), 20180032. doi:10.1515/hmbci-2018-0032
- Purohit, A., and Foster, P. A. (2012). Steroid Sulfatase Inhibitors for Estrogen- and Androgen-dependent Cancers. *J. Endocrinol.* 212 (2), 99–110. doi:10.1530/joe-11-0266
- Qaiser, M. Z., Dolman, D. E. M., Begley, D. J., Abbott, N. J., Cazacu-Davidescu, M., Corol, D. I., et al. (2017). Uptake and Metabolism of Sulphated Steroids by the Blood-Brain Barrier in the Adult Male Rat. *J. Neurochem.* 142 (5), 672–685. doi:10.1111/jnc.14117

- Ramsaransing, G. S. M., Heersema, D. J., and De Keyser, J. (2005). Serum Uric Acid, Dehydroepiandrosterone Sulphate, and Apolipoprotein E Genotype in Benign vs. Progressive Multiple Sclerosis. *Eur. J. Neurol.* 12 (7), 514–518. doi:10.1111/j.1468-1331.2005.01009.x
- Reed, M. J., Purohit, A., Woo, L. W. L., Newman, S. P., and Potter, B. V. L. (2005). Steroid Sulfatase: Molecular Biology, Regulation, and Inhibition. *Endocr. Rev.* 26 (2), 171–202. doi:10.1210/er.2004-0003
- Reitz, C., and Mayeux, R. (2014). Alzheimer Disease: Epidemiology, Diagnostic Criteria, Risk Factors and Biomarkers. *Biochem. Pharmacol.* 88 (4), 640–651. doi:10.1016/j.bcp.2013.12.024
- Rhodes, M. E., Li, P. K., Burke, A. M., and Johnson, D. A. (1997). Enhanced Plasma DHEAS, Brain Acetylcholine and Memory Mediated by Steroid Sulfatase Inhibition. *Brain Res.* 773 (1–2), 28–32. doi:10.1016/s0006-8993(97)00867-6
- Riches, Z., Stanley, E. L., Bloomer, J. C., and Coughtrie, M. W. H. (2009). Quantitative Evaluation of the Expression and Activity of Five Major Sulfotransferases (SULTs) in Human Tissues: The SULT "Pie". *Drug Metab. Dispos.* 37 (11), 2255–2261. doi:10.1124/dmd.109.028399
- Rižner, T. L., and Penning, T. M. (2014). Role of Aldo-Keto Reductase Family 1 (AKR1) Enzymes in Human Steroid Metabolism. *Steroids* 79, 49–63. doi:10.1016/j.steroids.2013.10.012
- Rupprecht, R., Berning, B., Hauser, C. A. E., Holsboer, F., and Reul, J. M. H. M. (1996). Steroid Receptor-Mediated Effects of Neuroactive Steroids: Characterization of Structure-Activity Relationship. *Eur. J. Pharmacol.* 303 (3), 227–234. doi:10.1016/0014-2999(96)00036-2
- Rupprecht, R. (2003). Neuroactive Steroids: Mechanisms of Action and Neuropsychopharmacological Properties. *Psychoneuroendocrinology* 28 (2), 139–168. doi:10.1016/s0306-4530(02)00064-1
- Salman, E. D., Faye-Petersen, O., and Falany, C. N. (2011). Hydroxysteroid Sulfotransferase 2B1b Expression and Localization in normal Human Brain. *Horm. Mol. Biol. Clin. Investig.* 8 (1), 445–454. doi:10.1515/hmbci.2011.117
- Salman, E. D., Kadlubar, S. A., and Falany, C. N. (2009). Expression and Localization of Cytosolic Sulfotransferase (SULT) 1A1 and SULT1A3 in normal Human Brain. *Drug Metab. Dispos.* 37 (4), 706–709. doi:10.1124/dmd.108.025767
- Sánchez, J. C., López-Zapata, D. F., and Pinzón, O. A. (2014). Effects of 17 β -Estradiol and IGF-1 on L-type Voltage-Activated and Stretch-Activated Calcium Currents in Cultured Rat Cortical Neurons. *Neuro Endocrinol. Lett.* 35 (8), 724–732. <https://www.nel.edu/userfiles/articlesnew/NEL350814A09.pdf>
- Sánchez-Guijo, A., Neunzig, J., Gerber, A., Oji, V., Hartmann, M. F., Schuppe, H.-C., et al. (2016). Role of Steroid Sulfatase in Steroid Homeostasis and Characterization of the Sulfated Steroid Pathway: Evidence from Steroid Sulfatase Deficiency. *Mol. Cell Endocrinol.* 437, 142–153. doi:10.1016/j.mce.2016.08.019
- Sarkar, S. N., Huang, R.-Q., Logan, S. M., Yi, K. D., Dillon, G. H., and Simpkins, J. W. (2008). Estrogens Directly Potentiate Neuronal L-type Ca²⁺ Channels. *Proc. Natl. Acad. Sci.* 105 (39), 15148–15153. doi:10.1073/pnas.0802379105
- Schiffer, L., Barnard, L., Baranowski, E. S., Gilligan, L. C., Taylor, A. E., Arlt, W., et al. (2019). Human Steroid Biosynthesis, Metabolism and Excretion Are Differentially Reflected by Serum and Urine Steroid Metabolomes: A Comprehensive Review. *J. Steroid Biochem. Mol. Biol.* 194, 105439. doi:10.1016/j.jsbmb.2019.105439
- Schuler, G. (2021). Steroid Sulfates in Domestic Mammals and Laboratory Rodents. *Domest. Anim. Endocrinol.* 76, 106622. doi:10.1016/j.domaniend.2021.106622
- Serra, M., Pisu, M. G., Littera, M., Papi, G., Sanna, E., Tuveri, F., et al. (2000). Social Isolation-Induced Decreases in Both the Abundance of Neuroactive Steroids and GABAA Receptor Function in Rat Brain. *J. Neurochem.* 75 (2), 732–740. doi:10.1046/j.1471-4159.2000.0750732.x
- Shimizu, M., and Tamura, H.-o. (2002). Identification and Localization of Two Hydroxysteroid Sulfotransferases in the Human Brain. *J. Health Sci.* 48 (5), 467–472. doi:10.1248/jhs.48.467
- Shirakawa, H., Katsuki, H., Kume, T., Kaneko, S., and Akaike, A. (2005). Pregnenolone Sulphate Attenuates AMPA Cytotoxicity on Rat Cortical Neurons. *Eur. J. Neurosci.* 21 (9), 2329–2335. doi:10.1111/j.1460-9568.2005.04079.x
- Smith, C. C., Gibbs, T. T., and Farb, D. H. (2014). Pregnenolone Sulfate as a Modulator of Synaptic Plasticity. *PSYCHOPHARMACOLOGY* 231 (17), 3537–3556. doi:10.1007/s00213-014-3643-x
- Sodani, K., Patel, A., Kathawala, R. J., and Chen, Z.-S. (2012). Multidrug Resistance Associated Proteins in Multidrug Resistance. *Chin. J. Cancer* 31 (2), 58–72. doi:10.5732/cjc.011.10329
- Spence, R. D., and Voskuhl, R. R. (2012). Neuroprotective Effects of Estrogens and Androgens in CNS Inflammation and Neurodegeneration. *Front. Neuroendocrinology* 33 (1), 105–115. doi:10.1016/j.yfrne.2011.12.001
- Sribnick, E. A., Del Re, A. M., Ray, S. K., Woodward, J. J., and Banik, N. L. (2009). Estrogen Attenuates Glutamate-Induced Cell Death by Inhibiting Ca²⁺ Influx through L-type Voltage-Gated Ca²⁺ Channels. *Brain Res.* 1276, 159–170. doi:10.1016/j.brainres.2009.04.022
- Srinivasan, R., Sailasuta, N., Hurd, R., Nelson, S., and Pelletier, D. (2005). Evidence of Elevated Glutamate in Multiple Sclerosis Using Magnetic Resonance Spectroscopy at 3 T. *Brain* 128 (Pt 5), 1016–1025. doi:10.1093/brain/awh467
- Stárka, L., Dušková, M., and Hill, M. (2015). Dehydroepiandrosterone: a Neuroactive Steroid. *J. Steroid Biochem. Mol. Biol.* 145, 254–260. doi:10.1016/j.jsbmb.2014.03.008
- Steckelbroeck, S., Nassen, A., Ugele, B., Ludwig, M., Watzka, M., Reissinger, A., et al. (2004). Steroid Sulfatase (STS) Expression in the Human Temporal Lobe: Enzyme Activity, mRNA Expression and Immunohistochemistry Study. *J. Neurochem.* 89 (2), 403–417. doi:10.1046/j.1471-4159.2004.02336.x
- Steckelbroeck, S., Watzka, M., Lütjohann, D., Makiola, P., Nassen, A., Hans, V. H. J., et al. (2002). Characterization of the Dehydroepiandrosterone (DHEA) Metabolism via Oxysterol 7 α -Hydroxylase and 17-ketosteroid Reductase Activity in the Human Brain. *J. Neurochem.* 83 (3), 713–726. doi:10.1046/j.1471-4159.2002.01187.x
- Stein, C., Hille, A., Seidel, J., Rijnbout, S., Waheed, A., Schmidt, B., et al. (1989). Cloning and Expression of Human Steroid-Sulfatase. *J. Biol. Chem.* 264 (23), 13865–13872. doi:10.1016/s0021-9258(18)80080-1
- Strömberg, J., Bäckström, T., and Lundgren, P. (2005). Rapid Non-genomic Effect of Glucocorticoid Metabolites and Neurosteroids on the γ -aminobutyric Acid-A Receptor. *Eur. J. Neurosci.* 21 (8), 2083–2088. doi:10.1111/j.1460-9568.2005.04047.x
- Strott, C. A. (2002). Sulfonation and Molecular Action. *Endocr. Rev.* 23 (5), 703–732. doi:10.1210/er.2001-0040
- Sun, T., Liu, Z., Liu, M., Guo, Y., Sun, H., Zhao, J., et al. (2019). Hippocampus-specific Rictor Knockdown Inhibited 17 β -Estradiol Induced Neuronal Plasticity and Spatial Memory Improvement in Ovariectomized Mice. *Behav. Brain Res.* 364, 50–61. doi:10.1016/j.bbr.2019.02.014
- Téllez, N., Comabella, M., Julià, E. v., Rio, J., Tintoré, M. a., Brieua, L., et al. (2006). Fatigue in Progressive Multiple Sclerosis Is Associated with Low Levels of Dehydroepiandrosterone. *Mult. Scler.* 12 (4), 487–494. doi:10.1191/135248505ms1322oa
- Tomassini, V., Onesti, E., Mainero, C., Giugni, E., Paolillo, A., Salvetti, M., et al. (2005). Sex Hormones Modulate Brain Damage in Multiple Sclerosis: MRI Evidence. *J. Neurol. Neurosurg. Psychiatry* 76 (2), 272–275. doi:10.1136/jnnp.2003.033324
- Tozzi, A., Bellingacci, L., and Pettorossi, V. E. (2020). Rapid Estrogenic and Androgenic Neurosteroids Effects in the Induction of Long-Term Synaptic Changes: Implication for Early Memory Formation. *Front. Neurosci.* 14, 572511. doi:10.3389/fnins.2020.572511
- Trent, S., Cassano, T., Bedse, G., Ojarikre, O. A., Humby, T., and Davies, W. (2012). Altered Serotonergic Function May Partially Account for Behavioral Endophenotypes in Steroid Sulfatase-Deficient Mice. *Neuropsychopharmacol* 37 (5), 1267–1274. doi:10.1038/npp.2011.314
- Tuckey, R. C. (1990). Side-chain Cleavage of Cholesterol Sulfate by Ovarian Mitochondria. *J. Steroid Biochem. Mol. Biol.* 37 (1), 121–127. doi:10.1016/0960-0760(90)90380-4
- Turner, D. M., Ransom, R. W., Yang, J. S., and Olsen, R. W. (1989). Steroid Anesthetics and Naturally Occurring Analogs Modulate the Gamma-Aminobutyric Acid Receptor Complex at a Site Distinct from Barbiturates. *J. Pharmacol. Exp. Ther.* 248 (3), 960–966.
- Valera, S., Ballivet, M., and Bertrand, D. (1992). Progesterone Modulates a Neuronal Nicotinic Acetylcholine Receptor. *Proc. Natl. Acad. Sci.* 89 (20), 9949–9953. doi:10.1073/pnas.89.20.9949
- Vallée, M., Mayo, W., Darnaudéry, M., Corpéchet, C., Young, J., Koehl, M., et al. (1997). Neurosteroids: Deficient Cognitive Performance in Aged Rats Depends on Low Pregnenolone Sulfate Levels in the hippocampus. *Proc. Natl. Acad. Sci.* 94 (26), 14865–14870. doi:10.1073/pnas.94.26.14865

- Vaňková, M., Hill, M., Velíková, M., Včelák, J., Vacínová, G., Dvořáková, K., et al. (2016). Preliminary Evidence of Altered Steroidogenesis in Women with Alzheimer's Disease: Have the Patients "OLDER" Adrenal Zona Reticularis. *J. Steroid Biochem. Mol. Biol.* 158, 157–177. doi:10.1016/j.jsbmb.2015.12.011
- Vaňková, M., Hill, M., Velíková, M., Včelák, J., Vacínová, G., Lukášová, P., et al. (2015). Reduced Sulfotransferase SULT2A1 Activity in Patients with Alzheimer's Disease. *Physiol. Res.* 64 (Suppl. 2), S265–S273. doi:10.33549/physiolres.933160
- Vega-Vela, N. E., Osorio, D., Avila-Rodriguez, M., Gonzalez, J., García-Segura, L. M., Echeverria, V., et al. (2017). L-type Calcium Channels Modulation by Estradiol. *Mol. Neurobiol.* 54 (7), 4996–5007. doi:10.1007/s12035-016-0045-6
- Wagner, T. F. J., Loch, S., Lambert, S., Straub, I., Mannebach, S., Mathar, I., et al. (2008). Transient Receptor Potential M3 Channels Are Ionotropic Glutamate Receptors in Pancreatic β Cells. *Nat. Cell Biol.* 10 (12), 1421–1430. doi:10.1038/ncb1801
- Wang, M.-D., Wahlström, G., and Bäckström, T. (1997). The Regional Brain Distribution of the Neurosteroids Pregnenolone and Pregnenolone Sulfate Following Intravenous Infusion. *J. Steroid Biochem. Mol. Biol.* 62 (4), 299–306. doi:10.1016/s0960-0760(97)00041-1
- Wang, M., Bäckström, T., Sundström, I., Wahlström, G., Olsson, T., Zhu, D., et al. (2001). Neuroactive Steroids and central Nervous System Disorders. *Int. Rev. Neurobiol.* 46, 421–459. doi:10.1016/s0074-7742(01)46071-5
- Wang, M. D., Bäckström, T., and Landgren, S. (2000). The Inhibitory Effects of Allopregnanolone and Pregnanolone on the Population Spike, Evoked in the Rat Hippocampal CA1 Stratum Pyramidale *In Vitro*, Can Be Blocked Selectively by Epiallopregnanolone. *Acta Physiol. Scand.* 169 (4), 333–341. doi:10.1046/j.1365-201x.2000.00744.x
- Wang, M., He, Y., Eisenman, L. N., Fields, C., Zeng, C.-M., Mathews, J., et al. (2002). β -Hydroxypregnanone Steroids Are Pregnenolone Sulfate-like GABA_A Receptor Antagonists. *J. Neurosci.* 22 (9), 3366–3375. doi:10.1523/jneurosci.22-09-03366.2002
- Weaver, C. E., Land, M. B., Purdy, R. H., Richards, K. G., Gibbs, T. T., and Farb, D. H. (2000). Geometry and Charge Determine Pharmacological Effects of Steroids on N-Methyl-D-Aspartate Receptor-Induced Ca^{2+} Accumulation and Cell Death. *J. Pharmacol. Exp. Ther.* 293 (3), 747–754. https://jpet.aspetjournals.org/content/293/3/747
- Weaver, C. E., Jr., Park-Chung, M., Gibbs, T. T., and Farb, D. H. (1997). 17β -Estradiol Protects against NMDA-Induced Excitotoxicity by Direct Inhibition of NMDA Receptors. *Brain Res.* 761 (2), 338–341. doi:10.1016/s0006-8993(97)00449-6
- Weill-Engerer, S., David, J.-P., Sazdovitch, V., Liere, P., Eyche, B., Pianos, A., et al. (2002). Neurosteroid Quantification in Human Brain Regions: Comparison between Alzheimer's and Nondemented Patients. *J. Clin. Endocrinol. Metab.* 87 (11), 5138–5143. doi:10.1210/jc.2002-020878
- Weir, C. J., Ling, A. T. Y., Belevi, D., Wildsmith, J. A. W., Peters, J. A., and Lambert, J. J. (2004). The Interaction of Anaesthetic Steroids with Recombinant glycine and GABA_A Receptors. *Br. J. Anaesth.* 92 (5), 704–711. doi:10.1093/bja/ae125
- Wetzel, C. H. R., Hermann, B., Behl, C., Pestel, E., Rammes, G., Ziegglänsberger, W., et al. (1998). Functional Antagonism of Gonadal Steroids at the 5-hydroxytryptamine Type 3 Receptor. *Mol. Endocrinol.* 12 (9), 1441–1451. doi:10.1210/mend.12.9.0163
- Willemsen, R., Kroos, M., Hoogeveen, A. T., van Dongen, J. M., Parenti, G., van der Loos, C. M., et al. (1988). Ultrastructural Localization of Steroid Sulphatase in Cultured Human Fibroblasts by Immunocytochemistry: a Comparative Study with Lysosomal Enzymes and the Mannose 6-phosphate Receptor. *Histochem. J.* 20 (1), 41–51. doi:10.1007/bf01745968
- Wong, P., Sze, Y., Chang, C. C. R., Lee, J., and Zhang, X. (2015). Pregnenolone Sulfate Normalizes Schizophrenia-like Behaviors in Dopamine Transporter Knockout Mice through the AKT/GSK3 β Pathway. *Transl Psychiatry* 5 (3), e528. doi:10.1038/tp.2015.21
- Wu, F.-S., and Chen, S.-C. (1997). Mechanism Underlying the Effect of Pregnenolone Sulfate on the Kainate-Induced Current in Cultured Chick Spinal Cord Neurons. *Neurosci. Lett.* 222 (2), 79–82. doi:10.1016/s0304-3940(97)13350-x
- Wu, F. S., Chen, S. C., and Tsai, J. J. (1997). Competitive Inhibition of the Glycine-Induced Current by Pregnenolone Sulfate in Cultured Chick Spinal Cord Neurons. *Brain Res.* 750 (1–2), 318–320. doi:10.1016/s0006-8993(97)00053-x
- Wu, F. S., Gibbs, T. T., and Farb, D. H. (1990). Inverse Modulation of Gamma-Aminobutyric Acid- and Glycine-Induced Currents by Progesterone. *Mol. Pharmacol.* 37 (5), 597–602.
- Wu, F. S., Gibbs, T. T., and Farb, D. H. (1991). Pregnenolone Sulfate: a Positive Allosteric Modulator at the N-Methyl-D-Aspartate Receptor. *Mol. Pharmacol.* 40 (3), 333–336.
- Wu, F. S., Lai, C. P., and Liu, B. C. (2000). Non-competitive Inhibition of 5-HT₃ Receptor-Mediated Currents by Progesterone in Rat Nodose Ganglion Neurons. *Neurosci. Lett.* 278 (1–2), 37–40. doi:10.1016/s0304-3940(99)00883-6
- Wu, F. S., Yu, H. M., and Tsai, J. J. (1998). Mechanism Underlying Potentiation by Progesterone of the Kainate-Induced Current in Cultured Neurons. *Brain Res.* 779 (1–2), 354–358. doi:10.1016/s0006-8993(97)01312-7
- Wu, M., Fang, K., Wang, W., Lin, W., Guo, L., and Wang, J. (2019). Identification of Key Genes and Pathways for Alzheimer's Disease via Combined Analysis of Genome-wide Expression Profiling in the hippocampus. *Biophys. Rep.* 5 (2), 98–109. doi:10.1007/s41048-019-0086-2
- Wu, T.-W., Wang, J. M., Chen, S., and Brinton, R. D. (2005). 17β -estradiol Induced Ca^{2+} Influx via L-type Calcium Channels Activates the Src/ERK/cyclic-AMP Response Element Binding Protein Signal Pathway and BCL-2 Expression in Rat Hippocampal Neurons: A Potential Initiation Mechanism for Estrogen-Induced Neuroprotection. *Neuroscience* 135 (1), 59–72. doi:10.1016/j.neuroscience.2004.12.027
- Xu, B., Yang, R., Chang, F., Chen, L., Xie, G., Sokabe, M., et al. (2012). Neurosteroid PREGS Protects Neurite Growth and Survival of Newborn Neurons in the Hippocampal Dentate Gyrus of APP^{swe}/PS1^{dE9} Mice. *Curr. Alzheimer Res.* 9 (3), 361–372. doi:10.2174/156720512800107591
- Xu, S., Cheng, Y., Keast, J. R., and Osborne, P. B. (2008). 17β -Estradiol Activates Estrogen Receptor β -Signalling and Inhibits Transient Receptor Potential Vanilloid Receptor 1 Activation by Capsaicin in Adult Rat Nociceptor Neurons. *Endocrinology* 149 (11), 5540–5548. doi:10.1210/en.2008-0278
- Yaghoubi, N., Malayev, A., Russek, S. J., Gibbs, T. T., and Farb, D. H. (1998). Neurosteroid Modulation of Recombinant Ionotropic Glutamate Receptors. *Brain Res.* 803 (1–2), 153–160. doi:10.1016/s0006-8993(98)00644-1
- Yanase, T., Fukahori, M., Taniguchi, S., Nishi, Y., Sakai, Y., Takayanagi, R., et al. (1996). Serum Dehydroepiandrosterone (DHEA) and DHEA-Sulfate (DHEA-S) in Alzheimer's Disease and in Cerebrovascular Dementia. *Endocr. J.* 43 (1), 119–123. doi:10.1507/endocrj.43.119
- Yang, L., Zhou, R., Tong, Y., Chen, P., Shen, Y., Miao, S., et al. (2020). Neuroprotection by Dihydrotestosterone in LPS-Induced Neuroinflammation. *Neurobiol. Dis.* 140, 104814. doi:10.1016/j.nbd.2020.104814
- Yilmaz, C., Karali, K., Fodelianaki, G., Gravanis, A., Chavakis, T., Charalampopoulos, I., et al. (2019). Neurosteroids as Regulators of Neuroinflammation. *Front. Neuroendocrinology* 55, 100788. doi:10.1016/j.yfrne.2019.100788
- Ysraelit, M. C., Gaitán, M. I., Lopez, A. S., and Correale, J. (2008). Impaired Hypothalamic-Pituitary-Adrenal axis Activity in Patients with Multiple Sclerosis. *Neurology* 71 (24), 1948–1954. doi:10.1212/01.wnl.0000336918.32695.6b
- Yue, X.-H., Tong, J.-Q., Wang, Z.-J., Zhang, J., Liu, X., Liu, X.-J., et al. (2016). Steroid Sulfatase Inhibitor DU-14 Protects Spatial Memory and Synaptic Plasticity from Disruption by Amyloid β Protein in Male Rats. *Horm. Behav.* 83, 83–92. doi:10.1016/j.yhbeh.2016.05.019
- Zhai, G., Teumer, A., Stolk, L., Perry, J. R. B., Vandenput, L., Coviello, A. D., et al. (2011). Eight Common Genetic Variants Associated with Serum DHEAS Levels Suggest a Key Role in Ageing Mechanisms. *Plos Genet.* 7 (4), e1002025. doi:10.1371/journal.pgen.1002025

Conflict of Interest: The authors declare that the research was conducted in the absence of any commercial or financial relationships that could be construed as a potential conflict of interest.

Publisher's Note: All claims expressed in this article are solely those of the authors and do not necessarily represent those of their affiliated organizations, or those of the publisher, the editors, and the reviewers. Any product that may be evaluated in this article, or claim that may be made by its manufacturer, is not guaranteed or endorsed by the publisher.

Copyright © 2022 Vitku, Hill, Kolatorova, Kubala Havrdova and Kancheva. This is an open-access article distributed under the terms of the Creative Commons Attribution License (CC BY). The use, distribution or reproduction in other forums is permitted, provided the original author(s) and the copyright owner(s) are credited and that the original publication in this journal is cited, in accordance with accepted academic practice. No use, distribution or reproduction is permitted which does not comply with these terms.



Profiling Urinary Sulfate Metabolites With Mass Spectrometry

Christopher C. J. Fitzgerald¹, Rikard Hedman¹, Dimanthi R. Uduwela¹, Bettina Paszerbovics¹, Adam J. Carroll¹, Teresa Neeman¹, Adam Cawley², Lance Brooker³ and Malcolm D. McLeod^{1*}

¹Research School of Chemistry, Australian National University, Acton, ACT, Australia, ²Australian Racing Forensic Laboratory, Racing NSW, Sydney, NSW, Australia, ³Australian Sports Drug Testing Laboratory, National Measurement Institute, Sydney, NSW, Australia

OPEN ACCESS

Edited by:

Tarsis G. Ferreira,
University of Houston, United States

Reviewed by:

Ernesto Satoshi Nakayasu,
Pacific Northwest National Laboratory
(DOE), United States
Fernando Ogata,
Federal University of São Paulo, Brazil

*Correspondence:

Malcolm D. McLeod
malcolm.mcleod@anu.edu.au

Specialty section:

This article was submitted to
Cellular Biochemistry,
a section of the journal
Frontiers in Molecular Biosciences

Received: 05 December 2021

Accepted: 12 January 2022

Published: 23 February 2022

Citation:

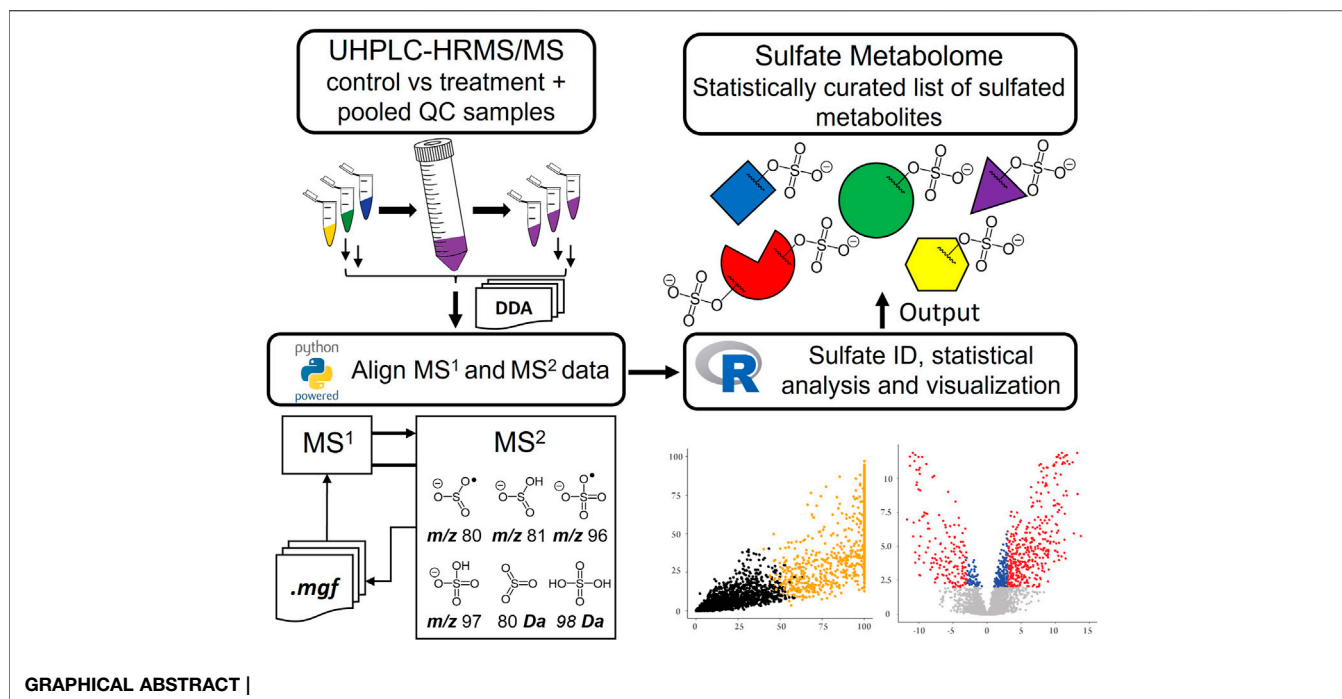
Fitzgerald CCJ, Hedman R, Uduwela DR, Paszerbovics B, Carroll AJ, Neeman T, Cawley A, Brooker L and McLeod MD (2022) Profiling Urinary Sulfate Metabolites With Mass Spectrometry. *Front. Mol. Biosci.* 9:829511. doi: 10.3389/fmolb.2022.829511

The study of urinary phase II sulfate metabolites is central to understanding the role and fate of endogenous and exogenous compounds in biological systems. This study describes a new workflow for the untargeted metabolic profiling of sulfated metabolites in a urine matrix. Analysis was performed using ultra-high-performance liquid chromatography-high resolution tandem mass spectrometry (UHPLC-HRMS/MS) with data dependent acquisition (DDA) coupled to an automated script-based data processing pipeline and differential metabolite level analysis. Sulfates were identified through *k*-means clustering analysis of sulfate ester derived MS/MS fragmentation intensities. The utility of the method was highlighted in two applications. Firstly, the urinary metabolome of a thoroughbred horse was examined before and after administration of the anabolic androgenic steroid (AAS) testosterone propionate. The analysis detected elevated levels of ten sulfated steroid metabolites, three of which were identified and confirmed by comparison with synthesised reference materials. This included 5 α -androstane-3 β ,17 α -diol 3-sulfate, a previously unreported equine metabolite of testosterone propionate. Secondly, the hydrolytic activity of four sulfatase enzymes on pooled human urine was examined. This revealed that *Pseudomonas aeruginosa* arylsulfatases (PaS) enzymes possessed higher selectivity for the hydrolysis of sulfated metabolites than the commercially available *Helix pomatia* arylsulfatase (HpS). This novel method provides a rapid tool for the systematic, untargeted metabolic profiling of sulfated metabolites in a urinary matrix.

Keywords: sulfation, mass spectrometry, metabolomics, steroid, anti-doping, sulfatase, sulfate ester

INTRODUCTION

The study of phase II metabolism is essential to understand the biochemical role and fate of endogenous and exogenous compounds and is dominated by the two major classes of conjugates: sulfates and glucuronides (Schänzer, 1996). A compelling example of the importance of phase II conjugation is provided by the field of steroid metabolism, with the conjugates accounting for up to 97% of excreted urinary metabolites (Pranata et al., 2019). Glucuronylation, performed by uridine 5'-diphospho-glucuronosyltransferases (UGTs) has traditionally been the main focus of these investigations, as the major excretory phase II pathway, and due to the ready availability of β -glucuronidase enzymes for selective deconjugation. More recently, the study of sulfate conjugates has gained prominence due to the intriguing interplay between sulfotransferase (SULT) mediated



synthesis, sulfatase promoted hydrolysis and a range of transport phenomena (Foster and Mueller, 2018; Uduwela et al., 2018; Günel et al., 2019). The systematic study of the sulfated metabolome in a variety of contexts will be pivotal in revealing the roles of sulfation pathways in biology.

The field of metabolomics initially emerged as a complementary approach to genomics and proteomics (Fiehn et al., 2000; Lafaye et al., 2004). However, metabolic profiling has grown into its own field and serves as a powerful way to identify biomarkers in an unbiased fashion, including with relative quantification (Fiehn et al., 2000; Tolstikov and Fiehn, 2002). Metabolomic methods can be applied to the study of disease states or perturbations to homeostasis, giving unprecedented insight into biological processes (Antignac et al., 2005; Pozo et al., 2018). The study of sulfate conjugated metabolites has been of particular interest in metabolomics and found useful applications in applied sciences such as anti-doping and medical research (Pranata et al., 2019; Mueller et al., 2021). A range of tools are available, including the use of nuclear magnetic resonance (NMR), and various hyphenated chromatographic-tandem mass spectrometry (MS/MS) techniques (Lafaye et al., 2004). Early approaches to examine the sulfate metabolome employed gas chromatography-mass spectrometry (GC-MS) techniques, however, these suffered from various limitations due to the polar character of the conjugates, challenges with reliable enzymatic or chemical cleavage of sulfate esters, and loss of information about conjugation sites and levels (Gomes et al., 2009). This directed research towards liquid chromatography-mass spectrometry (LC-MS) techniques, which permit the direct detection of the intact sulfate conjugates, allowing the sulfate fraction to be specifically targeted during analysis. This type of analysis heavily relies on MS/MS techniques driven by the

capacity of sulfate conjugates to readily undergo ionisation during electrospray ionisation (ESI), and display distinctive fragmentation behavior (Thevis et al., 2011; Gómez et al., 2012; Balcells et al., 2017a). Approaches based on tandem mass spectrometry include, multiple reaction monitoring (MRM), precursor ion scanning, or constant ion loss (CIL) scanning, which have all been used to selectively and directly detect sulfate conjugated metabolites (Bowers and Sanaullah, 1996; Bean and Henion, 1997; Hintikka et al., 2008; Gómez et al., 2013; Balcells et al., 2017a; McLeod et al., 2017; Schänzer and Thevis, 2017).

An early example of LC-MS based profiling of sulfate conjugates was in human and rat urine. Here sulfated molecules were identified by monitoring the neutral loss of 80 Da (SO_3), precursors of m/z 80 ($^*\text{SO}_3^-$) and of m/z 97 (HSO_4^-), using ESI triple-quadrupole MS/MS (Lafaye et al., 2004). These methods were used to identify tens of sulfate metabolites, some of which were then confirmed through synthesis of the corresponding reference materials (Lafaye et al., 2004). A similar study used ultra-high-performance liquid chromatography (UHPLC)/negative ion matrix-assisted laser desorption ionization tandem time-of-flight high resolution mass spectrometry (MALDI-TOF/TOF-MS) to identify 1,129 potential sulfate candidates from the urine of pregnant women with detection based on the neutral loss of 80 Da and/or the formation of the m/z 97 product ion. Database matches were investigated for these candidates but none were confirmed against reference materials (Yao et al., 2016). More recently a method for the detection of sulfated metabolites in gut-microbiota using UHPLC-MS in an untargeted fashion was reported (Ballet et al., 2018). In this study sulfated metabolites were identified by comparing

features that underwent change after treatment with a purified preparation of the commercially available sulfatase enzyme *Helix pomatia* arylsulfatase (HpS). Structural validation was then achieved through MS/MS fragment identification, by comparison with reference materials or through data base matching. The method was able to confirm the structures of 36 from 206 putative sulfated metabolites identified (Ballet et al., 2018). Although collectively these approaches provide useful tools to study sulfate metabolites, they also have some limitations. In general, these approaches monitor only a selection of the known sulfate ester fragmentation modes and as a result may miss important classes of conjugate or not report information that could aid in characterizing different classes of conjugate. Furthermore, methods such as enzyme hydrolysis, that assess conversions of sulfate esters to their non-sulfated counterparts, only report on species that change and do not necessarily report on those that do not change. Moreover, they may also miss those product species with low ionisation efficiencies. Herein, we report the development of an untargeted metabolomics approach to comprehensively profile the sulfate metabolome in a urinary matrix. It employs ultra-high performance liquid chromatography-tandem high resolution mass spectrometry (UHPLC-HRMS/MS) with data dependent acquisition (DDA) and a novel data analysis pipeline to systematically identify sulfated metabolites by studying fragmentation behavior. The suitability of the method was evaluated in two applications: firstly, as a screening tool to identify potential steroid markers in equine urine post doping with testosterone propionate; and secondly, to monitor the performance of sulfatase enzymes for the hydrolysis of sulfate esters in pooled human urine. This method increases the utility of untargeted metabolomics for sulfate biomarker discovery in a urinary matrix.

MATERIALS AND METHODS

Animal Administration

Animal administration was approved by both Charles Sturt University (Wagga Wagga, NSW, Australia) and Racing NSW Animal Care and Ethics Committees. Testoprop® (testosterone propionate, 250 mg) was administered by intramuscular injection in the neck, opposite to the sampling jugular catheter to a thoroughbred gelding (635 kg, 14-year-old). Urine samples were collected at -72, -48, -24, 0, 2, 4, 6, 8, 12, 24, 36, 48, 72 h and then daily to 28 days after administration. Samples were stored at -20°C at the Racing NSW or the Australian National University (ANU) in sterile Falcon tubes (polypropylene, centrifuge tubes, 50 ml).

Equine Urine Sample Preparation

The method has been reported previously and adapted according to our work (Waller et al., 2016). To an aliquot of urine (1.1 ml), phosphate buffer (0.55 ml, 100 mM, pH 7.4) was added and the samples were centrifuged (1,100 x g, 5 min) to pellet solids. Each supernatant was fortified with a mixture of analytical internal standards nandrolone sulfate (**S1**), cholane diol bis(sulfate) (**S2**), epiandrosterone ($^{18}\text{O}_3$)-sulfate (**S3**) and 5 α -androstane-3 β ,17 β -

diol 3, ($^{18}\text{O}_3$)-17-bis(sulfate) (**S4**) (0.150 ml, final concentration equivalent to 300 ng/ml original urine volume (1.1 ml) per standard). At this stage, the supernatants were split equally into biological samples and pooled quality control (QC) samples (0.818 ml, equivalent to 0.5 ml of original urine volume). The latter were pooled and then redistributed as pooled QC aliquots (0.818 ml). Both supernatant and pooled QC samples (0.818 ml) were then loaded onto a Waters Oasis™ WAX SPE cartridge (3 cc), that was pre-conditioned with methanol (2 ml) and water (2 ml). Samples were washed with NaOH (2 ml, 0.1 M), phosphate buffer (2 ml, 100 mM, pH 7.4), and Milli-Q water (2 ml) before elution with a mixture of ethyl acetate: methanol: diethyl amine (25:25:1 v/v/v, 3 ml) into clean 10 ml glass tubes. Samples were then evaporated to dryness under a reduced pressure at 40°C and stored at -20°C. The dried samples were re-dissolved with acetonitrile: water (20% v/v, 50 μL), filtered using 0.2 μm spin filters and stored at 5°C for analysis.

Enzyme Hydrolysis in Human Urine Sample Preparation

The human urine samples used in this study were collected with approval by the ANU Human Research Ethics Committee, in accordance with the 2007 National Statement on Ethical Conduct in Human Research (approval number 2013/654). Volunteers gave written informed consent prior to participation; they were all healthy and reported not using steroids within 1 month of supplying a sample. Urine was taken from six subjects (three females and three males ranging between 20–50 years old) and pooled, into phthalate free plastic containers (Nalgene® bottles, style 2110) and stored at -20°C. The following procedure was based on an established method (Stevenson et al., 2015). Aliquots of pooled human urine (2.1 ml) were pipetted into 15 ml falcon tubes. The samples were either adjusted to a pH of 7.5 ± 0.2 (PaS enzymes and control) or to 4.0 ± 0.2 (HpS enzyme) with the addition of Tris buffer (1.5 ml, 0.2 M) or acetate buffer (1.5 ml, 0.2 M) with mixing, respectively. To their respective tubes, preparations of purified WT-PaS, PVFV-PaS, LEF-PaS, or crude HpS (0.4 ml, PaS preparations 2.0 mg/ml, HpS 5.9 mg/ml) and for the control sample enzyme storage buffer (0.4 ml, 0.1 mM Tris-HCl, pH 7.5 in 50% v/v glycerol) were added. The quantities of enzyme were normalized according to their rates of *para*-nitrophenyl sulfate hydrolysis (**Supplementary Table S7**) (Stevenson et al., 2015). Hydrolysis reactions were performed in triplicate for a total of 15 samples and controls by overnight incubation at 37°C. Samples were centrifuged (1,100 x g, 5 min) and the supernatants were split equally (1.9048 ml each, equivalent to 1 ml of original urine volume) into biological and pooled QC samples. All pooled QC samples were pooled and redistributed into 1.9048 ml pooled QC aliquots. Each supernatant and pooled QC were fortified with a mixture of analytical internal standards nandrolone sulfate (**S1**), cholane diol bis(sulfate) (**S2**), epiandrosterone ($^{18}\text{O}_3$)-sulfate (**S3**) and 5 α -androstane-3 β ,17 β -diol 3, ($^{18}\text{O}_3$)-17-bis(sulfate) (**S4**) (0.300 ml, final concentration equivalent to 300 ng/ml urine volume (1 ml) per standard). The treatments, control and pooled QC samples were then subjected to SPE as above, with tris-HCl buffer (2 ml, 0.2 M) being used in place of phosphate

TABLE 1 | Masses used to identify sulfate-derived fragments and neutral losses (Attygalle et al., 2001; Yi et al., 2006; Farrell et al., 2011; Balcells et al., 2017b; McLeod et al., 2017; Esquivel et al., 2018).

Ion (<i>m/z</i>)	Nominal	Accurate
•SO ₃ [−]	80	79.9573
HSO ₃ [−]	81	80.9652
•SO ₄ [−]	96	95.9523
HSO ₄ [−]	97	96.9601
Neutral loss (Da)		
SO ₃	80	79.9568
H ₂ SO ₄	98	97.9674

buffer in the wash phase. Samples were then evaporated to dryness under reduced pressure at 40°C, and the dried samples were stored at −20°C until analysis. For analysis samples were reconstituted in MeOH: water (20% v/v, 100 µL).

UHPLC-HRMS/MS Analysis

The study was carried out using a Q-Exactive Plus Orbitrap mass spectrometer equipped with a heated electrospray ionisation source (HESI-II) interfaced to an Ulti-Mate 3000 system for chromatographic separation (all from Thermo Fisher, Scoresby, Australia). For equine urine samples: the column used was an Acquity UPLC CSH phenyl-hexyl column (2.1 × 100 mm, i.d., 1.7 µm) fixed to an Acquity UPLC CSH phenyl-hexyl VanGuard Pre-Column (2.1 × 5 mm i.d., 1.7 µm). The UHPLC separation was performed at flow rate 0.4 ml/min, using gradient mixing of two mobile phase components. Solution A: 20 mM ammonium formate in water; and solution B: 20 mM ammonium formate in acetonitrile: water (90% v/v). The gradient was 0–0.5 min (20% B), 0.5–15 min (20–58% B), 15–20.5 min (58–100% B), 20.5–21.5 min (100–20% B), 21.5–30.0 min (20% B). The injection volume was 5 µL and the column oven temperature was 40°C. For human urine samples: the column used was a polar end capped Thermo Accucore aQ C18 column (2.1 × 100 mm, 2.6 µm). The UHPLC separation was performed at a flow rate 0.4 ml/min, using gradient mixing of two mobile phase components; solution A: 5 mM ammonium formate in water; and solution B: 5 mM ammonium formate in methanol: water (99% v/v). The gradient was 0–20 min (1–100% B), 20–25 min (100% B), 25–26 min (100–1% B) and 26–35 min (1% B). The injection volume was 5 µL and the column oven temperature was 40°C. For HRMS analysis: the spray voltage was 2.50 kV, capillary temperature 250°C, S-lens RF level 50, and auxiliary heater temperature 350°C. Mass calibration was performed in negative mode: using propionic acid (*m/z* 73.0295), isobutyric acid (*m/z* 87.0452), heptanoic acid (*m/z* 129.0921), in addition to Pierce ESI negative ion calibration solution. Scan spectrum acquisition with a resolution of 70,000 (Full Width at Half Maximum; FWHM) and scan range of *m/z* 200 to 2000 was used in negative mode. The automatic gain control (AGC) was set to 3 × 10⁶. Data dependent acquisition (DDA) MS/MS spectra (*m/z* 50–500) were collected, between 1 and 20 min, with a resolution of 17,500 (FWHM) on the top 10 precursors in each scan window. The intensity threshold (minimum intensity to initiate a DDA scan) was 8.0 × 10⁴. The

apex trigger was set to 2–6 s, and dynamic exclusion was used to exclude already selected ions for the following 3 s. A static exclusion list was also used to exclude precursor ions from DDA that did not emanate from the urine samples but were instead derived from solvents and other method components that were observed in extraction blank samples. This list consisted of the 1,000 most abundant ions detected from two incubated water extraction blank samples, which were taken through the whole sample treatment. For experiments with pooled QC samples, the injection sequence started by running two blanks followed by running at least 10 system suitability samples and two pooled QC samples, followed by the main sequence. For both applications: biological samples were performed in triplicate and analysed in a random order, with pooled QC samples dispersed evenly throughout. In targeted parallel reaction monitoring (PRM) MS/MS experiments for metabolite confirmation, a list of single *m/z* was selected and fragmented over multiple NCE's, for both reference material and biological samples.

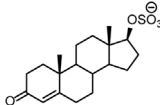
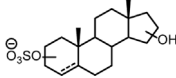
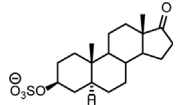
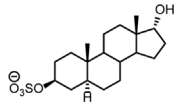
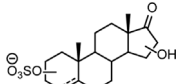
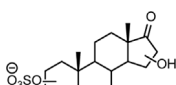
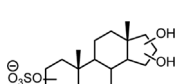
Data Workflow Pipeline and Processing

Data alignment, LOWESS normalization of total ion chromatograms (TIC), and Principal Component Analysis (PCA) analysis was performed in MS-DIAL by applying tolerances to both retention time (RT) (±3 s) and mass accuracy ($\Delta m/z \pm 5$ ppm), alongside the recommended settings for DDA-HRMS systems (Tsugawa et al., 2015). Further data analysis was performed either in python or R (**Supplementary Section S3**). A Python script was used to extract and append MS/MS data for each aligned feature that contained a sulfate-derived fragment. The *k*-means clustering function in R was used to sort metabolic features (Hartigan and Wong, 1979; Team, 2017). Two clusters were chosen as they represented the data appropriately (**Supplementary Figures S3, S4**) (Kaufman and Rousseeu, 2009). Clustering was performed based on the normalized data of eight unique parameters all derived from the MS/MS spectra. These included the six characteristic sulfate-derived fragments (**Table 1**). (Attygalle et al., 2001; Yi et al., 2006; Farrell et al., 2011; Balcells et al., 2017b; McLeod et al., 2017; Esquivel et al., 2018) The remaining two parameters were Intensity Ratio (IR): the total sum of sulfate-derived fragments divided by the sum of all fragments, and Maximum Abundance (MA): the normalized relative abundance (%) of the largest sulfate-derived fragment. Data were clustered into non-sulfate and sulfate groupings. High throughput differential metabolite level analysis and data visualization was performed in R, using the *limma* and *ggplot2* packages, respectively (Ginestet, 2011; Ritchie et al., 2015; Team, 2017). The output gives a final curated list of metabolic features that were sorted into sulfate and non-sulfate metabolites, with associated statistics [e.g., adjusted *p*-value, log₂ Fold Change (FC)], UHPLC-HRMS/MS data (RT and *m/z*), and product ion data for any sulfate-derived fragments detected by MS/MS (see **Supplementary Table S14** for an example).

Synthesis of Anabolic Androgenic Steroid Sulfate Metabolite Reference Materials

Briefly, the synthesis of sulfated reference materials was performed as follows and was adapted from previous work

TABLE 2 | Structures of steroid sulfate metabolites and associated high throughput differential level analysis data from the untargeted profiling (\log_2 fold change and adjusted p -value). Identified structures were confirmed against synthesized reference materials according to AORC retention time and MS/MS criteria, see **Supplementary Table S6**.

m/z	RT (min)	\log_2FC	Adjusted p -value	Structure	Identity
367.1583	8.77	10	2E-07		testosterone sulfate (1)
369.1739	7.69	9	6E-06		unidentified
369.1739	10.16	6	5E-06		epiandrosterone sulfate (2)
371.1895	10.53	8	2E-05		5α-androstane-3β-17α-diol-3-sulfate (3)
383.1537	6.37	7	1E-03		unidentified
385.1690	6.74	4	7E-08		unidentified
387.1845	7.59	10	2E-05		unidentified
387.1846	7.39	8	8E-03		unidentified
387.1846	4.56	9	5E-05		unidentified
387.1849	4.48	9	2E-05		unidentified

(Waller and McLeod, 2014): $\text{SO}_3\bullet\text{py}$ (30 mg, 188 mmol) was added to a solution of free steroid (5 mg) in dimethylformamide (0.5 ml) the resulting reaction mixture was capped and stirred at room temperature for 3 h. The reaction was then quenched with water (10 ml) and loaded onto a pre-conditioned Waters Oasis C18 SPE cartridge (3 cc). The reaction mixture was washed with aqueous ammonia solution (2 ml, 5% v/v) followed by water (2 ml). Steroid sulfates were then eluted in aqueous ammonia methanol solution (3 ml, 5% v/v). The methanolic ammonia fraction was then concentrated in vacuo to yield the desired steroid sulfate as an ammonium salt.

RESULTS AND DISCUSSION

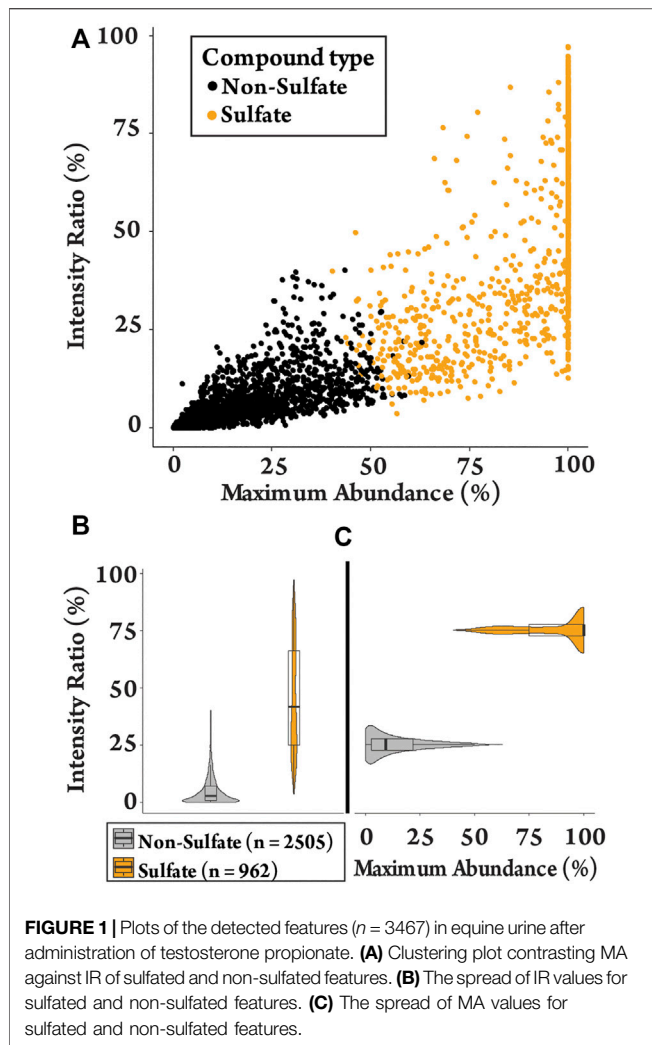
Application 1: The effects of Testosterone Propionate Doping on the Urinary Sulfate Metabolome in the Equine

Anabolic androgenic steroids (AAS) and their metabolites are routinely detected in anti-doping urinary analysis (Schänzer and Thevis, 2017). Intact phase II AAS metabolites such as sulfate esters play an important role in anti-doping analysis as long-term biomarkers for both exogenous and endogenous steroids

(Schänzer et al., 2013; Piper et al., 2016; Kiouisi et al., 2021). Further, sulfation of metabolites is reported to predominate in horses when compared to humans (Scarth et al., 2011). In this application we use the untargeted profiling workflow to assess change in the sulfate urinary metabolome after the intramuscular administration of the AAS testosterone propionate in a thoroughbred gelding (horse 1). This study included a comparison of pre (−24 h) and post (+12 h) administration urine samples, performed in triplicate. These samples were also compared against samples from a non-drug treated gelding (horse 2) at three time points, to assess natural variability over time. Samples were extracted using weak anion exchange (WAX) solid phase extraction (SPE) to isolate the sulfated fraction from the urine.

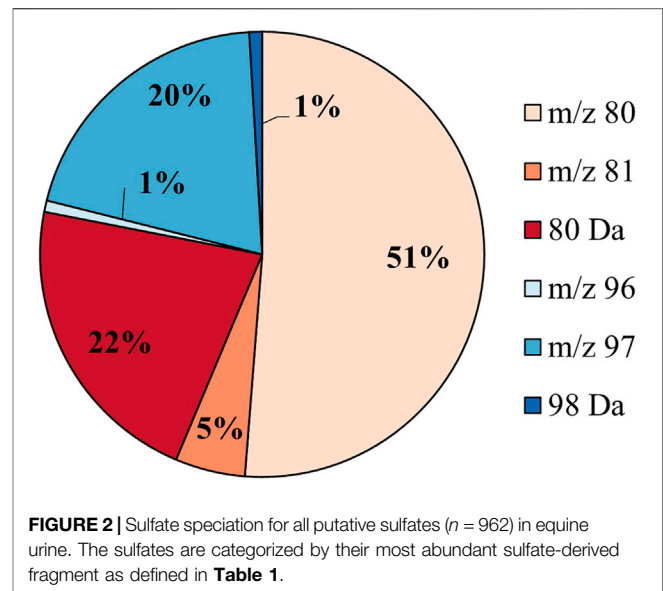
Data Acquisition, Batch Analysis and Alignment

Metabolomic data was acquired using UHPLC-HRMS/MS with data dependent acquisition. The normalized collision energy (NCE) for MS/MS analysis was optimized by studying fragmentation patterns of 20 steroid monosulfate and bis(sulfate) reference materials (**Supplementary Table S1**). An NCE of 60 eV was chosen for the DDA experiments as all sulfate-derived fragments could be observed with high relative abundance (**Table 1**). Following data acquisition, detected features were aligned using suitable tolerances ($\text{RT} \pm 3$ s and



$\Delta m/z \pm 5$ ppm) in MS-DIAL. Normalization was performed by the use of locally weighted scatterplot smoothing (LOWESS) program (Sangster et al., 2006; Godzien et al., 2015; Broadhurst et al., 2018; Considine et al., 2018; Dudzik et al., 2018). This gave an initial list of 6,230 total detected features. Following this, features without MS/MS spectra, an S/N ratio below three and peaks that appeared in less than two samples, were excluded giving a final curated list of 3467 features. Data was assessed through PCA with good quality data indicated by the tight clustering of replicate samples and pooled QC samples (**Supplementary Figure S1**) (Broadhurst et al., 2018).

To allow identification of sulfated metabolites, MS/MS spectra of LC/MS features from pooled QC samples were exported to Mascot Generic Format files (.MGF) and analyzed with a custom Python script (**Supplementary Section S7**) designed to search for accurate mass evidence of known sulfate-associated ions and neutral losses from the precursor ion. During this process two new parameters termed intensity ratio (IR) and maximum abundance (MA) were calculated for each detected feature. These parameters were simple ratios generated from the



sulfate-derived fragment ions observed in MS/MS spectra. The IR was the ratio of sulfate-derived fragment ions as a percentage of all product ions in the MS/MS spectrum. The MA was the relative abundance of the sulfate reporter ion with the highest relative abundance. As sulfate metabolites typically display MS/MS spectra dominated by characteristic product ions or neutral losses these ratios were used to help identify sulfate metabolites. These data on sulfate-derived fragments were mapped onto the alignment results from MS-DIAL on the basis of retention time and accurate precursor m/z (closest retention time match within tight m/z and RT error tolerance limits) using a second custom Python script. (**Supplementary Section S7**).

Identification of Sulfated Metabolites

k -means clustering was used to differentiate between sulfated and non-sulfated features in the samples in an unbiased manner. This aims to partition data into groups based on the minimization of the sum of squares to their assigned cluster center. Grouping was based on the six sulfate-derived fragments (**Table 1**) together with the ratios MA and IR, and were grouped to the nearest center (mean) across the eight parameters, clustered into two groups (**Supplementary Figure S3**) (Hartigan and Wong, 1979). This separated the 3467 features into 2,505 non-sulfates and 962 sulfates (28%). The clustering of features is visualised with a plot of MA vs. IR (**Figure 1A**), with a full summary of clustering provided in the supplementary information (**Supplementary Table S2**). As expected, sulfated features tended to have a larger MA value (i.e., a sulfate-derived fragment is a major peak) and a larger IR value (i.e., sulfate-derived fragments make up a relatively large proportion of total product ions). The distributions of these ratios are visualised as violin plots (**Figures 1B,C**). They show that the IR of sulfated molecules were spread with a median IR of 42% (**Figure 1B**, mean = 46%, range = 4–97%) contrasted with the non-sulfated features with a median IR of 3% (mean = 5%, range = 0–40%). The median MA of 99%

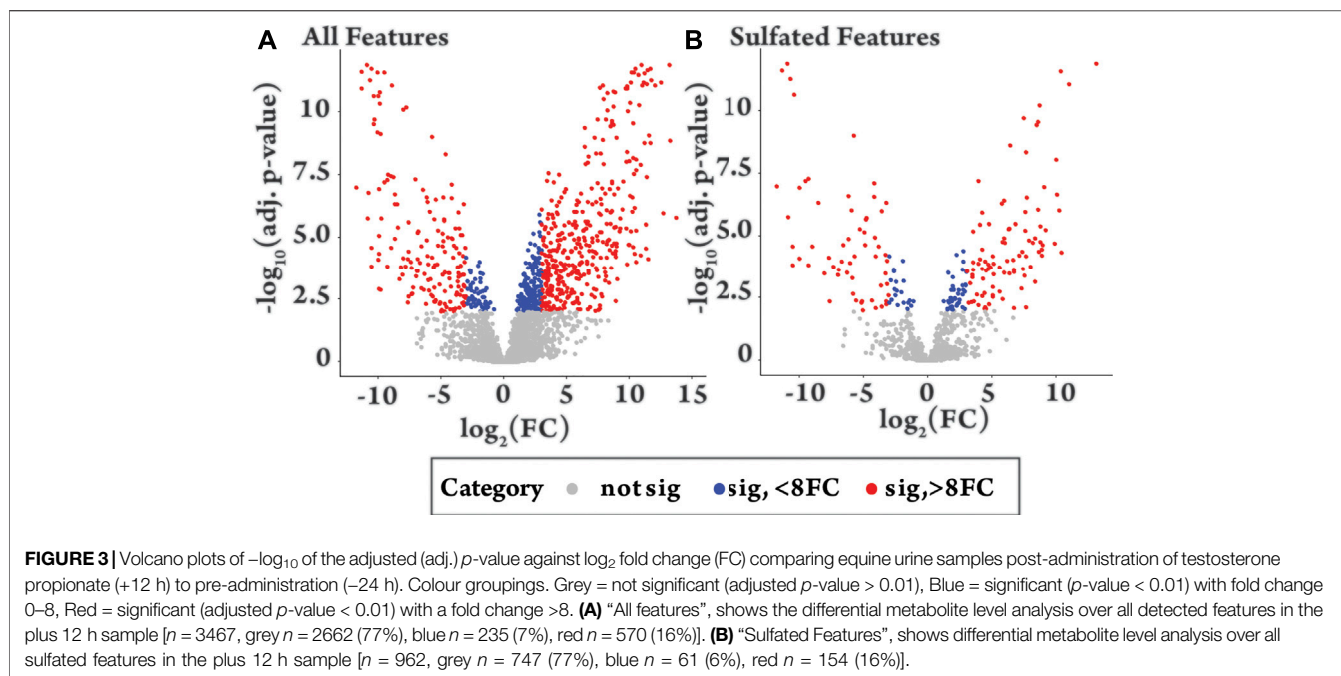


(Figure 1C, mean = 88%, range = 40–100%) also contrasted to the non-sulfated features with a median MA of 9% (mean = 5%, range = 0–63%). This clustering of sulfated and non-sulfated features was later used to prioritizise sulfated metabolites for further investigation.

Speciation of Sulfates

The putative sulfated metabolites can be differentiated further based on the observed major sulfate-derived transition (Table 1). In the equine urine samples (total sulfates, $n = 962$), the dominant sulfate-derived transition was the $^{\bullet}\text{SO}_3^-$ ion (m/z 80, $n = 493$, 51%), with the HSO_4^- ion (m/z 97, $n = 194$, 20%), and the neutral loss of SO_3 (80 Da, $n = 209$, 22%) also prominent. Other sulfate-derived fragments including the HSO_3^- (m/z 81, $n = 49$, 5%), $^{\bullet}\text{SO}_4^-$ (m/z 96, $n = 8$, 1%) ions, and H_2SO_4 neutral loss (98 Da, $n = 9$, 1%) were observed at a lower frequency (Figure 2). The sulfate-derived ions $^{\bullet}\text{SO}_3^-$, HSO_3^- and neutral loss SO_3 are typically associated with phenolic and other unsaturated sulfate metabolites, while the ion HSO_4^- is associated with saturated sulfates (McLeod et al., 2017). The majority of sulfate metabolites (78%) showed two or more sulfate derived fragments on applying a relative abundance threshold of 5% (data not shown).

High Throughput Differential Metabolite Level Analysis

To identify features that change significantly following drug administration, a high throughput differential analysis, commonly used to assess gene expression, was applied using the packages *Limma* and *Glimma* in R, from Bioconductor (Supplementary Section S7) (Ritchie et al., 2015; Su et al., 2017; Team, 2017). The results of the analysis comparing the pre- (–24 h) and post drug-administration samples (+12 h) are

shown as volcano plots for all features (Figure 3A) and sulfated features (Figure 3B), with the results summarized in Supplementary Table S3. Similar patterns were observed for all features and sulfated features in terms of significant change (red and blue, Figure 3) and positive and negative fold change. Of the 962 sulfated features, 215 had significantly changed (adjusted p -value < 0.01) (red and blue, Figure 3B) representing 6% of the total detected features in equine urine after doping. Of these, a larger proportion were upregulated, specifically 136 were upregulated and 79 were downregulated, as indicated by the direction of their fold change. The analysis also showed relatively large inter-horse variation in detected features, which is likely due to individual differences in metabolism between the two horses (Supplementary Figure S8). Comparisons also revealed limited intra-horse variation over time (horse 2, Supplementary Figure S9), but a relatively large intra-horse variation pre- and post-drug administration (Supplementary Figure S8), a pattern of change that could be indicative of increased metabolic activity following administration of the AAS testosterone propionate.

Discovery of a Novel Steroid Sulfate Metabolite in Equine Urine

The 215 LC/MS features found to display significant changes in relative signal intensity following testosterone propionate administration could represent direct metabolites of testosterone propionate or other metabolites modulated indirectly in response to testosterone propionate administration. However, this study specifically sought to identify sulfated metabolites derived from the direct metabolism of testosterone propionate. A list of possible

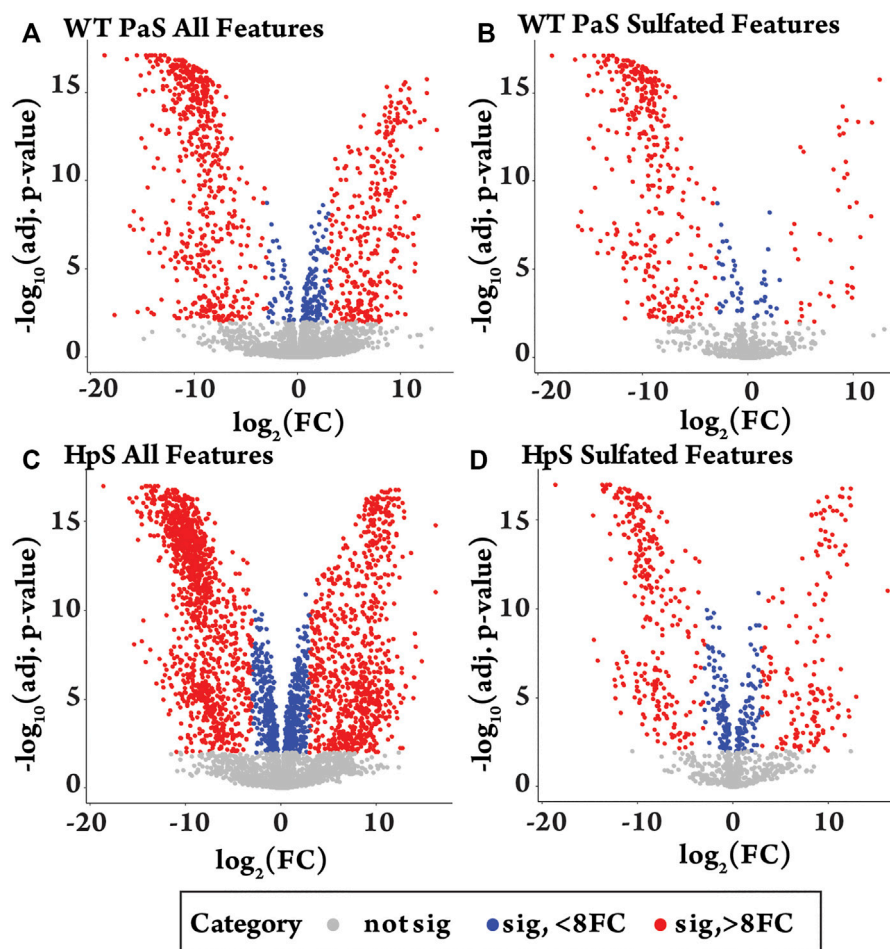
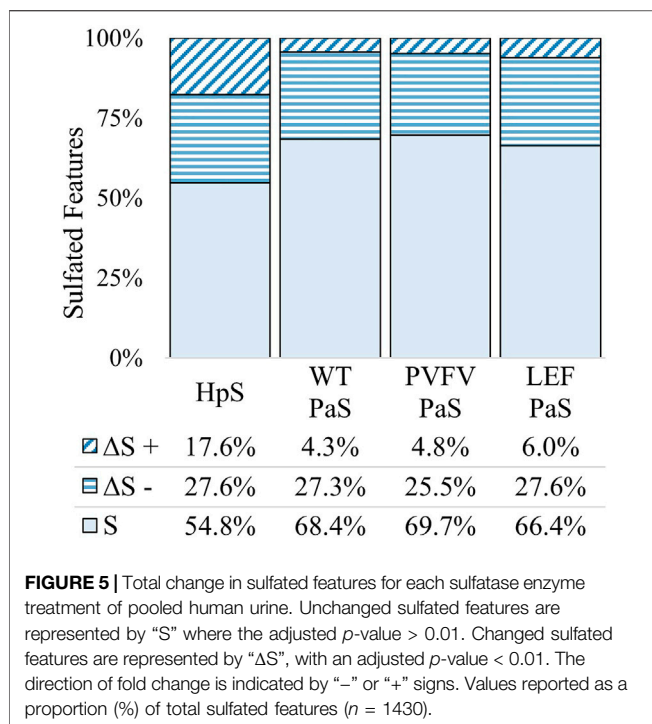


FIGURE 4 | Differential metabolite level analysis for enzyme hydrolysis of pooled human urine. **(A)** All detected features ($n = 5774$) in the WT-PaS treated urine relative to a control sample. **(B)** Sulfate features ($n = 1430$) in WT-PaS treated sample. **(C)** All detected features ($n = 5774$) in the HpS treated urine relative to a control sample. **(D)** Sulfate features ($n = 1430$) in HpS treated sample.

metabolites was generated by applying combinations of up to three phase I metabolic transformations, including hydroxylation, bond oxidation and reduction to testosterone, followed by sulfation (**Supplementary Table S4**). Steroid sulfates in the 215 molecules matching the accurate mass ($m/z \pm 5$ ppm) against the generated list of predicted metabolites were identified, using R. Where possible these putative metabolites were confirmed against synthetically derived reference materials by comparison of UHPLC retention time and MS/MS behaviour (Aru et al., 2020).

From this search 30 possible steroid sulfates were identified with theoretical accurate mass matching proposed metabolic transformations (**Supplementary Table S4**). Of these molecules, 10 were found to be elevated in the range of 16–1024-fold after testosterone propionate administration (+24 h) and by comparison to the control (horse 2), **Supplementary Table S5**. The identities of testosterone sulfate (1) (m/z 367.1583), epiandrosterone sulfate (2) (m/z 369.1739), and 5 α -androstane-3 β ,17 α -diol 3-sulfate (3) (m/z 371.1895) were

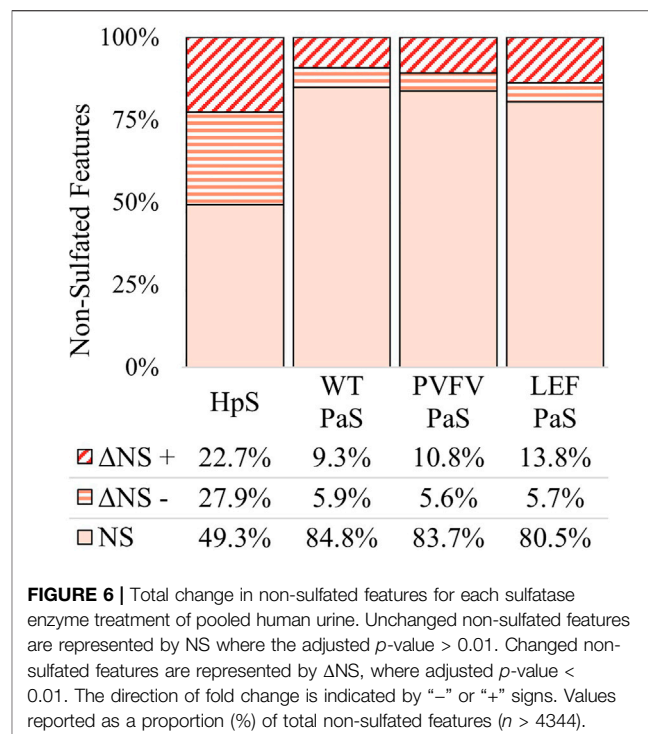
established after comparison to synthesised reference materials (**Table 2**, for synthesis of reference materials see **Supplementary Section S4**). Confirmation was performed according to criteria set out by the Association of Official Racing Chemists (AORC) for UHPLC retention times and MS/MS transitions (**Supplementary Table S6**) (Association of Official Racing Chemist, 2020). Scan MS data showed the expected isotope signatures. Of the three confirmed structures, the first two are known biomarkers of testosterone metabolism in equine and human systems (Piper et al., 2017; Esquivel et al., 2019). The final metabolite 5 α -androstane-3 β ,17 α -diol 3-sulfate (3) has not been described in literature or in online data bases such as ChEBI (Hastings et al., 2016). The upregulated nature of these steroid sulfates also support the general idea of perturbation caused by doping with testosterone propionate (Pozo et al., 2010; Scarth et al., 2011; Vimercati et al., 2017). Future directions for this work could aim at identifying the remaining seven putative steroid sulfate metabolites against reference materials. Longitudinal or population studies would also be required to assess the



importance of these markers in doping with testosterone propionate.

Application 2: Profiling in Sulfatase Treated Human Urine

Hydrolysis is frequently used prior to the analysis of conjugated steroids. In GC-MS analysis, sulfate conjugates are typically hydrolysed to the free steroid and derivatised in analytical workflows, to improve thermal stability and volatility. Hydrolysis is also commonly used in both GC-MS and LC-MS approaches to aid confirmation of metabolites against the more readily available unconjugated steroid reference materials. For sulfated conjugates, hydrolysis is often performed using the commercially available *Helix pomatia* aryl sulfatase (HpS). However, without extensive purification (Ballet et al., 2018), these crude enzyme preparations are known to contain additional enzyme activities such as glucuronidase, oxidase, and reductase, making it unsuitable for many applications (Gomes et al., 2009). Alternatively, chemical solvolysis can be used as a means of deconjugation, however, this can lead to analyte degradation and increased matrix interference (Gomes et al., 2009). Recently, a new recombinantly expressed and purified arylsulfatase from *Pseudomonas aeruginosa* has been investigated for the selective hydrolysis of sulfatase esters (Stevenson et al., 2015). Directed evolution was employed to improve the catalytic efficiency of testosterone sulfate hydrolysis, with improvements in substrate scope and thermostability relative to the wild-type (WT-PaS) enzyme also observed (Uduwela et al., 2018). This application sought to compare the performance of a commercially available HpS preparation to

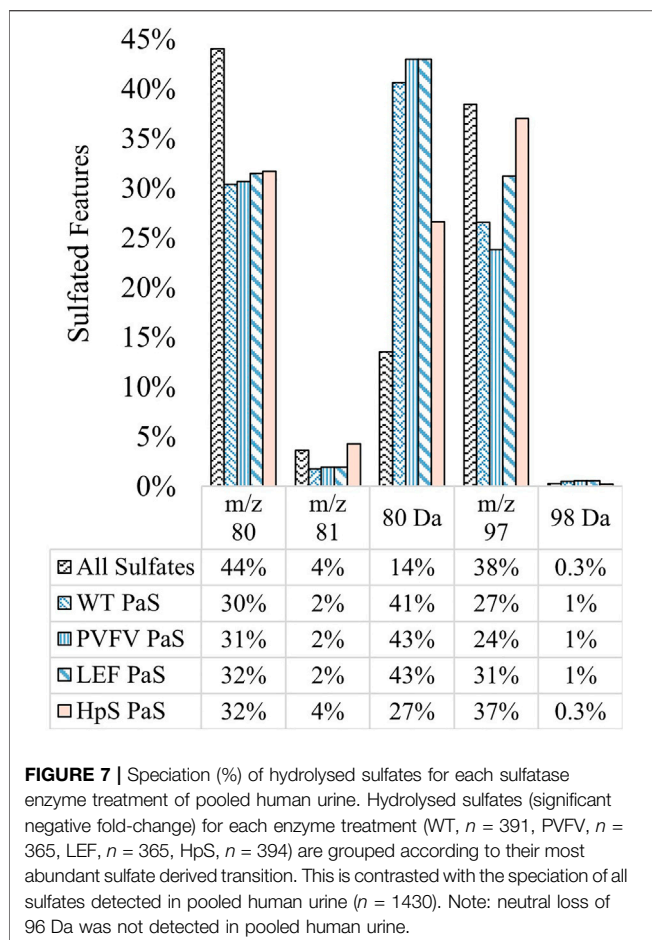


three PaS preparations for hydrolysis of urinary sulfates. Two improved mutants PVFV-PaS and LEF-PaS along with WT-PaS were selected for this evaluation, representing different points along the evolutionary pathway (Uduwela et al., 2018).

Profiling the Hydrolytic Activity of Sulfatases in Pooled Human Urine

The workflow described above was used to assess the change in the sulfate metabolome in pooled human urine after incubation with each enzyme preparation. For the hydrolysis study, aliquots of pooled human urine from six healthy people (three females and three males ranging between 20–50 years old) were treated with each enzyme preparation or a control in triplicate and incubated overnight. Enzyme activity was normalized for the hydrolysis of the common p -nitrophenyl sulfate prior to the experiment using recommended pH ranges (Supplementary Table S7) (Stevenson et al., 2015). Following this, samples were extracted and then subjected to the described workflow.

Implementing the analytical workflow resulted in 5,774 features with associated MS/MS data from an initial 15,608 detected features in the pooled human urine. The PCA analysis showed tight grouping of all PaS enzyme mutants, distinct from the control, HpS and pooled QC samples (Supplementary Figure S2) (Broadhurst et al., 2018). k -means clustering resulted in a total of 1,430 putative sulfates (25%) being identified from the 5,774 features (Supplementary Figure S5). In this, sulfate-derived fragment speciation was dominated by the ions m/z 80 ($n = 630$, 44%) and m/z 97 ($n = 550$, 38%), with other minor species also observed including neutral loss 80 Da ($n = 194$, 14%), m/z 81 ($n = 52$, 4%), neutral loss 98 Da ($n = 4$, 0.3%) and m/z 96 ($n = 8$, 1%)



(Supplementary Figure S6). In contrast to the equine urine samples this showed (Supplementary Figure S10) a higher proportion of saturated sulfates (m/z 97) than unsaturated sulfates (m/z 80, m/z 81 and 80 Da). The majority of sulfate metabolites (64%) showed two or more sulfate derived fragments on applying a relative abundance threshold of 5% (data not shown).

The differential metabolite level analysis revealed that of the four enzyme treatments, the crude HpS preparation had distinct activity from the three PaS treatments (Figures 4–6). HpS possessed the largest number of significantly changed molecules in both the non-sulfated and sulfated fraction of the urinary metabolome. In the sulfated fraction (Figure 5), HpS had a total of 45% (646/1,430) of total sulfates significantly changed, which contrasts with the three PaS treatments displaying changes ranging from 30 to 34% (WT, 452/1430, PVFV, 433/1430, LEF, 481/1430). In the non-sulfated fraction (Figure 6), HpS resulted in 50.6% (2,202/4344) of molecules undergoing significant change compared to the PaS treatments, 15–20% (WT, 662/4344, PVFV, 710/4344, LEF, 848/4344).

In terms of enzyme hydrolysis, both HpS and the PaS enzymes showed a similar proportion (25.5–27.6%, Figure 5) of the sulfated features with a significant negative fold change, consistent with sulfatase enzyme hydrolysis. However, in the



case of HpS treatment, this was accompanied by a greater proportion of sulfated features with a positive fold change (Figure 5) as well as a greater proportion of non-sulfated features undergoing both positive and negative fold change (Figure 6), which was inconsistent with simple sulfate ester hydrolysis and suggested significant levels of alternative enzyme activity. For the PaS enzyme treatments 82–87% (WT, 391/452, PVFV, 365/433, LEF, 365/481) of significantly changed sulfated features underwent a negative fold change consistent with enzyme hydrolysis compared to only 63% (394/646) for HpS treated samples (Figure 6 and Supplementary Table S3). Taken together, these observations show similar levels of sulfate hydrolysis for the four enzyme treatments but also clearly show higher selectivity for sulfate hydrolysis by the recombinantly expressed and purified PaS enzymes relative to the HpS crude enzyme preparation.

The substrate scope for each sulfatase treatment was assessed by comparing the sulfate-derived fragment speciation for hydrolysed sulfates. **Figure 7** shows the fragment speciation for all hydrolysed sulfates in comparison to the speciation of all detected sulfates ($n = 1,430$) in pooled human urine. Both enzyme classes displayed a preference for hydrolysis of sulfates, 27–43%, characterised by the neutral loss of SO_3 (80 Da), when compared to the total proportion of sulfate species 14%. This may indicate a preference for the hydrolysis of electron deficient unsaturated sulfate esters, such as phenolic sulfates, through a process of bond homolysis (to give $^{\bullet}\text{SO}_3^-$) followed by electron transfer to give SO_3 and the corresponding oxy-anion fragment. There were also distinct differences between the two classes of enzyme treatments. Specifically, the PaS treatments hydrolysed a smaller proportion of saturated sulfates compared to the HpS treatment, as indicated by the proportion of the m/z 97 ion. Within the PaS enzyme classes, there was also a small observed increase in the hydrolysis of saturated sulfates (m/z 97) from the WT-PaS to the LEF-PaS mutant. This trend aligned with the aims of the previous directed evolution study, which sought to improve the catalytic efficiency of the PaS enzyme for the hydrolysis of the saturated alkyl sulfate ester testosterone sulfate (Uduwela et al., 2018).

Evidence for Glucuronidase Activity in Crude HpS Extract

The results clearly show the HpS enzyme had lower selectivity for the hydrolysis of sulfated metabolites, as a large proportion, 55% (1,214/2,202), of non-sulfated metabolites underwent significant change, **Figure 6**. A large part of this non-specific activity is attributable to the crude nature of the HpS extract that contains a range of enzyme activities including glucuronidase, oxidase and reductase activities (Stevenson et al., 2015; Ballet et al., 2018; Uduwela et al., 2018).

To investigate the possible glucuronidase activity of the crude HpS extract, a semi-targeted search was adapted in a retrospective fashion on the data acquired for application 2. The search was performed against a list of putative steroid glucuronides either derived from known steroids or from metabolic transformations of testosterone glucuronide, in a similar approach to that adopted in application 1 (**Supplementary Table S8**). Each of the 1,214 significantly changed non-sulfated features was matched in MS and MS/MS using accurate mass (± 5 ppm) and assigned as glucuronides by matching to characteristic MS/MS transitions (Fabregat et al., 2013). These transitions included neutral loss of 194 Da (loss of glucuronic acid) and 176 Da [loss of glucuronic acid- H_2O (gluc)], and the fragment ions m/z 175 [(gluc-H) $^+$], m/z 157 [(gluc-H- H_2O) $^+$], m/z 113 [(gluc-H- H_2O - CO_2) $^+$], m/z 85 [(gluc-H- H_2O - CO_2 -CO) $^+$] and m/z 75 [(HOCH $_2$ CO $_2$) $^+$]. Unlike, Fabregat et al. (2013), matching was done at high resolution, allowing for accurate masses to be used in both MS and MS/MS dimensions (**Supplementary Table S9**).

From this search 96/1,214 molecules were identified as putative steroid glucuronides and had at least two characteristic MS/MS transitions. Of these, 90/96 underwent

significant hydrolysis in the HpS treated sample, while none of these 96 molecules underwent hydrolysis in the PaS treatments (**Supplementary Tables S8, S10**). The hydrolysis of glucuronide metabolites by HpS enzyme was not unexpected, with the product information sheet indicating at least 30 units of β -glucuronidase for every unit of sulfatase activity. Due to this, it has routinely been used in drug metabolism studies in both medical and anti-doping fields due to this broad substrate scope (Houghton and Maynard, 2010; Garg et al., 2018). A four-step purification of the crude HpS extract to generate higher selectivity for sulfate ester hydrolysis has recently been described, and the resulting preparation used to screen for unsaturated sulfate esters in human urine (Ballet et al., 2018). However, this purified HpS preparation is not commercially available. The PaS variants evaluated in this study show high levels of selectivity as expected for recombinantly expressed and purified enzymes and provide a convenient alternative for the study of the sulfated metabolome.

Substrate Selectivity of PaS

To demonstrate the selectivity of the PaS enzymes a targeted GC-MS analysis of free steroids was performed in treated urine (**Figure 8, Supplementary Table S11**). In this experiment we measured the concentrations of 33 free steroids in pooled human urine after treatment with either the PaS enzymes or with *Escherichia coli* (*E.coli*) β -glucuronidase (**Supplementary Section S3**). This β -glucuronidase was specifically chosen as that mandated for glucuronide deconjugation by the steroid module of the World Anti-Doping Agency athlete biological passport (World Anti-Doping Agency WADA, 2017). The concentration of 14 of these free steroids significantly increased after treatment with the PaS enzymes indicating some level of sulfate conjugation. This included testosterone sulfate that showed expected improvements in hydrolysis in moving from WT-PaS to PVFV-PaS and LEF-PaS mutants. Also, for these 14, the concentration of eight steroids, clustered in blue (**Figure 8**), showed a greater increase in concentration following PaS hydrolysis than observed for *E. coli* β -glucuronidase suggesting higher levels of sulfate conjugation. High levels of sulfate conjugation have also recently been reported for a range of circulating vitamin D metabolites (Jenkinson et al., 2021). These results were also compared against those from the metabolic profiling. Using an accurate mass search ($m/z \pm 5$ ppm) potential matches were found to each of these eight steroid sulfates in the UHPLC-HRMS/MS data set (**Supplementary Table S12**). Although the majority of these remain unconfirmed, epiandrosterone sulfate, was matched against an isotope labelled internal standard [epiandrosterone ($^{18}\text{O}_3$)-sulfate (**S3**)] used in the initial metabolic profiling. Epiandrosterone sulfate was found to undergo full hydrolysis for each enzyme treatment (**Supplementary Table S13**).

In this application we have demonstrated the selectivity of the PaS enzymes towards sulfated metabolites when compared to the commercially available crude HpS extract. As recombinantly expressed and purified enzymes, PaS is recommended as a preferred enzyme for studies of the sulfated metabolome. Overall, the results of this study demonstrate the usefulness of

untargeted metabolic profiling methods to monitor minute differences in the sulfate metabolome in urine. Its strength lies in the deconvolution of sulfated from non-sulfated metabolites by monitoring sulfate-derived fragment ions.

CONCLUSION

There are several clear pathways forward for this type of untargeted metabolic profiling. Due to its simplicity and relative ease of use it could be employed as a screen to look for new metabolites in applications such as in disease diagnosis or anti-doping. It is also conceivable that similar filters and scripts could be applied to related urinary metabolites such as glucuronides and phosphates, and dianionic metabolites (McLeod et al., 2017). Limitations of this approach lie with the acquisition speeds of the MS instrumentation and the DDA method. The DDA method suffers from only sampling higher abundance ions per duty cycle, which can lead to missed detection or the misassignment of a molecule.

Overall, we have presented a novel workflow for the untargeted profiling of sulfated metabolites in urine matrices that combines UHPLC-HRMS/MS instrumentation and a new data processing pipeline. This provided a rapid tool for the qualitative assessment of the sulfate metabolome in equine and human urine. In equine urine 215 of 962 putative sulfate metabolites were found to significantly change after testosterone propionate administration in a single horse. Of these, 10 upregulated features were predicted to be steroid sulfate metabolites based on accurate mass searches. The identity of three steroid sulfates were confirmed as testosterone sulfate (1), epiandrosterone sulfate (2), and a new metabolite, 5 α -androstane-3 β -17 α -diol-3-sulfate (3), according to AORC retention time and MS/MS criteria (Association of Official Racing Chemist, 2020). The profiling method was also used to examine sulfatase activity in pooled human urine. The new workflow identified 1,430 putative sulfated metabolite features in pooled urine from a total of 5,774 features. Qualitatively, it was observed that the three PaS enzymes selectively hydrolysed sulfate esters and may be preferred in applications targeting the sulfate metabolome. Alternative β -glucuronidase activity associated with the HpS enzyme was also demonstrated. The use of our profiling-based approach could be of value in the identification and monitoring of endogenous and exogenous sulfated metabolites in urine.

REFERENCES

- Antignac, J. P., Brosseau, A., Gaudin-Hirret, I., André, F., and Bizet, B. Le. (2005). Analytical Strategies for the Direct Mass Spectrometric Analysis of Steroid and Corticosteroid Phase II Metabolites. *Steroids* 70, 205–216. doi:10.1016/j.steroids.2004.11.009
- Aru, V., Motawie, M. S., Khakimov, B., Sørensen, K. M., Møller, B. L., and Engelsen, S. B. (2020). First-principles Identification of C-Methyl-Scyllo-Inositol

DATA AVAILABILITY STATEMENT

The datasets presented in this study can be found in online repositories. The names of the repository/repositories and accession number(s) can be found in the article/Supplementary Material.

ETHICS STATEMENT

The studies involving human participants were reviewed and approved by the ANU Human Research Ethics Committee. The patients/participants provided their written informed consent to participate in this study. The animal study was reviewed and approved by the Charles Sturt University (Wagga Wagga, NSW, Australia) Animal Care and Ethics Committee and the Racing NSW Animal Care and Ethics Committee.

AUTHOR CONTRIBUTIONS

CF: Conceptualization, Methodology, Script, Validation, and Writing—Original Draft. RH: Conceptualization and Methodology. DU: Conceptualization and Methodology. BP: Methodology. AC: Conceptualization and Script. TN: Methodology and Script. AC: Conceptualization and Funding. LB: Conceptualization and Methodology. MM: Conceptualization, Methodology, Funding, and Writing—Supervision, review and editing CF

FUNDING

We thank Thermo Fischer Scientific for supporting the Charles Hocart Award to DU and the Australian Research Council Linkage Project scheme (LP180100421) for financial support.

ACKNOWLEDGMENTS

Bradley Stevenson for guidance of PaS synthesis and related assays. Alex Chen for initial methodological development of UHPLC and HRMS/MS systems.

SUPPLEMENTARY MATERIAL

The Supplementary Material for this article can be found online at: <https://www.frontiersin.org/articles/10.3389/fmolb.2022.829511/full#supplementary-material>

(Mytilitol) - A New Species-specific Metabolite Indicator of Geographic Origin for marine Bivalve Molluscs (Mytilus and Ruditapes spp.). *Food Chem.* 328, 126959. doi:10.1016/j.foodchem.2020.126959

Association of Official Racing Chemist (2020). AORC MS Criteria. Association of Official Racing Chemists. Available at: <http://www.aorc-online.org/documents/aorc-ms-criteria-modified-23-aug-16/>.

Attygalle, A. B., García-Rubio, S., Ta, J., and Meinwald, J. (2001). Collisionally-induced Dissociation Mass Spectra of Organic Sulfate Anions. *J. Chem. Soc. Perkin Trans. 2* 24, 498–506. doi:10.1039/b009019k

- Balcells, G., Gómez, C., Garrosta, L., Pozo, O. J., and Ventura, R. (2017). Sulfate Metabolites as Alternative Markers for the Detection of 4-chlorometandienone Misuse in Doping Control. *Drug Test. Anal.* 9 (7), 983–993. doi:10.1002/dta.2101
- Balcells, G., Matabosch, X., and Ventura, R. (2017). Detection of Stanozolol O- and N- Sulfate Metabolites and Their Evaluation as Additional Markers in Doping Control. *Drug Test. Anal.* 9 (7), 1001–1010. doi:10.1002/dta.2107
- Ballet, C., Correia, M. S. P., Conway, L. P., Locher, T. L., Lehmann, L. C., Garg, N., et al. (2018). New Enzymatic and Mass Spectrometric Methodology for the Selective Investigation of Gut Microbiota-Derived Metabolites. *Chem. Sci.* 9 (29), 6233–6239. doi:10.1039/c8sc01502c
- Bean, K. a., and Henion, J. D. (1997). *J. Chromatogr. B* 690 (1–2), 65–75. doi:10.1016/s0378-4347(96)00403-3
- Bowers, L. D., and Sanaullah, fnm. (1996). Direct Measurement of Steroid Sulfate and Glucuronide Conjugates with High-Performance Liquid Chromatography-Mass Spectrometry. *J. Chromatogr. B: Biomed. Sci. Appl.* 687 (1), 61–68. doi:10.1016/s0378-4347(96)00232-0
- Broadhurst, D., Goodacre, R., Reinke, S. N., Kuligowski, J., Wilson, I. D., Lewis, M. R., et al. (2018). Guidelines and Considerations for the Use of System Suitability and Quality Control Samples in Mass Spectrometry Assays Applied in Untargeted Clinical Metabolomic Studies. *Metabolomics* 14 (6), 72. doi:10.1007/s11306-018-1367-3
- Hastings, J., Owen, G., Dekker, A., Ennis, M., Kale, N., Muthukrishnan, V., et al. (2016). ChEBI in 2016: Improved Services and an Expanding Collection of Metabolites. *Nucleic Acids Research* 44 (Database issue), D1214–D1219. doi:10.1093/nar/gkv1031
- Considine, E. C., Thomas, G., Boulesteix, A. L., Khashan, A. S., and Kenny, L. C. (2018). *Metabolomics* 14 (1). doi:10.1007/s11306-017-1299-3
- Dudzick, D., Barbas-Bernardos, C., García, A., and Barbas, C. (2018). Quality Assurance Procedures for Mass Spectrometry Untargeted Metabolomics. A Review. *J. Pharm. Biomed. Anal.* 147, 149–173. doi:10.1016/j.jpba.2017.07.044
- Esquivel, A., Alechaga, E., Monfort, N., and Ventura, R. (2018). *Drug Test. Anal.* 10 (11–12), 1734–1743. doi:10.1002/dta.2413
- Esquivel, A., Alechaga, E., Monfort, N., and Ventura, R. (2019). Sulfate Metabolites Improve Retrospectively after Oral Testosterone Administration. *Drug Test. Anal.* 11 (3), 392–402. doi:10.1002/dta.2529
- Fabregat, A., Pozo, O. J., Marcos, J., Segura, J., and Ventura, R. (2013). Use of LC-MS/MS for the Open Detection of Steroid Metabolites Conjugated with Glucuronic Acid. *Anal. Chem.* 85 (10), 5005–5014. doi:10.1021/ac4001749
- Farrell, T., Poquet, L., Dionisi, F., Barron, D., and Williamson, G. (2011). Characterization of Hydroxycinnamic Acid Glucuronide and Sulfate Conjugates by HPLC-DAD-MS2: Enhancing Chromatographic Quantification and Application in Caco-2 Cell Metabolism. *J. Pharm. Biomed. Anal.* 55 (5), 1245–1254. doi:10.1016/j.jpba.2011.03.023
- Fiehn, O., Kopka, J., Dörmann, P., Altmann, T., Trethewey, R. N., and Willmitzer, L. (2000). Metabolite Profiling for Plant Functional Genomics. *Nat. Biotechnol.* 18 (11), 1157–1161. doi:10.1038/81137
- Foster, P. A., and Mueller, J. W. (2018). SULFATION PATHWAYS: Insights into Steroid Sulfation and Desulfation Pathways. *J. Mol. Endocrinol.* 61 (2), T271–T283. doi:10.1530/jme-18-0086
- Garg, N., Hansson, A., Knych, H. K., Thevis, M., Hedeland, U., Globisch, D., et al. (2018). Structural Elucidation of Major Selective Androgen Receptor Modulator (SARM) Metabolites for Doping Control. *Org. Biomol. Chem.* 16 (5), 698–702. doi:10.1039/c7ob03030d
- Ginestet, C. (2011). ggplot2: Elegant Graphics for Data Analysis. *Stat. Soc. Ser. A. (Statistics Soc.)* 174 (1), 245–246. doi:10.1111/j.1467-985x.2010.00676.9.x
- Godzien, J., Alonso-Herranz, V., Barbas, C., Armitage, E. G., and Armitage, G. (2015). Controlling the Quality of Metabolomics Data: New Strategies to Get the Best Out of the QC Sample. *Metabolomics* 11, 518–528. doi:10.1007/s11306-014-0712-4
- Gomes, R. L., Meredith, W., Snape, C. E., and Sephton, M. A. (2009). Analysis of Conjugated Steroid Androgens: Deconjugation, Derivatisation and Associated Issues. *J. Pharm. Biomed. Anal.* 49, 1133–1140. doi:10.1016/j.jpba.2009.01.027
- Gómez, C., Pozo, O. J., Geyer, H., Marcos, J., Thevis, M., Schänzer, W., et al. (2012). Steroid Biochem. Mol. Biol. 132 (3–5), 239–246. doi:10.1016/j.jsbmb.2012.05.010
- Gómez, C., Pozo, O. J., Marcos, J., Segura, J., and Ventura, R. (2013). Alternative Long-Term Markers for the Detection of Methyltestosterone Misuse. *Steroids* 78 (1), 44–52. doi:10.1016/j.steroids.2012.10.008
- Günal, S., Hardman, R., Kopriva, S., and Mueller, J. W. (2019). Sulfation Pathways from Red to green. *J. Biol. Chem.* 294 (33), 12293–12312. doi:10.1074/jbc.rev119.007422
- Hartigan, J. A., and Wong, M. A. (1979). Algorithm AS 136: A K-Means Clustering Algorithm. *Appl. Stat.* 28 (1), 100. doi:10.2307/2346830
- Hintikka, L., Kuuranne, T., Leinonen, A., Thevis, M., Schänzer, W., Halket, J., et al. (2008). Liquid Chromatographic-Mass Spectrometric Analysis of Glucuronide-conjugated Anabolic Steroid Metabolites: Method Validation and Interlaboratory Comparison. *J. Mass. Spectrom.* 43 (7), 965–973. doi:10.1002/jms.1434
- Houghton, E., and Maynard, S. (2010). Some Aspects of Doping and Medication Control in Equine Sports. *Handb. Exp. Pharmacol.* 195, 369–409. doi:10.1007/978-3-540-79088-4_17
- Jenkinson, C., Desai, R., McLeod, M. D., Mueller, J. W., Hewison, M., and Handelsman, D. J. (2021). Circulating Conjugated and Unconjugated Vitamin D Metabolite Measurements by Liquid Chromatography Mass Spectrometry. *J. Clin. Endocrinol. Metab.* 107 (2), 435–449. doi:10.1210/clinem/dgab708
- Kaufman, L., and Rousseeu, P. (2009). *Finding Groups in Data: An Introduction to Cluster Analysis*, Vol. 344. John Wiley & Sons.
- Kioui, P., Fraggaki, A. G., Kioukia-Fougia, N., and Angelis, Y. S. (2021). Liquid Chromatography-Mass Spectrometry Behavior of Girard's Reagent T Derivatives of Oxosteroid Intact Phase II Metabolites for Doping Control Purposes. *Drug Test. Anal.* 13, 1822–1834. doi:10.1002/dta.3056
- Lafaye, A., Junot, C., Ramounet-Le Gall, B., Fritsch, P., Ezan, E., and Tabet, J.-C. (2004). Profiling of Sulfoconjugates in Urine by Using Precursor Ion and Neutral Loss Scans in Tandem Mass Spectrometry. Application to the Investigation of Heavy Metal Toxicity in Rats. *J. Mass. Spectrom.* 39 (6), 655–664. doi:10.1002/jms.635
- McLeod, M. D., Waller, C. C., Esquivel, A., Balcells, G., Ventura, R., Segura, J., et al. (2017). Constant Ion Loss Method for the Untargeted Detection of Bis-Sulfate Metabolites. *Anal. Chem.* 89 (3), 1602–1609. doi:10.1021/acs.analchem.6b03671
- Mueller, J. W., Vogg, N., Lightning, T. A., Weigand, I., Ronchi, C. L., Foster, P. A., et al. (2021). Steroid Sulfation in Adrenal Tumors. *J. Clin. Endocrinol. Metab.* 106 (12), 3385–3397. doi:10.1210/clinem/dgab18
- Piper, T., Putz, M., Schänzer, W., Pop, V., McLeod, M. D., Uduwela, D. R., et al. (2017). *Drug Test. Anal.* 9 (11–12), 1695–1703. doi:10.1002/dta.2291
- Piper, T., Schänzer, W., and Thevis, M. (2016). Revisiting the Metabolism of 19-nortestosterone Using Isotope Ratio and High Resolution/high Accuracy Mass Spectrometry. *J. Steroid Biochem. Mol. Biol.* 162, 80–91. doi:10.1016/j.jsbmb.2015.12.013
- Pozo, O. J., Marcos, J., Khymenets, O., Pranata, A., Fitzgerald, C. C., McLeod, M. D., et al. (2018). *J. Mol. Endocrinol.* 61 (2). doi:10.1530/jme-17-0286
- Pozo, O. J., Marcos, J., Ventura, R., Fabregat, A., and Segura, J. (2010). Testosterone Metabolism Revisited: Discovery of New Metabolites. *Anal. Bioanal. Chem.* 398 (4), 1759–1770. doi:10.1007/s00216-010-4082-0
- Pranata, A., Fitzgerald, C. C., Khymenets, O., Westley, E., Anderson, N. J., Ma, P., et al. (2019). *Steroids*, 143.
- Ritchie, M. E., Phipson, B., Wu, D., Hu, Y., Law, C. W., Shi, W., et al. (2015). Limma powers Differential Expression Analyses for RNA-Sequencing and Microarray Studies. *Nucleic Acids Res.* 43 (7), e47. doi:10.1093/nar/gkv007
- Sangster, T., Major, H., Plumb, R., Wilson, A. J., and Wilson, I. D. (2006). A Pragmatic and Readily Implemented Quality Control Strategy for HPLC-MS and GC-MS-based Metabonomic Analysis. *Analyst* 131 (10), 1075. doi:10.1039/b604498k
- Scarh, J. P., Teale, P., and Kuuranne, T. (2011). Drug Metabolism in the Horse: a Review. *Drug Test. Anal.* 3 (1), 19–53. doi:10.1002/dta.174
- Schänzer, W., Guddat, S., Thomas, A., Opfermann, G., Geyer, H., and Thevis, M. (2013). *Drug Test. Anal.* 5 (11–12), 810–818. doi:10.1002/dta.1516
- Schänzer, W. (1996). Metabolism of Anabolic Androgenic Steroids. *Clin. Chem.* 42 (7), 1001–1020. doi:10.1093/clinchem/42.7.1001
- Schänzer, W., and Thevis, M. (2017). Human Sports Drug Testing by Mass Spectrometry. *Mass. Spec. Rev.* 36, 16–46. doi:10.1002/mas.21479
- Stevenson, B. J., Waller, C. C., Ma, P., Li, K., Cawley, A. T., Ollis, D. L., et al. (2015). Pseudomonas Aeruginosaarylsulfatase: A Purified Enzyme for the Mild Hydrolysis of Steroid Sulfates. *Drug Test. Anal.* 7 (10), 903–911. doi:10.1002/dta.1782
- Su, S., Law, C. W., Ah-Cann, C., Asselin-Labat, M.-L., Blewitt, M. E., and Ritchie, M. E. (2017). Glimma: Interactive Graphics for Gene Expression Analysis. *Bioinformatics* 33 (13), 2050–2052. doi:10.1093/bioinformatics/btx094
- Team, R. C. R. (2017). *Foundation for Statistical Computing*. Vienna, Austria.
- Thevis, M., Thomas, A., and Schänzer, W. (2011). Current Role of LC-MS(/MS) in Doping Control. *Anal. Bioanal. Chem.* 401 (2), 405–420. doi:10.1007/s00216-011-4859-9

- Tolstikov, V. V., and Fiehn, O. (2002). Analysis of Highly Polar Compounds of Plant Origin: Combination of Hydrophilic Interaction Chromatography and Electrospray Ion Trap Mass Spectrometry. *Anal. Biochem.* 301 (2), 298–307. doi:10.1006/abio.2001.5513
- Tsugawa, H., Cajka, T., Kind, T., Ma, Y., Higgins, B., Ikeda, K., et al. (2015). MS-DIAL: Data-independent MS/MS Deconvolution for Comprehensive Metabolome Analysis. *Nat. Methods* 12 (6), 523–526. doi:10.1038/nmeth.3393
- Uduwela, D. R., Pabis, A., Stevenson, B. J., Kamerlin, S. C. L., and McLeod, M. D. (2018). Enhancing the Steroid Sulfatase Activity of the Arylsulfatase from *Pseudomonas aeruginosa*. *ACS Catal.* 8 (9), 8902–8914. doi:10.1021/acscatal.8b02905
- Vimercati, S., Büchi, M., Zielinski, J., Peduto, N., and Mevissen, M. (2017). Testosterone Metabolism of Equine Single CYPs of the 3A Subfamily Compared to the Human CYP3A4. *Toxicol. Vitro* 41, 83–91. doi:10.1016/j.tiv.2017.02.017
- Waller, C. C., Cawley, A. T., Suann, C. J., Ma, P., and McLeod, M. D. (2016). *In Vivo* and *In Vitro* Metabolism of the Designer Anabolic Steroid Furazadrol in Thoroughbred Racehorses. *J. Pharm. Biomed. Anal.* 124, 198–206. doi:10.1016/j.jpba.2016.02.031
- Waller, C. C., and McLeod, M. D. (2014). A Simple Method for the Small Scale Synthesis and Solid-phase Extraction Purification of Steroid Sulfates. *Steroids* 92, 74–80. doi:10.1016/j.steroids.2014.09.006
- World Anti-Doping Agency Wada (2017). *Athlete Biological Passport Operating Guidelines*.
- Yao, Y., Wang, P., Shao, G., Del Toro, L. V. A., Codero, J., and Giese, R. W. (2016). Nontargeted Analysis of the Urine Nonpolar Sulfateome: a Pathway to the Nonpolar Xenobiotic Exposome. *Rapid Commun. Mass. Spectrom.* 30 (21), 2341–2350. doi:10.1002/rcm.7726
- Yi, L., Dratter, J., Wang, C., Tunge, J. A., and Desaire, H. (2006). Identification of Sulfation Sites of Metabolites and Prediction of the Compounds' Biological Effects. *Anal. Bioanal. Chem.* 386 (3), 666–674. doi:10.1007/s00216-006-0495-1

Conflict of Interest: The authors declare that the research was conducted in the absence of any commercial or financial relationships that could be construed as a potential conflict of interest.

Publisher's Note: All claims expressed in this article are solely those of the authors and do not necessarily represent those of their affiliated organizations, or those of the publisher, the editors and the reviewers. Any product that may be evaluated in this article, or claim that may be made by its manufacturer, is not guaranteed or endorsed by the publisher.

Copyright © 2022 Fitzgerald, Hedman, Uduwela, Paszerbovics, Carroll, Neeman, Cawley, Brooker and McLeod. This is an open-access article distributed under the terms of the Creative Commons Attribution License (CC BY). The use, distribution or reproduction in other forums is permitted, provided the original author(s) and the copyright owner(s) are credited and that the original publication in this journal is cited, in accordance with accepted academic practice. No use, distribution or reproduction is permitted which does not comply with these terms.



Human Sulfotransferase Assays With PAPS Production *in situ*

Yanan Sun^{1,2†}, Lukas Corbinian Harps^{1†}, Matthias Bureik^{2*} and Maria Kristina Parr^{1*}

¹Pharmaceutical and Medicinal Chemistry (Pharmaceutical Analyses), Institute of Pharmacy, Freie Universität Berlin, Berlin, Germany, ²School of Pharmaceutical Science and Technology, Health Sciences Platform, Tianjin University, Tianjin, China

OPEN ACCESS

Edited by:

Jon Wolf Mueller,
University of Birmingham,
United Kingdom

Reviewed by:

Yang Xie,
Brigham and Women's Hospital and
Harvard Medical School, United States
Christoph Müller,
Ludwig Maximilian University of
Munich, Germany

*Correspondence:

Matthias Bureik
matthias@tju.edu.cn
Maria Kristina Parr
maria.parr@fu-berlin.de

[†]These authors have contributed
equally to this work and share first
authorship

Specialty section:

This article was submitted to
Cellular Biochemistry,
a section of the journal
Frontiers in Molecular Biosciences

Received: 02 December 2021

Accepted: 24 January 2022

Published: 28 February 2022

Citation:

Sun Y, Harps LC, Bureik M and
Parr MK (2022) Human
Sulfotransferase Assays With PAPS
Production *in situ*.
Front. Mol. Biosci. 9:827638.
doi: 10.3389/fmolb.2022.827638

For *in vitro* investigations on human sulfotransferase (SULT) catalyzed phase II metabolism, the costly cofactor 3'-phosphoadenosine-5'-phosphosulfate (PAPS) is generally needed. In the present study, we developed and optimized a new approach that combines SULT-dependent biotransformation using recombinant and permeabilized fission yeast cells (enzyme bags) with PAPS production *in situ* applying quality by design principles. In the initial application of the procedure, yeast cells expressing human SULT1A3 were used for the production of 4'-hydroxypropranolol-4-O-sulfate from 4-hydroxypropranolol. The optimized protocol was then successfully transferred to other sulfonation reactions catalyzed by SULT2A1, SULT1E1, or SULT1B1. The concomitant degradation of some sulfoconjugates was investigated, and further optimization of the reaction conditions was performed in order to reduce product loss. Also, the production of stable isotope labelled sulfoconjugates was demonstrated utilizing isotopically labelled substrates or ³⁴S-sulfate. Overall, this new approach results in higher space-time yields while at the same time reducing experimental cost.

Keywords: fission yeast, *in vitro* metabolism, method optimization, PAPS, sulfonation, SULT, quality by design, isotopic labelling

INTRODUCTION

The study of metabolic pathways of drug substances in humans relies both on *in vivo* and *in vitro* experiments. After administration drugs are either directly excreted unchanged or metabolized first. The main specimen for excretion of most drugs and metabolites is urine. The parent drugs often show shorter detection windows due to extensive metabolism. Therefore, in toxicological, forensic or doping control analysis metabolites are often used as target analytes in urine samples (Balcels et al., 2017; Esquivel et al., 2019). Even though *in vivo* techniques are widely applied in anti-doping research, the high expenditure and unpredicted toxicological effect of many prohibited drugs are considerable drawbacks. In the last two decades, modern *in vitro* techniques became a viable alternative and furthermore a great extension to *in vivo* studies (Ekins et al., 2000). Moreover, they allow for precise reaction phenotyping. In *in vitro* studies, tissues or fractions of tissues like liver microsomes or homogenized liver fractions are commonly applied. In recent years, biosynthesis of sulfoconjugates using genetically modified microorganisms has been developed as well (Taskinen et al., 2003; Nishikawa et al., 2018). Metabolism of drug substances occurs in the complementary phases I and II. While enzymes of phase I metabolism transform parent compounds by hydroxylation, oxidation, or reduction, phase II metabolism consists of the attachment of small moieties to the target molecules, thus allowing them to be excreted from the body rapidly and efficiently. The majority of phase II metabolites are glucuronide- or sulfoconjugates. The formation of the latter species is catalyzed

by sulfotransferases (SULTs), which for their activity depend on the cofactor 3'-phosphoadenosine-5'-phosphosulfate (PAPS).

For laboratory use PAPS is highly expensive (approx. 286 US\$/mg). This fact might contribute to the limited number of sulfonation studies as compared with research on glucuronidation. In biological sulfonation, conversion of inorganic sulfate into the high-energy cofactor PAPS is a prerequisite. In this pathway, adenosine triphosphate (ATP) sulfonation is initially catalyzed by ATP-sulfurylase to generate adenosine-5'-phosphosulfate (APS), which is subsequently phosphorylated by APS kinase to yield PAPS (Burkart et al., 2000). Afterwards, the sulfo-group is transferred from PAPS to the parent drug or its phase I metabolite in a reaction catalyzed by a SULT enzyme. The released 3'-phosphoadenosine-5'-phosphate (PAP) is subsequently dephosphorylated and re-phosphorylated in several enzymatically catalyzed steps to regenerate ATP (Robbins and Lipmann, 1958). In animal cells, ATP sulfurylase and APS kinase are expressed as a bifunctional enzyme named PAPS synthase (PAPSS), whereas in bacteria, yeasts, fungi, and plants, the two enzymes are generally encoded by separate genes (Besset et al., 2000).

In the budding yeast *Saccharomyces cerevisiae* ATP sulfurylase and APS kinase are encoded by the genes MET3 and MET14, respectively (Masselot and Surdin-Kerjan, 1977; Cherest et al., 1985; Cherest et al., 1987; Mountain and Korch, 1991). In the fission yeast *Schizosaccharomyces pombe* there is a MET14 homologue which is predicted to encode a APS kinase (Lock et al., 2019). While this has yet to be demonstrated experimentally, PAPS synthesis in *S. pombe* as such has already been reported (Song and Roe, 2008). Previously, all 14 human SULTs have been functionally expressed in *S. pombe* and, moreover, using this microbial host the functionality of SULT4A1 and SULT6B1 was demonstrated for the first time (Sun et al., 2020). In comparison to whole-cell biotransformation, sulfonation of drugs with permeabilized recombinant fission yeast cells (enzyme bags) provided higher sensitivity and shorter reaction times. However, the required PAPS addition makes this approach expensive for extensive substrate screening or for up-scaling of biosynthetic metabolite production. In this study, we investigated the possibility of generating PAPS by endogenous fission yeast enzymes in the presence of (comparatively cheaper) ATP and ammonium sulfate. For this purpose, the experimental conditions were first optimized using SULT1A3 and 4-hydroxypropranolol (4HP) as model compound. Further verification was then performed with several other SULTs and substrates.

MATERIAL AND METHODS

Chemicals and Reagents

Na_2HPO_4 and $\text{CaCl}_2 \cdot 2 \text{H}_2\text{O}$ were purchased from Riedel de Haen (Seelze, Germany). KH_2PO_4 , $\text{CuSO}_4 \cdot 5 \text{H}_2\text{O}$, H_3BO_3 , potassium hydrogen phthalate, Na_2SO_4 , nicotinic acid, $\text{MnSO}_4 \cdot \text{H}_2\text{O}$, and KI were from Merck (Darmstadt, Germany). $\text{ZnSO}_4 \cdot 7 \text{H}_2\text{O}$ was purchased from Acros (Geel, Belgium). Tris, agar,

NH_4HCO_3 , NH_4Cl , $\text{FeCl}_3 \cdot 6 \text{H}_2\text{O}$, $\text{MgCl}_2 \cdot 6 \text{H}_2\text{O}$, glucose, Triton-X100, and biotin were from Roth (Karlsruhe, Germany). Inositol was from Th.Geyer (Berlin, Germany), and $\text{MoO}_4 \cdot 2 \text{H}_2\text{O}$ was purchased from Alfa Aesar (Kandel, Germany). Dehydroepiandrosterone (DHEA) was obtained from Steraloids (Newport, RI, United States). 4HP, ATP, and citric acid were purchased from Sigma Aldrich (Steinheim, Germany). 7-Hydroxycoumarin (7HC) and formic acid were purchased from TCI (Zwijndrecht, Belgium). ^{34}S labelled $(\text{NH}_4)_2\text{SO}_4$ and D_9 -Salbutamol (D_9 -SA) were purchased from Sigma-Aldrich (Taufkirchen, Germany), D_6 -DHEA was obtained from Sigma-Aldrich (Saint Louis, MO, United States). Acetonitrile was from Fischer Scientific (Geel, Belgium), and HCOONH_4 was from VWR Chemicals (Damstadt, Germany). Ultrapure water was prepared with a Milli-Q water purification system LaboStar 2-DI/UV from SG Wasseraufbereitung und Regenerierstation GmbH (Barsbüttel, Germany). All other chemicals and reagents used were also of the highest grade available.

Fission Yeast Strains, Media and General Techniques

The recombinant fission yeast strains YN3, YN4, YN20, and YN25 used in this project were described before (Sun et al., 2020). The preparation of media and basic manipulation methods of *S. pombe* were carried out as described (Alfa et al., 1993). Briefly, strains were generally cultivated at 30°C in Edinburgh Minimal Medium (EMM). EMM was prepared with NH_4Cl (93.5 mM), glucose (2% w/v), Na_2HPO_4 (15.5 mM), potassium hydrogen phthalate (14.7 mM) and standard amounts of salt, vitamin and mineral stock solutions. Liquid cultures were kept shaking at 230 rpm.

Biotransformation With Enzyme Bags

This was essentially done as described before (Sun et al., 2020) with slight modifications. Briefly, fission yeast strains were grown in 10 ml liquid culture of EMM at 30°C and 230 rpm for 24 h. Incubation of main cultures in 250 ml Erlenmeyer flasks was performed subsequently. For each assay a certain number of cells were transferred to micro centrifuge tubes or falcons, pelleted and incubated in 0.3% Triton-X100 in Tris-KCl buffer (200 mM KCl, 100 mM Tris-Cl pH 7.8) at 30°C for 60 min at 230 rpm to allow for permeabilization. Cells were then washed thrice with NH_4HCO_3 buffer (50 mM, pH 7.8) and directly used for SULT-dependent reactions. Enzyme bags were resuspended in 200 μL of aqueous NH_4HCO_3 buffer (50 mM, pH 7.8) or phosphate buffer (50 mM, pH 7.8) containing PAPS or ATP, ammonium sulfate, magnesium chloride and substrate as indicated. Biotransformations were carried out at 37°C in a shaking incubator (300 rpm). Enzymatic reactions were stopped by short sharp centrifugation at 14,100 rcf for 2 min and 200 μL of sample in 1.5 ml micro centrifuge tubes were directly frozen at -20°C. After defrosting, samples were centrifuged again (14,100 rcf, 2 min). Supernatants were directly analyzed by ultra-high performance liquid chromatography tandem mass spectrometry (UHPLC-MS/MS) or diluted with a mixture of acetonitrile and ultrapure water

(50/50, v/v) prior to analysis. Negative control samples were incubated without cofactors (ATP, $(\text{NH}_4)_2\text{SO}_4$, and MgCl_2) or without cells, respectively.

Multifactorial Optimization

The optimization process was performed applying quality-by-design (QbD) principles. Design of experiments (DoE) was used for multivariate statistical analysis aiming to ensure robust protocol conditions. It started with a broad systematic screening of the influence of several factors on the incubation of 4HP with YN20 (SULT1A3): ATP concentration (1–50 mM, while $(\text{NH}_4)_2\text{SO}_4$ concentration was always kept to the half of ATP concentration), incubation time (3–72 h), cell number per incubation, pre-incubation time, and magnesium chloride concentration (1–100 mM) were altered. Results of the pre-screening disclosed some limits and trends of the factors. For further optimization a Box-Behnken design was used to investigate the effect of the five dependent variables in biotransformation and to optimize the experimental conditions to achieve the highest yield. The variables in this design involved ATP concentration (11–20 mM), magnesium chloride concentration (10–100 mM), pre-incubation time (i.e. incubation without substrate for either 0, 3, or 5 h), incubation time (3–24 h), and cell number (either 5×10^7 , 1.25×10^8 , 2.5×10^8 , or 5×10^8 per 200 μL). Considering the outcome and prediction of pre-screening and first round of optimization two further rounds of fine tuning were performed subsequently. The best conditions of round two and three as well as predicted optimal conditions were then compared as proof of concept and re-evaluated focusing on incubation time in particular. Also, both NH_4HCO_3 and phosphate buffer systems were evaluated. Product formation was monitored by UHPLC-MS/MS and results of the same analytes were compared *via* peak area. Statistical data analysis and parts of experimental design were carried out using Minitab (RRID: SCR_014483, Statistical Software, Coventry, United Kingdom) software program.

Biosynthesis of Isotope-Labelled Metabolites and Evaluation of *in situ* PAPS Generation

D₆-DHEA (100 μM) and D₉-SA (100 μM) were used as substrates in enzyme bags experiments. Enzyme bags experiments were also carried out with DHEA (100 μM) and SA (100 μM) utilizing $(\text{NH}_4)_2^{34}\text{SO}_4$ (5.5 mM) and ATP (11 mM) as educts for the cofactor PAPS. Production of labelled sulfoconjugates was monitored by UHPLC-MS/MS.

Degradation Experiments

Degradation of an already sulfonated metabolite in enzyme bags experiment was tested by incubating 7-hydroxycoumarin sulfate (7HCSU) with either YN3 or YN4 for 5 h at 37°C. All experiments were carried out in duplicates.

Optimized Enzyme Bags Biosynthesis

Based on the optimization experiments the final enzyme bag method used 2.5×10^8 precultured and pelleted fission yeast cells that are permeabilized using 200 μL of Triton-X100 [0.3% in

Tris-KCl buffer (200 mM KCl, 100 mM Tris-Cl pH 7.8)] at 30°C for 60 min at 230 rpm. After washing with NH_4HCO_3 buffer (50 mM, pH 7.8, three times) enzyme bags were resuspended in 200 μL of aqueous NH_4HCO_3 buffer (50 mM, pH 7.8) and supplied with ATP at 11 mM, ammonium sulfate at 22 mM, and magnesium chloride at 20 mM. Following substrate addition (final concentration of 100 μM in incubation solution) mixtures are incubated at 37°C at 300 rpm. Sharp centrifugation at 14,100 rcf for 2 min followed by a freeze-thaw cycle at –20°C and a second centrifugation at 14,100 rcf for 2 min yielded the sulfoconjugates in the supernatant.

UHPLC-MS/MS Instrumentation and Analytical Methods

Separation was conducted on a 1290 Infinity UHPLC System (Agilent Technologies, Waldbronn, Germany) with an Agilent InfinityLab Poroshell 120 Phenyl Hexyl (100 \times 2.1 mm, 2.7 μm) column or an Agilent InfinityLab Poroshell 120 C18-EC (2.1 \times 50 mm, 1.9 μm) column. As mass detector an Agilent 6495 Triple Quadrupole MS/MS was utilized. The details of the chromatographic separation conditions, the MS/MS operating parameters and the transitions for all analytes are listed in the supplemental information (Supplementary Tables S1–S3). Presented peak areas were provided by transitions of highest intensity (quantifier).

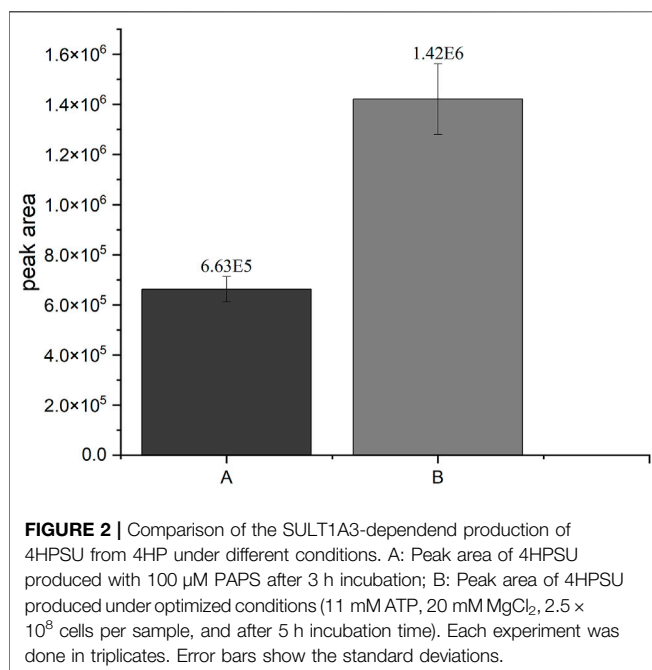
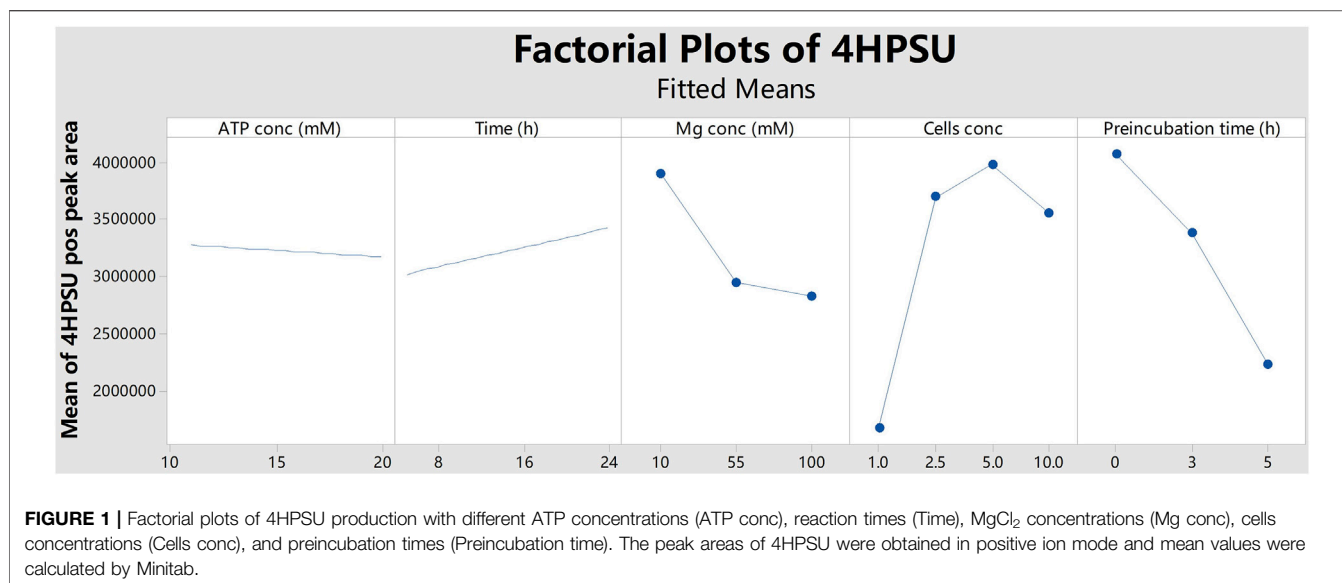
Statistical Analysis

All data are presented as mean \pm SD. Statistical analysis was done using Origin 2021 (Originlab Corporation, Northampton, MA, United States).

RESULTS

Optimization of Reaction Conditions for Sulfoconjugate Production With Enzyme Bags

Initially, a sulfonation assay of 4HP (for reaction schemes see Supplementary Figure S1) by SULT1A3 (strain YN20) with external PAPS (100 μM) was carried out as described (Sun et al., 2020). For substitution of the cofactor PAPS by ATP and SO_4^{2-} and optimization of the product yields multifactorial screening supported by Minitab software was started with five factors: ATP concentration, MgCl_2 concentration, number of cells, reaction incubation time, and time of preincubation without substrate. Initial results indicated that a reduction of yield was correlated with longer preincubation time (Figure 1). Therefore, later rounds were performed without any preincubation. Two optimization rounds were conducted within a more targeted range of each factor using Box-Behnken design. More specifically, ATP concentrations of 11 mM or 15 mM, cell numbers of 1.25×10^8 , 2.5×10^8 , or 5×10^8 per assay, MgCl_2 concentrations of 10 mM, 20 mM or 30 mM, and incubation times from 5 to 72 h were tested. The optimal conditions obtained were 11 mM ATP, 2.5×10^8 cells per sample, 20 mM MgCl_2 , and 5 h incubation time. The experiments under the optimal conditions gave over two times



higher peak areas of 4-hydroxypropanolol-4-O-sulfate (4HPSU) in comparison to the initial reaction with external PAPS (**Figure 2**). Thus, a standard protocol was established which allows substrate sulfonation with human SULTs recombinantly expressed in fission yeast using ATP and $(\text{NH}_4)_2\text{SO}_4$ instead of PAPS.

Evaluation of Optimal Conditions for Additional Substrates and Enzyme Isoforms

As proof of concept the above-mentioned standard protocol developed with the SULT1A3 (YN20) and 4HP was then applied to 7HC, DHEA, salbutamol (SA) and 4HP using

various SULTs (**Figure 3**). Experimental conditions were as follows: 11 mM ATP, 5.5 mM $(\text{NH}_4)_2\text{SO}_4$, 100 μM substrate, 20 mM MgCl_2 , and 2.5×10^8 cells per sample in NH_4HCO_3 buffer (pH 7.8). Substrates were incubated with SULTs reported in literature to metabolize the respective substrates (Miyano et al., 2005; Gamage et al., 2006; Ko et al., 2012; Nishikawa et al., 2018). DHEA was transformed to dehydroepiandrosterone sulfate (DHEASU) by SULT1E1 (YN25) and SULT2A1 (YN4). The strain with the latter enzyme provided a higher space-time yield. In case of the substrates SA, 7HC, and 4HP with various enzyme isoforms phenolic sulfonated metabolites were found in all experiments except in incubations of 7HC with SULT2A1 (YN4). The generation of 4HPSU was catalysed by SULT1B1 (YN3), SULT1E1 (YN25), and SULT1A3 (YN20). In same order yields were ascending. SA sulfonation to salbutamol sulfate (SASU) was successfully performed by SULT1A3 (YN20). 7HCSU was generated by SULT1B1 (YN3). Blank incubations served as negative controls. All blank incubations either without cofactors (-CoF) or without cells (-C) did not result in any detection of sulfonated metabolites.

In the past, recombinant fission yeast strains that express human UDP glucuronosyltransferases were successfully used for the production of stable isotope-labelled glucuronides (Dragan et al., 2010; Buchheit et al., 2011). In order to demonstrate the usefulness of our new protocol for the production of stable isotope-labelled sulfometabolites, biotransformations with D_6 -DHEA, D_9 -salbutamol (D_9 -SA), and $(\text{NH}_4)_2^{34}\text{SO}_4$ were conducted in the present study (**Figure 4** and **Figure 5**). Non-labelled DHEA or D_6 -DHEA were subjected to SULT2A1-dependent enzyme bag biotransformations either with $(\text{NH}_4)_2\text{SO}_4$ or $(\text{NH}_4)_2^{34}\text{SO}_4$. Results of UHPLC-MS/MS analysis proved same retention time of DHEASU, D_6 -DHEASU, and DHEA- ^{34}S -SU (**Figures 4A,C,E**) the respective pattern of mass transitions (**Figures 4B,D,F**) showed the successful production of non-labelled and isotope-labelled

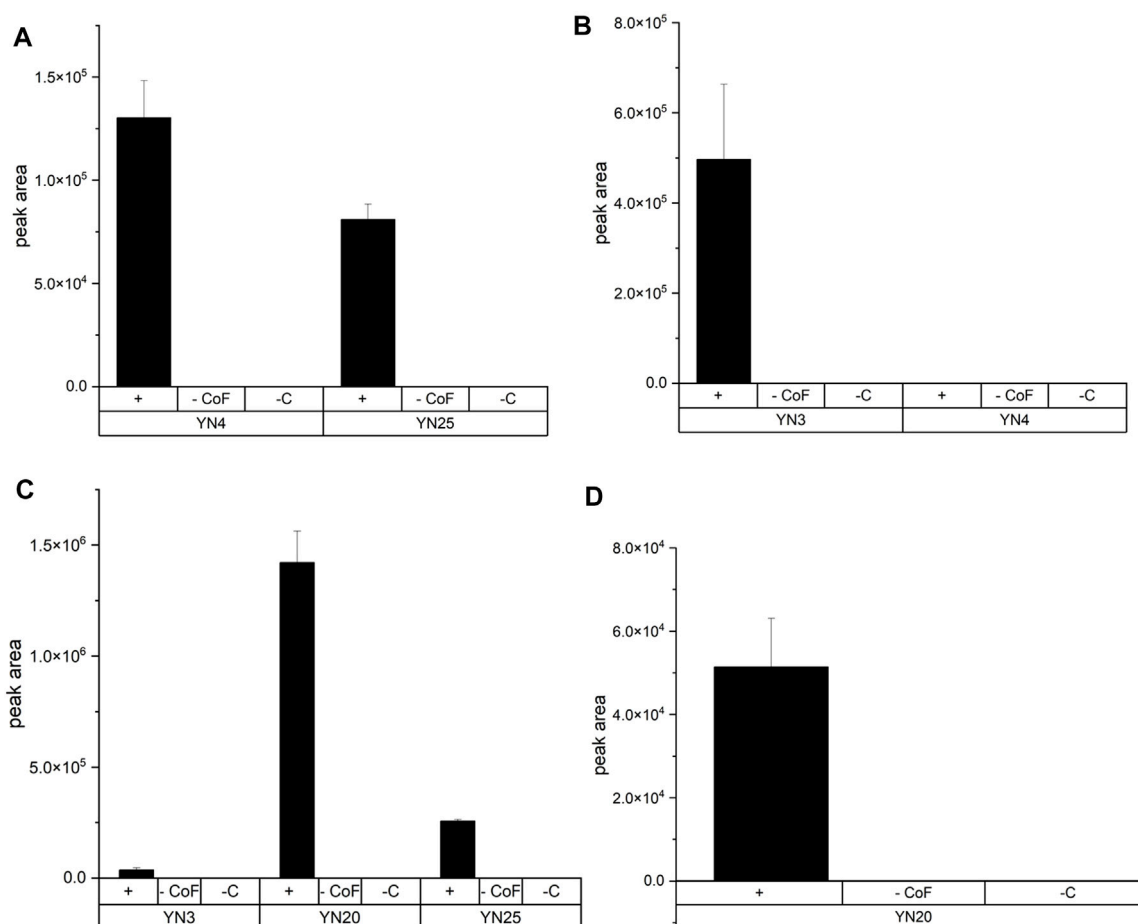


FIGURE 3 | Production of three different sulfoconjugated metabolites by various human SULTs. Experimental conditions are described in the text. Names of fission yeast strain are given in brackets. +: incubation with cells and cofactors—CoF: incubation without cofactors but with cells—C: incubation without cells but with cofactors. **(A)** Production of DHEASU from DHEA. **(B)** Production of 7HCSU from 7HC. **(C)** Production of 4HPSU from 4HP. Each experiment was done in triplicates. **(D)** Production of SASU from SA.

sulfometabolites. The same strategy was performed using non-labelled SA and D₉-SA with SULT1A3 (YN20) as well (Figure 5).

Further Optimization of Buffer, (NH₄)₂SO₄ and Substrate Concentrations

Unexpectedly, the sulfonation of 7HC by SULT2A1 (YN4) could not be shown using above mentioned conditions, even though the enzyme is known to metabolize this substrate (Nishikawa et al., 2018; Sun et al., 2020). It was suspected that product lability might be a reason. In order to confirm this suspicion, degradation assays were performed. Indeed, the incubation of 7HCSU with enzyme bags generated using YN3 at pH 7.8 led to more than 99% loss of the compound within 5 hours. By contrast, degradation tests in buffer without cells proved good stability of 7HCSU (Supplementary Figure S2). Apparently, there are endogenous fission yeast enzymes which can catalyze a cleavage of this sulfated metabolite.

Further investigations of the degradation of 7HCSU were performed by incubating permeabilized YN3 cells either in

NH₄HCO₃ buffer (at pH 7.8 or 7.4) or in phosphate buffer (at pH 7.8, 7.4, or 6.5). The results showed that in pH 7.8 phosphate buffer 7HCSU displays the smallest amount of degradation (Supplementary Figure S3). With the intention of avoiding total degradation of 7HCSU and increasing sulfonation yield of 7HC by SULT2A1 (YN4), and also with the purpose for exploring the possibility of further optimization of the general protocol, enzyme bag assays were subsequently conducted at higher substrate concentrations (7HC at 100 μM or 1 mM), higher (NH₄)₂SO₄ concentrations (5.5, 22, 33, or 44 mM), and also in phosphate buffer (pH 7.8). The results demonstrated that the peak area of 7HCSU reached the highest levels at 1 mM substrate concentration, while the influence of the (NH₄)₂SO₄ concentration on the yield was minor (Figure 6). The same optimization with higher substrate and ammonium sulfate concentrations was performed for the biotransformation of 4HP with SULT1A3 (YN20) as well. In this case, no particularly obvious differences were found among the different conditions (Supplementary Figure S4).

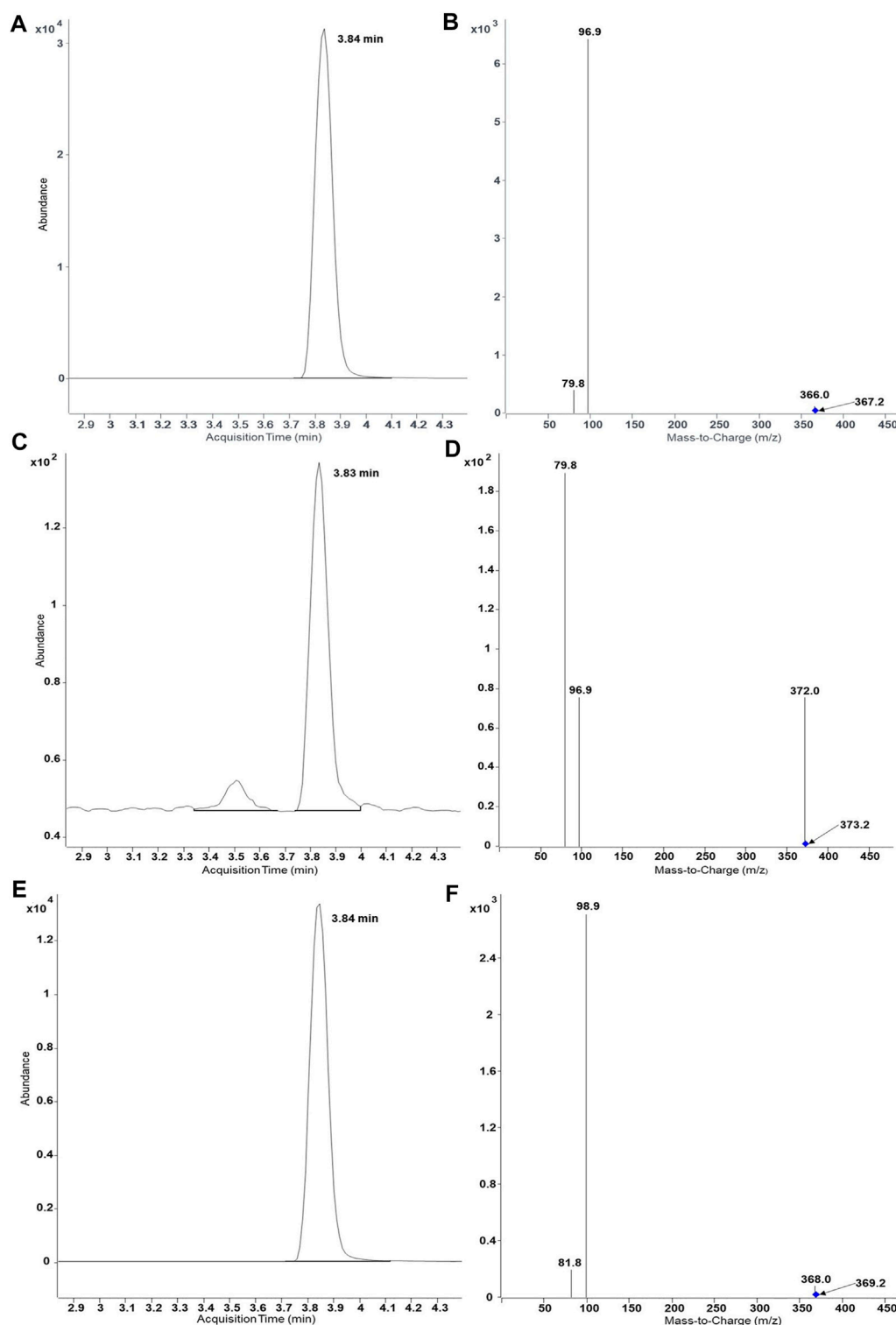


FIGURE 4 | UHPLC-MS/MS results of biosynthesis of DHEASU, D₆-DHEASU, and DHEA-³⁴S-SU by SULT2A1 (YN4). Product ion spectra generated in ESI⁻ are dominated by the fragment HSO₄⁻ (96.9) or H³⁴SO₄⁻ (98.9). **(A)** Chromatogram of DHEASU displaying qualifier transition m/z 367.2 → 96.9; **(B)** MRM transitions in DHEASU assay (m/z 367.2→366, 367.2→96.9 and 367.2→79.8); **(C)** Chromatogram of D₆-DHEASU displaying qualifier transition m/z 373.2 → 96.9 **(D)** MRM transitions in D₆-DHEASU assay (m/z 373.2→372, 373.2→96.9 and 373.2→79.8); **(E)** Chromatogram of DHEA-³⁴S-SU displaying qualifier transition m/z 369.2 → 98.9; **(F)** MRM transitions in DHEA-³⁴S-SU assay (m/z 369.2→368, 369.2→98.9 and 369.2→81.8).

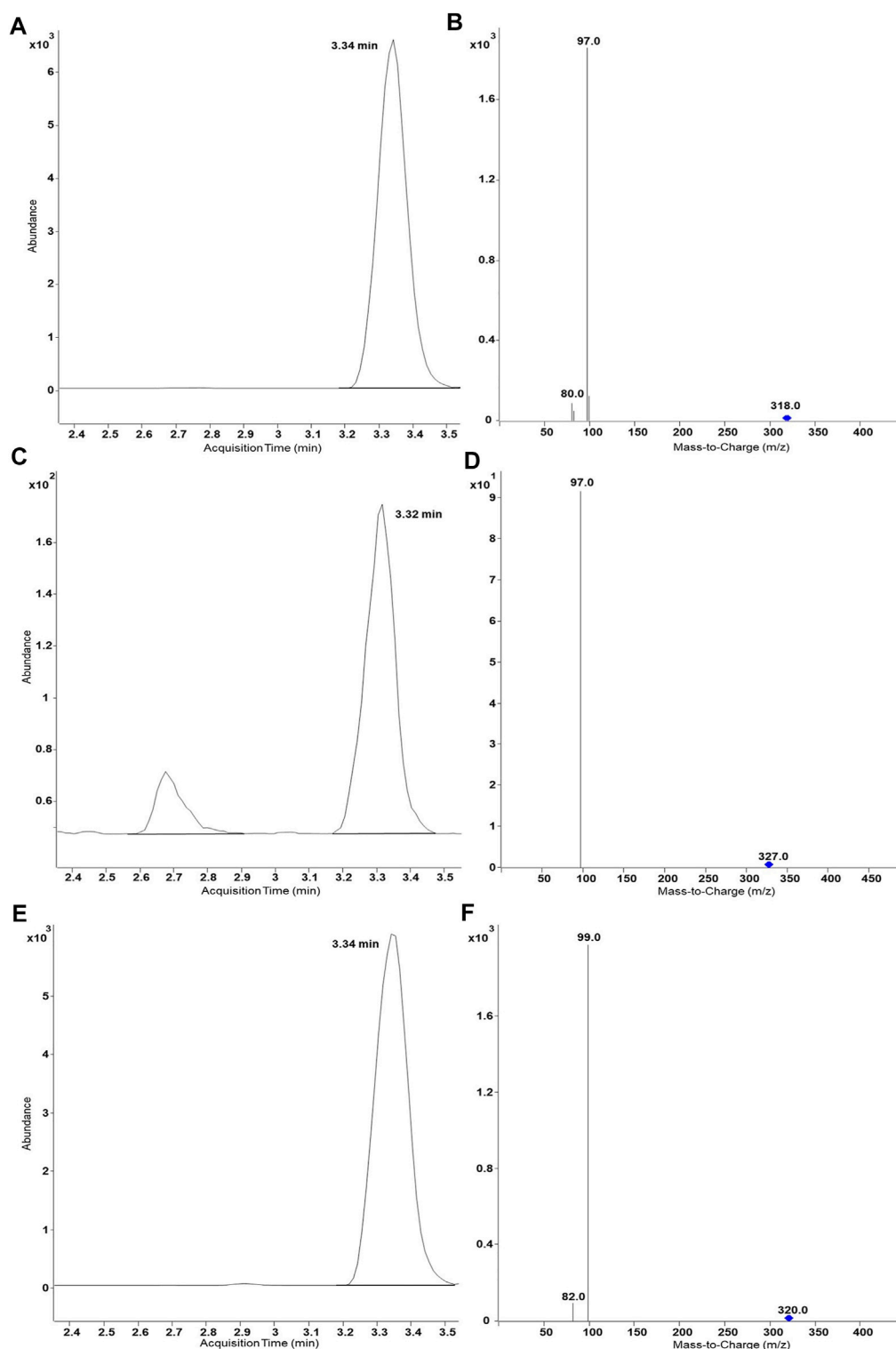
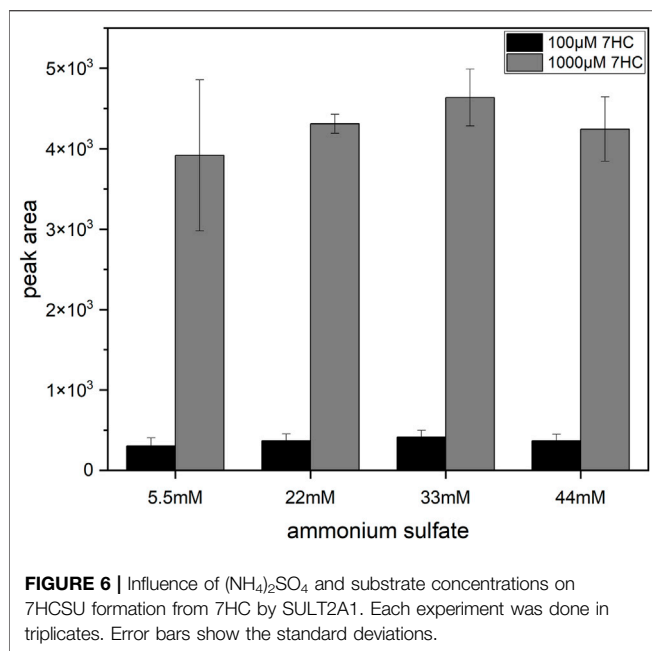


FIGURE 5 | UHPLC-MS/MS results of biosynthesis of SASU, D₉-SASU, and SA-³⁴S-SU by SULT1A3 (YN20). Product ion spectra generated in ESI⁻ are dominated by the fragment HSO₄⁻ (96.9) or H³⁴SO₄⁻ (98.9). **(A)** Chromatogram of SASU shows ion transition m/z 318.0 → 97; **(B)** MRM transitions in SASU assay (m/z 318.0 → 97.0 and 318.0 → 80.0); **(C)** Chromatogram of D₉-SASU shows m/z 327.0 → 97.0; **(D)** MRM transitions in D₉-SASU assay (m/z 327.0 → 97.0 and 327.0 → 79.8); **(E)** Chromatogram of SA-³⁴S-SU shows m/z 320.0 → 99.0; **(F)** MRM transitions in SASU assay (m/z 320.0 → 99.0 and 320.0 → 82.0).



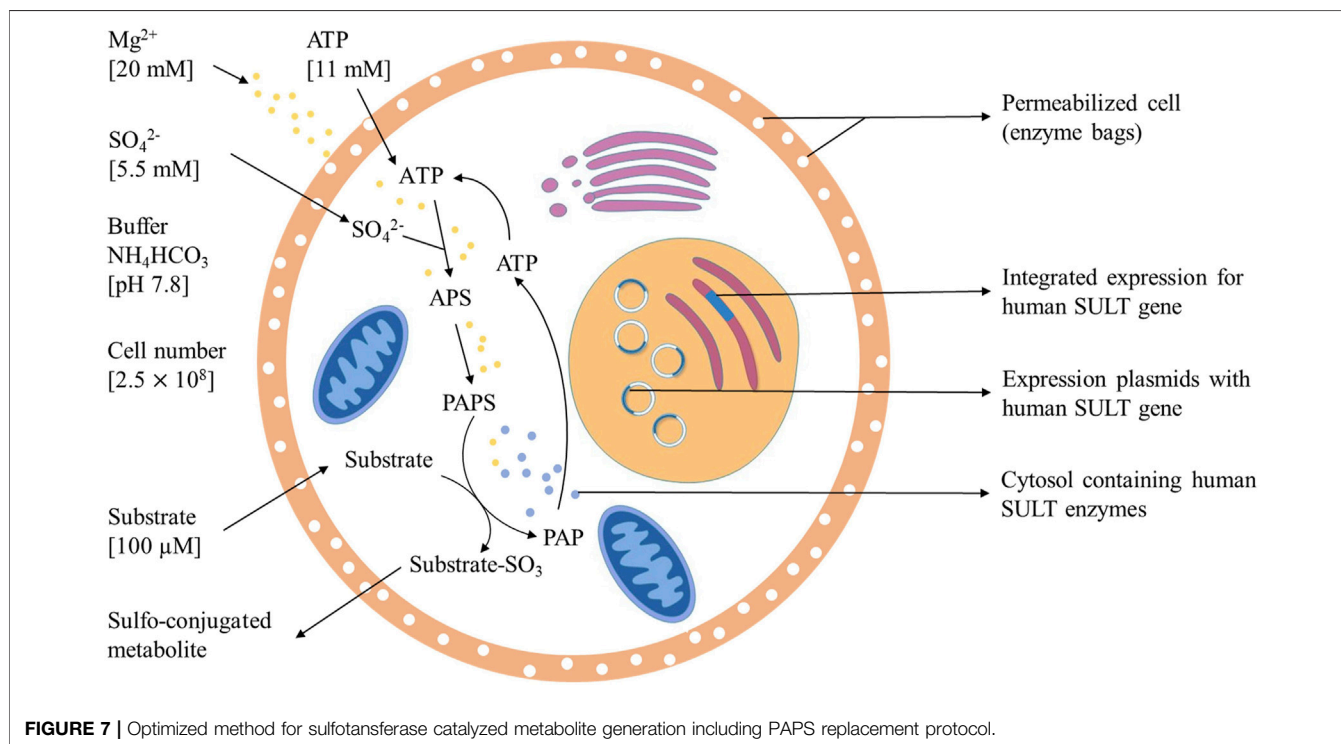
Final Protocol

The final protocol (Figure 7) for this sulfonation assay uses 20 mM Mg^{2+} , 11 mM ATP, 5.5 mM SO_4^{2-} , and 2.5×10^8 cells per incubation in ammonium bicarbonate buffer at pH 7.8 for 5 h at 37°C. In the case of 4HP, the most efficient substrate concentration was 100 µM. Sulfonation of compounds with a low affinity to a SULT can be achieved by enhancing substrate concentration to 1 mM.

DISCUSSION

In this study, the successful replacement of the SULT cofactor PAPS by ATP and $(\text{NH}_4)_2\text{SO}_4$ in a recombinant sulfoconjugate biosynthesis system is reported. While production and regeneration of PAPS were previously described in a chemoenzymatic approach (An et al., 2017), in an enzymatic approach (Burkart et al., 2000), and in liver S9 fraction-based biosynthesis (Weththasinghe et al., 2018), this assay successfully combines both, PAPS (re-)generation and sulfonation of xenobiotics. Multifactorial optimization was performed applying DoE principles using the model substrate 4HP and human SULT1A3, which is expressed by recombinant fission yeast strain YN20 (Figure 1). Compared with the biosynthesis where PAPS was used as cofactor, the optimized method with ATP and $(\text{NH}_4)_2\text{SO}_4$ resulted in a more than doubled yield of product (Figure 2). At the same time, the cost per experiment was reduced by a factor of 60. Further optimization was performed using 4HP with SULT1A3 and 7HC with SULT2A1. Permeabilized fission yeast (enzyme bags) assays with PAPS regeneration combine the advantage of high sensitivity and low cost. Small molecules like substrates, cofactors, and products can move in and out of the cells freely. Meanwhile, the enzymes needed for sulfonation remain trapped within the enzyme bags and can therefore be employed to catalyze the reactions of interest.

The concentration of magnesium ions was observed to be one of the most crucial parameters in the optimization process. Magnesium is an essential electrolyte in the human body. As a cofactor, magnesium participates in more than 300 enzyme systems that modulate multiple biochemical reactions in the body (Gröber



et al., 2015a). In biological systems that generate PAPS or sulfonated metabolites, magnesium functions as an assistant inorganic ion (Burkart et al., 2000; Weththasinghe et al., 2018). In this study, the concentration of MgCl_2 was tested in a range from 1 to 100 mM. Ultimately, 20 mM was found to be the optimal concentration. The results demonstrated that within certain limits, the MgCl_2 concentration had an evident impact on the yield of 4HPSU. Although the mechanism of magnesium in biological sulfonation is not yet completely understood, magnesium is reported to be essential for the pathway of PAPS synthesis in *S. cerevisiae* (Thomas and Surdin-Kerjan, 1997). It is reasonable to assume that magnesium either functions as an enzyme activator or is involved in ATP production within the sulfonation system (Swaminathan, 2003; Gröber et al., 2015b).

By screening several ATP concentrations, it was observed that higher ATP concentrations (≥ 50 mM) led to a significant decline of yield in sulfonated product formation. As a structural analogue of PAPS, ATP has been reported to competitively inhibit the sulfonation of human M and P phenol sulfotransferase (SULT1A3, SULT1A1) (Rens-Domiano and Roth, 1987; Dooley et al., 1994). This property might be responsible for the effects observed in here as well.

Afterwards, the standard protocol was applied to additional substrates and SULTs (Figure 3). Furthermore, production of stable isotope-labelled sulfometabolites, with D_6 -DHEA, D_9 -salbutamol (SA), and $(\text{NH}_4)_2^{34}\text{SO}_4$ were achieved applying the established protocol as well (Figures 4, 5). The competence of SULT2A1 to sulfonate 7HC was reported by Nishikawa (Nishikawa et al., 2018) and Sun (Sun et al., 2020). However, using our PAPS replacing protocol, the enzymatic activity of SULT2A1 towards 7HC could not be demonstrated under initial standard protocol conditions. A possible reason is a rapid degradation of the product 7HCSU, presumably by cleavage of the sulfate group. Therefore, the degradation of 7HCSU was subsequently investigated in reaction mixtures with and without cells (Supplementary Figure S1). Degradation was only found in assays with cells, which indicated that the degradation of 7HCSU is a result of enzymatic catalysis rather than of chemical instability. Less degradation was observed when phosphate buffer (pH 7.8) was used instead of hydrogen carbonate buffer, which is in line with earlier reports of sulfatase inhibition by phosphate (Lee and Van Etten, 1975; Bostick et al., 1978; Metcalfe et al., 1979). Furthermore, using phosphate buffer higher product yields were obtained with both SULT2A1 and SULT1B1. Therefore, for 7HC sulfonation experiments with enzyme bags, the usage of phosphate buffer (pH 7.8) is superior to that of NH_4HCO_3 buffer (pH 7.8).

In a previous study by Burkart et al. (2000) the generation of PAPS from ATP and inorganic sulfate was also achieved using genetically modified *E. coli*. Highest yields were obtained when the sulfate concentration dramatically exceeded that of ATP. Consequently, we increased the $(\text{NH}_4)_2\text{SO}_4$ concentration to 44 mM. However, the yield of 4HPSU did not show a significant rise with increasing $(\text{NH}_4)_2\text{SO}_4$ concentrations. This might indicate that the concentration of PAPS is not the main limiting factor of 4HPSU yield in this case.

Being a known hydroxysteroid converting SULT, SULT2A1 shows low affinity to phenolic compounds like 7HC (Tibbs et al.,

2015), which might explain the lack of sulfoconjugated metabolite in initial experiments. Therefore, the concentration of 7HC was increased to 1 mM to facilitate the enzymatic reaction. A remarkable increase of 7HCSU production (Figure 6) was observed. In this manner, the standard protocol was modified for biotransformation of low affinity substrates in enzyme bags.

The developed assay allows to determine whether a substrate is sulfonated by any one of the 14 human SULTs and also permits a comparison of their sulfonation activity. Due to the fact that the biosynthesized sulfoconjugates are not available as references, a quantitation of the results by UHPLC-MS/MS is not possible. Therefore, metabolite formation rates cannot be given in absolute values in this study.

The successful development of an optimized PAPS replacement protocol (details in Figure 7) provides an economic and efficient way for further research of SULT-dependent phase II metabolism pathways of drugs. Bigger scale screening experiments will be performed to demonstrate broad applicability and to further evaluate the possibilities of this great sulfonation technique. The biotechnological generation of sulfonated compounds and metabolites may be achieved on reasonable costs applying this assay.

DATA AVAILABILITY STATEMENT

The original contributions presented in the study are included in the article/Supplementary Material, further inquiries can be directed to the corresponding authors.

AUTHOR CONTRIBUTIONS

Conceptualization, MP and MB; methodology, YS, LH, MB and MP; software, YS and LH; investigation, YS and LH, resources, MP, and MB; data curation, MP and MB; writing—original draft preparation, YS and LH; writing—review and editing, MP, and MB; visualization, YS and LH; supervision, MP, and MB; project administration, MP and MB; funding acquisition, MP and MB. All authors have read and agreed to the published version of the manuscript.

FUNDING

This research was funded by the World Anti-Doping Agency (WADA grant 19A10MP). The APC was funded by the Open Access Publication Fund of the Freie Universität Berlin. We would like to acknowledge the assistance of the Core Facility BioSupraMol supported by the DFG.

SUPPLEMENTARY MATERIAL

The Supplementary Material for this article can be found online at: <https://www.frontiersin.org/articles/10.3389/fmolb.2022.827638/full#supplementary-material>

REFERENCES

- Alfa, C., Fantes, P., Hyams, J., McLeod, M., and Warbrick, E. (1993). *Experiments with Fission yeast A Laboratory Course Manual*. NY: Cold Spring Harbor Press, Cold Spring Harbor.
- An, C., Zhao, L., Wei, Z., and Zhou, X. (2017). Chemoenzymatic Synthesis of 3'-Phosphoadenosine-5'-Phosphosulfate Coupling with an ATP Regeneration System. *Appl. Microbiol. Biotechnol.* 101, 7535–7544. doi:10.1007/s00253-017-8511-2
- Balcells, G., Gómez, C., Garrosta, L., Pozo, Ó. J., and Ventura, R. (2017). Sulfate Metabolites as Alternative Markers for the Detection of 4-chlorometandienone Misuse in Doping Control. *Drug Test. Anal.* 9, 983–993. doi:10.1002/dta.2101
- Besset, S., Vincourt, J.-B., Amalric, F., and Girard, J.-P. (2000). Nuclear Localization of PAPS Synthetase 1: a Sulfate Activation Pathway in the Nucleus of Eukaryotic Cells. *FASEB J.* 14, 345–354. doi:10.1096/fasebj.14.2.345
- Bostick, W. D., Dinsmore, S. R., Mrochek, J. E., and Waalkes, T. P. (1978). Separation and Analysis of Arylsulfatase Isoenzymes in Body Fluids of Man. *Clin. Chem.* 24, 1305–1316. doi:10.1093/clinchem/24.8.1305
- Buchheit, D., Drăgan, C.-A., Schmitt, E. I., and Bureik, M. (2011). Production of Ibuprofen Acyl Glucosides by Human UGT2B7. *Drug Metab. Dispos.* 39, 2174–2181. doi:10.1124/dmd.111.041640
- Burkart, M. D., Izumi, M., Chapman, E., Lin, C.-H., and Wong, C.-H. (2000). Regeneration of PAPS for the Enzymatic Synthesis of Sulfated Oligosaccharides. *J. Org. Chem.* 65, 5565–5574. doi:10.1021/jo000266o
- Cherest, H., Nguyen, N. T., and Surdin-Kerjan, Y. (1985). Transcriptional Regulation of the MET3 Gene of *Saccharomyces cerevisiae*. *Gene* 34, 269–281. doi:10.1016/0378-1119(85)90136-2
- Cherest, H., Kerjan, P., and Surdin-Kerjan, Y. (1987). The *Saccharomyces cerevisiae* MET3 Gene: Nucleotide Sequence and Relationship of the 5' Non-coding Region to that of MET25. *Mol. Gen. Genet.* 210, 307–313. doi:10.1007/bf00325699
- Dooley, T. P., Mitchison, H. M., Munroe, P. B., Probst, P., Neal, M., Siciliano, M. J., et al. (1994). Mapping of Two Phenol Sulfotransferase Genes, STP and STM, to 16p: Candidate Genes for Batten Disease. *Biochem. Biophysical Res. Commun.* 205, 482–489. doi:10.1006/bbrc.1994.2691
- Dragan, C. A., Buchheit, D., Bischoff, D., Ebner, T., and Bureik, M. (2010). Glucuronide Production by Whole-Cell Biotransformation Using Genetically Engineered Fission Yeast *Schizosaccharomyces pombe*. *Drug Metab. Dispos.* 38, 509–515. doi:10.1124/dmd.109.030965
- Ekins, S., Ring, B. J., Grace, J., McRobie-Belle, D. J., and Wrighton, S. A. (2000). Present and Future *In Vitro* Approaches for Drug Metabolism. *J. Pharmacol. Toxicol. Methods* 44, 313–324. doi:10.1016/s1056-8719(00)00110-6
- Esquivel, A., Alechaga, E., Monfort, N., Yang, S., Xing, Y., Moutian, W., et al. (2019). Evaluation of Sulfate Metabolites as Markers of Intramuscular Testosterone Administration in Caucasian and Asian Populations. *Drug Test. Anal.* 11, 1218–1230. doi:10.1002/dta.2598
- Gamage, N., Barnett, A., Hempel, N., Dugleby, R. G., Windmill, K. F., Martin, J. L., et al. (2006). Human Sulfotransferases and Their Role in Chemical Metabolism. *Toxicol. Sci.* 90, 5–22. doi:10.1093/toxsci/kfj061
- Gröber, U., Schmidt, J., and Kisters, K. (2015). Magnesium in Prevention and Therapy. *Nutrients* 7, 8199–8226. doi:10.3390/nu7095388
- Gröber, U., Schmidt, J., and Kisters, K. (2015). Magnesium in Prevention and Therapy. *Nutrients* 7, 8199–8226. doi:10.3390/nu7095388
- Ko, K., Kurogi, K., Davidson, G., Liu, M.-Y., Sakakibara, Y., Suiko, M., et al. (2012). Sulfation of Ractopamine and Salbutamol by the Human Cytosolic Sulfotransferases. *J. Biochem.* 152, 275–283. doi:10.1093/jb/mvs073
- Lee, G. D., and Van Etten, R. L. (1975). Purification and Properties of a Homogeneous Aryl Sulfatase A from Rabbit Liver. *Arch. Biochem. Biophys.* 166, 280–294. doi:10.1016/0003-9861(75)90389-6
- Lock, A., Rutherford, K., Harris, M. A., Hayles, J., Oliver, S. G., Bähler, J., et al. (2019). PomBase 2018: User-Driven Reimplementation of the Fission Yeast Database Provides Rapid and Intuitive Access to Diverse, Interconnected Information. *Nucleic Acids Res.* 47, D821–D827. doi:10.1093/nar/gky961
- Masselot, M., and Surdin-Kerjan, Y. (1977). Methionine Biosynthesis in *Saccharomyces cerevisiae*. *Mol. Gen. Genet.* 154, 23–30. doi:10.1007/bf00265572
- Metcalfe, D. D., Corash, L. M., and Kaliner, M. (1979). Human Platelet Arylsulphatases: Identification and Capacity to Destroy SRS-A. *Immunology* 37, 723–729.
- Miyano, J., Yamamoto, S., Hanioka, N., Narimatsu, S., Ishikawa, T., Ogura, K., et al. (2005). Involvement of SULT1A3 in Elevated Sulfation of 4-hydroxypropenolol in Hep G2 Cells Pretreated with β -naphthoflavone. *Biochem. Pharmacol.* 69, 941–950. doi:10.1016/j.bcp.2004.12.012
- Mountain, H. A., and Korch, C. (1991). TDH2 Is Linked to MET3 on Chromosome X of *Saccharomyces Cerevisiae*. *Yeast* 7, 873–880. doi:10.1002/yea.320070814
- Nishikawa, M., Masuyama, Y., Nunome, M., Yasuda, K., Sakaki, T., and Ikushiro, S. (2018). Whole-cell-dependent Biosynthesis of Sulfo-Conjugate Using Human Sulfotransferase Expressing Budding Yeast. *Appl. Microbiol. Biotechnol.* 102, 723–732. doi:10.1007/s00253-017-8621-x
- Rens-Domiano, S. S., and Roth, J. A. (1987). Inhibition of M and P Phenol Sulfotransferase by Analogues of 3'-Phosphoadenosine-5'-Phosphosulfate. *J. Neurochem.* 48, 1411–1415. doi:10.1111/j.1471-4159.1987.tb05679.x
- Robbins, P. W., and Lipmann, F. (1958). Enzymatic Synthesis of Adenosine-5'-Phosphosulfate. *J. Biol. Chem.* 233, 686–690. doi:10.1016/s0021-9258(18)64728-3
- Song, J.-Y., and Roe, J.-H. (2008). The Role and Regulation of Trx1, a Cytosolic Thioredoxin in *Schizosaccharomyces pombe*. *J. Microbiol.* 46, 408–414. doi:10.1007/s12275-008-0076-4
- Sun, Y., Machalz, D., Wolber, G., Parr, M. K., and Bureik, M. (2020). Functional Expression of All Human Sulfotransferases in Fission Yeast, Assay Development, and Structural Models for Isoforms SULT4A1 and SULT6B1. *Biomolecules* 10, 1517. doi:10.3390/biom10111517
- Swaminathan, R. (2003). Magnesium Metabolism and its Disorders. *Clin. Biochem. Rev.* 24, 47–66.
- Taskinen, J., Ethell, B. T., Pihlavisto, P., Hood, A. M., Burchell, B., and Coughtrie, M. W. H. (2003). Conjugation of Catechols by Recombinant Human Sulfotransferases, UDP-Glucuronosyltransferases, and Soluble Catechol O-Methyltransferase: Structure-Conjugation Relationships and Predictive Models. *Drug Metab. Dispos.* 31, 1187–1197. doi:10.1124/dmd.31.9.1187
- Thomas, D., and Surdin-Kerjan, Y. (1997). Metabolism of Sulfur Amino Acids in *Saccharomyces cerevisiae*. *Microbiol. Mol. Biol. Rev.* 61, 503–532. doi:10.1128/mmbr.61.4.503-532.1997
- Tibbs, Z. E., Rohn-Glowacki, K. J., Crittenden, F., Guidry, A. L., and Falany, C. N. (2015). Structural Plasticity in the Human Cytosolic Sulfotransferase Dimer and its Role in Substrate Selectivity and Catalysis. *Drug Metab. Pharmacokinet.* 30, 3–20. doi:10.1016/j.dmpk.2014.10.004
- Wethrasinghe, S. A., Waller, C. C., Fam, H. L., Stevenson, B. J., Cawley, A. T., and McLeod, M. D. (2018). Replacing PAPS: In Vitro Phase II Sulfation of Steroids with the Liver S9 Fraction Employing ATP and Sodium Sulfate. *Drug Test. Anal.* 10, 330–339. doi:10.1002/dta.2224

Conflict of Interest: The authors declare that the research was conducted in the absence of any commercial or financial relationships that could be construed as a potential conflict of interest.

Publisher's Note: All claims expressed in this article are solely those of the authors and do not necessarily represent those of their affiliated organizations, or those of the publisher, the editors and the reviewers. Any product that may be evaluated in this article, or claim that may be made by its manufacturer, is not guaranteed or endorsed by the publisher.

Copyright © 2022 Sun, Harps, Bureik and Parr. This is an open-access article distributed under the terms of the Creative Commons Attribution License (CC BY). The use, distribution or reproduction in other forums is permitted, provided the original author(s) and the copyright owner(s) are credited and that the original publication in this journal is cited, in accordance with accepted academic practice. No use, distribution or reproduction is permitted which does not comply with these terms.



Disease-Related Protein Variants of the Highly Conserved Enzyme PAPSS2 Show Marginal Stability and Aggregation in Cells

Oliver Brylski^{1,2†}, Puja Shrestha^{1†}, Philip J. House³, Patricia Gnutz², Jonathan Wolf Mueller^{3,4*} and Simon Ebbinghaus^{1,2*}

¹Institute of Physical and Theoretical Chemistry, TU Braunschweig, Braunschweig, Germany, ²Institute of Physical Chemistry II, Ruhr University, Bochum, Germany, ³Institute of Metabolism and Systems Research (IMSR), University of Birmingham, Birmingham, United Kingdom, ⁴Centre for Endocrinology, Diabetes and Metabolism (CEDAM), Birmingham Health Partners, Birmingham, United Kingdom

OPEN ACCESS

Edited by:

Giuseppe Calamita,
University of Bari Aldo Moro, Italy

Reviewed by:

Annarita Di Mise,
University of Bari Aldo Moro, Italy
Antonio Rossi,
University of Pavia, Italy

*Correspondence:

Jonathan Wolf Mueller
j.w.mueller@bham.ac.uk
Simon Ebbinghaus
s.ebbinghaus@tu-braunschweig.de

[†]These authors have contributed
equally to this work

Specialty section:

This article was submitted to
Cellular Biochemistry,
a section of the journal
Frontiers in Molecular Biosciences

Received: 22 January 2022

Accepted: 28 February 2022

Published: 08 April 2022

Citation:

Brylski O, Shrestha P, House PJ,
Gnutz P, Mueller JW and Ebbinghaus S
(2022) Disease-Related Protein
Variants of the Highly Conserved
Enzyme PAPSS2 Show Marginal
Stability and Aggregation in Cells.
Front. Mol. Biosci. 9:860387.
doi: 10.3389/fmolb.2022.860387

Cellular sulfation pathways rely on the activated sulfate 3'-phosphoadenosine-5'-phosphosulfate (PAPS). In humans, PAPS is exclusively provided by the two PAPS synthases PAPSS1 and PAPSS2. Mutations found in the PAPSS2 gene result in severe disease states such as bone dysplasia, androgen excess and polycystic ovary syndrome. The APS kinase domain of PAPSS2 catalyzes the rate-limiting step in PAPS biosynthesis. In this study, we show that clinically described disease mutations located in the naturally fragile APS kinase domain are associated either with its destabilization and aggregation or its deactivation. Our findings provide novel insights into possible molecular mechanisms that could give rise to disease phenotypes associated with sulfation pathway genes.

Keywords: PAPS synthase, sulfation pathways, in-cell spectroscopy, protein folding, stability and aggregation

INTRODUCTION

Sulfation is a highly important biological process where a sulfate moiety from the activated sulfate donor 3'-phosphoadenosine-5'-phosphosulfate (PAPS) is transferred onto acceptor molecules. Adding the negatively charged sulfate group to a hydroxyl-group induces significant changes in the chemical properties of the acceptor molecule with a major impact on their function. It is the sheer variety of sulfated metabolites that makes sulfation impactful on numerous biological systems. Sulfotransferases use activated sulfate to modify proteins, glycans and other biomolecules like steroid hormones (Klassen and Boles, 1997; Strott, 2002; Mueller et al., 2015).

Active PAPS synthase enzymes generate active sulfate in the form of PAPS. In humans, there are two isoforms PAPSS1 and PAPSS2 (van den Boom et al., 2012). Nevertheless, disease-related protein variants have been exclusively reported for PAPSS2.

In a variety of human genetics studies, a total of 65 individuals with various inactivating alleles of the human PAPSS2 gene have been described (Ahmad et al., 1998; Haque et al., 1998; Noordam et al., 2009; Miyake et al., 2012; Iida et al., 2013; Tüysüz et al., 2013; Oostdijk et al., 2015; Handa et al., 2016; Bownass et al., 2019; Eltan et al., 2019; Perez-Garcia et al., 2021). These have been analyzed and summarized recently (Baranowski et al., 2018; Brylski et al., 2019; Paganini et al., 2020). An additional PAPSS2 variant is known for brachymorphic mice (Kurima et al., 1998).

Recently, several studies investigated the essential steps in sulfation pathways, whose malfunction is correlated with disease symptoms (Mueller et al., 2015; Foster and Mueller, 2018). Among these symptoms are bone and cartilage dysplasia (Oostdijk et al., 2015), as well as androgen excess and polycystic ovary syndrome (PCOS) (Noordam et al., 2009; Oostdijk et al., 2015), all caused by point-mutations in the *PAPSS2* gene encoding for the PAPS synthase 2 enzyme. These point mutations diminish the enzyme activity and they are mainly located within the kinase domain of *PAPSS2* (Kurima et al., 1998; Noordam et al., 2009; Iida et al., 2013).

It is evident that *PAPSS2* plays a vital role in skeletal development as well as steroid hormones regulation (Kurima et al., 1998; Noordam et al., 2009; Iida et al., 2013). Kurima and coworkers linked the mutation G78R within the nucleotide kinase domain of the *PAPSS2* isoform, with the bone phenotype seen in the brachymorphic mouse (*bm*) (Kurima et al., 1998). G78R is located in the adenosine-5'-phosphosulfate (APS) kinase domain, close to the ligand-binding site. The mutation causes catalytic inactivation and hence lowered intracellular PAPS availability. As a consequence, *bm* mice show reduced postnatal growth that was ascribed to under-sulfation of the extracellular matrix; they also show abnormal hepatic detoxification and prolonged bleeding times (Kurima et al., 1998). One of the most prominent roles of sulfation is the modification of glycosaminoglycans (GAGs) by Golgi-residing carbohydrate sulfotransferases (Gesteira et al., 2021). Sulfated GAGs play a vital role in cell signaling to regulate many biochemical processes like cell growth and proliferation, promotion of cell adhesion, anticoagulation and wound repair (Raman et al., 2005; Prydz, 2015). In brachymorphic cartilage, GAGs are found at normal level but significantly under-sulfated, affecting the formation of connective tissue, such as, cartilage (Kurima et al., 1998; Cho et al., 2004).

More recently, Noordam and coworkers reported a case study of a girl with premature pubarche, hyperandrogenic anovulation, very low level of dehydro-epiandrosterone sulfate (DHEAS) and high level of androgen. The steroid sulfation defect of this patient was associated with a T48R mutation found in the APS kinase domain. Due to this mutation, PAPS synthesis is affected, leading to incompetent DHEA inactivation, with the latter resulting in increased levels of androgens causing PCOS-like phenotypes (Noordam et al., 2009). In 2013, Iida and coworkers reported more *PAPSS2* mutations (C43Y, L76Q, E183K, V540D) out of which three, C43Y, L76Q and E183K, were found in the APS kinase domain. C43Y and L76Q cause loss of function leading to brachyolmia and abnormal androgen metabolism (Iida et al., 2013).

Eukaryotic cells express another PAPS synthase gene, *PAPSS1*, that shares 78% identity at the level of amino acid sequence (van den Boom et al., 2012). However, this protein isoform cannot compensate for the loss of the other (Mueller et al., 2018). This lack of compensation raises the question of whether the two isoforms impact differently on subsets of sulfation pathways. Subcellular localization sequences (Schröder et al., 2012) were identified in both PAPS synthases and dimer formation (Sekulic et al., 2007; Grum et al., 2010; Brylski et al., 2019) was observed, both features proposed to be crucial for proper localization and

activity of the enzyme. In addition to these physiological aspects, *in vitro* biophysical studies focused on the stability of PAPS synthases revealed that isoforms of this enzyme are only marginally stable as recombinant proteins (van den Boom et al., 2012). However, PAPS synthase proteins can be stabilized by preferential binding of their substrates to the APS kinase domain, namely PAPS, adenosine diphosphate (ADP) and APS (van den Boom et al., 2012; Mueller and Shafqat, 2013).

Using a recently developed folding sensor of the APS kinase domain of the human PAPS synthase *PAPSS2* (Brylski et al., 2021), we investigate how clinically reported single-point-mutations change the in-cell stability of the APS kinase domain and if destabilization could lead to aggregation and thus loss of metabolic activity.

MATERIALS AND METHODS

Construction of *PAPSS2* and *APSK37* Variants

The pEGFP-C1-*PAPSS2* plasmid encoding human full-length *PAPSS2b* C-terminally fused to an EGFP fluorescent protein (Schröder et al., 2012), was used for DpnI-based site-directed mutagenesis and subsequently for cell counting experiments. To generate the *APSK37* sensor, the APS kinase domain of *PAPSS2* was PCR-subcloned into a modified pDream2.1 vector with an N-terminal AcGFP1 and a C-terminal mCherry (Ebbinghaus et al., 2010). The APSK enzyme was truncated between the two isoleucine residues I220 and I221, within the flexible linker that connects the kinase and the sulfurylase domains (Harjes et al., 2005). Furthermore, the flexible and disordered N-terminal region, which is known to assist in the dimerization of the protein (Sekulic et al., 2007; Grum et al., 2010), was truncated by 37 amino acids ($\Delta 37$). Further, DpnI-based site-directed mutagenesis was used to introduce different disease related point mutations (G78R, L76Q, C43Y and T48R). All constructs were verified by Sanger DNA sequencing.

Cell Culture and Plasmid Transfection

HeLa cells were grown at 5% CO₂ at 37°C in DMEM supplemented with 10% FBS, 100 U/ml penicillin and 0.1 mg/ml streptomycin. Cells were passaged at a 1:4 or 1:6 ratios at 80–90% confluence, using trypsin digestion. For transfection, cells were seeded in six-well plates (Sarstedt). Using Lipofectamine 3000 (Thermo Fisher), cells were transfected according to the manufacturers protocol. Concisely, a mixture of 125 μ l Opti-MEM (Thermo Fisher) with 2 μ g of the respective plasmid DNA and 4 μ l P3000 reagents was prepared. After 5 min of incubation, the mixture was transferred to another solution containing 125 μ l Opti-MEM supplemented with 4 μ l Lipofectamine3000 reagent. Cells were incubated for 6 h after the addition of transfection mixture to the cellular growth medium at 5% CO₂, 37°C. The cells were passaged using trypsin digestion and seeded in 35 mm glass bottom dishes (Fluorodish, World Precision Instruments). Cells were grown for 2 days at standard cell culture conditions before imaging.

Sample Preparation

Fast Relaxation Imaging (FReI) was performed with transfected cells grown on 35 mm glass bottom dishes (Fluorodish, World Precision Instruments). Cells were washed with Dulbecco's Phosphate Buffered Saline (DPBS) (Sigma-Aldrich) after removing the growth medium. 30 μ L Leibovitz's L15 medium supplemented with 30% FBS were sealed between a glass cover slip (Menzel #1.0) with a 120 μ m thick imaging spacer (Sigma-Aldrich) and a glass bottom dish with cells.

Fast Relaxation Imaging Measurements

FReI is a combination of wide field fluorescence microscopy with millisecond temperature jumps induced by an IR diode laser (m2k-Laser, 2200 nm). The technique was previously described (Ebbinghaus et al., 2010; Gnutt et al., 2019a). Shortly, fluorescent light was split by a dichroic beam splitter into donor and acceptor signal that was recorded using CCD cameras while the sample is rapidly heated by an IR laser. The temperature sensitive dye Rhodamine B (Sigma Aldrich) was used for the calibration of temperature jumps (Vöpel et al., 2015; Gao et al., 2016; Büning et al., 2017). The heat profile used in this study showed an average temperature increase of 2.2°C per jump at intervals of 50 s, covering a range from 23.0 to 58.2°C in 16 steps. Image acquisition was performed at one frame per second (fps) with LED exposure times typically between 50 and 200 ns. Data was recorded using AxioVision software and the images were processed and analyzed using ImageJ (National Institute of Health, United States) and further evaluated using self-written MatLab (Mathworks) codes and GraphPad Prism 6 (GraphPad).

For data analysis, fluorescence intensities were averaged throughout the cytoplasmic region for each channel individually (Dhar et al., 2011). Further, background subtraction was performed for the individual channels and the ratio of the donor and acceptor channel (D/A) calculated. The changes of D/A ratio upon temperature jump yield information about the associated conformational change. An increase in D/A refers a decrease in FRET that may be attributed to protein unfolding. To analyze the kinetics of protein unfolding, the individual channel intensities were used as D- α A according to (Dhar et al., 2011). To determine the melting point (T_M) of the protein, the thermodynamic model introduced as *Better thermodynamics from kinetics* (Girdhar et al., 2011) was used:

$$D - \alpha A(T) = \frac{-\delta g_1 \Delta T \cdot T_m}{R(T - \Delta T/2)^2} \cdot (A_0 + m_A(T - T_m)) \cdot \frac{\exp(-\delta g_1(T - (\Delta T/2) - T_m) \cdot (R(T - \Delta T/2))^{-1})}{(1 + \exp(-\delta g_1(T - (\Delta T/2) - T_m) \cdot (R(T - \Delta T/2))^{-1}))^2}$$

Where, δg_1 is pre-factor of the linear Taylor approximation of the two-state populations. ΔT is the amplitude of the temperature jump (set to 2.2°C) and A_0 and m_A are fitting parameters of the underlying baseline (with m_A set to 0).

HEK293 Cell Culture and Wide Field Microscopy

HEK293 cells were cultured in DMEM with high glucose (Gibco, United Kingdom), supplemented with 10% fetal FBS and penicillin/

streptomycin at 1%. Cells were passaged at 80–90% confluence, using trypsin digestion. Regular checks ensured that all cells were mycoplasma-free. Cells were seeded 1:8 or 1:10 in culture flasks or maintaining stocks or at 200,000 cells per well into six-well plates with microscopic slides in them. Transfection of these HEK293 cells 24 h after seeding on cover slips was performed using the XtremeGENE HP DNA transfection reagent (Roche, United Kingdom), according to manufacturer's instructions. Cells were left growing for 24 or 48 h, then washed with ice-cold PBS and incubated with ice-cold methanol, followed by three further washing steps using PBS. Finally, cover slips with cells were mounted on microscopic slides, using fluorescence mounting media, and fixed with nail varnish. The slides were anonymized to enable blind, non-biased analysis. The slides were then viewed under a wide-field fluorescent microscope and scored at least three different sections using a $\times 20$ objective. Cells were imaged with a $\times 20$ objective. The number of speckles per cell was scored in large numbers of cells, in a blinded fashion. As a control, fluorescence intensity was ranked as well (low/medium/high). No correlation was found between fluorescence intensity and number of speckles, suggesting that protein over-expression levels were not linked to the observed patterns of speckles. Significant changes of population of non-speckled cells have been determined using two-way ANOVA with a *post-hoc* Holm-Sidak's test correcting for multiple comparisons.

RESULTS

Mutations in APSK37 Reveal Distinct Folding Stabilities

We analyzed the effect of disease-related mutations on the folding stability and aggregation of the APS kinase domain of the bifunctional PAPSS2 protein, using our recently established APSK folding sensor (APSK37) (Brylski et al., 2021). The sensor reports intramolecular FRET between the N-terminal AcGFP1 and the C-terminal mCherry fusion proteins (see Materials and Methods for details).

We analyzed PAPS synthase disease point mutations located in the APS kinase domain to understand whether the phenotypes seen clinically correlate with misfolded, destabilized or inactive protein. Therefore, we created the variants G78R, L76Q, T48R and C43Y within APSK37 (Oostdijk et al., 2015), expressed them in HeLa cells and studied their in-cell protein stability in comparison to the wt protein using Fast Relaxation Imaging (FReI). In FReI, a rapid perturbation of temperature is applied by absorption of infrared light (IR) by the sample (Ebbinghaus et al., 2010; Vöpel et al., 2017; Gnutt et al., 2019b) (Figures 1A,B). Dual-color imaging allows to measure changes in donor-to-acceptor intensity ratio (D/A) (Figure 1C) that display unfolding kinetics and thermodynamics of the protein in the cell (see Materials and Methods for details) (Figure 1D).

A structural analysis of the surface exposure of the disease-related mutants revealed that C43Y, T48R and L76Q are deeply buried in the protein core (solvent accessible surface area (SASA) $\leq 1 \text{ \AA}^2$) compared to G78R (Kabsch and Sander, 1983; Brylski et al., 2019); all of them located in close proximity in the central beta-sheet of the APSK (Figure 1E).

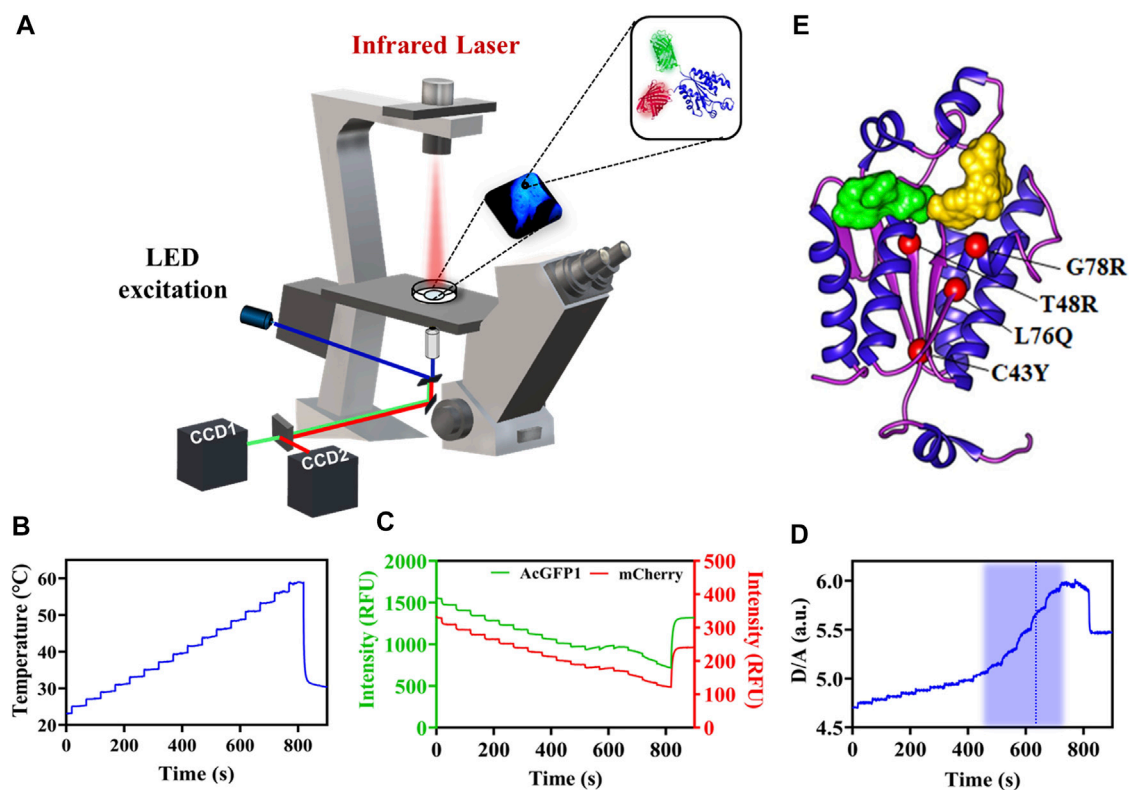


FIGURE 1 | In-cell thermal unfolding of APSK37 wt using Fast Relaxation Imaging. **(A)** Schematic representation of the Fast Relaxation Imaging setup. **(B)** Induced temperature profile calculated by the calibration procedure published in Büning et al., 2017. **(C)** Change in fluorescence according to the temperature profile in B of the APSK37 AcGFP1 FRET donor (D) and the mCherry FRET acceptor (A). **(D)** D/A ratio calculated from the intensity data in (C). The thermal unfolding region is shaded in blue and the calculated T_M is displayed by a dash blue line. **(E)** Crystal structure of the APSK domain of PAPSS2 (PDB:2AX4). Studied mutations are shown as red spheres. ADP/ATP (green) and APS/PAPS (yellow) binding sites are indicated by the substrates surface representation.

For APSK37 wt, we observed an increase of the normalized D/A ratio upon IR-laser heating and decrease after returning to the starting temperature (Figure 2A). This behavior is also evident for G78R mutant (Figure 2B), which exhibits an apparent two-state folding behavior as the respective unfolding kinetics can be fitted by a single exponential function. Plotting and fitting the respective amplitudes against temperature (Figures 2C,D) allowed the determination of a $T_M = 46.1 \pm 2.1^\circ\text{C}$ which is similar to wt ($48.0 \pm 1.7^\circ\text{C}$) (Figure 2E). Additionally, no significant differences were found with respect to the modified standard state free energies of folding ΔG_f^0 , suggesting that this mutation does not affect the stability of the protein (Figure 2F).

For the mutations C43Y, T48R and L76Q, we did not detect any unfolding transitions, impeding the determination of T_M . We rather observed a strong decrease in the D/A ratio (Figures 3A–C) that can be attributed to an increase in FRET by intermolecular energy transfer due to self-association (Ebbinghaus et al., 2010; Büning et al., 2017).

Self-Association and Aggregation of C43Y, T48R and L76Q

We then investigated if the self-association events observed in FRET result in the formation of microscopically visible aggregates.

We monitored their formation by wide-field fluorescence microscopy of EGFP-labeled full-length human PAPS synthase 2 carrying the disease mutants, expressed in HEK293 cells along with PAPSS 2 wt proteins. The cellular distribution pattern of the protein and degree of aggregate formation was scored by classifying individual cells according to the number of speckles that were visible inside each cell (Figure 4A). Figure 4B illustrates the cellular distribution pattern of the protein and the degree of aggregate formation for different mutants compared to PAPSS2 wt. The mutants C43Y, T48R and L76Q caused a higher number of aggregates compared to PAPSS2 wt. The level of aggregate formation of the G78R mutation is not significantly different from wt. Thus, the results show that the self-association of the C43Y, T48R and L76Q APSK37 proteins measured by FRET is in accordance with protein aggregation of the respective mutants in the full-length PAPSS2 protein. On the other hand, the G78R mutant is stable and does not lead to aggregation both in APSK37 and PAPSS2 proteins.

DISCUSSION

Generally, proteins with disease-related mutations either show a loss of catalytic function, a gain of toxic function (Winklhofer

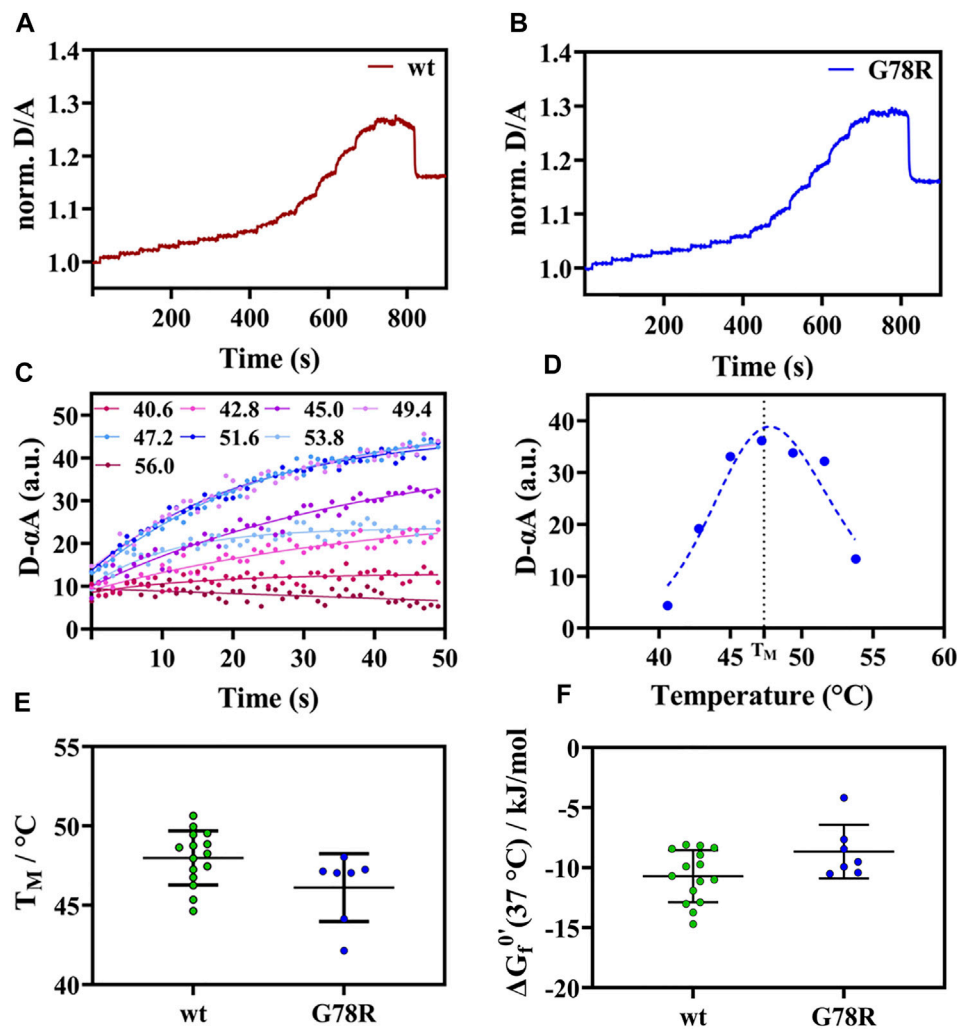


FIGURE 2 | Thermal unfolding curve APSK37 wt and mutants (G78R). **(A)** Exemplary temperature induced thermal unfolding curves of wt (data shown from (Brylski et al., 2021)). **(B)** Exemplary temperature induced thermal unfolding curves of G78R. **(C)** Exponential unfolding curves of single temperature jumps from panel (B) showing the relaxations kinetics at the respective temperatures. **(D)** Kinetic amplitudes as a function of temperature to determine the T_m (dashed line). **(E)** Thermal stability comparison of the mutant G78R with APSK37 wt: Melting points of APSK37 (green) and melting point of G78R (blue) derived from FRel measurement showing average \pm s.d. **(F)** Folding free energy $\Delta G_f^{0'}$ for both APSK37 wt and G78R mutant with mean \pm s.d. There are no statistically significant differences between wt and G78R. Significance were tested via one-way ANOVA with a *post-hoc* Holm-Sidak test correcting for multiple comparisons (no significant changes observed).

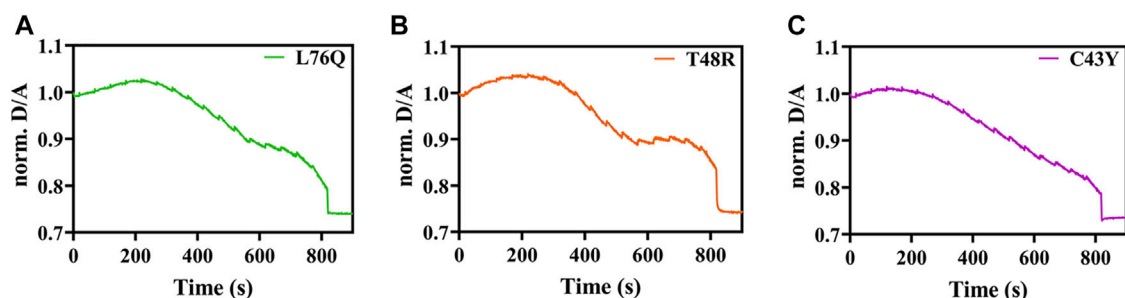


FIGURE 3 | Exemplary temperature-induced thermal unfolding curves of the L76Q, T48R, and C43Y mutants are visible in Figures 3A–C, respectively.

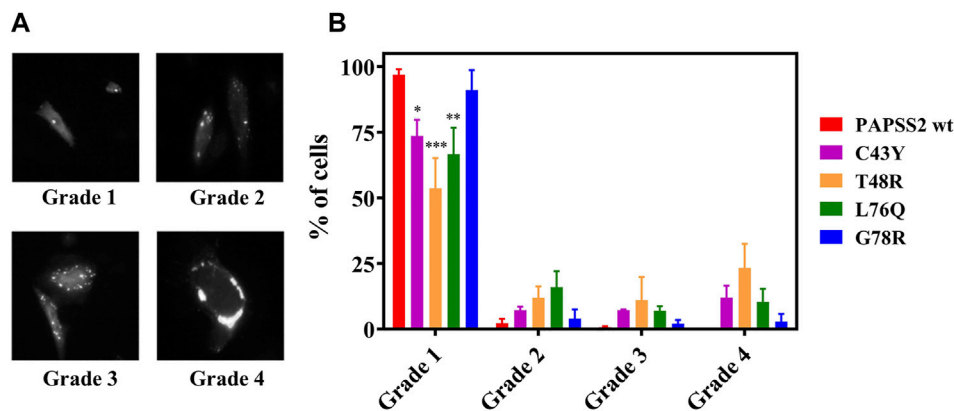


FIGURE 4 | Expression and distribution of recombinant human PAPSS in HEK293 cells. **(A)** Exemplary fluorescence image of HEK293 cells showing fluorescence spots classified according to three categories. **(B)** Even distribution; no speckles: grade 1, 1–3 speckles: grade 2, 4–10 speckles: grade 3 and more than 10 speckles or large clumps: grade 4. Data is presented as average \pm s.e.m. Cells were counted from four different slides ($N = 4$) with $n > 200$ cells in total for each protein variant. Asterisks indicate significant differences of the fraction of cells showing no speckles compared to PAPSS2 wt (* $p < 0.05$, *** $p < 0.001$). Additional statistical significance within grade 1 was found between G78R and T48R(***) or G78R and L76Q(*).

et al., 2008; De Baets et al., 2015) or a significant loss in stability of the protein leading to misfolding and aggregation (Waters, 2001; Denny et al., 2013; Gandhi et al., 2019). For PAPSS2, many studies have shown that disease-related gene defects cause different forms of bone and cartilage malformation (Kurima et al., 1998; Iida et al., 2013), as a consequence of under-sulfation of extracellular matrix. Dysregulation of steroid metabolism causing an increase in androgen activation is further associated with diseases like PCOS and premature pubarche (Noordam et al., 2009).

The results of this study show that PAPSS2 disease-related mutations cause a destabilization and aggregation of the enzyme in cellular environments for the mutants C43Y, T48R, L76Q. The G78R mutation however shows a folding stability that is comparable to wt, preventing aggregation. Regarding catalysis, Kurima and coworkers have reported that the G78R variant has very little residual APS kinase activity, but the ATP sulfurylase activity was comparable to wt (Kurima et al., 1998). Conformational changes of the APS binding site upon mutation, modifying the interaction between the ATP γ -phosphate group, the magnesium ion and the DGDN-loop can be a potential reason for the catalytic inhibition APS kinase (Kurima et al., 1998). The mutation may not disrupt the native fold, however, a catalytic conversion, for example due to a loss in flexibility within the DGDN-loop, may not be possible anymore.

The mutations C43Y, T48R, and L76Q destabilize APSK37 and lead to aggregation of both APSK37 and full-length PAPS synthase. All three mutations reside in the central β -sheet region of the protein (Figure 1E), suggesting that this is a sensitive region that maintains the native fold and prevents self-association and aggregation. Changes in the protein's native structure, protein-protein interactions and many other sequential and parallel events can lead to misfolded/unfolded conformations, resulting in aggregation. Protein aggregation is often linked with various pathologies, including neurodegenerative diseases, such

as Alzheimer's, Parkinson's and Huntington's. These disease-related aggregates are generally sub-divided into loss-of-function and gain-of- toxic function effects (Ross and Poirier, 2004; Wang, 2005; Soto and Pritzkow, 2018). Indeed, the three above-mentioned PAPSS mutations were previously classified as "missense mutants," causing its loss of function (Noordam et al., 2009; Iida et al., 2013). Missense mutations in nuclear deubiquitinase BAP1 were previously shown to induce destabilization and aggregation of this enzyme, with the latter being suggested as the main cause of its functional loss (Bhattacharya et al., 2016). In fact, this hypothesis is further supported by our previous studies (Brylski et al., 2021) using an alanine scanning mutagenesis of the substrate binding site of APSK37 in HeLa cells. The results revealed a large range of different in-cell stabilities for the single point mutations ($\Delta G_f^0 = -10.7$ to $+13.8$ kJ/mol).

Our results suggest two distinct possible disease mechanisms, one related to misfolding and aggregation, and the other one related to inhibition of catalytic function. However, whether these processes are causal for the different pathologies needs to be elucidated in future studies.

CONCLUSION

So far, many sulfotransferase-related mutations are known to be associated with the sulfation pathway but a lot less is reported for PAPSS. Our results report that PAPSS2 disease-related mutations cause misfolding and aggregation (L76Q, T48R, and C43Y), and inhibition of the catalytic function (G78R). Even though our study showed that the three missense mutants (L76Q, T48R and C43Y) lead to aggregation, the molecular details of this process remains to be explored, particularly putative cytotoxic effects of amyloid formation. Therapeutic approaches against the rare diseases that are associated with these mutations may thus be different, encompassing supplementation of lacking compounds

(Klinge et al., 2018) or inhibitors to reduce aggregation (Vöpel et al., 2017).

DATA AVAILABILITY STATEMENT

The original contributions presented in the study are included in the article/Supplementary Material, further inquiries can be directed to the corresponding authors.

AUTHOR CONTRIBUTIONS

JWM and SE, designed the study; OB, PS, PJH, and PG, acquired data. OB, PS, PJH, PG, JWM, and SE, analyzed and interpreted data. OB and JWM, drafted the work. OB, PS, JWM, and SE,

revised it critically for important intellectual content. All authors approved the final version of the manuscript and agreed to be accountable for all aspects of the work in ensuring that questions related to the accuracy or integrity of any part of the work are appropriately investigated and resolved.

FUNDING

We acknowledge funding from the Cluster of Excellence RESOLV (EXC 1069) and the Human Frontier Science Program (Research Grant RGP0022/2017). OB was supported by the Graduate School of Solvation Science (Ruhr University Bochum). JWM was supported by the European Commission Marie Curie Fellowship SUPA-HD (625451).

REFERENCES

- Ahmad, M., Ul Haque, M. F., Ahmad, W., Abbas, H., Haque, S., Krakow, D., et al. (1998). Distinct, Autosomal Recessive Form of Spondyloepimetaphyseal Dysplasia Segregating in an Inbred Pakistani kindred. *Am. J. Med. Genet.* 78, 468–473. doi:10.1002/(sici)1096-8628(19980806)78:5<468:aid-ajmg13>3.0.co;2-d
- Baranowski, E. S., Arlt, W., and Idkowiak, J. (2018). Monogenic Disorders of Adrenal Steroidogenesis. *Horm. Res. Paediatr.* 89, 292–310. doi:10.1159/000488034
- Bhattacharya, S., Hanpude, P., and Maiti, T. K. (2016). Cancer Associated Missense Mutations in BAP1 Catalytic Domain Induce Amyloidogenic Aggregation: A New Insight in Enzymatic Inactivation. *Sci. Rep.* 5, 18462. doi:10.1038/srep18462
- Bownass, L., Abbs, S., Armstrong, R., Baujat, G., Behzadi, G., Berentsen, R. D., et al. (2019). PAPSS2-related Brachyolmia: Clinical and Radiological Phenotype in 18 New Cases. *Am. J. Med. Genet.* 179, 1884–1894. doi:10.1002/ajmg.a.61282
- Brylski, O., Ebbinghaus, S., and Mueller, J. W. (2019). Melting Down Protein Stability: PAPS Synthase 2 in Patients and in a Cellular Environment. *Front. Mol. Biosci.* 6, 31. doi:10.3389/fmolb.2019.00031
- Brylski, O., Shrestha, P., Gnut, P., Gnut, D., Mueller, J. W., and Ebbinghaus, S. (2021). Cellular ATP Levels Determine the Stability of a Nucleotide Kinase. *Front. Mol. Biosci.* 8, 790304. doi:10.3389/fmolb.2021.790304
- Büning, S., Sharma, A., Vachharajani, S., Newcombe, E., Ormsby, A., Gao, M., et al. (2017). Conformational Dynamics and Self-Association of Intrinsically Disordered Huntingtin Exon 1 in Cells. *Phys. Chem. Chem. Phys.* 19, 10738–10747. doi:10.1039/C6CP08167C
- Cho, Y. R., Lee, S. J., Jeon, H. B., Park, Z. Y., Chun, J.-S., and Yoo, Y. J. (2004). Under-sulfation by PAPS Synthetase Inhibition Modulates the Expression of ECM Molecules during Chondrogenesis. *Biochem. Biophysical Res. Commun.* 323, 769–775. doi:10.1016/j.bbrc.2004.08.173
- De Baets, G., Van Doorn, L., Rousseau, F., and Schymkowitz, J. (2015). Increased Aggregation Is More Frequently Associated to Human Disease-Associated Mutations Than to Neutral Polymorphisms. *PLOS Comput. Biol.* 11, e1004374. doi:10.1371/journal.pcbi.1004374
- Denny, R. A., Gavrín, L. K., and Saiah, E. (2013). Recent Developments in Targeting Protein Misfolding Diseases. *Bioorg. Med. Chem. Lett.* 23, 1935–1944. doi:10.1016/j.bmcl.2013.01.089
- Dhar, A., Girdhar, K., Singh, D., Gelman, H., Ebbinghaus, S., and Gruebele, M. (2011). Protein Stability and Folding Kinetics in the Nucleus and Endoplasmic Reticulum of Eucaryotic Cells. *Biophysical J.* 101, 421–430. doi:10.1016/j.bpj.2011.05.071
- Ebbinghaus, S., Dhar, A., McDonald, J. D., and Gruebele, M. (2010). Protein Folding Stability and Dynamics Imaged in a Living Cell. *Nat. Methods* 7, 319–323. doi:10.1038/nmeth.1435
- Eltan, M., Yavas Abali, Z., Arslan Ates, E., Kirkgoz, T., Kaygusuz, S. B., Türkylmaz, A., et al. (2019). Low DHEAS Concentration in a Girl Presenting with Short Stature and Premature Pubarche: A Novel PAPSS2 Gene Mutation. *Horm. Res. Paediatr.* 92, 262–268. doi:10.1159/000502114
- Foster, P. A., and Mueller, J. W. (2018). SULFATION PATHWAYS: Insights into Steroid Sulfation and Desulfation Pathways. *J. Mol. Endocrinol.* 61, T271–T283. doi:10.1530/JME-18-0086
- Gandhi, J., Antonelli, A. C., Afridi, A., Vatsia, S., Joshi, G., Romanov, V., et al. (2019). Protein Misfolding and Aggregation in Neurodegenerative Diseases: a Review of Pathogeneses, Novel Detection Strategies, and Potential Therapeutics. *Rev. Neurosci.* 30, 339–358. doi:10.1515/revneuro-2016-0035
- Gao, M., Gnut, D., Orban, A., Appel, B., Righetti, F., Winter, R., et al. (2016). RNA Hairpin Folding in the Crowded Cell. *Angew. Chem. Int. Ed.* 55, 3224–3228. doi:10.1002/anie.201510847
- Gesteira, T. F., Marforio, T. D., Mueller, J. W., Calvaresi, M., and Coulson-Thomas, V. J. (2021). Structural Determinants of Substrate Recognition and Catalysis by Heparan Sulfate Sulfotransferases. *ACS Catal.* 11, 10974–10987. doi:10.1021/acscatal.1c03088
- Girdhar, K., Scott, G., Chemla, Y. R., and Gruebele, M. (2011). Better Biomolecule Thermodynamics from Kinetics. *J. Chem. Phys.* 135, 015102. doi:10.1063/1.3607605
- Gnut, D., Sistemich, L., and Ebbinghaus, S. (2019a). Protein Folding Modulation in Cells Subject to Differentiation and Stress. *Front. Mol. Biosci.* 6, 38. doi:10.3389/fmolb.2019.00038
- Gnut, D., Timr, S., Ahlers, J., König, B., Manderfeld, E., Heyden, M., et al. (2019b). Stability Effect of Quinary Interactions Reversed by Single Point Mutations. *J. Am. Chem. Soc.* 141, 4660–4669. doi:10.1021/jacs.8b13025
- Grum, D., van den Boom, J., Neumann, D., Matena, A., Link, N. M., and Mueller, J. W. (2010). A Heterodimer of Human 3'-Phospho-Adenosine-5'-Phosphosulphate (PAPS) Synthases Is a New Sulphate Activating Complex. *Biochem. Biophysical Res. Commun.* 395, 420–425. doi:10.1016/j.bbrc.2010.04.039
- Handa, A., Tham, E., Wang, Z., Horemuzova, E., and Grigeliuniene, G. (2016). Autosomal Recessive Brachyolmia: Early Radiological Findings. *Skeletal Radiol.* 45, 1557–1560. doi:10.1007/s00256-016-2458-8
- Haque, M. F. u., King, L. M., Krakow, D., Cantor, R. M., Rusiniak, M. E., Swank, R. T., et al. (1998). Mutations in Orthologous Genes in Human Spondyloepimetaphyseal Dysplasia and the Brachymorphic Mouse. *Nat. Genet.* 20, 157–162. doi:10.1038/2458
- Harjes, S., Bayer, P., and Scheidig, A. J. (2005). The Crystal Structure of Human PAPS Synthetase 1 Reveals Asymmetry in Substrate Binding. *J. Mol. Biol.* 347, 623–635. doi:10.1016/j.jmb.2005.01.005
- Iida, A., Simsek-Kiper, P. Ö., Mizumoto, S., Hoshino, T., Elcioglu, N., Horemuzova, E., et al. (2013). Clinical and Radiographic Features of the Autosomal Recessive Form of Brachyolmia Caused by PAPSS2 Mutations. *Hum. Mutat.* 34, 1381–1386. doi:10.1002/humu.22377
- Kabsch, W., and Sander, C. (1983). Dictionary of Protein Secondary Structure: Pattern Recognition of Hydrogen-Bonded and Geometrical Features. *Biopolymers* 22, 2577–2637. doi:10.1002/bip.360221211

- Klassen, C. D., and Boles, J. W. (1997). Sulfation and Sulfotransferases 5: the Importance of 3'-phosphoadenosine 5'-phosphosulfate (PAPS) in the Regulation of Sulfation. *FASEB J.* 11, 404–418. doi:10.1096/fasebj.11.6.9194521
- Klinge, C. M., Clark, B. J., and Prough, R. A. (2018). "Dehydroepiandrosterone Research: Past, Current, and Future," in *Vitamins and Hormones* (Cambridge, MA: Elsevier), 108.1–28. doi:10.1016/bs.vh.2018.02.002
- Kurima, K., Warman, M. L., Krishnan, S., Domowicz, M., Krueger, R. C., Deyrup, A., et al. (1998). A Member of a Family of Sulfate-Activating Enzymes Causes Murine Brachypodism. *Proc. Natl. Acad. Sci.* 95, 8681–8685. doi:10.1073/pnas.95.15.8681
- Miyake, N., Elcioglu, N. H., Iida, A., Isguven, P., Dai, J., Murakami, N., et al. (2012). PAPSS2 mutations Cause Autosomal Recessive Brachyolmia. *J. Med. Genet.* 49, 533–538. doi:10.1136/jmedgenet-2012-101039
- Mueller, J. W., Gilligan, L. C., Idkowiak, J., Arlt, W., and Foster, P. A. (2015). The Regulation of Steroid Action by Sulfation and Desulfation. *Endocr. Rev.* 36, 526–563. doi:10.1210/er.2015-1036
- Mueller, J. W., Idkowiak, J., Gesteira, T. F., Vallet, C., Hardman, R., van den Boom, J., et al. (2018). Human DHEA Sulfation Requires Direct Interaction between PAPS Synthase 2 and DHEA Sulfotransferase SULT2A1. *J. Biol. Chem.* 293, 9724–9735. doi:10.1074/jbc.RA118.002248
- Mueller, J. W., and Shafqat, N. (2013). Adenosine-5'-phosphosulfate - a Multifaceted Modulator of Bifunctional 3'-Phospho-Adenosine-5'-Phosphosulfate Synthases and Related Enzymes. *FEBS J.* 280, 3050–3057. doi:10.1111/febs.12252
- Noordam, C., Dhir, V., McNelis, J. C., Schlereth, F., Hanley, N. A., Krone, N., et al. (2009). Inactivating PAPSS2 Mutations in a Patient with Premature Pubarche. *N. Engl. J. Med.* 360, 2310–2318. doi:10.1056/NEJMoa0810489
- Oostdijk, W., Idkowiak, J., Mueller, J. W., House, P. J., Taylor, A. E., O'Reilly, M. W., et al. (2015). PAPSS2 Deficiency Causes Androgen Excess via Impaired DHEA Sulfation-In Vitro and In Vivo Studies in a Family Harboring Two Novel PAPSS2 Mutations. *J. Clin. Endocrinol. Metab.* 100, E672–E680. doi:10.1210/jc.2014-3556
- Paganini, C., Gramegna Tota, C., Superti-Furga, A., and Rossi, A. (2020). Skeletal Dysplasias Caused by Sulfation Defects. *Ijms* 21, 2710. doi:10.3390/ijms21082710
- Perez-Garcia, E. M., Whalen, P., and Gurtunca, N. (2021). Novel Inactivating Homozygous PAPSS2 Mutation in Two Siblings with Disproportionate Short Stature. *AACE Clin. Case Rep.* doi:10.1016/j.aace.2021.11.003 [https://www.aaceclinicalcasereports.com/article/S2376-0605\(21\)00121-8/fulltext](https://www.aaceclinicalcasereports.com/article/S2376-0605(21)00121-8/fulltext).
- Prydz, K. (2015). Determinants of Glycosaminoglycan (GAG) Structure. *Biomolecules* 5, 2003–2022. doi:10.3390/biom5032003
- Raman, R., Sasisekharan, V., and Sasisekharan, R. (2005). Structural Insights into Biological Roles of Protein-Glycosaminoglycan Interactions. *Chem. Biol.* 12, 267–277. doi:10.1016/j.chembiol.2004.11.020
- Ross, C. A., and Poirier, M. A. (2004). Protein Aggregation and Neurodegenerative Disease. *Nat. Med.* 10, S10–S17. doi:10.1038/nm1066
- Schröder, E., Gebel, L., Eremeev, A. A., Morgner, J., Grum, D., Knauer, S. K., et al. (2012). Human PAPS Synthase Isoforms Are Dynamically Regulated Enzymes with Access to Nucleus and Cytoplasm. *PLoS ONE* 7, e29559. doi:10.1371/journal.pone.0029559
- Sekulic, N., Dietrich, K., Paarmann, I., Ort, S., Konrad, M., and Lavie, A. (2007). Elucidation of the Active Conformation of the APS-Kinase Domain of Human PAPS Synthetase 1. *J. Mol. Biol.* 367, 488–500. doi:10.1016/j.jmb.2007.01.025
- Soto, C., and Pritzkow, S. (2018). Protein Misfolding, Aggregation, and Conformational Strains in Neurodegenerative Diseases. *Nat. Neurosci.* 21, 1332–1340. doi:10.1038/s41593-018-0235-9
- Strott, C. A. (2002). Sulfonation and Molecular Action. *Endocr. Rev.* 23, 703–732. doi:10.1210/er.2001-0040
- Tüysüz, B., Yılmaz, S., Gül, E., Kolb, L., Bilguvar, K., Evliyaoğlu, O., et al. (2013). Spondyloepimetaphyseal Dysplasia Pakistani Type: Expansion of the Phenotype. *Am. J. Med. Genet.* 161, 1300–1308. doi:10.1002/ajmg.a.35906
- van den Boom, J., Heider, D., Martin, S. R., Pastore, A., and Mueller, J. W. (2012). 3'-Phosphoadenosine 5'-Phosphosulfate (PAPS) Synthases, Naturally Fragile Enzymes Specifically Stabilized by Nucleotide Binding. *J. Biol. Chem.* 287, 17645–17655. doi:10.1074/jbc.M111.325498
- Vöpel, T., Bravo-Rodriguez, K., Mittal, S., Vachharajani, S., Gnutt, D., Sharma, A., et al. (2017). Inhibition of Huntingtin Exon-1 Aggregation by the Molecular Tweezer CLR01. *J. Am. Chem. Soc.* 139, 5640–5643. doi:10.1021/jacs.6b11039
- Vöpel, T., Scholz, R., Davico, L., Groß, M., Büning, S., Kareth, S., et al. (2015). Infrared Laser Triggered Release of Bioactive Compounds from Single Hard Shell Microcapsules. *Chem. Commun.* 51, 6913–6916. doi:10.1039/C4CC09745A
- Wang, W. (2005). Protein Aggregation and its Inhibition in Biopharmaceutics. *Int. J. Pharmaceutics* 289, 1–30. doi:10.1016/j.ijpharm.2004.11.014
- Waters, P. J. (2001). Degradation of Mutant Proteins, Underlying "Loss of Function" Phenotypes, Plays a Major Role in Genetic Disease. *Curr. Issues Mol. Biol.* 3 (3), 57–65. doi:10.21775/cimb.003.057
- Winklhofer, K. F., Tatzelt, J., and Haass, C. (2008). The Two Faces of Protein Misfolding: Gain- and Loss-Of-Function in Neurodegenerative Diseases. *EMBO J.* 27, 336–349. doi:10.1038/sj.emboj.7601930

Conflict of Interest: The authors declare that the research was conducted in the absence of any commercial or financial relationships that could be construed as a potential conflict of interest.

Publisher's Note: All claims expressed in this article are solely those of the authors and do not necessarily represent those of their affiliated organizations, or those of the publisher, the editors and the reviewers. Any product that may be evaluated in this article, or claim that may be made by its manufacturer, is not guaranteed or endorsed by the publisher.

Copyright © 2022 Brylski, Shrestha, House, Gnutt, Mueller and Ebbinghaus. This is an open-access article distributed under the terms of the Creative Commons Attribution License (CC BY). The use, distribution or reproduction in other forums is permitted, provided the original author(s) and the copyright owner(s) are credited and that the original publication in this journal is cited, in accordance with accepted academic practice. No use, distribution or reproduction is permitted which does not comply with these terms.



Sulfation Pathways During Neurodevelopment

Taylor Clarke¹, Francesca E. Fernandez¹ and Paul A. Dawson^{2*}

¹School of Behavioural and Health Sciences, Faculty of Health Sciences, Australian Catholic University, Banyo, QLD, Australia,

²Mater Research Institute, University of Queensland, Brisbane, QLD, Australia

Sulfate is an important nutrient that modulates a diverse range of molecular and cellular functions in mammalian physiology. Over the past 2 decades, animal studies have linked numerous sulfate maintenance genes with neurological phenotypes, including seizures, impaired neurodevelopment, and behavioral abnormalities. Despite sulfation pathways being highly conserved between humans and animals, less than one third of all known sulfate maintenance genes are clinically reportable. In this review, we curated the temporal and spatial expression of 91 sulfate maintenance genes in human fetal brain from 4 to 17 weeks post conception using the online Human Developmental Biology Resource Expression. In addition, we performed a systematic search of PubMed and Embase, identifying those sulfate maintenance genes linked to atypical neurological phenotypes in humans and animals. Those findings, together with a search of the Online Mendelian Inheritance in Man database, identified a total of 18 candidate neurological dysfunction genes that are not yet considered in clinical settings. Collectively, this article provides an overview of sulfate biology genes to inform future investigations of perturbed sulfate homeostasis associated with neurological conditions.

Keywords: sulfate, brain, embryological, fetal, gene expression, neurological dysfunction

OPEN ACCESS

Edited by:

Tarsis G. Ferreira,
Optimvia, United States

Reviewed by:

William Davies,
Cardiff University, United Kingdom
Antonio Rossi,
University of Pavia, Italy

*Correspondence:

Paul A. Dawson
paul.dawson@mater.uq.edu.au

Specialty section:

This article was submitted to
Cellular Biochemistry,
a section of the journal
Frontiers in Molecular Biosciences

Received: 30 January 2022

Accepted: 24 March 2022

Published: 14 April 2022

Citation:

Clarke T, Fernandez FE and
Dawson PA (2022) Sulfation Pathways
During Neurodevelopment.
Front. Mol. Biosci. 9:866196.
doi: 10.3389/fmolb.2022.866196

INTRODUCTION

Sulfate is essential for healthy growth and development (Dawson, 2011). Supplied from the diet and catabolism of sulfur-containing amino acids, intracellular sulfate is transformed into 3'-phosphoadenosine 5'-phosphosulfate (PAPS) which is the universal sulfate donor for sulfate conjugation (sulfonation) to a wide range of endogenous and exogenous molecules via sulfotransferases (Mulder and Jakoby, 1990). Sulfonation biotransforms the physiological properties of molecules, including: (i) inactivation of steroids, thyroid hormone and neurotransmitters (Darras et al., 1999; Richard et al., 2001; Dawson, 2012); (ii) detoxification of xenobiotics and certain pharmaceutical drugs (McCarver and Hines, 2002); and (iii) maintenance of tissue structure and function via the sulfate content of glycosaminoglycans (Yamaguchi, 2001). Sulfatases remove sulfate from substrates to maintain the required balance of sulfonated to unconjugated substrates (Hanson et al., 2004). Disturbances in any of these sulfation pathways has the potential for adverse physiological consequences.

In recent years, interest in human sulfate biology has expanded following animal studies that show adverse phenotypes linked to sulfate biology genes (Langford et al., 2017). Neurological dysfunction is one of the most predominant phenotypes linked to disturbances of sulfate biology. This is not surprising when considering that sulfonation biotransforms numerous target molecules in the brain, including inactivation of thyroid hormone, metabolism of neurotransmitters (e.g., serotonin, noradrenaline and dopamine) and modulation of neurosteroid actions on GABA_A, N-methyl-D-

TABLE 1 | Sulfate biology genes that are either clinically reportable or not yet captured in clinical genetics.

^aClinically reportable genes			Genes that have been investigated in research settings but are not yet captured in clinical resources
Green	Amber	Red	
Sulfate transporters			
<i>SLC4A1</i>	<i>SLC26A1</i>		<i>SLC13A1, SLC13A4, SLC26A6, SLC26A9, SLC26A11</i>
<i>SLC26A2</i>			
<i>SLC26A3</i>			
<i>SLC26A7</i>			
<i>SLC26A8</i>			
PAPS synthetases			
<i>PAPSS2</i>			<i>PAPSS1</i>
PAPS transporters			
			<i>SLC35B2, SLC35B3</i>
Key enzymes in the pathways of sulfate generation			
^b <i>CBS</i>	^b <i>CTH</i>		<i>CDO1, SQOR, TST</i>
<i>GOT1</i>			
^b <i>SUOX</i>			
Cytosolic sulfotransferases			
<i>SULT2B1</i>			<i>SULT1A1, SULT1A2, SULT1A3, SULT1A4, SULT1B1</i> <i>SULT1C2, SULT1C3, SULT1C4, SULT1E1, SULT2A1</i> <i>SULT4A1, SULT6B1</i>
Membrane-bound sulfotransferases			
^b <i>CHST3</i>	<i>CHST11</i>	^b <i>CHST8</i>	<i>CHST2, CHST4, CHST5, CHST7, CHST9</i>
^b <i>CHST6</i>	^b <i>HS2ST1</i>		<i>HS3ST6, CHST10, CHST12, CHST13, CHST15, GAL3ST1</i>
^b <i>CHST14</i>		^b <i>HS6ST1</i>	<i>GAL3ST2, GAL3ST3, GAL3ST4, HS3ST1, HS3ST2</i>
^b <i>NDST1</i>			<i>HS3ST3A1, HS3ST3B1, HS3ST4, HS3ST5, HS6ST2, HS6ST3, NDST2, NDST3, NDST4, TPST1, TPST2, UST</i>
Sulfatases and sulfatase modifying factors			
^b <i>ARSA</i>			<i>ARSD, ARSF, ARSG, ARSH, ARSJ, ARSK, SULF1, SULF2</i>
^b <i>ARSB</i>			<i>SUMF2</i>
^b <i>STS</i>			
^b <i>ARSE</i>			
^b <i>ARSI</i>			
^b <i>GALNS</i>			
^b <i>GNS</i>			
^b <i>IDS</i>			
^b <i>SGSH</i>			

^aGenes captured in clinical resources and coded green (high level of evidence), amber (medium level evidence, not yet used) and red (no strong evidence, do no use) by searching the online PanelAPP (<https://panelapp.gha.umccr.org/>) consensus diagnostic gene panels (Martin et al., 2019) 18–19 January 2022.

^bLinked to adverse neurological phenotype.

aspartate (NMDA) glutamergic and σ -opioid receptors (Rivett et al., 1982; Kríz et al., 2008). Sulfonation of proteoglycans (e.g., heparan sulfate) and cerebroside sulfate also plays an important role in maintaining the structure and function of brain tissue (Schwartz and Domowicz, 2018). Animal studies have also shown that hyposulfataemia leads to reduced sulfonation capacity and abnormal behavioral phenotypes, including impaired memory, increased anxiety and seizures in mice (Dawson et al., 2003; Dawson et al., 2004; Dawson et al., 2005). More recent studies have shown that reduced transfer of sulfate across the blood-brain barrier of neonatal mice leads to: (i) decreased heparan sulfate levels in the subventricular zone (SVZ) and rostral migratory stream; (ii) impairment in perineuronal net formation (which contains sulfonated proteoglycans) in the hippocampus and somatosensory cortex; (iii) increased neural stem cell proliferation and decreased neuronal maturation in the SVZ; (iv) seizures; and (v) impaired behavioral phenotypes, including impaired long-term spatial memory and defects in social interaction and social memory (Zhang et al., 2020). Despite the diverse roles for sulfate during neurodevelopment, most

human sulfate biology genes have not yet been considered in clinical genetics.

To date, 91 genes are known to contribute to maintaining sulfate homeostasis, including those encoding: sulfate transporters; PAPS synthetases and transporters; enzymes in the pathway of sulfate generation; cytosolic and membrane-bound sulfotransferases; and sulfatases (Langford et al., 2017). However, only 24 of these genes are currently considered in clinical genetics, with 16 of those genes linked to neurological dysfunction (Table 1). Animal studies have shown additional sulfate biology genes are linked to adverse neurological phenotypes (Langford et al., 2017), suggesting that the number of clinically reportable genes is currently underestimated. This warrants further investigation into the role of sulfate biology genes in human neurophysiology.

In this study, we curated the temporal and spatial mRNA expression patterns of all known sulfate biology genes in the developing human fetal brain between 4 and 17 weeks gestation, corresponding to a critical time for nervous system formation *in utero*. We show moderate to abundant mRNA expression levels

of 62 genes, suggesting a critical role of sulfate in early neurodevelopment. Additionally, we collated 18 sulfate biology genes implicated in atypical neurological function from the animal and human research literature which are currently not captured in clinical resources. Overall, these findings provide data for future investigations of sulfate biology genes associated with neurological dysfunction.

SULFATE BIOLOGY GENE EXPRESSION IN HUMAN FETAL BRAIN

We obtained data of gene expression in the human fetal brain from the online Human Developmental Biology Resource (HDBR) Expression (Lindsay et al., 2016) (<https://www.hdb.org/>) from 6 November 2021 to 12 January 2022. The HDBR is one of the rare human fetal tissue databases providing gene expression under 8 weeks post-conception compared to other databases (Johnson et al., 2009; Sunkin et al., 2013), which is essential for getting a better understanding of brain development since neurulation starts after 3 weeks post conception (O'Rahilly and Müller, 1994). Taking in account that brain development is dynamic, HDBR reports anatomical regionalisation gene expression results, which is also essential for mapping the differential pattern of gene expression related to selected brain regions compared to using full brain tissues (Ono et al., 2017). Data were available for four brain regions (cerebrum, brainstem, diencephalon and cerebellum) from 4 to 17 weeks post-conception. The gene expression levels for each tissue sample were averaged for each set of technical replicates, and then quantile normalized within each set of biological replicates using limma. Finally, they are averaged for all biological replicates. Specifically, we used transcripts per million (TPM) mapped reads-normalized RNA-Seq data to plot results for each gene. Of the 91 sulfate biology genes, 16 were abundantly expressed (>100 TPM) in at least one brain region at one gestational time point, 46 genes had moderate (>10 to 100 TPM) mRNA expression, and 15 genes had lower (≥ 0.1 to 10 TPM) mRNA expression levels (Figures 1–4). Fourteen genes (*SLC13A1*, *SLC26A3*, *SLC26A9*, *SULT1A4*, *SULT1C3*, *SULT2A1*, *SULT2B1*, *SULT6B1*, *CHST4*, *CHST13*, *GAL3ST2*, *HS3ST6*, *ARSH* and *ARSJ*) had undetectable or negligible (<0.1 TPM) mRNA expression levels (data not shown). The limitations of these data are that mRNA levels may: (i) not be representative of encoded protein level; (ii) not be predictive of functional impact when abnormal, for example altered expression of highly-expressed genes does not necessarily result in a more severe neurodevelopmental phenotype than altered expression of lowly-expressed genes; (iii) be redundant as other family member genes may compensate for altered expression level of a particular gene; (iv) not identify any sex-specific effects as the data are derived from pooled samples, which warrants future investigations to compare sulfate biology gene expression between male and female samples. Furthermore, our focus on genes expressed in the brain doesn't take into account any of the sulfate biology genes expressed in other tissues that may influence neurodevelopment, such as the thyroid or adrenal gland or testis

that could theoretically influence neurodevelopment through endocrine effects. Nonetheless, the temporal and spatial mRNA expression profiles of sulfate biology genes reported in the present study provide information for the next phase of research into understanding the regulation of sulfate homeostasis in the developing brain.

Genes Involved in Sulfate and PAPS Supply

Amongst the most abundantly expressed sulfate biology genes at all gestational time points are those involved in: (i) transporting sulfate from circulation to brain across the blood brain barrier (*SLC13A4*) (Zhang et al., 2020); (ii) the major (*CDO1*) and minor (*CTH*) biochemical pathways of sulfate generation (Dawson et al., 2020); and (iii) synthesis (*PAPSS1*) and transportation (*SLC35B2* and *SLC35B3*) of PAPS (Langford et al., 2017) (Figure 1). *SLC13A4* mRNA expression was specifically expressed in the cerebrum, indicating that sulfate transport from circulation likely contributes an important role in sulfate supply in early neurodevelopment. Of great interest are the data showing abundant mRNA expression of those genes involved in pathways of sulfate generation from the sulfur-containing amino acid cysteine. Previous studies suggested that the developing fetus has negligible capacity to generate sulfate, based on low *CDO1* and *CTH* mRNA expression levels in the liver (Gaull et al., 1972; Lorette and Chatagner, 1978). However, a more recent animal study showed the expression of *Cdo1* mRNA in the developing mouse fetus from mid-gestation (Rakoczy et al., 2015). The present study shows abundant expression of *CDO1*, suggesting that the fetal brain most likely generates sulfate, in addition to obtaining sulfate from circulation via *SLC13A4*. The present study also shows that *PAPSS1* is the most abundantly expressed sulfate biology gene in all four selected regions of the fetal brain, suggesting that this gene encodes for the predominant PAPS synthetase in fetal brain tissue, rather than *PAPSS2* which is expressed in cartilage and linked to developmental dwarfism disorders (Bownass et al., 2019). In addition, the findings of abundant *SLC35B2* and *SLC35B3* mRNA expression suggest that PAPS is actively transported in the golgi of fetal brain cells for sulfonation reactions via membrane-bound sulfotransferases. Collectively, these findings of abundant mRNA expression of genes involved in sulfate supply and generation, as well as generation and transport of PAPS, suggest that sulfate has an important physiological role in early fetal neurodevelopment.

Sulfotransferase Genes

There are two classes of sulfotransferases based on their protein sub-cellular localization: (i) cytosolic sulfotransferases which sulfonate neurotransmitters, bile acids, xenobiotics and steroids; and (ii) membrane-bound sulfotransferases that sulfonate proteoglycan and lipid molecules (Gamage et al., 2006). The present study shows abundant mRNA levels of four cytosolic (Figure 2) and 22 membrane-bound (Figure 3) sulfotransferases. *SULT4A1* is the most abundantly expressed cytosolic sulfotransferase mRNA in all four fetal brain regions. Whilst the substrate of *SULT4A1*-mediated sulfonation has not yet been identified, a recent study suggests it plays a role in the regulation of neuronal morphology and synaptic activity (Culotta

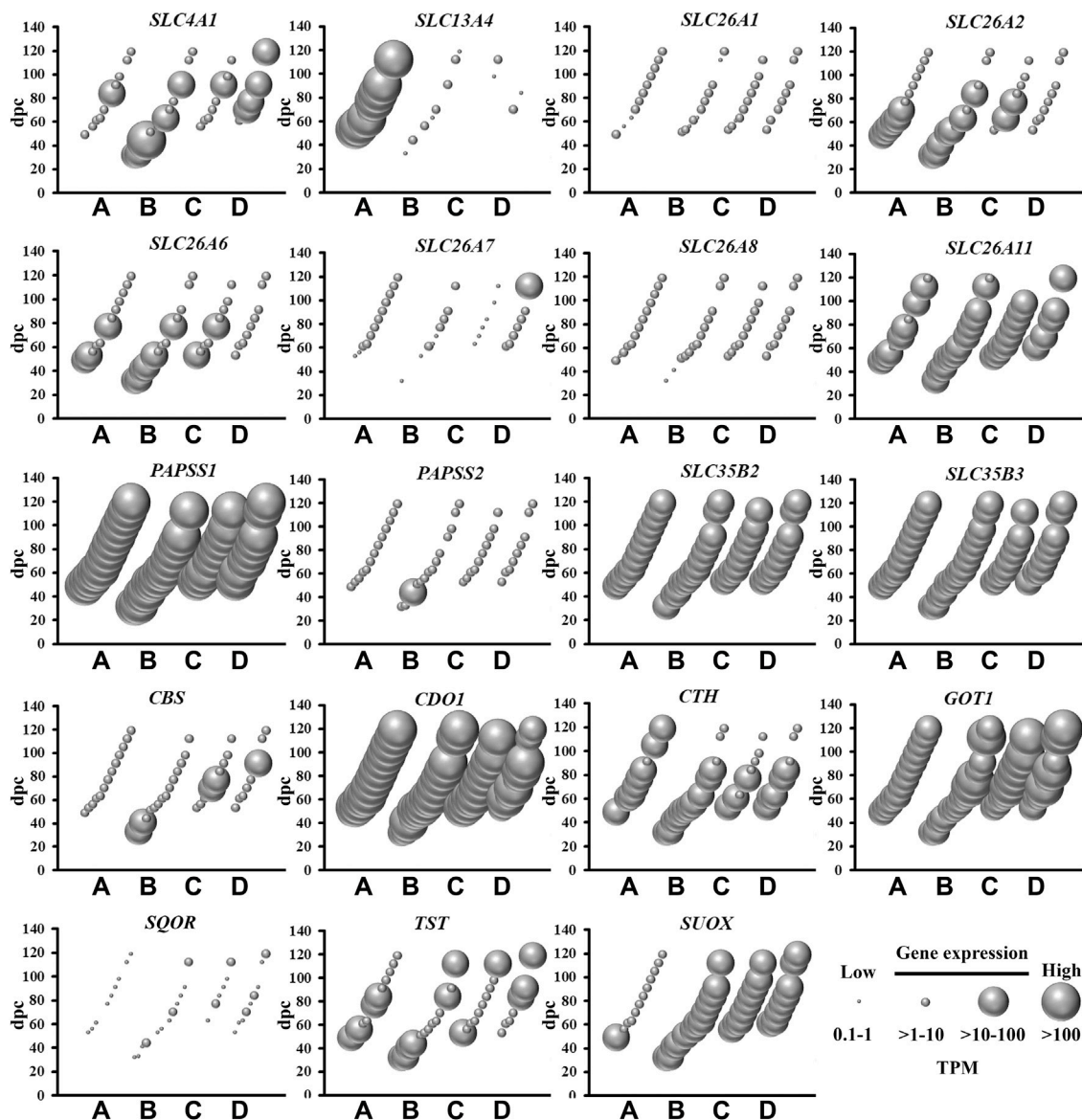
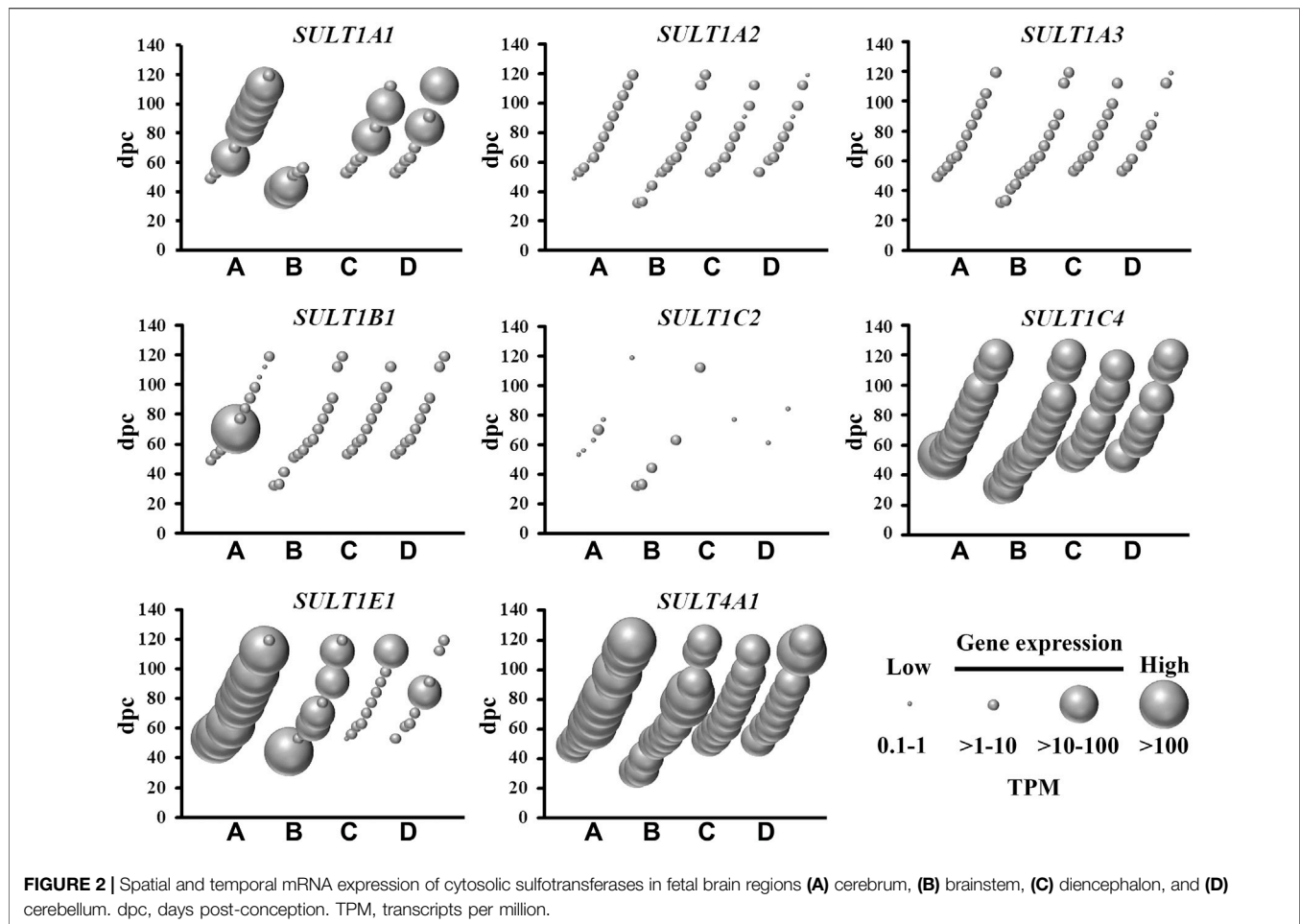


FIGURE 1 | Spatial and temporal mRNA expression of sulfate transporters, PAPS synthetases and transporters, and enzymes in the pathways of sulfate generation in fetal brain regions (A) cerebrum, (B) brainstem, (C) diencephalon, and (D) cerebellum. dpc, days post-conception. TPM, transcripts per million.

et al., 2020). Abundant mRNA levels of *SULT1E1* and *SULT1C4*, suggest that these two sulfotransferases, that sulfonate estrogenic compounds (Dawson, 2012), may regulate hormonal signalling pathways during fetal neurodevelopment. Interestingly, *SULT1E1* mRNA is mainly expressed in cerebrum, which is a critical region in hormonal regulation due to its development into the thalamic and hypothalamic structures modulating endocrine body system. *SULT1A1* mRNA expression was abundant in the cerebrum, with lower levels detected in the other three brain regions. *SULT1A1* sulfonates phenolic compounds, and while it has a major role of Phase II metabolism in the liver (Pacifci, 2005), it is also proposed to contribute to the detoxification and clearance of drugs and toxins in the brain (Salman et al., 2009). It is intriguing to see a single burst of abundant *SULT1B1*, iodothyronine

sulfotransferase (Stanley et al., 2005), mRNA expression at 10 weeks post-conception. This time point coincides with the early stage of neuronal migration, a neurodevelopmental process that relies on the action of thyroid hormone which is regulated by *SULT1B1*-mediated sulfonation (Wang et al., 1998; Morreale de Escobar et al., 2004). In addition to the cytosolic sulfotransferases, the majority of all known membrane-bound sulfotransferases were abundantly expressed (Figure 3), including: carbohydrate sulfotransferases *CHST1*, *CHST2*, *CHST3*, *CHST8*, *CHST10*, *CHST11*, *CHST14*, and *CHST15*; galactose 3-O-sulfotransferases *GAL3ST3* and *GAL3ST4*; heparan sulfate 2-O-sulfotransferase *HS2ST1*; heparan sulfate 3-O-sulfotransferases *HS3ST2*, *HS3ST4*, and *HS3ST5*; heparan sulfate 6-O-sulfotransferases *HS6ST1*, *HS6ST2* and *HS6ST3*;



heparan N-deacetylase/N-sulfotransferases *NDST1* and *NDST2*; tyrosylprotein sulfotransferase *TPST1*; and uronyl 2-sulfotransferase *UST*. Overall, these findings suggest the sulfonation of numerous substrates in the developing fetal brain.

Sulfatase Genes

The removal of sulfate from lipids, glycosaminoglycans and steroids is mediated by sulfatases (Hanson et al., 2004), of which nine are abundantly expressed in the fetal brain (Figure 4). This is relevant to sulfatases that target a range of substrates in the central nervous system, including sulfoglycolipids (*ARSA*), proteoglycans (*ARSB*, *ARSK*, *GNS*, *IDS*, *SULF1* and *SULF2*) and steroids (*STS*). With the exception of *STS*, all of these sulfatase genes were expressed in all four brain regions over the 4–17 weeks gestational period. *STS* mRNA level is low in cerebrum when compared to brainstem, diencephalon and cerebellum, suggesting that steroid activity is spatially confined to the latter three brain regions during early neurodevelopment. *SULF1* and *SULF2* mRNA, highly expressed in developing fetal brain, lead to the formation of enzyme removing 6-O-sulfate groups of proteoglycans and modulating morphogen Shh gradient during embryonic development. By modifying the Shh gradient in the embryo, the regulation of motorneuron to oligodendrocyte precursor cell fate change is

significantly affected in the developing ventral spinal cord (Jiang et al., 2017). The present study also shows abundant sulfatase modifying factor 2 (*SUMF2*) mRNA levels in comparison to low *SUMF1* mRNA levels, indicating that *SUMF2* is the major sulfatase regulating factor in early fetal brain tissue. There were short bursts of increased *ARSI*, *GALNS* and *SGSH* mRNA expression that were spatially enriched, suggesting a localized and temporary requirement for these glycosaminoglycans metabolizing sulfatases. Taken together, the abundant mRNA expression of numerous sulfatases indicates an active process of regulating sulfate content in the developing fetal brain.

CANDIDATE NEUROLOGICAL DYSFUNCTION SULFATE BIOLOGY GENES

Despite the mRNA expression of 62 sulfate biology genes in the fetal brain (Figures 1–4), only 12 of these genes are considered for neurological dysfunction in routine clinical genetics (Table 1). As an approach to inform clinical geneticists and potentially expand the list of clinically reportable genes, we undertook a systematic online search (10–23 September 2021). We used PubMed and Medline to identify sulfate biology genes reported to be associated with atypical neurological phenotypes in humans using the search

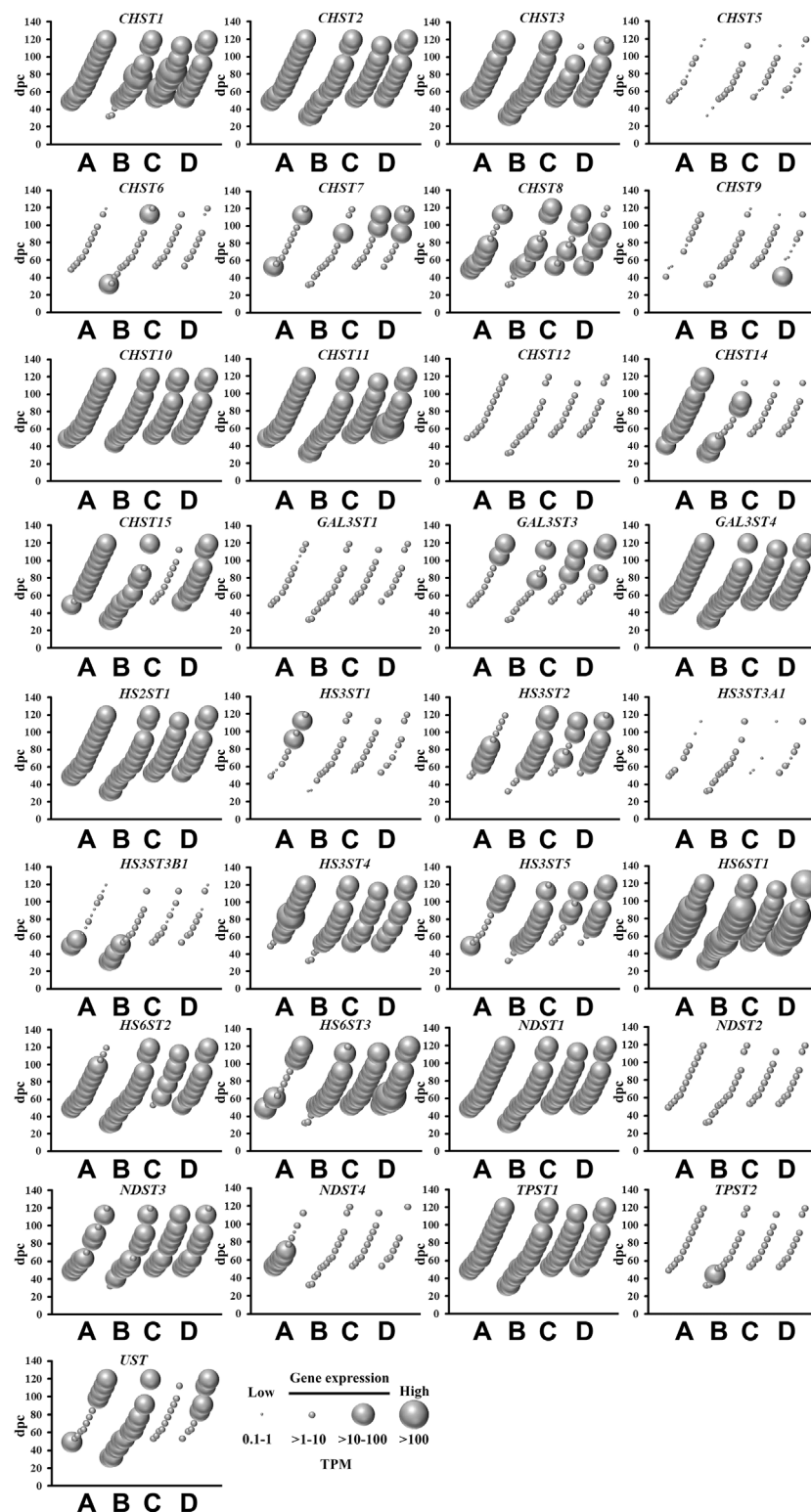


FIGURE 3 | Spatial and temporal mRNA expression of membrane-bound sulfotransferases in fetal brain regions (A) cerebrum, (B) brainstem, (C) diencephalon, and (D) cerebellum. dpc, days post-conception. TPM, transcripts per million.

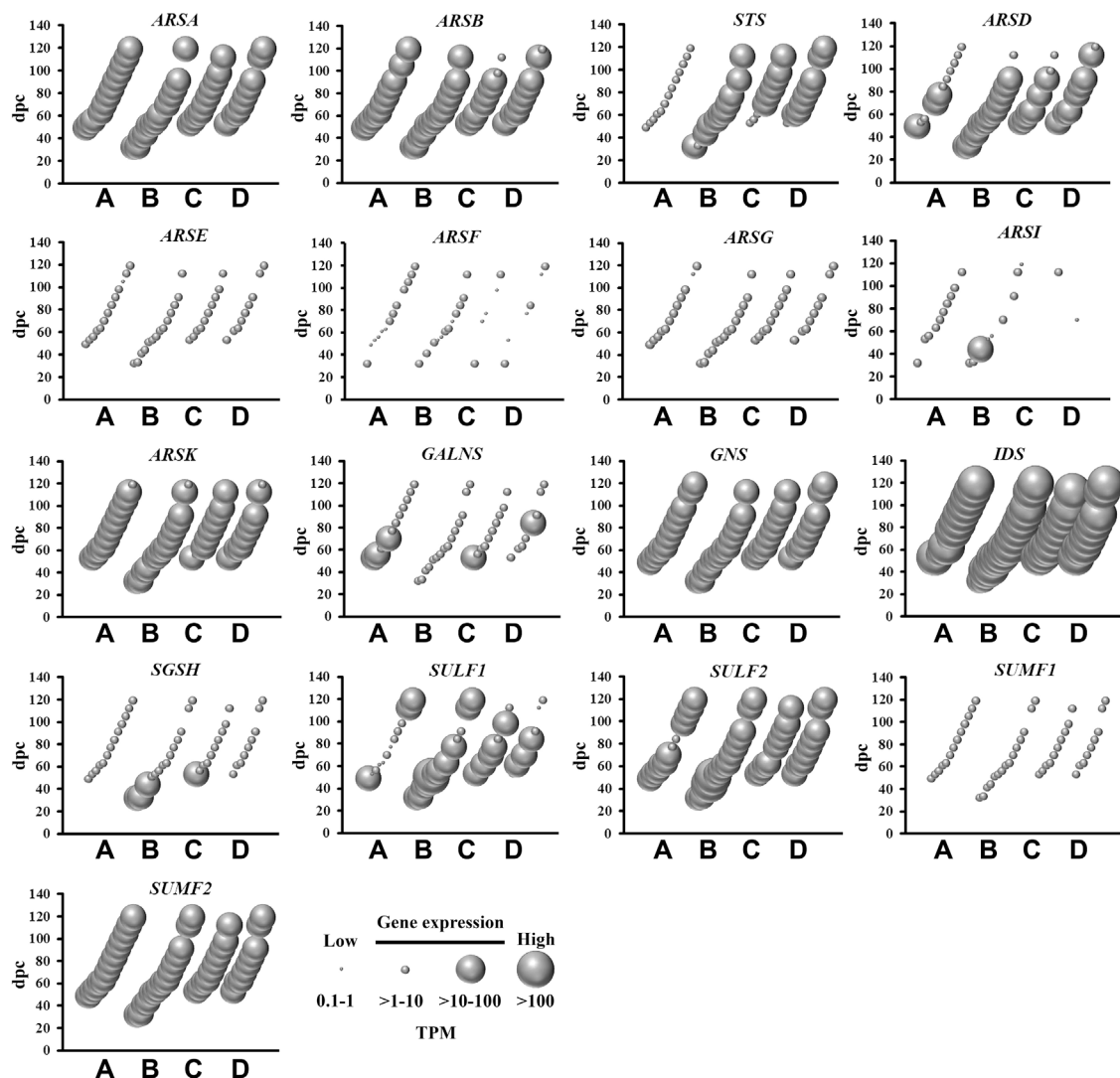


FIGURE 4 | Spatial and temporal mRNA expression of sulfatases and sulfatase modifying factors in fetal brain regions (A) cerebrum, (B) brainstem, (C) diencephalon, and (D) cerebellum. dpc, days post-conception. TPM, transcripts per million.

terms: (“brain” or “cerebellum” or “cerebral” or “neurodevelop”) and (“gene” or “dna” or “gene expression regulation” or “gene expression” or “gene genetic regulation”) and (“sulphate” or “sulfate” or “SO₄”). We included articles that associated any of the sulfate biology genes with neurological conditions. All references used in this study were peer-reviewed research articles published in English between January 2001 and September 2021. In addition, we used OMIM (<https://www.ncbi.nlm.nih.gov/omim/?term=>) to expand our search prior to 2001 and to include any research articles not captured in our literature search. Overall, our research literature and OMIM searches identified 42 research articles that report the involvement of sulfate biology genes in neurological dysfunction.

From the curated list of research articles, we identified 18 candidate neurological dysfunction genes that are not yet clinically reportable (Table 2). Ten of these genes were

reported from animal studies (*SLC13A1*, *SLC13A4*, *SLC35B2*, *CDO1*, *CHST12*, *CHST15*, *NDST2*, *NDST3*, *SULF2* and *UST*), 2 from human and animal studies (*ARSG* and *SULF1*) and 6 from human research studies (*SQOR*, *TST*, *SULT4A1*, *CHST10*, *HS6ST2* and *ARSK*). Thirteen of these genes are abundantly expressed in the human brain between 4 and 17 weeks gestation, whereas *SQOR*, *CHST12*, *NDST2* and *ARSG* are expressed at low level (Figures 1–4) and *SLC13A1* mRNA level is negligible (data not shown). The *SLC13A1* gene is primarily expressed in the proximal tubule of the kidney where it mediates sulfate reabsorption (Ullrich and Murer, 1982; Lee et al., 2005). Disruption of human *SLC13A1* and mouse *Slc13a1* causes renal sulfate wasting and hyposulfataemia, which is proposed to reduce sulfate supply to the brain (Dawson et al., 2003; Bowling et al., 2012). Sulfide: quinone oxidoreductase (*SQOR*) is an enzyme in the minor

TABLE 2 | Neurological phenotypes reported for sulfate biology genes that are not yet captured in clinical genetics.

Gene	Phenotypes (References)
Sulfate transporters	
<i>SLC13A1</i>	Mice: seizures, behavioural abnormalities (Dawson et al., 2003; Dawson et al., 2004; Dawson et al., 2005)
<i>SLC13A4</i>	Mice: impaired social behavior and neurogenesis (Zhang et al., 2019; Zhang et al., 2020)
PAPS transporters	
<i>SLC35B2</i>	<i>Drosophila</i> : pupal lethality (Kamiyama et al., 2003)
Key enzymes in the pathways of sulfate generation	
<i>CDO1</i>	Mice: fetal death and irregular shaped cranium (Ueki et al., 2011)
<i>SQOR</i>	Human: encephalopathy, seizures, coma, Leigh syndrome-like brain lesions (Friederich et al., 2020)
<i>TST</i>	Human: Leber optic atrophy (Cagianut et al., 1981)
Cytosolic sulfotransferases	
<i>SULT4A1</i>	Human: perturbed dendritic morphology and synaptic activity (Culotta et al., 2020)
Membrane-bound sulfotransferases	
<i>CHST10</i>	Human: T cell invasion and nerve damage during inflammation (Dasgupta et al., 2009)
<i>CHST12</i>	Mice: adverse cerebellar development (Ishii and Maeda, 2008)
<i>CHST15</i>	Mice: adverse cerebellar development (Ishii and Maeda, 2008)
<i>HS6ST2</i>	Human: Global developmental delay, intellectual disability, enlarged lateral ventricles (Paganini et al., 2019)
<i>NDST2</i>	Mice: Induction of neural cells (Forsberg et al., 2012)
<i>NDST3</i>	Mice: subtle behavioral abnormalities (Pallerla et al., 2008)
<i>UST</i>	Mice: adverse cerebellar development (Ishii and Maeda, 2008)
Sulfatases and sulfatase modifying factors	
<i>ARSG</i>	Human: Usher syndrome, Type IV (Abad-Morales et al., 2020; Fowler et al., 2021; Peter et al., 2021). Dog: cerebellar ataxia, neuronal ceroid lipofuscinosis (Abitbol et al., 2010)
<i>ARSK</i>	Human: Mucopolysaccharidosis type X (Verheyen et al., 2021)
<i>SULF1</i>	Human: microcephaly, diffuse or multifocal cerebral dysfunction (Day-Salvatore and McLean, 1998). Mice: Reduced hippocampal spine density and impaired long-term potentiation in CA1 (Kalus et al., 2009)
<i>SULF2</i>	Mice: Impaired generation of Olig2-expressing pMN-derived cell subtype (Ohayon et al., 2019). Mice: Congenital hydrocephalus and impaired spatial learning (Kalus et al., 2009)
<i>SULF1/2</i>	Mice: Corticospinal tract defects (Okada et al., 2017)

pathway of sulfate generation (Dawson, 2013) and its loss leads to excess hydrogen sulfide levels that cause encephalopathy and Leigh disease (Friederich et al., 2020). Individuals with *SQOR* mutations first present with coma in early childhood (Friederich et al., 2020), suggesting a physiological role for *SQOR* in the brain beyond the 17-week gestational end point used to assess gene expression in the present study. Increasing *CHST12*, *NDST2* and *ARSG* mRNA levels in brain at developmental ages beyond 17 weeks gestation (Humphries et al., 1998; Hiraoka et al., 2000; Khateb et al., 2018), also explains their low mRNA levels presented in this study. Nonetheless, the 18 genes listed in **Table 2**, warrant further research to determine whether these candidate neurological dysfunction genes are to be considered in clinical genetics.

SUMMARY

In this study, we show the moderate to abundant mRNA expression of 62 sulfate biology genes in the human fetal brain between 4 and 17 weeks post-conception, a critical period in nervous system formation. This relatively large number of genes highlights the physiological relevance of sulfate in neurodevelopment and is a testament to the genetic complexity of maintaining sulfate homeostasis. However, sulfate biology is underappreciated in clinical settings, with only 12 genes routinely considered for certain neurological conditions. Our finding of an additional 18 genes reported in the research literature with neurological dysfunction, warrants

future studies to validate the pathogenetics of these genes in human brain. Expanding the list of clinically reportable sulfate biology genes has the potential for improved genetic counselling, and potentially for developing therapeutic approaches towards clinical treatments. Overall, this study curated a list of sulfate biology genes involved in early brain development that provide information for future research of the physiological roles and regulation of sulfate homeostasis in human brain.

AUTHOR CONTRIBUTIONS

This study was designed by TC, FEF and PAD. Online searches were conducted by TC and PAD and all authors contributed to the preparation of the manuscript and approved the final version.

FUNDING

This study was funded by the Mater Foundation. PAD is supported by a Mater Foundation Principal Research Fellowship.

ACKNOWLEDGMENTS

We acknowledge the administrative and IT support of Mater Research Ltd. for this research that was carried out in part at the Translational Research Institute (TRI), which is supported by a grant from the Australian Government.

REFERENCES

- Abad-Morales, V., Navarro, R., Burés-Jelstrup, A., and Pomares, E. (2020). Identification of a Novel Homozygous ARSG Mutation as the Second Cause of Usher Syndrome Type 4. *Am. J. Ophthalmol. Case Rep.* 19, 100736. doi:10.1016/j.ajoc.2020.100736
- Abitol, M., Thibaud, J.-L., Olby, N. J., Hitte, C., Puech, J.-P., Maurer, M., et al. (2010). A Canine Arylsulfatase G (ARSG) Mutation Leading to a Sulfatase Deficiency Is Associated with Neuronal Ceroid Lipofuscinosis. *Proc. Natl. Acad. Sci. U.S.A.* 107 (33), 14775–14780. doi:10.1073/pnas.0914206107
- Bowling, F. G., Heussler, H. S., McWhinney, A., and Dawson, P. A. (2012). Plasma and Urinary Sulfate Determination in a Cohort with Autism. *Biochem. Genet.* 51 (1–2), 147–153. doi:10.1007/s10528-012-9550-0
- Bownass, L., Abbs, S., Armstrong, R., Baujat, G., Behzadi, G., Berentsen, R. D., et al. (2019). PAPSS2 -related Brachyolmia: Clinical and Radiological Phenotype in 18 New Cases. *Am. J. Med. Genet.* 179 (9), 1884–1894. doi:10.1002/ajmg.a.61282
- Cagianut, B., Rhyner, K., Furrer, W., and Schnebli, H. P. (1981). Thiosulphate-sulphur Transferase (Rhodanese) Deficiency in Leber's Hereditary Optic Atrophy. *The Lancet* 318 (8253), 981–982. doi:10.1016/s0140-6736(81)91171-5
- Culotta, L., Scalmani, P., Vinci, E., Terragni, B., Sessa, A., Broccoli, V., et al. (2020). SULT4A1 Modulates Synaptic Development and Function by Promoting the Formation of PSD-95/NMDAR Complex. *J. Neurosci.* 40 (37), 7013–7026. doi:10.1523/jneurosci.2194-19.2020
- Darras, V. M., Hume, R., and Visser, T. J. (1999). Regulation of Thyroid Hormone Metabolism during Fetal Development. *Mol. Cell. Endocrinol.* 151 (1–2), 37–47. doi:10.1016/s0303-7207(99)00088-x
- Dasgupta, S., Silva, J., Wang, G., and Yu, R. K. (2009). Sulfoglucuronosyl Paragloboside Is a Ligand for T Cell Adhesion: Regulation of Sulfoglucuronosyl Paragloboside Expression via Nuclear Factor κ B Signaling. *J. Neurosci. Res.* 87 (16), 3591–3599. doi:10.1002/jnr.22153
- Dawson, P. A., Beck, L., and Markovich, D. (2003). Hyposulfatemia, Growth Retardation, Reduced Fertility, and Seizures in Mice Lacking a Functional NaS I -1 Gene. *Proc. Natl. Acad. Sci. U.S.A.* 100 (23), 13704–13709. doi:10.1073/pnas.2231298100
- Dawson, P. A. (2013). Role of Sulphate in Development. *Reproduction* 146 (3), R81–R89. doi:10.1530/REP-13-0056
- Dawson, P. A., Steane, S. E., and Markovich, D. (2004). Behavioural Abnormalities of the Hyposulphataemic NaS1 Knock-Out Mouse. *Behav. Brain Res.* 154 (2), 457–463. doi:10.1016/j.bbr.2004.03.013
- Dawson, P. A., Steane, S. E., and Markovich, D. (2005). Impaired Memory and Olfactory Performance in NaSi-1 Sulphate Transporter Deficient Mice. *Behav. Brain Res.* 159, 15–20. doi:10.1016/j.bbr.2004.09.020
- Dawson, P. A. (2011). Sulfate in Fetal Development. *Semin. Cell Developmental Biol.* 22 (6), 653–659. doi:10.1016/j.semcdb.2011.03.004
- Dawson, P. A. (2012). "The Biological Roles of Steroid Sulfonation," in *Steroids - from Physiology to Clinical Medicine*. Editor S. M. Ostojic (Rijeka: Intech), 45–64.
- Dawson, P. A., Weerasekera, S. J., Atcheson, R. J., Twomey, S. A., and Simmons, D. G. (2020). Molecular Analysis of the Human Placental Cysteine Dioxygenase Type 1 Gene. *Mol. Genet. Metab. Rep.* 22, 100568. doi:10.1016/j.ymgmr.2020.100568
- Day-Salvatore, D., and McLean, D. (1998). Blepharophimosis, Hypoplastic Radius, Hypoplastic Left Heart, Telecanthus, Hydronephrosis, Fused Metacarpals, and ?prehensile? Halluces: A New Syndrome? *Am. J. Med. Genet.* 80 (4), 309–313. doi:10.1002/(sici)1096-8628(19981204)80:4<309::aid-ajmg2>3.0.co;2-j
- Forsberg, M., Holmborn, K., Kundu, S., Dagälv, A., Kjellén, L., and Forsberg-Nilsson, K. (2012). Undersulfation of Heparan Sulfate Restricts Differentiation Potential of Mouse Embryonic Stem Cells. *J. Biol. Chem.* 287 (14), 10853–10862. doi:10.1074/jbc.M111.337030
- Fowler, N. H., El-Rashedy, M. I., Chishti, E. A., Vander Kooi, C. W., and Maldonado, R. S. (2021). Multimodal Imaging and Genetic Findings in a Case of ARSG-Related Atypical Usher Syndrome. *Ophthalmic Genet.* 42 (3), 338–343. doi:10.1080/13816810.2021.1891552
- Friederich, M. W., Elias, A. F., Kuster, A., Laugwitz, L., Larson, A. A., Landry, A. P., et al. (2020). Pathogenic Variants in SQOR Encoding Sulfide:quinone Oxidoreductase Are a Potentially Treatable Cause of Leigh Disease. *Jrnl Inher Metab. Disea* 43 (5), 1024–1036. doi:10.1002/jimd.12232
- Gamage, N., Barnett, A., Hempel, N., Duggleby, R. G., Windmill, K. F., Martin, J. L., et al. (2006). Human Sulfotransferases and Their Role in Chemical Metabolism. *Toxicol. Sci.* 90 (1), 5–22. doi:10.1093/toxsci/kfj061
- Gaull, G., Sturman, J. A., and Räihä, N. C. R. (1972). Development of Mammalian Sulfur Metabolism: Absence of Cystathionase in Human Fetal Tissues. *Pediatr. Res.* 6 (6), 538–547. doi:10.1203/00006450-197206000-00002
- Hanson, S. R., Best, M. D., and Wong, C.-H. (2004). Sulfatases: Structure, Mechanism, Biological Activity, Inhibition, and Synthetic Utility. *Angew. Chem. Int. Ed.* 43 (43), 5736–5763. doi:10.1002/anie.200300632
- Hiraoka, N., Nakagawa, H., Ong, E., Akama, T. O., Fukuda, M. N., and Fukuda, M. (2000). Molecular Cloning and Expression of Two Distinct Human Chondroitin 4-O-Sulfotransferases that Belong to the HNK-1 Sulfotransferase Gene Family. *J. Biol. Chem.* 275 (26), 20188–20196. doi:10.1074/jbc.M002443200
- Humphries, D. E., Lanciotti, J., and Karlinsky, J. B. (1998). cDNA Cloning, Genomic Organization and Chromosomal Localization of Human Heparan Glucosaminyl N-deacetylase/N-Sulphotransferase-2. *Biochem. J.* 332 (Pt 2), 303–307. doi:10.1042/bj320303
- Ishii, M., and Maeda, N. (2008). Spatiotemporal Expression of Chondroitin Sulfate Sulfotransferases in the Postnatal Developing Mouse Cerebellum. *Glycobiology* 18 (8), 602–614. doi:10.1093/glycob/cwn040
- Jiang, W., Ishino, Y., Hashimoto, H., Keino-Masu, K., Masu, M., Uchimura, K., et al. (2017). Sulfatase 2 Modulates Fate Change from Motor Neurons to Oligodendrocyte Precursor Cells through Coordinated Regulation of Shh Signaling with Sulfatase 1. *Dev. Neurosci.* 39 (5), 361–374. doi:10.1159/000464284
- Johnson, M. H., Grossmann, T., and Kadosh, K. C. (2009). Mapping Functional Brain Development: Building a Social Brain through Interactive Specialization. *Developmental Psychol.* 45 (1), 151–159. doi:10.1037/a0014548
- Kalus, I., Salmen, B., Viebahn, C., Figura, K. v., Schmitz, D., D'Hooge, R., et al. (2009). Differential Involvement of the Extracellular 6-O-Endosulfatases Sulf1 and Sulf2 in Brain Development and Neuronal and Behavioural Plasticity. *J. Cell Mol Med* 13 (11–12), 4505–4521. doi:10.1111/j.1582-4934.2008.00558.x
- Kamiyama, S., Suda, T., Ueda, R., Suzuki, M., Okubo, R., Kikuchi, N., et al. (2003). Molecular Cloning and Identification of 3'-Phosphoadenosine 5'-Phosphosulfate Transporter. *J. Biol. Chem.* 278 (28), 25958–25963. doi:10.1074/jbc.M302439200
- Khateb, S., Kowalewski, B., Bedoni, N., Damme, M., Pollack, N., Saada, A., et al. (2018). A Homozygous Founder Missense Variant in Arylsulfatase G Abolishes its Enzymatic Activity Causing Atypical Usher Syndrome in Humans. *Genet. Med.* 20 (9), 1004–1012. doi:10.1038/gim.2017.227
- Kříž, L., Bičíková, M., and Hampl, R. (2008). Roles of Steroid Sulfatase in Brain and Other Tissues. *Physiol. Res.* 57 (5), 657–668. doi:10.33549/physiolres.931207
- Langford, R., Hurrión, E., and Dawson, P. A. (2017). Genetics and Pathophysiology of Mammalian Sulfate Biology. *J. Genet. Genomics* 44, 7–20. doi:10.1016/j.jgg.2016.08.001
- Lee, A., Dawson, P. A., and Markovich, D. (2005). NaSi-1 and Sat-1: Structure, Function and Transcriptional Regulation of Two Genes Encoding Renal Proximal Tubular Sulfate Transporters. *Int. J. Biochem. Cell Biol.* 37 (7), 1350–1356. doi:10.1016/j.biocel.2005.02.013
- Lindsay, S. J., Xu, Y., Lisgo, S. N., Harkin, L. F., Copp, A. J., Gerrelli, D., et al. (2016). HDBR Expression: A Unique Resource for Global and Individual Gene Expression Studies during Early Human Brain Development. *Front. Neuroanat.* 10, 86. doi:10.3389/fnana.2016.00086
- Loriette, C., and Chatagner, F. (1978). Cysteine Oxidase and Cysteine Sulfenic Acid Decarboxylase in Developing Rat Liver. *Experientia* 34 (8), 981–982. doi:10.1007/BF01915299
- Martin, A. R., Williams, E., Foulger, R. E., Leigh, S., Daugherty, L. C., Niblock, O., et al. (2019). PanelApp Crowdsources Expert Knowledge to Establish Consensus Diagnostic Gene Panels. *Nat. Genet.* 51 (11), 1560–1565. doi:10.1038/s41588-019-0528-2
- McCarver, D. G., and Hines, R. N. (2002). The Ontogeny of Human Drug-Metabolizing Enzymes: Phase II Conjugation Enzymes and Regulatory Mechanisms: Table 1. *J. Pharmacol. Exp. Ther.* 300 (2), 361–366. doi:10.1124/jpet.300.2.361

- Morreale de Escobar, G., Obregon, M., and Escobar del Rey, F. (2004). Role of Thyroid Hormone during Early Brain Development. *Eur. J. Endocrinol.* 151 (Suppl. 3), U25–U37. doi:10.1530/eje.0.151u025
- Mulder, G. J., and Jakoby, W. B. (1990). "Sulfation," in *Conjugation Reactions in Drug Metabolism: An Integrated Approach: Substrates, Co-substrates, Enzymes and Their Interactions in Vivo and in Vitro*. Editor G. J. Mulder (London: Taylor & Francis), 107–161.
- O'Rahilly, R., and Müller, F. (1994). Neurulation in the normal Human Embryo. *Ciba Found. Symp.* 181, 70–89. ; discussion 82–79. doi:10.1002/9780470514559.ch5
- Ohayon, D., Escalas, N., Cochard, P., Glise, B., Danesin, C., and Soula, C. (2019). Sulfatase 2 Promotes Generation of a Spinal Cord Astrocyte Subtype that Stands Out through the Expression of Olig2. *Glia* 67 (8), 1478–1495. doi:10.1002/glia.23621
- Okada, T., Keino-Masu, K., Nagamine, S., Kametani, F., Ohto, T., Hasegawa, M., et al. (2017). Desulfation of Heparan Sulfate by Sulf1 and Sulf2 Is Required for Corticospinal Tract Formation. *Sci. Rep.* 7 (1), 13847. doi:10.1038/s41598-017-14185-3
- Ono, H., Ogasawara, O., Okubo, K., and Bono, H. (2017). RefEx, a Reference Gene Expression Dataset as a Web Tool for the Functional Analysis of Genes. *Sci. Data* 4, 170105. doi:10.1038/sdata.2017.105
- Pacifici, G. M. (2005). Sulfation of Drugs and Hormones in Mid-gestation Human Fetus. *Early Hum. Development* 81 (7), 573–581. doi:10.1016/j.earlhumdev.2004.10.021
- Paganini, L., Hadi, L. A., Chetta, M., Rovina, D., Fontana, L., Colapietro, P., et al. (2019). A HS6ST2 Gene Variant Associated with X-linked Intellectual Disability and Severe Myopia in Two Male Twins. *Clin. Genet.* 95 (3), 368–374. doi:10.1111/cge.13485
- Pallerla, S. R., Lawrence, R., Lewejohann, L., Pan, Y., Fischer, T., Schlomann, U., et al. (2008). Altered Heparan Sulfate Structure in Mice with Deleted NDST3 Gene Function. *J. Biol. Chem.* 283 (24), 16885–16894. doi:10.1074/jbc.M709774200
- Peter, V. G., Quinodoz, M., Sadio, S., Held, S., Rodrigues, M., Soares, M., et al. (2021). New Clinical and Molecular Evidence Linking Mutations in ARSG to Usher Syndrome Type IV. *Hum. Mutat.* 42 (3), 261–271. doi:10.1002/humu.24150
- Rakoczy, J., Lee, S., Weerasekera, S. J., Simmons, D. G., and Dawson, P. A. (2015). Placental and Fetal Cysteine Dioxygenase Gene Expression in Mouse Gestation. *Placenta* 36 (8), 956–959. doi:10.1016/j.placenta.2015.06.003
- Richard, K., Hume, R., Kaptein, E., Stanley, E. L., Visser, T. J., and Coughtrie, M. W. H. (2001). Sulfation of Thyroid Hormone and Dopamine during Human Development: Ontogeny of Phenol Sulfotransferases and Arylsulfatase in Liver, Lung, and Brain1. *J. Clin. Endocrinol. Metab.* 86 (6), 2734–2742. doi:10.1210/jcem.86.6.7569
- Rivett, A. J., Eddy, B. J., and Roth, J. A. (1982). Contribution of Sulfate Conjugation, Deamination, and O-Methylation to Metabolism of Dopamine and Norepinephrine in Human Brain. *J. Neurochem.* 39 (4), 1009–1016. doi:10.1111/j.1471-4159.1982.tb11490.x
- Salman, E. D., Kadlubar, S. A., and Falany, C. N. (2009). Expression and Localization of Cytosolic Sulfotransferase (SULT) 1A1 and SULT1A3 in normal Human Brain. *Drug Metab. Dispos* 37 (4), 706–709. doi:10.1124/dmd.108.025767
- Schwartz, N. B., and Domowicz, M. S. (2018). Proteoglycans in Brain Development and Pathogenesis. *FEBS Lett.* 592 (23), 3791–3805. doi:10.1002/1873-3468.13026
- Stanley, E. L., Hume, R., and Coughtrie, M. W. H. (2005). Expression Profiling of Human Fetal Cytosolic Sulfotransferases Involved in Steroid and Thyroid Hormone Metabolism and in Detoxification. *Mol. Cell Endocrinol.* 240 (1–2), 32–42. doi:10.1016/j.mce.2005.06.003
- Sunkin, S. M., Ng, L., Lau, C., Dolbeare, T., Gilbert, T. L., Thompson, C. L., et al. (2013). Allen Brain Atlas: an Integrated Spatio-Temporal portal for Exploring the central Nervous System. *Nucleic Acids Res.* 41, D996–d1008. doi:10.1093/nar/gks1042
- Ueki, I., Roman, H. B., Valli, A., Fieselmann, K., Lam, J., Peters, R., et al. (2011). Knockout of the Murine Cysteine Dioxygenase Gene Results in Severe Impairment in Ability to Synthesize Taurine and an Increased Catabolism of Cysteine to Hydrogen Sulfide. *Am. J. Physiology-Endocrinology Metab.* 301 (4), E668–E684. doi:10.1152/ajpendo.00151.2011
- Ullrich, K. J., and Murer, H. (1982). Sulphate and Phosphate Transport in the Renal Proximal Tubule. *Phil. Trans. R. Soc. Lond. B* 299, 549–558. doi:10.1098/rstb.1982.0151
- Verheyen, S., Blatterer, J., Speicher, M. R., Bhavani, G. S., Boons, G.-J., Ilse, M.-B., et al. (2021). Novel Subtype of Mucopolysaccharidosis Caused by Arylsulfatase K (ARSK) Deficiency. *J. Med. Genet.*, 16, jmedgenet–2021. doi:10.1136/jmedgenet-2021-108061
- Wang, J., Falany, J. L., and Falany, C. N. (1998). Expression and Characterization of a Novel Thyroid Hormone-Sulfating Form of Cytosolic Sulfotransferase from Human Liver. *Mol. Pharmacol.* 53 (2), 274–282. doi:10.1124/mol.53.2.274
- Yamaguchi, Y. (2001). Heparan Sulfate Proteoglycans in the Nervous System: Their Diverse Roles in Neurogenesis, Axon Guidance, and Synaptogenesis. *Semin. Cell Developmental Biol.* 12 (2), 99–106. doi:10.1006/scdb.2000.0238
- Zhang, Z., Dawson, P. A., Piper, M., and Simmons, D. G. (2019). Postnatal N-Acetylcysteine Administration Rescues Impaired Social Behaviors and Neurogenesis in Slc13a4 Haploinsufficient Mice. *EBioMedicine* 43, 435–446. doi:10.1016/j.ebiom.2019.03.081
- Zhang, Z., Jhaveri, D., Sharmin, S., Harvey, T. J., Dawson, P. A., Piper, M., et al. (2020). Cell-extrinsic Requirement for Sulfate in Regulating Hippocampal Neurogenesis. *Biol. Open* 9 (7). doi:10.1242/bio.053132

Conflict of Interest: The authors declare that the research was conducted in the absence of any commercial or financial relationships that could be construed as a potential conflict of interest.

Publisher's Note: All claims expressed in this article are solely those of the authors and do not necessarily represent those of their affiliated organizations, or those of the publisher, the editors and the reviewers. Any product that may be evaluated in this article, or claim that may be made by its manufacturer, is not guaranteed or endorsed by the publisher.

Copyright © 2022 Clarke, Fernandez and Dawson. This is an open-access article distributed under the terms of the Creative Commons Attribution License (CC BY). The use, distribution or reproduction in other forums is permitted, provided the original author(s) and the copyright owner(s) are credited and that the original publication in this journal is cited, in accordance with accepted academic practice. No use, distribution or reproduction is permitted which does not comply with these terms.



Role of the Steroid Sulfate Uptake Transporter Soat (*Slc10a6*) in Adipose Tissue and 3T3-L1 Adipocytes

Emre Karakus¹, Andreas Schmid², Silke Leiting¹, Bärbel Fühler¹, Andreas Schäffler², Thilo Jakob³ and Joachim Geyer^{1*}

¹Institute of Pharmacology and Toxicology, Faculty of Veterinary Medicine, Justus Liebig University, Giessen, Germany, ²Department of Internal Medicine III, Giessen University Hospital, Justus Liebig University, Giessen, Germany, ³Department of Dermatology and Allergology, Giessen University Hospital, Justus Liebig University, Giessen, Germany

OPEN ACCESS

Edited by:

Jon Wolf Mueller,
University of Birmingham,
United Kingdom

Reviewed by:

Paul Dawson,
The University of Queensland,
Australia
Paul Alexander Foster,
University of Birmingham,
United Kingdom

*Correspondence:

Joachim Geyer
Joachim.M.Geyer@vetmed.uni-
giessen.de

Specialty section:

This article was submitted to
Cellular Biochemistry,
a section of the journal
Frontiers in Molecular Biosciences

Received: 27 January 2022

Accepted: 24 March 2022

Published: 28 April 2022

Citation:

Karakus E, Schmid A, Leiting S,
Fühler B, Schäffler A, Jakob T and
Geyer J (2022) Role of the Steroid
Sulfate Uptake Transporter Soat
(*Slc10a6*) in Adipose Tissue and 3T3-
L1 Adipocytes.
Front. Mol. Biosci. 9:863912.
doi: 10.3389/fmolb.2022.863912

In addition to the endocrine and paracrine systems, peripheral tissues such as gonads, skin, and adipose tissue are involved in the intracrine mechanisms responsible for the formation of sex steroids via the transformation of dehydroepiandrosterone and dehydroepiandrosterone sulfate (DHEA/DHEAS) into potent androgenic and estrogenic hormones. Numerous studies have examined the relationship between overweight, central obesity, and plasma levels of DHEA and DHEAS. The sodium-dependent organic anion transporter Soat (*Slc10a6*) is a plasma membrane uptake transporter for sulfated steroids. Significantly increased expression of *Slc10a6* mRNA has been previously described in organs and tissues of lipopolysaccharide (LPS)-treated mice, including white adipose tissue. These findings suggest that Soat plays a role in the supply of steroids in peripheral target tissues. The present study aimed to investigate the expression of Soat in adipocytes and its role in adipogenesis. Soat expression was analyzed in mouse white intra-abdominal (WAT), subcutaneous (SAT), and brown (BAT) adipose tissue samples and in murine 3T3-L1 adipocytes. In addition, adipose tissue mass and size of the adipocytes were analyzed in wild-type and *Slc10a6*^{-/-} knockout mice. Soat expression was detected in mouse WAT, SAT, and BAT using immunofluorescence. The expression of *Slc10a6* mRNA was significantly higher in 3T3-L1 adipocytes than that of preadipocytes and was significantly upregulated by exposure to lipopolysaccharide (LPS). *Slc10a6* mRNA levels were also upregulated in the adipose tissue of LPS-treated mice. In *Slc10a6*^{-/-} knockout mice, adipocytes increased in size in the WAT and SAT of female mice and in the BAT of male mice, suggesting adipocyte hypertrophy. The serum levels of adiponectin, resistin, and leptin were comparable in wild-type and *Slc10a6*^{-/-} knockout mice. The treatment of 3T3-L1 adipocytes with DHEA significantly reduced lipid accumulation, while DHEAS did not have a significant effect. However, following LPS-induced Soat upregulation, DHEAS also significantly inhibited lipid accumulation in adipocytes. In conclusion, Soat-mediated import of DHEAS and other sulfated steroids could contribute to the complex pathways of sex steroid intracrinology in adipose tissues. Although in cell cultures the Soat-mediated uptake of DHEAS appears to reduce lipid accumulation, in *Slc10a6*^{-/-} knockout mice, the Soat deletion induced adipocyte hyperplasia through hitherto unknown mechanisms.

Keywords: SOAT, *Slc10a6*, DHEAS, transport, knockout mouse, 3T3-L1, adipocytes, adipogenesis

INTRODUCTION

Steroid hormones play a vital role in the regulation of many physiological processes, including mineral and glucose homeostasis and sexual differentiation. In addition to gonadal steroid secretion, humans and other species have evolved intracrine mechanisms of androgenic and estrogenic steroid formation in peripheral tissues such as skin and adipose tissue (Labrie et al., 1991, Labrie et al., 2005; Dhatriya and Nair, 2003; Nawata et al., 2004). The sulfated form of dehydroepiandrosterone (DHEA), namely, DHEAS is the most abundant circulating steroid hormone in humans and is secreted exclusively by adrenal glands. The precursor hormone DHEAS acts as a large reservoir for the synthesis of potent androgens and estrogens in peripheral tissues (Labrie et al., 1991, Labrie et al., 2005), which naturally possess the enzymatic machinery to transform DHEAS into active sex steroids (Killinger et al., 1995; Labrie et al., 2001). The plasma levels of DHEA and DHEAS decrease with aging in both men and women (Labrie et al., 2003). Furthermore, a reduction in DHEA and/or DHEAS levels has been linked to age-related conditions such as cardiovascular disease (Wu et al., 2017), prostate and breast tumors (Zumoff et al., 1981; Schwartz et al., 1986; Stahl et al., 1992), immune deficiency (Casson et al., 1993), poor mental health (Haren et al., 2007; Wong et al., 2011), and insulin resistance. Low serum levels of DHEAS have also been associated with rheumatoid arthritis (Deighton et al., 1992) and with certain features of obesity, such as high body mass index (Tchernof et al., 1995), central fat accumulation (De Pergola et al., 1991, De Pergola et al., 1996), and the increase in visceral fat in men and waist-to-hip ratio in women (Hernández-Morante et al., 2008; Sayin et al., 2020). These correlations remained significant after adjustment for age. Interestingly, *in vitro* studies on adipocytes have revealed the stimulatory effect of DHEAS on lipolysis, suggesting that elevated levels of DHEAS negatively influence lipid accumulation (Hernández-Morante et al., 2008).

Clinical trials have also demonstrated that the administration of DHEA has beneficial effects on several obesity-associated pathologies, including improving insulin resistance and glucose metabolism in type 2 diabetic patients, decreasing body fat mass, and even decreasing abdominal visceral and subcutaneous fat in elderly men and women (Nestler et al., 1988; Yen et al., 1995; Morales et al., 1998; Yamaguchi et al., 1998; Villareal and Holloszy, 2004; Weiss et al., 2011). Moreover, in rat and mouse studies, DHEA or DHEAS treatment reduced body weight gain, lipid accumulation, number of fat pads, body fat percentage, and adipocyte levels (Tagliaferro et al., 1986; Muller and Cleary, 1985; Lea-Currie et al., 1997a, Lea-Currie et al., 1997b). In addition, DHEAS was found to reduce adipocyte hyperplasia in rats on a high-fat diet (Lea-Currie et al., 1997b). Furthermore, *in vitro* DHEA decreased the proliferation of preadipocytes and reduced their differentiation into mature adipocytes (Gordon et al., 1986; Shantz et al., 1989; Lea-Currie et al., 1998).

DHEAS is negatively charged at physiological concentrations and, therefore, cannot enter cells by diffusion, which is a key point that has not been sufficiently considered in these studies. Specific uptake transporters are required to transport DHEAS from the extracellular to intracellular compartment. The steroid sulfate uptake transporters belonging to the solute carrier families of organic anion transporting polypeptides (OATPs) and organic anion transporters (OATs) all represent multispecific carriers (Roth et al., 2012). However, the sodium-dependent organic anion transporter SOAT (gene symbol *SLC10A6* in humans and *Slc10a6* in animals) that belongs to the solute carrier family SLC10 is a specific uptake transporter for sulfated steroid hormones. DHEAS, 16 α -hydroxy-DHEAS, pregnenolone sulfate, 17 α -hydroxypregnenolone sulfate, androstenediol-3-sulfate, epiandrosterone-3 β -sulfate, androsterone-3 α -sulfate, testosterone-17 β -sulfate, epitestosterone-17 α -sulfate, 5 α -dihydrotestosterone sulfate, estrone-3-sulfate, and 17 β -estradiol-17-sulfate, representing the physiologically most relevant sulfated steroids, all have been identified as SOAT substrates (Geyer et al., 2004, Geyer et al., 2006, Geyer et al., 2007; Fietz et al., 2013; Schweigmann et al., 2014; Grosser et al., 2018). After their cellular uptake through SOAT/Soat transporters and intracellular desulfation by steroid sulfatase (STS), these sulfated steroids contribute to the steroid regulation of peripheral tissues such as adipose tissue or skin in an intracrine manner (Reed et al., 2005; Labrie et al., 1991, Labrie et al., 1998, Labrie et al., 2005). *SLC10A6* mRNA is highly expressed in the testes, pancreas, placenta, breast, lung, heart, skin, vagina, and kidney in humans (Geyer et al., 2007; Fietz et al., 2013). According to data from the Human Protein Atlas (2022), SOAT protein is present in the breast, bronchus, cervix, esophagus, nasopharynx, oral mucosa, prostate, skin, stomach, tonsil, and vagina, all at medium score expression levels. In addition, SOAT protein is highly expressed in various breast pathologies, including ductal hyperplasia, intraductal papilloma, and intraductal carcinoma (Karakus et al., 2018). In mice, the expression of *Slc10a6* mRNA has been detected in the lungs, testes, heart, bladder, pancreas, gall bladder, and skin. Furthermore, by immunohistochemistry, Soat protein was localized in bronchial epithelial cells of the lung, in primary and secondary spermatocytes, in the round spermatids within the seminiferous tubules of the testis, in the epidermis of the skin, and in the urinary epithelium of the bladder (Grosser et al., 2013). In a recent study, *Slc10a6* mRNA was among the most strongly induced transcripts in mice exposed to lipopolysaccharide (LPS), suggesting that *Slc10a6* represents an inflammation-responsive gene (Kosters et al., 2016).

Based on these previous findings, the present study aimed to extend our knowledge of the role of Soat in adipogenesis by investigating the mRNA and protein expression pattern of *Slc10a6*/Soat in adipocytes. The experiments were performed *in vivo* in *Slc10a6*^{-/-} knockout and wild-type mice and in LPS-treated mice and *in vitro* using the 3T3-L1 adipocyte cell line.

MATERIALS AND METHODS

Materials

All chemicals, unless otherwise stated, were obtained from Sigma-Aldrich (Taufkirchen, Germany).

Cell Culture

Murine 3T3-L1 preadipocytes were cultured at 37 °C and 5% CO₂ in DMEM (Dulbecco's modified Eagle medium, Biochrom AG, Berlin, Germany) supplemented with 10% newborn calf serum (NCS; Sigma-Aldrich) and 1% penicillin/streptomycin (PAN-Biotech, Aidenbach, Germany). At confluence, the cells were differentiated into mature adipocytes by culturing in DMEM/F12/glutamate medium (Lonza, Basel, Switzerland) supplemented with 20 µM 3-Isobutylmethylxanthine (Serva, Heidelberg, Germany), 1 µM corticosterone, 100 nM insulin, 200 µM ascorbate, 2 µg/ml apo-transferrin, 5% fetal calf serum (FCS, PAN-Biotech), 1 µM biotin, 17 µM pantothenate, 1% penicillin/streptomycin, and 300 µg/ml Pedersen fetuin (MP Biomedicals, Illkirch, France) (Zaitsev and Serrero, 1990; Bachmeier and Löffler, 1994) for 9 days using a slightly modified protocol as reported previously (Hochberg et al., 2021). The cell cultures were supplemented with adipogenesis-inducing medium (AIM) from day 0 to day 8 of differentiation, when the cell culture medium was switched to serum-free conditions (with increased insulin supplementation to a concentration of 1 µM). On day 9, the mature adipocytes were switched to serum-free DMEM/F12/glutamate-medium lacking insulin for 3–5 h. With the start of the simulation experiments, the cells were supplied with a fresh serum-free medium. The cell phenotypes were established by light microscopy as having the appearance of extensive accumulation of lipid droplets. The mature adipocytes on day 9 of differentiation were used for stimulation experiments after overnight incubation under serum-free culture conditions.

Real-Time PCR Analysis

The cells were stimulated with 10 ng/ml LPS (Sigma-Aldrich) for different periods of time. The cells were harvested and total mRNA was extracted using the Maxwell RSC simplyRNA Tissue Kit (Promega). Complementary DNA (cDNA) was synthesized from 1 µg total RNA using 8 µL of RT-mix SuperScript III Reverse Transcriptase (18080044, Invitrogen, Darmstadt, Germany). For quantitative analysis of the expression of the *Slc10a6*, *Slco1a1*, *Slco1a4*, and *Slco1b2* mRNA transcripts, gene-specific TaqMan Gene Expression Assays Mm00512730_m1, Mm01267415_m1, Mm00453136_m1, and Mm00451510_m1 (Thermo Fisher Scientific, Waltham, Massachusetts, United States) were used, respectively. The Mm99999915-g1 assay (Thermo Fisher Scientific) was used for the control amplification of glyceraldehyde-3-phosphate dehydrogenase (*Gapdh*). In the case of *Slco2b1* mRNA, real-time PCR was performed using the fluorescent dye SYBR Green PCR Master Mix (PowerUp SYBR Master Mix A25742, Thermo Fisher Scientific) and the following primers: *Slco2b1* forward 5'-AGT TTG AGC AGG

GCT TCT ACC-3' and *Slco2b1* reverse 5'-CTG TGA CAT AGG ACA AAG AAC TTG A-3'. The results were normalized to the mRNA expression of *Gapdh* (forward primer 5'-ACG GGA AGC TCA CTG GCA TG-3' and reverse primer 5'-CCA CCA CCC TGT TGC TGT AG-3'). A standard curve analysis with these primer pairs revealed r^2 of 0.999 and PCR efficiency of 106.6% for *Slco2b1* and r^2 of 0.999 and PCR efficiency of 99.6% for *Gapdh*. The TaqMan expression assay efficiencies were as follows: r^2 of 0.998 and PCR efficiency of 97.2% for *Slc10a6*, r^2 of 0.994 and PCR efficiency of 96.5% for *Slco1a1*, r^2 of 0.996 and PCR efficiency of 103.6% for *Slco1a4*, r^2 of 0.991 and PCR efficiency of 98.7% for *Slco1b2*, and r^2 of 0.997 and PCR efficiency of 98.5% for *Gapdh*. Real-time amplification was performed on an Applied Biosystems 7300 Real-Time PCR System in 96-well optical plates using 5 µL cDNA, 1.25 µL TaqMan Gene Expression Assay, 12.5 µL TaqMan Universal PCR Master Mix, and 6.25 µL water in each 25 µL reaction. The plates were heated for 10 min at 95 °C, and then 40 cycles of 15 s at 95 °C and 60 s at 60 °C were applied. All data were expressed as fold changes using the $2^{-\Delta\Delta C_t}$ method with the calibrator indicated in the *Figure legends*. In the case of carrier expression profiling, ΔC_t values are presented.

Immunofluorescence

The cells were grown on poly-L-lysine-coated 8-well µ-slides (80826, IBIDI, Gräfelfing, Germany). After 48 h, the cells were incubated with or without 10 ng/ml LPS for 24 h and, afterward, were fixed with 2% paraformaldehyde (PFA) and blocked with blocking buffer containing 1% bovine serum albumin and 4% goat serum in phosphate-buffered saline (PBS, containing 137 mM NaCl, 2.7 mM KCl, 1.5 mM KH₂PO₄ (Roth), 7.3 mM Na₂HPO₄ (Roth), pH 7.4) for 30 min at room temperature. Then, 3T3-L1 cells were incubated at 4°C overnight with an antibody against murine Soat₃₂₉₋₃₄₄ (1:500 dilution, Eurogentec, Seraing, Belgium), followed by labeling with the secondary antibody Alexa Fluor 488 goat anti-rabbit (1:800 dilution, A-11008, Invitrogen) and the nuclear marker Hoechst 33342 (1:5000, H1399, Invitrogen). Cell imaging was performed at room temperature on an inverted Leica DM5500 fluorescence microscope (Leica Microsystems, Wetzlar, Germany).

Oil Red O Staining and the Triglyceride Assay

During adipocyte differentiation (days 0–9), the cells were treated with 1 µM DHEA, 100 nM testosterone, 10 µM DHEAS, 10 µM STX64, or 1 µM flutamide in the presence or absence of LPS (10 ng/ml) in 6-well plates. The cells were then washed with cold PBS and fixed with 4% formalin (v/v) for 30 min. After Oil Red O staining, the cells were photographed using a phase-contrast microscope (DMI1, Leica Microsystems) at ×10 magnification. For quantitative measurement of lipid accumulation, the stained cells were dried, Oil Red O was extracted in isopropanol, and absorbance was determined at 520 nm using a microplate reader.

Sample Preparation From Mouse Tissues

Male C57BL/6 wild-type mice (age 8–12 weeks, bred on standard chow) received an intraperitoneal injection of 1 µg LPS per animal after overnight fasting. The control animals received intraperitoneal injections of the corresponding volume of H₂O instead of LPS. The mice were euthanized for organ and tissue resection 2 h after injections. Epididymal (intra-abdominal) and subcutaneous adipose tissue specimens were resected and shock-frozen in liquid nitrogen for subsequent analysis of mRNA expression. Animal experiments were performed at the University of Regensburg, Germany, and all the animal studies were approved by the local government agency (approval no. 54-2532, 1.14/10). Furthermore, the organ samples were obtained from wild-type (WT) and *Slc10a6*^{-/-} knockout mice after anesthesia with ketamine (120 mg/kg) and xylazine (16 mg/kg) and exsanguination by heart puncture. These experiments, including euthanasia and tissue preparations, were approved by the local regulatory authority (Regierungspräsidium Giessen) with the reference number V54-19 c 20 15 h 02 GI 20/23 Nr. A8/2013.

Immunofluorescence Analysis on Tissue Sections

For histological analyses, the tissue samples from WT and *Slc10a6*^{-/-} knockout mice were fixed for 10 min in 4% PFA and embedded in Tissue-Tek O.C.T. (Sakura Finetek Germany GmbH, Staufen, Germany). The fixed sections were permeabilized, blocked with 5% goat serum in PBS-TritonX-100 (0.1%), and incubated with the primary Soat antibody (mSoat₃₂₉₋₃₄₄, 1:400 dilution, Eurogentec) overnight at 4°C. Subsequently, the tissue sections were incubated with the secondary antibody Alexa Fluor 488 goat anti-rabbit (1:800 dilution, A-11008, Invitrogen). The slides were counterstained with Hoechst 33342 and analyzed on a Leica DM5500 B microscope. The captured images were analyzed with Leica Fluorescence Workstation LAS AF 6000 software (Leica Microsystems).

Measurement of Adipocyte Size

The adipose tissues from WT and *Slc10a6*^{-/-} knockout mice were fixed in 10% formalin and processed for paraffin embedding. Paraffin tissue sections were cut into 3.5-µm slices and processed for hematoxylin and eosin (H&E) staining. For quantification of the size of the adipocytes, six tissue sections of each group were selected and photographed using the DMi1 microscope (Leica Microsystems) at ×10 magnification. Finally, the adipocyte size was quantified using Fiji which is ImageJ software with the add-on Adiposoft plugin (NIH, Bethesda, MD, United States).

Quantification of Adiponectin, Resistin, and Leptin Concentrations in Mice

Concentrations of the adipokines adiponectin, resistin, and leptin were measured in the serum of WT and *Slc10a6*^{-/-} knockout mice

in duplicate by ELISA (DuoSet ELISA development systems, R&D Systems, Wiesbaden, Germany). The measurements were repeated for samples exceeding an intra-duplicate variation of 20%.

Statistical Analysis

All graphs and calculations were prepared using GraphPad Prism software 6.07 (GraphPad Software, La Jolla, CA, United States). Student's unpaired *t*-test and one-way ANOVA with Tukey's multiple comparison tests were performed to determine statistical significance. All data were expressed as mean ± standard deviation (SD). *P* < 0.05 was considered statistically significant.

RESULTS

Soat Expression in Adipose Tissue

To explore the role of Soat in intracrine steroid production in peripheral tissues, a *Slc10a6*^{-/-} knockout mouse model was established in a previous study by our group (Bakhaus et al., 2018). In the present study, the expression of Soat protein was investigated in adipose tissues, namely, in white intra-abdominal adipose tissue (WAT), subcutaneous adipose tissue (SAT), and brown adipose tissue (BAT) from WT and *Slc10a6*^{-/-} knockout mice. As shown in **Figure 1**, Soat is abundantly expressed in WAT (**Figure 1A**), SAT (**Figure 1B**), and BAT (**Figure 1C**) in WT mice. As expected, no Soat immunoreactivity was observed in the *Slc10a6*^{-/-} knockout mice, which clearly indicated the specificity of the anti-Soat antibody.

Adipose Tissue Morphology and Serum Adipokine Levels in *Slc10a6*^{-/-} Knockout Mice

A closer analysis of body weight, adipose tissue weight, and adipocyte size was then carried out in groups of 10 WT (four female and six male) mice and 10 *Slc10a6*^{-/-} knockout (four female and six male) mice. All were derived from het × het breeding and were genotyped as previously reported (Bakhaus et al., 2018). All mice were fed *ad libitum*. As indicated in **Figure 2A**, all mice showed comparable body weight. WAT, SAT, and BAT specimens were dissected from all mice, and the weights of the adipose tissue were normalized for the total body weight. Although there was a trend for higher WAT, SAT, and BAT ratios in the male *Slc10a6*^{-/-} knockout mice, these differences did not reach the level of significance. In female mice, the WAT, SAT, and BAT ratios were nearly identical between the WT and the *Slc10a6*^{-/-} knockout mice. In addition, serum levels of classical adipokines, namely, adiponectin, leptin, and resistin were analyzed in WT and *Slc10a6*^{-/-} knockout mice by ELISA. As indicated in **Figure 2B**, there was no significant difference in serum concentrations of adiponectin, leptin, and resistin in female or male mice. In the next step, histological sections after H&E

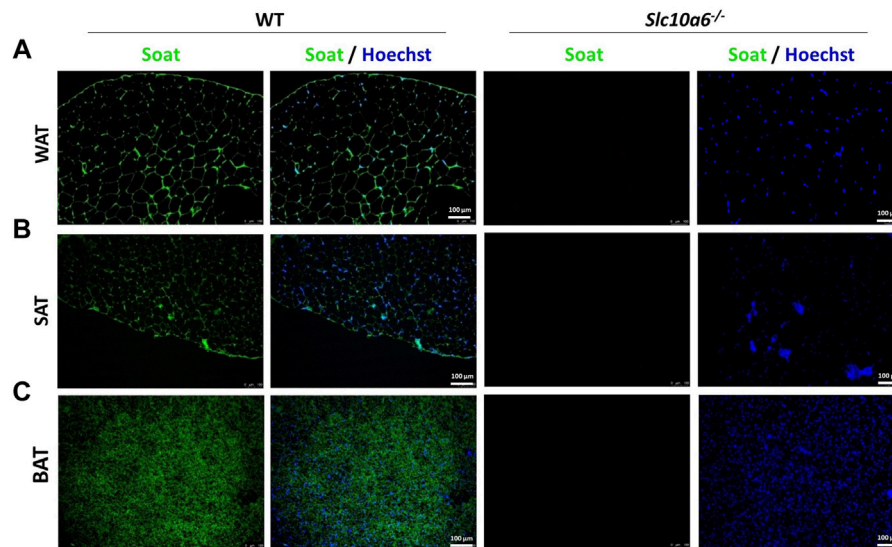


FIGURE 1 | Soat expression in mouse adipose tissues. Immunostaining of the Soat protein in WAT (A), SAT (B), and BAT (C) of wild-type and *Slc10a6*^{-/-} knockout mice with the anti-Soat antibody (green). Scale bar: 100 μ m. Blue: nuclear counterstaining with Hoechst 33342. WT, wild type; WAT, white adipose tissue; SAT, subcutaneous adipose tissue; BAT, brown adipose tissue.

staining (shown in **Figure 2C**) were used to quantify the mean areas of WAT, SAT, and BAT adipocytes (**Figure 2D**, data in μm^2). Interestingly, WAT and SAT in female mice and BAT in male mice showed significantly larger adipocyte size in the *Slc10a6*^{-/-} knockout mice than that in the WT mice.

LPS Upregulated Soat Expression in 3T3-L1 Adipocytes

Soat expression and lipid accumulation were then analyzed in an adipocyte cell culture model. 3T3-L1 preadipocytes were used and differentiated to adipocytes as described in the *Materials and Methods* section. To examine whether Soat is expressed in 3T3-L1 cells, we first measured *Slc10a6* mRNA levels using qPCR. *Slc10a6* mRNA was detected in 3T3-L1 preadipocytes and showed a significant 46.4-fold upregulation during differentiation into 3T3-L1 adipocytes (**Figure 3A**). This was confirmed at the protein level by significantly higher immunofluorescence signals with the anti-Soat antibody in mature adipocytes than those in 3T3-L1 preadipocytes (**Figure 3B**). For comparison, mRNA expression of other steroid sulfate uptake carrier candidates from the Oatp family, namely, *Oatp2b1*, *Oatp1a1*, *Oatp1a4*, and *Oatp1b2* was analyzed in 3T3-L1 adipocytes using qPCR. As shown in **Figure 3C**, only the expression of the *Slco2b1* and *Slco1a4* mRNAs was detected, while the *Slco1a1* and *Slco1b2* mRNAs were not expressed in the 3T3-L1 adipocytes. Unlike *Slc10a6*, *Slco2b1* (**Figure 3D**) and *Slco1a4* (**Figure 3E**) mRNAs were not detected in 3T3-L1 preadipocytes.

A previous study showed that *Slc10a6* mRNA levels were significantly induced by LPS in the mouse liver and WAT (Kosters et al., 2016). To further investigate the response of peripheral intracrine tissues to inflammation, gene expression

analysis of steroid sulfate carriers was performed in LPS-induced 3T3-L1 adipocytes and mouse adipose tissues. As shown in **Figure 4**, LPS treatment of 3T3-L1 adipocytes significantly increased *Slc10a6* mRNA (**Figure 4A**) and Soat protein expressions (**Figure 4E**). In contrast, LPS treatment of the 3T3-L1 adipocytes significantly induced downregulation of the *Slco2b1* (**Figure 4C**) and *Slco1a4* (**Figure 4D**) mRNA expression at least at 16 h, indicating that LPS-induced upregulation was specific for Soat. In addition, *Slc10a6* mRNA expression was analyzed in WAT, SAT, and PAT specimens of LPS-treated WT mice and in untreated control mice. LPS was injected intraperitoneally at 1 μ g LPS per animal. As shown in **Figure 4B**, *Slc10a6* mRNA expression was significantly induced by LPS treatment in all types of adipose tissue, namely, WAT, SAT, and PAT.

DHEAS-Induced Lipolysis in LPS-Treated 3T3-L1 Adipocytes

To investigate the role of Soat in modulating DHEAS-mediated effects on adipogenesis, 3T3-L1 cells were treated with LPS through the entire differentiation process of 9 days. Furthermore, DHEA, DHEAS, testosterone, STX64, and flutamide were incubated as indicated in the experimental procedure scheme (**Figure 5**). Lipid accumulation was measured by extraction and quantification of Oil Red O dye after completion of 3T3-L1 differentiation on day 9. Representative images of Oil Red O dye staining are presented in **Figure 5A,B**. Treatment with DHEA and testosterone significantly reduced the accumulation of intracellular lipid droplets. Treatment with DHEAS alone also reduced the lipid accumulation but without reaching statistical significance. However, DHEAS also significantly reduced lipid

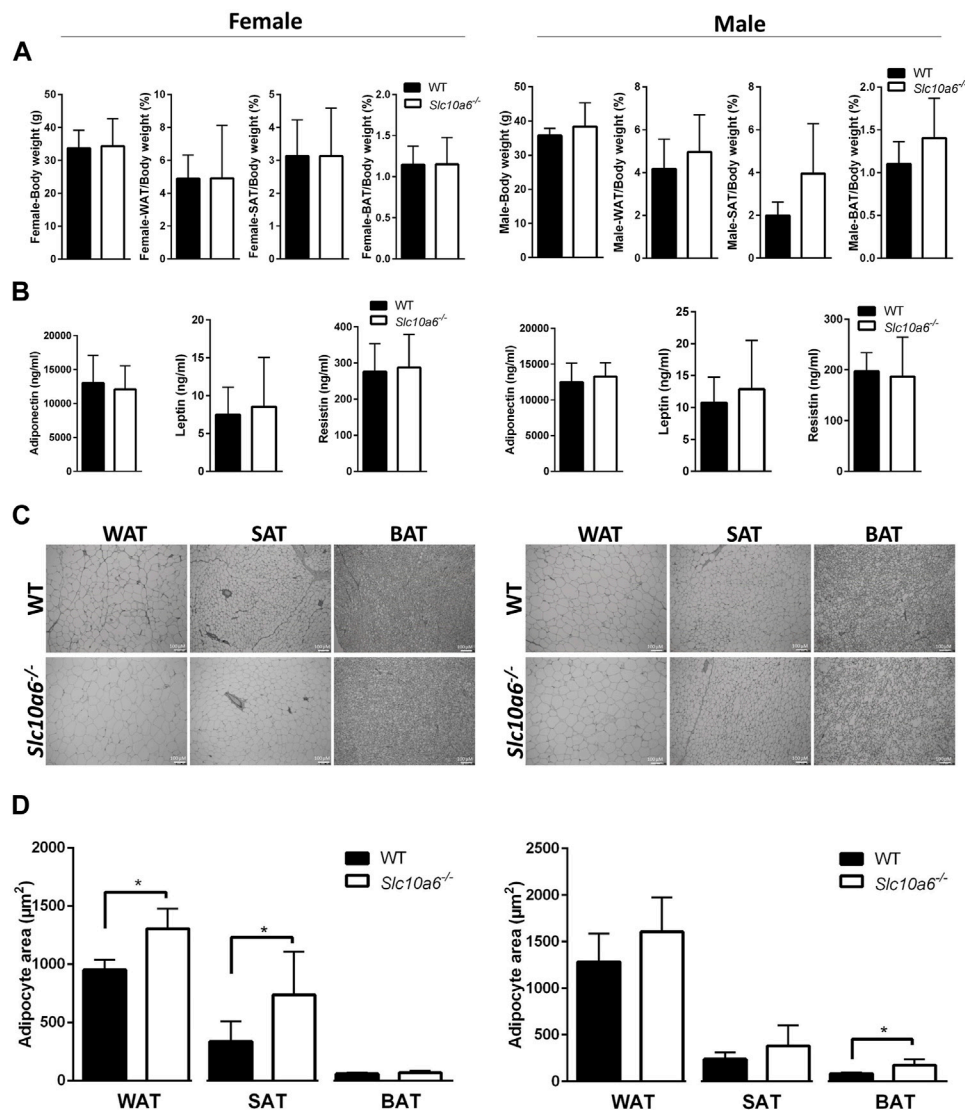


FIGURE 2 | Effects of Soat knockout on body weight, fat tissue weight, and adipocyte size. Adipose tissues of female (left panel) and male (right panel) WT and *Slc10a6*^{-/-} knockout mice were analyzed. **(A)** Weight of adipose tissues (WAT, SAT, and BAT) was normalized for total body weight. Results are shown as means \pm SD. **(B)** Serum levels of adiponectin, leptin, and resistin. Data are presented as means \pm SD of $n = 4$ female and $n = 6$ male mice per genotype. **(C)** Histological presentation and **(D)** quantitative examination of WAT, SAT, and BAT cell morphology. Histological slides after H&E staining were used for quantitative analysis of the mean adipocyte size expressed in μm^2 . Scale bars: 100 μm . Data are presented as mean \pm SD. *Significant differences between WT and *Slc10a6*^{-/-} knockout mice indicated by $p < 0.05$ according to Student's *t*-test. WT, wild type; WAT, white adipose tissue; SAT, subcutaneous adipose tissue; BAT, brown adipose tissue.

accumulation after co-incubation with LPS, and this effect was significantly stronger than that with LPS treatment alone. These results suggest that DHEAS negatively regulates lipid accumulation in differentiated adipocytes through LPS-induced Soat expression. The DHEAS-mediated inhibition of lipid accumulation observed in the LPS-exposed 3T3-L1 cells was reversed in the presence of STX64, a specific inhibitor of STS (**Figure 5B**), suggesting that conversion of DHEAS to DHEA by STS is essential for this process. In addition, the androgen receptor (AR) antagonist flutamide reversed this effect (**Figure 5B**), suggesting that an AR-dependent pathway is involved.

DISCUSSION

In the present study, we characterized for the first time the potential role of the SOAT/Soat steroid sulfate uptake carrier in adipose tissue and adipocytes. Transporters such as Soat are responsible for the cellular uptake of negatively charged sulfated steroids and, therefore, can be regarded as gatekeepers in the plasma membrane for the intracellular functions of these precursor molecules. In principle, there are several candidates for steroid sulfate uptake carriers from the OATP/Oatp and OAT/Oat carrier families that show widespread tissue expression (Roth et al., 2012). Furthermore, the hepatic bile acid carrier Na^+ /taurocholate co-transporting polypeptide (NTCP/

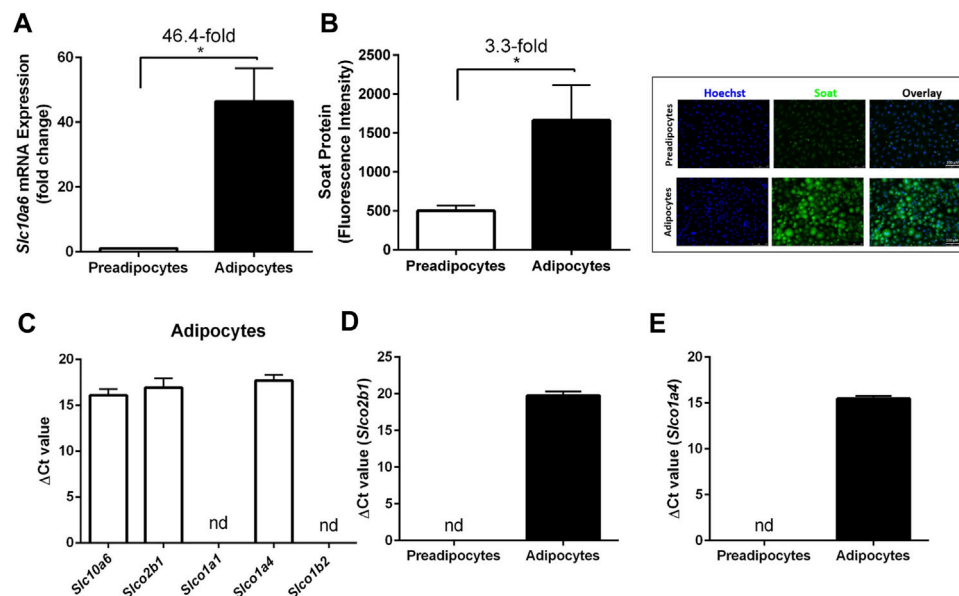


FIGURE 3 | Expression of Soat and other steroid sulfate transporters in 3T3-L1 preadipocytes and adipocytes. **(A)** *Slc10a6* mRNA levels were quantified by qPCR in 3T3-L1 preadipocytes and adipocytes using a *Slc10a6*-specific TaqMan probe. *Gapdh* expression was used to normalize *Slc10a6* expression (Δ Ct), and the Δ Ct value in preadipocytes was set as the calibrator for $2^{-\Delta\Delta Ct}$ calculation of the fold expression change during adipocyte differentiation. **(B)** Anti-Soat immunofluorescence analysis and quantification of fluorescence intensity in 3T3-L1 preadipocytes and adipocytes. Data in **(B)** represent means \pm SD of three independent areas of view (each with 60–74 cells) of three independent replicates. Representative immunofluorescence images of preadipocytes and adipocytes are shown. The cells were fixed and stained with the anti-Soat antibody and the secondary Alexa Fluor 488 goat anti-rabbit antibody (green fluorescence). Hoechst 33342 was used for nuclei staining (blue fluorescence). **(C)** Expression profile of 3T3-L1 adipocytes for different steroid sulfate uptake carriers. **(D)** *Slco2b1* and **(E)** *Slco1a4* mRNA expression in preadipocytes and differentiated adipocytes. Expression data in **(C–E)** are presented as Δ Ct values from qPCR analysis and represent carrier expression normalized to *Gapdh* expression. Data are expressed as means \pm SD. *Significant differences between preadipocytes and adipocytes indicated by $p < 0.05$ according to Student's t-test.

Ntcp) is involved in the uptake of sulfated steroids by hepatocytes (Geyer et al., 2006). The Soat carrier is unique among these carriers for several reasons: (I) In contrast to OATPs/Oatps and OATs/Oats, SOAT/Soat mediates a sodium-coupled active transport of its substrates into cells; (II) this carrier is very substrate-specific and exclusively transports sulfated steroid hormones, whereas the other carriers also have bile acids and drugs among their substrates and, thus, are multispecific; (III) SOAT/Soat is highly expressed in many peripheral tissues known to be steroid responsive, and in some of these tissues SOAT/Soat is even coexpressed with STS (e.g. in the placenta) (Geyer et al., 2007; Fietz et al., 2013; Grosser et al., 2013; Schweigmann et al., 2014; Bakhaus et al., 2018). All these points make SOAT/Soat an interesting candidate for intracrine steroid regulation in peripheral tissues and organs, such as adipose tissue.

SOAT/Soat transports all 3' and 17' monosulfated steroids that are physiologically relevant and of these, in humans, DHEAS is quantitatively the most relevant and dominant precursor (Orentreich et al., 1984) that is used to synthesize androgens and estrogens, such as testosterone, dihydrotestosterone, estrone, and 17 β -estradiol, *via* STS and other steroidogenic enzymes (Khalil et al., 1993; Labrie et al., 1995; Reed et al., 2005). STS is expressed in preadipocytes and mature adipocytes (Marwah et al., 2006; McNelis et al., 2013) and, thus, could exert intracrine effects on adipogenesis in combination with Soat, which is highly expressed in WAT, SAT, and BAT adipose tissue, at least in mice (Figure 1).

Considering our current knowledge about SOAT/Soat, we assume a functional role in the local supply of adipose tissue with sulfated steroids, which could then be involved in the regulation of various physiopathological processes such as obesity (Figure 6). There are numerous studies showing that serum DHEAS levels are negatively correlated with obesity (Al-Harithy, 2003; Hernández-Morante et al., 2008; Gómez-Santos et al., 2012; Jaff et al., 2015; Sayın et al., 2020). However, the role of SOAT in this process is difficult to demonstrate in human patients. Thus, effects of DHEA/DHEAS on adipocytes are often analyzed in the mouse 3T3-L1 cell line to investigate adipogenesis, lipogenesis, and lipolysis (Green and Meuth, 1974; Green and Kehinde, 1975), considering that rodents have much lower circulating concentrations of these hormones (Guillemette et al., 1996). In addition, much of our knowledge concerning preadipocyte biology and adipocyte differentiation has been obtained using 3T3-L1 cells. In the present study, we also used WT and *Slc10a6*^{-/-} knockout mice to investigate the role of Soat on body weight, fat tissue weight, adipocyte size, and serum adipokine levels *in vivo* in male and female mice. Our results demonstrate that the knockout of Soat expression did not influence total body weight and the weight of adipose tissues in mice fed *ad libitum*. These results are consistent with our previous findings in *Slc10a6*^{-/-} knockout mice (Bakhaus et al., 2018). We also did not find any significant differences in the gain or loss of fat-free mass with weight changes and the serum levels

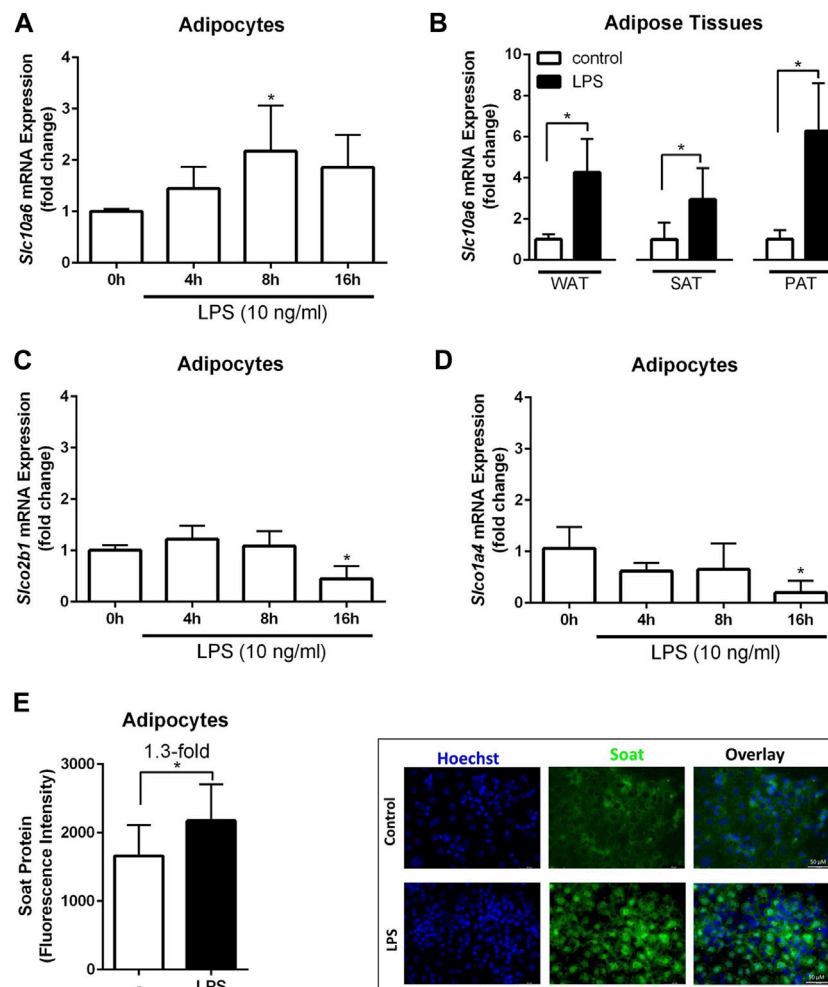


FIGURE 4 | Expression analysis of steroid sulfate uptake carriers in adipocytes and adipose tissue in response to LPS. The mRNA expression levels of *Slc10a6* (A), *Slco2b1* (C), and *Slco1a4* (D) were quantified using qPCR in LPS-induced 3T3-L1 adipocytes. 3T3-L1 adipocytes were treated with 10 ng/ml LPS for the indicated time periods. Data represent means \pm SD of triplicate determination of representative experiments (B) *Slc10a6* mRNA expression in LPS-treated mice for WAT, SAT, and PAT (n = 6). Data represent means \pm SD. All carrier mRNA expression levels were normalized to *Gapdh* expression. Soat protein expression in (E) represents means \pm SD of three independent areas of view (each with 60–74 cells) of three independent replicates. The mature adipocytes were treated with 10 ng/ml LPS for 24 h. Representative immunofluorescence images are shown. Cells were fixed and stained with the anti-Soat antibody and the secondary Alexa Fluor 488 goat anti-rabbit antibody (green fluorescence). Hoechst 33342 was used for nuclei staining (blue fluorescence). *Significant differences indicated by $p < 0.05$ using one-way ANOVA (A, C and D) or Student's t-test (B and E). LPS, lipopolysaccharide; WAT, white intra-abdominal adipose tissue; SAT, subcutaneous adipose tissue; PAT, perirenal adipose tissue.

of the adipokines leptin, adiponectin, and resistin (Figure 2). These adipokines originate primarily from fat deposits and exert essential regulatory functions in adipose tissue, especially under different metabolic conditions such as obesity, fasting, and diabetes (Galic et al., 2010; Coelho et al., 2013; Leal and Mafra, 2013). Adiponectin is the most abundant circulating adipokine (Yamauchi et al., 2001). In some studies, the serum levels of adiponectin are inversely correlated with those of adipose tissue. Arita et al. (1999) reported that plasma adiponectin concentrations decrease with obesity in humans. Similarly, male patients with morbid obesity present higher serum levels of DHEAS than obese women, while women exhibit higher plasma adiponectin values than male patients (Hernández-Morante et al., 2006). This study by Hernández-Morante et al. (2006)

also demonstrated the significant effect of DHEAS on the upregulation of adiponectin in visceral adipose tissue. Furthermore, DHEAS replacement therapy in postmenopausal women resulted in decreased plasma levels of adiponectin (Gómez-Santos et al., 2012). Conversely, reduction in leptin and an upregulation of resistin gene expression have been described in adipose tissue after DHEA administration (Kochan and Karbowska, 2004). One study reported that rats treated with DHEA express elevated serum concentrations of resistin and DHEAS but decreased serum levels of leptin and adiponectin (Pérez-de-Heredia et al., 2008). It is noteworthy that the lack of *Soat* *per se* had no effect on serum adiponectin, leptin, and resistin in our study. However, it must be considered that these mice were fed a standard diet *ad*

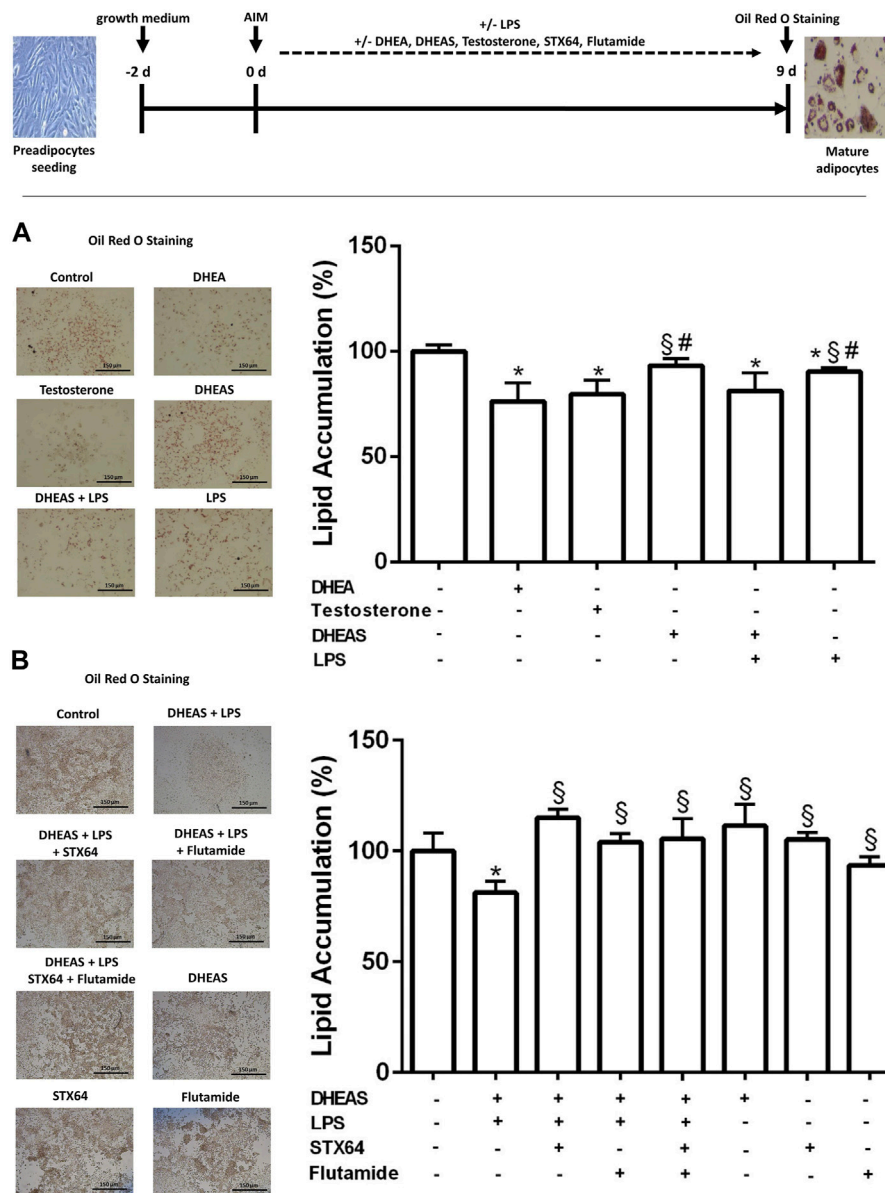


FIGURE 5 | Effect of DHEAS on lipid accumulation in LPS-induced 3T3-L1 adipocytes. Scheme of the experimental procedure for 3T3-L1 differentiation from preadipocytes to mature adipocytes over 9 days and cell treatment. Cell differentiation was induced by hormonal supplementation (AIM) as described in the *Materials and Methods* section. 3T3-L1 preadipocytes were incubated with DHEA (1 μ M), testosterone (100 nM), DHEAS (10 μ M), STX64 (10 μ M), or flutamide (1 μ M) in the presence or absence of LPS for the entire 9-day differentiation period, and every 2 days the medium was changed with fresh AIM containing the respective compounds. On day 9, the cells were stained with Oil Red O. Representative photomicrographs of Oil Red O staining in mature 3T3-L1 adipocytes are shown (scale bar: 150 μ m). Lipid accumulation was measured by Oil Red O extraction and quantification using a microplate reader. Data are expressed as mean \pm SD of three replicates from (A) three independent experiments and from (B) one representative experiment. Significant differences are indicated by $p < 0.05$ using one-way ANOVA with Tukey's multiple comparisons test: *significantly different compared to control; §significantly different compared to LPS + DHEAS; #significantly different compared to DHEA and testosterone. AIM, adipogenesis-inducing media.

libitum. Future experiments including high-fat diet feeding of *Slc10a6*^{-/-} knockout mice and additional DHEAS treatment could be helpful in fully elucidating the role of Soat in adipogenesis.

It is noteworthy that *Slc10a6*^{-/-} knockout mice were characterized by a significant increase in adipocyte size in WAT and SAT of female and in BAT of male mice compared to WT control animals (Figure 2D). The large interindividual

variability observed in adipocyte size suggests that the propensity for fat cell hypertrophy in each fat compartment may differ between the groups studied. Interestingly, male *Slc10a6*^{-/-} knockout mice showed significantly higher serum cholesterol sulfate levels than their wild type controls, with no significant difference found for female mice (Bakhaus et al., 2018). Approximately, 25% of total cholesterol is stored in adipose

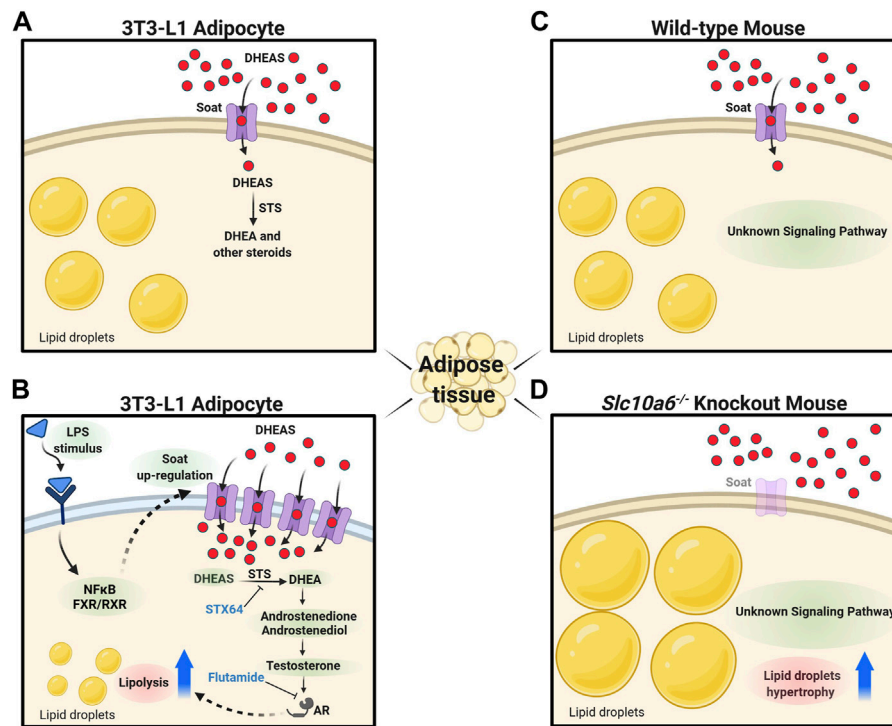


FIGURE 6 | Proposed role of Soat in lipid droplet formation and steroid-triggered lipolysis. **(A)** Soat expression in the plasma membrane of 3T3-L1 adipocytes and uptake of DHEAS under physiological conditions. **(B)** Upregulation of Soat expression by LPS treatment through JNK and NF- κ B-dependent pathways increases DHEAS uptake and stimulation of lipolysis via an AR-dependent pathway. The lipolytic effect of DHEAS could be blocked by STX64 and flutamide. **(C)** As DHEAS levels are low in mice, Soat may mediate uptake of other relevant sulfated steroids here. **(D)** Absence of steroid sulfate uptake through Soat in *Slc10a6*^{-/-} knockout mice could lead to the hypertrophy of lipid droplets in adipocytes via hitherto unknown signaling pathways. DHEAS, dehydroepiandrosterone sulfate; DHEA, dehydroepiandrosterone; STS, steroid sulfatase; STX64, STS inhibitor; LPS, lipopolysaccharide; NF- κ B, nuclear factor “kappa-light-chain-enhancer” of activated B-cells; FXR, farnesoid X receptor; RXR, retinoid X receptor; AR, androgen receptor; flutamide, androgen receptor antagonist. The figure was created with biorender.com.

deposits in normal weight humans, while this rate can rise to 50% in obese individuals (Prattes et al., 2000). Lipid droplet expansion requires substantial amounts of cholesterol, triggering the transfer of caveolin proteins from the plasma membrane to lipid droplets to facilitate their enlargement (Chui et al., 2005; Robenek et al., 2011). Furthermore, Dalla Valle et al. (2006) demonstrated STS expression at the levels of mRNA, protein, and catalytic activity in human adipose tissue, whereas sulfotransferase expression was not found. Thus, higher serum cholesterol sulfate levels in males may have masked differences in adipocyte size. In this context, further studies are needed including analytical steroid profiling of serum and adipose tissue from WT and *Slc10a6*^{-/-} knockout mice.

The expression of *Slc10a6* mRNA and Soat protein was upregulated in 3T3-L1 cells after differentiation from preadipocytes into mature adipocytes (Figure 3). In addition, the mRNA expression of other potential steroid sulfate uptake carriers in adipocytes was analyzed, and *Slco2b1* and *Slco1a4* were also found to be expressed at low levels, while *Slco1a1* and *Slco1b2* mRNAs are not detectable in mature adipocytes. Dalla Valle et al. (2006) and McNelis et al. (2013) reported that mRNA expression of the human OATP carriers OATP-B (*SLCO2B1*), OATP-D (*SLCO3A1*), OATP-E

(*SLCO4A1*), and of STS, could be detected in human adipose tissue and in cultured preadipocytes and adipocytes, whereas OATP-A (*SLCO1A2*), OATP-C (*SLCO1B1*), OATP-8 (*SLCO1C3*), OAT3 (*SLC22A8*), and OAT4 (*SLC22A11*) were not detected. In addition, Dalla Valle et al. (2006) analyzed the expression of steroidogenic enzymes and related proteins such as cytochromes P450_{scc}, P450_{c17}, P450_{arom}, steroidogenic factor 1 (SF-1), and steroidogenic acute regulatory protein (StAR), which are involved in the *de novo* biosynthesis of steroid hormones from cholesterol. They showed that none of these enzymes could be detected at the mRNA level, while STS mRNA was expressed in samples from cultured preadipocytes, adipocytes, and adipose tissues. The absence of these essential enzymes required for cholesterol-mediated estrogen and androgen biosynthesis suggests that uptake carriers for sulfated steroid precursors, indeed, might be essential for the regulation of the adipose tissue by steroids.

A global gene expression analysis in mice demonstrated that Soat is among the most strongly induced genes by LPS in the liver and macrophages (Kosters et al., 2016). In addition, *Slc10a6* mRNA expression was upregulated in the liver of mice treated with the cytokine IL-1 β . The inflammation-mediated upregulation of Soat expression was likely modulated by the

nuclear receptor farnesoid X receptor (FXR), the retinoid X receptor (RXR), and glucocorticoid receptor (GR), which were expressed by all tissues, including white and brown adipose tissues. Since the testes have higher Soat expression than other tissues, the testes were used in this study as the control tissue. However, Soat shows higher expression in the BAT and is less expressed in WAT of untreated mice when compared to that in the testes. In contrast, *Slc10a6* mRNA levels are upregulated in WAT and downregulated in BAT specimens of LPS-induced mice (Kosters et al., 2016). We found that LPS-elicited inflammation induced a significant increase in *Slc10a6* mRNA expression in WAT, SAT, and PAT specimens of mice *in vivo* and in mature 3T3-L1 adipocytes *in vitro* (Figure 4). In contrast, the mRNA transcripts for *Slco2b1* and *Slco1a4* were downregulated in LPS-treated mature 3T3-L1 adipocytes.

DHEA treatment suppresses both proliferation and adipocyte differentiation of 3T3-L1 cells and inhibits AIM-induced lipid accumulation in 3T3-L1 adipocytes (Lea-Currie et al., 1998; Fujioka et al., 2012; Yokokawa et al., 2020). This finding was confirmed in the present study. Marwah et al. (2006) showed that DHEA is metabolized into adiol and testosterone in 3T3-L1 adipocytes. Furthermore, Singh et al. (2006) demonstrated that testosterone and dihydrotestosterone, in a dose-dependent manner, caused inhibition of lipid accumulation in 3T3-L1 differentiated for 12 days. Moreover, this inhibitory effect was significantly blocked by the AR antagonist flutamide (Singh et al., 2006). These studies suggest that testosterone and dihydrotestosterone both play a role in adipogenic differentiation of 3T3-L1 cells *via* the AR. Lea-Currie et al. (1998) showed that DHEAS, in contrast to DHEA, had no impact on preadipocyte proliferation and differentiation. These studies corroborate our findings in adipocytes, demonstrating that DHEA, but not DHEAS, suppresses both proliferation and lipid accumulation. The lack of effects of DHEAS on murine 3T3-L1 preadipocytes and adipocytes may be due to the low expression levels of steroid sulfate uptake transporters. In this context, another interesting observation of our study was the LPS-induced upregulation of Soat in adipocytes and the decrease in adipocyte differentiation and AIM-induced lipid accumulation by DHEAS, accompanied by LPS-mediated upregulation of Soat in 3T3-L1 cells (Figure 5). Although lipid accumulation was also significantly reduced by LPS treatment alone, we observed a significantly stronger effect of LPS treatment combined with DHEAS. Moreover, we tested whether DHEAS-mediated inhibition of lipid accumulation was related to downstream steroid metabolites. We observed that both STS inhibition by STX64 and AR inhibition by flutamide completely abolished the DHEAS-mediated effects, clearly indicating that conversion of DHEAS to DHEA and subsequent androgens is involved in this process (Figure 5B). It is well known that obesity due to excess fat accumulation is associated with varying degrees of chronic inflammation in adipose tissue. This leads to hypoxia, adipocyte cell death, and modified secretion of adipokines (Sanada et al., 2016) and finally ends in chronic morbidities characterized by metabolic inflammation (Handschin and Spiegelman, 2008; Makki et al., 2013). The results of the present study suggest that the inflammation-mediated

overexpression of Soat and subsequently increased uptake of DHEAS finally lead to inhibition of adipocyte differentiation and reduced lipid accumulation *via* the AR, as depicted in Figure 6.

In conclusion, Soat is a specific uptake carrier for sulfated steroids with significant expression levels in adipose tissues and a proposed role in obesity. To clarify this role *in vivo*, *Slc10a6*^{-/-} knockout mice were analyzed. We observed that LPS-induced inflammation increased the expression of Soat in adipocytes and adipose tissues, contributing to lipolysis by increased uptake of the Soat substrate DHEAS, while deletion of Soat caused adipocyte hyperplasia in mice. We are aware that our study has some limitations. The most important is that the steroid profiles in the adipocytes could not be analyzed, so it was not possible to determine how DHEAS was exactly converted to active androgens.

DATA AVAILABILITY STATEMENT

The original contributions presented in the study are included in the article/Supplementary Material, further inquiries can be directed to the corresponding author.

ETHICS STATEMENT

The animal study was reviewed and approved by the University of Regensburg, local government agency, approval no. 54-2532, 1.14/10 and Regierungspräsidium Giessen, reference number V54-19 c 20 15 h 02 GI 20/23 Nr. A8/2013.

AUTHOR CONTRIBUTIONS

EK, AS, SL, BF, and JG: acquisition and analysis of data; EK, AS, and JG: interpretation of data; EK, AS, and JG: study concept, design and supervision, and writing of the manuscript. TJ and ASä: resources and review and editing of the manuscript.

FUNDING

This study was supported in part by the grants to EK from the Scholar Rescue Fund and from the Philipp Schwartz-Initiative of the Alexander von Humboldt-Stiftung.

ACKNOWLEDGMENTS

We thank Frank Hanses (University of Regensburg) for excellent advice and practical support in animal experiments and Britta Dorn (Department of Dermatology and Allergology, Justus Liebig University Giessen) for excellent technical assistance in histological analysis of murine adipose tissues.

REFERENCES

- ## REFERENCES
- Al-Harithy, R. N. (2003). Dehydroepiandrosterone Sulfate Levels in Women. Relationships with Body Mass index, Insulin and Glucose Levels. *Saudi Med. J.* 24 (8), 837–841.
- Arita, Y., Kihara, S., Ouchi, N., Takahashi, M., Maeda, K., Miyagawa, J.-i., et al. (1999). Paradoxical Decrease of an Adipose-specific Protein, Adiponectin, in Obesity. *Biochem. Biophysical Res. Commun.* 257 (1), 79–83. doi:10.1006/bbrc.1999.0255
- Bachmeier, M., and Löffler, G. (1994). Adipogenic Activities in Commercial Preparations of Fetuin. *Horm. Metab. Res.* 26 (2), 92–96. doi:10.1055/s-2007-1000780
- Bakhaus, K., Bennien, J., Fietz, D., Sánchez-Guijo, A., Hartmann, M., Serafini, R., et al. (2018). Sodium-dependent Organic Anion Transporter (Slc10a6–Slc10a6pendent Organic Anion Transporter (SlstyledeuinReplaced] Refstyledsrity Giessen) for excellent technical. *J. Steroid Biochem. Mol. Biol.* 179, 45–54. doi:10.1016/j.jsmb.2017.07.019
- Casson, P. R., Andersen, R. N., Herrod, H. G., Stentz, F. B., Straughn, A. B., Abraham, G. E., et al. (1993). Oral Dehydroepiandrosterone in Physiologic Doses Modulates Immune Function in Postmenopausal Women. *Am. J. Obstet. Gynecol.* 169 (6), 1536–1539. doi:10.1016/0002-9378(93)90431-h
- Chui, P. C., Guan, H.-P., Lehrke, M., and Lazar, M. A. (2005). PPARγ Regulates Adipocyte Cholesterol Metabolism via Oxidized LDL Receptor 1. *J. Clin. Invest.* 115 (8), 2244–2256. doi:10.1172/JCI24130
- Coelho, M., Oliveira, T., and Fernandes, R. (2013). State of the Art Paper Biochemistry of Adipose Tissue: an Endocrine Organ. *aoms* 2 (92), 191–200. doi:10.5114/aoms.2013.33181
- De Pergola, G., Zamboni, M., Sciaraffia, M., Turcato, E., Pannacciulli, N., Armellini, F., et al. (1996). Body Fat Accumulation Is Possibly Responsible for Lower Dehydroepiandrosterone Circulating Levels in Premenopausal Obese Women. *Int. J. Obes. Relat. Metab. Disord.* 20 (12), 1105–1110.
- De Pergola, G., Giagulli, V. A., Garruti, G., Cospite, M. R., Giorgino, F., Cignarelli, M., et al. (1991). Low Dehydroepiandrosterone Circulating Levels in Premenopausal Obese Women with Very High Body Mass index. *Metabolism* 40 (2), 187–190. doi:10.1016/0026-0495(91)90172-s
- Deighton, C. M., Watson, M. J., and Walker, D. J. (1992). Sex Hormones in Postmenopausal HLA-Identical Rheumatoid Arthritis Discordant Sibling Pairs. *J. Rheumatol.* 19 (11), 1663–1667.
- Dhatariya, K. K., and Nair, K. S. (2003). Dehydroepiandrosterone: Is There a Role for Replacement? *Mayo Clinic Proc.* 78, 1257–1273. doi:10.4065/78.10.1257
- Fietz, D., Bakhaus, K., Wapelhorst, B., Grosser, G., Günther, S., Alber, J., et al. (2013). Membrane Transporters for Sulfated Steroids in the Human Testis - Cellular Localization, Expression Pattern and Functional Analysis. *PLoS One* 8 (8), e62638. doi:10.1371/journal.pone.0062638
- Fujioka, K., Kajita, K., Wu, Z., Hanamoto, T., Ikeda, T., Mori, I., et al. (2012). Dehydroepiandrosterone Reduces Preadipocyte Proliferation via Androgen Receptor. *Am. J. Physiology-Endocrinology Metab.* 302 (3026), E694–E704. doi:10.1152/ajpendo.00112.2011
- Galic, S., Oakhill, J. S., and Steinberg, G. R. (2010). Adipose Tissue as an Endocrine Organ. *Mol. Cell Endocrinol.* 316 (3162), 129–139. doi:10.1016/j.mce.2009.08.018
- Geyer, J., Döring, B., Meerkamp, K., Ugele, B., Bakhiya, N., Fernandes, C. F., et al. (2007). Cloning and Functional Characterization of Human Sodium-dependent Organic Anion Transporter (SLC10A6). *J. Biol. Chem.* 282 (28227), 19728–19741. doi:10.1074/jbc.M702663200
- Geyer, J., Godoy, J. R., and Petzinger, E. (2004). Identification of a Sodium-dependent Organic Anion Transporter from Rat Adrenal Gland. *Biochem. Biophysical Res. Commun.* 316 (3162), 300–306. doi:10.1016/j.bbrc.2004.02.048
- Geyer, J., Wilke, T., and Petzinger, E. (2006). The Solute Carrier Family SLC10: More Than a Family of Bile Acid Transporters Regarding Function and Phylogenetic Relationships. *Naunyn Schmied Arch. Pharmacol.* 372, 413–431. doi:10.1007/s00210-006-0043-8
- Gómez-Santos, C., Hernández-Morante, J. J., Tébar, F. J., Granero, E., and Garaulet, M. (2012). Differential Effect of Oral Dehydroepiandrosterone-Sulphate on Metabolic Syndrome Features in Pre- and Postmenopausal Obese Women. *Clin. Endocrinol.* 77 (4), 548–554. doi:10.1111/j.1365-2265.2011.04306.x
- Gordon, G. B., Newitt, J. A., Shantz, L. M., Weng, D. E., and Talalay, A. (1986). Inhibition of the Conversion of 3T3 Fibroblast Clones to Adipocytes by Dehydroepiandrosterone and Related Anticarcinogenic Steroids. *Cancer Res.* 46 (7), 3389–3395.
- Green, H., and Kehinde, O. (1975). An Established Preadipose Cell Line and its Differentiation in Culture II. Factors Affecting the Adipose Conversion. *Cell* 5 (1), 19–27. doi:10.1016/0092-8674(75)90087-2
- Green, H., and Meuth, M. (1974). An Established Pre-adipose Cell Line and its Differentiation in Culture. *Cell* 3 (2), 127–133. doi:10.1016/0092-8674(74)90116-0
- Grosser, G., Bennien, J., Sánchez-Guijo, A., Bakhaus, K., Döring, B., Hartmann, M., et al. (2018). Transport of Steroid 3-sulfates and Steroid 17-sulfates by the Sodium-dependent Organic Anion Transporter SOAT (SLC10A6). *J. Steroid Biochem. Mol. Biol.* 179, 20–25. doi:10.1016/j.jsmb.2017.09.013
- Grosser, G., Fietz, D., Günther, S., Bakhaus, K., Schweigmann, H., Ugele, B., et al. (2013). Cloning and Functional Characterization of the Mouse Sodium-dependent Organic Anion Transporter Soat (Slc10a6). *J. Steroid Biochem. Mol. Biol.* 138, 90–99. doi:10.1016/j.jsmb.2013.03.009
- Guillemette, C., Hum, D. W., and Bélanger, A. (1996). Levels of Plasma C19 Steroids and 5 Alpha-Reduced C19 Steroid Glucuronides in Primates, Rodents, and Domestic Animals. *Am. J. Physiology-Endocrinology Metab.* 271 (2 Pt 1), E348–E353. doi:10.1152/ajpendo.1996.271.2.E348
- Handschin, C., and Spiegelman, B. M. (2008). The Role of Exercise and PGC1α in Inflammation and Chronic Disease. *Nature* 454 (4547203), 463–469. doi:10.1038/nature07206
- Haren, M. T., Malmstrom, T. K., Banks, W. A., Patrick, P., Miller, D. K., and Morley, J. E. (2007). Lower Serum DHEAS Levels Are Associated with a Higher Degree of Physical Disability and Depressive Symptoms in Middle-Aged to Older African American Women. *Maturitas* 57 (574), 347–360. doi:10.1016/j.maturitas.2007.03.003
- Hernandez-Morante, J. J., Milagro, F., Gabaldon, J. A., Martinez, J. A., Zamora, S., and Garaulet, M. (2006). Effect of DHEA-Sulfate on Adiponectin Gene Expression in Adipose Tissue from Different Fat Depots in Morbidly Obese Humans. *Eur. J. Endocrinol.* 155 (4), 593–600. doi:10.1530/eje.1.02256
- Hernández-Morante, J. J., Pérez-de-Heredia, F., Luján, J. A., Zamora, S., and Garaulet, M. (2008). Role of DHEA-S on Body Fat Distribution: Gender- and Depot-specific Stimulation of Adipose Tissue Lipolysis. *Steroids* 73 (2), 209–215. doi:10.1016/j.steroids.2007.10.005
- Hochberg, A., Patz, M., Karrasch, T., Schäffler, A., and Schmid, A. (2021). Serum Levels and Adipose Tissue Gene Expression of Cathelicidin Antimicrobial Peptide (CAMP) in Obesity and during Weight Loss. *Horm. Metab. Res.* 53 (3), 169–177. doi:10.1055/a-1323-3050
- Human Protein Atlas (2022). Human Protein Atlas. SLC10A6. Available at: <https://www.proteinatlas.org/ENSG00000145283-SLC10A6/tissue> (Accessed January 27, 2022).
- Jaff, N. G., Norris, S. A., Snyman, T., Toman, M., and Crowther, N. J. (2015). Body Composition in the Study of Women Entering and in Endocrine Transition (SWEET): A Perspective of African Women Who Have a High Prevalence of Obesity and HIV Infection. *Metabolism* 64 (9), 1031–1041. doi:10.1016/j.metabol.2015.05.009
- Karakus, E., Zahner, D., Grosser, G., Leidolf, R., Gundogdu, C., Sánchez-Guijo, A., et al. (2018). Estrone-3-Sulfate Stimulates the Proliferation of T47D Breast Cancer Cells Stably Transfected with the Sodium-dependent Organic Anion Transporter SOAT (SLC10A6). *Front. Pharmacol.* 9 (9), 941. doi:10.3389/fphar.2018.00941
- Khalil, M. W., Strutt, B., Vachon, D., and Killinger, D. W. (1993). Metabolism of Dehydroepiandrosterone by Cultured Human Adipose Stromal Cells: Identification of 7α-Hydroxydehydroepiandrosterone as a Major Metabolite Using High Performance Liquid Chromatography and Mass Spectrometry. *J. Steroid Biochem. Mol. Biol.* 46 (5), 585–595. doi:10.1016/0960-0760(93)90186-z
- Killinger, D. W., Strutt, B. J., Roncari, D. A., and Khalil, M. W. (1995). Estrone Formation from Dehydroepiandrosterone in Cultured Human Breast Adipose Stromal Cells. *J. Steroid Biochem. Mol. Biol.* 52 (2), 195–201. doi:10.1016/0960-0760(94)00164-h
- Kochan, Z., and Karbowska, J. (2004). Dehydroepiandrosterone Up-Regulates Resistin Gene Expression in white Adipose Tissue. *Mol. Cell Endocrinol.* 218 (1–2), 21857–21864. doi:10.1016/j.mce.2003.12.012

- Kosters, A., Abebe, D. F., Felix, J. C., Dawson, P. A., and Karpen, S. J. (2016). Inflammation-associated Upregulation of the Sulfated Steroid Transporter Slc10a6 in Mouse Liver and Macrophage Cell Lines. *Hepatol. Res.* 46 (8), 794–803. doi:10.1111/hepr.12609
- Labrie, F., Bélanger, A., Luu-The, V., Labrie, C., Simard, J., Cusan, L., et al. (1998). DHEA and the Intracrine Formation of Androgens and Estrogens in Peripheral Target Tissues: its Role during Aging. *Steroids* 63 (5–6), 322–328. doi:10.1016/s0039-128x(98)00007-5
- Labrie, F., Simard, J., Luu-The, V., Trudel, C., Martel, C., Labrie, C., et al. (1991). Expression of 3 Beta-Hydroxysteroid Dehydrogenase/delta 5-delta 4 Isomerase (3 Beta-HSD) and 17 Beta-Hydroxysteroid Dehydrogenase (17 Beta-HSD) in Adipose Tissue. *Int. J. Obes.* 15 Suppl 2 (Suppl. 2), 91–99.
- Labrie, F., Bélanger, A., Simard, J., Luu-The, V., and Labrie, C. (1995). DHEA and Peripheral Androgen and Estrogen Formation: Intracrinology. *Ann. NY Acad. Sci.* 774 (774), 16–28. doi:10.1111/j.1749-6632.1995.tb17369.x
- Labrie, F., Luu-The, V., Bélanger, A., Lin, S.-X., Simard, J., Pelletier, G., et al. (2005). Is Dehydroepiandrosterone a Hormone? *J. Endocrinol.* 187 (2), 169–196. doi:10.1677/joe.1.06264
- Labrie, F., Luu-The, V., Labrie, C., Bélanger, A., Simard, J., Lin, S.-X., et al. (2003). Endocrine and Intracrine Sources of Androgens in Women: Inhibition of Breast Cancer and Other Roles of Androgens and Their Precursor Dehydroepiandrosterone. *Endocr. Rev.* 24 (2), 152–182. doi:10.1210/er.2001-0031
- Labrie, F., Luu-The, V., Labrie, C., and Simard, J. (2001). DHEA and its Transformation into Androgens and Estrogens in Peripheral Target Tissues: Intracrinology. *Front. Neuroendocrinology* 22 (3), 185–212. doi:10.1006/frne.2001.0216
- Lea-Currie, Y. R., Wen, P., and McIntosh, M. K. (1998). Dehydroepiandrosterone Reduces Proliferation and Differentiation of 3T3-L1 Preadipocytes. *Biochem. Biophysical Res. Commun.* 248 (3), 497–504. doi:10.1006/bbrc.1998.8996
- Lea-Currie, Y., Wen, P., and McIntosh, M. (1997a). Dehydroepiandrosterone-sulfate (DHEAS) Reduces Adipocyte Hyperplasia Associated with Feeding Rats a High-Fat Diet. *Int. J. Obes.* 21 (11), 1058–1064. doi:10.1038/sj.ijo.0800516
- Lea-Currie, Y., Wu, S.-M., and McIntosh, M. (1997b). Effects of Acute Administration of Dehydroepiandrosterone-Sulfate on Adipose Tissue Mass and Cellularity in Male Rats. *Int. J. Obes.* 21 (2), 147–154. doi:10.1038/sj.ijo.0800382
- Leal, V. d. O., and Mafra, D. (2013). Adipokines in Obesity. *Clinica Chim. Acta* 419 (419), 87–94. doi:10.1016/j.cca.2013.02.003
- Makki, K., Froguel, P., and Wolowczuk, I. (2013). Adipose Tissue in Obesity-Related Inflammation and Insulin Resistance: Cells, Cytokines, and Chemokines. *ISRN Inflamm.* 2013, 1–12. doi:10.1155/2013/139239
- Marwah, A., Gomez, F. E., Marwah, P., Ntambi, J. M., Fox, B. G., and Lardy, H. (2006). Redox Reactions of Dehydroepiandrosterone and its Metabolites in Differentiating 3T3-L1 Adipocytes: A Liquid Chromatographic-Mass Spectrometric Study. *Arch. Biochem. Biophys.* 456 (1), 1–7. doi:10.1016/j.abb.2006.09.023
- McNelis, J. C., Manolopoulos, K. N., Gathercole, L. L., Bujalska, I. J., Stewart, P. M., Tomlinson, J. W., et al. (2013). Dehydroepiandrosterone Exerts Antigluco-corticoid Action on Human Preadipocyte Proliferation, Differentiation, and Glucose Uptake. *Am. J. Physiology-Endocrinology Metab.* 305 (9), E1134–E1144. doi:10.1152/ajpendo.00314.2012
- Morales, A. J., Haubrich, R. H., Hwang, J. Y., Asakura, H., and Yen, S. S. C. (1998). The Effect of Six Months Treatment with a 100 Mg Daily Dose of Dehydroepiandrosterone (DHEA) on Circulating Sex Steroids, Body Composition and Muscle Strength in Age-Advanced Men and Women. *Clin. Endocrinol.* 49 (4), 421–432. doi:10.1046/j.1365-2265.1998.00507.x
- Muller, S., and Cleary, M. P. (1985). Glucose Metabolism in Isolated Adipocytes from Lean and Obese Zucker Rats Following Treatment with Dehydroepiandrosterone. *Metabolism* 34 (3), 278–284. doi:10.1016/0026-0495(85)90013-7
- Nawata, H., Yanase, T., Goto, K., Okabe, T., Nomura, M., Ashida, K., et al. (2004). Adrenopause. *Horm. Res. Paediatr.* 62 (Suppl. 3), 110–114. doi:10.1159/000080509
- Nestler, J. E., Barlascini, C. O., Clore, J. N., and Blackard, W. G. (1988). Dehydroepiandrosterone Reduces Serum Low Density Lipoprotein Levels and Body Fat but Does Not Alter Insulin Sensitivity in Normal Men*. *J. Clin. Endocrinol. Metab.* 66 (1), 57–61. doi:10.1210/jcem-66-1-57
- Orentreich, N., Brind, J. L., Rizer, R. L., and Vogelmann, J. H. (1984). Age Changes and Sex Differences in Serum Dehydroepiandrosterone Sulfate Concentrations throughout Adulthood. *J. Clin. Endocrinol. Metab.* 59 (3), 551–555. doi:10.1210/jcem-59-3-551
- Pérez-de-Heredia, F., Sánchez, J., Priego, T., Nicolás, F., Portillo, M. d. P., Palou, A., et al. (2008). Adiponectin Is Involved in the Protective Effect of DHEA against Metabolic Risk in Aged Rats. *Steroids* 73 (11), 1128–1136. doi:10.1016/j.steroids.2008.04.011
- Prattes, S., Hörl, G., Hammer, A., Blaschitz, A., Graier, W. F., Sattler, W., et al. (2000). Intracellular Distribution and Mobilization of Unesterified Cholesterol in Adipocytes: Triglyceride Droplets Are Surrounded by Cholesterol-Rich ER-like Surface Layer Structures. *J. Cell. Sci.* 113 (Pt 17), 2977–2989. doi:10.1242/jcs.113.17.2977
- Reed, M. J., Purohit, A., Woo, L. W. L., Newman, S. P., and Potter, B. V. L. (2005). Steroid Sulfatase: Molecular Biology, Regulation, and Inhibition. *Endocr. Rev.* 26 (2), 171–202. doi:10.1210/er.2004-0003
- Robenek, H., Buers, I., Robenek, M. J., Hofnagel, O., Ruebel, A., Troyer, D., et al. (2011). Topography of Lipid Droplet-Associated Proteins: Insights from Freeze-Fracture Replica Immunogold Labeling. *J. Lipids* 2011, 1–10. doi:10.1155/2011/409371
- Roth, M., Obaidat, A., and Hagenbuch, B. (2012). OATPs, OATs and OCTs: the Organic Anion and Cation Transporters of the SLCO and SLC22A Gene Superfamilies. *Br. J. Pharmacol.* 165 (5), 1260–1287. doi:10.1111/j.1476-5381.2011.01724.x
- Sanada, Y., Yamamoto, T., Satake, R., Yamashita, A., Kanai, S., Kato, N., et al. (2016). Serum Amyloid A3 Gene Expression in Adipocytes Is an Indicator of the Interaction with Macrophages. *Sci. Rep.* 6, 38697. doi:10.1038/srep38697
- Sayin, S., Kutlu, R., and Kulaksizoglu, M. (2019). The Relationship between Sex Steroids, Insulin Resistance and Body Compositions in Obese Women: A Case-Control Study. *J. Med. Biochem.* 39 (1), 25–31. doi:10.2478/jomb-2019-0009
- Schwartz, A. G., Pashko, L., and Whitcomb, J. M. (1986). Inhibition of Tumor Development by Dehydroepiandrosterone and Related Steroids. *Toxicol. Pathol.* 14 (3), 357–362. doi:10.1177/019262338601400312
- Schweiggmann, H., Sánchez-Guijo, A., Ugele, B., Hartmann, K., Hartmann, M. F., Bergmann, M., et al. (2014). Transport of the Placental Estradiol Precursor 16 α -Hydroxy-Dehydroepiandrosterone Sulfate (16 α -OH-DHEAS) by Stably Transfected OAT4-, SOAT-, and Ntcp-Hek293 Cells. *J. Steroid Biochem. Mol. Biol.* 143, 259–265. doi:10.1016/j.jsbmb.2014.03.013
- Shantz, L. M., Talalay, P., and Gordon, G. B. (1989). Mechanism of Inhibition of Growth of 3T3-L1 Fibroblasts and Their Differentiation to Adipocytes by Dehydroepiandrosterone and Related Steroids: Role of Glucose-6-Phosphate Dehydrogenase. *Proc. Natl. Acad. Sci. U.S.A.* 86 (10), 3852–3856. doi:10.1073/pnas.86.10.3852
- Singh, R., Artaza, J. N., Taylor, W. E., Braga, M., Yuan, X., Gonzalez-Cadavid, N. F., et al. (2006). Testosterone Inhibits Adipogenic Differentiation in 3T3-L1 Cells: Nuclear Translocation of Androgen Receptor Complex with β -Catenin and T-Cell Factor 4 May Bypass Canonical Wnt Signaling to Down-Regulate Adipogenic Transcription Factors. *Endocrinology* 147 (1), 141–154. doi:10.1210/en.2004-1649
- Stahl, F., Schnorr, D., Pilz, C., and Dörner, G. (1992). Dehydroepiandrosterone (DHEA) Levels in Patients with Prostatic Cancer, Heart Diseases and under Surgery Stress. *Exp. Clin. Endocrinol.* 99 (2), 68–70. doi:10.1055/s-0029-1211136
- Tagliaferro, A. R., Davis, J. R., Truchon, S., and Van Hamont, N. (1986). Effects of Dehydroepiandrosterone Acetate on Metabolism, Body Weight and Composition of Male and Female Rats. *J. Nutr.* 116 (10), 1977–1983. doi:10.1093/jn/116.10.1977
- Tchernof, A., Després, J.-P., Bélanger, A., Dupont, A., Prud'homme, D., Moorjani, S., et al. (1995). Reduced Testosterone and Adrenal C19 Steroid Levels in Obese Men. *Metabolism* 44 (4), 513–519. doi:10.1016/0026-0495(95)90060-8
- Valle, L. D., Toffolo, V., Nardi, A., Fiore, C., Bernante, P., Di Liddo, R., et al. (2006). Tissue-specific Transcriptional Initiation and Activity of Steroid Sulfatase Complementing Dehydroepiandrosterone Sulfate Uptake and Intracrine Steroid Activations in Human Adipose Tissue. *J. Endocrinol.* 190 (1), 129–139. doi:10.1677/joe.1.06811
- Villareal, D. T., and Holloszy, J. O. (2004). Effect of DHEA on Abdominal Fat and Insulin Action in Elderly Women and Men. *JAMA* 292 (18), 2243–2248. doi:10.1001/jama.292.18.2243

- Weiss, E. P., Villareal, D. T., Fontana, L., Han, D.-H., and Holloszy, J. O. (2011). Dehydroepiandrosterone (DHEA) Replacement Decreases Insulin Resistance and Lowers Inflammatory Cytokines in Aging Humans. *Aging* 3 (5), 533–542. doi:10.18632/aging.100327
- Wong, S. Y., Leung, J. C., Kwok, T., Ohlsson, C., Vandenput, L., Leung, P. C., et al. (2011). Low DHEAS Levels Are Associated with Depressive Symptoms in Elderly Chinese Men: Results from a Large Study. *Asian J. Androl.* 13 (6), 898–902. doi:10.1038/aja.2011.116
- Wu, T. T., Chen, Y., Zhou, Y., Adi, D., Zheng, Y. Y., Liu, F., et al. (2017). Prognostic Value of Dehydroepiandrosterone Sulfate for Patients with Cardiovascular Disease: A Systematic Review and Meta-Analysis. *Jaha* 6 (5), e004896. doi:10.1161/JAHA.116.004896
- Yamaguchi, Y., Tanaka, S.-i., Yamakawa, T., Kimura, M., Ukawa, K., Yamada, Y., et al. (1998). Reduced Serum Dehydroepiandrosterone Levels in Diabetic Patients with Hyperinsulinaemia. *Clin. Endocrinol.* 49 (3), 377–383. doi:10.1046/j.1365-2265.1998.00533.x
- Yamauchi, T., Kamon, J., Waki, H., Terauchi, Y., Kubota, N., Hara, K., et al. (2001). The Fat-Derived Hormone Adiponectin Reverses Insulin Resistance Associated with Both Lipodystrophy and Obesity. *Nat. Med.* 7 (8), 941–946. doi:10.1038/90984
- Yen, S. S. C., Morales, A. J., and Khorram, O. (1995). Replacement of DHEA in Aging Men and Women. *Ann. NY. Acad. Sci.* 774 (774), 128–142. doi:10.1111/j.1749-6632.1995.tb17377.x
- Yokokawa, T., Sato, K., Narusawa, R., Kido, K., Mori, R., Iwanaka, N., et al. (2020). Dehydroepiandrosterone Activates 5'-adenosine Monophosphate-Activated Protein Kinase and Suppresses Lipid Accumulation and Adipocyte Differentiation in 3T3-L1 Cells. *Biochem. Biophysical Res. Commun.* 528 (3), 612–619. doi:10.1016/j.bbrc.2020.05.136
- Zaitzu, H., and Serrero, G. (1990). Pedersen Fetuin Contains Three Adipogenic Factors with Distinct Biochemical Characteristics. *J. Cell. Physiol.* 144 (3), 485–491. doi:10.1002/jcp.1041440316
- Zumoff, B., Levin, J., Rosenfeld, R. S., Markham, M., Strain, G. W., and Fukushima, D. K. (1981). Abnormal 24-hr Mean Plasma Concentrations of Dehydroisoandrosterone and Dehydroisoandrosterone Sulfate in Women with Primary Operable Breast Cancer. *Cancer Res.* 41 (9Pt 1), 3360–3363.

Conflict of Interest: The authors declare that the research was conducted in the absence of any commercial or financial relationships that could be construed as a potential conflict of interest.

Publisher's Note: All claims expressed in this article are solely those of the authors and do not necessarily represent those of their affiliated organizations, or those of the publisher, the editors, and the reviewers. Any product that may be evaluated in this article, or claim that may be made by its manufacturer, is not guaranteed or endorsed by the publisher.

Copyright © 2022 Karakus, Schmid, Leiting, Fühler, Schäffler, Jakob and Geyer. This is an open-access article distributed under the terms of the Creative Commons Attribution License (CC BY). The use, distribution or reproduction in other forums is permitted, provided the original author(s) and the copyright owner(s) are credited and that the original publication in this journal is cited, in accordance with accepted academic practice. No use, distribution or reproduction is permitted which does not comply with these terms.



Site-Specific Regulation of Sulfatase and Aromatase Pathways for Estrogen Production in Endometriosis

Katiane de Almeida Da Costa^{1†}, Helena Malvezzi^{1†}, Cristine Dobo^{1,2}, Rosa Maria Neme^{1,3}, Renée Zon Filippi^{1,2}, Thiago Pinheiro Arrais Aloia¹, Elisa Rampazo Prado¹, Juliana Meola⁴ and Carla de Azevedo Piccinato^{1,4*}

¹Hospital Israelita Albert Einstein, São Paulo, Brazil, ²Department of Clinical Pathology, Hospital Israelita Albert Einstein, São Paulo, Brazil, ³Centro de Endometriose São Paulo, Av. República Do Libano, São Paulo, Brazil, ⁴Department of Gynaecology & Obstetrics, School of Medicine of Ribeirão Preto, University of São Paulo, Ribeirão Preto, Brazil

OPEN ACCESS

Edited by:

Jon Wolf Mueller,
University of Birmingham,
United Kingdom

Reviewed by:

Andrea Romano,
Maastricht University, Netherlands
Maire Peters,
University of Tartu, Estonia

*Correspondence:

Carla de Azevedo Piccinato
cpiccinato@uwalumni.com

[†]These authors have contributed
equally to this work and share the first
authorship

Specialty section:

This article was submitted to
Cellular Biochemistry,
a section of the journal
Frontiers in Molecular Biosciences

Received: 14 January 2022

Accepted: 04 April 2022

Published: 03 May 2022

Citation:

Da Costa KdA, Malvezzi H, Dobo C,
Neme RM, Filippi RZ, Aloia TPA,
Prado ER, Meola J and Piccinato CdA
(2022) Site-Specific Regulation of
Sulfatase and Aromatase Pathways for
Estrogen Production in Endometriosis.
Front. Mol. Biosci. 9:854991.
doi: 10.3389/fmolb.2022.854991

Endometriosis is a highly prevalent gynecological disease characterized by lesions in different sites. Regulation of specific estrogen pathways may favor the formation of distinct microenvironments and the progression of endometriosis. However, no study has simultaneously evaluated the gene and protein regulation of the main estrogen-synthesizing enzymes in endometriosis. Thus, our goals were to study the relationship between gene and protein expression of aromatase (*CYP19A1* or *ARO*), steroid sulfatase (*STS*), and hydroxysteroid 17-beta dehydrogenase (*HSD17B1*) in superficial (*SUP*), ovarian (*OMA*), and deep infiltrating (*DIE*) endometriotic lesion sites as well as in the eutopic endometrium of patients with (*EE*) and without (control) endometriosis in the same and large cohort of patients. The site-specific expression of these enzymes within different cells (glandular and stromal components) was also explored. The study included 108 patients surgically diagnosed with endometriosis who provided biopsies of *EE* and endometriotic lesions and 16 disease-free patients who collected normal endometrium tissue. Our results showed that *CYP19A1* was detected in all endometriosis tissues and was in higher levels than in control. Unique patterns of the *STS* and *HSD17B1* levels showed that they were most closely regulated in all tissues, with manifestation at greater levels in *DIE* compared to the other endometriotic lesion sites, *OMA* and *SUP*. Gene and protein expression of *ARO*, *STS*, and *HSD17B1* occurred at different rates in endometriotic sites or *EE*. The distinctive levels of these estrogen-synthesizing enzymes in each endometriotic site support the hypothesis of a tissue microenvironment that can both influence and be influenced by the expression of different estrogenic pathways, locally affecting the availability of estrogen needed for maintenance and progression of endometriotic lesions.

Keywords: aromatase, *CYP19A1*, *STS*, *HSD17B1*, estradiol, stromal cells, glandular cells, endometrium

INTRODUCTION

Endometriosis is the most prevalent gynecological disease in women of reproductive age (Taylor et al., 2021), and it is an important worldwide public health problem (Olive and Schwartz, 1993; Signorile and Baldi, 2010). Endometriosis is characterized by endometrial tissue localized outside the uterus (ectopic lesions), usually at several sites, that causes a chronic inflammatory process predisposing to adhesion formation (Jackson and Telner, 2006; Vermeulen et al., 2021). The current estimation of endometriosis prevalence is around 10–15% of women of childbearing age (Eskenazi and Warner, 1997; Giudice and Kao, 2004) of whom 20–50% present infertility-related symptoms (Smolarz et al., 2021).

Intracrinology of endometriosis debates on the balance between estrogen biosynthesis and metabolism that determines local estrogen availability in the tissues (Piccinato et al., 2018a). Evidence of this mechanism was revealed by data showing that the levels of estradiol and estrone remained constant in the lesions, despite the menstrual cyclical changes in circulating levels and the eutopic endometrium (Huhtinen et al., 2012). Such features indicate that, within the lesions, there are intrinsic regulatory pathways, which maintain high tissue availability of estrogen necessary for disease progression. As reported in previous studies, there are controversial data on gene regulation and protein levels of estradiol-synthesizing enzymes. Some studies have shown that, in endometriotic lesions, there are enzymes that synthesize estrogen from androgenic precursors as well as for *de novo* synthesis from cholesterol (Cornillie et al., 1990; Nap et al., 2004; Attar and Bulun, 2006; Kamergorodsky et al., 2009; Gibson et al., 2018; Mori et al., 2018; Mori et al., 2019). Conversely, estrogen-inactivating enzymes are clearly dysregulated in endometrial and/or endometriotic tissues evidencing a putative compensatory mechanism in view of the increased local estrogen concentrations (Piccinato et al., 2016b, 2017; 2018b).

Overall, two estrogen synthesizing pathways stand out: the aromatase (ARO)-dependent pathway and the steroid sulfatase (STS)-dependent pathway (Piccinato et al., 2018a). Briefly, ARO catalyzes the aromatization of androstenedione and testosterone to E1 or E2, respectively. STS mediates the local desulphonation of inactive circulating steroids, called estrogen sulfates, to their unconjugated, biologically active forms (Miller and Fraser, 2015; Foster, 2021). Interestingly, both pathways share a common final step through the action of hydroxysteroid 17-beta dehydrogenase (HSD17B1). This reducing enzyme belongs to the HSD17B family with high specificity for steroid substrates and high catalytic activity for the conversion of E1 to E2; therefore, HSD17B1 is an important regulator of intracellular steroid hormone concentration at the final stages of biosynthesis (Konings et al., 2018; Foster et al., 2019).

Although no clear association between lesion sites and enzymes function has been described in endometriosis, different types of lesions, as well as different localizations, seem to directly determine the dynamics of the disease (Taylor et al., 2021). Considering that endometriosis is an estrogen-dependent disease, the expression regulation of estrogen-

synthesizing enzymes may have an even more pre-eminent impact on endometriosis dynamics. In this context, although sometimes with contradicting results, some studies have focused on site-specific regulation of aromatase. A couple of studies have described ovarian lesions/endometriomas (OMA) express high levels of aromatase gene (*CYP19A1*) and protein (ARO) (Heilier et al., 2006; Szaflik et al., 2020), whereas deep infiltrating endometriotic lesions (DIE) either fail to express ARO or show reduced expression (Bulun et al., 2004). Another example of site-specific regulation occurs with STS, which is highly expressed in DIE and OMA (Šmuc et al., 2007; Šmuc et al., 2009; Piccinato et al., 2016b) but is minimally present or even absent (Colette et al., 2009) in the eutopic endometrium of endometriosis-affected women (Dassen et al., 2007). The unbalanced redox metabolism of enzymes belonging to the HSD17B1 family is the putative cause of the higher E2 synthesis that has been detected in ectopic and eutopic endometrium. Expression of reducing type- *HSD17B1* mRNA was significantly higher in the ectopic tissue (superficial peritoneal endometriosis: SUP, DIE, and OMA), whereas no difference was seen in the expression of *HSD17B1*-oxidizing types 2 and 4 (Šmuc et al., 2007; Bulun et al., 2010; Delvoux et al., 2014). Altogether, these observations strengthen the idea that the production of estrogen, which takes place through complex enzymatic pathways, is site-specific.

There is no consensus among published studies regarding the expression of estradiol-synthesizing enzymes in endometriotic lesions. Furthermore, there are no published studies simultaneously investigating the expression of these enzymes, ARO, STS, and HSD17B1, in endometriotic tissue samples obtained from a large cohort of patients. The present study explores previous significant reports that demonstrate high and constant levels of estrogens (estradiol and estrone) in different endometriotic tissues (Huhtinen et al., 2012). We, thus, hypothesize that the observed site-specific variations in estrogen concentrations are a result of differential expression regulation of estrogen-synthesizing enzymes, namely, ARO and STS, and also HSD17B1.

Although intracrine estrogen concentration depends on the complex interaction of synthesizing and metabolizing enzymes, our aim was to evaluate gene and protein expression of the synthesizing part (ARO, STS, and HSD17B1) in different types of endometriotic lesions (SUP, OMA, and DIE) as well as in samples of eutopic endometrium (EE) obtained from the same patients with endometriosis. Patients without endometriosis were donors of nonendometriosis eutopic endometrial tissue, here called the control group. In addition, we investigated by laser-capture microdissection and immunohistochemistry the cellular expression of the chosen enzymes.

MATERIALS AND METHODS

Patients and Samples

One hundred and ten women (94 with endometriosis and 16 without endometriosis: control group) were screened at the Assisted Reproduction Centre of the tertiary hospital of

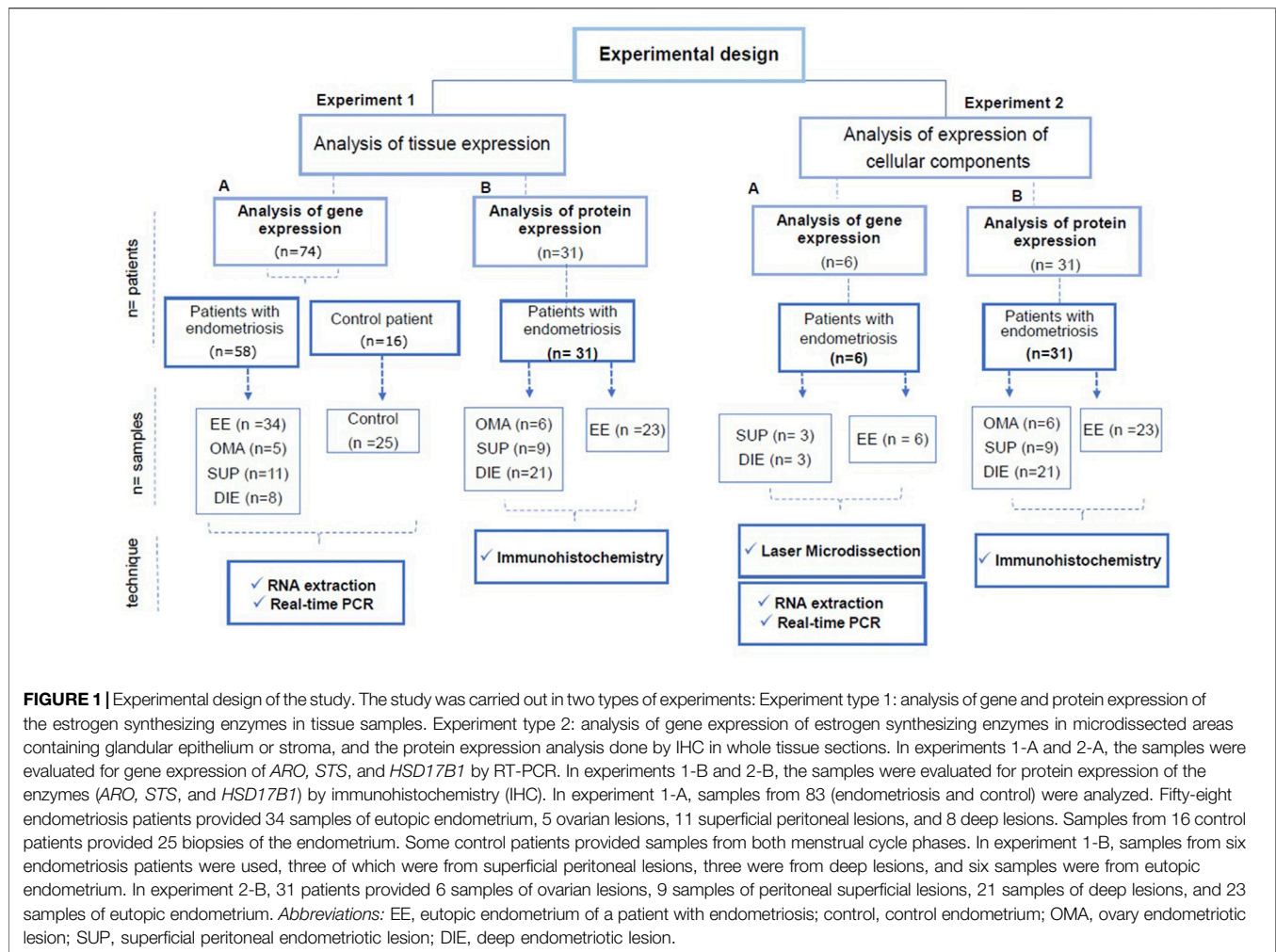


FIGURE 1 | Experimental design of the study. The study was carried out in two types of experiments: Experiment type 1: analysis of gene and protein expression of the estrogen synthesizing enzymes in tissue samples. Experiment type 2: analysis of gene expression of estrogen synthesizing enzymes in microdissected areas containing glandular epithelium or stroma, and the protein expression analysis done by IHC in whole tissue sections. In experiments 1-A and 2-A, the samples were evaluated for gene expression of *ARO*, *STS*, and *HSD17B1* by RT-PCR. In experiments 1-B and 2-B, the samples were evaluated for protein expression of the enzymes (*ARO*, *STS*, and *HSD17B1*) by immunohistochemistry (IHC). In experiment 1-A, samples from 83 (endometriosis and control) were analyzed. Fifty-eight endometriosis patients provided 34 samples of eutopic endometrium, 5 ovarian lesions, 11 superficial peritoneal lesions, and 8 deep lesions. Samples from 16 control patients provided 25 biopsies of the endometrium. Some control patients provided samples from both menstrual cycle phases. In experiment 1-B, samples from six endometriosis patients were used, three of which were from superficial peritoneal lesions, three were from deep lesions, and six samples were from eutopic endometrium. In experiment 2-B, 31 patients provided 6 samples of ovarian lesions, 9 samples of peritoneal superficial lesions, 21 samples of deep lesions, and 23 samples of eutopic endometrium. **Abbreviations:** EE, eutopic endometrium of a patient with endometriosis; control, control endometrium; OMA, ovary endometriotic lesion; SUP, superficial peritoneal endometriotic lesion; DIE, deep endometriotic lesion.

Faculdade de Medicina de Ribeirão Preto (Universidade de São Paulo, FMRP-USP), at the São Paulo Endometriosis Centre and Hospital Israelita Albert Einstein (HIAE), between the years 2011–2019. Biopsies of eutopic endometrium (control = control eutopic endometrium without endometriosis and EE = eutopic endometrium of a patient with endometriosis), superficial peritoneal endometriosis (SUP), deeply infiltrating endometriosis (DIE) (rectum, rectosigmoid, retrocervical, vesical, and uterosacral ligament lesions), and ovarian endometrioma (OMA) together with 5 ml of peripheral blood were collected in surgery.

The majority of patients enrolled for gene expression assessment are an extension of our sample cohort previously described (Piccinato et al., 2016b; Piccinato et al., 2018b), which includes proliferative and secretory phase samples. **Figure 1** depicts the control patients provided biopsies from both menstrual cycle phases; thus, out of 16 patients enrolled, 25 biopsies were collected (12 nonsecretory and 13 secretory). Endometriosis patients provided together 34 eutopic endometria (8 nonsecretory and 26 secretory), 5

endometrioma (2 nonsecretory and 3 secretory), 11 superficial lesions (1 nonsecretory and 10 secretory), and 8 deep infiltrating lesions (3 nonsecretory and 5 secretory). For protein expression evaluation, 34 endometriosis patients (19 nonsecretory and 15 secretory) provided 23 eutopic endometria, 6 endometriomas, 9 superficial lesions, and 21 deep infiltrating lesions. No difference in age was observed among patients (average of 35.5 ± 5 years).

All samples were collected after a written, informed consent form was signed by all patients. The study was approved by the Committee on Human Research of the Hospital Albert Einstein (FR-30468, 12/16/2009; São Paulo, Brazil), which is affiliated to the Ethics Committee of the Brazilian Ministry of Health (CONEP), upon signing the informed consent form.

The diagnosis of endometriosis was made by visualizing the lesions during surgery, which was further confirmed by histopathological analysis at the Pathological Anatomy Laboratory of FMRP-USP or HIAE. Nonendometriosis patients had confirmed the absence of endometriotic foci by inspection during tubal ligation surgery.

Inclusion criteria for both groups were reproductive age, nonsmokers, non-menopause, and no use of any hormonal therapy for at least 3 months before collection. Exclusion criteria were the presence of other reproductive disorders such as polycystic ovary syndrome, myoma, or any tumors.

Experimental Design

A diagram of the experimental design is shown in **Figure 1**. Basically, two types of experiments were performed. The gene and protein expression of estrogen synthesizing enzymes quantified by RT-PCR and immunohistochemistry (IHC) with the histometric analysis in extracted fragments from the lesion biopsies or, as a second approach, in the thereof microdissected or immunohistochemistry-stained endometrial glandular and stromal regions.

In all experiments, gene expression analyses were performed by RT-PCR and protein expression analyses were by immunohistochemistry. The patients' menstrual cycle phase was considered in all protein assessments. The menstrual cycle phase was defined by the dosage of progesterone: secretory (progesterone >1 ng) and nonsecretory (progesterone <1 ng).

Laser Capture Microdissection

The laser capture microdissection (LCM) technique was used to obtain separate samples of regions containing glandular cells or stromal cells. The preparation of histological slides (Membrane Slide NF 1.0 PEN D Zeiss, Munich, Germany) for LCM was performed in a cryostat (Leica CM 1860; Buffalo Grove, IL, United States), following the manufacturer's instructions. The samples were embedded, with the aid of an Optimal Cutting Temperature (OCT) compound (Sakura Finetek, Torrance, CA, United States), and cut into 10 μm sections. The slides were stained with Crystal Violet (Sigma Aldrich, MERK SA, Darmstadt, Germany) according to a protocol already tested by our group (Da Costa et al., 2019). The LCM was performed with the computerized system PALM RoboSoftWare 4.6 MicroBeam LSM 710 visualized with a 20x objective. Areas larger than 50 μm^2 were microdissected according to previous standardization of the LCM technique (Da Costa et al., 2019). The microdissected materials were collected in microdissection tubes (Sample AdhesiveCap 500 clear D Zeiss, Munich, Germany) and immediately frozen at -80°C .

Whenever needed, a pathologist validated the identification of the two areas, glandular and stromal, in the microdissected samples of EE and endometriotic lesions. Glandular and stromal areas from EE were, respectively, compared with glandular and stromal areas from endometrial lesions.

RNA Extraction

The PicoPure RNA Isolation Kit (Life Technologies, MERK SA, Darmstadt, Germany) was used to extract RNA from whole biopsy samples, whereas for the microdissected samples, a specific kit for microdissected samples, RNAaqueous Micro Total RNA Isolation Kit (ThermoFisher Scientific, Waltham, MA, United States) was used. The extracted total RNA was quantified by spectrophotometry using a NanoDrop One Microvolume UV-Vis Spectrophotometer (ThermoFisher Scientific, Waltham, MA, United States) at an absorbance of 260 nm and frozen at -80°C .

cDNA Synthesis and Real-Time Polymerase Chain Reaction (RT-PCR in Real Time)

Reverse transcription of RNA samples was performed using the SuperScript III First-Strand Synthesis SuperMix Kit (Invitrogen, ThermoFisher Scientific, Waltham, MA, United States) with oligo-dT primers. Some RNA samples needed dilution in DNase/RNase free ultrapure water and others were concentrated using a vacuum concentrator (Refrigerator Centrivap Vacuum Concentrators- Labconco, Kansas City, MO, United States). The final reaction volume was 14 μl per sample. The samples were placed in a thermocycler (Master Cycler-Nexus, Eppendorf Sigma Aldrich, MERK SA, Darmstadt, Germany) at 50°C for 50 min.

The sequences of genes analyzed and synthesized by Invitrogen Brazil were CYP19A1 forward = 5-CACAGAAGA GAACTGGAAGAA-3 and reverse = 5- TCCAATATGCAC TGGTTCAC-3, STS forward = 5-GGAGTGAGAAGGGCATGG TA-3 and reverse = 5-CTCCAGCAGCCTCTTTATGG-3, HSD17 β 1 forward = 5-TCGCGTTAGCCAGTTTTACC-3 and reverse = 5-TCGCGTTAGCCAGTTTTACC-3, and GAPDH (housekeeping) forward = 5-GAAGGTGAAGGTCGGAGTCA-3 and reverse = 5-TGAGGTCAATGAAGGGGTCA-3.

Real-time amplification was performed according to the SYBRGreen Master Mix assay protocol (Thermo Fisher Scientific, Waltham, MA, United States). Briefly, 1.5 μl of cDNA was added to 13.5 μl of the mix, totaling the final volume of 15 μl of reaction per well of the plate. The specificity of the generated product was confirmed by analyzing the dissociation curve of the primers (melting curve) of the formed products as well as by electrophoretic running of the material amplified on a 2.5% horizontal agarose gel. The calculations of the relative gene expression of the samples were made using the $\Delta\Delta\text{Ct}$ method with the housekeeping gene *GAPDH* as normalizer. The normalizer was determined based on the coefficient of variation (CV) obtained in similar datasets, being the lowest when compared to other candidate housekeeping genes (Piccinato et al., 2016b; Piccinato et al., 2018b).

To calculate $\Delta^{-\text{Ct}}$ as well as to control intra-assay variation, placental cDNA was used as a reference sample for the analysis of gene expression of the biopsy (whole tissue) (Piccinato et al., 2016a). For the analysis of gene expression of cellular components, a pool of samples of 2 μl of cDNA from tissue samples (non-microdissected) was used as a reference sample.

Immunohistochemistry and Histometric Analysis

Paraffin-embedded blocks were used. 3 μm thick sections spaced by 9 μm were obtained (microtome: Leica RM2125 RTS, Buffalo Grove, IL, United States).

Immunohistochemistry was performed using the BenchMarck ULTRA IHC/ISH labeling platform from Ventana Medical System Inc. (Tucson, Arizona, United States) using the ultraView Universal DAB Detection kit, following the manufacturer's guidelines. In brief, slides were blocked with hydrogen peroxide and incubated at 35°C with 100 μl of

primary antibody 1:200 anti-ARO (ab18995, Abcam, Cambridge, United Kingdom) and 1:200 anti-HSD17B1 antibodies (ab51045, Abcam, Cambridge, United Kingdom) for 1 h and antiSTS 1:100 (ab62219, Abcam, Cambridge, United Kingdom) for 2 h. The samples were incubated with polymer, chromogen, and stained with hematoxylin. At the end of the procedure, the slides were washed in a solution with Tween 20 detergent (Sigma-Aldrich, MERK SA, Darmstadt, Germany), dehydrated to 100% alcohol, and mounted with coverslips and mounting medium (Dako, Mounting Medium).

The stained slides were analyzed using the IX51 Microscope and Olympus cellSens Dimension 1.16 software (Shinjuku, Tokyo, Japan). To evaluate the protein expression of the whole tissue samples, three different fields from each section were photomicrographed at $\times 10$ magnification, resulting in nine images per sample. To evaluate protein expression, two different fields of each section were photomicrographed (at $\times 20$), resulting in six photomicrographs per sample. Similarly, the same photomicrographs were used to determine enzyme staining at different cellular components: glandular or stromal areas. Protein expression values were determined from the histometric analysis of the percentage of the stained area for each of the proteins (ARO, STS, and HSD17B1) (Bartels et al., 1995).

Statistical Analysis

The variables of interest in the present study, gene and protein expression of ARO, STS, and HSD17B1 and their ratios, were continuous, nonnormal, and asymmetrically distributed, being analyzed by generalized models with Weibull distribution or generalized estimating equation models with Tweedie distribution, in order to compare groups (EE, SUP, OMA, and DIE) and menstrual cycle phase (secretory and nonsecretory). The ratio between enzymes (ARO:STS, ARO:HSD17B1, and STS:HSD17B1) was a mathematical strategy to evaluate the relative expression level between enzymes per sample. The models adjusted considered the interaction effect between the groups and menstrual cycle phase, the dependence between the measurements of the same patient in different tissues (e.g., EE and lesions), and the multiple comparisons were corrected by the sequential Bonferroni method. The results are presented as estimated means and 95% confidence intervals (CI). Spearman's correlation was applied to evaluate the relationship among variables. Analyses were performed using the SPSS program, R, and GAMLSS package, considering a p value of less than 0.05 statistically significant.

RESULTS

Higher *CYP19A1* Expression Occurs in Endometriosis Tissue, and Higher ARO Occurs in Eutopic Endometrium as Compared to Lesions

We compared the gene expression between endometriosis tissues and control and protein expression among endometriotic lesions

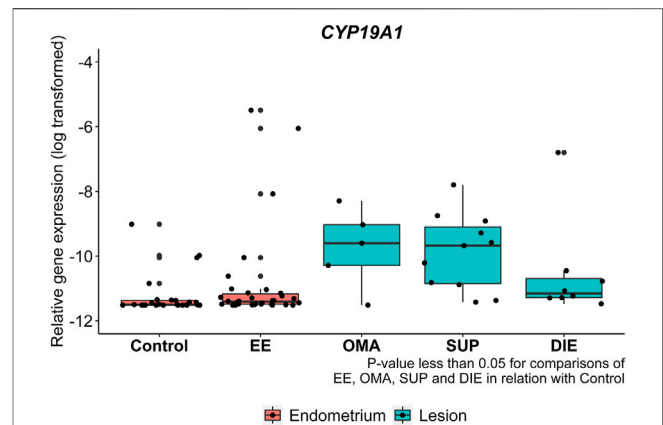


FIGURE 2 | *CYP19A1* mRNA expression from endometriotic samples.

Gene expression levels of *CYP19A1* were analyzed by real-time polymerase chain reaction in eutopic endometrium from control patients (control), eutopic endometrium from endometriosis patients (EE), and in ovarian (OMA), superficial (SUP), and deep-infiltrating (DIE) lesions. Relative gene expression levels were normalized by *GAPDH*. Bars represent the \log_{10} mean fold change of the normalized gene expression relative to a reference sample and 95% CI. Statistical differences between groups are indicated by * $p < 0.005$.

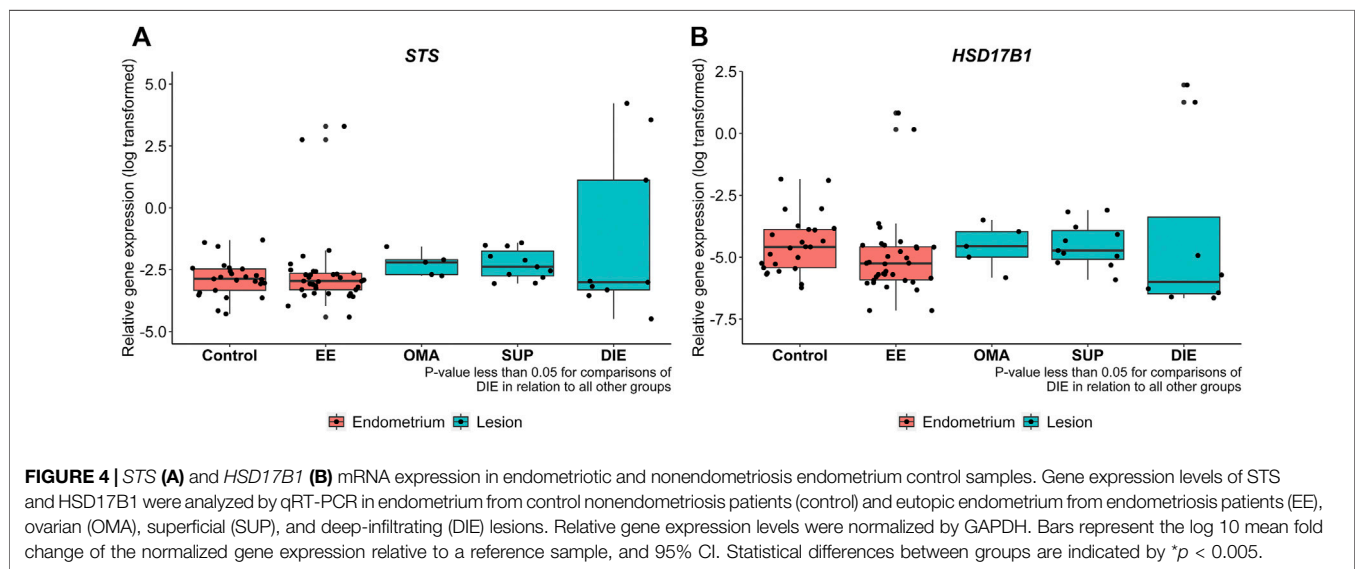
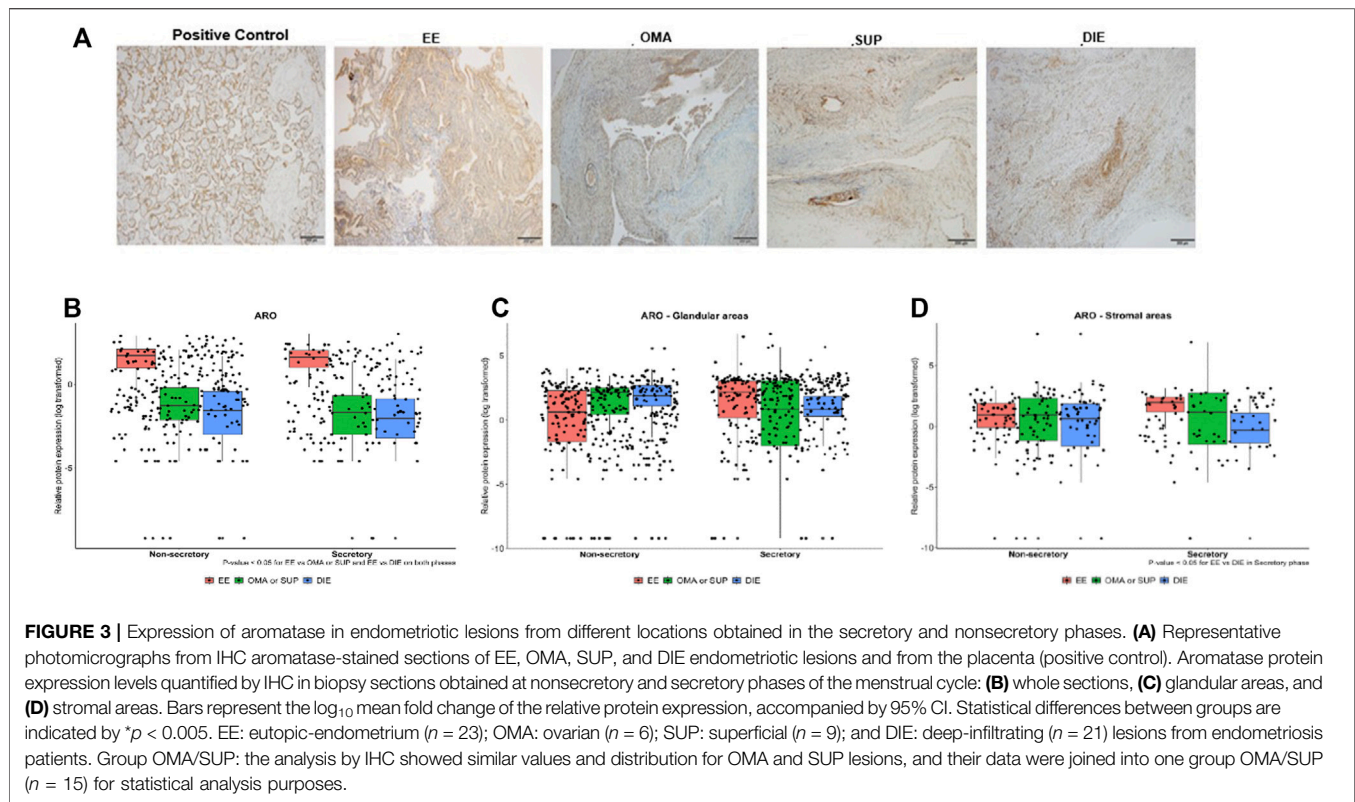
and EE. Notably, expression levels of *CYP19A1* were significantly higher in all types of endometriotic lesions OMA (12 times, $p = 0.0390$), SUP (31 times, $p = 0.0171$), and DIE (16 times, $p = 0.0446$), as well as in the EE (4 times, $p = 0.039$), compared to control endometrium (Figure 2).

When whole sections were analyzed by IHC (Figure 3A) for ARO protein expression, higher expression of this enzyme was detected in EE compared to OMA/SUP ($p < 0.003$) and DIE ($p < 0.001$) at both menstrual phases (Figure 3B).

Next, we looked at ARO protein expression in the stromal and glandular regions of EE, OMA/SUP, and DIE biopsies (Figure 3C and 3 days). Both regions, stromal and glandular, of the three types of biopsy locations, expressed ARO at similar levels, at both menstrual phases (Figure 3C and 3 days). The only significant difference in ARO expression was detected in the stromal area of DIE (circa 10-fold higher) vs. EE at the secretory phase (Figure 3D).

Gene and Protein Expression of STS and HSD17B1 Are Higher in Endometriotic Lesions Than in EE

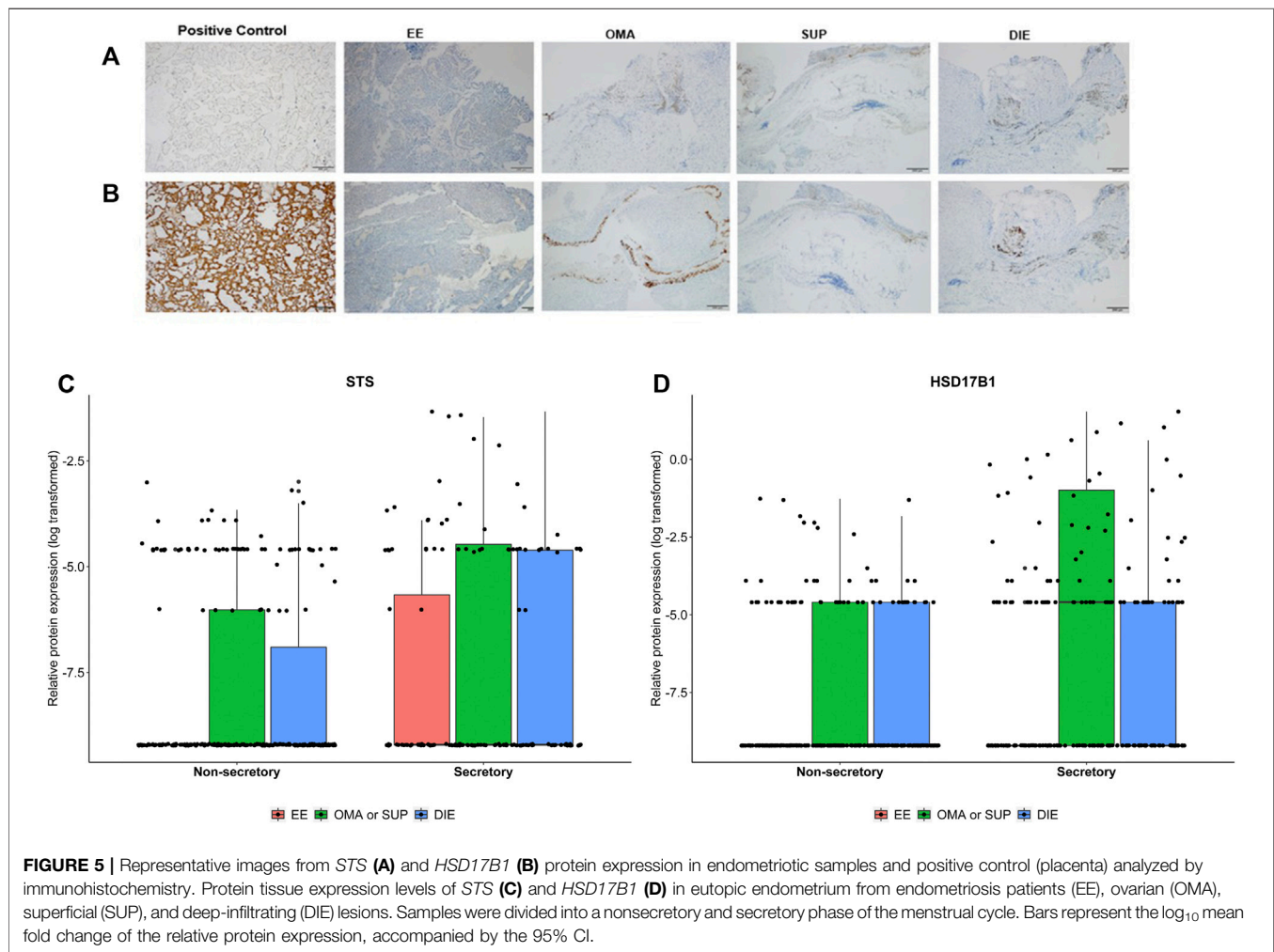
Figure 4 depicts RT-qPCR results regarding tissue STS and HSD17B1 gene expression. Only DIE had significantly higher expression levels of STS and HSD17B1 in comparison to all other collected samples including control ($p = 0.0003$ and $p = 0.0163$, respectively), EE ($p = 0.018$ and $p = 0.0035$, respectively), and other endometriotic sites (OMA: $p = 0.0223$ and $p = 0.0201$, respectively, and SUP: $p = 0.0004$ and $p = 0.0035$, respectively). Apart from DIE, all other groups showed similar levels of STS or HSD17B1 mRNA expression. Tissue protein analyses by IHC done on whole tissue sections



for either *STS* (**Figure 5A**) or *HSD17B1* (**Figure 5B**) showed no statistical differences among groups (**Figure 5C,D**).

However, when areas of sections were analyzed for *STS* protein expression, OMA/SUP and DIE groups had (**Supplementary Figure S1**), in the glandular areas, higher values than in eutopic endometrium from patients (EE) at

both menstrual cycle phases (**Figures 6A,B**). In the stromal areas, again OMA/SUP ($p = 0.018$) and DIE ($p = 0.012$) groups had *circa* two-fold higher values for *STS* expression than EE. In contrast, *HSD17B1* was present in the glandular and stromal areas, but differences between groups of *circa* two-fold were detected only at nonsecretory-phase samples for



OMA/SUP ($p < 0.001$) or DIE ($p = 0.012$) vs. EE (Figures 6A,B).

STS Is the Most Expressed Gene in Endometriosis, but ARO Is the Most Expressed Enzyme

Ratio analyses were employed to compare groups regarding enzyme relationships. The gene and protein ratios between estrogen-synthesizing enzymes were chosen to evaluate the regulation of ARO, STS, and HSD17B1. For these analyses, the interaction effect between the group and the cycle phase classification was taken into consideration. As shown, STS had the highest values for gene expression, and ARO had the highest ones for protein comparisons (Tables 1,2). The gene expression ratios, *CYP19A1:STS* and *CYP19A1:HSD17B1*, were significantly higher in endometriotic lesions compared to EE and control. These results indicate that *CYP19A1* was lower than STS in OMA ($p = 0.022$) e SUP ($p = 0.004$) compared to control, and in SUP ($p = 0.012$) compared to EE. In addition, *CYP19A1* was lower than HSD17B1 in OMA ($p = 0.005$), SUP ($p = 0.0005$), and DIE

($p = 0.039$) in relation to control, and lower in SUP ($p = 0.049$) when compared to EE. There was also a difference in *CYP19A1:HSD17B1* ratio between EE and control ($p = 0.011$) (Table 1).

At the protein level, comparisons of the ARO:STS ratio among all groups highlighted that the ARO expression was consistently greater than the STS expression (Table 2). The ARO expression prevailed over the STS expression in EE, in both cycle phases, with higher ratio in EE as compared to OMA:SUP lesions ($p < 0.001$ in the nonsecretory phase; $p = 0.017$ in the secretory phase) and DIE ($p < 0.001$ in the nonsecretory phase; $p = 0.017$ in the secretory phase). In all compared groups, the ARO: HSD17B1 ratios indicate that ARO was greater than the expression of HSD17B1 (Table 2). The ARO: HSD17B1 ratio was higher in EE when compared to DIE ($p = 0.032$) in the secretory phase but not among the other experimental groups. No other differences were detected among endometriotic sites. Notably, the STS: HSD17B1 ratio did not vary among all compared groups ($p > 0.05$).

The Spearman correlation analysis was employed to evaluate the relationship among gene and protein expression of enzymes regardless of groups. The results of mRNA expression showed

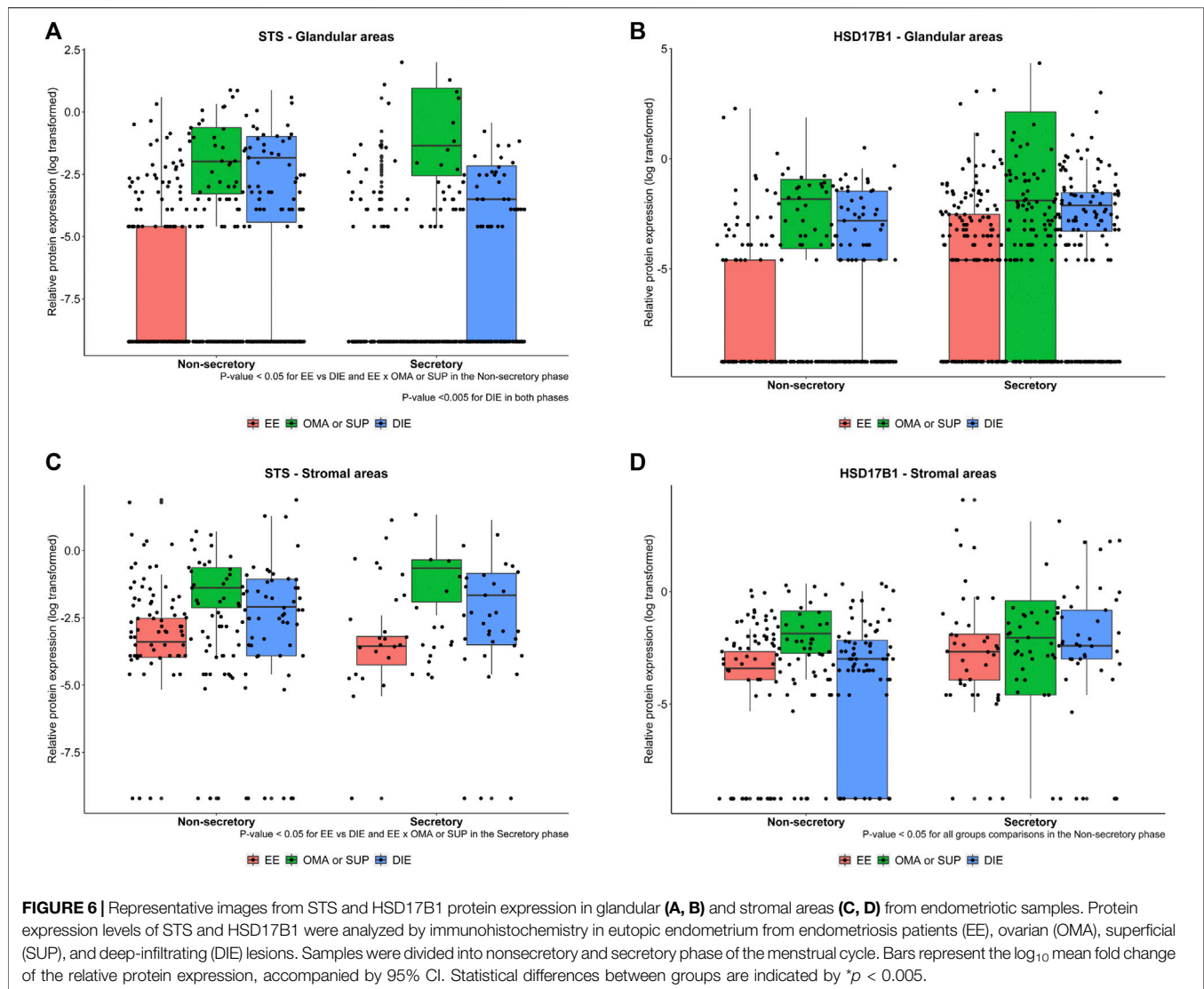


TABLE 1 | Gene expression ratio among *CYP19A1*, *STS*, and *HSD17B1* in biopsies from endometriotic lesions and from eutopic endometrium of non-endometriosis patients (control).

	Ratio <i>CYP19A1</i> : <i>STS</i> ($\times 10^{-5}$)	Ratio <i>CYP19A1</i> : <i>HSD17B1</i> ($\times 10^{-5}$)	Ratio <i>HSD17B1</i> : <i>STS</i> ($\times 10^{-8}$)
Control	2.4 (0.6; 10.5)	9.9 (2.3; 41.7)	39.4 (21.6; 71.8)
EE	6.7 (2.9; 15.5)	76.1 (25.9; 223.5) [*]	14.7 (10.9; 19.9)
OMA	21.4 (0.9; 526.5) [*]	146.5 (3.2; 6682.5) [*]	15.3 (7.5; 31.6)
SUP	65.2 (22.6; 188.1) ^{*#}	584.2 (210.3; 1623.1) ^{**}	15.9 (10.5; 24.0)
DIE	11.0 (5.3; 23.0)	155.7 (49.8; 487.3) [*]	10.4 (7.0; 15.6)

Results are expressed as mean and 95% CI. **p* < 0.01 vs. control. #*p* < 0.01 vs. EE. ^{*}*p* < 0.05 vs. EE within cycle phase. ^{*}*p* < 0.05 vs. control. ^{*}*p* < 0.001 vs. control. ^{**}*p* < 0.05 vs. EE.

weak and positive correlation between *CYP19A1* and *STS* ($\rho = 0.052$, $p = 0.001$) and between *CYP19A1* and *HSD17B1* ($\rho = 0.033$, $p = 0.0005$). Furthermore, there was a stronger and positive correlation between *STS* and *HSD17B1* ($\rho = 0.402$, $p < 0.001$). Correlation among protein levels demonstrated weak and

negative correlation between ARO and *HSD17B1* ($\rho = -0.152$, $p = 0.001$) and weak and positive correlation between *STS* and *HSD17B1* ($\rho = 0.133$, $p = 0.009$). ARO e *STS* demonstrated weak negative correlation with no statistical difference ($\rho = -0.051$ e $p = 0.310$).

TABLE 2 | Protein expression ratio among *ARO*, *STS*, and *HSD17B1* in biopsies from endometriotic lesions and from eutopic endometrium of nonendometriosis patients (control).

	Cycle phase	Ratio ARO:STS ($\times 10^{-1}$)	Ratio ARO:HSD17B1 ($\times 10^{-1}$)	Ratio STS:HSD17B1
EE	Nonsecretory	59.8 (42.1; 84.8)	57.3 (25.2; 130.6)	0.38 (0.05; 0.89)
	Secretory	57.8 (28.6; 117.0)	66.7 (31.8; 139.6)	0.43 (0.1; 0.84)
SUP-OMA	Nonsecretory	11.9 (6.0; 23.8)*	7.1 (2.7; 18.7)	0.31 (0.13; 0.59)
	Secretory	1.8 (1.0; 3.1) #	8.2 (2.7; 25.1)	0.36 (0.11; 0.72)
DIE	Nonsecretory	3.3 (1.0; 11.3)*	3.4 (1.6; 7.2)	0.31 (0.11; 0.63)
	Secretory	1.3 (0.7; 2.4)#	3.9 (2.1; 7.4)**	0.36 (0.15; 0.65)

Results are expressed as mean (95% CI). *p < 0.01 vs. EE within cycle phase. #p < 0.05 vs. EE within cycle phase. *p < 0.05 nonsecretory vs. secretory phase. **p < 0.05 vs. EE within cycle phase.

No Detectable Differences in the Expression of *CYP19A1*, *STS*, and *HSD17B1* mRNA Were Observed at Cellular Levels

CYP19A1 was detected in 20.8% of samples, while *STS* was identified in 83% of stromal and 66% of epithelial cells. *HSD17B1* expression was present in almost all samples: 91.6% stromal and 91.6% epithelial (Supplementary Figure S2).

DISCUSSION

Our hypothesis in this study was that previously reported estrogen levels detected in endometriosis sites (Huhtinen et al., 2012) are different in function of the distinct expression of estrogen-synthesizing enzymes in each lesion site. Our data show that the relative expression of *ARO*, *STS*, and *HSD17B1* vary in endometriotic tissue obtained from deep infiltrating lesions (DIE), superficial (SUP), ovarian (OMA), and eutopic endometrium from endometriosis patients (EE) lend support to the hypothesis. The expression of those enzymes in endometriosis was also compared to endometrium samples of nonendometriosis patients (control). It should be mentioned that we analyzed material from a large number of patients taking into account the patients' menstrual cycle phases.

The gene encoding *ARO*, *CYP19A1*, was detected in all endometriosis tissue at levels all greater than found in control; *STS* and *HSD17B1* presented consistently higher mRNA expression levels in DIE. In addition, analysis of gene expression levels applied to the dataset indicated that *STS* and *HSD17B1* genes were the most closely regulated. Overall, for protein expression, EE presented higher levels of *ARO* and endometriotic lesions had superior levels of *STS* and *HSD17B1*. Particularly, unique patterns of mRNA expression levels of the *STS* and *HSD17B1* were described in DIE when compared to OMA and SUP lesion sites; EE gene and protein expression regulations of *ARO*, *STS*, and *HSD17B1* were distinct from those of the endometriotic sites. Taken together, the findings of different levels of the estrogen-synthesizing enzymes in distinct lesion sites support the hypothesis that the local tissue microenvironment can influence and be influenced by the regulation of different estrogenic pathways. Ultimately, this determines the local availability of estrogen, previously reported in other studies (Huhtinen et al., 2012), which in turn directly affects the local growth of ectopic endometrium.

Gene expression (mRNA) and tissue protein expression (as measured in IHC stained sections) of *ARO*, *STS*, and *HSD17B1*, as well as their relative ratios, did not always match. *STS* mRNA was more expressed in relation to the others enzymes, in all sample groups analyzed, followed by *HSD17B1* and finally by *CYP19A1*. *ARO* protein expression was higher among groups, followed by *STS* and *HSD17B1*. We detected differences between *CYP19A1*:*STS* ratios, *CYP19A1*:*HSD17B1* (gene expression), *ARO*:*STS*, and *ARO*:*HSD17B1* (protein expression) in different sites of endometriosis. This would reinforce the idea that there is a regulation of enzymes in a site-specific manner, as the proportions are variable among sites. On the other hand, the lack of difference between gene and protein expression for the ratio *HSD17B1*:*STS*, in different endometriosis sites indicates that these enzymes are more closely regulated, as they show less expression variation. Supporting this observation, the Spearman correlation analysis of gene expression between *STS* and *HSD17B1* revealed a positive, moderate correlation between these same enzymes, not seen between them and *CYP19A1*. Correlation among protein levels was, in general, weak and, although significant, might not be clinically relevant.

It seems that endometriotic lesion sites' estrogen synthesis is more closely regulated by the enzymes *STS* and *HSD17B1*, whereas in the EE, *ARO* is the dominant regulator. Although *STS* expressed higher mRNA but not protein in comparison with the other enzymes, the stromal areas of OMA/SUP and DIE lesions showed *STS* elevated levels of protein. Conversely, *ARO* was significantly more expressed at the protein level, and it was prominent in stromal areas of EE.

The existence of tissues similar to the endometrium in sites other than the uterine cavity implies that there are local and specific mechanisms that support the survival and growth of the ectopic tissue in an otherwise alien environment. Comparative to the other sites, DIE presented the most distinct and elevated *STS* and *HSD17B1* mRNA expression levels. This suggests that a unique hormonal environment developed in this lesion type favoring high estrogen-synthesis enzymes. Indeed, estradiol measurements by HPLC-MSMS showed its high and persistent concentrations in endometriotic lesions, including deep lesions (Huhtinen et al., 2012). Because vascularization is limited in the DIE (Liu et al., 2008) and the antagonizing enzyme, sulfotransferase is upregulated (Piccinato et al., 2016a), and it seems reasonable to propose that regulatory mechanisms might exist to maintain estradiol levels and disease progression despite poor blood irrigation. In OMA and largely in SUP lesions, blood supply is more pronounced favoring the mRNA

expression of *CYP19A1*, allowing the use of the precursor's testosterone/androstenedione from circulation to synthesize estradiol.

Either higher levels, or no difference, or absence of *CYP19A1* mRNA was previously described in endometriotic lesions in comparison with the endometrium of disease-free, women-control, or of endometriosis patients, EE (Noble et al., 1997; Matsuzaki et al., 2006; Dassen et al., 2007; Colette et al., 2009; Mori et al., 2018). Despite having verified that there is *CYP19A1* expression in control endometrium (although at lower levels compared to EE), this study corroborates previous findings showing increased gene and protein expression of ARO in EE (Hudelist et al., 2007; Aghajanova et al., 2009).

The enzymes STS and HSD17B1 have been considered important in the pathogenesis of endometriosis, as indicated by the use of their inhibitors in the treatment of endometriosis (Purohit et al., 2008; Salah et al., 2017; Maltais et al., 2018; Barra et al., 2019). Our data evidenced a parallel regulation between them suggesting a local combined relationship. Thus, STS and HSD17B1 together can play an important role in estrogen production by desulfating sulfated steroidogenic compounds (DHEAS, E2S, and E1S) into active compounds that reach endometriotic tissues in the bloodstream (Purohit et al., 2008). Expression of STS (gene and protein), being greater than of HSD17B1, may provide more E1 or E2, but the final balance between these two estrogens depends on HSD17B1 regulating the formation of the more active estradiol, namely, E2.

In consonance with other authors (Konings et al., 2018), we found in a larger cohort of patients that the expression of STS and HSD17B1 genes was much higher in DIE compared to all other endometriotic lesion types and EE or endometrium from nonaffected women. Increased STS mRNA expression has also been demonstrated in OMA, whereas HSD17B1 expression was higher in all types of endometriotic lesions when compared to control (Šmuc et al., 2007) or EE (Mori et al., 2015). In fact, only low levels of the HSD17B1 gene and protein (Dassen et al., 2007) or total absence of this enzyme (Utsunomiya et al., 2001) were reported in the endometrium of nonaffected women. Colette et al. (2013) described similar levels of 1 HSD17B1 gene and protein expressions among different types of lesions.

The elevated expression of STS and HSD17B1 genes in DIE lesions in comparison to other lesion types was not paralleled by the corresponding protein expression of these enzymes. Although staining by IHC was present for both enzymes, there were no significant quantitative differences between the analyzed groups (EE, SUP, OMA, and DIE). Other studies have also failed to find significant differences in STS protein expression among different endometriotic lesions and EE (Dassen et al., 2007).

The lack of association between the results of gene and protein expressions of the analyzed estradiol-producing enzymes can be explained by posttranscriptional regulatory events, which can prevent the formation of functional proteins from the mRNA transcript. Estrogens are consistently present in endometriotic tissue, regardless of the menstrual cycle phases (Huhtinen et al., 2012). Interestingly, the stability of several mRNAs is regulated by estrogens (Ing, 2005). Several microRNAs (miRNA) control gene expression at the posttranscriptional level and can be induced or inhibited by estrogen (Klinge, 2012; Kolanska et al., 2021). In addition,

E2 canonical signaling pathways mainly mediated by nuclear estrogen receptors can perform as transcription factors to stabilize or destabilize mRNAs via miRNAs modifying gene expression (Kim et al., 2021). These controls promote the expression of genes that are critical to either strengthen or diminish the effects of steroid hormones that depend on the feedback of the same enzymes they regulate. Furthermore, estrogen-regulated expression of miRNA is both cell- and tissue-specific (Cohen et al., 2008).

Regarding the participation of the glandular versus stromal areas of endometriotic lesions in estrogen synthesis, we looked at the expression of ARO, STS, and HSD17B1 in the various types of endometriotic lesions and of eutopic endometrium, EE. Molecular and histophysiological differences between stromal and glandular cells from EE or endometriotic lesions have already been described such as alterations in prosurvival enzymes, cytoskeletal proteins, proteasomes, and cell repair mechanisms (Bastos Wolff et al., 2012). It was suggested that endometrial stromal cells responsive to progesterone could induce HSD17B2 (i.e., inactivation of E2) in epithelial cells (Yang et al., 2001) via paracrine factors. However, primary cultures of OMA stromal cells stimulated with progesterone resulted in the suppression of HSD17B2 expression in epithelial Ishikawa cells (Cheng et al., 2007).

We found higher protein expression of HSD17B1 in the stromal cell regions from endometriotic lesions. This result lends support to the idea that the regulation of estrogen secretion in endometriotic lesions is cell-specific. A pilot study detected, by immunofluorescence, the presence of stromal cells (but not epithelial cells) in the bloodstream of women with endometriosis, suggesting that endometrial stromal cells may migrate from the EE to distant sites via the bloodstream (Lin et al., 1995). It may also suggest that stromal cells could participate in the maintenance of endometriotic lesions. For the STS pathway, both stromal and epithelial cells seem to act at maintaining high levels of estrogen-synthesizing enzymes, as observed in our results. It appears that stromal cells are more susceptible to deficient steroid hormonal secretion.

Because steroid hormones regulate the expression of some estrogen metabolizing and synthesizing enzymes, which could be present at different levels throughout the menstrual cycle, the experimental design of our study included samples from progesterone-secretory and nonsecretory phases. Although the menstrual cycle phase was taken into account in the statistical analysis, it was not always possible to separate the main findings of the study considering this variable, especially for the gene analysis. Interestingly, stromal STS secretion was higher during the secretory phase, when compared to glandular STS expression in the nonsecretory phase. Furthermore, DIE lesions expressed more STS protein in the secretory phase than in the nonsecretory phase. These results agree with previously published results (Simpson et al., 1994) and with those from our group (Piccinato et al., 2016b), in which increased STS expression levels were seen in the secretory phase of the cycle. In contrast, other authors have reported that STS expression levels are not altered in the different phases of the menstrual cycle (Šmuc et al., 2007; Colette et al., 2013).

The higher protein expression of ARO was found in stromal EE in relation to DIE, in secretory phase samples, which agrees with the results of ARO tissue protein expression, suggesting that the stromal cells in the endometrium may be the main site of

estrogen production. However, some authors have found ARO mRNA and protein expressed preferentially in glandular cells (Aghajanova et al., 2009; Wang et al., 2010). It is known that the endometrial tissue undergoes cyclical changes according to systemic hormonal variation (Foti et al., 2018). However, our findings suggest that the EE may be autonomous with regard to regulation of the ARO pathway, maintaining its expression, and the increased local estrogen production, regardless of systemic hormonal variations. Considering the basic characterization of endometriosis, such as the presence of endometrial tissue in other sites, it is important to understand not only the ectopic behavior of the endometrial-like tissue but also the behavior of that tissue in its place of origin (uterus) during the onset of the disease.

We found high variability among samples in the gene expression of all enzymes in stromal and glandular cell areas. Of note, most samples did not express detectable levels of *CYP19A1* mRNA. The absence of *CYP19A1* in some microdissected biopsies may signify no expression or expression below the detection levels of RT-PCR. In fact, LCM yields small amounts of microdissected material (Matsuzaki et al., 2004) and, consequently, amplification of genes with a low expression such as *CYP19A1* might not reach detectable levels. It is important to consider that the number of microdissected samples for the experiments on gene expression was rather small. Despite having generated interesting primary results, we have to consider them preliminary and subject to confirmation.

CONCLUSION

Although the level of the single enzymes in the intracrine machinery varies with apparently no clear association with the localization of endometriotic lesions, a combination of enzymes and site intracrinology may explain site-specific characteristics of the disease. The results of the present study support this idea, as endometriotic sites present, at both gene and protein levels, higher *STS* and *HSD17B1*, whereas in EE, there was increased ARO expression. The cellular compartment of *in situ* protein expression seems to emphasize the importance of cell regulation in a paracrine manner. Finally, even though *STS* was the most expressed gene, ARO was the most expressed protein, revealing a complex site-specific system of transcript activation. Although enzyme activity studies are still required to fully understand how estrogen biosynthesis is regulated in the distinct sites where endometriosis occurs, it was possible to substantiate the pronounced gene and protein regulation of *STS* and *HSD17B1*, in endometriotic sites (particularly, in DIE) and of ARO in EE. It is apparent that endometriotic lesions at different sites correspond to different facets of the same disease and develop site-dependent intrinsic regulatory mechanisms.

DATA AVAILABILITY STATEMENT

The original contributions presented in the study are included in the article/**Supplementary Material**, further inquiries can be directed to the corresponding author.

ETHICS STATEMENT

The studies involving human participants were reviewed and approved by the Research Ethics Committee of the Hospital Israelita Albert Einstein (CAAE: 56229916.9.0000.0071). The patients/participants provided their written informed consent to participate in this study.

AUTHOR CONTRIBUTIONS

KC and HM made a substantial contribution to the acquisition, analysis, and interpretation of data; and the draft and revision of the manuscript. CD, RN, RF, TA, and EP made a substantial contribution to the acquisition and analysis of data. JM revised the manuscript. CP made a substantial contribution to the conception and design of the work, analysis, interpretation of data, and the draft and revision of the manuscript. All authors have approved the submitted manuscript and are accountable for their contributions and ensured that questions related to the accuracy or integrity of any part of the work were appropriately investigated, resolved, and documented in the literature.

FUNDING

KAC was supported by the Coordenação de Aperfeiçoamento de Pessoal de Nível Superior (CAPES); HM received support from the Fundação de Amparo a Pesquisa do Estado de São Paulo (FAPESP: 2018/11042-0).

ACKNOWLEDGMENTS

The authors would like to acknowledge the Department of Gynaecology & Obstetrics of FMRP-USP for the technical assistance offered during sample collection and hormonal analyses. We thank Bruno G. Vianna for the support with LCM and samples storage. We also thank Elivane Silva Victor (HIAE) for the statistical analyses and Prof. Ises de Almeida Abrahamsohn for critically reviewing the manuscript.

SUPPLEMENTARY MATERIAL

The Supplementary Material for this article can be found online at <https://www.frontiersin.org/articles/10.3389/fmolb.2022.854991/full#supplementary-material>

Supplementary Figure S1 | Representative images from *STS* and *HSD17B1* protein expression in both menstrual cycle phases analysed by immunohistochemistry.

Supplementary Figure S2 | Relative gene expression in glandular and stromal areas in endometriosis tissue. Gene expression levels of *CYP19A1*, *STS* and *HSD17B1* were analysed by qRT-PCR in eutopic endometrium from endometriosis patients (EE) and lesions. Relative gene expression levels were normalised by *GAPDH*. Bars represent the absolute CT values from each patient individually.

REFERENCES

- Aghajanova, L., Hamilton, A., Kwintkiewicz, J., Vo, K. C., Giudice, L. C., and Jaffe, R. B. (2009). Steroidogenic Enzyme and Key Decidualization Marker Dysregulation in Endometrial Stromal Cells from Women with versus without Endometriosis. *Biol. Reprod.* 80, 105–114. doi:10.1095/biolreprod.108.070300
- Attar, E., and Bulun, S. E. (2006). Aromatase Inhibitors: the Next Generation of Therapeutics for Endometriosis? *Fertil. Sterility* 85, 1307–1318. doi:10.1016/j.fertnstert.2005.09.064
- Barra, F., Romano, A., Grandi, G., Facchinetti, F., and Ferrero, S. (2019). Future Directions in Endometriosis Treatment: Discovery and Development of Novel Inhibitors of Estrogen Biosynthesis. *Expert Opin. Investig. Drugs* 28, 501–504. doi:10.1080/13543784.2019.1618269
- Bartels, P. H., Thompson, D., Bartels, H. G., Montironi, R., Scarpelli, M., and Hamilton, P. W. (1995). Machine Vision-Based Histometry of Premalignant and Malignant Prostatic Lesions. *Pathol. - Res. Pract.* 191, 935–944. doi:10.1016/s0344-0338(11)80979-9
- Bastos Wolff, R., Teixeira Gomes, R. C., Verna, C., Cristofani Maioral, G. C. C., Cristina Rampazo, T., Santos Simões, R., et al. (2012). Molecular Features of Sexual Steroids on Cartilage and Bone. *Revista da Associação Médica Brasileira (English Edition)* 58, 493–497. doi:10.1016/s2255-4823(12)70235-7
- Bulun, S. E., Cheng, Y. H., Pavone, M. E., Yin, P., Imir, G., Utsunomiya, H., et al. (2010). 17 β -Hydroxysteroid Dehydrogenase-2 Deficiency and Progesterone Resistance in Endometriosis. *Semin. Reprod. Med.* 28, 44–50. doi:10.1055/s-0029-1242992
- Bulun, S. E., Fang, Z., Imir, G., Gurates, B., Tamura, M., Yilmaz, B., et al. (2004). Aromatase and Endometriosis. *Semin. Reprod. Med.* 22, 45–50. doi:10.1055/s-2004-823026
- Cheng, Y. H., Imir, A., Fenkci, V., Yilmaz, M. B., and Bulun, S. E. (2007). Stromal Cells of Endometriosis Fail to Produce Paracrine Factors that Induce Epithelial 17 β -Hydroxysteroid Dehydrogenase Type 2 Gene and its Transcriptional Regulator Sp1: a Mechanism for Defective Estradiol Metabolism. *Am. J. Obstet. Gynecol.* 196, 391–398. doi:10.1016/j.ajog.2006.12.014
- Cohen, A., Shmoish, M., Levi, L., Cheruti, U., Levavi-Sivan, B., and Lubzens, E. (2008). Alterations in Micro-ribonucleic Acid Expression Profiles Reveal a Novel Pathway for Estrogen Regulation. *Endocrinology* 149, 1687–1696. doi:10.1210/en.2007-0969
- Colette, S., Defrère, S., Van Kerk, O., Van Langendonck, A., Dolmans, M.-M., and Donnez, J. (2013). Differential Expression of Steroidogenic Enzymes According to Endometriosis Type. *Fertil. Sterility* 100, 1642–1649. doi:10.1016/j.fertnstert.2013.08.003
- Colette, S., Lousse, J. C., Defrère, S., Curaba, M., Heilier, J. F., Van Langendonck, A., et al. (2009). Absence of Aromatase Protein and mRNA Expression in Endometriosis. *Hum. Reprod.* 24, 2133–2141. doi:10.1093/humrep/dep199
- Cornillie, F. J., Oosterlynck, D., Lauweryns, J. M., and Koninck, P. R. (1990). Deeply Infiltrating Pelvic Endometriosis: Histology and Clinical Significance. *Fertil. Steril* 53, 978. doi:10.1016/S0015-0282(16)53570-5
- Da Costa, K. A., Malvezzi, H., Viana, B. G., Filippi, R. Z., Neme, R. M., Aloia, T. P. A., et al. (2019). Validation of Laser Capture Microdissection Protocol in Endometriosis Studies. *Medicina (Kaunas)* 55, 1–12. doi:10.3390/medicina55090520
- Dassen, H., Punyadeera, C., Kamps, R., Delvoux, B., Van Langendonck, A., Donnez, J., et al. (2007). Estrogen Metabolizing Enzymes in Endometrium and Endometriosis. *Hum. Reprod.* 22, 3148–3158. doi:10.1093/humrep/dem310
- Delvoux, B., D'Hooghe, T., Kyama, C., Koskimies, P., Hermans, R. J. J., Dunselman, G. A., et al. (2014). Inhibition of Type 1 17 β -Hydroxysteroid Dehydrogenase Impairs the Synthesis of 17 β -Estradiol in Endometriosis Lesions. *J. Clin. Endocrinol. Metab.* 99, 276–284. doi:10.1210/jc.2013.2851
- Eskenazi, B., and Warner, M. L. (1997). Epidemiology of Endometriosis. *Obstet. Gynecol. Clin. North America* 24, 235–258. doi:10.1016/s0889-8545(05)70302-8
- Foster, P. A. (2021). Steroid Sulphatase and its Inhibitors: Past, Present and Future. *Molecules* 26, 2852. doi:10.3390/molecules26102852
- Foti, P. V., Farina, R., Palmucci, S., Vizzini, I. A. A., Libertini, N., Coronella, M., et al. (2018). Endometriosis: Clinical Features, MR Imaging Findings, and Pathologic Correlation. *Insights Imaging* 9, 149–172. doi:10.1007/s13244-017-0591-0
- Gibson, D., Simitsidellis, I., Collins, F., and Saunders, P. (2018). Endometrial Intracrinology: Oestrogens, Androgens, and Endometrial Disorders. *Ijms* 19, 3276. doi:10.3390/ijms19103276
- Giudice, L. C., and Kao, L. C. (2004). Endometriosis. *Lancet* 364 (04), 1789–1799. doi:10.1016/S0140-6736(04)17403-5
- Heilier, J.-F., Donnez, O., Van Kerckhove, V., Lison, D., and Donnez, J. (2006). Expression of Aromatase (P450 aromatase/CYP19) in Peritoneal and Ovarian Endometriotic Tissues and Deep Endometriotic (Adenomyotic) Nodules of the Rectovaginal Septum. *Fertil. Sterility* 85, 1516–1518. doi:10.1016/j.fertnstert.2005.10.041
- Hudelist, G., Czerwenka, K., Keckstein, J., Haas, C., Fink-Retter, A., Gschwanter-Kaulich, D., et al. (2007). Expression of Aromatase and Estrogen Sulfotransferase in Eutopic and Ectopic Endometrium: Evidence for Unbalanced Estradiol Production in Endometriosis. *Reprod. Sci.* 14, 798–805. doi:10.1177/1933719107309120
- Huhtinen, K., Desai, R., Stähle, M., Salminen, A., Handelsman, D. J., Perheentupa, A., et al. (2012). Endometrial and Endometriotic Concentrations of Estrone and Estradiol Are Determined by Local Metabolism rather Than Circulating Levels. *J. Clin. Endocrinol. Metab.* 97, 4228–4235. doi:10.1210/jc.2012-1154
- Ing, N. H. (2005). Steroid Hormones Regulate Gene Expression Posttranscriptionally by Altering the Stabilities of Messenger RNAs. *Biol. Reprod.* 72, 1290–1296. doi:10.1095/biolreprod.105.040014
- Jackson, B., and Telnor, D. E. (2006). Managing the Mispliced: Approach to Endometriosis. *Can. Fam. Physician* 52, 1420–1424.
- Kamergorodsky, G., Ribeiro, P. A. A., Galvão, M. A. L., Abrão, M. S., Donadio, N., de Barros Moreira Lemos, N. L., et al. (2009). Histologic Classification of Specimens from Women Affected by Superficial Endometriosis, Deeply Infiltrating Endometriosis, and Ovarian Endometriomas. *Fertil. Sterility* 92, 2074–2077. doi:10.1016/j.fertnstert.2009.05.086
- Kim, C. K., Linscott, M. L., Flury, S., Zhang, M., Newby, M. L., and Pak, T. R. (2021). 17 β -Estradiol Regulates miR-9-5p and miR-9-3p Stability and Function in the Aged Female Rat Brain. *Noncoding RNA* 7, 53. doi:10.3390/ncrna7030053
- Klinge, C. M. (2012). miRNAs and Estrogen Action. *Trends Endocrinol. Metab.* 23, 223–233. doi:10.1016/j.tem.2012.03.002
- Kolanska, K., Bendifallah, S., Canlorbe, G., Mekinian, A., Touboul, C., Aractingi, S., et al. (2021). Role of miRNAs in normal Endometrium and Endometrial Disorders: Comprehensive Review. *J. Clin. Med.* 10, 3457. doi:10.3390/jcm10163457
- Konings, G., Brentjens, L., Delvoux, B., Linnanen, T., Cornel, K., Koskimies, P., et al. (2018). Intracrine Regulation of Estrogen and Other Sex Steroid Levels in Endometrium and Non-gynecological Tissues; Pathology, Physiology, and Drug Discovery. *Front. Pharmacol.* 9, 940. doi:10.3389/fphar.2018.00940
- Lin, D., Sugawara, T., Strauss, J. F., Clark, B. J., Stocco, D. M., Saenger, P., et al. (1995). Role of Steroidogenic Acute Regulatory Protein in Adrenal and Gonadal Steroidogenesis. *Science* 267, 1828–1831. doi:10.1126/science.7892608
- Liu, A. J., Guan, Z., Zhang, Z. M., Wei, L. X., and Li, Y. L. (2008). Study on Expression of Estrogen Receptor Isoforms in Eutopic and Ectopic Endometrium of Ovarian Endometriosis. *Zhonghua Bing Li Xue Za Zhi* 37, 584–588.
- Maltais, R., Trottier, A., Roy, J., Ayan, D., Bertrand, N., and Poirier, D. (2018). Pharmacokinetic Profile of PBRM in Rodents, a First Selective Covalent Inhibitor of 17 β -HSD1 for Breast Cancer and Endometriosis Treatments. *J. Steroid Biochem. Mol. Biol.* 178, 167–176. doi:10.1016/j.jsbmb.2017.12.007
- Matsuzaki, S., Canis, M., Pouly, J.-L., Déchelotte, P. J., and Mage, G. (2006). Analysis of Aromatase and 17 β -Hydroxysteroid Dehydrogenase Type 2 Messenger Ribonucleic Acid Expression in Deep Endometriosis and Eutopic Endometrium Using Laser Capture Microdissection. *Fertil. Sterility* 85, 308–313. doi:10.1016/j.fertnstert.2005.08.017
- Matsuzaki, S., Canis, M., Vaur-Barrière, C., Pouly, J. L., Boespflug-Tanguy, O., Penault-Llorca, F., et al. (2004). DNA Microarray Analysis of Gene Expression Profiles in Deep Endometriosis Using Laser Capture Microdissection. *Mol. Hum. Reprod.* 10, 719–728. doi:10.1093/molehr/gah097
- Miller, E. J., and Fraser, I. S. (2015). The Importance of Pelvic Nerve Fibers in Endometriosis. *Women's Health (Lond Engl)* 11, 611–618. doi:10.2217/whe.15.47
- Mori, T., Ito, F., Koshiba, A., Kataoka, H., Takaoka, O., Okimura, H., et al. (2019). Local Estrogen Formation and its Regulation in Endometriosis. *Reprod. Med. Biol.* 18, 305–311. doi:10.1002/rmb2.12285

- Mori, T., Ito, F., Koshiba, A., Kataoka, H., Tanaka, Y., Okimura, H., et al. (2018). Aromatase as a Target for Treating Endometriosis. *J. Obstet. Gynaecol. Res.* 44, 1673–1681. doi:10.1111/jog.13743
- Mori, T., Ito, F., Matsushima, H., Takaoka, O., Koshiba, A., Tanaka, Y., et al. (2015). Dienogest Reduces HSD17 β 1 Expression and Activity in Endometriosis. *J. Endocrinol.* 225, 69–76. doi:10.1530/joe-15-0052
- Nap, A. W., Groothuis, P. G., Demir, A. Y., Evers, J. L. H., and Dunselman, G. A. J. (2004). Pathogenesis of Endometriosis. *Best Pract. Res. Clin. Obstet. Gynaecol.* 18, 233–244. doi:10.1016/j.bpobgyn.2004.01.005
- Noble, L. S., Takayama, K., Zeitoun, K. M., Putman, J. M., Johns, D. A., Hinshelwood, M. M., et al. (1997). Prostaglandin E 2 Stimulates Aromatase Expression in Endometriosis-Derived Stromal Cells. *J. Clin. Endocrinol. Metab.* 82, 600. doi:10.1210/jcem.82.2.3783
- Olive, D. L., and Schwartz, L. B. (1993). Endometriosis. *N. Engl. J. Med.* 328, 1759–1769. doi:10.1056/NEJM199306173282407
- Piccinato, C. A., Malvezzi, H., Gibson, D. A., and Saunders, P. T. K. (2018a). SULFATION PATHWAYS: Contribution of Intracrine Oestrogens to the Aetiology of Endometriosis. *J. Mol. Endocrinol.* 61, T253–T270. doi:10.1530/jme-17-0297
- Piccinato, C. A., Neme, R. M., Torres, N., Sanches, L. R., Cruz Derogis, P. B. M., Brudniewski, H. F., et al. (2016b). Increased Expression of CYP1A1 and CYP1B1 in Ovarian/peritoneal Endometriotic Lesions. *Reproduction* 151, 683–692. doi:10.1530/rep-15-0581
- Piccinato, C. A., Neme, R. M., Torres, N., Sanches, L. R., Derogis, P. B. M. C., Brudniewski, H. F., et al. (2016a). Effects of Steroid Hormone on Estrogen Sulfotransferase and Steroid Sulfatase Expression in Endometriosis Tissue and Stromal Cells. *J. Steroid Biochem. Mol. Biol.* 158, 117–126. doi:10.1016/j.jsbmb.2015.12.025
- Piccinato, C. A., Neme, R. M., Torres, N., Silvério, R., Pazzini, V. B., Rosa e Silva, J. C., et al. (2017). Is Cytochrome P450 3A4 Regulated by Menstrual Cycle Hormones in Control Endometrium and Endometriosis? *Mol. Cell Biochem* 427, 81–89. doi:10.1007/s11010-016-2899-3
- Piccinato, C. A., Neme, R. M., Torres, N., Victor, E. d. S., Brudniewski, H. F., Silva, J. C. R. e., et al. (2018b). Enhanced UGT1A1 Gene and Protein Expression in Endometriotic Lesions. *Reprod. Sci.* 25, 1371–1375. doi:10.1177/1933719118764255
- Purohit, A., Fusi, L., Brosens, J., Woo, L. W., Potter, B. V., and Reed, M. J. (2008). Inhibition of Steroid Sulphatase Activity in Endometriotic Implants by 667 COUMATE: A Potential New Therapy. *Hum. Reprod.* 23, 290–297. doi:10.1093/humrep/dem308
- Salah, M., AbdelsamieAhmed, A. S., and Frotscher, M. (2017). First Dual Inhibitors of Steroid Sulfatase (STS) and 17 β -Hydroxysteroid Dehydrogenase Type 1 (17 β -HSD1): Designed Multiple Ligands as Novel Potential Therapeutics for Estrogen-dependent Diseases. *J. Med. Chem.* 60 (9), 4086–4092. doi:10.1021/acs.jmedchem.7b00062
- Signorile, P. G., and Baldi, A. (2010). Endometriosis: New Concepts in the Pathogenesis. *Int. J. Biochem. Cell Biol.* 42, 778–780. doi:10.1016/j.biocel.2010.03.008
- Simpson, E. R., Mahendroo, M. S., Means, G. D., Kilgore, M. W., Hinshelwood, M. M., Graham-Lorence, S., et al. (1994). Aromatase Cytochrome P450, the Enzyme Responsible for Estrogen Biosynthesis. *Endocr. Rev.* 15, 342–355. doi:10.1210/edrv-15-3-342
- Smolarz, B., Szylo, K., and Romanowicz, H. (2021). Endometriosis: Epidemiology, Classification, Pathogenesis, Treatment, and Genetics (Review of Literature). *Int. J. Mol. Sci.* 22, 1054. doi:10.3390/ijms221910554
- Šmuc, T., Hevir, N., Ribic-Pucelj, M., Husen, B., Thole, H., and Rižner, T. L. (2009). Disturbed Estrogen and Progesterone Action in Ovarian Endometriosis. *Mol. Cell Endocrinol.* 301, 59–64. doi:10.1016/j.mce.2008.07.020
- Šmuc, T., Pucelj, M. R., Šinkovec, J., Husen, B., Thole, H., and Lanisnik Rizner, T. (2007). Expression Analysis of the Genes Involved in Estradiol and Progesterone Action in Human Ovarian Endometriosis. *Gynecol. Endocrinol.* 23, 105–111. doi:10.1080/09513590601152219
- Szaflik, T., Smolarz, B., Mroczkowska, B., Kulig, B., Soja, M., Romanowicz, H., et al. (2020). An Analysis of ESR2 and CYP19A1 Gene Expression Levels in Women with Endometriosis. *In Vivo* 34, 1765–1771. doi:10.21873/invivo.11970
- Taylor, H. S., Kotlyar, A. M., and Flores, V. A. (2021). Endometriosis Is a Chronic Systemic Disease: Clinical Challenges and Novel Innovations. *The Lancet* 397, 839–852. doi:10.1016/s0140-6736(21)00389-5
- Utsunomiya, H., Suzuki, T., Kaneko, C., Takeyama, J., Nakamura, J., Kimura, K., et al. (2001). The Analyses of 17-Hydroxysteroid Dehydrogenase Isozymes in Human Endometrial Hyperplasia and Carcinoma. *J. Clin. Endocrinol. Metab.* 86, 3436–3443. doi:10.1210/jc.86.7.3436
- Vermeulen, N., Abrao, M. S., Einarsson, J. I., Horne, A. W., Johnson, N. P., Lee, T. T. M., et al. (2021). Endometriosis Classification, Staging and Reporting Systems: a Review on the Road to a Universally Accepted Endometriosis Classification. *Facts, Views Vis. ObGyn* 13, 1–26. doi:10.52054/fvvo.13.3.025
- Wang, S., Wang, L., Zhu, T., Gao, X., Li, J., Wu, Y., et al. (2010). Improvement of Tissue Preparation for Laser Capture Microdissection: Application for Cell Type-specific miRNA Expression Profiling in Colorectal Tumors. *BMC Genomics* 11, 163. doi:10.1186/1471-2164-11-163
- Yang, S., Fang, Z., Gurates, B., Tamura, M., Miller, J., Ferrer, K., et al. (2001). Stromal PRs Mediate Induction of 17 β -Hydroxysteroid Dehydrogenase Type 2 Expression in Human Endometrial Epithelium: A Paracrine Mechanism for Inactivation of E2. *Mol. Endocrinol.* 15, 2093–2105. doi:10.1210/mend.15.12.0742

Conflict of Interest: The authors declare that the research was conducted in the absence of any commercial or financial relationships that could be construed as a potential conflict of interest.

Publisher's Note: All claims expressed in this article are solely those of the authors and do not necessarily represent those of their affiliated organizations, or those of the publisher, the editors, and the reviewers. Any product that may be evaluated in this article, or claim that may be made by its manufacturer, is not guaranteed or endorsed by the publisher.

Copyright © 2022 Da Costa, Malvezzi, Dobo, Neme, Filippi, Aloia, Prado, Meola and Piccinato. This is an open-access article distributed under the terms of the Creative Commons Attribution License (CC BY). The use, distribution or reproduction in other forums is permitted, provided the original author(s) and the copyright owner(s) are credited and that the original publication in this journal is cited, in accordance with accepted academic practice. No use, distribution or reproduction is permitted which does not comply with these terms.

Advantages of publishing in Frontiers



OPEN ACCESS

Articles are free to read
for greatest visibility
and readership



FAST PUBLICATION

Around 90 days
from submission
to decision



HIGH QUALITY PEER-REVIEW

Rigorous, collaborative,
and constructive
peer-review



TRANSPARENT PEER-REVIEW

Editors and reviewers
acknowledged by name
on published articles

Frontiers

Avenue du Tribunal-Fédéral 34
1005 Lausanne | Switzerland

Visit us: www.frontiersin.org

Contact us: frontiersin.org/about/contact



REPRODUCIBILITY OF RESEARCH

Support open data
and methods to enhance
research reproducibility



DIGITAL PUBLISHING

Articles designed
for optimal readership
across devices



FOLLOW US

@frontiersin



IMPACT METRICS

Advanced article metrics
track visibility across
digital media



EXTENSIVE PROMOTION

Marketing
and promotion
of impactful research



LOOP RESEARCH NETWORK

Our network
increases your
article's readership